UNIVERSITY OF CALIFORNIA
ENGINEERING AND PHYSICAL SCIENCES EXTENSION SERIES

UNIVERSITY
OF FLORIDA
LIBRARIES

1853

Digitized by the Internet Archive
in 2013

http://archive.org/details/ballisticmissile00seif

BALLISTIC
MISSILE
AND
SPACE
VEHICLE
SYSTEMS

Engineering and Physical Science Extension Series,
University of California, Los Angeles

Howard Seifert, Editor
SPACE TECHNOLOGY

Robert L. Pecsok, Editor
PRINCIPLES AND PRACTICE OF GAS CHROMATOGRAPHY

Howard Seifert and Kenneth Brown, Editors
BALLISTIC MISSILE AND SPACE VEHICLE SYSTEMS

BALLISTIC MISSILE AND SPACE VEHICLE SYSTEMS

HOWARD S. SEIFERT

Professor, Aeronautical Engineering, Stanford University
Director of Professional Development, United Technology Corporation

KENNETH BROWN

Editor, John Wiley & Sons, Inc., Member of Instructional Staff
Engineering and Physical Science Extension
University of California, Los Angeles

New York • London, John Wiley & Sons, Inc.

Copyright © 1961 by John Wiley & Sons, Inc.

All Rights Reserved

This book or any part thereof must not
be reproduced in any form without the
written permission of the publisher.

Library of Congress Catalog Card Number: 61-11496
Printed in the United States of America

PREFACE

The course entitled "Space Technology" which was offered at the University of California in 1957-58 under the auspices of the UCLA Engineering Extension Department enjoyed considerable popularity, and was documented in a Wiley book of the same title. However, it was felt that a second course of greater depth but more limited breadth was needed, in which the relationships among the various parts of a missile or space system were emphasized. Accordingly, the course "Ballistic Missile and Space Vehicle Systems," from which this book is derived, was given (to duplicate sections) on the UCLA campus under the Engineering Extension Rocket Propulsion Certificate Program, and ultimately was filmed for distribution by UCLA to industrial and educational organizations.

The philosophy of "Ballistic Missile and Space Vehicle Systems" differs from that of "Space Technology" in that the engineering design aspects of vehicle mechanical systems are stressed, whereas space biology, space physics, and space communications are not treated. The content was outlined by the editors to cover the subject as fully as possible, and individual chapters were supplied by specialists, each of whom has made significant contributions to his special subfield of space technology. The lecturers include many men with major responsibilities in academic, government, and industrial research organizations doing work in aerospace engineering. This composite or "team" effort in authorship, just as in research, provides a result more authoritative, effective, and up-to-date than any single individual could produce.

The text includes the fundamental laws of propulsion, structures, trajectories, guidance and control, and states many of the interface problems which result when two or more of the subsystems interact. The engineering design principles of each subsystem are discussed, and the treatment has been expanded to include a survey of vehicle reentry stabilization and of vehicle support systems.

4.24.62 Publ. astronomy

Propulsion is treated in five chapters, under the headings of propulsion fundamentals, liquid propellant engines, solid propellant engines, nuclear propulsion, and electric propulsion. The section on structures includes fundamentals, as well as static and dynamic vehicle analysis. Flight dynamics begins with fundamental ballistics and extends through satellites, satellite interceptors, and lunar probes. A special chapter discusses the relation between vehicle mission and vehicle design. Finally, a comprehensive discussion of control system theory prefaces an analysis of radio and of inertial guidance systems.

We would like to express sincere appreciation to all of the authors who, although they were harassed by a host of professional duties, took time to make worthy contributions to this book. Special thanks should be given also to Mr. John Dillon, Head of the Engineering Extension Department, to Dr. Clifford Bell, Head of the Physical Science Extension Department, and to Mr. Oscar Patterson of the Department of Visual Communication, University of California, for handling the complex arrangements of filming the twenty-one lecturers and distributing the film series throughout the country, and to Barbara Peer, Aerospace Corporation, for handling the innumerable details involved in communicating with the twenty-one authors and keeping their efforts on schedule. Finally, we wish to express appreciation to our wives, Mary Seifert and Jerre Brown, for their patience during the hours we spent coordinating the lecture series, filming the lectures, and editing and proofreading the manuscript.

May, 1961

HOWARD SEIFERT

KENNETH BROWN

CONTENTS

Chapter 1 Systems Engineering, *E. B. Doll* 1

1.1 An Introduction to Systems Engineering 1
1.2 The Concept of Systems Engineering 4
1.3 The Application of Systems Engineering to Ballistic Missiles 4
1.4 The Systems Engineer 14

Chapter 2 Rocket Propulsion Fundamentals, *H. S. Seifert* 15

2.1 Introduction 15
2.2 The Magnitude of Rocket Thrust 16
2.3 Determination of the Jet Velocity 20
2.4 Flow Through De Laval Nozzles 24
2.5 Mass Flow Through the Nozzle 25
2.6 Nozzle Area Ratio ϵ as a Function of Pressure Ratio 28
2.7 Thrust Coefficient C_F 28
2.8 Design and Performance Criteria 34
2.9 Effect of System on Motor Design 39
2.10 Fundamental Design Procedure 43
2.11 Propellant Injector Design 47
2.12 Commercial Specifications 50

Chapter 3 Liquid Engine Design Parameters, *J. O. Crum* 54

3.1 Introduction 54
3.2 Engine Components 55

Chapter 4 Solid Engines and Their Design Parameters, *C. E. Bartley* 77

4.1 Introduction 77
4.2 Operation of the Solid Propellant Rocket Motor 80

4.3 Propellants and Their Characteristics 82
4.4 The Effect of Application on Rocket Design 86
4.5 Trends in Solid Propellant Rocket Development 88

Chapter 5 Nuclear Rocket Propulsion, *R. D. DeLauer* 90

5.1 Introduction to Nuclear Energy 90
5.2 Materials 93
5.3 Potential Performance 98
5.4 Reactor Design Problems 103
5.5 Vehicle Design Problem Areas 108
5.6 Testing 109
5.7 Power Density 114

Chapter 6 Plasma Propulsion Systems, *D. B. Langmuir* 119

6.1 Introduction 119
6.2 General Theory 120
6.3 Performance Properties of the Electrically Propelled Rocket 124
6.4 The Plasma Engine 127
6.5 Electrostatic Propulsion 128
6.6 Conclusion 136

Chapter 7 Propulsion Interface, *J. E. Brooks* 138

7.1 Interface Concept 138
7.2 Synthesis of System Interfaces 142
7.3 Engineering of Interface Problems 144
7.4 System Performance and Trajectory Considerations 144
7.5 Propellant Utilization and Mixture Ratio Control 146
7.6 Thrust Vector Control by Gimbaling 148
7.7 Transient Operation 150
7.8 Staging Problems 151
7.9 Support System Considerations 152

Chapter 8 Fundamental Flight Dynamics and Staging, *A. R. Hibbs* 155

8.1 Vacuum Velocity Law 155
8.2 Vertical Flight Near the Earth's Surface 158
8.3 Motion Over a Spherical Nonrotating Earth 159
8.4 Motion in an Inverse Square Field 161
8.5 Interplanetary Flight 164

Chapter 9 Mission and Vehicle Design, *W. H. Amster* 168

9.1 Introduction 168
9.2 Analysis of Ballistic Flight 169
9.3 Missions for Space Vehicles 176
9.4 Velocity Capability of Space Vehicles 191
9.5 Mission and Vehicle Size 197
9.6 Systems Integration of Vehicles, Stages, and Payloads 199
9.7 Symbols 204

Chapter 10 Structure Fundamentals, *A. Kaplan* 207

10.1 Introduction 207
10.2 Trajectory Characteristics 207
10.3 Principal Loads 212
10.4 Typical Structural Elements 221

Chapter 11 Structures: Static Integrated Analysis, *H. W. Johnson* 232

11.1 Introduction 232
11.2 Structural Design Requirements and System Interactions 233
11.3 Parametric Missile Design Analysis 237

Chapter 12 Structures: Integrated Dynamic Analysis, *J. G. Berry, H. E. Lindberg, and J. D. Wood* 253

12.1 Introduction 253
12.2 In-Flight Dynamic Loads 254
12.3 Simplified Equations of Motion 261
12.4 Illustrative Example 274
12.5 Prelaunch-Postlaunch Dynamic Loads 275

Chapter 13 Estimating Performance Capabilities of Boost Rockets, *P. Dergarabedian, and R. P. Ten Dyke* 296

13.1 Introduction 296
13.2 Velocity Versus Burnout Angle 299
13.3 Burnout Altitude Versus Burnout Angle 306
13.4 Burnout Surface Range 307
13.5 Free-Flight Trajectory 307
13.6 Range Equation 308
13.7 Selection of Missile Design Parameters 314
13.8 Symbols 322

Chapter 14 Trajectory Analysis, *A. B. Mickelwait* 324

14.1 Introduction 324
14.2 Uniform Gravitational Field 325
14.3 Motion in General Gravitational Field 329
14.4 Elementary Trajectory and Guidance Analysis for Ground-to-Ground Vehicles 333
14.5 Earth Satellite Orbital Analysis 336

Chapter 15 Control System Theory and Components, *J. R. Burnett* 345

15.1 Introduction 345
15.2 Control System Theory 345
15.3 Transfer Functions 349

15.4 Complex Frequency Domain 351
15.5 Feedback Concept 352
15.6 Stability 357
15.7 Ballistic Missile Control Systems 362
15.8 Inputs 367
15.9 Other Considerations 369
15.10 Summary 370

Chapter 16 Radio Guidance Fundamentals, *R. B. Muchmore* 372

16.1 Introduction 372
16.2 Electromagnetic Theory 373
16.3 Radio Measurements 379
16.4 Radio Guidance Errors 386
16.5 System Design for a Hypothetical System 395
16.6 Conclusion 400

Chapter 17 Inertial Guidance for Ballistic Vehicles, *W. T. Russell* 402

17.1 Introduction 402
17.2 Gyroscopes 404
17.3 Accelerometers 415
17.4 Stabilized Platforms 420
17.5 Attitude Control System 424
17.6 Gravity 426
17.7 Guidance Schemes 430
17.8 Ballistic Missile Example 432
17.9 Sounding Rocket Problem 437

Chapter 18 Re-entry and Recovery, *J. R. Sellars* 448

18.1 Introduction 448
18.2 General Trajectory Considerations 449
18.3 Flow Around Bodies at Hypersonic Speeds 453

18.4 Heat Transfer Calculations 456
18.5 Heat Protection Systems 459
18.6 Satellite Re-entries 461
18.7 Satellite Heat Shielding Techniques 467

Chapter 19 Auxiliary Subsystems, *D. E. Shonerd* 470

19.1 Introduction 470
19.2 Objectives of Auxiliary Subsystems 479
19.3 Description of Typical Auxiliary Subsystems 481
19.4 Countdown Procedures 486
19.5 Data Acquisition 492
19.6 Range Safety 499

Chapter 20 The Missile as an Integrated Space Vehicle System, *K. Brown* 503

20.1 Introduction 503
20.2 Performance Parameters 504
20.3 Over-all Systems Analysis 506
20.4 Specific Design Parameters 512
20.5 Conclusion 514

Index 517

1

SYSTEMS ENGINEERING

E. B. Doll

1.1 AN INTRODUCTION TO SYSTEMS ENGINEERING

1.1.1 A Definition of Systems Engineering

Systems engineering is the job of integrating the whole, as distinct from the invention and design of its parts; the creation and analysis of the over-all answer to a problem; the breaking down of the total into a set of harmonious, specified parts; the assurance of compatibility and consistency in the ensemble; and the relating of that ensemble to the outside world that has originated the need and that will employ the final result. These considerations are present in varying degrees in the production of every piece or group of equipment, from a chair to a transcontinental railroad. Always some fraction of every engineering effort has in effect been devoted to this systems engineering.

The top systems engineer must be a good manager. Furthermore, he must be a good scientist and engineer with considerable breadth. In each project a large number of specialized fields of engineering and science are involved. The systems engineering task usually involves integration of several fields—aerodynamics, electronics, chemistry, metallurgy, astronomy, and hydraulics; a systems engineering team must include experts in the scientific fundamentals of these specialized fields. The top engineer of each specialty or component field making up the system must be basically a good systems engineer, even though his major detailed knowledge may be in the field of his specialty. Below him are the specialists, experts in the different fields that are a part of the total system. The relationship among these experts cannot be smooth and cannot be kept in proper balance for the good of the system as a whole unless there is at least one expert in each of the component areas who is basically a systems man.

As the individual specialties unfold in this book, we can look back and recognize that in missile and space system problems the role of systems engineering cannot be discounted. We can readily see the relation of systems engineering to space missions as well as to missile systems. It is probable that the ballistic missile, developed for military purposes, will be the basic instrument that will permit the initial conquest of space. In the interest of simplicity, the following comments will be devoted to ballistic missile systems.

1.1.2 What Is a System ?

A system is a purposeful aggregation of subsystems which are functionally and sometimes physically interdependent. The operation of any subsystem is affected by one, several, or all the other subsystems. For example, an industrial refinery, an automobile manufacturing plant, a transcontinental railroad, and many other complex industrial activities can be categorized as systems and lend themselves, especially in their development period, to the same analytical and investigative techniques that have been applied successfully to the development of missiles. The ballistic missile is a representative system, part of a large system which is called a weapon system.

1.1.3 What Is a Missile Subsystem?

Within a system there are several subsystems. The Atlas ICBM, for example (Fig. 1.1), contains the re-entry vehicle or payload, the prime purpose of the missile. It includes an airframe which is a series of tanks and a certain amount of plumbing. It houses a guidance system, which is in evidence from some of the antenna structures on the side. It contains a propulsion system, represented by the engine at the base and by the small vernier engines. There are other elements on board the missile, each one a staggering engineering task

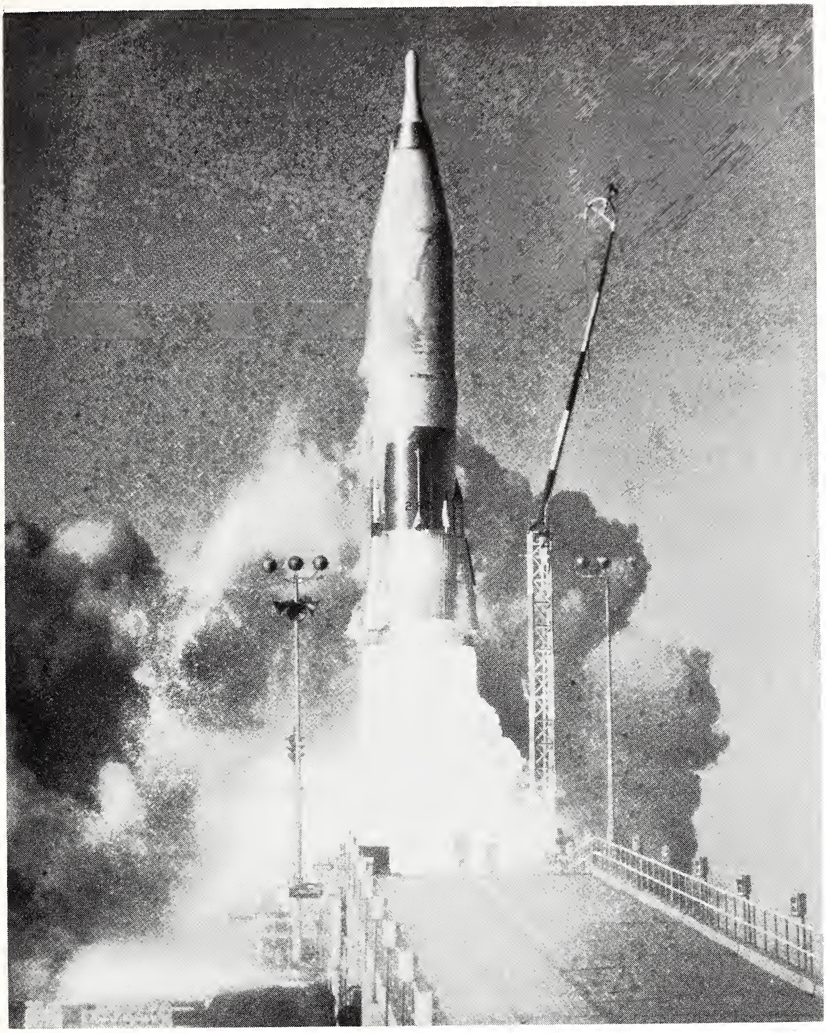

Fig. 1. 1

in itself. The Atlas is a truly integrated system.

The Atlas weapon system consists of not only the missile but also a ground support system, including in part a launcher, a propellant supply, a propellant-handling system, ground checkout equipment, ground launch control equipment, maintenance equipment, and a chain of supplies that goes all the way back to the factories. Thus the system problem is complicated greatly by the fact that, along with the design of a missile, a ground support system has to be developed, people must be trained, technical manuals must be written.

In addition, there are major systems on the ground which are directly related to the Atlas—the radar station and the very complex computer which operates in conjunction with the guidance. The complete system is an extremely complex device. All the elements are integrated together for one sole purpose, to perform a specified mission.

1.2 THE CONCEPT OF SYSTEMS ENGINEERING

1.2.1 The Importance of Optimization

The mission of a ballistic missile is to deliver a relatively small payload to a target area. The ratio between total gross weight at take-off and payload is far larger than for a conventional aircraft. Consequently, the efficiency is small, and a few errors one way or another can be the difference between success and failure.

1.2.2 Technical Disciplines

The ballistic missile system uses many of the technical disciplines from university curricula—electrical engineering, electronic engineering, mechanical engineering, thermodynamics, chemical engineering, aerodynamics. The system is characterized by the pulling together of a large number of scientific disciplines, with the highest qualities of performance or intellectual capacity available in each area brought into focus on an over-all systems problem. Working together are specialists in individual technical fields and a number of people with sufficient breadth to appreciate interface problems between the many technical disciplines and to act as "referees" in applying the various technologies.

1.3 THE APPLICATION OF SYSTEMS ENGINEERING TO BALLISTIC MISSILES

1.3.1 Required Specifications

The first consideration is the customer's needs. In industry money is not invested for pleasure or satisfaction; money is invested to supply products that someone will buy. As for the military situation, this consideration is what the Air Force calls a GOR, or general operational requirement. Such customer requirements, such specifications, are dependent on the state of the art, the anticipated capability of the component, and the success that can be achieved in a properly conducted development program. Once the customer's basic need is established, a development or systems effort must be organized to produce a system to meet the need.

The project goal is to supply the customer's requirements by an established time, recognizing the constant changes inevitably associated with major systems such as a ballistic missile or space vehicle system. The element of urgency is ever present since having the missile ready by the date set for completion is the most important criterion of performance.

1.3.2 Urgency

In the missile business it is said, "If it wasn't required yesterday, it isn't worth doing." There is constant pressure to meet a certain time schedule. As far as military technology is concerned, today is a revolutionary period and we are constantly threatened with the problems of obsolescence. If the efforts are improperly directed, the end product is obsolete before it is finished. Today's military technology is exceedingly more complicated than in World War II. We are living in an era in which, if the wrong guess is made during peacetime, there will never be enough time to make a right guess during wartime. Every effort is directed toward having a military weapons deterrent capability which will make it impractical for an aggressor to engage in hostilities.

1.3.3 Operations Analysis

The military does not request the best missile that can be designed. It must consider the technical state of the art and understand what is most reasonable. The military must look at its requirements and, at the same time, at the potential enemy capability. The program is guided by intelligence, by experience with the kind of achievement that can be consolidated as a function of time. This technique is called "war gaming" or, when applied to a whole society, operations analysis.

Operations analysis is a portion of over-all systems engineering. In verifying our own military capability, such parameters are used as circular probable error (CEP) or the miss distance that can be expected on a probability function basis; the yield, which is the size of the explosion; the reliability or number of units that will succeed; the cost; the maintenance capability; and a similar estimate of the enemy's capability. On paper it can be proved that anyone might have won any war at any particular time. The results of an operations analysis technique are only as good as the assumptions that are made.

1.3.4 Anticipating Technological Breakthroughs

Since in this book you will be perusing a number of individual technical areas, it is important to remind you that in a systems effort, such as a major missile program, it is necessary to act both with knowledge of the current state of the art and on the basis of the forecast state of the art. No matter what approach is taken to a large program, it will be a matter of several years before the end product is operational and in the hands of the customer. Designs are not made to meet today's requirements but to meet the requirement anticipated to be established at the time the system becomes available. Equally, designs are drawn to take advantage of the state of technology which exists at that time.

There is nothing new about the idea of rockets, nothing new about the idea of military ballistic missiles. The V-2 rocket during World War II is a classic example. However, the systems engineering in the postwar period showed that an intercontinental ballistic missile using the then existing chemical propellant could not sensibly be expected to deliver a large enough payload to be worthwhile in a military sense. Obviously, it could not carry enough TNT to do any damage. It could not even carry enough fissionable nuclear material, the kind of bomb explosive material available in World War II, to make it worthwhile. So it was said to be useless to work on ballistic missiles. This is an example of a failure to anticipate technical breakthroughs. It was not very much later that the breakthrough did come and a technique was developed whereby a thermonuclear warhead could be made in relatively small packages. The yield per pound went up by a factor of a thousand, and the ballistic missile became a very effective device.

The systems engineer, above everything else, must attempt to anticipate these technological breakthroughs. There have been many in military past history. Poison gas in World War I could have been a military breakthrough had it been utilized. The V-2 could easily have been a breakthrough in World War II. To go further back, there was armor plate, the crossbow, and then the field artillery which Napoleon exploited. The communication reaction times in those days were long but the development lead times were short, and the enemy could use them to advantage. Perhaps one side had a large standing army and the opponent did not, but by the time the army got moving and a certain amount of time had been lost doing necessary things, the other side could form one. This is what happened in 1917 and again in 1941. The next time, if war is anticipated, preparations must be made in advance for there will be no time to catch up.

1.3.5 Parametric Studies

A parametric study involves creating a mathematical model of the system of interest and then varying the important variables to determine an optimum set of specifications. In a parametric study various engineering parameters—such as specific impulse, mass ratio, thrust-to-weight ratio, guidance accuracy versus weight, effects of countermeasures—are subjected to thorough analysis. A large number of configurations, many different assemblies, are postulated, and by these engineering studies several broad avenues of approach are identified. This engineering synthesis is conducted to narrow down to a small number a series of competing configurations. At first this synthesis is performed on paper because there is not time or money to find an optimum design empirically. Technical know-how, the ability to estimate uncertainties and tolerances, and the ability to estimate future weight savings all make it possible to set up analytical models and study them for performance and for characteristics, and to investigate certain major elements such as the control system, which is the autopilot for stabilizing the flight of a basically unstable missile. (Raising a missile may be likened to lifting a pencil up by pushing on the bottom of it with a finger.) With an analytic model, which is sometimes a true mechanical analog, it becomes possible, for example, to analyze the behavior of the control system, which in turn may be affected by the way fuel sloshes inside the tank—a highly complicated integral feedback action. This process is carried out both for subsystems and systems.

One complex example of a missile systems problem is its trajectory, the path the missile follows from the time it leaves the launcher until it reaches the target area. One item affected by the trajectory, for instance, is the guidance antenna. In the days before inertial systems, when radio signals were transmitted to the ground stations to adjust the attitude and trajectory of the missile, there was concern lest the absorption of these signals in the highly ionized gases in the missile exhaust flame cause loss of communication. The flame attenuation was a function of the trajectory shape. Because a trajectory involves practically every element of the missile program, it is one of the best subjects for parametric studies.

1.3.6 The Process of Iteration

In making systems studies by means of analytic models, knowledge of many technical fields is required. Propulsion, guidance, structural stability, nuclear physics, and practically everything else imaginable are investigated. The systems engineer cannot afford to be a specialist; he has to be a "jack of all trades." He has to have intellectual curiosity, and he has to be able to solve problems in areas in which he is not necessarily trained in great detail. In the process, extensive computers are used, analytic models are used, sometimes a small-scale experiment is used. An "iterative" process is used. The problem is hit from all sides and tried over and over again. To save money, the principal systems characteristics must be determined by analytical or small-scale tests before the large development hardware program can begin. In this process a basic configuration is settled upon for a particular mission. Sometimes when the systems are more complicated and the state of the art is more difficult to guarantee, a parallel back-up program is instituted.

Sometimes it becomes necessary to "back-up" whole programs. In the missile program for the ICBM there are two configurations, the Atlas and the Titan. With something as important as the ICBM, as vital to the welfare of this nation, it was not prudent at the beginning of the program to rely on only one configuration (Fig. 1.2).

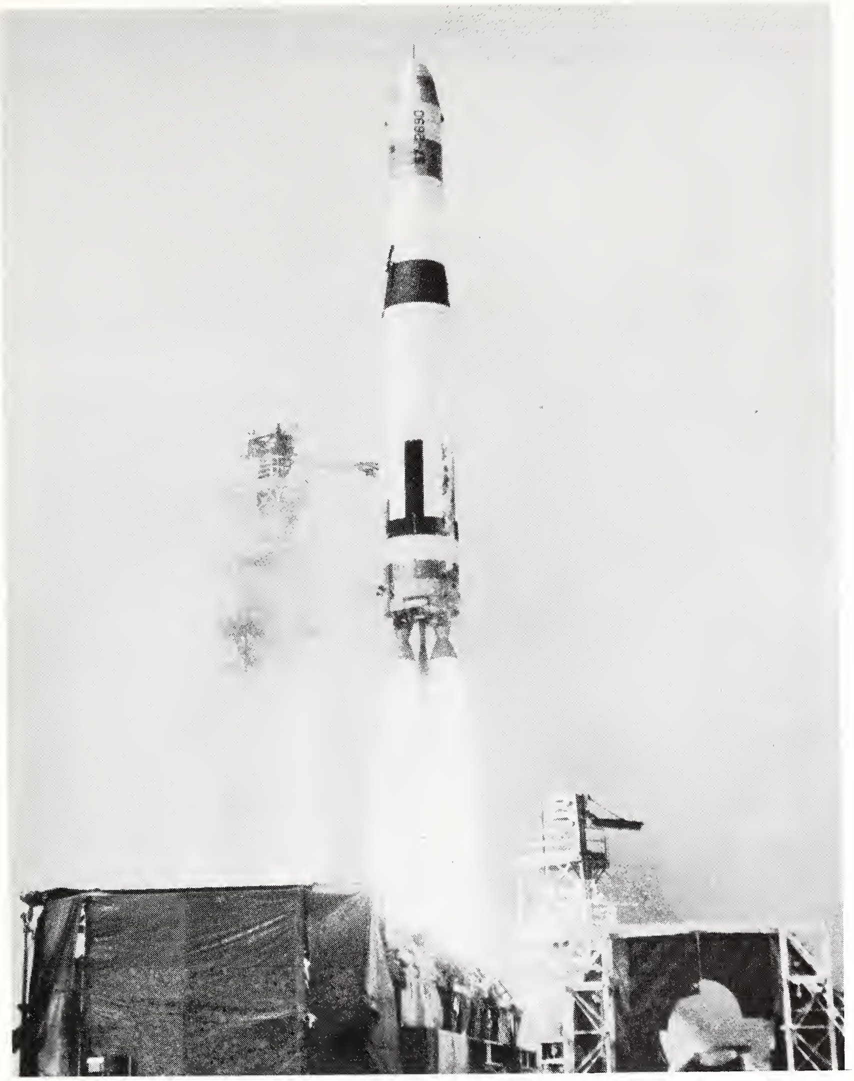

Fig. 1. 2

1.3.7 Economic Considerations

Military economics is not so much a matter of supply and demand as of having a certain amount of resources—dollars, manpower—and of deciding where they are to be spent. Time is a critical factor, for if a system were postulated that would require fifteen years to develop, it might be decided to adopt another system that takes only five years because only five years is available before the need becomes acute.

In the final analysis the success of the program is measured by its cost, by the performance achieved, and by the time needed to complete it. The national need for these weapons is, of course, justification for the expense involved.

1.3.8 Individual Subsystems Approach

The missile problem could be approached by doing the maximum possible work on the individual system elements. The guidance supervisor could be directed to produce the best possible guidance system for the missile. The airframe department could be asked to produce the best airframe. The propulsion man could design an advanced engine. The result would probably be chaos. Without one man knowing what the other is doing, each will assume that he has certain privileges which are incompatible with the assumptions of the other. Thus it is apparent that, in tackling a program such as outlined here, a major synthesis task is required.

1.3.9 Principle of Concurrency

To save years of time in a development program, the principle of concurrency, or parallel development of the various subsystems, is applied. The engine is not developed and then the airframe built around it; the completed engine and airframe are not flown before the guidance system is planned. Work on all major systems must be done in parallel rather than in sequence. The systems engineer has the task of seeing that each of the independent development programs is properly directed so that, when they come together, the ultimate systems objectives will be met. A schedule is prepared of what are believed to be problems, and milestone dates are established for the solutions. Any failure to keep up with these dates will cause extra emphasis on that area. The systems engineer must parcel out performance and weight allotments in a budget which comprises not only dollars but weight, the cornerstone of the missile program, and accuracy requirements. He will divide weight allowances between the different elements of the system. Above all, he must portion out reliability. There are 50,000 components on board a missile, any one of which could fail and abort the mission. If there are 100 items, each of which is 99 per cent reliable, the over-all reliability is 0.99 raised to the hundredth power, a very small number.

1.3.10 Authority of the Systems Engineer: Interface Problems

It is essential for someone who is not responsible for the individual elements of the system to exercise the total control. The systems engineer plays this role in the initial outlining of a program and in the continual day-to-day development and production because, as the program progresses, the best estimates of original designers will turn out to be incorrect in some areas. It is the constant interaction, constant trade-off, constant evaluation that keeps the systems engineer active.

The technical budgets for weight and reliability are established, and the systems engineer then sets up what is called a systems test program. Only the systems engineer can properly plan, conduct, and evaluate the tests in which subsystems are brought together. A new word has been developed in the missile industry, "interface," referring to the phenomena or the places at which two subsystems are coupled together or interact. Interface can be a piece of paper; it can be a mechanical latching arrangement; it can be an electrical induction circuit; it can be heat flow; it can be almost any means of coupling if it is a boundary for interactions between two or more of the systems. In the language of missilemen, interface is described as the relation between two major subsystems and the interaction between them. The systems engineer controls the interface between the re-entry vehicle, the nose cone, and the missile itself, to be sure that the two pieces fit, that the plugs tie together, that if the weight of the re-entry vehicle is changed the autopilot will still be stable owing to the change in the dynamics of the systems. On occasion the systems engineer must compromise the performance of one subsystem in order to make it possible for another to be acceptable. The systems engineer must have the authority for directing the subsystem methods in a technical sense, or he will be essentially helpless to perform the job properly and arrive at a successful product.

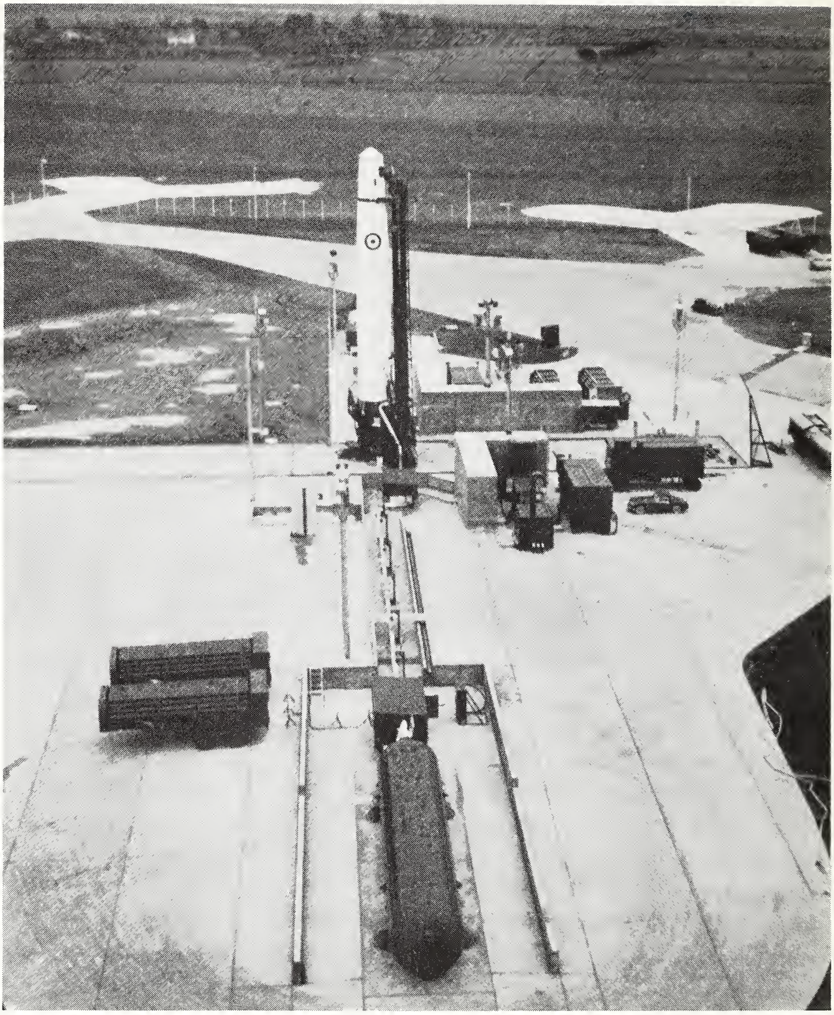

Fig. 1.3a

1.3.11 Associated Ground Support System

Usually the center of attention is the missile. However, the missile is essentially useless without a ground system. For the earliest use of the missile, it is necessary that other groups of engineers work on "the brick and mortar" to support installations in general. It is mandatory for these engi-

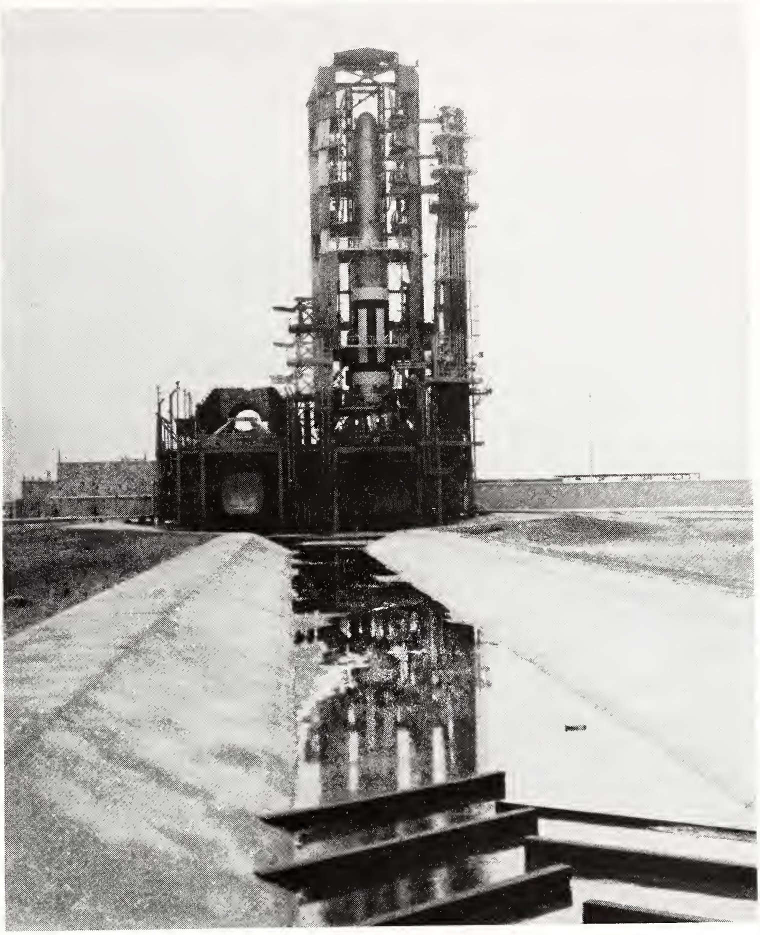

Fig. 1. 3b

neers to begin work early, often before the missile itself has been built, and to know the characteristics of the missile so that they can design the ground support system, procure it, install it, check it out, and have it ready to receive missiles as soon as they have completed successful flight testing (Fig. 1.3).

One of the most complex systems engineering jobs is the integration or marriage of the missile to its ground system.[1] It is sometimes necessary to make significant trade-offs between the air-borne system and the ground system; it is essential always to make appropriate trade-offs between the man and the machine. In addition, operating personnel must be organized, trained, and integrated with the system, a major task.

1.4 THE SYSTEMS ENGINEER

The systems engineer must first be a very good engineer in at least one particular field of technology. He must exercise intellectual curiosity and be concerned with the other fields. When called on to exercise judgment, he should have the ability to make the decisions on trade-offs between the various elements of the system, including human factors, economics, political requirements. In the broadest interpretation, the systems engineer is the key element in the development of either a complex military system or a complex industrial system.

This outline has concentrated on the systems engineering problem of the ballistic missile because it encompasses all the various areas of technology to be discussed in the text. The problem is challenging to engineers because it is quite clear that for weapon systems and space vehicle systems it will be necessary to extend every discipline to its limit. The engineer and scientist must push to the frontiers of knowledge and exploit to the fullest the state of the art.

REFERENCE

1. K. Brown and P. Weiser, Ground Support Systems for Missiles and Space Vehicles, McGraw-Hill, New York, 1961.

2

ROCKET PROPULSION FUNDAMENTALS*

H. S. Seifert

2.1 INTRODUCTION

A rocket is a container filled with matter and energy, so arranged that a portion of the matter can receive energy in kinetic form and then be ejected at a controlled rate in a desired direction. This part, originally at rest in relation to the container, is transformed into the gaseous state and escapes with a high velocity. The remaining nongaseous part of the system undergoes a time rate of change of momentum, and hence the container experiences a reaction force or useful thrust.

An optimum rocket produces high thrust per unit rate of mass expenditure. If the thrust is held constant, the rate at which kinetic energy is supplied to the expended mass must vary inversely as the mass flow rate. Since an effective rocket should spend mass frugally, it must squander energy prodigally. This high rate of evolution of energy implies that the ejected matter is subjected to high temperatures. The task of the rocket ‘‘motor’’ is to convert the random thermal energy of this gaseous working fluid into an ordered state in which the velocities of as many of the gas molecules as possible have been aligned in a specific direction. In this ideal condition their total momentum in the reference direction will be a maximum, but their temperature and pressure, as measured by an observer traveling with the stream, will be zero.

---

* Portions of this chapter have been taken from Space Technology, John Wiley and Sons, New York, Chapter 14, 1959.

One hundred per cent efficiency cannot be achieved in the earth's atmosphere, since expansion into a vacuum would be required. The expansion process must finally stop when the ''free stream'' pressure of the emerging jet approaches that of the surrounding atmosphere, in which state considerable energy of random motion which cannot produce useful thrust remains in the gas.

The rocket container or ''motor,'' since it utilizes a working fluid operating between combustion pressure and ambient pressure, may be regarded as a heat engine, and an analysis of its operation should consider the thermodynamic process involved. The basic physical phenomenon under consideration is the flow of fluid through a duct with concurrent changes in the form of the energy contained in the fluid. This may occur as injection of fluid into a combustion chamber with subsequent efflux through an orifice, as in the liquid propellant rocket, or as evolution of gas from the surface of a solid, as in the solid propellant rocket.

The process will be assumed to be steady; that is, the various physical parameters will not be rapidly varying functions of time. Since steady processes usually occur with constant local pressures, equilibrium thermodynamics will be applied, although chemical equilibrium is not completely achieved in nozzles.

This chapter will discuss how the magnitude of the thrust of a rocket is determined from the velocity and mass rate of flow of the expellant fluid, and how in turn these quantities are determined by the nozzle dimensions and the fluid properties of pressure, temperature, molecular weight, and ratio of specific heats.

It will conclude with a discussion of the fundamental system interface relations which involve the rocket engine as one subsystem, as well as comments on some less fundamental but nevertheless practically important interface problems.

2.2 THE MAGNITUDE OF ROCKET THRUST

2.2.1 Reaction of a Fluid Jet

The calculation of the thrust caused by the ejection of a compressible fluid is more complicated than that of a simple series of particles because of the addition of pressure forces to the momentum forces. We begin the thrust computation[1, 2] by invoking the "momentum theorem" for fluids, which states that the vector net time rate of change of momentum, or flux of momentum, through a fixed (mathematical) surface enclosing a steadily flowing fluid equals the vector area integral of pressure, or net force, acting on the surface. This fixed closed surface may, for example, be the interior of a rocket motor together with its nozzle exit plane and is defined in coordinates fixed with respect to the rocket.

The thrust F acting on a rocket shell is the sum of all pressure forces acting on its inner and outer surfaces[3] (Fig. 2.1). Thus

$$F = \int_s p\, \vec{ds} = \int_{s_i} p_i\, \vec{ds}_i + \int_{s_o} p_o\, \vec{ds}_o \qquad (2.1)$$

where p is the (scalar) pressure on the motor wall and $\vec{ds}$ is a vector element of wall surface area. Subscripts i and o refer to the inside and outside surfaces, respectively. If the motor is a surface of revolution, it is clear that F will be directed along the axis of symmetry.

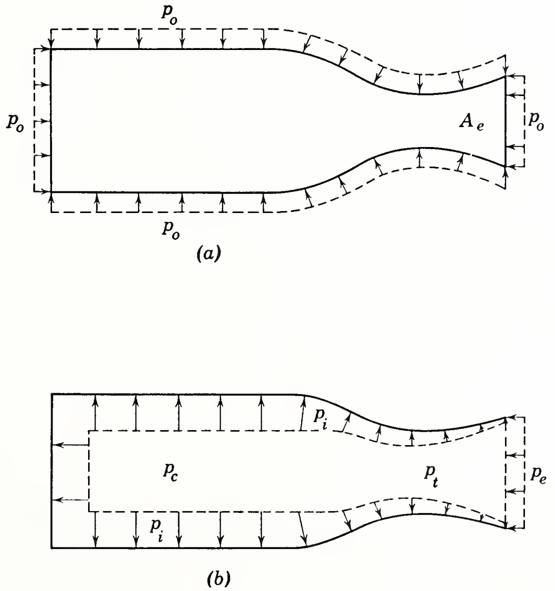

Fig. 2.1 Pressure forces acting on a rocket motor to produce the thrust: (a) the external forces due to atmospheric pressure, (b) the internal forces due to the combustion gases.

To evaluate the integral over the inner surface in eq. 2.1, let us apply the momentum theorem to the gas contained within the rocket motor and the nozzle exit plane of area A_e (Fig. 2.1). The axial flux of momentum through the exit plane is $\dot{m}v_{xe}$, where v_{xe} is the average axial component of the exhaust velocity relative to the rocket. The pressure acting on the contained gas is the reaction $-p_i$ to the pressure p_i on the motor wall, and the average pressure opposing the flow through the exit section of area A_e is the static or free-stream pressure p_e of the gas at the plane of the exit. This pressure p_e in conjunction with p_o gives rise to the "pressure" component of the thrust mentioned at the beginning of this section. Note that p_e is not usually equal to p_o, the atmospheric or ambient pressure. Assuming that the pressure forces are axially symmetrical, and equating the total force on the gas in the motor volume to its axial time rate of change or flux of momentum, we obtain the scalar equation

$$\int (-p_i)\,ds_i + A_e p_e = \dot{m}v_{xe}$$

$$\int p_i\,ds_i = A_e p_e - \dot{m}v_{xe} \qquad (2.2)$$

The integral $\int_{s_o} p_o\,\vec{ds}_o$ over the outer surface S_o, considered here to be axially symmetric so that a scalar equation may be written, may be readily evaluated as follows. The resultant force caused by uniform atmospheric pressure p_o on any completely closed vessel at rest is zero. If we now take an enclosure the shape of the rocket, this force may be resolved into (a) the axial force acting on the plane area A_e of the nozzle exit section and (b) the sum of all the remaining symmetrical external pressure forces. Hence (Fig. 2.1).

$$p_o A_e + \int p_o\,\vec{ds}_o = 0$$

or

$$\int p_o\,\vec{ds}_o = -p_o A_e \qquad (2.3)$$

The effect of nonclosure of area A_e is to create an unbalanced force of magnitude $-p_o A_e$ acting on the rocket shell in opposition to the useful thrust.

We may now evaluate the thrust expression 2.1 by eliminating the integrals with the help of eqs. 2.2 and 2.3. There results

$$F = -\dot{m}v_{xe} + A_e(p_e - p_o) \qquad (2.4)$$

This useful equation shows that the thrust law for a compressible fluid differs from that for a particle jet by adding a "pressure thrust" term $A_e(p_e - p_o)$ in addition to the "momentum thrust" $-\dot{m}v_{xe}$. The sign conventions in this derivation have been so chosen that v_{xe} is considered to be evaluated by a negative number, although all other algebraic symbols in eq. 2.4 are evaluated with positive numbers.

The average velocity component v_{xe} in the axial direction is usually less than the true velocity of efflux v_e, which often has a component perpendicular to the axis. A factor λ may be applied to correct v_e for this divergence of flow; thus we write

$$v_{xe} = \lambda v_e \qquad (2.5)$$

The value of λ depends on the angle of divergence of the exit cone of the nozzle, and if we assume uniform conical flow, λ may be approximated closely by the relation

$$\lambda = \tfrac{1}{2}(1 + \cos \alpha) \qquad (2.6)$$

where α is the half-angle of the nozzle exit cone. It is possible to redirect radial flow so that it is approximately parallel to the axis by the use of a suitably curved bell-shaped nozzle similar to that of a supersonic wind tunnel. In this manner a given expansion ratio may be achieved together with parallel flow in a shorter and lighter nozzle than in an equivalent simple cone of small divergence angle.

2.2.2 Conditions for Maximum Thrust

It will be shown that when p_e equals p_o in the thrust eq. 2.4 the thrust F is a maximum. A nozzle for which p_e equals p_o is said to be "correctly" expanded. If p_e is smaller than p_o, the gases are "overexpanded" and the pressure thrust will be negative, although partially compensated by an increased momentum thrust. If p_e is larger than p_o, the gases are "underexpanded." Although the pressure thrust will then be positive—that is, in the same sense as the velocity thrust—it will not compensate completely for loss in exhaust velocity v_e owing to inadequate expansion. Because pressure and momentum thrusts tend to compensate, the net thrust F is rather insensitive to variations in the expansion pressure ratio p_c/p_e. For example, a nozzle correctly expanded at sea level gives about 6 per cent less thrust at an elevation of 40,000 ft (pressure = 2.72 psia) than one correctly designed for that altitude, although both nozzles will increase thrust with altitude because of the decrease in ambient pressure p_o.

A physical proof of the fact that thrust F is a maximum at $p_e = p_o$ may be seen by referring to Fig. 2.2. The pressure field p_e on the divergent conical part of a nozzle is represented. Section A is chosen so that p_e equals p_o at that point. If we start with a definitely underexpanded nozzle, such that p_e is larger than p_o, and imagine small extensions such as B added to it, each extension will contribute to the net thrust owing to the pressures upon it. So long as p_e is larger than p_o, the force acting on the nozzle increment assists the total thrust. After the point A is reached, p_e is smaller than p_o, and further increments subtract from the total thrust. Consequently, maximum thrust is attained when just enough nozzle cone is used to make p_e equal to p_o.

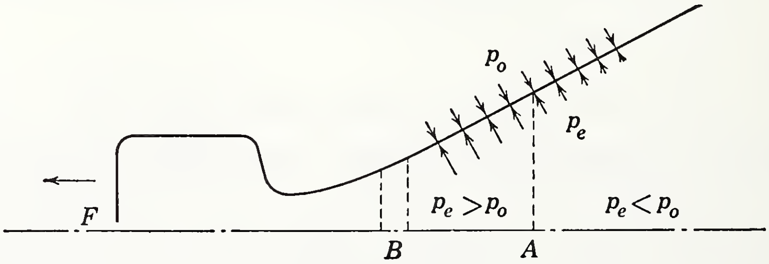

Fig. 2.2 Graphical demonstration that choice of expansion ratio for maximum thrust is at $p_c = p_o$.

2.3 DETERMINATION OF THE JET VELOCITY

Although eq. 2.4 for thrust F is simple in form, it is expressed in terms of variables which are not directly measurable, namely mass flow and velocity. It is therefore useful to compute these quantities in terms of known pressures and gas properties.

2.3.1 Conservation Law for Enthalpy and Kinetic Energy

Let postulate flow in a duct which is one-dimensional, parallel, and adiabatic. It can be shown from conservation of energy[5] that

$$v^2/2 = c_p(T_c - T) \tag{2.7}$$

in which T_c is chamber temperature (where $v = 0$) and T is the static temperature at the point of the nozzle where the velocity is v. By further specializing the fluid to be an ideal gas, we may use well-known relations[11] to replace specific heat c_p, leading to

$$v = \left[\frac{2\gamma}{\gamma - 1} \cdot \frac{R'T_c}{M}\left(1 - \frac{T}{T_c}\right)\right]^{1/2} \tag{2.8}$$

in which $\gamma = c_p/c_v$ = ratio of specific heats,
R' = universal gas constant,
M = molecular weight of gases.

In order to calculate the v obtainable from a given chemical reaction, it is necessary to know the chamber temperature T_c, as well as the average molecular weight $\overline{M}$ and specific heat ratio γ of the products of combustion. Both T_c and $\overline{M}$ may be calculated by successive approximation using the following steps.

1. Choose reactants (and their proportion by weight).
2. Postulate the important reactions.
3. Estimate a reaction temperature T_c.
4. Assuming equilibrium, use the laws of mass action and of conservation of matter to balance the postulated chemical equations.
5. Correct T_c by trial until the equations in step 4 are consistent.
6. Calculate $\overline{M}$ and γ from the composition of combustion products.

2.3.2 Gas Velocity as a Function of Pressure Ratio

Using the ideal gas equation of state

$$\frac{p}{\rho} = \frac{R'}{M} \cdot T$$

and assuming that the adiabatic expansion is also isentropic, so that the conventional relation

$$\frac{T}{T_c} = \left(\frac{p}{p_c}\right)^{(\gamma - 1)/\gamma} \tag{2.9}$$

may be used, together with the equation of state, we may express the velocity v in the forms

$$v = \left\{ \frac{2\gamma}{\gamma - 1} \cdot \frac{p_c}{\rho_c} \left[1 - \left(\frac{p}{p_c} \right)^{(\gamma - 1)/\gamma} \right] \right\}^{1/2} \tag{2.10}$$

$$v = \left\{ \frac{2\gamma}{\gamma - 1} \cdot \frac{R'T_c}{M} \left[1 - \left(\frac{p}{p_c} \right)^{(\gamma - 1)/\gamma} \right] \right\}^{1/2} \tag{2.11}$$

The factor in brackets is the ideal cycle efficiency of the expansion process,

$$\eta_i = \left[1 - \left(\frac{p}{p_c} \right)^{(\gamma - 1)/\gamma} \right] \tag{2.12}$$

and represents the fraction of the total enthalpy which is converted to ordered kinetic energy. It approaches unity as p/p_c approaches zero.

It will be well to review here the assumptions on which eqs. 2.10 and 2.11 rest. They are (a) one-dimensional flow, (b) parallel flow, (c) ideal gas equation of state, (d) constant specific heats, (e) adiabatic expansion, (f) isentropic expansion, (g) nonreacting (frozen) flow, and (h) zero nozzle entry velocity.

Although this may seem like a restrictive array, the resulting equations correspond to experiment to within 2 or 3 per cent in most measurements.

2.3.3 The Role of Specific Heat Ratio γ

The dimensionless ratio $\gamma = c_p/c_v$ occurs very frequently in all equations involving gas flow. It is in order, therefore, to examine γ as a physical concept in which c_v is a measure of the energy required to raise the temperature (i.e., translational kinetic energy) of a unit mass of gas a unit amount with volume held fixed; and c_p is a measure of the energy required to increase the temperature by one unit and in addition to perform work by expansion, such as to maintain a constant pressure on the surroundings, whether they are gaseous or solid. Therefore, the more nearly $\gamma = c_p/c_v$ approaches unity, the larger the amount of thermal energy associated with a given mass of gas per unit amount of mechanical work performed adiabatically.

The equipartition theory[6] of gases states that the internal energy of a molecule tends to divide equally among its several degrees of freedom in translation, rotation, and vibration, if given a sufficient time. Under equilibrium conditions each degree of freedom can possess energy $\frac{1}{2}kT$, where k is Boltzmann's constant. Thus a simple molecule has no reservoir of energy and loses thermal energy (temperature) rapidly as it goes through the expansion process and does work on its surroundings. On the other hand, a complex molecule with many degrees of freedom has a greater ability to store energy in other than translational modes at a given temperature (γ approaches unity), and it loses temperature (translational kinetic energy) slowly as it does work in expanding. This is indicated in the adiabatic expansion law eq. 2.9. For example, if $\gamma = 1.25$, then eq. 2.9 gives

$$\frac{T_e}{T_c} = \left(\frac{p_e}{p_c}\right)^{1/5} \tag{2.13}$$

and a 97 per cent drop in pressure results in only a 50 per cent decrease in temperature. The dependence on γ of thrust coefficient C_F, to be discussed in Section 2.7.2, is shown in Fig. 2.5 (p. 31).

2.3.4 The Role of Molecular Weight M

Equation 2.11 indicates that the chamber temperature T_c should be high and the molecular weight M of the products of combustion should be low to secure a high exhaust velocity v. In general, if samples of two gas species of different molecular weights are at the same temperature, the individual molecules of different species will possess the same translational kinetic energy, by virtue of the equipartition of energy principle. Consequently, if they are allowed to expand into a vacuum, the ratio of their velocities will be inversely proportional to the square roots of the ratio of their molecular weights, and their individual momenta will be directly proportional to the square roots of their molecular weights. For equal temperatures, mass flow rates, and pressures, more thrust can be secured from the matter of lower molecular weight. This fact is important in determining the choice of rocket propellants and favors those that contain a high percentage of hydrogen.

The most suitable working fluid for a nuclear reactor, heat exchanger type rocket is seen from these considerations to be hydrogen, since the molecular weight in such a rocket may be chosen independently of temperature.

2.4 FLOW THROUGH DE LAVAL NOZZLES

2.4.1 The Supersonic (de Laval) Nozzle Contour

As was stated in Section 2.3, it is necessary in designing rockets to express the thrust, which is proportional to the product of mass flow rate and exhaust velocity, in terms of pressure and known properties of the combustion products. This has already been done for the exhaust velocity v in eq. 2.11. It remains to be shown how the mass flow rate $\dot{m}$ can be expressed in the same terms and what effect the back pressure of the atmosphere has on thrust before it can be calculated explicitly in terms of dimensions and pressures.

The geometrical form of the orifice through which the compressible gases escape is important in determining both mass flow rate and thrust. It is not evident a priori what the shape of this "nozzle" should be.[8-10, 12] For example, the velocity of an incompressible fluid such as water flowing through a converging-diverging venturi tube first increases and then decreases, with a maximum at the smallest cross section. The mass flow rate is proportional to the over-all pressure difference. On the other hand, a compressible fluid undergoing adiabatic expansion through a similar venturi will behave in the same manner only as long as the velocity at all points is less than the local velocity of sound. As soon as sonic velocity is reached, which occurs first at the narrowest cross section, or "throat," the behavior changes entirely. The mass flow rate (but not the velocity) is now unaffected by any changes in pressure downstream from the throat. This effect is sometimes called "nozzling." Moreover, the gas velocity downstream of the throat will increase (becoming supersonic) to a value determined by the pressure at the nozzle exit. The pressure ratio p_e/p_c necessary to cause sonic flow is called the critical pressure ratio. The pressure ratio in most rocket motors is well above this minimum value.

2.4.2 Behavior of a Nozzle at Various Back Pressures

If with a given nozzle we maintain a fixed chamber pressure, and, starting with a like exit pressure, gradually reduce this exit pressure to a value only a little below chamber pressure, the flow is at first all subsonic and the nozzle is actually a venturi tube. As we follow the flow downstream, the velocity at first increases but decreases again beyond the throat section. The velocity at the throat section will increase with continued reduction of the exit pressure, and hence the mass flow rate in through the nozzle will also increase. After sonic velocity is reached at the throat section, further reduction in exit pressure will not increase $\dot{m}$, which will remain constant. However, the velocity at the exit will be increased by decreasing the pressure at the nozzle exit[10,12,13,16-18] and, as long as the exit area is the corresponding size, may be computed from eq. 2.10. Figure 2.3 shows how the parameters p, ρ, v, and T vary throughout a nozzle relative to their values in the throat section.

2.5 MASS FLOW THROUGH THE NOZZLE

2.5.1 Mass Flow in Terms of Chamber Parameters

The two important terms in thrust eq. 2.4 are exhaust velocity v and mass flow $\dot{m}$. It is desirable to derive a relationship for mass flow, expressed in terms of measurable conditions such as chamber pressure p_c and throat area A_t, similar to eq. 2.11 for exhaust velocity.

We begin by applying the equation of continuity to the throat section of the nozzle, which results in

$$\dot{m} = A_t \rho_t v_t \tag{2.14}$$

If v_t and ρ_t are evaluated in terms of chamber conditions, this finally leads to

$$\dot{m} = \left[\gamma\left(\frac{2}{\gamma+1}\right)^{\frac{\gamma+1}{2(\gamma-1)}}\right] \cdot \left(\frac{A_t p_c}{\gamma \cdot R/M'T_c}\right)^{1/2}$$

$$\dot{m} = \Gamma' \frac{A_t p_c}{a_c} \tag{2.15}$$

where we define Γ' as

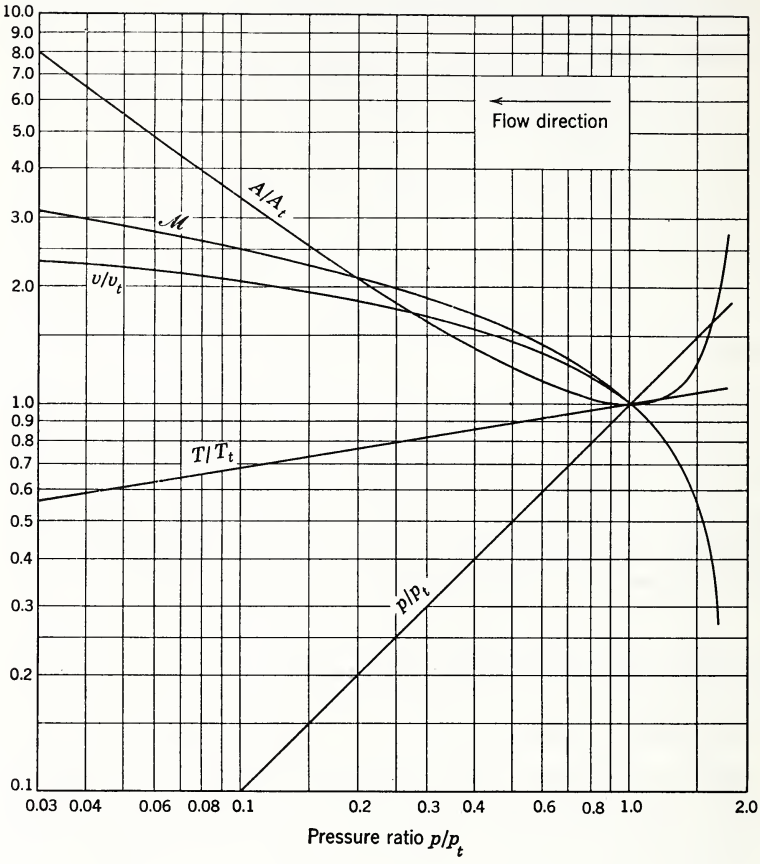

Fig. 2.3 Dependence of temperature T, velocity v, area A, density ρ, and Mach number $\mathcal{M}$ on pressure p in nozzle flow. All magnitudes are relative to their values at the throat; $\gamma = 1.2$.

$$\Gamma' = \gamma\left(\frac{2}{\gamma + 1}\right)^{\frac{\gamma+1}{2(\gamma-1)}} \tag{2.16}$$

and a_c is the velocity of sound in the chamber.

2.5.2 The Characteristic Velocity c*

The denominator of eq. 2.15 has the dimensions of velocity, and we may rewrite this equation in such a way as to define a useful new parameter c*, called the "characteristic velocity";

thus

$$\dot{m} = \frac{\Gamma'}{a_c} \cdot p_c A_t = \frac{p_c A_t}{c^*} \tag{2.17}$$

where

$$c^* = \frac{p_c A_t}{\dot{m}} = \frac{a_c}{\Gamma'} = \frac{(\gamma R' T_c / M)^{1/2}}{\Gamma'} \tag{2.18}$$

Since Γ' is a constant of the order of unity, c^* is nearly equal to sonic velocity in the chamber gases. It may also be regarded as the chamber pressure required to force unit mass flow through unit throat area.

The characteristic velocity is readily measured experimentally for a given propellant burning at a definite pressure. It is evident from eq. 2.18 that c^* is independent of nozzle exit pressures and diameters and may be considered as the parameter indicating the efficacy of the gas generation or combustion process. The quantity c^* is commonly used as a measure of the merit of a propellant, although its value may be affected adversely by poor combustion chamber design. By using physicochemical methods to calculate T_c, γ, and M in eq. 2.18, a theoretical value of c^* may be found. Experimental measurements of $p_c A_t/\dot{m}$ are usually over 90 per cent of this theoretical value for a well-designed motor. Such laboratory measurements are often made the basis of rocket motor design. Table 2.1 lists the c^* values for several propellants.

TABLE 2.1
Typical Values of Characteristic Velocity c^*

	Mixture Ratio R, oxid./fuel	Characteristic[a] Velocity c^*, ft/sec	Combustion Temperature T_c, °F
LOX[b] -alcohol (75%)	1.3	5537	5079
LOX-gasoline	2.5	5540	5470
LOX-hydrazine	0.33	5610	3632
LOX-ammonia	1.4	5840	4951
LOX-hydrogen	3.0	8345	4290
RFNA[c] -aniline	3.0	5015	5065

[a] Values taken from G. P. Sutton, Rocket Propulsion Elements, second edition, John Wiley and Sons, New York, 1956.

[b] LOX = liquid oxygen.

[c] RFNA = red fuming nitric acid.

The characteristic velocity c^* has the dimensions of feet per second when $\dot{m}$ is expressed in slugs per second, A_t in square inches, and p_c in pounds per square inch.

2.6 NOZZLE AREA RATIO ϵ AS A FUNCTION OF PRESSURE RATIO

In order to determine how well nozzle exit pressure matches ambient pressure, and hence how closely optimum design is approached by a particular nozzle, it is useful to have the nozzle area ratio $\epsilon = A_e/A_t$ expressed as a function of the pressure ratio p_c/p_e. (Note that p_c/p_e is more convenient than p_t/p_e.)

The expression for ϵ may be found by taking the equation for the area of any nozzle section in terms of the pressure at that section and eliminating the unknown mass flow term $\dot{m}$ by means of equation 2.15. The result is

$$\epsilon = \frac{A_e}{A_t} = \frac{\Gamma'}{\gamma} \cdot \left(\frac{p}{p_c}\right)^{1/2} \left\{ \frac{2}{\gamma - 1} \left[1 - \left(\frac{p}{p_c}\right)^{(\gamma - 1)/\gamma} \right] \right\}^{-1/2} \tag{2.19}$$

with Γ' as already defined in eq. 2.16. The chamber temperature (or its equivalents a_c or p_c/p_e), which is usually inaccessible to measurement, has canceled out of eq. 2.19. Values of $\epsilon = A_e/A_t$ versus p_e/p_c for various values of the parameter γ have been plotted in Fig. 2.4. This relation gives the area A corresponding to any free-stream nozzle pressure p, whether or not the cross section is at the exit. At the exit, A equals A_e and p equals p_e. To find ϵ for a "properly" expanded nozzle, simply set $p_e = p_o$, the ambient atmospheric pressure.

2.7 THRUST COEFFICIENT C_F

2.7.1 Empirical Definition of C_F

It is often desirable to express thrust F in terms of combustion chamber pressure p_c and throat area A_t rather than in terms of $\dot{m}$ and v as was done in eq. 2.4, since p_c and A_t may be considered independently adjustable variables on which F depends. It is found experimentally that F follows a relationship of the form

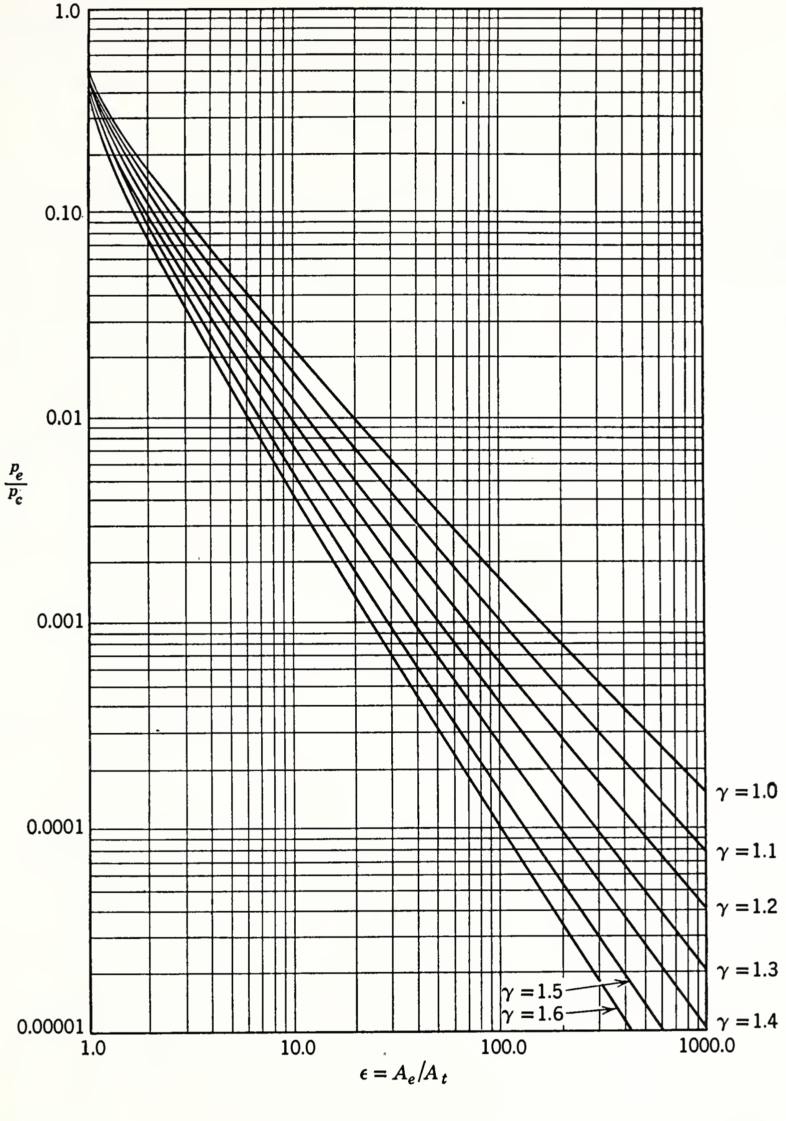

Fig. 2.4 Values of pressure ratio p/p_c as a function of area ratio A/A_t for various values of the parameter γ.

$$F = C_{FX} p_c A_t \tag{2.20}$$

where C_{FX} is an experimental thrust coefficient readily determined by measuring the remaining quantities of eq. 2.20.

The measured value of C_{FX} may then be applied to determine the throat area of a rocket having any desired thrust, providing the variables on which C_{FX} depends (A_e/A_t, p_c/p_e, λ, γ, and frictional effects) are kept constant.

2.7.2 Analytical Definition of C_F

An analytical expression for the thrust coefficient C_F as a function of γ, p_c/p_o, and ϵ (= A_e/A_t) will now be written, assuming isentropic flow and no separation. Then C_F may be compared with the experimental value of C_{FX} to indicate the magnitude of the frictional and divergence effects. In a well-designed nozzle, C_{FX} is less than 3 per cent smaller than C_F.

If the fundamental thrust eq. 2.4 is expressed in terms of pressure by substituting for mass flow $\dot{m}$ from eq. 2.15 and for velocity v_e from eq. 2.11, we obtain

$$F = \Gamma' \left\{ \frac{2}{\gamma - 1} \left[1 - \left(\frac{p_e}{p_c} \right)^{(\gamma - 1)/\gamma} \right] \right\}^{1/2} p_c A_t + (p_e - p_o) A_e \quad (2.21)$$

Dividing this by $p_c A_t$ gives C_F:

$$C_F = F/p_c A_t$$

$$C_F = \Gamma' \left\{ \frac{2}{\gamma - 1} \left[1 - \left(\frac{p_e}{p_c} \right)^{(\gamma - 1)/\gamma} \right] \right\}^{1/2} + \left(\frac{p_e - p_o}{p_c} \right) \frac{A_e}{A_t} \quad (2.22)$$

$$C_F = C_F(\gamma, \epsilon, p_c/p_o, p_c/p_e)$$

Since ϵ (= A_e/A_t) and p_c/p_e are uniquely related by eq. 2.19, C_F is actually a function of only four independent quantities (γ, ϵ, p_c, p_o). As was shown in Section 2.2.2, thrust, and hence C_F, has a maximum with respect to p_e when p_e equals p_o. However, C_F approaches an upper limit asymptotically as p_e and p_o together approach zero, that is, for a large expansion ratio exhausting into a near vacuum. For example, at $\gamma = 1.25$ this upper limit is about 2.1 (see Fig. 2.7).

We see from eq. 2.22 that as a rocket with a fixed ϵ rises through the atmosphere, C_F increases steadily in spite of the fact that ϵ can be optimum for only one altitude. At nonoptimum altitudes, C_F could be improved a few per cent by adjusting ϵ. For example, in the typical case in which $\gamma = 1.25$, C_F increases 8 per cent from sea level to 40,000 ft ($\frac{1}{4}$ atm) if the nozzle is fixed and 12 per cent if it is a "rubber" nozzle adjusted to the optimum expansion ratio at each altitude.

If the altitude increase were "infinite" (zero atmospheric pressure), the fixed nozzle C_F would increase 12 per cent, whereas that of the "rubber" nozzle would increase nearly 50 per cent.

Curves of ϵ versus p_c/p_e have been given in Fig. 2.4. Figure 2.5 gives curves of C_F versus ϵ for an ideal (i.e., no divergence or friction loss) nozzle in vacuum ($p_o = 0$). Figure 2.6 gives curves of C_F versus ϵ for an ideal nozzle which is matched (i.e., $p_o = p_e$) to its environment. Figure 2.7 gives sets of curves of C_F versus ϵ for mismatched (i.e., $p_o \neq p_e$) ideal nozzles in which the parameter p_o/p_c or atmosphere-to-chamber pressure ratio is given values of 10^{-1}, 10^{-2}, 10^{-3}, and 10^{-4}. All these curves are drawn for $\gamma = 1.0, 1.2, 1.4$, and 1.6. Figure 2.8 is a nomograph for finding the quantity $\Delta C_F = -(p_o/p_c)$ to correct vacuum C_F to any specified atmospheric pressure or altitude.

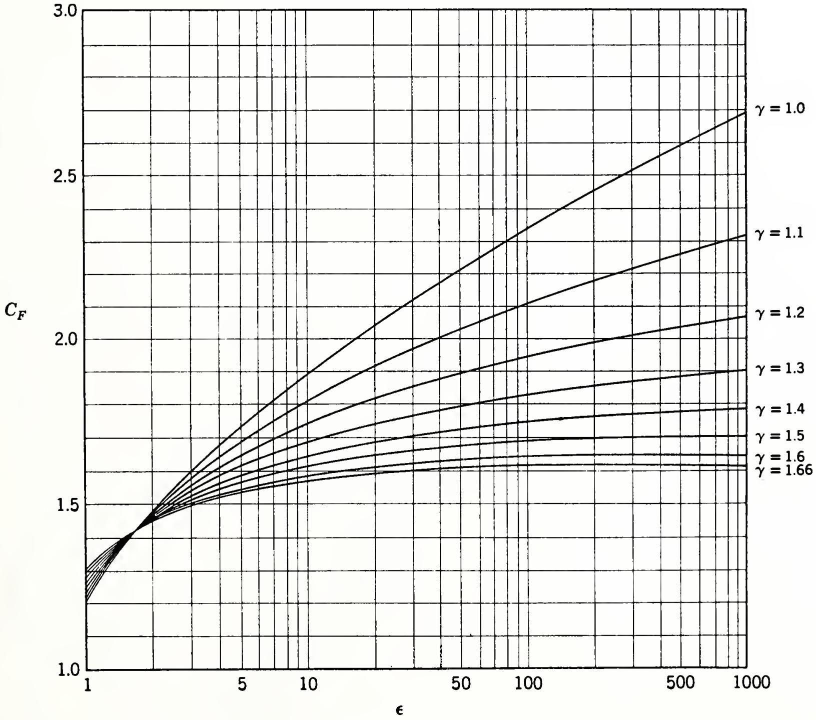

Fig. 2.5 C_F versus ϵ for lossless nozzle in vacuum, with γ as a parameter.

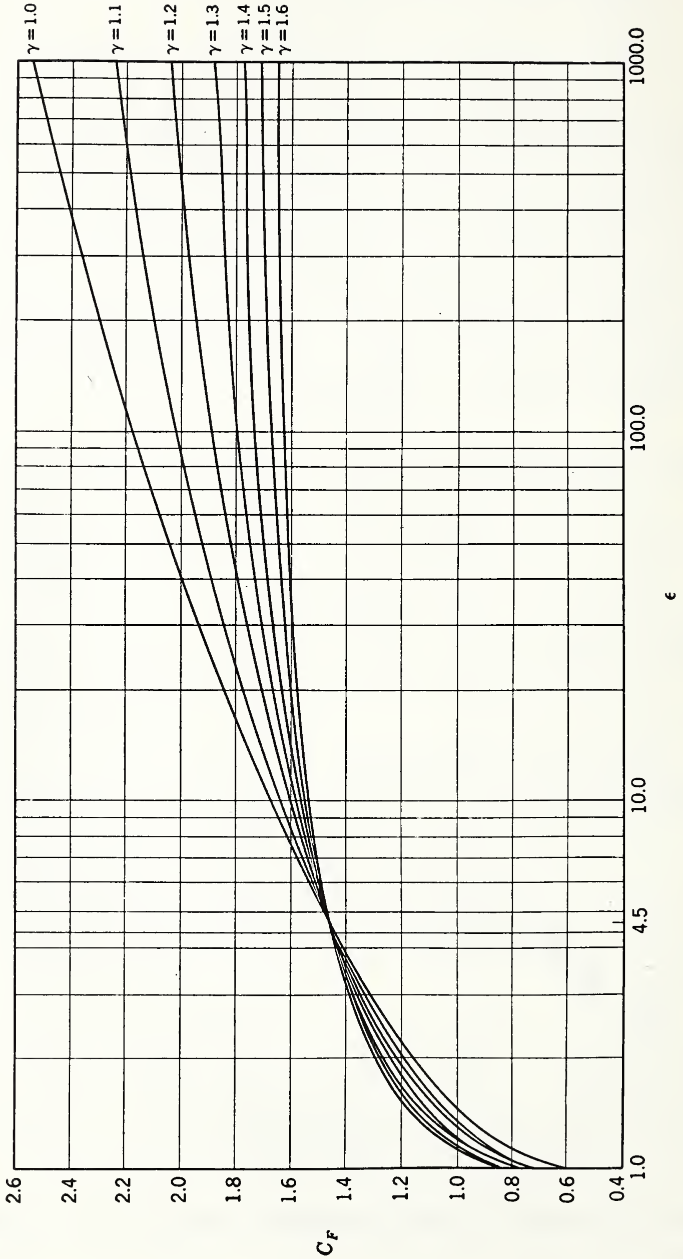

Fig. 2.6 C_F versus ϵ for a lossless nozzle in which p_e equals p_o (matched nozzle) and γ is a parameter.

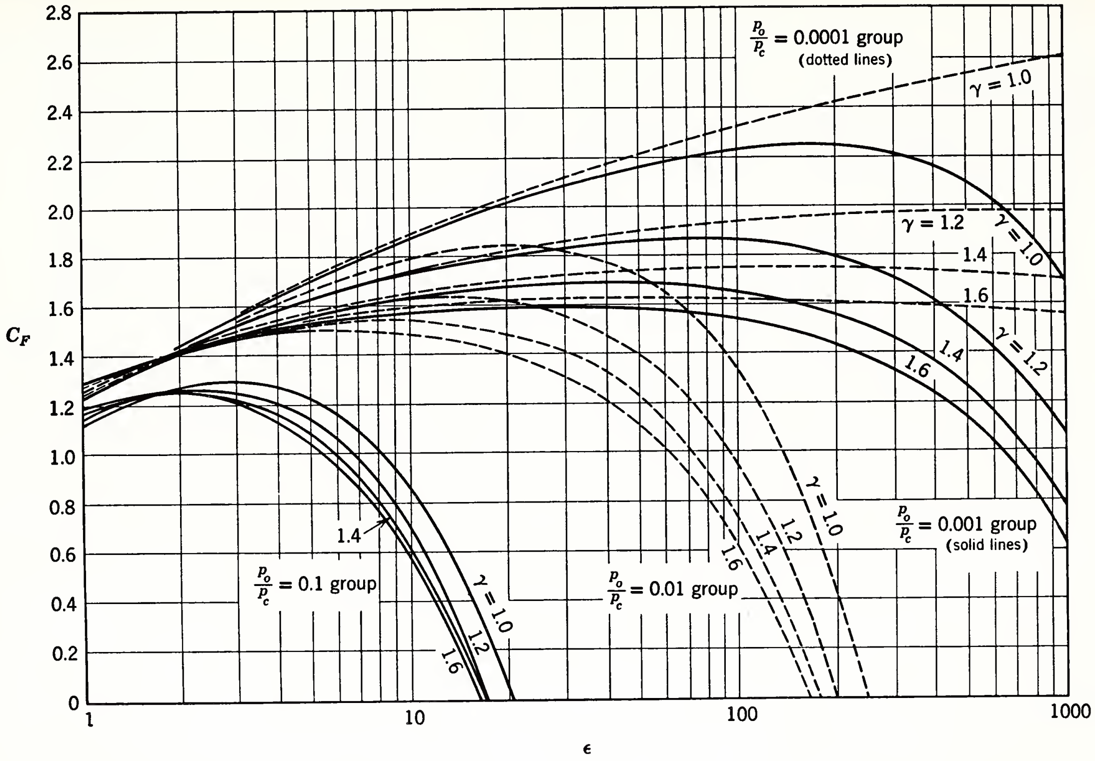

Fig. 2.7 C_F versus ϵ with both γ and atmosphere-to-chamber ratio p_o/p_c as parameters, assuming no separation.

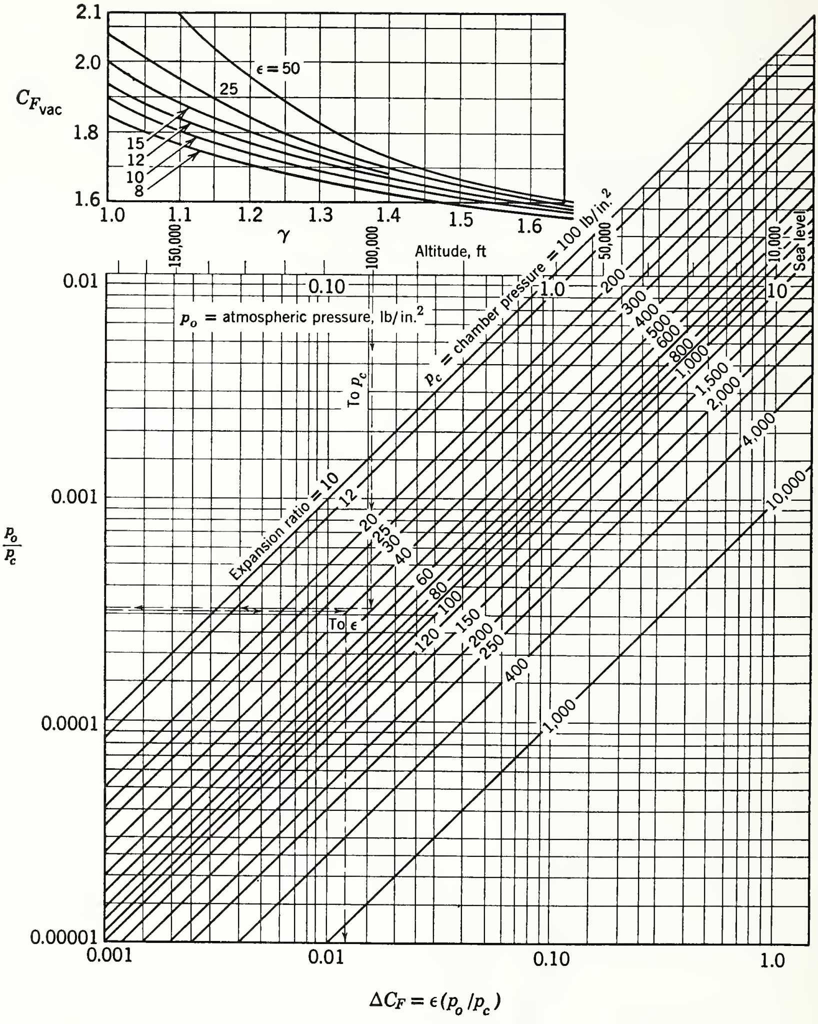

Fig. 2.8 Nomograph for correcting vacuum C_F to specified atmospheric pressure or altitude. (Courtesy J. B. Kendrick of Space Technology Laboratories, Inc.)

2.8 DESIGN AND PERFORMANCE CRITERIA

2.8.1 Specific Impulse

The rocket is unusual in the field of propulsion in that its thrust is independent of its velocity and does not require the presence of surrounding matter. In contrast, in the airplane power plant, for example, the thrust of the airplane decreases with increasing relative velocity and decreasing density of the atmosphere. Conventional motors normally propel their loads at a constant speed; rocket motors are usually accelerating a free body of rapidly decreasing mass. The goal of a conventional motor is to exert a force through a distance, that of a rocket to produce an acceleration during a time interval, that is, to achieve a given terminal velocity. Therefore, impulse (or momentum change) is a more significant parameter in rating rockets than energy dissipated, and the thrust per unit weight rate of flow—called the "specific impulse"—

$$I_{sp} = F/\dot{m}_{av}\, g = Ft/m_p g \tag{2.23}$$

is a more useful measure of performance than is the power generated. Typical units for I_{sp} are seconds or pound-seconds per pound.

The reciprocal of I_{sp} is the "specific propellant consumption" w_{sp} $(= 1/I_{sp})$. Although I_{sp} is primarily a measure of propellant performance, its value is affected by the geometric design of the rocket, the combustion pressure, and the external atmospheric pressure. This fact must be remembered when comparing propellants.

2.8.2 The Impulse-Weight Ratio

A measure of the performance of the rocket, in which the nonexpendable mass m_o is taken into account, is

$$\frac{Ft}{(m_p + m_o)g} = \frac{\text{total impulse}}{\text{total weight}} \tag{2.24}$$

It indicates the excellence of the over-all design of container-plus-propellant as a unit. Certain rocket propellants whose specific impulses are higher than those of others may lose their advantage when compared on the basis of impulse-weight ratio, owing to their low density. This parameter is particularly useful in rating solid propellant rocket propulsors, since the combustion chambers and propellant container are an integral unit. The impulse-weight ratio I/W is related to the specific impulse I_{sp} through the "loading factor" ν which is simply the fraction of the rocket vehicle mass expendable as propellant. Thus

$$I/W = \nu I_{sp} \tag{2.25}$$

Another useful parameter which takes into account the importance of propellant density is the impulse-volume ratio I/V which is simply related to the impulse-weight ratio as follows:

$$I/V = \rho \cdot I/W \tag{2.26}$$

2.8.3 Effective Exhaust Velocity

It is difficult to measure v_{xe} and p_e of eq. 2.4 experimentally. Moreover, the expansion is not strictly adiabatic, frictionless, and "perfect." It is convenient then to define an effective exhaust velocity,

$$c_{eff} = v_{xe} - A_e(p_c - p_o)/\dot{m} \tag{2.27}$$

which makes it possible to write the thrust eq. 2.4 in the simple form of

$$F = \dot{m}c_{eff} \tag{2.28}$$

even though it is understood that c_{eff} is not equal to the true efflux velocity $v_{xe} = \lambda v_e$. It is now possible to compute a useful engineering parameter c_{eff} simply by measuring the readily observable quantities F and $\dot{m}$. The effective exhaust velocity may be used to compare the relative performance efficiencies of motors operating under similar geometric, chemical, and pressure conditions, even though they may be of different scale.

2.8.4 Thrust Coefficient C_{FX}

The coefficient C_{FX} which is defined by the relation

$$F = C_{FX}\, p_c A_t$$

and which was discussed in detail in Section 2.7 is important in design calculations. The coefficient C_{FX} is a figure of merit for the performance of the nozzle. It is useful in determining the throat area A_t since F and p_c are often specified in advance.

2.8.5 Characteristic Velocity c*

The quantity c^* which is defined by the relation

$$c^* = \frac{p_c A_t}{\dot{m}} = \frac{p_c A_t g}{\dot{w}}$$

has the dimensions of velocity. It was discussed in detail in Section 2.5.2 and is useful in the prediction of mass flow rate when p_c and A_t are specified. The characteristic velocity c^* is a figure of merit for the performance of the propellant and is proportional to the square root of the energy released in the chamber reaction inversely to the molecular weight.

2.8.6 Relations among c_{eff}, C_{FX}, and c^*

The effective exhaust velocity c_{eff} is related simply to C_{FX} and c^* as follows:

$$c_{eff} = \frac{F}{\dot{m}} = \frac{F/p_c A_t}{\dot{m}/p_c A_t} = C_{FX} c^* \qquad (2.29)$$

It is evident from eq. 2.29 that the effective exhaust velocity c_{eff} (or specific impulse $I_{sp} = c_{eff}/g$) is proportional to two factors, C_{FX} and c^*, of which C_{FX} is a function of nozzle efficiency and c^* is a function of combustion efficiency.

2.8.7 Characteristic Length L^*

A somewhat less basic, but nevertheless useful, design parameter is the "characteristic length" L^* which is defined as

$$L^* = \frac{\text{Combustion volume}}{A_t} \qquad (2.30)$$

where combustion volume is understood to extend only to the plane of the nozzle throat. It can be shown that L^* is proportional to the residence time of an element of propellant during combustion in the chamber and hence is determined by the chemical composition and pressure of the propellant gases. The "characteristic length" L^* is used to determine the needed combustion volume and thus determines the size of the chamber.

A list of the most important design parameters is given in Table 2.2. Examination of this table will give a certain perspective of rocket performance.

TABLE 2.2

Summary of Performance Parameters

Parameter	Symbol	Unit	Typical Values
Effective exhaust velocity	c_{eff}	ft/sec	3,000-12,000
Specific impulse	I_{sp}	sec	100-400
Thrust coefficient	C_F	—	1.1-2.0
Characteristic velocity	c*	ft/sec	2,000-6,000
Characteristic length	L*	in.	10-500

2.8.8 Simplified Liquid Rocket Design Procedure

Three sets of quantities that must be known accurately in order to design a liquid rocket motor are (a) the chamber and nozzle dimensions, (b) the heat transfer and cooling system specifications, and (c) the hydraulic and geometrical parameters of the injector. Only the basic motor dimensions will be considered here.

The quantities that are usually specified initially are thrust F (lb); combustion pressure p_c (psi); external pressure p_o(psi); and propellant chemicals. The c* and L* data for specific propellants must be collected empirically in advance.

From the given conditions we wish to find values of throat area A_t (in.^{2}); exit area A_e (in.^{2}); chamber volume V_c (in.^{3}); and propellant weight flow rate $\dot{m}$ (lb/sec). The following procedure may be used.

1. Select a value of thrust F, combustion pressure p_c, and external pressure p_o; determine the propellant combination and, if a bipropellant, the mixture ratio r.

2. Using empirical data collected from static rocket motor tests with the propellant at the values of p_c and r just chosen, in conjunction with thermochemical calculations, determine the ratio of specific heats γ, characteristic length L*, and characteristic velocity c*. The value of γ is usually between 1.1 and 1.3, and L* often lies between 40 and 100 in.

3. Use the ratio of specific heats γ and the pressure ratio p_c/p_o to calculate the nozzle coefficient C_F and the ideal nozzle expansion ratio ϵ, as in eqs. 2.22 and 2.19. Graphs of C_F and ϵ are shown in Figs. 2.5 and 2.4. The theoretical values of C_F must be corrected slightly for friction and divergence of the nozzle, $C_{FX} = \lambda \eta C_F$.

4. Use the basic relation $F = C_{FX} p_c A_t$ to compute the throat area A_t and the known ratio $\epsilon = A_e/A_t$ to compute the exit area A_e.

5. Use the definition of characteristic velocity c* to calculate the total mass flow rate $\dot{m}$; thus, $\dot{m} = p_c A_t / c^*$.

6. Determine the combustion volume V_c from the relation $V_c = L^* A_t$ using the empirically measured characteristic length L*.

7. The ratio of combustion chamber cross-sectional area A_c to throat area A_t is determined from a knowledge of heat transfer and structural strength factors. Heat transfer is increased if A_c is small; stress is increased if A_c is large. A typical range of A_c/A_t is 2 to 6. When this ratio is fixed, the chamber length l_c is also determined. Using as an example a 1500-lb-thrust acid-aniline motor, we arrive by this process at a set of specifications, listed in Table 2.3 in the order in which they must logically be calculated.

TABLE 2.3

Typical Rocket Engine Specifications

Initial specifications	
Thrust at sea level, F	1500 lb
Combustion pressure, p_c	300 psia
Average external pressure, p_o	8.5 psia
Propellant	acid-aniline
Mixture ratio, r	2.75
Empirical data	
Ratio of specific heats, γ	1.25
Characteristic velocity, c*	4600 ft/sec
Characteristic length, L*	73.4 in.
Calculated data	
Corrected thrust coefficient, C_{FX}	1.35
Expansion ratio, ϵ	5.0
Throat area, A_t	3.7 in.^{2}
Exit area, A_e	18.5 in.^{2}
Total weight flow rate, $\dot{m}g$	7.8 lb/sec
Oxidizer flow rate, $\dot{m}_o g$	5.72 lb/sec
Fuel flow rate, $\dot{m}_f g$	2.08 lb/sec
Combustion volume, V_c	272 in.^{3}
Chamber area ratio, A_c/A_t	5.85
Chamber diameter, d_c	5.25 in.
Chamber length, l_c	11.0 in.

2.9 EFFECT OF SYSTEM ON MOTOR DESIGN

The goal of this book is to discuss the systems aspects of ballistic vehicles, so it is appropriate here to review the effect of the mission on the rocket engine design.

The fundamental requirement of nearly every chemical rocket engine is to accelerate a specified mass to a specified velocity or range. These basic specifications in turn influence the magnitude and duration of thrust produced by the engine. Durations typical of different missions are listed in Table 2.4.

TABLE 2.4

Application	Duration, sec
Artillery rockets	0.1-1.0
Short-range missile boosters	0.5-5.0
Aircraft take-off	10.0-45.0
Long-range missile propulsion	30-300
Aircraft propulsion	300-3600
Space propulsion	60- ?

The magnitude of thrust is determined by the product of the mass to be accelerated and the maximum acceleration which this mass can tolerate. Thrust may range from 1 g or less for a vulnerable payload (such as a human passenger) to 100g or more for an insensitive payload. Rockets have been constructed with thrusts ranging from less than an ounce (for model aircraft) to significant multiples of a million pounds.

After the duration and magnitude of thrust have been chosen (or thrust as a function of time, if a "programmed" thrust is to be used), the designer has to choose approximately a dozen sets of quantities or "inputs," which are variable within limited ranges, and which he determines from his experience and knowledge of the state of the art (see Section 2.8 and Table 2.2). These include propellant chemicals, their mixture ratio, combustion and atmospheric pressure; materials of construction and allowable stresses therein; permissible dry weight of the engine; means of propellant feed and flow control; and acceptable tolerances of the dimensions, pressures, flow rates, and properties of materials and propellants and other engineering parameters.

After making an appropriate first estimate of the "input" quantities, the designer may by suitable calculations arrive at such dependent or "output" quantities as throat area, nozzle expansion ratio, combustion chamber proportions, propellant flow rates, injector hydraulics, feed system power requirements, and heat flow into the combustion chamber. These first estimates may not be acceptable or may not be optimum values, whereupon changes are made in the original assumptions, and by an iterative process an acceptable solution is found or its existence is shown to be impossible.

There are many interactions among the variables. For example, an increase in nozzle exit diameter may increase drag and weight so that an increase in thrust is necessary, which may require a still greater nozzle diameter. Or an increase in chamber pressure may require heavier pumps while allowing smaller tanks. A tolerance in relative mass flow rates which permits the fuel tank to empty before the oxidizer tank may decrease available impulse to a point at which the vehicle will not perform its mission.[20]

A skilled designer whose intuitions have been developed by experience can perform studies that will reveal the effects of changes in such major parameters as chamber pressure or propellant density. Another way in which nearly all important quantities can be taken into account is to devise a mathematical model of the rocket engine; that is, to write down explicit equations relating the various "input" and "output" quantities. These are then solved simultaneously on a large computing machine, and various parameters are changed until optimum solutions (maximum velocity, minimum structural weight) are found. This procedure requires that specific numerical values be chosen for all parameters (i.e., c^*, fuel density, etc.) and that "scaling laws" for the weight of various assemblies as a function of pressure, size, heat transfer, etc., be adopted. These must usually be somewhat simplified in order to make the equations manageable. A typical rocket engine might be represented by a system of 25 to 50 simultaneous equations.[21, 22]

It should be emphasized that much careful thought must precede a machine optimization study, and that most of the qualitative and logical decisions, the "physics" of the problem, must be postulated before appealing to the machine for quantitative answers. On the other hand, machine calculations can reveal the importance (or insignificance) of factors that might otherwise escape notice because of the complexity of the mathematics.

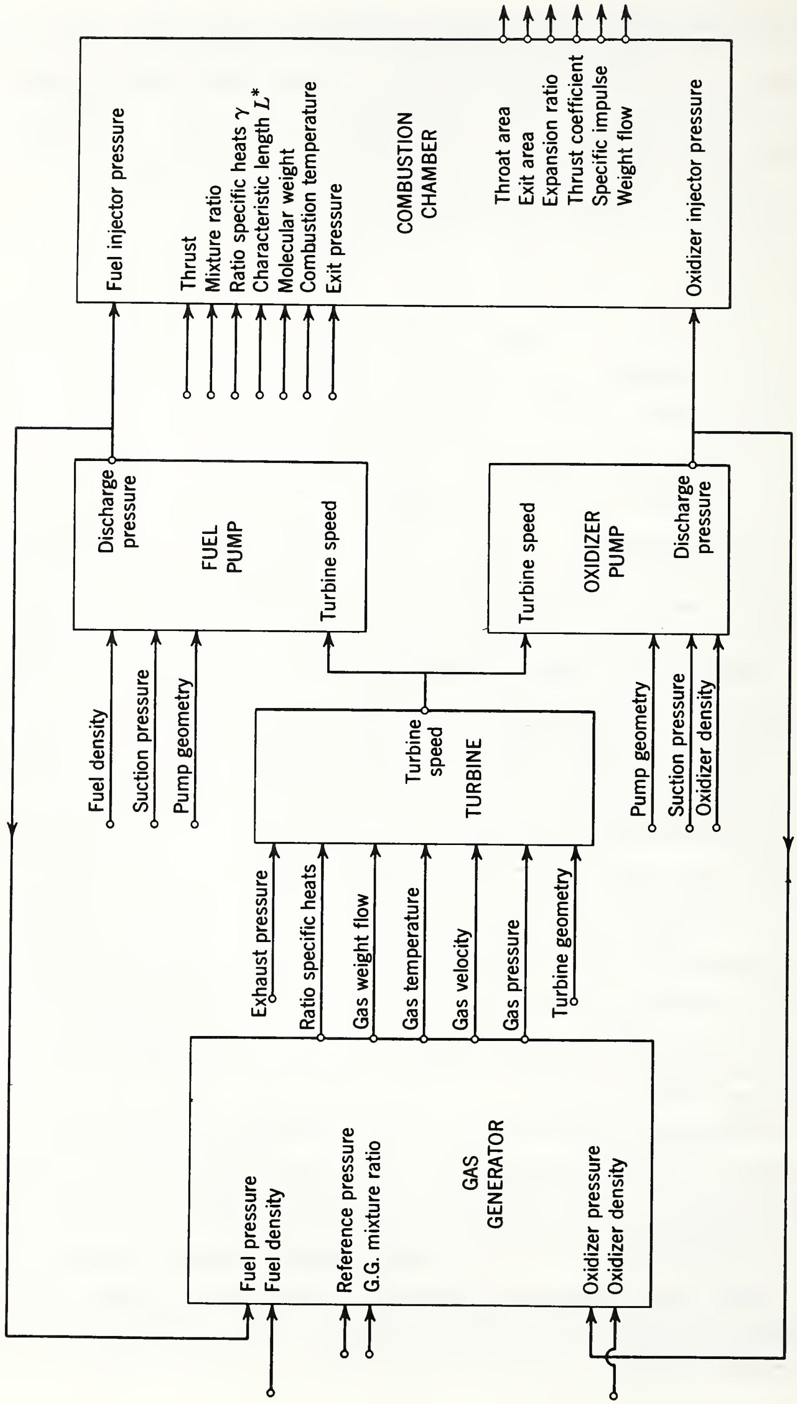
COMBUSTION CHAMBER
Fuel injector pressure
Thrust
Mixture ratio
Ratio specific heats γ
Characteristic length L^*
Molecular weight
Combustion temperature
Exit pressure
Throat area
Exit area
Expansion ratio
Thrust coefficient
Specific impulse
Weight flow
Oxidizer injector pressure
FUEL PUMP
Discharge pressure
Turbine speed
Fuel density
Suction pressure
Pump geometry
OXIDIZER PUMP
Turbine speed
Discharge pressure
Pump geometry
Suction pressure
Oxidizer density
TURBINE
Turbine speed
Exhaust pressure
Ratio specific heats
Gas weight flow
Gas temperature
Gas velocity
Gas pressure
Turbine geometry
GAS GENERATOR
Fuel pressure
Fuel density
Reference pressure
G.G. mixture ratio
Oxidizer pressure
Oxidizer density

Fig. 2.9 Rocket engine system relations.

A way of visualizing the relationships that exist in a typical rocket engine system is shown in Fig. 2.9. In this diagram a box is used to symbolize a set of equations connecting certain "input" variables with other "output" variables. For example, a box labeled "combustion chamber" might have as inputs thrust F, chamber pressure p_c, mixture ratio r, ratio of specific heats γ, characteristic length L*, combustion temperature T_c, and mean molecular weight of chamber gases M. The outputs might include throat area A_t, exit area A_e, weight flow $\dot{w}$, expansion ratio ϵ, and thrust coefficient C_F. These remarks assume that combustion chamber heat transfer, stress, and weight interact but little with the thrust chamber geometry and combustion parameters, thus simplifying the analytical model.

In this chapter we do not discuss propellant feed systems but confine our attention to the rocket motor proper, which includes the injector, combustion chamber, and nozzle. Each of these is a separate design problem.

2.10 FUNDAMENTAL DESIGN PROCEDURE

2.10.1 Basic Parameters

In making quick estimates of rocket sizes, designers are often interested in knowing what mass flow $\dot{m}$ and throat area A_t correspond to a specified thrust, chamber pressure, and propellant combination. These are readily found from

$$A_t = \frac{F}{p_c C_F} \qquad \text{(see eq. 2.20)}$$

and

$$\dot{m} = \frac{p_c A_t}{c^*} \qquad \text{(see eq. 2.17)}$$

The parameters C_F and c* are estimated as follows. Since the reacting chemicals are given, the ratio of specific heats γ and the characteristic velocity c* of the combustion products can be estimated from Table 2.1 (γ will often lie between 1.16 and 1.25). By using the selected γ and a reasonable choice of area ratio ϵ and pressure ratio p_c/p_o (ambient pressure values of interest are $p_o \simeq 0$ psia for altitude above 100,000 ft), a value of thrust coefficient C_F may be found in

Figs. 2.5, 2.6, 2.7, and 2.8. This C_F will always lie between the extremes of 1.2 and 2.7; usually it will be between 1.3 and 1.9. An experienced designer will often be able to estimate C_F to within 10 per cent; however, there are instances in which C_F must be known to ±0.1 per cent. An orderly procedure for arriving at the fundamental parameters of the combustion chamber is given in Section 2.8.8.

Two examples of typical short calculations will now be given.

EXAMPLE I

Given: Thrust $F = 1500$ lb at sea level
Pressure $p_c = 240$ psia
Ambient $p_o = 14.7$
Divergence[19] factor $\lambda = 0.98$
Loss factor $\eta = 0.95$
Ratio specific heats $\gamma = 1.25$
Find: (Assume optimum nozzle for sea-level operation)
Experimental thrust coefficient C_{FX}
Expansion ratio ϵ
Throat area A_t

The pressure ratio p_o/p_c equals $14.7/240 = 0.0613$

From the curves, we find for $\gamma = 1.25$ that $C_F = 1.363$ and $\epsilon = 2.98$.

The experimental thrust coefficient is

$$C_{FX} = \lambda\eta C_F$$
$$C_{FX} = 0.98 \times 0.95 \times 1.363$$
$$C_{FX} = 1.27$$

The throat area is

$$A_t = \frac{F}{p_c C_{FX}} = \frac{1500}{240 \times 1.27} = 4.92 \text{ in.}^2$$

There is no need here to know I_{sp} or mass flow to find A_t.

EXAMPLE II

Given: Thrust $F = 100{,}000$ lb at altitude
Pressure $p_c = 300$ psia
Ambient $p_o = 8.5$ psia
Specific impulse $I_{sp} = 250$ sec

$$\lambda = 0.98$$
$$\eta = 0.98$$
$$\gamma = 1.21$$

Find: Mass flow $\dot{m}$
Throat area A_t

The pressure ratio p_o/p_c equals $8.5/300 = 0.0283$.

As in Example I, we find from the curves that C_F equals 1.50 and

$$C_{FX} = \lambda\eta C_F = 1.50 \times 0.98 \times 0.98 \times 1.44$$

$$A_t = \frac{F}{p_c C_{FX}} = \frac{100{,}000}{300 \times 1.44} = 232 \text{ in.}^2$$

From eq. 2.23,

$$\dot{m} = \frac{F}{gI_{sp}}$$

$$\dot{m} = \frac{100{,}000}{32.2 \times 250}$$

$$\dot{m} = 12.44 \text{ slugs/sec}$$

$$\dot{w} = 400 \text{ lb/sec}$$

There is no need to know C_F to find $\dot{m}$ when F and I_{sp} are given.

2.10.2 Combustion Chamber Proportions

The principal design criterion for the rocket chamber upstream of the throat is that it enclose sufficient volume for the chemical reaction to have time to go to completion before the combustion products accelerate to sonic velocity. Other secondary design criteria are that the surface of the chamber be sufficiently small for the total heat flow through its walls to be absorbed by the available coolant, that its weight be kept as low as possible, and that its geometrical form be such that violent acoustical oscillations (combustion instability) are minimized.

The volume of the combustion chamber is conveniently estimated by the use of the ratio $V_c/A_t = L^*$ which was defined in Section 2.8.7 as the characteristic length. L^* is characteristic of a specific chemical reaction occurring at a specific pressure, proportional to the time of residence of a molecule in the chamber. L* is determined by experiment. If A_t and L* are known, it is easy to calculate chamber volume V_c, which is here defined to include all volume up to the plane of the nozzle throat.

Values of L* range widely from those of most volatile and easily burned propellants, such as gaseous hydrogen and gaseous oxygen with an L* of 10 in., through acid-aniline and oxygen-kerosene with L*'s of 30 to 80 in., to monopropellants which burn at low pressures only with difficulty, such as nitromethane with L*'s of 300 to 600 in.

The fact that L* is taken as a fixed number independent of F for a particular p_c and reaction means that the proportions of a rocket chamber vary as it is scaled up or down.

Figure 2.10 shows the relative proportions of L* = 40 chambers in which the throat radii are 1 in., 5 in., and 10 in. These would yield thrusts (with fixed p_c) of ratio 1 : 25 : 100.

2.10.3 Choice of Combustion Pressure Level

Two conflicting sets of requirements must be met in selecting the combustion pressure p_c. If p_c is too low, the ideal thermodynamic efficiency n_i of the expansion process will be reduced and quite possibly the required L* for good combustion will be increased. If p_c is too high, the weight of the propellant feed system (and the power it requires) will be increased. The compromise used in the German V-2, a pump-fed system, was $p_c = 225$ psia. As pump efficiencies and designs have improved, pressure has been increased to $p_c =$ 650 psia in several modern engines, and still higher pressures are in prospect. When the entire propellant tank must be pressurized to a value above p_c, as in gas-pressurized systems, a suitable compromise (used, for instance, in the American-made Corporal) is $p_c = 300$ psia. Space vehicle systems may use even lower pressures, for if the environmental pressure p_o is low, as it is for rockets operating entirely at very high altitudes, a large pressure ratio p_c/p_o and consequent good cycle efficiency η_i can be achieved without the necessity for large values of p_c. The size and weight of a low-pressure chamber go up as p_c decreases. However, the use of low p_c opens up the possibility of designing a simple gas-pressurized system without the complication and weight of pumps and

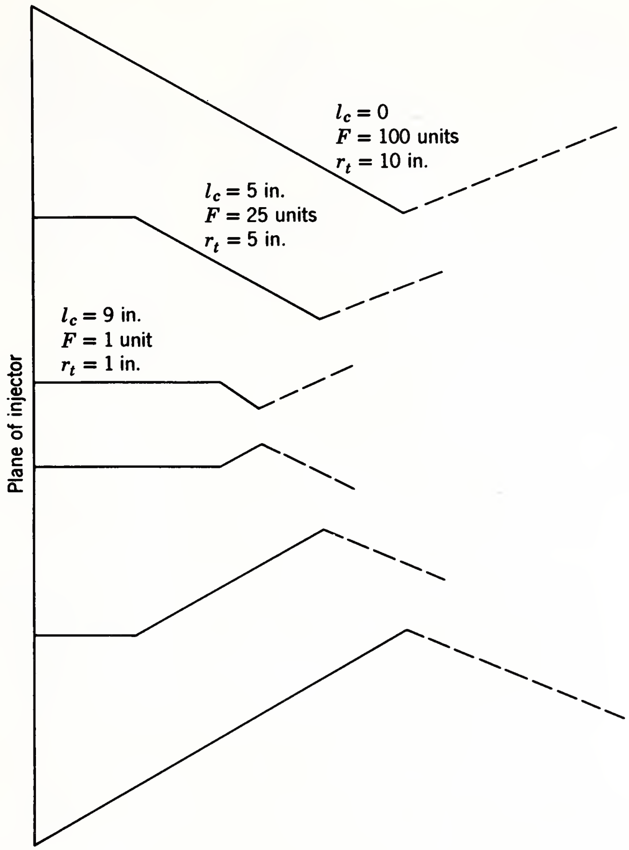
$l_c = 0$
F = 100 units
r_t = 10 in.
l_c = 5 in.
F = 25 units
r_t = 5 in.
l_c = 9 in.
F = 1 unit
r_t = 1 in.
Plane of injector

Fig. 2.10 Effect of scale on chamber aspect ratio; L* = 40 in.; $\beta = 30°$; p_c = constant. Thrust units arbitrary.

without excessive weight penalty for the propellant tanks. A series of engines of constant thrust and bounded exit diameter covering the range $p_c = 7.5$ psia to $p_c = 350$ psia are shown in Fig. 2.11.

Conclusions made without taking into account heat transfer and coolant pressures and weights are not completely realistic and must be regarded as tentative.

2.11 PROPELLANT INJECTOR DESIGN

2.11.1 Design Philosophy

The design of a rocket motor injector head—that simple

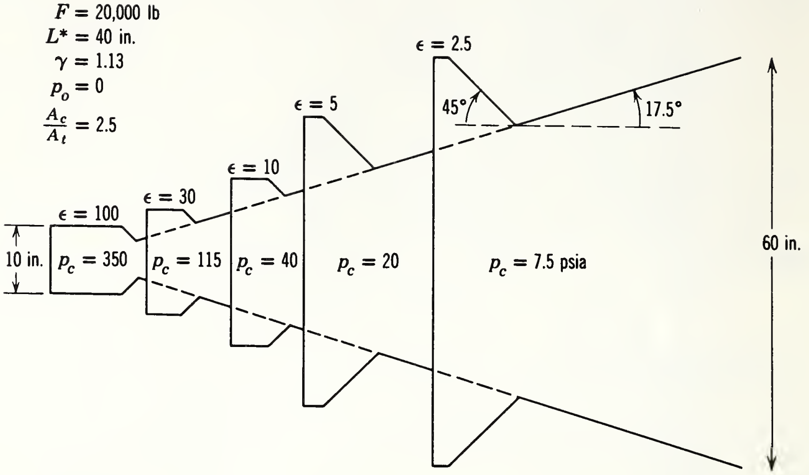

Fig. 2.11 Effect of varying p_c on engine contour (constant thrust and exit diameter).

component consisting of a manifold and some holes--remains almost entirely empirical even after 15 years of experience. Even the vocabulary by which different types are described is far from standardized. Designs that work at one scale do not necessarily work well at another scale. The number of ways in which one or two liquids may be injected into a chamber in order to be mixed and atomized is very large. These ways may be sorted out after a fashion by considering the geometry and dynamics of the flow, respectively.

2.11.2 Flow Geometry

Typical injector stream cross sections may be cylindrical, annular, conical, flat (this last either by impingement or extrusion), or some other shape. Streams may be combined in pairs or triplets or other multiples at any orientation and allowed to impinge at any point in combustion space. The relative diameters of streams may have any value, although there is evidence that, if they match, better mixing is secured. Figure 2.12 shows schematically some geometries that have been found workable.

2.11.3 Flow Dynamics

Significant dynamical variables describing an injected

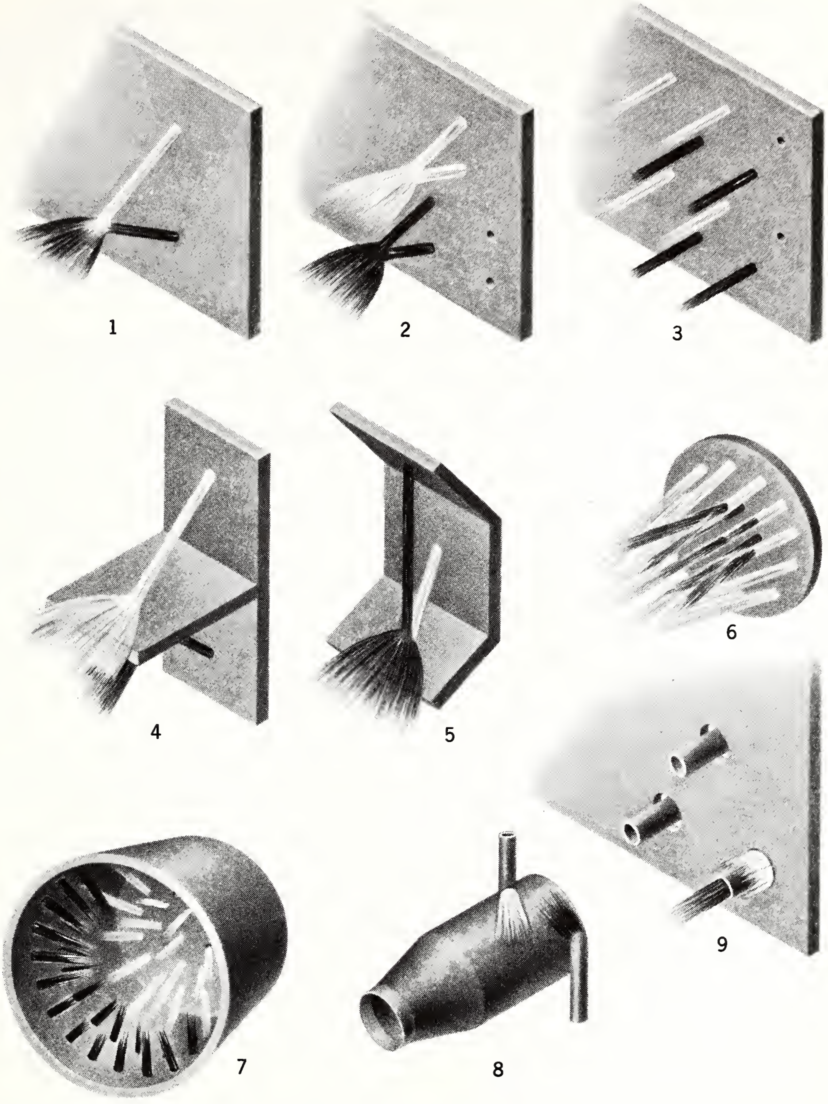

Fig. 2.12 Configurations of fluid jets used in liquid propellant injector heads. (1) Unlike impinging. (2) Like-on-like impinging. (3) Nonimpinging (showerhead). (4) Splash plate. (5) Mix-plate (Enzian). (6) Converging-diverging cones. (7) Intersecting cones and jets (V-2 Rosette) with O_2 in center. (8) Premix. (9) Coaxial.

stream are its average velocity, momentum, and its velocity profile. When streams are combined, important parameters are the degree of mixing, degree of atomization (particle-size distribution), and spatial distribution of particles. Rather careful measurements of these quantities have been made for flow in the absence of combustion. How these results are affected by the thermal and pressure disturbances of combustion is not well understood, although efforts have been made to evaluate the relative importance of mixing and atomization during actual firing tests. These results show that mixing and atomization must both be present for efficient hydrocarbon-liquid oxygen reaction.

The ideal injector should provide (a) high specific impulse, (b) stable combustion over a wide range of chamber pressure, (c) an acceptable rate of heat flow to the chamber walls, (d) smooth transition from ignition to full combustion, (e) uniform (not streaky or localized) combustion, (f) minimum erosion of injector face, chamber wall, or nozzle throat, (g) low injection pressure drop, (h) steady fluid jets, and (i) insensitivity to vibration and acoustic waves. In addition, it should be light in weight and easy to fabricate, and it should be made of noncritical materials.

2.12 COMMERCIAL SPECIFICATIONS

The road from prototype laboratory model to well-tried reliable, "work-horse" rocket is a long one and involves many tests. The ultimate user—for example, a commercial airline wishing to use jet-assisted take-off regularly from some high-altitude airfield—wishes to be assured that the rocket is safe and reliable. Therefore a long list of specifications must be met by any really practical engine, most of which have some repercussion on the design. Some of the more important requirements which may be demanded by a customer are now listed.

2.12.1 Performance

1. Curves showing actual thrust data versus p_c over the extreme operating limits of p_c, with randomness in p_c guaranteed to ± 10 per cent or less, depending on the application.

2. Curves showing actual sea level I_{sp} versus mixture ratio r, at nominal p_c with Δr guaranteed to be within specified limits.

3. Actual head versus flow curves for the pumps, if any, for rated design speed and for values deviating from it by ±10 per cent.

4. Flow calibrations for injector and coolant ducts to be supplied.

2.12.2 Operation

5. Engine to start successfully on the first try a specified number of times and to reach 100 per cent thrust each time within a specified time interval. Starting sequence of control actions such as pressurizing, valving, and ignition to be precisely stated.

6. Engine to shut down safely and reliably within a specified time of the control signal. "Safely" may be defined to include absence of dribbling propellants and fire.

7. In event of certain agreed upon malfunctions, such as loss of electrical control power to valves, ignition failure, etc., engine guaranteed to stop in a "fail-safe" manner.

8. Draining and filling connections to be located with maximum convenience and minimum hazard, preferably at a single point. Pilot control to be of maximum simplicity and located on a single panel.

9. No external or internal leakage permitted that might produce hazard.

2.12.3 Environment

10. Completely loaded engine to be exposed to temperature extremes ranging from subzero to tropical for long enough to reach thermal equilibrium, followed by successful operation.

11. Engine to operate at any attitude to be encountered in flight.

12. Engine to withstand handling shocks, dropping, axial accelerations and decelerations of a specified number of g's (say not less than 10), as well as rotational accelerations around three perpendicular axes (of say 10 radians/sec^2) followed by satisfactory operation. This test has particular reference to relays and valves.

13. Engine to operate under flight exposure, that is, with conditions of airspeed or vacuum and temperature combination expected in flight.

14. Engine to be subjected to protracted periods of rains, sand, dust, fungus, salt spray, and vibration with satisfactory inspection to follow.

2.12.4 Reliability and Quality Control

15. Engine to operate over a specified time duration for a specified number of consecutive operations with standard parts and no failure, or alternatively a specified number of engines to operate once with no failures (acceptance and qualification tests).

16. Clear statement of maximum acceptable limits on propellant composition, such as per cent water in H_2O_2, per cent NO_2 in HNO_3, specific gravity range of kerosene, etc.

17. Dry weight equal to or less than specified value by actual weighing.

18. Major components interchangeable.

19. Packaging such that engine may be stored for extended period before installation without deterioration.

REFERENCES

1. R. K. Sherburne and W. L. Weeks, "Momentum Thrust of a Rocket," Am. J. Phys., **21**, 139-140 (1953).
2. W. F. Durand, Aerodynamic Theory, Durand Reprinting Committee, California Institute of Technology, Vol. 1, 1943, p. 118; or R. H. Sabersky, Elements of Engineering Thermodynamics, McGraw-Hill, New York, p. 281, 1957.
3. F. J. Malina, "Characteristics of a Rocket Motor Unit Based on the Theory of Perfect Gases," J. Franklin Institute, **230**, No. 4, 449 (1940).
4. G. V. R. Rao, "Exhaust Nozzle Contour for Optimum Thrust," Jet Propulsion, **28**, No. 6, 377 (1958).
5. R. H. Sabersky, Elements of Engineering Thermodynamics, McGraw-Hill, New York, Chapter 7, 1957.
6. J. H. Jeans, Kinetic Theory of Gases, Cambridge University Press, London, 1940.
7. A. E. H. Love, Mathematical Theory of Elasticity, Cambridge University Press, London, 1927; or H. Lamb, Hydrodynamics, sixth edition, republished by Dover, New York, 1945.
8. A. W. Wundheiler, "On Instruction in Supersonic Flow," Am. J. Phys., **15**, No. 6, 512 (1947).
9. R. N. Wimpress, Internal Ballistics of Solid Fuel Rockets, McGraw-Hill, New York, 1950, p. 40.
10. M. Summerfield, C. R. Foster, and W. C. Swan, "Flow Separation

in Over-expanded Supersonic Exhaust Nozzles," *Jet Propulsion*, **24**, 319 (1954).

11. G. P. Sutton, *Rocket Propulsion Elements*, second edition, John Wiley and Sons, New York, 1956, p. 94.
12. H. W. Liepmann and A. E. Puckett, *Introduction to Aerodynamics of a Compressible Fluid*, John Wiley and Sons, New York, 1947, Chapter 4.
13. H. R. Ivey, "A Mechanical Analogy for Hypersonic Flow," *J. Aeronaut. Sci.*, **17**, No. 8, 519-523 (1950).
14. W. J. M. Rankine, "Theory of Waves of Finite Disturbance," *Trans. Roy. Soc.* (London), **160**, 277-288 (1870).
15. F. P. Bundy, H. M. Strong, and A. B. Gregg, "Measurement of Velocity and Pressure of Gases in Rocket Flames by Spectroscopic Methods," *J. Appl. Phys*., 22, 1069-1077 (1951).
16. D. Altman, "An Investigation of Shock Waves in Jets," Jet Propulsion Laboratory, Progress Report 9-3, May 1947, p. 12.
17. J. D. McKenney, "An Investigation of Flow Separation in a Two-Dimensional Transparent Nozzle," Jet Propulsion Laboratory, Progress Report 20-129, April 4, 1951.
18. C. R. Foster, "Experimental Study of Gas Flow Separation in Overexpanded Exhaust Nozzles for Rocket Motors," Jet Propulsion Laboratory, Progress Report 4-103, May 9, 1949.
19. C. R. Foster, "Experimental Study of the Divergence-Angle Effect in Rocket Motor Exhaust Nozzles," Jet Propulsion Laboratory, Progress Report 20-134, January 16, 1951.
20. J. A. Brousseau, Jr., "Optimum Ratio of Propellants," *Jet Propulsion*, **26**, No. 2, 106 (1956); and R. H. Reichel, "Importance of Mixture Ratio Control," *Jet Propulsion*, **25**, No. 6, 291 (1955).
21. Carl H. Builder, "General Solutions for Optimization of Staging of Multistage Boost Vehicle," *ARS Journal*, **29**, No. 7, p. 497-499.
22. B. N. Smith, "Perturbation Analysis of Low-Frequency Rocket Engine System Dynamics on an Analog Computer," *Jet Propulsion*, **26**, No. 1, 40-45 (1956).

3

LIQUID ENGINE DESIGN PARAMETERS

J. O. Crum

3.1 INTRODUCTION

In the discussion of liquid engine design parameters this chapter will:

1. Identify the components of a liquid rocket vehicle which may be considered part of the liquid rocket engine.
2. Enumerate differences in liquid rocket engine systems resulting from major design concepts of the vehicle.
3. Discuss the parameters which affect the design of various engine components.
4. Consider problems arising from the interface between the vehicle and the rocket engine.

3.1.1 Components of a Liquid Propellant Rocket

From a functional viewpoint, a liquid rocket is a vehicle which moves a payload from one point in space to another. This definition implies a vehicle consisting of (a) a payload, (b) guidance equipment, (c) an airframe, (d) propellant tanks, (e) a rocket engine, and (f) a thrust vector control system. The latter three components will be discussed in this chapter as the liquid engine system.

3.1.2 Basic Parameters Influencing Sizing

The performance of a rocket vehicle can be expressed as a function of (a) its specific impulse, a composite figure relating to the energy content of the propellant and the expansion efficiency of the nozzle; (b) the ratio of the total weight of the vehicle divided by its empty weight; and (c) drag and gravity factors. For high performance the specific impulse and the ratio of the total to the empty weight should be maximal, and the integrated effect of drag and gravity should be minimal. These requirements conflict, and for any given rocket application an optimum compromise is sought. Some of the factors relating to the selection and design of rocket engines which must be considered in establishing the optimum rocket are discussed in the following paragraphs.

3.2 ENGINE COMPONENTS

3.2.1 Configuration of a Typical Engine (Pressure-Fed)

Figure 3.1 is a schematic of a pressure-fed liquid rocket engine, utilizing alcohol and liquid oxygen as its propellants. A pump-fed system will be discussed later.

The main elements of this system are (a) the propellant tanks; (b) a propellant feed mechanism, a supply of high-pressure helium to force the propellants out of the tanks and into the thrust chamber; (c) the thrust chamber, and (d) a multiplicity of valves.

3.2.2 Parameters Influencing Design of Liquid Rocket Engines

A. General Parameters. The volume of the propellant tanks depends on the density and the total weight of propellant. For a bipropellant system as shown in Fig. 3.1, the ratio of the sizes of the propellant tanks is dependent on the mixture ratio selected. The thrust required of the rocket engine is proportional to the weight rate of flow of propellants. The larger the weight rate of flow the larger and heavier will be the propellant feed mechanism, thrust chamber, and plumbing. Hence, a high propellant density and a low thrust-to-weight ratio would be advantageous for a liquid rocket vehicle.

Let us now examine the parameters influencing the design of the typical pressurized liquid engine system of Fig. 3.1. For this configuration the combustion pressure in the thrust

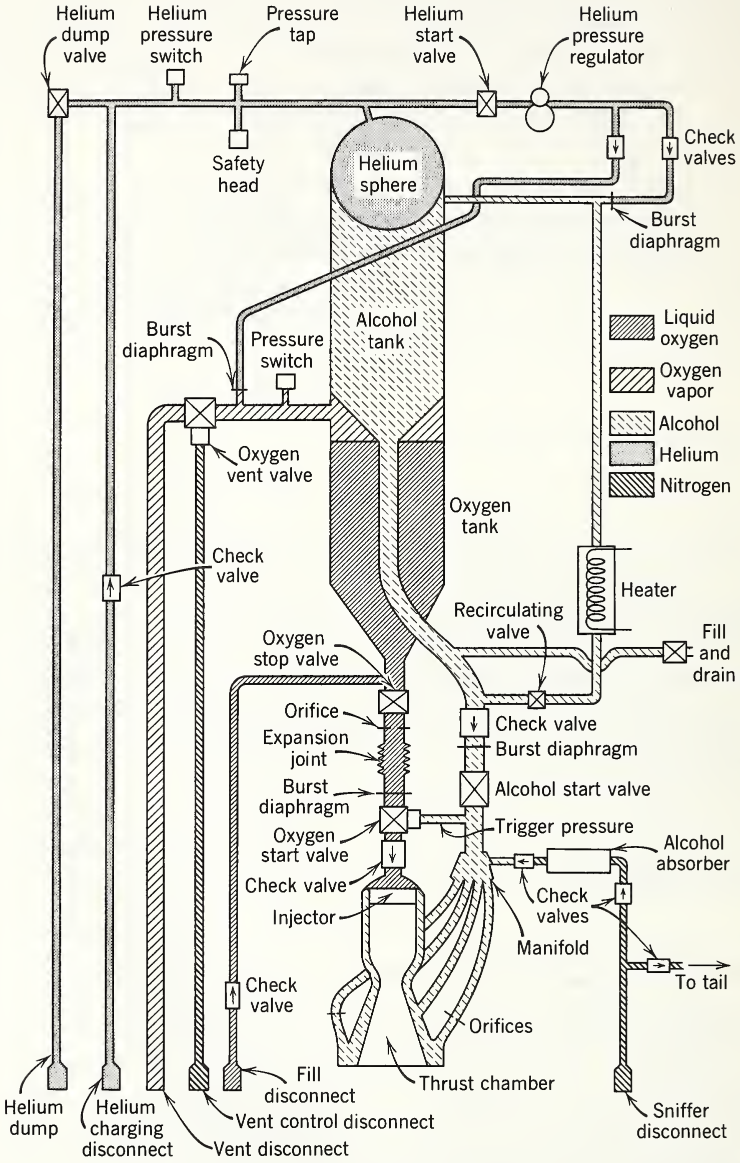
Helium dump valve
Helium pressure switch
Pressure tap
Helium start valve
Helium pressure regulator
Safety head
Helium sphere
Check valves
Burst diaphragm
Liquid oxygen
Oxygen vapor
Alcohol
Helium
Nitrogen
Alcohol tank
Burst diaphragm
Pressure switch
Oxygen vent valve
Oxygen tank
Check valve
Heater
Recirculating valve
Fill and drain
Oxygen stop valve
Orifice
Expansion joint
Burst diaphragm
Oxygen start valve
Check valve
Injector
Check valve
Burst diaphragm
Alcohol start valve
Trigger pressure
Alcohol absorber
Check valves
Manifold
To tail
Check valve
Orifices
Thrust chamber
Fill disconnect
Vent control disconnect
Vent disconnect
Helium dump
Helium charging disconnect
Sniffer disconnect

Fig. 3.1 Schematic diagram of pressurized liquid propellant feed system for missile application. (Courtesy General Electric Company.)

chamber is approximately 300 psi. Combustion temperatures approach 5000° F. The pressure drop of the liquid oxygen flowing through the injector orifices is about 50 psi, resulting in liquid oxygen pressure at the inlet to the thrust chamber of about 350 psi at a temperature of about –280° F. The pressure drop of the alcohol flowing through the injector and the thrust chamber cooling jacket (alcohol acts as the thrust chamber coolant) is about 100 psi, resulting in an alcohol pressure at the inlet to the thrust chamber of about 400 psi at room temperature. These factors suggest that equal propellant tank pressures of about 400 psi would be selected for this application.

An orifice is installed in the liquid oxygen line to reduce the 400-psi pressure in the liquid oxygen tank to the 350 psi required at the liquid oxygen inlet to the thrust chamber. The mixture ratio at which propellants are consumed is a function of the size of this orifice. The orifice is selected so that the engine operates at the desired mixture ratio. The pressure in the propellant tanks must be constant in order to operate the engine at a constant combustion chamber pressure (the usual mode of operation). Helium is provided at an initial pressure of about 2000 psi at the helium sphere. Helium flows through the regulator which reduces the pressure to 400 psi. At the end of a firing when the propellants have been consumed, the helium sphere and both propellant tanks will contain helium at 400 psi.

Because of the high pressures, the tanks and plumbing for a pressurized rocket are relatively heavy. When a rocket vehicle becomes large a turbopump feed system can replace the pressurized feed system at a weight saving; however, we must consider the increased complexity and relative reliability of the turbopump system.

B. Significance of the Propellant Mixture Ratio. Figure 3.2 shows the variation with mixture ratio of several important rocket parameters. This graph applies only to the 75 per cent ethanol-liquid oxygen propellant combination at a combustion pressure of 200 psia, in a rocket engine perfectly expanded to a pressure ratio of 13.6; however, it adequately simulates the characteristics of many propellant combinations under reasonable operating conditions. The following important information can be derived from this graph:

1. As the mixture ratio (pounds of oxidizer consumed per pound of fuel burned) increases, the flame temperature increases. (If the mixture ratio were further increased beyond

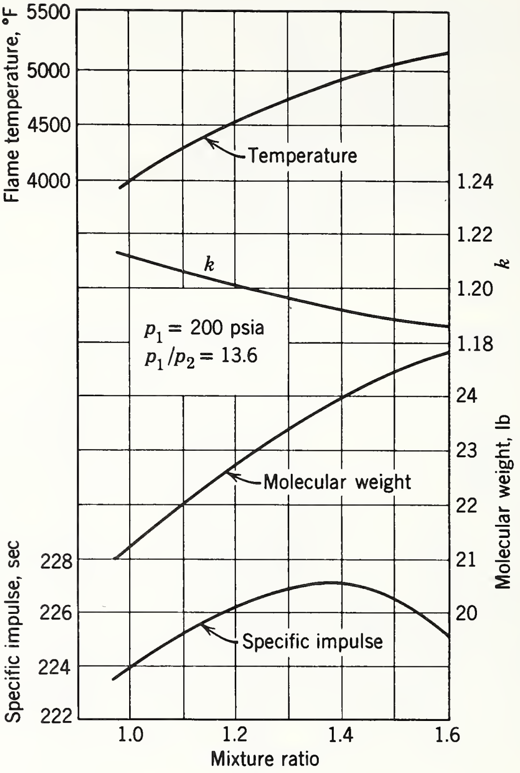

Fig. 3.2 Calculated performance of a liquid oxygen—75 per cent ethanol propellant system.

the limits of the graph, the flame temperature would be found to increase until the mixture ratio reached the stoichiometric value and then decrease for higher values of the mixture ratio.)

2. The molecular weight of the products of combustion increases with increasing mixture ratio. No maximum is observed in this case.

3. The value of the ratio of the specific heats k decreases with increasing mixture ratio.

4. The specific impulse, which is a function of k and the ratio of the flame temperature and the molecular weight, varies with the mixture ratio and reaches a maximum value at a lower mixture ratio than the maximum flame temperature.

The volume of the propellant tanks will be determined by the amount of propellant needed for a mixture ratio yielding maximum specific impulse. In addition, the orifice in the liquid oxygen line should be adjusted so that the engine will operate at this optimal mixture ratio and the propellant tanks will empty simultaneously. Since a pound of dead weight has a significant effect on range, on very high-performance vehicle, this orifice is replaced by a controllable valve. This valve is operated by a sensing system which senses the quantity of each propellant remaining and adjusts the valve position so that both propellants are exhausted simultaneously.

3.2.3 Operation of the Pressure-Fed Rocket Engine

In the system depicted in Fig. 3.1, initially all the tanks are empty, all valves are closed, and burst diaphragms are intact. The fuel, alcohol, is introduced at atmospheric pressure by opening the alcohol fill and drain valve, electrically controlled and actuated either by electrical power or by pneumatic or hydraulic pressure. A pressure relief (or vent) valve on the alcohol tank permits the filling of the tank. After filling, both the fill and drain valve and the vent valve are closed.

The oxidant, liquid oxygen, is introduced at atmospheric pressure through the fill disconnect and check valve. The oxygen vent valve (pneumatically operated) is opened to permit the escape of gaseous oxygen. The liquid oxygen tank is filled to the appropriate level and maintained at that level until firing preparations are completed.

Finally, helium at approximately 2000 psi is introduced through the helium charging disconnect and check valve.

Firing procedure can now begin. First, the liquid oxygen vent valve is closed and the remotely controlled alcohol start valve and the oxygen stop valve are opened by pneumatic or hydraulic pressure through the action of a pilot valve. The remotely controlled helium start valve is opened, allowing helium to flow through the pressure regulator and the check valves and, as the pressure builds up, to burst the burst diaphragms and pressurize the propellant tanks. When the pressure builds up in the propellant tanks, the diaphragms in the propellant outlet lines burst. Alcohol flows through the engine cooling jacket and the injector. The igniter (which is not shown) is activated. Pressure builds up in the alcohol inlet line to activate the oxygen start valve. The valve opens and allows liquid oxygen to flow to the engine and support combustion. It should be noted that the alcohol is permitted to enter the combustion chamber first to insure adequate cooling; however, the other propellant must follow closely to prevent an accumulation of unburned coolant in the chamber, a condition which could result in an explosion.

The engine continues to operate until shutdown time, when first the oxygen stop valve is closed and then the alcohol start valve.

3.2.4 The Turbopump-Fed Rocket Engine

Most modern large rockets are turbopump-fed, rather than pressure-fed. When a turbopump is used to raise the propellant pressure from propellant tank (of the order of 30 psia) to engine operation pressure (300-400 psia), thin-walled propellant tanks can be used, resulting in an over-all reduction of vehicle empty weight. On the other hand, the turbopump, a complex, high-speed, high-energy device, is more difficult to control and operate reliably in the flight environment. Figure 3.3 is a schematic of a turbopump-fed rocket. In addition to the valves and plumbing ordinarily associated with a pressure-fed rocket, this system contains a turbopump, a gas generator which is in itself a miniature pressure-fed rocket, and a third propellant (hydrogen peroxide).

Additional features of the turbopump system of Fig. 3.3 are

1. An independent pressure regulator to pressurize the peroxide tank and thus force peroxide into the peroxide decomposer (operates at about 300 psi and 1200-1500°F).
2. A means of ducting the turbine exhaust gases overboard. This is necessary to prevent an accumulation of combustible hot gases in the engine compartment where a spark or main engine ignition may cause fire or an explosion.
3. An oxygen boiler operating in the turbine exhaust. The oxygen boiler serves to vaporize a portion of the high-pressure liquid oxygen, and thus provide gaseous oxygen to pressurize the liquid oxygen tank.

Some designers have applied the bootstrap principle to supply propellants for the gas generator (Fig. 3.4), thereby both reducing the dry weight of the vehicle and simplifying logis-

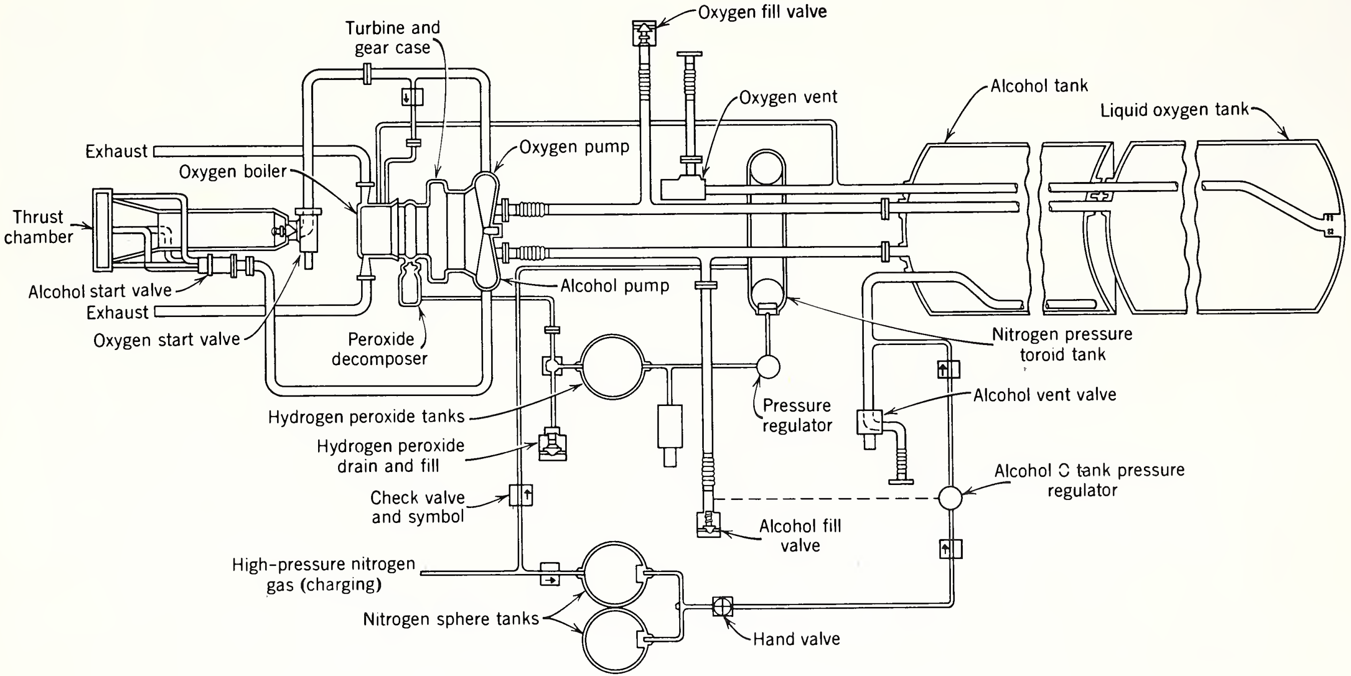
Turbine and gear case
Oxygen fill valve
Oxygen vent
Alcohol tank
Liquid oxygen tank
Exhaust
Oxygen boiler
Oxygen pump
Thrust chamber
Alcohol start valve
Alcohol pump
Exhaust
Oxygen start valve
Peroxide decomposer
Nitrogen pressure toroid tank
Alcohol vent valve
Pressure regulator
Hydrogen peroxide tanks
Hydrogen peroxide drain and fill
Alcohol C tank pressure regulator
Check valve and symbol
Alcohol fill valve
High-pressure nitrogen gas (charging)
Nitrogen sphere tanks
Hand valve

Fig. 3.3 Schematic diagram of missile rocket system using a turbopump. The turbine is driven by the decomposition products of hydrogen peroxide, which in turn comes from a pressurized tank. (Courtesy General Electric Company.)

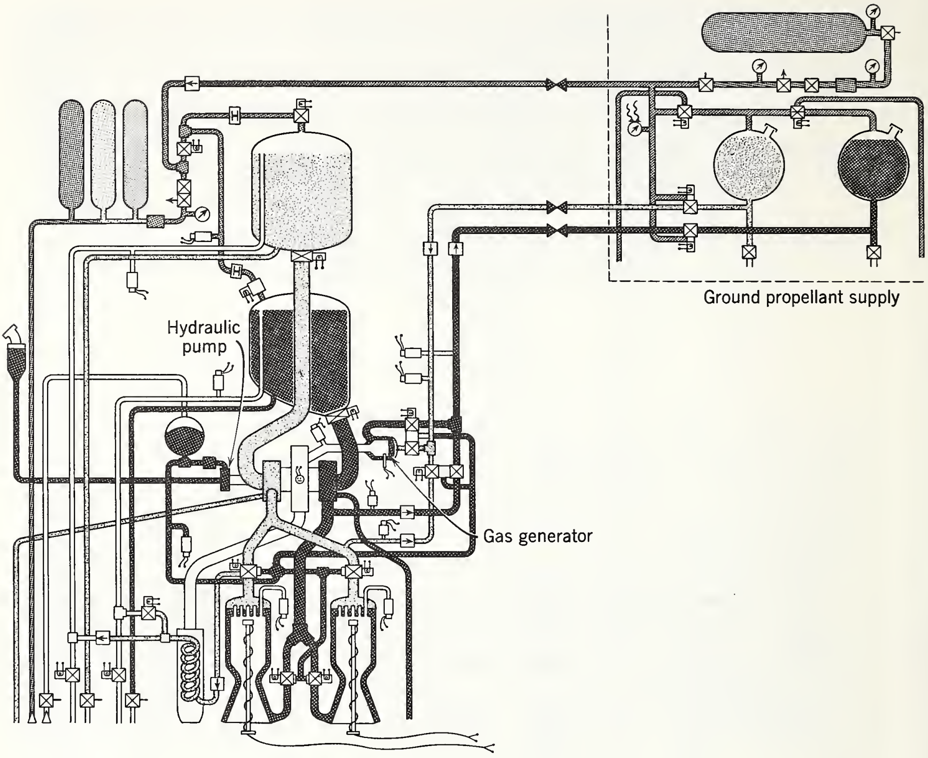

Fig. 3.4 Schematic diagram of missile rocket system using "bootstrap" turbopump.

tics by eliminating the need for the third propellant. With this principle, separate flight-borne propellant tanks and a pressurizing system for the gas generator are not required. High-pressure oxidizer and fuel are bled from the pump outlet to supply the gas generator. Once the turbopump starts, it bootstraps to the operating point. To start the turbopump, fuel and oxidizer are supplied from a pressurized ground supply. As soon as the gas generator is supplying sufficient hot gas and the turbopump is providing fuel and oxidizer at a reasonable pressure, the ground supply is removed and the engine bootstraps to its operating point.

This figure also shows a hydraulic pump being driven from a power take-off pad on the turbopump. The hydraulic pressure is used to actuate various valves which require large actuating forces.

Figure 3.5 is a cutaway section of the turbopump used on the German V-2 rocket. The turbopump consists of two centrifugal pumps, one for alcohol and one for liquid oxygen, and a two-stage impulse-type turbine. This is an example of a direct-drive turbopump (one in which the pumps are on the same shaft as the turbine and turn at the same speed as the turbine).

A. Pumps. Pumps used in rocket vehicles are generally of the centrifugal kind. These are efficient and economical in weight and space for the large flows and high pressures they must handle. A centrifugal pump is particularly attractive when a liquefied gas is one of the components of the propellant system, since with such a pump the liquid cannot become trapped in an enclosed pump space, as it could with a piston-type pump.

The pumping action of a centrifugal pump may be understood as follows. Assume that the pump intake is connected to a supply of fluid and that the pump is primed (the fluid passages in the pump are filled). When the pump impeller begins to rotate, it imparts a radial and tangential velocity to the fluid in the channels of the impeller. As the fluid leaves the impeller tip, it is moving at a high velocity (has a high kinetic energy). The pump volute, which surrounds the impeller, acts as a diffuser to convert this kinetic energy into potential energy or pressure, and the discharge from the volute is the high-pressure discharge from the pump.

A few of the parameters which influence the design of pumps are now listed.

Discharge flow. Each pump of a turbopump delivers a certain number of pounds per second of propellant. This is the flow rate at which the engine, gas generator, and auxiliaries consume the propellant and is, therefore, a major factor in determinating the flow passage areas in the pump.

Required output head. The sum of the combustion chamber pressure, the injector pressure drop, the cooling system pressure drop, and the pressure drop through various valves and plumbing determines the required output head or pump discharge pressure. Since the pump discharge pressure represents the conversion of kinetic energy to potential energy, and the kinetic energy is imparted to the fluid by the rotation of the pump impeller, it is apparent that the discharge pressure will define the impeller configuration—that is, the im-

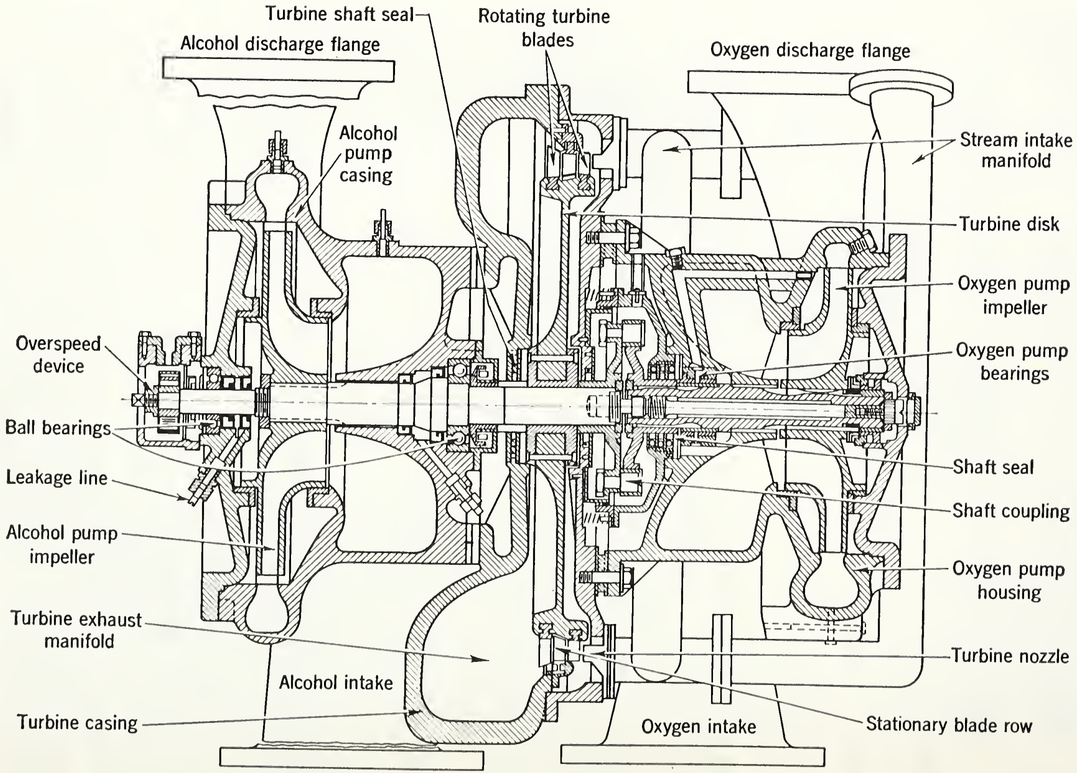
Turbine shaft seal
Alcohol discharge flange
Rotating turbine blades
Oxygen discharge flange
Alcohol pump casing
Stream intake manifold
Turbine disk
Oxygen pump impeller
Overspeed device
Oxygen pump bearings
Ball bearings
Leakage line
Shaft seal
Shaft coupling
Alcohol pump impeller
Oxygen pump housing
Turbine exhaust manifold
Turbine nozzle
Alcohol intake
Turbine casing
Oxygen intake
Stationary blade row

Fig. 3.5 V-2 turbopump assembly.

peller radius for a given pump speed.

Internal leakage. Maintaining close clearances between the rotating and stationary parts of the centrifugal pump at the wearing surfaces minimizes the internal leakage [the circulation between the high pressure (discharge) side to the low pressure (suction) side].

External leakage. The use of a stuffing box or shaft seal prevents external leakage (leakage from the inside of the pump to the outside along the rotating shaft).

Inlet head. One of the main interfaces between the turbopump and the rocket vehicle is the inlet head interface. Pump performance is limited by cavitation, a phenomenon which occurs when the static pressure at any point in a fluid flow passage becomes less than the fluid vapor pressure. The formation of vapor bubbles causes cavitation. These bubbles collapse when they reach a region of high pressure, that is, when the static pressure becomes greater than the vapor pressure. In centrifugal pumps cavitation is most likely to occur in the pump impeller inlet, since this is the point at which the lowest absolute pressure is encountered. The excessive formation of vapor causes the pump discharge to fluctuate and makes the combustion both erratic and dangerous.

The suction head above vapor pressure required by the pump must always be less than the available or net positive suction head furnished at the pump inlet in order to avoid cavitation. The requirement for suction head above vapor pressure results from the design of the pump. The available suction head is a value determined from the tank pressure (the absolute gas pressure in the tank above the liquid level), the elevation of the propellant level above the pump inlet, the friction losses in the line between the tank and the pump, and the vapor pressure of the fluid. Various significant heads used in the design of liquid rockets are defined in Fig. 3.6. When the flying vehicle is accelerating, the elevation head will be the product of the measured head and the load factor.

Still greater head may be necessary to avoid pump cavitation. To supply this head, the propellant may have to be pressurized by external means, such as the addition of another pump in series (a booster pump) or by additional pressurization of the propellant tanks. Pressurization of the propellant tanks requires thicker tank walls, and therefore heavier tanks, which will increase the empty weight of the vehicle.

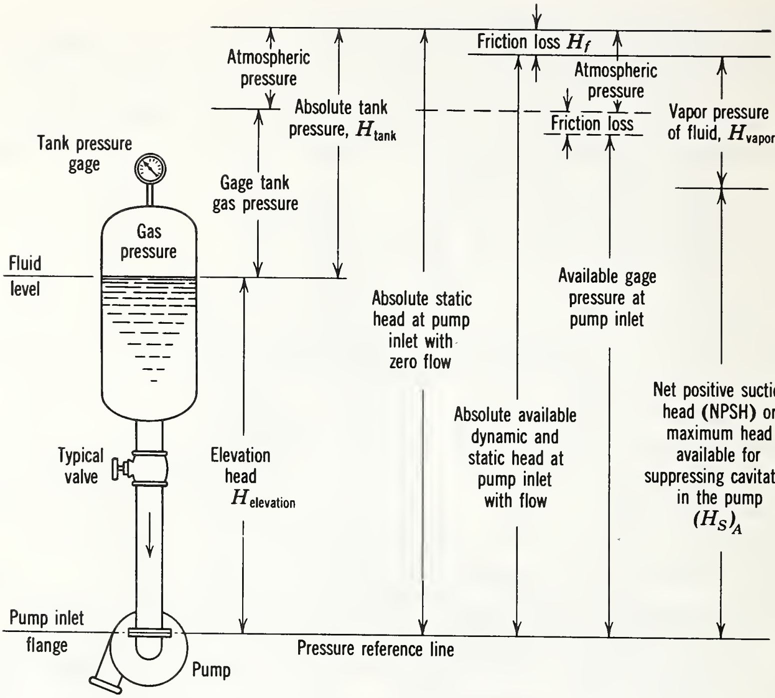
Atmospheric pressure
Absolute tank pressure, H_{tank}
Friction loss H_f
Atmospheric pressure
Friction loss
Vapor pressure of fluid, H_{vapor}
Tank pressure gage
Gage tank gas pressure
Gas pressure
Fluid level
Absolute static head at pump inlet with zero flow
Available gage pressure at pump inlet
Absolute available dynamic and static head at pump inlet with flow
Net positive suction head (NPSH) or maximum head available for suppressing cavitation in the pump $(H_S)_A$
Typical valve
Elevation head $H_{elevation}$
Pump inlet flange
Pressure reference line
Pump

Fig. 3.6 Definition of pump suction heads.

B. Turbines. Turning our attention to the turbine, Fig. 3.5 shows that the V-2 turbine was a two-stage impulse turbine. Impulse turbines are generally used in rocket applications since they are simpler and weigh less per unit horsepower in the significant power and pressure ratio range than reaction turbines. You will notice that high-pressure steam (in this case the decomposition products of hydrogen peroxide) is conducted by the steam intake manifold to a stationary ring of turbine nozzles. In the turbine nozzles the enthalpy of the working fluid is converted into kinetic energy—that is, the steam is given a high velocity. The high-velocity working fluid is delivered against the rotating blades of the turbine. Wheel rotation results from the impulse imparted by the momentum of the high-velocity fluid.

The efficiency of an impulse turbine is a function of the ratio of the tip speed of the turbine wheel to the inlet velocity of the working fluid. Since the V-2 turbopump is a direct drive configuration, and since the rotational speed is limited by the

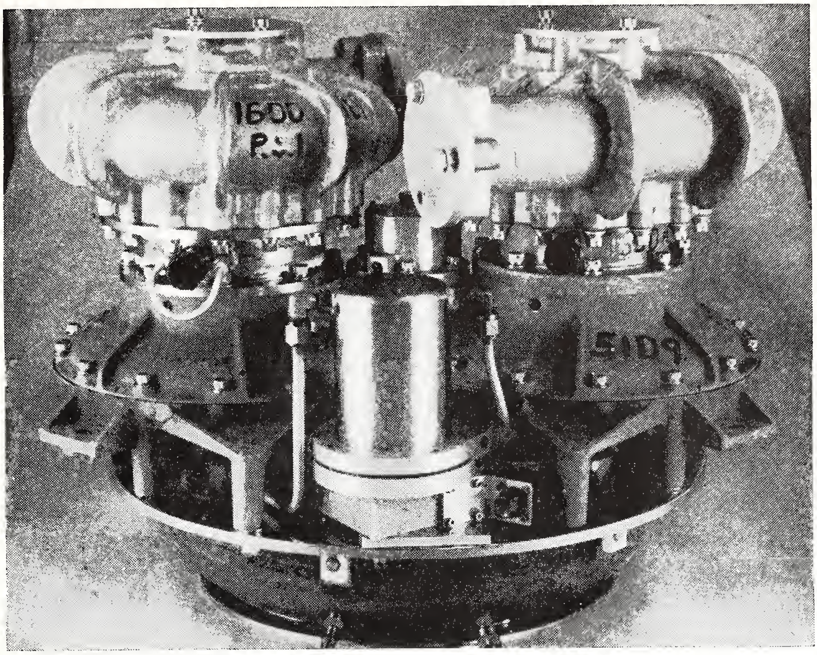

Fig. 3.7a Developmental turbopump assembly with geared turbine drive. (Courtesy General Electric Company.)

capabilities of the pumps, the turbine designers improved the efficiency of the turbine by removing the velocity of the working fluid in two stages. This design increased the weight and complexity of the turbine wheel and the turbine housing; however, compensatorily less working fluid is required.

Figure 3.7 is a more advanced turbopump configuration. In this assembly each pump and the turbine wheel are arranged to run at their optimum speeds by a system of gears. This geared system is more efficient than the direct-drive V-2 system.

C. The Gas Generator. The function of the gas generator is to generate gases by a chemical reaction of propellants and thus provide the working fluid for the turbine. The operating temperature of the turbine wheel is the limiting factor on the temperature of the gases provided by the gas generator, and if the bootstrap principle is used, this factor will define the mixture ratio at which the propellants consumed in the gas

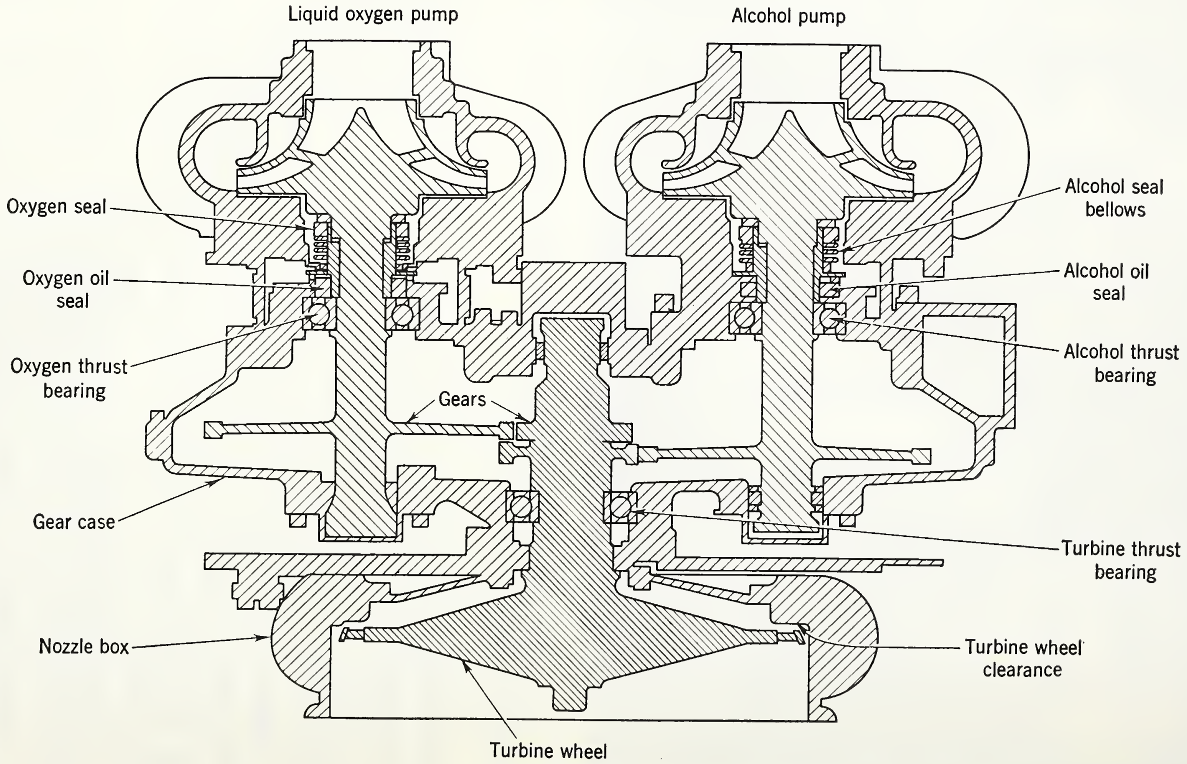
Liquid oxygen pump
Alcohol pump
Oxygen seal
Oxygen oil seal
Oxygen thrust bearing
Gears
Gear case
Nozzle box
Turbine wheel
Alcohol seal bellows
Alcohol oil seal
Alcohol thrust bearing
Turbine thrust bearing
Turbine wheel clearance

Fig. 3.7b Schematic of Fig. 3.7a.

generator are used (flame temperature is a function of propellant mixture ratio).

3.2.5 The Thrust Chamber

A. Dimensions. Having discussed the source of propellants, either pressure-fed or turbopump-fed, let us now examine the thrust chamber. The thrust chamber consists of four elements: (a) the nozzle where the enthalpy of the combustion products is converted into velocity, (b) the combustion chamber where the oxidizer and fuel are burned, (c) the injector which serves to inject and mix the oxidizer and the fuel so that combustion may take place, and (d) a cooling device. Figure 3.8 shows a system in which cooling is accomplished by circulating some coolant, perhaps water, in a spiral path between the inner and outer shell of the thrust chamber.

The parameters which control, to a great extent, the design of thrust chambers are (a) the propellant, (b) the thrust required, (c) the chamber pressure, (d) the trajectory, (e) the duration of burning, (f) the permissible drop in combustion chamber pressure.

If we know the trajectory which the vehicle is expected to

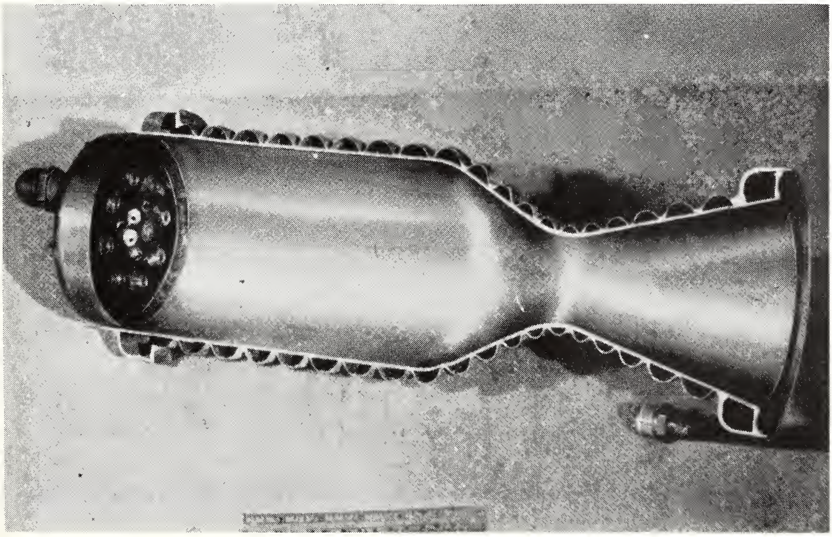

Fig. 3.8 Cutaway view of a small thrust chamber showing the helical cooling passages.

fly, we can select, after trial and error, an optimum expansion ratio for the nozzle. If we know the expansion ratio, that is, the ratio of the exit area to the throat area, we can determine the thrust coefficient of the nozzle. We can use this thrust coefficient, and the thrust and chamber pressure required, to determine the throat area of the nozzle. Elementary nozzle theory assumes that the flow velocity in the combustion chamber is zero. A zero velocity would be possible only if the ratio of the combustion chamber diameter and the throat diameter were infinite. This ratio is never infinite for a real rocket engine and, consequently, there is an approach velocity in the combustion chamber. The closer the ratio of the combustion chamber diameter and the throat diameter is to unity, the higher the velocity in the combustion chamber and the greater the pressure drop between the injector and the nozzle throat. The pressure drop appears as a loss of thrust or specific impulse. Thus, the permissible combustion chamber pressure drop in relation to the throat area determines the combustion chamber diameter.

A property of the propellant combination known as ''stay time'' is a parameter which must be determined experimentally. Stay time is the time required by a particular propellant combination to complete combustion after it has been injected. If the combustion chamber is constructed so that it ejects the products of combustion from the nozzle before complete combustion, the full specific impulse of the propellant will not be realized. If the products of combustion remain in the combustion chamber after the combustion process is complete, no further increase in specific impulse results. To correct the latter defect, we could make the thrust chamber smaller and possibly lighter without lowering thermodynamic performance. At any rate, by knowing the stay time of the particular propellant combination and the diameter of the combustion chamber, it is possible to derive the required length or volume of the combustion chamber.

B. Propellant Injectors. The function of the injector is to introduce and meter the propellant flow to the combustion chamber, and to atomize and mix the propellant into a correctly proportioned, homogeneous fuel-oxidizer mixture that can readily be vaporized and burned.

Figure 3.9 shows several injector configurations. The theory of injector design is not in an advanced state. Many different types of injectors have been tried, and the ones in Fig. 3.9 have all been used successfully for various applications to provide the maximum specific impulse with the minimum stay time.

The injector may also, in certain instances, be called upon to alleviate the cooling problem. Very frequently this is done by injecting an excess of fuel near the thrust chamber wall. In addition to the cooling obtained from the vaporization of this liquid, it is apparent that the local mixture ratio at which this propellant is burned will be much lower than normal, and thus the local flame temperature will be lower than normal. These relatively cool gases will form a curtain that partially insulates the chamber wall from the higher flame temperature near the center of the combustion chamber.

C. Cooling. In a regeneratively cooled engine, one or both components of the propellant system are forced, prior to entering the injector, to flow through channels in the thrust chamber walls and pick up heat released by the combustion process. Figure 3.8 is a cutaway of a thrust chamber showing

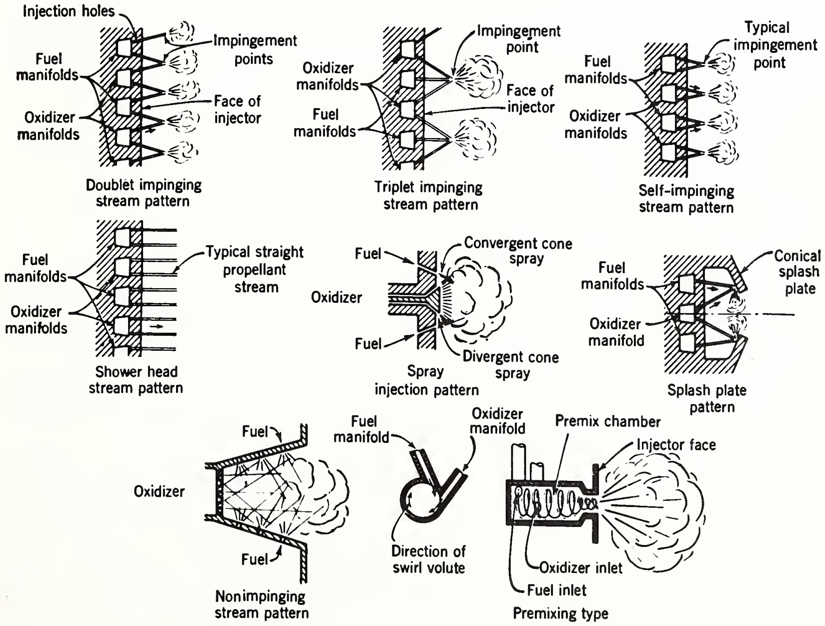
Injection holes
Fuel manifolds
Oxidizer manifolds
Impingement points
Face of injector
Doublet impinging stream pattern
Oxidizer manifolds
Fuel manifolds
Impingement point
Face of injector
Triplet impinging stream pattern
Fuel manifolds
Oxidizer manifolds
Typical impingement point
Self-impinging stream pattern
Fuel manifolds
Oxidizer manifolds
Typical straight propellant stream
Shower head stream pattern
Fuel
Oxidizer
Fuel
Convergent cone spray
Divergent cone spray
Spray injection pattern
Fuel manifolds
Oxidizer manifold
Conical splash plate
Splash plate pattern
Fuel
Oxidizer
Fuel
Nonimpinging stream pattern
Fuel manifold
Oxidizer manifold
Direction of swirl volute
Premix chamber
Injector face
Oxidizer inlet
Fuel inlet
Premixing type

Fig. 3.9 Schematic diagrams of several injector types.

the cooling passage—a single continuous channel which starts at the nozzle end, winds helically around the nozzle and combustion chamber, and ends at the head end of the rocket engine. Note that the cross section of the channel decreases as the nozzle throat area is approached. This increases the velocity of the coolant, thereby increasing the heat transfer rate in the critical throat region. At the head end of the motor the channel terminates in a ring which connects with the fuel inlet to the injector. The heat picked up in this way by the fuel during the cooling of the thrust chamber is returned to the system when the fuel is injected and burned.

As thrust chambers increase in size and propellant flow rates increase, it has become possible to utilize a series of longitudinal channels for cooling rather than a single helical channel. Most large modern thrust chambers are now cooled by the coolant flowing axially in a great many flow channels.

Sometimes it is not feasible to adequately cool a given thrust chamber by regenerative means alone. To aid in the cooling, fuel or oxidizer may be injected near the hot spot in order to provide a protective film of coolant over the hot spot. This technique was successfully used by the Germans in the V-2 combustion chamber where raw fuel was injected at appropriate points along the chamber wall to supplement regenerative cooling.

3.2.6 Thrust Vector Control

Finally we shall discuss that portion of the rocket engine system which may act or be acted upon to produce and apply control forces to the vehicle.

One means of altering the direction of the application of thrust from a thrust chamber is to mount the thrust chamber in a gimbal and through rotatable joints deliver propellants to the thrust chamber (Fig. 3.10). In this figure propellant is transferred through the gimbal housing to the thrust chamber.

In another system (Fig. 3.11) a universal or pin joint at the head end of the thrust chamber replaces the gimbal system. Flexible hoses are used to feed propellant to this thrust chamber. Both rotating seals and flexible hoses can be major problems when one of the propellants is a cryogenic fluid such as liquid oxygen, a corrosive fluid such as nitric acid or hydrogen peroxide, or perhaps even gasoline at a supply pressure of 500-1000 psi.

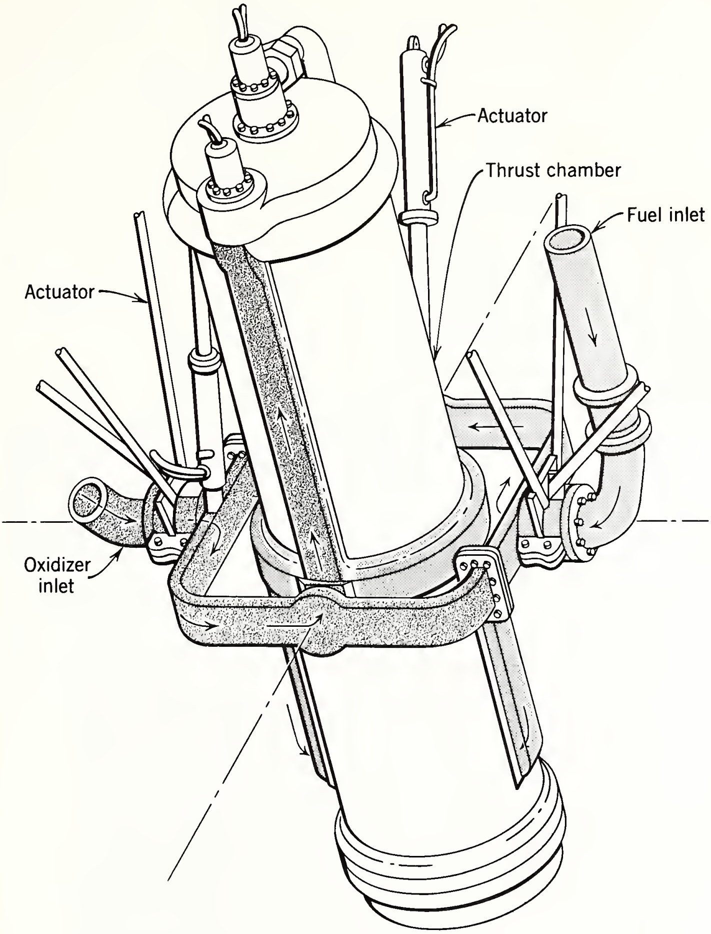

Fig. 3.10 Schematic diagram of a gimbal-mounted thrust chamber.

Figure 3.12 shows flow in a two-dimensional nozzle which is being operated at a back pressure much higher than optimum for the exit area to throat area ratio ($P_e < P_a$). Note that the flow has separated from the nozzle wall, well upstream from the nozzle exit. The flow velocity in the separated region is substantially zero. If a portion of a jet vane were located in the separated region, no usable control force would be obtained from that portion. As the vehicle rises in altitude and the back pressure becomes less and finally equals the nozzle exit pressure ($P_e = P_a$), the flow

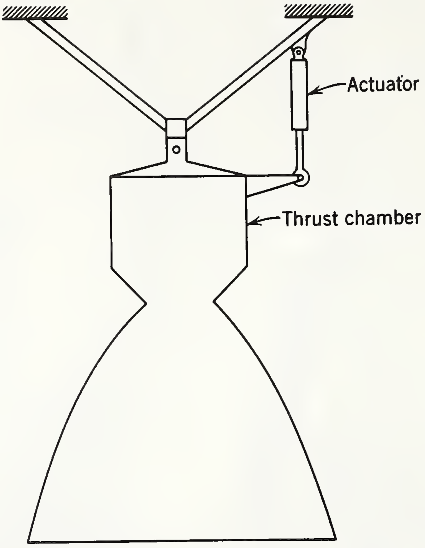
Actuator
Thrust chamber

Fig. 3.11 Schematic diagram of a "universal joint"—or "pin joint"—mounted thrust chamber.

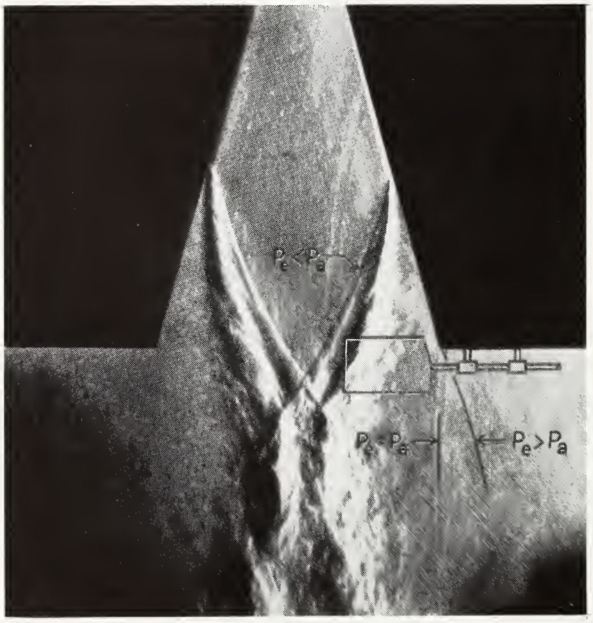
$P_e<P_a$
$P_e<P_a$
$P_e>P_a$

Fig. 3.12 Wind tunnel picture showing the separation of flow in the nozzle at high back pressure.

will not be separated and the jet boundary will be essentially cylindrical. At this time a controlled deflection of the vane will produce a control force. At any altitude in between, the amount of control force obtained from a movement of the vane will be a function of the back pressure existing at that altitude. With jet vanes the control force for a unit deflection is usually a function of altitude and increases with increasing altitude.

Figure 3.13 shows the jet vane installation used in the German V-2. Jet vanes are submerged in the jet of the thrust chamber, whether or not they are applying a control force. This imposes an unnecessary drag on the vehicle. In an ef-

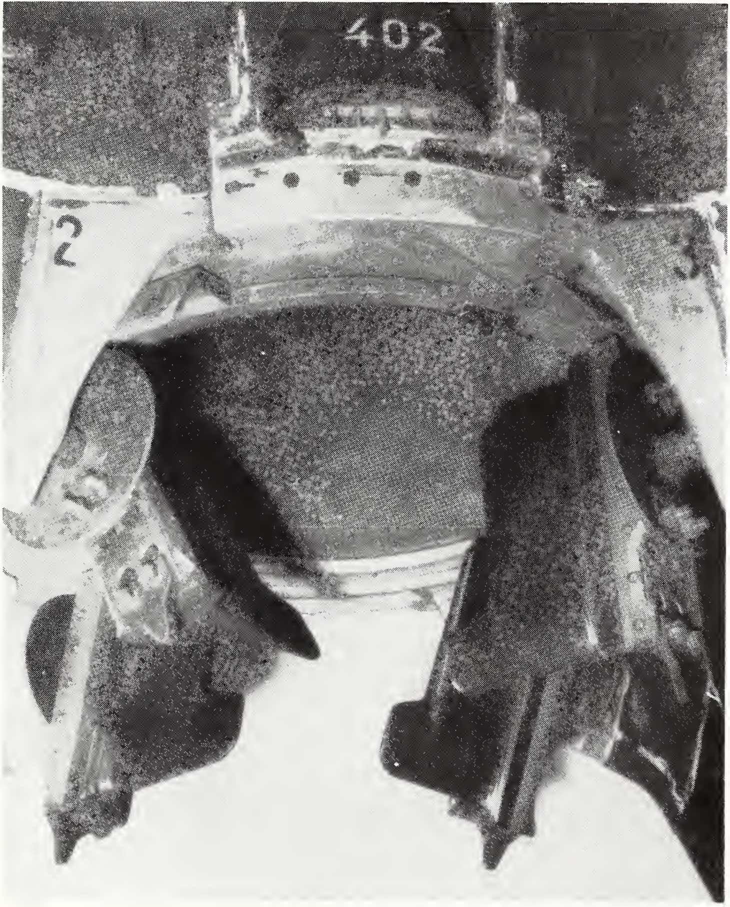

Fig. 3.13 Jet vane installation on V-2 rocket.

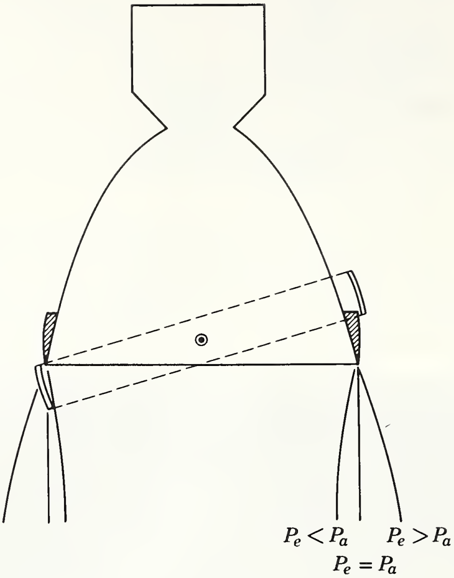

Fig. 3.14 Jetavator.

fort to provide a control device which would be submerged in the jet only during the time it was required to produce a control force, a device known as a jetavator has been proposed (Fig. 3.14). A jetavator is merely a ring surrounding the exit of the nozzle. This ring is mounted so that it can be deflected into the jet as needed. Notice that the control force available from a jetavator is also a function of the back pressure on the nozzle.

4

SOLID ENGINES AND THEIR DESIGN PARAMETERS

C. E. Bartley

4.1 INTRODUCTION

It is generally believed that solid propellant rockets were first invented by the Chinese and utilized in fireworks displays several centuries B.C. However, there is evidence[1] that rockets may have originated in India and been used in warfare as early as 2000 B.C. In the thirteenth and fourteenth centuries, rockets propelled by gunpowder were employed for signaling and illumination by European armies. Sir William Congreve developed artillery rockets which were utilized with devastating effect by the British armies in the siege of Copenhagen in 1807. During World War II intensive programs to develop artillery rockets were undertaken by most of the belligerents. Applications to long-range missiles, guided missiles, and boosting—such as the assisted take-off of aircraft—have grown with the continuing improvements in the art of rocketry.

Since 1950 in particular, the United States has increasingly focused attention on the development of solid propellants. Published lists of operational military missiles (Table 4.1) show that propulsion with solid propellants is favored by a wide margin over that with liquid propellants. This trend has been extended to even the largest missiles.

The solid propellant type of rocket has several advantages over the liquid propellant. The chief advantage is that it is

TABLE 4.1
Published Operational Missiles in U.S. and Type of Propulsion Used

U.S. Army		U.S. Navy		U.S. Air Force	
Missile[1]	Propulsion[2]	Missile	Propulsion	Missile	Propulsion
Nike-Ajax (Hercules)	S/L	Bullpup	S	Mighty-Mouse	S
Nike-Hercules	S	Polaris	S	Falcon	S
Hawk	S	Diamondback	S	Bomarc	S/A
Dart	S	Sidewinder	S	Rascal	L
La Crosse	S	Zuni	S	Matador	S/A
Little John	S	Sparrow	S	Snark	S/A
Honest John	S	Terrier	S	Thor (Polaris)	L
Corporal (Sergeant)	L	Tartar	S	Atlas (Minuteman)	L
Redstone	L	Regulus	S/A	Titan (Minuteman)	L
Jupiter (Polaris)	L	Talos	S/A		

[1] Name in parentheses shows advanced possible solid-propelled missile for liquid propelled missile shown.

[2] S = solid propellant, L = liquid propellant, A = air-breathing engine. Combinations will show both as S/L, etc.

easier to use. After preparation at the point of manufacture, the solid rocket is easily transported and may usually be fired with simple electrical circuits. Usually, elaborate field-servicing equipment is not needed. Because of the simplicity of design, the solid propellant rocket is cheaper for most one-shot uses. For many applications the solid propellant rocket is superior in total impulse to total weight ratio, primarily because of the greater energy available per unit volume (Table 4.2), thereby requiring less dead-weight structure to carry the propellant. However, many factors must be considered in detail design in order to select the proper propulsion system.[2]

The major advances in solid propellant rockets during World War II were the development of new propellants which were more suitable for rocket propulsion than gun propellants or black powder; the discovery and quantitative analysis of special characteristics of these propellants which strongly affect rocket design and performance; the invention of propellant materials with mechanical properties capable of withstanding pressure and acceleration forces without failure; the discovery of suitable techniques to limit burning to certain surfaces of the propellant charge; and the invention of propellants which could be made into almost unlimited sizes, thus paving the way for their use in long-range missiles and space vehicles.

TABLE 4.2

Comparison of Some Liquid and Solid Propellants at 300 psi, Optimum Expansion at Sea Level

Propellant	Aniline RFNA	Ethyl Alcohol Lox	Typical Solid Propellant
Specific impulse (sec)	220	244	220
Density, lb/ft^3	86.5	65.5	108
Impulse/unit volume, (lb)(sec)/ft^3	19,000	16,000	23,800

The theory and semitheoretical correlation of factors important for both exterior and interior ballistics have proceeded quite rapidly, and the fundamental understanding of rocket behavior and of the dependence of behavior on various parameters is quite good. Rocketry has changed from an art to a science, although much still remains to be understood.

4.2 OPERATION OF THE SOLID PROPELLANT ROCKET MOTOR

Before discussing solid propellant rockets further, it is desirable to describe their manner of operation and to outline the qualitative relationships which govern rocket performance.

The rocket unit consists of a charge of solid propellant within a combustion chamber and an exhaust nozzle through which the products of combustion escape (Fig. 4.1). The reaction caused by expulsion of the combustion products is the thrust of the rocket. The propellants used in rockets, just as those used in guns, do not explode but burn at a definite rate on the surfaces that are exposed to the hot gases or flame within the combustion chamber. The rate at which the surface of a propellant recedes in a direction normal to itself during burning is designated as the rate of burning and is usually expressed in inches per second. The burning rate depends on the chamber pressure and is usually expressed as

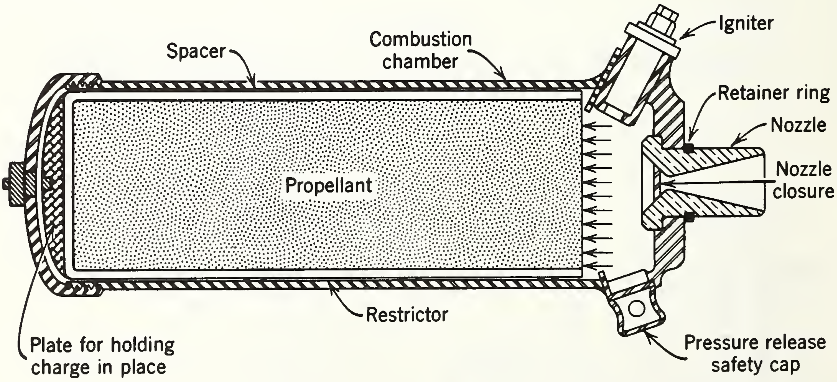

Fig. 4.1 Rocket motor assembly featuring supports for an end-burning charge (not sealed to combustion chamber), fixed nozzle end igniter, separable copper nozzle, and safety release cap.

$$r = ap^n \tag{4.1}$$

where r is the burning rate, p is the pressure, and a and n are characteristic of the particular propellant (a is a function of temperature and n is a fractional exponent usually less than one-half). The burning rates usually lie between 0.1 and 1.0 in./sec at 1000 psi at 70° F. The thrust of a rocket motor may be considered as equal to the product of exhaust velocity and mass flow; therefore, in order to obtain a high thrust from a given propellant, not only a high burning rate but also a large burning surface must be used to obtain the required mass flow. Since a combustion chamber of a given size and construction will withstand a limited pressure and contain only a certain volume of propellant, the thrust may be made large for a short time by providing a large burning surface, or small for a long time by providing a small burning surface. In order to further clarify these ideas, we now describe some types of solid propellant rockets.

Broadly speaking, solid propellant charges are commonly designated as restricted-burning or unrestricted-burning. A restricted-burning charge has the major portion of its surface coated so that this area will not burn, whereas the unrestricted charge has only a minor portion of its surface protected against burning.

In one type of a restricted-burning rocket, the propellant charge is made in the form of a solid right-circular cylinder. The cylindrical surface and one end face are restricted from burning. Consequently, burning is allowed to proceed from one end only. This type of rocket is sometimes called end-burning or cigarette-burning. The duration of thrust obtained from this restricted-burning rocket is proportional to the length of the charge and depends on the chamber pressure and the type of propellant used. The thrust obtained is proportional to the area of the circular burning surface and depends on the chamber pressure, the type of propellant, and the design of the rocket unit.

In one type of an unrestricted-burning rocket, the propellant charge is often in the form of a hollow right-circular cylinder. This charge, held in place by a suitable grid or trap, is unprotected except for the few support points required to mount it. The charge is ignited and allowed to burn on all surfaces without restriction. The thrust from such a unit is proportional to the burning surface and depends on the chamber pressure, the type of propellant used, and the design of the rocket unit and the powder charge. The duration is proportional to the thickness of the cylindrical wall (web thickness) and depends on the chamber pressure, the type of propellant, and the internal geometry of the combustion chamber and the powder charge. It should be noted that in this unrestricted-burning rocket the combustion gas must flow lengthwise through the unit, parallel to the burning surface of the powder charge.

The chamber pressure generated by either type of rocket unit is a function of the ratio of the burning surface area to the cross-sectional area of the exhaust nozzle throat. For the restricted- or unrestricted-burning rocket, where the gas flows parallel to the surface, the chamber pressure also depends to a marked degree on the geometry of the propellant charge and the internal geometry of the combustion chamber.

The types of solid propellant rockets described do not include all types by any means; these are simply two extremes of charge design. Figure 4.2 shows a variety of charge arrangements that have been used in rockets and their typical thrust-time characteristics.

Generally, unrestricted-burning rockets are used where application of thrust is required for periods ranging from 0.05 to 10 sec, and restricted-burning rockets are used where application of thrust is required for periods ranging from 1 to more than 100 sec.

4.3 PROPELLANTS AND THEIR CHARACTERISTICS

The solid propellant rocket is remarkably simple in its essential features. However, the development of a practical rocket motor that is reliable, convenient to use, and moderately easy to manufacture has been a long and complex process. Because of the importance of these practical considerations, discussion of solid propellant rockets must necessarily refer to the state of the art.

Table 4.3 lists some typical propellants and their manufacturing methods, with the ranges encountered for some of the most important propellant characteristics. Two types of

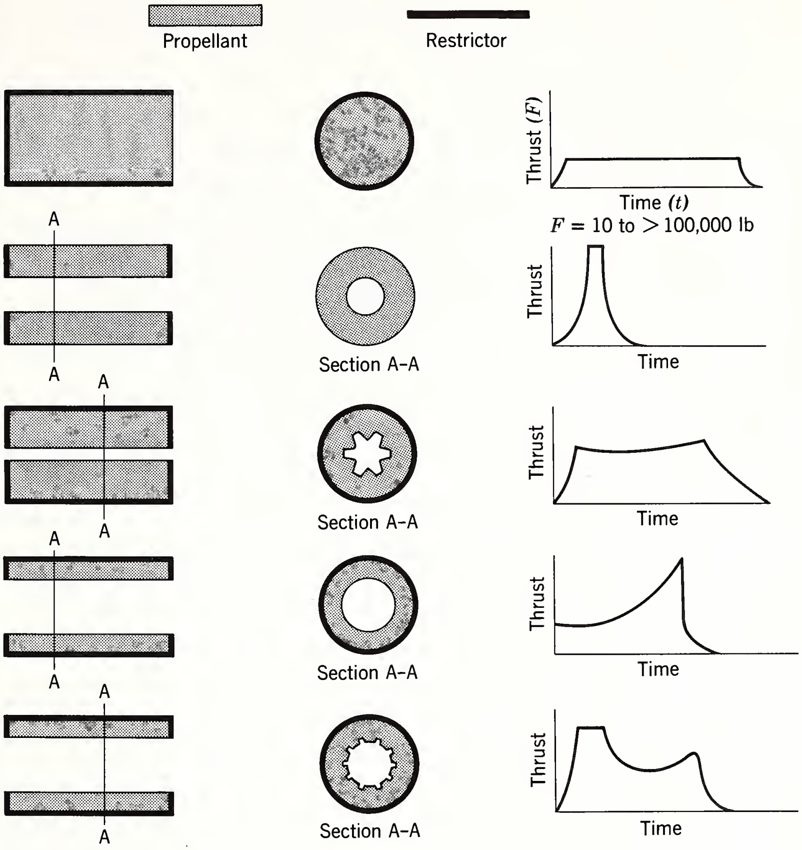
Propellant
Restrictor
Thrust (F)
Time (t)
F = 10 to > 100,000 lb
A
A
Section A-A
Thrust
Time
A
A
Section A-A
Thrust
Time
A
A
Section A-A
Thrust
Time
A
A
Section A-A
Thrust
Time

Fig. 4.2 The geometry of some solid propellant charges and their typical thrust time characteristics. Thrust may range from 1.0 lb to greater than 100,000 lb, and time from 0.05 sec to greater than 100 sec.

propellants are generally used: double-base and composite. The double-base propellants are so named because they are comprised of two primary compounds, nitroglycerin and nitrocellulose, each a self-sufficient combustible. The composite propellants include a granular oxidizer, such as ammonium perchlorate or ammonium nitrate, which is mixed into an organic fuel such as asphalt, synthetic rubber, or plastics. The wide range of burning rates and geometric possibilities affords great flexibility in design. Castable compositions allow fabrication of such large charges that thrusts

TABLE 4.3

Properties Found in Some Average Solid Propellants

System	Double-Base	Composite	
		No. 1	No. 2
Typical Ingredients[1]	N. G. 35 N. C. 55 Misc. 10	A. P. 75 $(CH_2)_x$ 20 Misc. 5	A. N. 85 $(CH_2)_x$ 10 Misc. 5
Mfg. methods	← Mold, Extrude, Cast →		
Flame temp., °F, example	← 4000 →		2500
Specific heat ratio	← 1.25 →		1.25
Average molecular wt.	← 25 →		21
Characteristic velocity, ft/sec	← 4500 →		4000
Specific wt, lb/in.^{3}	0.056	0.062	0.056
Mechanical properties	Hard, tough	← Soft, Pliable to Hard, Tough →	
Burning rate, in./sec at 1000 psi 70 °F	0.35	0.50	0.10
Burning rate exponent, n $(r = ap^n)$	← 0.1 to 0.8 →		

[1] N.G. = Nitroglycerine, N.C. = Nitrocellulose, A.P. = Ammonium perchlorate, A.N. = Ammonium nitrate.

and burning times up to and greater than 100,000 lb and 100 sec are realistic. No single propellant has all the ideal characteristics for any specific application; therefore, it is necessary to select the best combination of propellant characteristics for the proposed application. Ammonium nitrate composite propellants are suitable when low-cost, smokeless, noncorrosive properties are desirable but high-energy and high-density properties are not necessary. Double-base propellants are useful when smokeless, high-energy, noncorrosive properties are desirable but high-temperature storage is not a requirement. Ammonium perchlorate composite propellants are useful when high energy and high-temperature storage are required but smoke and corrosion can be tolerated.

Since the energy per unit mass that can be obtained from chemical fuels is limited, many features of rocket performance other than specific impulse receive considerable attention in order to achieve the desired results. For example, to preserve wall strength, the rocket motor may be designed so that the charge burns internally to shield the combustion chamber wall from the hot gases. Other important characteristics which must be taken into design consideration may be designated by the following terms.

Temperature sensitivity. This may also be called the variation of performance with propellant temperature. Temperature sensitivity is usually expressed as change in pressure with temperature under constant design conditions and may range from approximately zero to $\frac{1}{2}$ per cent/° F, depending on the pressure range.

Temperature limits. A rocket unit will malfunction if its temperature, before firing, does not lie between certain limits. The temperature limits are defined by propellant properties, size, design, and intended use. Some units have been qualified for both arctic and equatorial use; others have to be temperature-conditioned to perform satisfactorily.

Combustion limit. Some propellants do not burn satisfactorily at low pressures.

Resonance. Abnormal pressure peaks and oscillations occur in solid rocket units when critical combinations of propellant characteristics, size, and geometry are present. These oscillations impart vibrations which can destroy instrumentation or actually tear a missile apart. Resonance can usually be avoided by careful selection of propellant and design parameters.

Erosive burning. In almost all high-performance rocket motors it is necessary to shield the structural parts from the hot gases with the propellant by utilizing a radial-burning charge. This results in gases flowing at high speed parallel to the burning surface. The flow of the gas over the propellant surface influences the basic burning rate of the propellant, sometimes significantly, so the simple law $r = ap^n$ does not entirely apply. The relationship

$$r = ap^n (1 + k \rho_g V_g) \tag{4.2}$$

has been developed for composite propellants, where

k is an empirical constant called the "mass erosive burning" constant

ρ_g is the gas density
V_g is the velocity of the gas parallel to the burning surface.

When the factor $1 + k\rho_g V_g$ is significant, the equilibrium pressure of operation is markedly influenced and in particular cases the stability of operation may also be affected.

These characteristics may be interrelated and arise from various, and sometimes the same, fundamental causes.

4.4 THE EFFECT OF APPLICATION ON ROCKET DESIGN

The fundamental purpose of a rocket unit is to supply a required amount of impulse (force times duration or mass times velocity) to a vehicle. Rockets are seldom employed to do work (move a force through a distance). Usually they are used to accelerate a mass to some velocity. If the rocket is to be used efficiently, the final velocity should be moderately high (an appreciable fraction of the exhaust velocity of the rocket). In many cases, however, convenience rather than efficiency dictates the design of a rocket for a particular application.

Rockets are being used to assist the take-off of aircraft, to provide initial boosts to missiles, and to supply the main propulsive force for missiles. Through modification of rocket design the high-pressure gas resulting from combustion is now sometimes used to operate pneumatic devices. Such gas generation is, of course, at complete variance with the missile applications just mentioned; but gas generation has grown as a by-product of rocket development as the reliability of rocket devices has increased.

When rockets are employed as the dominant means of propelling a missile, its accuracy may be affected by such additional characteristics as burning time, proper alignment of the exhaust jet, and possible distortion of the rocket unit by pressure and temperature.

Performance requirements for rockets vary from those for a missile propelled by a very small motor, with a maximum velocity of 150 ft/sec, to those for a high-velocity missile consisting chiefly of a rocket motor, with a maximum velocity of more than 5000 ft/sec. Aerodynamic drag is relatively unimportant for low-speed missiles, but it becomes an important factor for high-velocity missiles. Rockets that are to be externally mounted on aircraft should also have minimum drag. Small frontal area, short burning time, and large impulse requirements lead to a long, slim missile with a large burning area for the charge. The large burning area and the small diameter require high-velocity internal gas flow. This internal gas flow sometimes makes stable combustion difficult to achieve and leads to heating of the motor tube, distortion of the charge by pressure forces, and erosion of internal fittings. It may also lead to failure of inhibitor strips placed upon the propellant charge to limit the burning surface area. For short-burning, high-performance missiles, the requirements of external and internal ballistics are usually opposite and create optimization problems.

An interesting optimization example is the common requirement to determine the maximum velocity possible with a given payload for a missile of a given diameter. The horizontal drag-free velocity equation for the rocket in such a case is

$$v_b = I_{sp}\, g \ln\left(1 + \frac{W_p}{W_e}\right) \tag{4.3}$$

where v_b = burned velocity
I_{sp} = specific impulse
g = gravitational constant
W_p = propellant weight
W_e = empty weight after the propellant is burned.

The optimization of v_b for a given propellant and pressure may be obtained by maximizing W_p/W_e. W_p/W_e can be expressed as a function of the length-to-diameter ratio (l/d) of the combustion chamber and maximized with respect to l/d; that is, the l/d value which will yield maximum W_p/W_e can be selected. As the pressure changes, the optimum l/d and maximum velocity attainable change, as illustrated by Fig. 4.3. It is seen that a definite optimum pressure does exist to give maximum velocity, depending on payload, type of propellant, and the ratio A_t/A_d where A_t is the cross-sectional area of the exhaust nozzle throat and A_d is the initial cross-sectional area of the gas duct (often called the port area) through the propellant. Optimization of specific problems such as the one cited illustrates how critical it is to integrate the solid propellant rocket motor into the entire missile system.

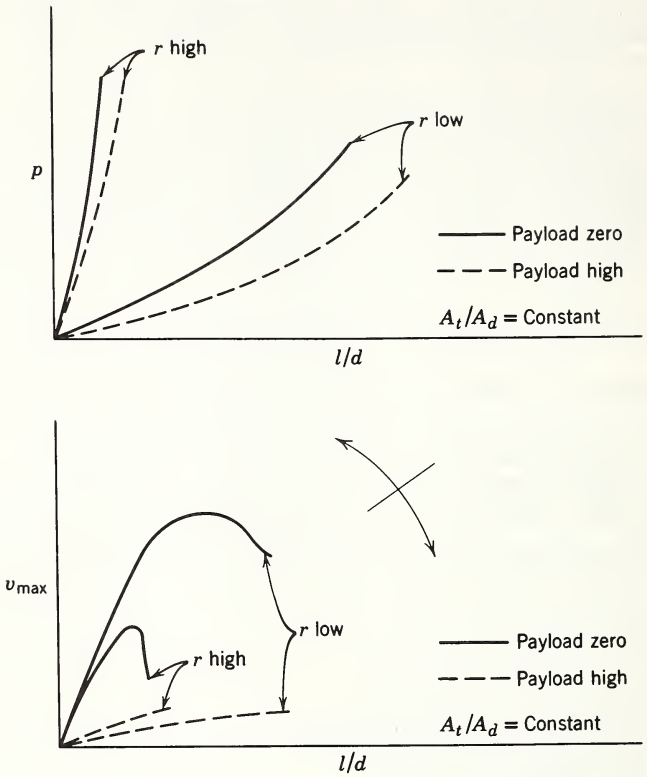

Fig. 4.3 Optimization curves showing pressure and maximum horizontal drag-free velocity versus length-to-diameter ratio for solid propellant rockets.

4.5 TRENDS IN SOLID PROPELLANT ROCKET DEVELOPMENT

Efforts in solid propellant rocket development are directed toward achieving flexibility in design, high performance, reliability, and low cost. In summary, the factors which at present are helping most to approach these ideals are:

1. Internal-burning charge design. (Combustion chamber case insulated from hot gases.)
2. Casting processes. (Large and small charges made with nearly equal ease.)
3. High-energy, high-density propellants. (High energy per unit volume and per unit weight results in decreased

over-all motor weight and, usually, decreased cost.)

4. Motor construction materials of high strength and low weight. (Improved fabrication techniques.)
5. High-strength, low-conductivity, heat-resistant materials. (Allows low weight for parts exposed to combustion gases, such as the exhaust nozzle.)
6. "Gasless" igniters. (Negligible ignition pressure peak, provides increased reliability.)

Design flexibility depends to a great extent on the ability to obtain a wide range of burning rates and still retain smokeless, noncorrosive exhaust gases; however, much research must be done in order to combine these desirable characteristics. The most important fundamental problem is the understanding and control of the burning rate.

The cost of solid propellants has been high because of the safety requirements necessary in their manufacturing processes and the high basic material cost. The trend is to attempt to use less expensive materials for some applications, even though relatively low performance results, and much progress has been made in this direction. Streamlining of manufacture is being perfected, with improvement in both safety and cost factors. The construction of the motor of a solid propellant rocket is so simple that the over-all cost of the complete rocket unit may be less than that for a comparable liquid propellant rocket which uses much less expensive propellant materials. Furthermore, the simplicity of operation makes the solid propellant rocket motor reliable, and, therefore, particularly desirable for field use. In addition to rocket propulsion, the gas generation capabilities of solid propellants indicate that they may be used for many novel applications in the future.

REFERENCES

1. J. Chem. Educ., 25 (1948).
2. John I. Shafer, Space Technology, John Wiley and Sons, New York, 1959.

5

NUCLEAR ROCKET PROPULSION

R. D. DeLauer

5.1 INTRODUCTION TO NUCLEAR ENERGY

The fission process has provided mankind with an almost weightless source of energy. Years of development since 1945 on the control of this energy have successfully substituted nuclear fuel for diesel oil or coal in the boilers of naval vessels (Nucleonics, July 1957) and ground-based power plants. Much progress has also been made toward nuclear-powered aircraft, and it now appears that nuclear energy will inevitably displace fossil fuel in nearly every form of heat engine.

There are two major reasons why the adaptation of nuclear energy to rocket propulsion is particularly appealing. First is the fact that the amount of energy which can be absorbed by a pound of working fluid passing through a rocket reactor, and subsequently extracted in the rocket nozzle expansion process, is limited only by the temperature and design limitations of the reactor employed, rather than by the energy content endowed by nature to combustible fuels, as used in chemical rockets. The second reason is simply that the rocket vehicle working fluid can be chosen independently of energy content considerations, thus giving predominant importance to such factors as coolant molecular weight, liquid density, ease of handling, etc.

Consider a rocket vehicle as shown schematically in Fig. 5.1. Here propellant (reactor coolant) is pumped to the reactor from the tank by a turbopump driven by reactor bleed gas. The reactor vaporizes and heats the propellant gas and exhausts it through a convergent-divergent nozzle. The vehicle itself is propelled by the net pressure force exerted on the rocket motor and nozzle structure by the exhausting propellant. The complete system of vehicle plus propellant gas follows the principle of conservation of momentum, which reduces in this case to Newton's third law of motion. Applying

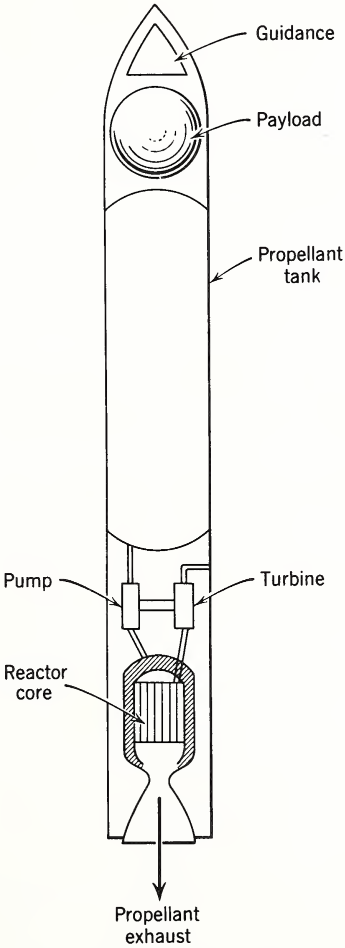
Guidance
Payload
Propellant tank
Pump
Turbine
Reactor core
Propellant exhaust

Fig. 5.1 Schematic nuclear rocket.

this principle to any rocket vehicle, we obtain the simple "mass ratio" equation

$$(m_0/m_b) = \exp\,(\Delta v_c/g_c I_{sp}) \tag{5.1}$$

where m_0 and m_b are "full" and "burnt" vehicle weight,
Δv_c is the vehicle velocity reached at "burnout" of the rocket (if moving in free space)
I_{sp} is the specific impulse of the propellant gas.

It is evident that for a fixed burnout velocity (thus also range) the vehicle weight and size will decrease with increasing I_{sp}. The specific impulse, however, is proportional to

$$I_{sp}\,\alpha\,\sqrt{T_e/M} \tag{5.2}$$

where T_e is the peak gas temperature (at reactor core exit)
M is the mean molecular weight of the exhaust gases

Evidently operation at high temperature with low molecular weight gases is most beneficial.

Both chemical and nuclear heat exchanger rockets are limited by the limiting temperatures of structural materials. In addition, chemical rockets are limited by the combustion temperatures which can be achieved with useful chemical fuel-oxidizer combinations. This latter temperature is about 6000°R, which also represents the approximate upper limit of operation of high-temperature refractory materials, so to a first approximation we can consider the gas operating temperature the same in both chemical and nuclear rocket systems. However, the nature of the combustion process restricts the chemical rocket to propellants with gaseous molecular weights of the order of 20, whereas the nuclear system can use hydrogen as its working fluid, with a molecular weight of 2, thus gaining a factor of $\sqrt{10}$ in specific impulse over conventional chemical rockets. The effect on gross vehicle weight is more profound than this, since I_{sp} enters exponentially into the mass ratio equation. Figure 5.2 illustrates this point, showing the relation between vehicle mass ratio and propellant specific impulse for an arbitrary vehicle "characteristic" velocity change of $\Delta v_c = 32{,}000$ ft/sec, typical of that required for intercontinental missile flights. Note how rapidly the mass ratio decreases with increasing specific impulse and the consequent potential margin of superiority of nuclear over chemical rockets.

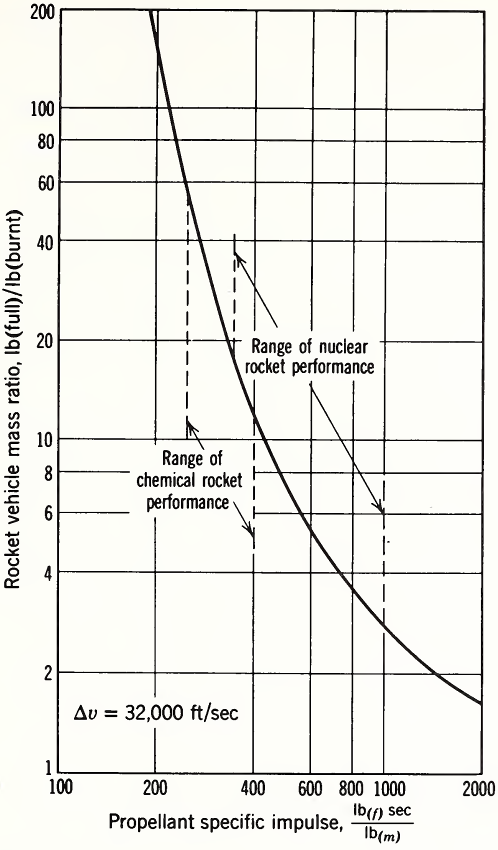

Fig. 5.2 Influence of specific impulse on vehicle gross weight.

5.2 MATERIALS

Propellants for nuclear rockets should be chosen from compounds or elements with low molecular weights at gaseous conditions. The obvious choice is thus from among the elements hydrogen, helium, lithium, and beryllium and their dissociable compounds such as the various hydrocarbons and hydrides. The easily dissociated compounds of nitrogen and hydrogen are also of interest, as are the alcohols. Practical consideration of material melting points rules out lithium and beryllium, and the difficult cryogenic problems associated with liquid helium make it appear unattractive. The list of potentially useful materials thus reduces to a single element, hydrogen, and its compounds. The physical properties of four of these propellants are shown in Table 5.1 together with their decomposed molecular weights at 5000°R gas temperature. The most difficult handling problem of the four propellants shown is that associated with use of liquid hydrogen which requires cryogenic handling facilities of high quality to minimize boil-off losses. Ammonia and ethyl alcohol are both powerful drying agents, having a great affinity for water, and can ''burn'' skin by local dehydration. They thus present a handling hazard. The most easily handled is octane, provided one avoids open flames in mixtures of octane vapor and air.

High performance also results from operation at high gas temperature. To achieve nuclear core temperatures comparable to those resulting from chemical combustion, the reactor fuel elements must be capable of operation close to the highest melting points of known materials. In addition, as discussed later, the core must operate at an extremely high power density in order to produce a motor thrust-to-weight ratio great enough to fly a large missile. The fuel element base material must thus have high strength at high temperature, high thermal conductivity, to reduce temperature gradients, and should

TABLE 5.1
Properties of Some Liquid Propellants

Propellant	Hydrogen	Ammonia	Ethyl Alcohol	Octane
Chemical formula	H_2	NH_3	C_2H_5OH	C_8H_{18}
Liquid molecular weight, lb/mole	2.016	17.03	46.07	114.23
Decomposed molecular weight, lb/mole	2.0	8.5	9.5	6.0
Melting point, °F	−434.5	−108	−180	−70
Boiling point, °F	−423	− 28	174	258
Heat of vaporization, Btu/lb	197	589	367	128
Critical pressure, atm	12.8	111.5	63.1	24.6
Liquid density, lb/ft^3	4.3 at −424°F	43 at − 30°F	55 at 60°F	47 at 60°F

be a poor absorber of neutrons but a good neutron moderator since it may occupy a large fraction of the core volume. It must also be proof against chemical attack by hot propellant gases. Of course, a base material with all these desirable properties must also be able to contain fissionable fuel without losing them, or it is of no value in rocket reactor construction.

Radiation damage problems are less severe in rocket reactors than in conventional power reactors because:
(a) rocket motor operating times are so short (order of minutes) that the total megawatt-hour output is small compared to that expected from long-lived ground power plants; and
(b) rocket motor operating temperatures are high enough to assure "annealing-out" of some effects (e.g., distortion of crystal lattice structures) that plague other reactors.

The choice of materials for operation at high temperature is extremely limited. Of the elements only carbon (graphite), tungsten, rhenium, tantalum, molybdenum, and niobium have sufficiently high melting temperatures to permit their consideration. The only compounds of potential practical value appear to be the carbides of these refractory metals, and of zirconium. Available information on the high-temperature physical characteristics of these materials is given in Table 5.2; however, little is known of the effects of adding fissionable fuel to the base material. In the absence of such information the designer must pick and choose on the ground of known base material characteristics, and must set up comprehensive experimental programs to study the effects of fuel loading on the material of interest. These can be profound, as shown by the uranium-tungsten system. Tungsten alone has a melting point of 6540°F, but the addition of more than about one atomic per cent uranium metal produces a tungsten-uranium mixture with a melting point of about 2530°R, far too low to be of value for rocket motor use.

For core-moderated thermal reactors the thermal neutron cross sections and the resonance absorption integral of the fuel element base material are of interest in comparing different materials for use. The former indicates the degree of competition for thermal neutrons offered by the fuel carrier as compared with the fuel itself, and the latter parameter is a measure of neutron absorption in the "slowing-down" or epithermal energy region. Values of these parameters are

TABLE 5.2

Properties of Some Fuel Element Base Materials

Material		Graphite (C)	Tungsten (W)	Rhenium (Re)	Tantalum (Ta)	Niobium Carbide (NbC)	Zirconium Carbide (ZrC)
Melting Point, °R		7000 (sublimes)	6550	6200	5850	7500	6250
Room temperature density, lb/ft^3		103	1190	1280	1040	490	425
Tensile strength at 5000°R, lb/in.^{2}		3000–6000	5000–9000	4000–6000	1000–5000	—	16,000[a]
Conductivity at 5000°R, Btu/(hr)(ft)(°F)		10–20	50	—	40	8.2[b]	12[b]
Atomic or molecular weight, lb/mole		12.0	183.9	186.3	180.9	104.9	103.2
Thermal neutron absorption cross section	Microscopic, barns/atom	0.0045	19.1	84	21	1.1	0.185
	Macroscopic, 1/cm	0.00037	1.19	0.56	1.16	0.049	0.0073
Resonance absorption integral, barns/atom		0	450	650	500	4	3

[a] At 2700°R [b] At 500°F

given in Table 5.2. Note that the macroscopic absorption cross section of tungsten is about 3000 times that for graphite. The resonance absorption integral of tungsten is also high, making it, as well as rhenium and tantalum, undesirable, neutron-wise, for use in regions of neutron slowing down. Maximum efficiency in the use of these materials as fuel carriers requires lumping of structure in a moderator matrix so that fast neutrons can be thermalized without "seeing" the high epithermal resonance absorption cross sections which are characteristic of these materials.

Because of the low atomic weight of C, any carbon-bearing material, such as the carbides listed, is potentially a moderator. Graphite, traditionally proposed for use in nuclear rocket reactors,[1,2] is unique among high-temperature materials in that it can be used both as a fuel element base material and as a neutron moderator. If the reactor core is sufficiently large, say 4 or 5 ft in diameter, graphite fuel elements can be used to achieve thermal cores that are nearly self-moderating. Smaller cores may require appreciable external moderation, by use of thermalizing neutron reflectors, to achieve criticality without excessively high fuel loadings. Requirements on uniformity or flatness of fission density distribution, dictated by considerations of propellant flow and over-all reactor performance which are discussed later, also necessitate the use of moderating reflectors around either type (matrix or homogeneous) of core assembly. On the bases of weight, volume, and high-temperature capabilities, beryllium metal, beryllium oxide, and graphite appear to be preferred materials for use as rocket reactor reflector moderators.

All propellant gases of interest contain hydrogen, which is why they are interesting as propellants. Unfortunately, high-temperature hydrogen is a very active material, embrittles some metals, forms hydrides with others, reduces some oxides, and reacts with carbon to form volatile hydrocarbons. A successful fuel element material must be able to withstand the attack of hot hydrogen without structural damage or significant loss of fissionable fuel. This can be accomplished either by the development of hydrogen-resistant protective coatings or by the use of hydrogen-reactive additives in the basic propellant to produce a "neutral" nonreactive propellant. Such an additive might be carbon (in the form of hydrocarbons) or oxygen (as in the alcohols). Both can react with hydrogen in the gas phase, thus reducing its ability to attack the hot surfaces of fuel elements.

The allowable peak performance of any heat exchanger rocket reactor is determined by the available solutions of the problems of various materials. These problems are formidable, covering the structural, nuclear, and chemical fields, and it is evident that much materials research must be carried out to permit the design and construction of successful high-performance nuclear rocket reactors.

5.3 POTENTIAL PERFORMANCE

Reactor operation at high temperature (ca. 5000°R) with low molecular weight propellants is alone not enough to ensure ‘‘useful’’ nuclear rocket vehicle performance. Another parameter of importance is the ratio of rocket motor thrust to reactor weight. Obviously this must be considerably greater than unity if the propulsion system is to lift a large missile off the surface of the earth. In order to determine minimal performance requirements for reactor design purposes, it is necessary to study the over-all change in characteristics of the complete vehicle as the parameters which describe reactor performance are varied. Even a simple vehicle system analysis will give a fairly clear picture of the variational trends to be expected from different reactor operating conditions.

The thrust-to-weight ratio of a nuclear system depends on the detailed reactor design; however, simple parametric equations can be used to describe the reactor weight, power, and thrust output in general terms. The reactor weight is equal to the total reactor volume multiplied by its average density. The reactor volume, in turn, is given by the ratio of power to average volumetric power density. The fission power is related linearly to the product of thrust and propellant exhaust velocity or specific impulse, and the initial vehicle acceleration (at take-off) is determined by the ratio of thrust to gross vehicle weight. By combining these functional relations with the mass ratio equation, the vehicle performance is related to the reactor specific power output by

$$\Delta v_c = g_c I_{sp} \left[\ln \left(A_1 + A_2 \frac{a_0 g_c I_{sp}}{2\eta K} \right)^{-1} \right] \tag{5.3}$$

where Δv_c is the vehicle "characteristic" velocity in feet per second

g_c is the force-to-mass conversion factor, 32.2 $(lb_m/lb_f)(ft/sec^2)$

η is the nozzle expansion efficiency (between 0.6 and 0.8 for large nozzles)

a_0 is the take-off acceleration in units of sea level gravity.

A_1 is the fraction of gross vehicle weight taken by all the structural, tankage, payload, and pumping components of the missile

A_2 is a conversion factor, 1.356×10^{-6} Mw-sec/ft-lb

K is the reactor specific power in megawatts per pound

I_{sp} is the propellant specific impulse in pound-force seconds per pound-mass

To illustrate the effect of varying K, let us consider the two "traditional" propellants, hydrogen and ammonia.[1, 2] For operation at a core pressure of 100 atm and with a nozzle expansion efficiency of about 70 per cent, the specific impulse of these two propellants varies with temperature about as shown in Table 5.3. Assuming a peak gas temperature of 5000°R and an initial force acceleration of 1.3 g, the performance of a nuclear rocket vehicle as described by eq. 5.3 is shown in Fig. 5.3 as a function of the reactor specific power output. In computing these curves, A_1 was arbitrarily assumed

TABLE 5.3
Propellant Specific Impulse

Peak Gas Temperature, °R	Specific Impulse,[a] lb_f-sec/lb_m	
	Ammonia	Hydrogen
4000	350	720
5000	400	825
6000	450	930

[a] P_c = 100 atm; η = 0.7

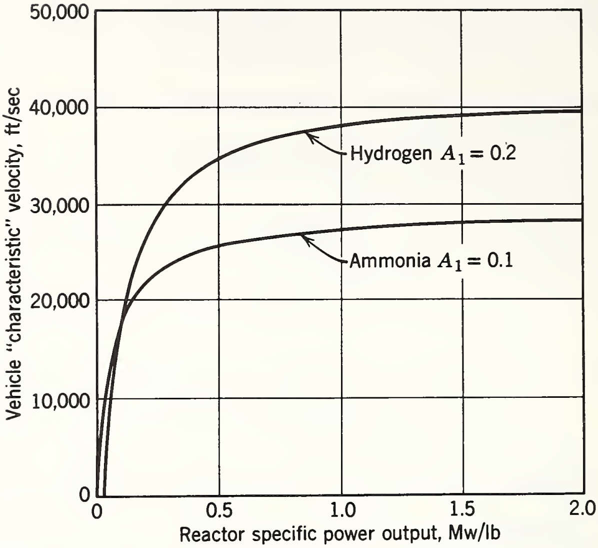

Fig. 5.3 Effect of reactor performance on vehicle performance.

to be 0.1 for ammonia and 0.2 for hydrogen rockets. This difference is a result of the lower density, hence larger missile volume and propellant tankage are required when liquid hydrogen, as compared with ammonia, is used for the same vehicle mission. Note completion of the break in the curves at a reactor specific power of about 0.6 Mw/lb. It is evident that little is to be gained by increasing the specific power much beyond this value. The reactor core power density must be at least 120 Mw/ft³ to achieve this value in a reactor with an average density of 100 lb/ft³ (about that for graphite and beryllium), whose core volume is half the total reactor volume.

By following a line of argument similar to that used in the analysis of reactor specific power, simple relations can be found which permit comparison of the performance capabilities of different vehicles. Two such relations are those between gross weight m_0, payload weight m_d, tankage volume V_t (indicates missile size), various component weight coefficients, and the vehicle characteristic velocity. These are

$$\frac{m_d}{m_0} = \exp\left(-\frac{\Delta v_c}{g_c I_{sp}}\right) - (A_1 + A_2) \qquad (5.4)$$

and

$$\frac{V_t}{m_d} = \frac{m_0}{m_d} \frac{m_p}{\rho_p m_0} \tag{5.5}$$

The actual burnout velocity, which determines the vehicle range, is approximately related to the characteristic velocity by

$$\Delta v_a = A_3 \, \Delta v_c - 0.5 g_c I_{sp} \left[1 - \exp\left(- \frac{\Delta v_c}{g_c I_{sp}} \right) \right] \tag{5.6}$$

The factor A_1 is the fraction of gross weight taken by structure, pumping equipment, and tankage, exclusive of payload weight, and A_2 is that taken by the nuclear rocket motor itself. The factor A_3 is used to account for degradation of performance by atmospheric effects, such as drag and increased nozzle back pressure at sea level.

By using these equations, a comparison was made between nuclear hydrogen, nuclear ammonia, and chemical oxygen-gasoline systems. Operating and performance conditions used in this analysis are shown in Table 5.4. Values given for the A_1 are different for the different vehicles because of the variation in relative importance of drag, tankage weight, etc., on low- versus high-density vehicles. The final results of this

TABLE 5.4

System Performance Parameters

Propellant	Chemical Oxygen-Gasoline	Nuclear	
		Ammonia	Hydrogen
Specific impulse, lb-sec/lb	315	400	825
Pumping, structure, and tankage weight coefficient A_1, lb/lb	0.04	0.06	0.12
Rocket motor weight coefficient A_2, lb/lb	0.013	0.026	0.054
Rocket motor thrust weight ratio, lb/lb	100	50	24
Atmospheric effects factor A_3	0.95	0.94	0.88
General conditions	$\eta = 0.7$: $a_0 = 1.3$: $T_{nuclear} = 5000°R$		

comparison are shown graphically in Fig. 5.4. Note from the figure that the single-stage chemical oxygen-gasoline rocket vehicle becomes excessively large and heavy for flight beyond about 18,000 ft/sec, whereas the nuclear hydrogen rocket appears to be satisfactory up to a burnout velocity of about

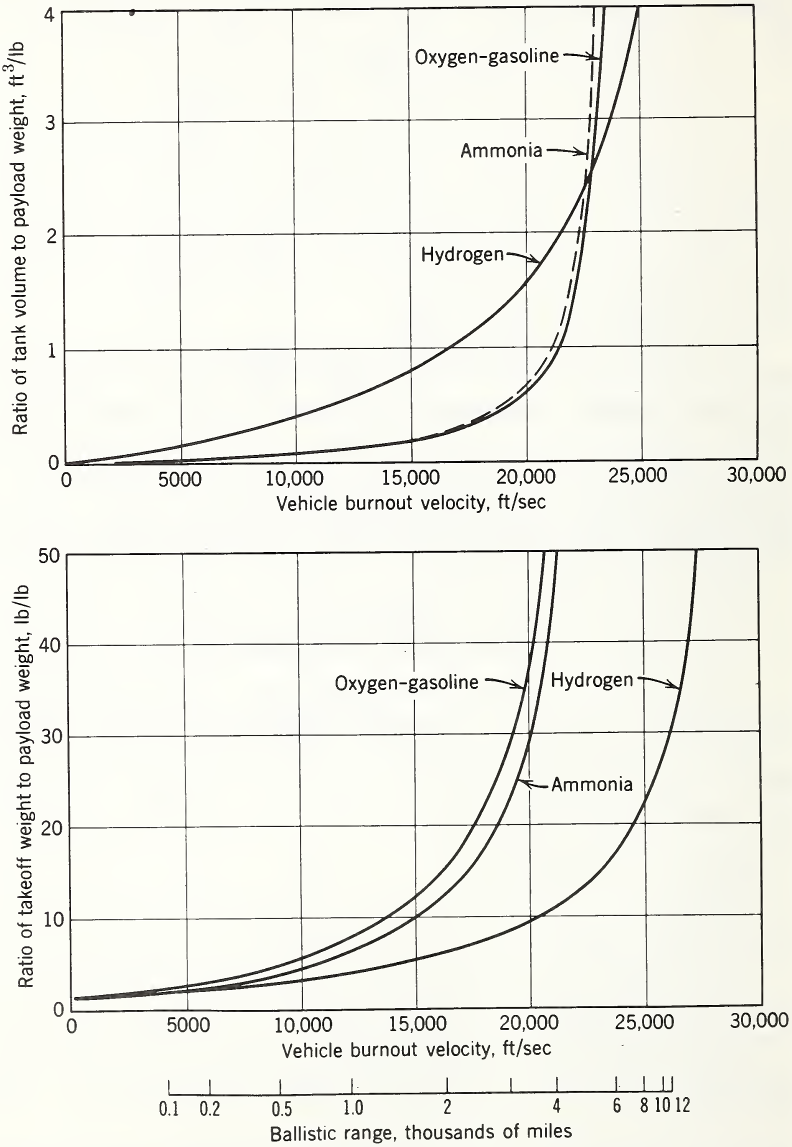

Fig. 5.4 Typical rocket vehicle performance.

23,000 ft/sec. Note also that the ammonia rocket vehicle is not significantly different in performance from the oxygen-gasoline rocket under the conditions assumed for this comparison. A different set of assumptions would, of course, yield a different comparative result.

Aside from the possible gross-weight advantage for long-range missions, nuclear rockets have several other desirable operating features. Unlike a chemical rocket motor, which is restricted by injection, mixing, and combustion problems to operation over a fairly narrow range about its design point, a gas-cooled nuclear reactor can be operated over a very wide range (e.g., 100 : 1) below its peak operating condition. This capability makes it possible to consider thrust-programmed flight, optimized to minimize vehicle structural stresses, for example, and thus to minimize the weight of structure. Another advantage is that single-stage nuclear rockets can be used for missions which would ordinarily require multiple-stage chemical vehicles. In a multistage rocket one stage is stacked on another, the stages are fired in succession, and the empty shells are dropped as each stage is "burnt." Proper performance from such a staged vehicle thus requires the successful operation of several independent vehicles in series, each one taking off from the nose of the last stage preceding it. It is obvious that this introduces an element of unreliability in the complete assembly which is not present in a single-stage missile.

These nonanalytical factors are often of great importance in reality; yet it is seldom possible to include quantitative assessment of them between competing systems on a comparative basis as clear-cut as that used for parameters such as gross weight, tank volume, range, etc. For this reason the results of systems studies should not be accepted as sound predictions of system performance; they should be viewed only as guideposts which indicate general trends of behavior.

5.4 REACTOR DESIGN PROBLEMS

As shown in Section 5.3, reduction in weight of components and the efficient utilization of propellant are important design criteria for any missile system. When applied to the design of a nuclear rocket these criteria immediately define three major problem areas that make nuclear rocket reactors unique as compared with more conventional types of reactor systems. These problem areas are (a) high core power density, (b) rapid reactor start-up operation, and (c) extreme sensitivity to fission density distribution.

5.4.1 Core Power Density

Since weight is so important, the designer is faced with the difficult situation of achieving maximum power with minimum reactor weight or volume. The power requirements for missile systems of interest are enormous, of the order of several thousand megawatts even for fairly small long-range missiles. As already discussed, this sort of power level coupled with the desirability of low rocket motor weight leads to a reactor specific power requirement greater than $\frac{1}{2}$ Mw/lb with a consequent bulk reactor power density greater than 50 Mw/ft^3 for a reactor material like graphite. If the neutron reflector volume is about equal to the core volume, the power density within the core (where the fissions are taking place) must then be greater than 100 Mw/ft^3. Achieving such a power density is roughly equivalent to obtaining the power output of Hoover Dam from the volume displaced by a small office desk.

Such a high power density is reflected in severe design requirements on the core structure. For fuel elements, high power density implies high heat transfer rates, which result in large temperature variations within the element volume. High heat transfer rates, in turn, result from high propellant flow rates, which lead to large structural loads on the hot fuel elements in the reactor. Even for materials with a fairly high thermal conductivity (such as graphite), the internal temperature differences resulting from volume heat generation can cause severe thermal strains. If the strain rates are high because of rapid power transients, for example, the induced thermal stresses will become large and can lead to failure of the reactor core fuel elements. This thermal strain problem also exists in other portions of the core structure owing to gamma and neutron heating and to differential thermal expansion of separate and possibly unequally cooled structures. Since a flying nuclear rocket reactor is basically a one-shot device, thermal stresses can be partially alleviated by permitting the material to creep. However, for test devices creep deformation of the core structure may not be acceptable, because of nonlinear, nonreversible, "hysteresis" effects which could lead to cumulative distortion of structure over many thermal cycles. Another consequence of the required high power density is the large neutron and gamma ray flux leakage to the structure external to the core. Here care must be taken in the selection of structural materials in order to minimize the heating which results from the attenuation of this radiation. Even with the most desirable materials, gamma and neutron heating power densities of several megawatts per cubic foot will be generated. This heat energy must be removed in order to keep the temperature rise in the structural materials at a low value so that highly stressed, low-weight structures may be used. In most cases such heat removal can be accomplished by regenerative cooling systems which use the primary propellant as the coolant.

In general, from a design point of view, for cores it is advantageous to use materials that possess high thermal conductivity, low thermal expansion coefficient, and low modulus of elasticity. Structural components, such as the pressure shell containing the reactor proper, need materials that have high modulus of elasticity and high strength at elevated temperatures. In this area considerable effort is required to develop fabrication techniques which will permit the employment of thin-walled construction while still retaining high-strength and low-deformation characteristics.

5.4.2 Start-up Operation

Another problem unique to rocket reactors results from the requirement of rapid start-up. In order to conserve propellant, the time on the launching pad during start-up must be minimized. For example, in the launching of some large chemical rocket vehicles propellant flow is maintained at a few per cent of full design flow for 10 to 30 sec prior to take-off. This "idling" period is followed by a rise to full flow as fast as the flow valves and turbopumps can be adjusted to design conditions. For a nuclear reactor system such a short start-up cycle to full power can be extremely difficult. An indication of the problem is shown by a simplified examination of the character of the time rate of change of neutron density within the core. Neglecting delayed neutrons, this is

$$\frac{dn}{dt} = \frac{\delta k}{l^*} n \tag{5.7}$$

where n is the number of neutrons per unit volume at a particular time t
δk is the excess multiplication factor of the assembly
l^* is the mean effective lifetime of the neutrons.

Integration of eq. 5.7 gives the relationship

$$n = n_0 \exp(\delta k/l^*)t \tag{5.8}$$

where n_0 is the initial number of neutrons per unit volume
n is the number after time t

Equation 5.8 shows that for a positive excess multiplication factor the number of neutrons and the power will rise exponentially with time.

The reactor period T is defined as the time required for the neutron level to change by a factor of e (2.718). It can be seen from eq. 5.8 that this is given by

$$T = \frac{l^*}{\delta k} \tag{5.9}$$

for a reactor in which all fissions are caused by prompt neutrons.

As a consequence of the exponential character of the rise in power, it is evident that the reactor control system must contain adequate safeguards to prevent runaways. However, the fission process itself contains a built-in safety feature. In eqs. 5.7 through 5.9 it was assumed that all fission neutrons are given off at the instant of fission and have a mean effective lifetime of l^*. In reality, a small fraction of the neutrons are given off at different discrete times after the fission process has occurred. These delayed neutrons provide a practical basis for reactor control by the introduction of a time delay in build-up of the neutron level.

To take account of the delayed neutron groups, the relation between reactivity, neutron lifetime, and the stable period of the reactor is[4]

$$\frac{\delta k}{k_{eff}} = \frac{l^*}{Tk_{eff}} + \sum_{d} \frac{\beta_i}{1 + \lambda_i T} \tag{5.10}$$

Here β_i and λ_i are the yield and decay constant respectively of the d delayed neutron groups. As is well known, it is possible to operate a reactor so that the effective multiplication factor k_{eff} (ratio of the number of neutrons in one generation to that in the preceding generation) becomes large enough that a chain reaction can be sustained without the need of the delayed neutrons. This condition occurs when k_{eff} equals 1.0075 and is called prompt critical. Now, for a neutron mean effective lifetime of 10^{-3} sec, typical of a well-moderated thermal reactor, solution of eq. 5.10 for the known delayed neutron groups shows that the reactor period will be about 0.68 sec at prompt critical. In this condition the power level will increase by a factor of 10 in 1.57 sec.

Now, to achieve a start-up condition which is desirable from the rocket vehicle performance standpoint, the propellant wastage during start-up should be less than 1 per cent of that required for propulsion of the vehicle. For a long-range missile this can be achieved by programmed operation of the reactor to go from 5 per cent to 100 per cent of full power in about 5 sec. In turn, this requires a start-up period of about 1.67 sec, which can be obtained only by operation at a reactivity within 25 per cent or less of the prompt critical condition. For comparison, conventional reactors are generally brought to full power with periods 10 to 100 times longer than that just given. Production of a control system capable of accomplishing this task requires considerable imagination in engineering development.

This fast start-up also results in severe thermal stress conditions on the volume-heated structural components. Very rapid thermal strain rates will occur with the rapid rise in power and temperature. Under these conditions it may be necessary to permit creep of the structural components in order to relieve thermal strains without component failure. Because of the nonreversibility of some creep phenomena, it is readily seen that the thermal cyclability of a flight-type rocket reactor may be extremely limited. As previously mentioned, this can be a great complication in the ground testing phase of a flight reactor development program.

5.4.3 Fission Density Distribution

The third major requirement to be met in achieving a compact and efficient core heat exchanger is that each segment of the reactor core transfer as much heat to the propellant as every other geometrically similar segment. For systems in which the flow passages are of uniform size and distribution, this requirement means that the fission density distribution must be uniform in the direction normal to the propellant flow. Thus in a cylindrical core with axial flow, the fission density must be uniform or ‘‘flat’’ at every axial station. For reactors with appreciable neutron moderation external to the core, or for cores with a high concentration of fissionable fuel, the fission density distribution tends to peak at the reflected boundaries of the core, necessitating a radial variation in the loading of fuel elements to achieve the desired flatness. This propellant flow-fission density matching poses a difficult design problem which is greater in matrix geometry than in homogeneous cores.

These three special problem areas are by no means the only ones confronting the designer of rocket reactors; however, they do show that the designing of high-power short-life, minimum-weight reactors requires a different philosophy from that successfully used for conventional, bulky, stationary, long-lived operating power reactor systems.

5.5 VEHICLE DESIGN PROBLEM AREAS

Large rockets, whether powered by chemical or nuclear energy, pose many difficult problems in minimum-weight stress-limit design of components such as turbopumps, propellant tanks, tank and payload support structure, motor mounting and thrust structure, etc. However, some problems arise in connection with the use of nuclear propulsion systems which are not found in large chemical rocket vehicles.

All of these are a result of the leakage of nuclear radiation from the reactor during operation. Gamma photons and fast neutrons carry the major portion of the radiation energy. Thermal neutron leakage is generally insignificant in energy content compared to these two but is of prime importance in analyzing activation of structures surrounding the reactor (test stands, instruments, etc.). The gamma rays and fast neutrons leaking forward out of the reactor lose almost all their energy in the structure (pumps, turbine, piping) between the reactor and propellant tanks and in the propellant itself. This leakage will vaporize some of the propellant before it reaches the pumping system unless shielding material is used to absorb the radiation energy before it gets to the tanks. A cooling system must be provided for any such shielding as well as for the missile skin and other gamma-absorbing structures near the reactor. To avoid an excessive weight penalty, the propellant must be used as the sink for this heat energy, but this in turn requires extra ducting and heat exchange piping. Another effect of gamma leakage is the ionization of air surrounding the missile in its flight through the atmosphere, resulting in a barrier to the transmission of low-frequency electromagnetic radiation to or from the missile, for guidance purposes, for example. For reactors of thousands of megawatts total power, electromagnetic wave frequencies of the order of hundreds to thousands of megacycles may be required for good communication. Since this is within the range of present standard microwave equipment, no serious difficulties should be encountered. Guidance equipment should be carried in the nose of a nuclear rocket, forward of the propellant, to minimize the radiation levels seen by the equipment during reactor operation as well as to remove it as far as possible from the region of maximum air ionization. In general, the propellant will provide sufficient shielding for the operation of conventional vacuum tubes, but probably not enough to permit the use of transistorized equipment without additional shielding.

5.6 TESTING

The testing program necessary for the successful development of a nuclear rocket motor encompasses the manifold problems of the reactor engineer as well as those of the chemical rocket designer.

In order to determine the nuclear characteristics of a device, tests must be carried out utilizing critical assembly mock-ups, zero power configurations of correctly detailed geometry, and the full-scale device. Many of these tests can be made with the reactor operating at very low power levels; however, full-scale full-power runs eventually must be made to prove the device at design point. It is during this last phase of the testing program that the major problems arise.

In static testing, the hazards and problems associated with nuclear radiation leakage from the reactor are the controlling factors in designing the test facilities and in conducting the test operation. The neutron and gamma ray radiation field adjacent to an operating rocket reactor can be of such magnitude that the test instrumentation and personnel must be either within heavily shielded structures, if close up, or separated by great distances from the device. Figure 5.5 shows the dose rates expected from a ground test reactor during operation as a function of receiver-source separation distance. It should be noted that the dose rates fall off very rapidly beyond a separation distance of about 1 mile, so that almost any power rocket reactor can be operated without personnel haz-

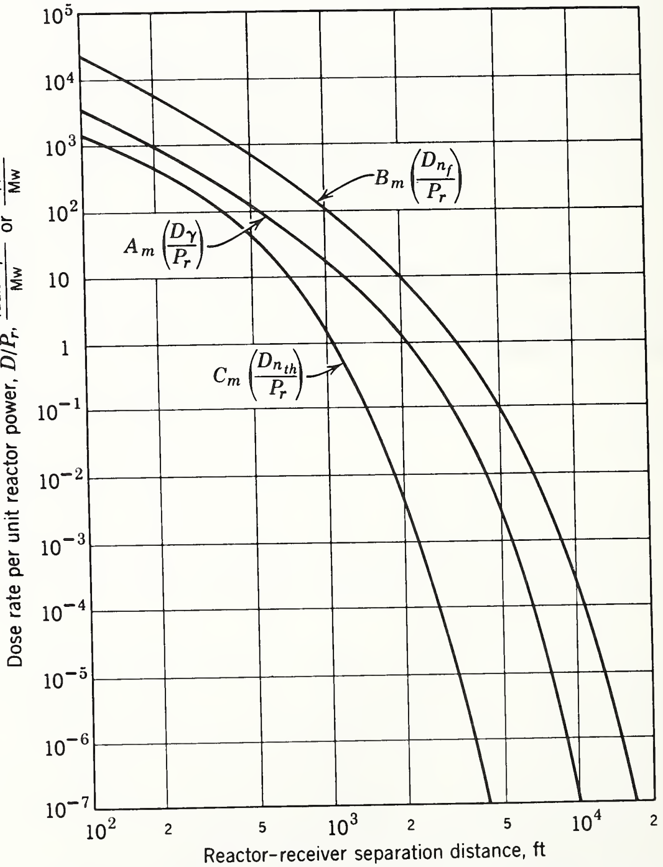

Fig. 5.5 Radiation dose rates during reactor static testing.

ard from a distance of a few miles. For flight testing of a complete missile, the control room doses will always be less than those from static tests because of the short length of time (compared to total operating time) that the reactor is on the launching pad. For this reason shield design based on static firing requirements is always conservative (thereby safe) from a flight test standpoint.

Another factor which can restrict the re-use of an expensive test stand is the neutron and gamma induced activation of the structural materials and auxiliary test equipment. To minimize this problem, care must be taken in the design of the test stand and its equipment and in the choice of materials in order that materials with long half-lived neutron-activated isotopes are avoided.

An additional problem associated with high-power test operation results from the large amount of gamma and beta decay power released within the reactor after shutdown. Figure 5.6 shows the decay power output as a function of "cooling" time, or time after reactor shutdown, for various reactor operating periods. The existence of this decay power can

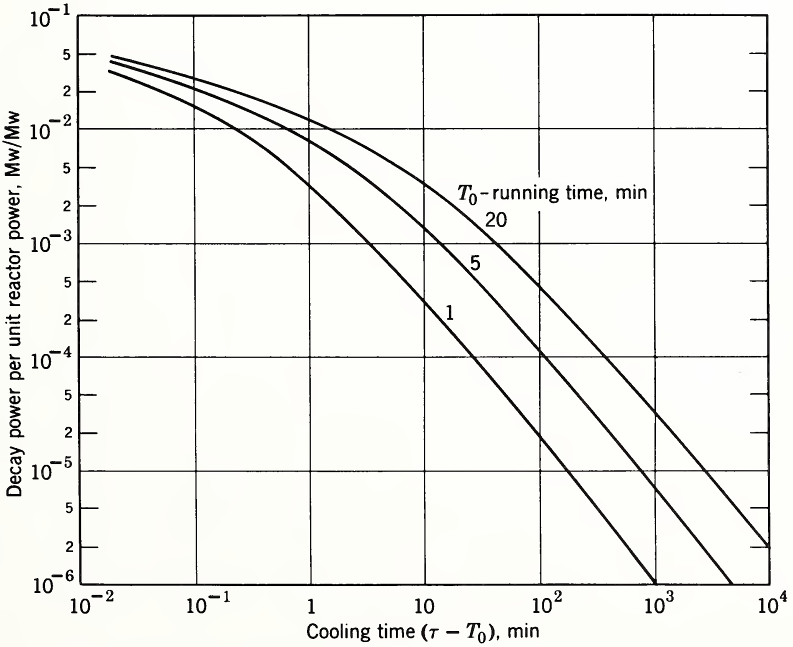

Fig. 5.6 Beta plus gamma decay power.

be either a blessing or a curse, depending on the particular situation of interest. For static testing, extensive cool-down systems and procedures are required to remove this decay power if the reactor is to be salvaged for post-test examination. In flight testing, as long as the reactor has been operating at full power for a sufficient period of time (e.g., more than 10 sec) the decay heat can be utilized to vaporize the reactor as a range safety feature. Indeed, unless special airborne shutdown cooling systems are carried in flight test vehicles, all flight test reactors will be vaporized within a few seconds after shutdown. In general, this vaporization will take place far above the atmosphere and thus no ‘‘fallout’’ or other radiation hazard is expected.

The success of any test program depends on the amount and accuracy of the diagnostic information obtained. This is especially true for nuclear rocket motors since they must be designed to operate at the very peak limits of material performance. Accurate and reliable test instrumentation, as well as detailed post-mortem examination, is required to extract the maximum amount of information from a given reactor test. Although some useful information on the ‘‘black-box’’ gross performance of a reactor can be obtained by instruments located outside the core, unfortunately very few instruments exist that can even survive, let alone perform, in the temperature, flow, and radiation environment of an operating rocket reactor core itself. In addition to the instrumentation problem, data recording is greatly complicated by the large distances required between recording-control rooms and the test stand.

Because of the difficulty of determining the core performance during reactor operation, much is necessarily left to the post-mortem examination of the core components to determine whether the design parameters have been met. By post-mortem examination it is possible to determine a general survival picture for the core materials and structures, and to ascertain the fission distribution in the core during high-temperature operation. This latter information can be found by analyzing the distribution of fission products throughout the fuel region; here the existence of fission product decay chains is welcome as a diagnostic tool to study reactor nuclear performance. Knowledge of the fission distribution is of interest because it provides a check on the behavior of the thermal neutron flux distribution as the thermal base (temperature) of the reactor is changed, thus permitting correlation of room temperature neutronic measurements with actual reactor operating conditions. Such correlations are needed in the design of rocket reactors to fit specified high-temperature fission density distributions. Visual determination of the erosion, corrosion, and deformation of core materials and structures can lead to a better understanding of creep reversibility and of the general limitations on materials performance. Obviously, this sort of knowledge is vitally important to the design of high power density rocket reactors.

It must be remembered that the post-mortem examination of a fired reactor is a difficult task. Because of the intense decay radiation, all disassembly and analysis work must be done remotely. For reasons of radiation safety all such "hot" disassembly and handling must be done in heavily shielded areas with remotely operated equipment. Elaborate radiation safety monitoring systems and procedures must also be provided to guard against contamination outside the shielded "hot" rooms. Since this type of facility represents a considerable dollar investment, the test area layout and test program scheduling must be based on efficient and continued use of such facilities.

Little has been said about the problems of flight-testing complete missile systems. The major physical difference between static and flight testing of nuclear rocket motors is that a greater separation distance (reactor to control room) is required for flight tests in order to minimize the effects of an accident resulting in flight failure immediately after launching. Another difference, common to flight testing of chemical missiles as well, is that all control and diagnostic information must be telemetered to the control center rather than carried by the direct cable connections that can be used for static test purposes. As previously discussed, air ionization around the missile by leakage radiation from the reactor adds only slight complication to the telemetering system requirements for nuclear missiles as compared with those for chemical missiles.

In general, developmental static testing of nuclear rocket motors poses more severe reactor instrumentation, radiation, and handling problems than does flight testing. The problems are more severe because the total radiation dose at any fixed ground point is greater from a ground test than from a flight test, and because static tests are inherently oriented more toward study of the propulsion system performance than are flight tests of a complete missile system.

5.7 POWER DENSITY

As previously discussed, the ratio of heat transfer surface to total volume is a means of comparing compact cores, but careful consideration must be given to the frictional losses within such cores. Since pump weights may be a considerable fraction of the total weight of a nuclear rocket motor system, the propellant pressure drop requirements for particular heat exchanger designs must be investigated before a true comparison can be made. Another factor arises from the possibility that the heat transfer rates are not the same for the different configurations. Therefore, it is convenient to make a comparison of cores of different geometry on the basis of bulk core power density. This comparison is simply the ratio of the power output of the reactor to the total volume of the core:

$$\eta = \frac{P_r}{V_c} \tag{5.11}$$

where P_r is the total power output of the reactor
V_c is the total volume of the core

For preliminary design purposes, it is reasonable to compute the over-all heat transfer by the relationship

$$\frac{Q}{A_T} = h_a \Delta T_{LM} \tag{5.12}$$

where Q = total heat transferred
h_a = average heat transfer coefficient
A_T = total heat transfer surface area
T_{LM} = logarithmic mean temperature

The reactor power in megawatts is related to the total heat transferred by

$$Q = K(1 - f_e) P_r \tag{5.13}$$

where K is the conversion factor 3.413×10^6 Btu/Mwhr

f_e is the fraction of the fission energy escaping from the reactor in photons and fast neutrons

The analysis herein assumes that f_e is zero or that the reactor power used is only that given up to the cooling fluid (propellant). Under this assumption, substituting eqs. 5.12 and 5.13 into eq. 5.11 along with $\zeta = A_T/V_c$, the power density becomes

$$\eta = \frac{1}{K} h_a \frac{A_T}{V_c} \Delta T_{LM}$$

$$\eta = \frac{1}{K} h_a \zeta \, \Delta T_{LM} \qquad (5.14)$$

with the average heat transfer coefficients being those associated with particular geometries.

The consequences of high core power density in terms of core geometry are best demonstrated by an example. Consider a case where it is desired to design a 5000-Mw nuclear rocket motor using hydrogen as the propellant with a core power density of 100 Mw eq'.

$P_r = 5000$ Mw
$\eta = 100$ Mw/ft^3

The volume of the core must therefore be $V_c = 50\,\text{ft}^3$ and the diameter and frontal area will be

$$D_c = \left(\frac{50 \times 4}{\pi}\right)^{1/3} = 4 \text{ ft}$$

$$A_c = 12.5 \text{ ft}^2$$

for a right-circular cylindrical geometry.

It can be shown that the critical mass is heavily dependent on the core fraction; therefore, this must be kept to a minimum. For this example assume $\epsilon = 0.30$. The propellant flow area A_f then becomes

$$A_f = \epsilon A_c = 3.75 \text{ ft}^2$$

In order to obtain 5000 Mw with a peak hydrogen temperature of 5000°R, the propellant flow rate, as determined from the power flow rate relationships must be

$$w = \frac{P_r}{20.8} = 240 \text{ lb/sec}$$

The specific mass flow rate for this particular core is thus

$$G = \frac{w}{A_f} = 2.30 \times 10^5 \text{ lb/(hr)(ft}^2\text{)}$$

For a constant wall temperature of 5500°R, a propellant inlet temperature of 500°R, and an exit temperature of 5000°R,

$$\Delta T_{LM} = \frac{\Delta T_e - \Delta T_i}{\ln (\Delta T_e/\Delta T_i)}$$

gives

$$\Delta T_{LM} = \frac{5000 - 500}{\ln (5000/500)} = 1950°\text{R}$$

and eq. 5.14 yields

$$h_a \zeta = \frac{100 \times 3.413 \times 10^6}{1950} = 1.75 \times 10^5 \text{ Btu/(hr)(ft}^3\text{)(°F)} \quad (5.15)$$

For a plate core the specific surface area is

$$\zeta = \frac{2}{t + u} = \frac{2}{u} \epsilon$$

and for the assumed 30 per cent void

$$\zeta = \frac{0.60}{u} \quad (5.16)$$

where u is the flow gap width
t is the plate thickness

Combining eq. 5.16 with eq. 5.15 gives a restrictive relation between the heat transfer coefficient and the flow passage width. This is

$$\frac{h}{u} = 2.92 \times 10^5 \quad (5.17)$$

Since the hydraulic or equivalent diameter is $D_e = 2u$ for flow between parallel plates, then

$$h = 1.46 \times 10^5 D_e \quad (5.18)$$

Now, by employing the correlation relationship equation

$$\frac{hD}{k_f} = 0.023 \left(\frac{DG}{\mu_f}\right)^{0.8} \left(\frac{c_{pf} \mu_f}{k_f}\right)^{1/3} \quad (5.19)$$

it is possible to obtain the proper hydraulic diameter, since

$$h = 0.023 \frac{G^{0.8}}{D_e^{0.2}} \frac{k_f}{\mu_f^{0.8}} \left(\frac{c_{pf}\mu_f}{R_f}\right)^{1/3}$$

$$D_e^{1.2} = 15.75 \times 10^{-8} G^{0.8} \frac{k_f}{\mu_f^{0.8}} \left(\frac{c_{pf}\mu_f}{k_f}\right)^{1/3} \qquad (5.20)$$

The film temperature needed to determine the physical properties of the propellant will be based on an average value of the fluid bulk temperature and the plate wall temperature. That is for a propellant inlet temperature of 500°R an exit 5000°R and a plate wall temperature of 5500°R

$$T_f = \frac{(T_i + T_e)/2 + T_w}{2} = \frac{2750 + 5500}{2} = 4125°R$$

For this temperature,

$\mu_f = 0.08$ lb/(hr)(ft)
$k_f = 0.46$ Btu/(hr)(ft)(°F)
$c_{p_f} = 3.78$ Btu/(lb)(°F)

Using these properties and the mass flow rate per unit area,

$G = 2.30 \times 10^5$ lb/(hr)(ft^2)

the required hydraulic diameter becomes, from eq. 5.20,

$D_e = 0.020$ ft

resulting in flow gap and plate thickness dimensions of

$u = 0.010$ ft $= 0.120$ in.
$t = 0.0233$ ft $= 0.280$ in.

Note that a tolerance of ±0.005 in. here can result in a 10 per cent variation in flow gap width, with a consequent variation in flow from one channel to the next. These dimensions, which are typical, and their consequences show that the achievement of high power density requires extreme care in the detailed design and construction of the nuclear reactor core.

REFERENCES

1. L. R. Shepherd and A. V. Cleaver, "The Atomic Rocket, 1, 2, 3, and 4," J. Brit. Interplanet. Soc., 7, Nos. 5, 6 (1948), and 8, Nos. 1, 2 (1949).
2. H. S. Tsien, "Rockets and Other Thermal Jets Using Nuclear Energy," Chapter 11 of The Science and Engineering of Nuclear Power, Vol. 11, edited by Clark Goodman, Addison-Wesley Press, Reading, Mass., 1949.
3. George P. Sutton, Rocket Propulsion Elements, 1st and 2nd editions, John Wiley and Sons, New York, 1956, Table 4-3, p. 112.
4. S. Glasstone and M. C. Edlund, The Elements of Nuclear Reactor Theory, D. Van Nostrand, Princeton, N. J., 1952, Sec. 10.29, p. 301.
5. R. Bussard and R. DeLauer, Nuclear Rocket Propulsion, McGraw-Hill, New York, 1958.

6

PLASMA PROPULSION SYSTEMS

D. B. Langmuir

6.1 INTRODUCTION

Previous chapters have discussed rocket propulsion fundamentals, liquid engine design, solid engine design, and nuclear engine design. In these discussions it was shown that specific impulse exerts a dominant effect on rocket performance and that achievable values of this parameter are limited by the energy content per unit mass of the fuel-propellant combination. The high specific energy content of nuclear fuels and the essentially unlimited velocities or momenta produced by electrical acceleration techniques, therefore, present an alluring combination to those surveying future rocket developments. In this chapter we discuss how nuclear energy or solar energy might be combined with modern mass expulsion systems to permit more effective space exploration than can be attained by ordinary rockets.

The material is discussed in three topics.

1. The general theory of this type of space propulsion, in which the mass and the energy are quite separate.
2. The performance properties of the electrically propelled spaceship, including some simple rules which permit a quick calculation of the over-all performance of this kind of a system.
3. Problems associated with the actual plasma acceleration device.

6.2 GENERAL THEORY

A plasma is a gas containing approximately equal densities of free electrons and positive ions. A fluorescent lamp, the sun's corona, and the interior of the stars are well-known examples. Most of the mass in the universe is in the form of plasma, "the fourth state of matter." What, then, does a plasma have to do with an engine or propulsion?

The answer is that since the plasma is susceptible to electric forces and (in the forms which can be made by man) has very low density, it should be possible by applying electric forces to make it move with a very high velocity. High specific impulse is the potential advantage which "plasma propulsion" offers, at the price of a separate electric power supply and many challenging difficulties of technique.

6.2.1 Electrically Propelled Rocket

Some major characteristics of any electrically propelled rocket are illustrated in Fig. 6.1. The most important differ-

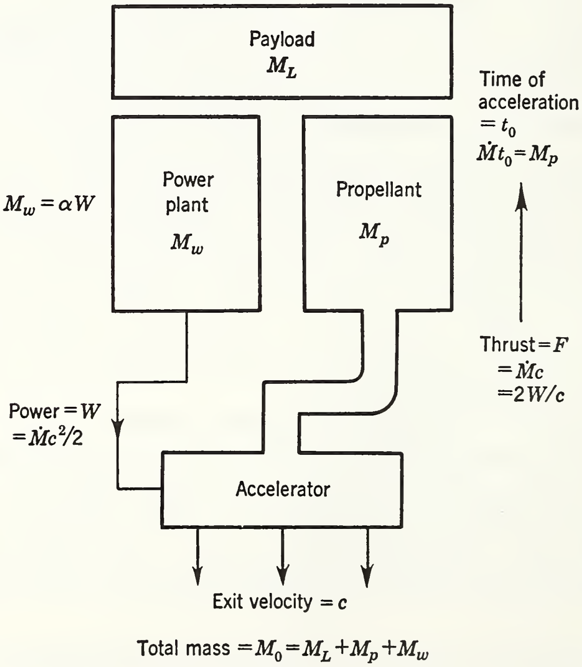
Payload
M_L
Time of acceleration $= t_0$
$\dot{M}t_0 = M_p$
$M_w = \alpha W$
Power plant
M_w
Propellant
M_p
Thrust $= F$
$= \dot{M}c$
$= 2W/c$
Power $= W$
$= \dot{M}c^2/2$
Accelerator
Exit velocity $= c$
Total mass $= M_0 = M_L + M_p + M_w$

Fig. 6.1

ence between this rocket and the chemical rocket is that its fuel is not used as a propellant. The propellant is the mass which is accelerated and expelled from the rocket in order to produce thrust, as contrasted with the fuel which supplies the necessary energy.

The electrically propelled rocket consists of four main divisions. As seen in Fig. 6.1, M_L represents the payload. The unit will have a power plant of mass M_w. The mass of the propellant, separate from the power plant, is designated M_p. This propellant will be conducted to an acceleration system or plasma acceleration device shown as the "accelerator." The power from the power plant will be fed to the accelerator and will be used to impart kinetic energy to the propellant which will be ejected with an exhaust velocity c.

In this discussion the performance of the separately powered rocket will be defined in terms of the ratio of initial mass to payload mass (M_0/M_L), the time of acceleration (t_0), and the velocity increment (ΔV) imparted to the final mass ($M_L + M_w$) of the rocket in field-free space. Other important parameters are the specific weight of the power plant α and the exhaust velocity c.

The simplified analysis which follows passes over several considerations which should be noted. Thus the power plant will often have value as part of the payload. If, for example, a replacement power plant had to be delivered to a space station, a useful mission would be performed even though M_L were equal to zero. The acceleration time t_0 will not generally be the total time for the mission. Care must be exercised in deducing performance of actual missions from the free-space velocity increment ΔV, since, when spiraling outward at low acceleration from a center of gravitational attraction, the ΔV required to escape may be as much as 2.4 times that needed with impulsive acceleration. The parameters chosen are, however, convenient and permit definite conclusions of broad, general accuracy to be drawn from a simple analysis.

6.2.2 Analysis of Performance[1, 2]

By using the notation of Fig. 6.1, the following equations define the performance of the separately powered rocket. The conservation of mass is stated by

$$M_0 = M_L + M_w + M_p \tag{6.1}$$

and

$$\dot{M}t_0 = M_p \tag{6.2}$$

The conservation of momentum is stated by

$$F = \dot{M}c = (M_w + M_p + M_L - \dot{M}t)\dot{V} \tag{6.3}$$

The conservation of energy is stated by

$$\dot{M}c^2/2 = W \tag{6.4}$$

From eqs. 6.3 and 6.4 we note that

$$F = 2W/c \tag{6.5}$$

The power plant has specific weight α so that

$$M_w = \alpha W \tag{6.6}$$

The α must be regarded as the effective specific weight, equal to the weight of the complete power plant and acceleration system divided by the kinetic energy actually delivered in 1 sec to the expelled mass. Generally α will vary only slowly with W.

A special case of the separately powered rocket is one with a payload of zero. This rocket is of interest as a limiting case and also for practical missions under some circumstances. If M_L equals zero, eqs. 6.1 and 6.3 become

$$M_0 = M_w + M_p \tag{6.7}$$

$$\dot{M}_c = (M_w + M_p - \dot{M}t)\dot{V} \tag{6.8}$$

$$= 2W/c = 2M_w/\alpha c \tag{6.9}$$

using eqs. 6.5 and 6.6. When eq. 6.9 is substituted into eq. 6.8, an integration gives

$$\Delta V = \sqrt{2t_0/\alpha}\,\sqrt{M_w/M_p}\,\ln\left(1 + \frac{M_p}{M_w}\right) \tag{6.10}$$

$$\frac{\Delta V}{c} = \ln\left(1 + \frac{2t_0/\alpha}{c^2}\right) \tag{6.11}$$

$$= \ln\left(1 + \frac{V_c^2}{c^2}\right) \tag{6.12}$$

where

$$V_c = \sqrt{2t_0/\alpha} \tag{6.13}$$

In practical units

$$V_c = \sqrt{t_0/500\alpha} \text{ km/sec} \tag{6.13a}$$

if t_0 is in seconds and α in kilograms per kilowatt. The symbol V_c is defined as a "characteristic velocity" and is discussed further in Section 6.3.1.

The independent variable in eq. 6.10 is M_p/M_w, the ratio of the mass of the power plant to that of the propellant. The value of this ratio determines the exhaust velocity c from eqs. 6.2, 6.4, and 6.6, as follows:

$$M_w/M_p = c^2/V_c^2 \tag{6.14}$$

This relation is plotted as the abscissa at the top of Fig. 6.2.

The performance of the separately powered rocket with zero payload, as expressed in eqs. 6.10 and 6.12, is shown as the top curve of Fig. 6.2. It is seen that as the exhaust velocity is increased the velocity increment ΔV reaches a maximum and then declines. An optimum value of c therefore exists. High specific impulse is a desirable aim in this type of space vehicle only up to a certain point.

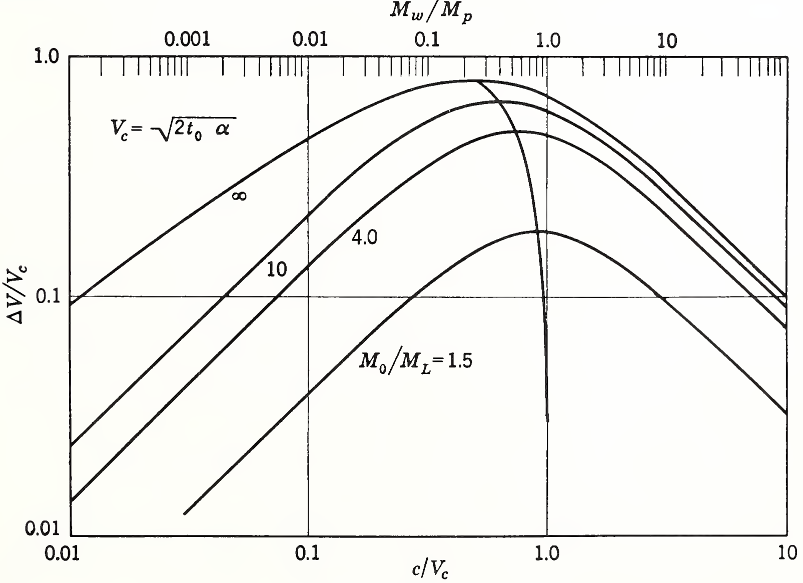

Fig. 6.2

In this special case of zero payload the conditions that apply at the optimum are

$$\begin{aligned} \Delta V &= 0.805 V_c \\ c &= 0.505 V_c = 0.627 \Delta V \\ M_p/M_0 &= 0.796 \\ M_w/M_0 &= 0.204 \end{aligned} \tag{6.15}$$

Analysis of the zero payload may seem to be primarily academic; however, it helps mathematically to illustrate the principles and, for the electrical or separately powered rocket, may have a specific use. Although the propellant is gone at the completion of acceleration, the power plant remains and need not be totally spent if nuclear or solar energy sources are used. The two most valuable commodities in outer space are undoubtedly energy and mass, and the spaceship is still equipped with one of them. If the rocket were propelled under its own power to its destination, its power plant would have great usefulness and should often therefore be counted as part of the payload.

If a payload M_L is carried, eq. 6.8 becomes

$$\dot{M} c = (M_w + M_p + M_L - \dot{M} t)\dot{V} \tag{6.16}$$

After integrating and substituting this leads to

$$\frac{\Delta V}{c} = \ln \frac{1 + M_w/M_p}{M_L/M_0 + M_w/M_p} \tag{6.17}$$

which can be put into the form

$$\frac{\Delta V}{V_c} = \frac{c}{V_c} \ln \frac{1 + c^2/V_c^2}{M_L/M_0 + c^2/V_c^2} \tag{6.18}$$

Compared to eq. 6.11 there is one more variable, the ratio of the payload to the initial mass. The lower curves in Fig. 6.2 represent the over-all performance of the separately powered rocket with a finite payload. The ordinate of this graph is $\Delta V/V_c$, the ratio of two velocities, whereas the abscissa is the exhaust velocity divided by the characteristic velocity.

6.3 PERFORMANCE PROPERTIES OF THE ELECTRICALLY PROPELLED ROCKET

This presentation of the over-all performance of the separately powered rocket in dimensionless form is convenient, because

1. The characteristic velocity V_c is easy to compute and has a clear physical significance.

2. Two of the most interesting characteristics of the electrically propelled rocket are numerically approximately equal to V_c, namely, the optimum exhaust velocity and the maximum attainable velocity increment.

6.3.1 The Characteristic Velocity V_c

Values of $V_c = \sqrt{2t_0/\alpha}$ are shown in Fig. 6.3. It is obviously reasonable that over-all performance should improve if, for the same power output, the power plant is made lighter or the duration of its operation is extended. Characteristic velocity V_c can be seen to be the velocity which the power plant would have if its full energy output $M_w t_0/\alpha$ were put in the form of kinetic energy of its own mass M_w.

The optimum value of ΔV drops from $0.805V_c$ as M_L is increased from zero. For large payloads an approximate formula is

$$\frac{\Delta V}{V_c} \simeq \frac{1}{2}\left(1 - \frac{M_L}{M_0}\right) \tag{6.19}$$

For small payloads an approximation is

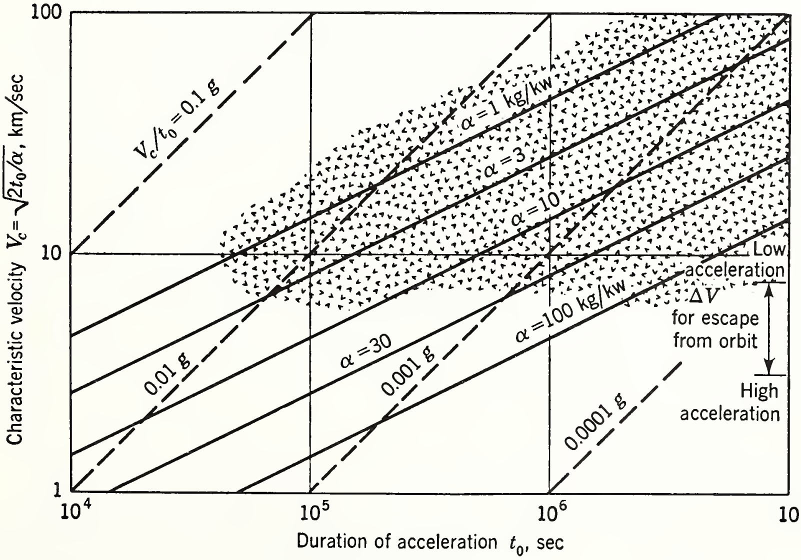

Fig. 6.3

$$\frac{\Delta V}{V_c} = 0.805 - 2\frac{M_L}{M_0} \tag{6.20}$$

6.3.2 Acceleration

The average acceleration during the time t_0 is given by $\bar{a} = \Delta V/t_0$,

$$\bar{a} = \frac{0.204(\Delta V/V_c)^2}{\alpha \Delta V} \tag{6.21}$$

in units of g (g = 981 cm/sec²). Inspection of this formula, and of Fig. 6.3 which shows lines of constant acceleration, could make it clear that for practical values of α ($\alpha > 1$ kg/kw) and for useful values of ΔV ($\Delta V > 10$ km/sec) the acceleration will be much less than 1. Values of 10^{-3} or 10^{-4} g may nevertheless give useful performance as compared to chemical rockets, provided the electrically propelled rocket can first be placed in a satellite orbit by a high-acceleration system.

6.3.3 Comparision with Chemical Rockets

The relative merits of an electrical rocket as compared with a chemical rocket can best be determined by comparing the payloads that can be delivered by the two methods for space missions which are identical in initial and final position and velocity and in elapsed time. Analysis shows that the comparison depends on the specific impulse I_{sp} of the chemical rocket and on the specific power available for the electrical rocket. For missions to Mars, Irving and Blum[3] have found that, compared to the chemical rocket of $I_{sp} = 600$ sec the electrically propelled rocket will have a superior performance if α is smaller than 20 kg/kw. For $I_{sp} = 300$ sec, α must be smaller than 50 kg/kw. These figures apply for a total round-trip time of about 15 months.

6.3.4 Relativistic Speeds

Although many interesting new possibilities would be offered by space vehicles which could approach the speed of light, it is easy to show that the electrically propelled rocket is of negligible interest in this connection. The reason is that fissionable fuel, with its output of about one megawatt day per gram of material fissioned, has insufficient specific energy content. The maximum speed to which a lump of such fuel could be accelerated by its own energy output would be the velocity of the fission fragments, about 10^4 km/sec, or one-thirtieth the velocity of light. Fusion processes impose about the same limitation. If, suitably stretching the imagination, we conceive of using the fission products themselves as the propellant in a conventional rocket, the formula $M_0/M_L = e^{\Delta V/c}$ applies, where c is the fragment velocity. Even in this case the mass ratio to achieve one-third the velocity of light would be 20,000. Relativistic rocket velocities appear to justify no serious consideration if the energy source is to be fission or fusion.

6.4 THE PLASMA ENGINE

This discussion shows that when a power supply is available that can deliver kilowatts of electricity in the environment of outer space for several months, and that weighs some tens of kilograms per kilowatt, the electrically propelled rocket will offer interesting possibilities for space travel. The next subject of attention must then be the thrust device, the function of which is to transform the electrical energy of the power supply to kinetic energy of the propellant, ejecting the latter with the optimum exhaust velocity. The value of the latter, approximately equal to $V_c = \sqrt{2t_0/\alpha}$, is in the range 10 to 50 km/sec for the most practicable space missions.

There are three main categories of thrust devices to accomplish this purpose.

6.4.1 Electrothermal Thrust Devices

In these an electric arc is used to heat the propellant, which is then accelerated by adiabatic expansion as in a chemical rocket. The thrust is exerted by impact of the atoms or molecules of the propellant on the walls of the combustion chamber and nozzle.

6.4.2 Electromagnetic Thrust Devices

In these an electric current which is caused to pass through the propellant gas interacts with a magnetic field so as to accelerate the propellant. The thrust is exerted by interaction between magnetic fields and currents in conductors which are part of the thrust device.

6.4.3 Electrostatic Thrust Devices

In these charged particles are accelerated by passage through a potential drop, and particles of opposite sign are subsequently added to neutralize the current flow and space charge. Thrust is exerted by termination of lines of electric force on electrodes which are part of the thrust device.

Each of these types of device produces a stream of gaseous propellant containing charged particles of opposite sign in approximately equal amounts. All may therefore be properly called "plasma engines."

Since an adequate treatment of all these methods is not possible in this chapter, the remainder of the discussion will be confined to electrostatic propulsion. This choice in no way represents any judgment about the relative merits of the other systems, which the author is not competent to discuss.

6.5 ELECTROSTATIC PROPULSION

6.5.1 Thrust, Mass Flow, and Aspect Ratio

The velocity of electrostatically accelerated ions is

$$c = \sqrt{2Vq/m} \text{ meters/sec} \tag{6.22}$$

where V is the accelerating potential in volts and q/m is the charge-to-mass ratio in coulombs per kilogram. In practical units

$$c = 13.8\sqrt{V/A} \text{ km/sec} \tag{6.23}$$

where V is the potential in volts and A is the atomic mass of the ion ($A = 1$ for proton).

The mass flow rate will be proportional to the current and to the ionic mass A. A basic limitation on mass flow rate will therefore be imposed by the laws governing the space charge current which can pass between electrodes in high vacuum. For flow between parallel planes the equation is[4]

$$j = \frac{4}{9} \epsilon_0 \sqrt{2q/m} \frac{V^{3/2}}{x_0^2} \text{ amp/cm}^2 \tag{6.24}$$

where j is the maximum space charge limited current density
x_0 is the separation between the planes in centimeters
ϵ_0 is the permittivity of free space $(= 8.85 \times 10^{-12})$

and the other variables are as defined earlier. In practical units the current is

$$j = 5.44 \times 10^{-8} \frac{V^{3/2}}{A^{1/2} x_0^{\,2}} \text{ amp/cm}^2 \tag{6.25}$$

and the mass flow is

$$\dot{M} = jm/q \tag{6.26}$$

$$= 5.71 \times 10^{-13} \frac{A^{1/2}\, V^{3/2}}{x_0^{\,2}} \tag{6.27}$$

The thrust will be

$$F = 10^5 \dot{M}c/g \tag{6.28}$$

$$= 102\dot{M}c \text{ grams/cm}^2 \tag{6.29}$$

if c is in kilometers per second and $\dot{M}$ is in grams per square centimeter per second; g in eq. 6.28 is the acceleration of gravity.

The power in the beam is

$$W = jV \text{ watts/cm}^2 \tag{6.30}$$

By suitable algebraic elimination we may obtain a simplified expression for the thrust per unit area

$$\frac{F}{A} = \frac{8}{9} \epsilon_0 \frac{V^2}{x_0^{\,2}} \tag{6.31}$$

$$= 8.01 \times 10^{-10} V^2/x_0^{\,2} \text{ grams/cm}^2 \tag{6.32}$$

Equations 6.31 and 6.32 make clear the fact that the force exerted as the thrust F is truly an electrostatic force. An electrostatic field intersecting a conducting surface exerts a force

$$F/A = \tfrac{1}{2} \epsilon_0 E^2 \tag{6.33}$$

if E is in volts per meter. This is in agreement with eq. 6.31, provided the value of E is taken as ${}^4/_3 (V/x_0)$. The following discussion shows that this is, in fact, the correct value to use and provides a physical interpretation of the electrostatic nature of the resultant force.

The potential distribution between parallel planes separated by a distance x_0, in the absence of space charge is

$$-V/V_0 = x/x_0 \tag{6.34}$$

shown by the straight line in Fig. 6.4. The field at the emitter is $-V_0/x_0$ and that at the accelerator is $+V_0/x_0$. Since these are equal in absolute value, eq. 6.33 shows that the forces on the two electrodes will be equal and opposite, making the net thrust zero in the absence of space charge.

Under space charge limited conditions the potential distribution is

$$-\frac{V}{V_0} = \left(\frac{x}{x_0}\right)^{4/3} \tag{6.35}$$

shown by the curve in Fig. 6.4. The field at the emitter is zero (the essential condition characteristic of space charge limited flow), whereas that at the accelerator is $\frac{4}{3}(V_0/x_0)$, in agreement with the previous paragraph. Since the force on

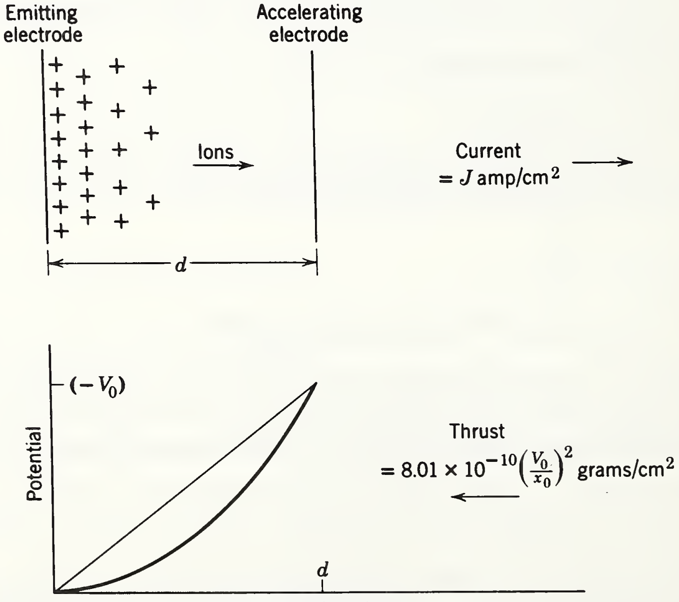
Emitting electrode
Accelerating electrode
Ions
Current = J amp/cm^2
d
$(-V_0)$
Potential
Thrust = $8.01 \times 10^{-10}\left(\frac{V_0}{x_0}\right)^2$ grams/cm^2
d
Distance along beam

Fig. 6.4

the emitter is zero, the net thrust is equal to the force on the accelerator electrode, thus confirming eq. 6.31. The lines of force which start on this electrode terminate on the charges distributed through the intervening space and impart acceleration to them.

Equation 6.31 can be put in the form

$$F = \frac{8}{9}\epsilon_0 V^2 \frac{A}{x_0^2} = \frac{2\pi}{9}\epsilon_0 V^2\left(\frac{D}{x_0}\right)^2 = \frac{2\pi}{9}\epsilon_0 V^2 R^2 \tag{6.36}$$

$$= 6.28 \times 10^{-10}\ V^2R^2 \text{ grams} \tag{6.37}$$

where $R = D/x_0$ may be defined as the "aspect ratio" of the diode emitting-accelerating system; R is the ratio of the (circular) diameter of the emitting area to the accelerating distance x_0.

A parameter useful in vacuum tube studies is the "perveance" P, defined as follows:

$$P = I/V^{3/2} \text{ amp/volts}^{3/2} \tag{6.38}$$

where I is the total space charge limited current which flows when voltage V is applied. The perveance is related to the aspect ratio as follows:

$$P = \frac{\pi}{9}\epsilon_0\sqrt{2q/m}\,R^2 = \begin{cases} 1.83 \times 10^{-6}R^2 \text{ for electrons} \\ 0.37 \times 10^{-3}R^2 \text{ for Cs ions} \end{cases} \tag{6.39}$$

The perveance depends on the shape, but not on the size scale, of the electrode configurations.

To obtain significant amounts of thrust in the useful range of exhaust velocities, R must be much larger than unity.[5] This may be shown by examples: for cesium with $I_s = 5000$ sec the thrust of a beam having an aspect ratio $R = 1$ is 0.0022 gram; the values of R required for thrusts of 1 and 100 grams are 21.4 and 214, respectively.

The maximum value of R which can be used for a single ion beam is about unity.[6,7] The basic reason for this limitation is that the space charge causes the potential within the beam to build up so that ions in the center of the beam are slowed to rest. From various calculations of the maximum perveance achievable in space charge limited beams[7] it can be readily calculated that a theoretical upper limit upon R is approximately 3. Practical considerations limit actual individual ion beams to a lower range of values. It is apparent that an ion beam of large aspect ratio can be produced only by forming a large number of parallel beams, each of which individually has a low aspect ratio. An alternative way of doing this would be to use a grid for the accelerating electrode. In the case of two-dimensional systems having cylindrical symmetry, such as the familiar Pierce gun, the width of the slit aperture d must be limited to $d \lesssim x_0$.

The current densities of cesium,[8, 9] potassium,[10] and rubidium[10] ions which can be produced with low atom-ion ratios by surface ionization on tungsten increase with tungstem temperatures from about 1 ma/cm^2 at 1200°K to 200 ma/cm^2 at 1600°K, all three alkalies giving about the same values. Porous tungsten of the type used in diffuser cathodes shows cesium ion emission comparable with solid tungsten and permits introduction of cesium from the rear. The power radiated from tungsten varies from 1.7 to 7.6 watts/cm^2 over this range, so that the associated ionization energy requirements are 1700 ev/ion at 1 ma/cm^2 and 38 ev/ion at 200 ma/cm^2.[2, 11, 5] The fact that these ionization energy requirements are a sensitive function of the current density makes the efficiency of the engine a sensitive function of its over-all size.

The behavior of an ion beam projected into space is crucially dependent on the value of its aspect ratio. If $R \lesssim 1$, the electric forces produced by the space charge are primarily radial in direction (perpendicular to the ion motion). As the beam expands under the influence of these forces, the radial fields diminish in intensity. The approximate shape of the outer trajectories of such a beam is given by the formula

$$\Theta \sim 0.24R\left(\ln \frac{r}{r_0}\right)^{1/2} \tag{6.40}$$

where r is the radius of the expanded beam
r_0 is the beam radius at the exit orifice
Θ is the angle between the outer trajectory and the axis.

The term in brackets varies so slowly that the beam will proceed many kilometers from the orifice without diverging more than 45° from the axis, if $R \leq 1$.[6]

The statements in the previous paragraph lose validity if ion beams are operated in parallel. If a large number of "narrow" ion flows are merged into a single region within which current density and direction of flow are approximately uniform, the radial fields will be canceled out except for fringe effects near the edge of the beam. Throughout most of the volume of the beam the electric fields will be either parallel or opposite to the direction of ion flow. The one-dimensional solution of the space charge equations which represent this case is well known, the most important feature being that a space charge potential equal to the full acceleration voltage builds up within one acceleration distance, causing the ions to be stopped and reflected back toward the source. This is the "ion turn-around" or "stalling" effect.[12–14, 6]

6.5.2 Charge Neutralization

The successful and efficient operation of an electrostatic propulsion system requires that the ions move off into space without serious loss in energy below the value corresponding to the final exit voltage V_0. The two conditions necessary for fulfillment of this condition are that the net current leaving the space vehicle be zero, and that the potential variations throughout the ion beam be small compared to V_0. The first, or "current neutralization" condition, is easy to achieve and has been repeatedly demonstrated in experiments,[15, 16] but is essentially independent of the second, or "charge neutralization," requirement. The latter exists automatically in a beam for which $R \overset{\sim}{<} 1$, with or without the addition of neutralizing charges, but such narrow beams are of small interest as thrust devices. Charge neutralization of a broad ($R \gg 1$) beam of accelerated ions resulting from addition of electrons in high-vacuum conditions which adequately simulate a space environment is therefore a subject of crucial current interest.

The simplest theoretical solution consists of an electron current density $j_e = -n_e e v_e$ equal to and flowing parallel to the ion current density $j_p = +n_p e v_p$. If v_e equals v_p and j_e equals n_p, the net charge will be everywhere zero, and perfect neutralization will be achieved.

A slight mismatch in initial velocities will cause an excess of one kind of charge at the exit plane. The space potential then fluctuates with a space wavelength $\lambda = 3\pi\sqrt{2m_e/m_p}\,x_0$, where m_e/m_p is the ratio of electron to ion mass and x_0 is the acceleration spacing of the equivalent space charge limited diode required to produce the ion beam.[17-21] For cesium m_p/m_e is 244,000 and λ is $0.027\,x_0$. If the initial electron velocity is more than double that of the ions, the voltage fluctuations in the beam reach an amplitude which brings the electrons to rest. The solution in this case has been discussed but is of small practical interest because the electron energy necessary to match the velocity of cesium ions is $V_0/244{,}000$, or about 0.01 ev if $I_s = 5000$ sec.[18,6] The initial thermal velocities of electrons from a cathode at 1000°K are much higher than this. The solution of the one-dimensional problem just given including a Maxwellian distribution of electron velocities has been investigated and found to involve fundamental complications of a physical nature, leading to the interesting doubt that any steady-state solution exists if the mean velocity of the electron is greater than that of the ions.[19,6] This theory is also probably of only academic interest, however. If neutralization of a 1000-volt beam were achieved with a perfection of 99 per cent, the remaining 10-volt fluctuations in potential would be two orders of magnitude greater than kT.

It appears that any realistic treatment of the charge neutralization problem should deal with the flow of the electrons in three dimensions, and in the presence of variations of space potential of appreciable amplitude, for example, at least several per cent of V_0. The speed of the electrons will then be, as seems inevitable, much higher than that of the ions. When adequate neutralization is achieved, the following conditions will then be fulfilled.

1. $n_e \sim n_p$, that is the charge densities will approximately balance.
2. $\overline{v_e} = v_p$, the drift velocity of the electron cloud will equal the ion velocity.
3. $\overline{j_e} = -j_p$, the net electron current will match the ion current.
4. $j_e \gg j_p$, the circulating current of electrons will be much larger than the ion current.

A positive fluctuation of space potential will produce two effects of opposite nature. First, electrons will be attracted to the positive region; if this effect causes a net increase in n_e, the result will be to reduce the positive fluctuation and to make the system stable. Second, the electrons passing through the region will move faster; if j_e is constant, n_e would thus be reduced. This would lead to a buildup of positive potential, with a tendency toward instability.

The question of how to ensure that the stabilizing tendency predominates over the other under the conditions and in the geometry which exist in a practical propulsion device appears to be essential to the neutralization problem.

A simple case which lends itself to calculation is that in which a thin slab of ions is projected between parallel electron-emitting plates.[20, 6] The electrons, drawn out by the positive ion space charge, move perpendicular to the plates and to the ion velocity. The electron current is assumed to be limited by the usual space charge condition of zero field at the emitter. Hopefully the electrons may also acquire a slight transverse drift parallel to the ion flow, so as to make $\bar{j}_e = -j_p$. Although the solutions to this simple case do not shed light on the last point, the results are instructive. If 2d is the thickness of the slab of ions, and x_0 is the acceleration distance, the potential at the center of the slab is $V_1 = 0.101 d^2 V_0/x_0^2$. This is slightly more than 40 per cent of the potential that would exist at the center of the slab without any electrons. The electron current density is

$$j_e = \frac{\sqrt{2}}{3\pi} \sqrt{M/m}\, \frac{d}{x_0}\, j_p \tag{6.41}$$

For cesium $j_e/j_p \sim 75 d/x_0$. Consideration of this one-dimensional model leads to conclusions as follows:

1. This neutralization system must have a modular size about equal to (or less than) x_0. It does not differ appreciably from the ion acceleration system in respect to the required fineness of structure.
2. The total electron circulating current must be many times the ion current. It appears that power requirements for emission of neutralizing electrons may be serious. Effective means of trapping electrons will be necessary so that the large circulating current can be maintained by injecting an electron current of much smaller magnitude.

It seems clear that any dissipative effects, such as collisions, which exist throughout the volume of the beam, will be stabilizing in nature, but since mean free paths are many meters in length for practical cases, it is difficult to see how such effects can produce results within the turn-around distances of a few millimeters.

6.6 CONCLUSION

It is hoped that this discussion will convey to the reader some of the alluring possibilities which electrical propulsion offers, together with some of the fundamental problems encountered in attempting to produce appreciable mass flows of drifting plasma.

REFERENCES

1. D. B. Langmuir, "Low-Thrust Flight: Constant Exhaust Velocity in Field-Free Space," Space Technology, John Wiley and Sons, New York, 1959, Chapter 9.
2. D. B. Langmuir, "Problems of Thrust Production by Electrostatic Fields," Vistas in Astronautics, Vol. 2, Pergamon Press, London, 1959, pp. 127-136.
3. J. H. Irving, Space Technology, John Wiley and Sons, New York, 1959, Chapter 10.
4. C. D. Child, Phys. Rev., **32**, 498 (1911).
5. J. M. Sellen, H. Shelton, and D. B. Langmuir, "Electrostatic Propulsion Design Principles and Problems," XIth International Astronautical Congress, Stockholm, August 15-20, 1960, RW-RL-175.
6. Ramo-Wooldridge Research Laboratory Staff, "Electrostatic Propulsion," Proc. IRE, **48**, No. 4, 477-491 (1960).
7. J. R. Pierce, Theory and Design of Electron Beams, D. Van Nostrand, Princeton, N. J., 1949, pp. 147-149, 161-164.
8. J. B. Taylor and I. Langmuir, "The Evaporation of Atoms, Ions, and Electrons from Cesium Films on Tungsten," Phys. Rev., **44**, 423-458 (1933).
9. J. B. Taylor and I. Langmuir, "Vapor Pressure of Cesium by the Positive Ion Method," Phys. Rev., **51**, 753-760 (1960).
10. T. J. Killian, "Thermionic Phenomena Caused by Vapors of Rubidium and Potassium," Phys. Rev., **27**, 578-587 (1926).
11. H. Shelton, R. F. Wuerker, and J. M. Sellen, "Generation and Neutralization of Ions for Electrostatic Propulsion," American Rocket Society Meeting, San Diego, Calif., ARS Preprint 882-59, June 1959.
12. C. E. Fay, A. L. Samuel, and W. Shockley, "On the Theory of Space Charge between Parallel Plane Electrodes," Bell System Tech. J., **17**, 49-79 (1938).

13. B. Salzberg and A. V. Haeff, "Effects of Space Charge in the Grid-Anode Region of Vacuum Tubes," *RCA Rev.*, **2**, 336-374 (1938).
14. E. Stuhlinger, "Electrical Propulsion System for Space Ships with Nuclear Power Source," *J. Astronautics*, 149-152(1955); 11-14 (1956).
15. R. C. Speiser, C. R. Dulgeroff, and A. T. Forrester, "Experimental Studies with Small Scale Ion Motors," American Rocket Society Meeting, Washington, D.C., ARS Preprint 926-59, November 1959.
16. J. M. Sellen and H. Shelton, "Space Charge Measurements in Expanding Ion Beams," ARS Semi-Annual Meeting, Los Angeles, Calif., ARS Preprint 1160-60, May 1960.
17. D. B. Langmuir and H. M. Wachowski, "A Note on the Charge Neutralization Problem in Electrostatic Ion Propulsion," ERL-131, October 1, 1958.
18. H. M. Wachowski, "Space Charge Neutralization in Ionic Propulsion—The Single Velocity Case," ERL-LM-171, September 29, 1958.
19. D. A. Geffen and P. Stehle, "Space Charge Neutralization in the Steady State," ERL-125, August 12, 1958.
20. S. Naiditch, et al., "Ion Propulsion Systems Experiment Studies," American Rocket Society Meeting, Washington, D.C., ARS Preprint 928-59, November 1959.
21. H. Mirels and B. M. Rosenbaum, "Analysis of One Dimensional Ion Rocket with Grid Neutralization," NASA TN D-266, 1960.

7

PROPULSION INTERFACE

J. E. Brooks

7.1 INTERFACE CONCEPT

In a general sense, "propulsion interface" means the complete set of interactions between propulsion and the rest of the system. A very significant feature of complex ballistic and space vehicle systems is the large number of interactions between the characteristics and parameters of the various elements of the total system. These interactions become especially important when the fundamental capabilities of such subsystems as propulsion and guidance are pushed to the utmost with very little design margin. Consequently, a fundamental aspect of systems engineering is the explicit consideration of these interactions in the design process. Such an interplay of the most significant parameters is obviously fundamental in the initial formulation of the system configuration, and a proper balance between the various competing factors in the preliminary design is an essential feature of a good system. For example, the main features of the propulsion system, such as thrust level, specific impulse, and propellant characteristics, are of prime importance in the preliminary system design. These features, which involve significant interaction with characteristics of the rest of the system, must be considered quantitatively in the initial system synthesis. However, there are other implicit interactions not so well recognized that must be dealt with on a system basis early in the development program to avoid subsequent difficulties. Hence, the considerable importance given in systems engineering to the "interface concept" and to the corresponding formulation and resolution of interface items.

Once the system has been blocked out, it is generally appropriate to break down the development task into subtasks which usually are designated as subsystems. It is also desirable to arrive at a breakdown that makes these subsystems as independent and self-contained as possible, whether the system development is a broad one, such as the original ICBM programs involving many separate corporations, or whether the development is to be done by a single company or department. For example, a typical liquid rocket ballistic missile system may be broken down into the following areas:

Structure and tankage
Propellant feed
Engine
Flight control
Guidance
Accessory systems (electrical, hydraulic, pneumatic)
Payload
Missile flight safety
Instrumentation (for R and D)

The advantages gained by having specialized groups concentrate on various tasks is obvious. A by-product, however, is the creation of somewhat artificial boundaries, or interfaces, between the various subsystems. These interfaces are particularly significant when the subsystem developers are separate companies. An important example is the customary breakdown of the propulsion function into an engine and a propellant feed subsystem. This is such a standard practice for liquid rockets that, generally, "engine interface" will be discussed here rather than "propulsion interface."

Thus the term "interface," when used in the system sense, refers specifically to interactions between the characteristics of one subsystem and those of one or more of the other subsystems. The distinguishing feature of this subclass is that these interactions are not the sole concern of any one development team. Therefore, the corresponding technical resolutions must be formulated at the outset of the main development effort to avoid later disruption of the various subsystem development programs. It is this type of system problem that we are most concerned with when we speak of interface

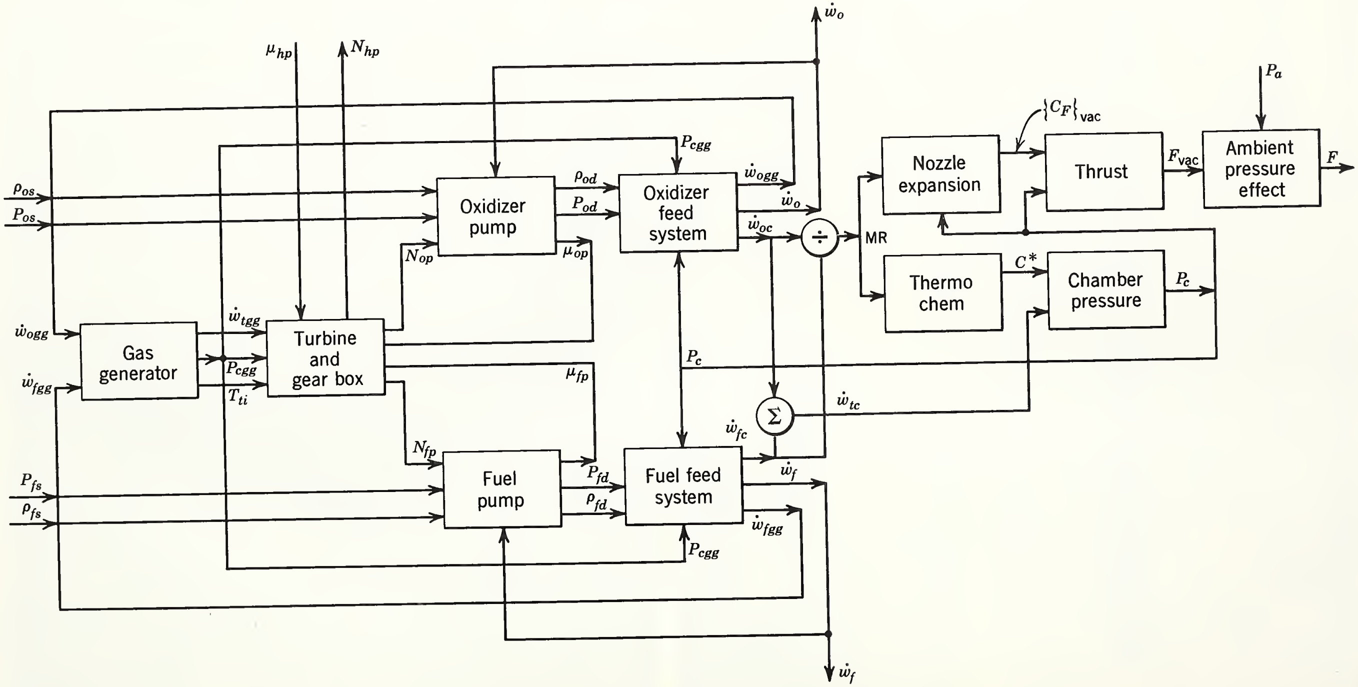
μ_{hp}
N_{hp}
$\dot{w}_o$
P_a
$\{C_F\}_{vac}$
P_{cgg}
ρ_{os}
P_{os}
Oxidizer pump
ρ_{od}
P_{od}
Oxidizer feed system
$\dot{w}_{ogg}$
$\dot{w}_o$
$\dot{w}_{oc}$
N_{op}
μ_{op}
÷
MR
Nozzle expansion
Thrust
F_{vac}
Ambient pressure effect
F
Thermo chem
C^*
Chamber pressure
P_c
$\dot{w}_{tgg}$
$\dot{w}_{ogg}$
Gas generator
$\dot{w}_{fgg}$
P_{cgg}
T_{ti}
Turbine and gear box
P_c
μ_{fp}
Σ
$\dot{w}_{tc}$
$\dot{w}_{fc}$
N_{fp}
Fuel pump
P_{fd}
ρ_{fd}
Fuel feed system
$\dot{w}_f$
$\dot{w}_{fgg}$
P_{fs}
ρ_{fs}
P_{cgg}
$\dot{w}_f$

Fig. 7.1 Interrelation diagram for single-chamber liquid rocket engine.

SYMBOLS FOR FIGURE 7.1

C^*	Characteristic velocity
$\{C_F\}_{vac}$	Vacuum thrust coefficient
F	Chamber thrust under ambient pressure
F_{vac}	Chamber thrust under vacuum
MR	Mixture ratio
N_{fp}	Fuel pump speed
N_{hp}	Hydraulic pump speed
N_{op}	Oxidizer pump speed
P_a	Ambient pressure
P_c	Chamber pressure
P_{cgg}	Gas generator pressure
P_{fd}	Fuel pump discharge pressure
P_{fs}	Fuel pump suction pressure
P_{od}	Oxidizer pump discharge pressure
P_{os}	Oxidizer pump suction pressure
T_{ti}	Turbine inlet temperature
$\dot{w}_f$	Total fuel mass flow rate
$\dot{w}_{fc}$	Chamber fuel mass flow rate
$\dot{w}_{fgg}$	Gas generator fuel mass flow rate
$\dot{w}_o$	Total oxidizer mass flow rate
$\dot{w}_{oc}$	Chamber oxidizer mass flow rate
$\dot{w}_{ogg}$	Gas generator oxidizer mass flow rate
$\dot{w}_{tc}$	Total chamber propellant mass flow rate
$\dot{w}_{tgg}$	Total gas generator mass flow rate
μ_{fp}	Fuel pump torque
μ_{hp}	Hydraulic pump torque
μ_{op}	Oxidizer pump torque
ρ_{fd}	Fuel pump discharge density
ρ_{fs}	Fuel pump suction density
ρ_{od}	Oxidizer pump discharge density
ρ_{os}	Oxidizer pump suction density

items. There are also routine items, involving relatively straightforward coordination rather than problem solving, that are classified as interface because of their connection with an arbitrary physical boundary. These routine items are easier to deal with and are not as significant as the implicit functional interactions.

7.2 SYNTHESIS OF SYSTEM INTERFACES

Successful handling of interface items that create system design problems requires technical competence and thorough knowledge of all the subsystems involved and their associated design problems. Invariably such system design problems cut across more than one technical discipline. The very concept of a "functional" interface rather than a physical one is significant because many subsystem characteristics important in the design of other elements in the system are customarily linked with subsystem design problems and interactions are apparent only when a detailed functional description of the system is given. Analytical models of the various subsystems which can be combined into a total system synthesis are useful in this connection. The emphasis is placed on input-output relationships and on the significant parameters or disturbance variables that affect these relationships. An example of such a model for a liquid rocket engine is blocked out in Fig. 7.1. Each internal input-output block represents a set of theoretical and/or empirical relationships as required. The understanding of such detailed relationships between the physical variables is the basis for thorough knowledge of the engine and is essential in the interpretation of test data for engine evaluation. The corresponding interrelation diagram for the missile system is shown in Fig. 7.2 where the individual subsystem models are combined.

A diagram representing an analytical system model is different from general system block diagrams because it shows relationships between specific physical variables rather than simply indefinite influences. Thus the systems engineer can achieve a comprehensive understanding and identification of significant interactions. In particular, such diagrams indicate the physical quantities that should be measured and how such data may be interpreted to evaluate the significant relationships throughout the system.

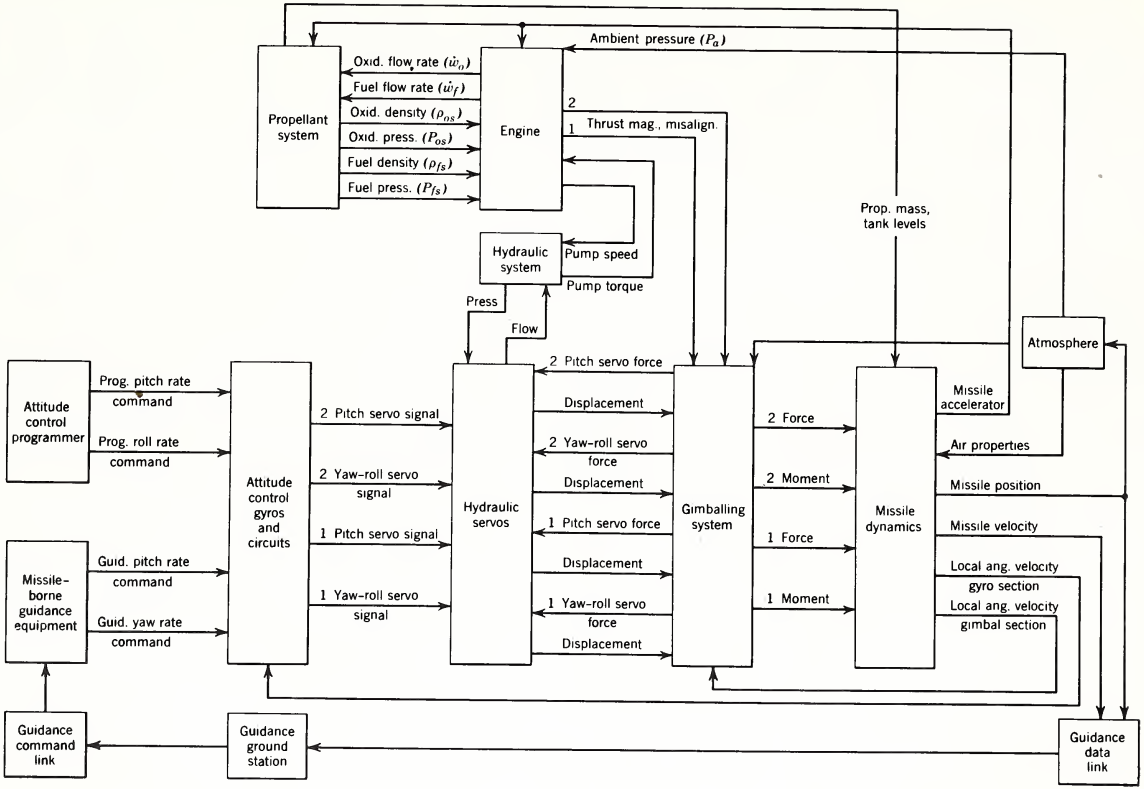

Propellant system
Engine
Oxid. flow rate ($\dot{w}_o$)
Fuel flow rate ($\dot{w}_f$)
Oxid. density (ρ_{os})
Oxid. press. (P_{os})
Fuel density (ρ_{fs})
Fuel press. (P_{fs})
Ambient pressure (P_a)
2
1
Thrust mag., misalign.
Hydraulic system
Pump speed
Pump torque
Press
Flow
Prop. mass, tank levels
Atmosphere
Attitude control programmer
Prog. pitch rate command
Prog. roll rate command
Missile-borne guidance equipment
Guid. pitch rate command
Guid. yaw rate command
Attitude control gyros and circuits
2 Pitch servo signal
2 Yaw-roll servo signal
1 Pitch servo signal
1 Yaw-roll servo signal
Hydraulic servos
2 Pitch servo force
Displacement
2 Yaw-roll servo force
Displacement
1 Pitch servo force
Displacement
1 Yaw-roll servo force
Displacement
Gimballing system
2 Force
2 Moment
1 Force
1 Moment
Missile dynamics
Missile accelerator
Air properties
Missile position
Missile velocity
Local ang. velocity gyro section
Local ang. velocity gimbal section
Guidance command link
Guidance ground station
Guidance data link

Fig. 7.2 Typical missile system utilizing two-chamber liquid rocket engine.

7.3 ENGINEERING OF INTERFACE PROBLEMS

Once the over-all interface picture is understood and formulated in the context of the total system design problem, a corresponding engineering effort is in order. More and more it has been recognized that an organizational systems engineering responsibility and activity is required to initiate, coordinate, and direct this program. The interface items must be identified for each development team, and the first approximations for achieving compatibility specified. As the system design progresses, these initial approximations will be refined and additional interface items identified. Thus the systems engineering is not static but is a continuously evolving effort of system evaluation and design decision. A large development program involving several corporations naturally imposes peculiar contractual and organizational problems.

Part of the basic problem in a large-scale systems development is disseminating engineering information and achieving coordinated direction of the total program. This is particularly necessary in the area of interface problems, for specialists in one subsystem area may not be aware of developments in the rest of the system. Working documents often prove useful and take the form of data books and subsystem integration information. Ultimately, the coordinated results of the interface engineering effort must appear in the appropriate contractually binding specifications, which generally take the form of system criteria documents. The implications to each subsystem are then covered in the corresponding procurement specification package.

7.4 SYSTEM PERFORMANCE AND TRAJECTORY CONSIDERATIONS

In the preliminary design phase for a complex system, an optimum solution is sought by comparing various grossly defined design configurations. Comparisons are usually sufficiently accurate if only "design-point" operation of the system—that is, operation with all quantities at some nominal or average value—is considered. In the final design, however, it is necessary to consider the performance degradation caused by "off-design-point" operation. Stated another way, there must be a satisfactory compromise between restrictive tolerances on the one hand and performance degradation on the other. An important example of this is found in the interface area where the effect of engine tolerances and uncertainties on system range capability must be considered.

When a mission has been assigned, the over-all performance problem for either a ballistic missile or a space vehicle is generally defined as follows. Starting from a designated launch site on the earth, the payload must be transported to a selected (moving) target in inertial space with some required (statistical) accuracy. For an orbital vehicle there is a corresponding performance problem, but for this vehicle it is associated with three position components and three velocity components. In the ballistic missile problem, the target is thought of as located at some particular latitude, longitude, and altitude.

In order to define the performance of a flight from a given launch site to a specific target, the terminal statistics--that is, the miss distance at some appropriate probability limit—must be examined. If we are concerned with maximum performance from a given launch site for targets of greater and greater ranges, the degradation in terminal statistics caused by propellant depletion must be examined. The range capability is then defined as those ranges for which the terminal statistical characteristics do not deteriorate outside of acceptable limits as a result of propellant depletion. In practice this amounts to defining maximum range capability as the range achievable with some high probability such as 0.99-0.999; otherwise terminal statistics would show an unacceptable deterioration from those that the guidance system is capable of.

In turn, defining maximum range capability gives rise to a system optimization problem in which the maximization criteria are not expressed in terms of design-point determination but in terms of statistical dispersion characteristics. These trajectory dispersion characteristics arise for a given target as a result of the variations in external conditions and in many parameters throughout the system. The resulting range distribution function can be derived in terms of the statistics of system tolerances and in terms of certain adjustable parameters. The optimum design then corresponds to selection of these parameters to give maximum range at the required probability.

Since acceleration and mass consumption will directly affect trajectory kinematics, so also will variations in thrust and specific impulse from their nominal values cause a corresponding dispersion in the trajectory. In addition to a significant effect on range statistics, these dispersions are important because they affect such factors as aero heating, structural loads, radar look angle, dynamic pressure at staging, re-entry angle, etc. Therefore, these variables must be restricted to stay within allowable design conditions called trajectory constraints. Thus tolerances on thrust and specific impulse are important in the trajectory synthesis problem; that is, it is necessary to establish definite nominal values for these quantities with variations about such nominals restricted to acceptable values. The process for adjusting engine thrust and flow rates to some range under standard conditions is called "engine balancing." The determination of quantitative results that make possible the prediction of a given engine's operation under various conditions is called "engine calibration." As prelaunch conditions and variations during flight must be taken into account, an analytical engine model is required to predict thrust and flow rates in terms of varying input conditions. Thus an important interface item exists in regard to engine balance and calibration requirements.

7.5 PROPELLANT UTILIZATION AND MIXTURE RATIO CONTROL

In bipropellant liquid rockets range dispersions arising from engine tolerances are influenced more by the effect of mixture ratio variations on propellant utilization than by thrust and specific impulse variations. For ideal propellant utilization, fuel and oxidizer consumption must be regulated so that both propellants are depleted to their respective minimum usable levels at the same time or to within some acceptable tolerance. For the systems discussed here this ideal ratio is difficult to achieve because small deviations between loaded mixture ratio and engine consumption mixture ratio will result in significant amounts of propellant outage. Outage is the amount of one usable propellant remaining when the other has been depleted to its minimum level. To illustrate, let

2.25 = loaded mixture ratio of usable oxidizer/usable fuel
112,500 lb = usable oxidizer loaded
50,000 lb = usable fuel loaded

It is assumed that a predicted in-flight average engine mixture ratio of 2.25 has been exactly loaded. Now, suppose the prediction of in-flight average engine mixture ratio (based on engine balance and calibration data) was high by 2 per cent (i.e., 2.295). Thus 112,500 lb of oxidizer would be combined in flight with 50,000/1.02 or 49,020 lb of fuel, leaving an outage of 980 lb of fuel. This outage corresponds to a shortened burning time, or is equivalent to a substantial amount of "dead weight." On the other hand, if the prediction were 2 per cent low (i.e., 2.205, which in general is equally as probable as 2 per cent high), an outage of 0.02 (112,500) or 2250 lb of oxidizer would be obtained. This example illustrates two salient features of the outage control problem.

1. The in-flight average engine mixture ratio must be predicted or controlled to "instrumentation" accuracy to prevent excessive outage.
2. The effect of a given prediction error in mixture ratio is more pronounced when it results in outage of the propellant required in the larger quantity.

Thus, in order to determine the correct amount of propellant to be loaded, a stringent interface requirement is placed on the engine in regard to mixture ratio predictability. In other words, an engine model is required to predict launch and in-flight variations, engine balance must be accomplished to establish a nominal mixture ratio for the engine, and tolerances must be established for mixture ratio statistics relative to repeatability. A high degree of loading accuracy is also required.

To compensate for an unfavorable outage, it is possible to off-load from the predicted mixture ratio to bias the statistics against this situation. Such an off-load quantity may be considered as an optimization parameter to be selected in terms of some system criterion, such as minimum outage or maximum range at a desired probability.

The inherent accuracy limitations of an open-loop outage control system based on mixture ratio predictability can be eliminated by a closed-loop propellant utilization system. In such a scheme, propellant sensors and a computer are used to determine any deviation from the desired program in propellant utilization. Such a derived error is used to operate a control feature in the engine, thus correcting its consumption mixture ratio to the programmed ratio. In designing such a system, a mixture ratio operating range, feedback gain, sensor accuracy, computer capability, and other factors must be considered. To achieve as simple and reliable a system as possible, only the capability that is required to cope with realistic error situations should be included in the design. Thus the various effects caused by trajectory dispersion must be studied.

Changes in thrust and specific impulse that are coupled with mixture ratio variations resulting from propellant utilization present a special problem. Such changes must be held to acceptable limits by proper system design, resulting in interface requirements on the engine that, for closed-loop outage control, can be met only if the designer has a comprehensive analytical understanding of engine operation. There is also the hardware interface requirement for in-flight feedback adjustment of engine mixture ratio.

7.6 THRUST VECTOR CONTROL BY GIMBALING

The basic principles of flight control by means of thrust vector gimbaling are discussed in Chapter 16, so this section will consider only the gimbaling characteristics of the engine system which create a number of significant interface items.

The total angular travel of the gimbaled chamber must be specified early in the design of the engine because of its fundamental role in determining engine geometry. The value for this total angular travel is set by the control requirement for overcoming the maximum disturbing moment on the missile during flight. This moment arises mainly from wind and aerodynamic effects in conjunction with thrust unbalance and misalignment. Since the missile is basically unstable, a disturbing moment in excess of that produced by maximum gimbaling could not be overcome by the control system and would cause the missile to tumble to destruction.

Other important geometry interface requirements concern engine alignment. If the thrust vector is misaligned from its nominal position, a disturbing moment and side force will result and can be corrected only by the control system after an attitude error has been produced. The effect is to cause a dispersion away from the desired flight path. The thrust vector alignment is particularly important in the initial launch transient in order to achieve proper clearance relative to the launcher. Thus there are interface requirements for alignment of the engine frame to the missile, alignment of the thrust chamber relative to the engine frame, and alignment of the thrust vector relative to the chamber. Similarly, there are requirements for the location of the gimbal point and the point of action of the thrust vector relative to the chamber, but such effects are usually not very significant. The alignment tolerance of the chamber must take into account any structural deflections under thrust loading.

The missile flight stability problem is a complex one that requires a comprehensive analytical model of all the important elements involved. In particular, the characteristics of the gimbaling servos must be known. These are affected by such inertial properties of the gimbaled chamber as moment of inertia, mass, and center of gravity location. Gimbal-bearing friction and backlash are other interface items that can also be important at low amplitude.

An even more important dynamic characteristic of the gimbaling system in regard to flight stability is the effect of compliance in the engine structure support arrangement for the servos. The natural resonance of this servo back-up spring with the chamber inertia can create significant dynamic effects in the effective servo transfer function. Thus there is an important or even critical interface requirement in regard to the engine frame-chamber natural frequency, which is usually the elastic mode of lowest frequency. Engine frame stiffness must be sufficient to maintain this frequency above some satisfactory value.

Rapid gimbaling of the chamber and oscillations of the missile will produce dynamic loads upon the chamber. Such motions must, of course, be specified as part of the interface data in order to estimate the corresponding engine structural loads. In practice, the chamber must be capable of surviving a hard-over actuation arising from servo failure.

7.7 TRANSIENT OPERATION

The most critical part of engine operation from the reliability point of view are start and shutdown transients. In addition, these transients are important for their interface effects.

Structural dynamic effects must be considered carefully to determine the corresponding loads. The launcher structure as well as the missile must be considered as elastic so that the suddenness of thrust build-up is significant in setting the magnitude of dynamic loads. In addition, the release mechanism and timing in relation to the thrust build-up transient are important, and necessitate certain specifications for thrust build-up characteristics. Limits must be set on the time rate of change for maximum thrust and/or times to build up to particular thrust levels.

The unbalance moment for a dual-chamber engine during transients can give the missile disturbing moments that are not desired. Thus this effect is usually specified to remain below some acceptable level.

Of particular importance are the shutdown characteristics in relation to velocity accuracy requirements. The residual impulse derived from the engine after the shutdown command is given must be predictable to within limits required for burnout velocity control. In general, some sort of vernier thrust phase is used to attain the accuracy required for ballistic missiles or space vehicles.

Some radio guidance schemes make use of ‘‘dead reckoning’’ calculations during the vernier phase, updating filtered radar data by using computer simulation of the response of the missile to guidance commands. Such a scheme requires predictability within certain limits of vernier acceleration and thus thrust, representing still another interface requirement on the engine.

Considering the engine and propellant feed as separate subsystems involves a corresponding interface. Thus transient hydraulic dynamic effects in the suction feed lines, such as pressure surges or oscillations, are interface items, and the net positive suction head required for pump-fed engines must be specified for both the transient condition and steady operation.

7.8 STAGING PROBLEMS

As discussed in Chapters 8 and 9, before firing the second- or third-stage engine, the engine of the preceding stage must be shut down and the structure housing that engine must be mechanically separated from the missile or vehicle. Staging thus creates many equipment design problems because, even though the expended stage is useless, the shutdown of its engine must be carefully controlled. Not only must a damaging explosion be avoided, but the shutdown transient must not produce unwanted disturbances. Furthermore, shutdown should be essentially complete before the connecting bolts between the stages are exploded; otherwise some undesirable bumping may occur.

To avoid the possibility of an explosion when the next engine starts, separation or some protection is required. Separation is more efficient when the thrust is applied to the lighter, expended stage. On the other hand, if the separating thrust is applied to the new stage, some needed suction head will be produced for the engine if it is pump-fed. During the low- (or zero) thrust period, the flight control system will probably be unable to maintain a stable attitude. Thus the staging sequence must often be completed within a short acceptable period, usually a few seconds. However, if a coast period is desired, then an effective attitude control system must be designed.

Perhaps the most critical part of the staging process during the flight of a liquid rocket engine is the engine start under low-thrust conditions. If a zero-thrust period is experienced, any drag will tend to cause the propellant to leave the aft end of its tank. With a cryogenic propellant, a zero-thrust period causes cavitation, with a gaseous condition in the pump suction inlet, and leads to improper flow of propellants to the chamber with the possibility of a disastrous explosion. Cavitation can be avoided by special design features such as a positive displacement feed for starting propellants, the addition of solid propellant rockets to maintain thrust during the staging period, etc. Solid propellant engines, of course, are not susceptible to this critical start problem.

The proper sequence for the staging events must be determined as a compromise between too short a separation distance at engine start and too much attitude error caused by the delay in reinstating thrust vector control. The uncertainties in the engine shutdown transient and in the subsequent engine start transient are very important to this problem. Accordingly, interface requirements are specified to limit the dispersion in these transients to acceptable limits. Since it may be difficult to control these characteristics tightly, the staging sequence should be designed to be as insensitive as practical to the engine transient time histories. This is particularly true with regard to shutdown which is very sensitive to altitude conditions. Consequently, applicable experimental altitude data cannot be obtained from prior ground testing.

7.9 SUPPORT SYSTEM CONSIDERATIONS

Many other interface problems are associated with ground activities in support of ballistic missile or space vehicle launchings, becoming particularly complex for fast-reacting military weapon systems, for which there must be clearly developed operational support concepts for maintenance, logistics, human engineering, and tactics.

Illustrative of the relationship between support concepts and engine design is the fact that engine calibration is usually invalidated by the replacement of a major element, such as a pump for a liquid rocket, unless interchangeability has been implemented in the development program. Similarly, decontamination of the thrust chamber after firings or transportation may be required unless techniques or design features are clearly specified and satisfied in the development program.

Accessibility to the engine after installation within the vehicle must always be taken into account during development. Lack of easy accessibility may give rise to complicated missile separation requirements for a staging vehicle having an internal engine. For safety, the amount of allowable propellant leakage must also be specified.

Support system interactions are especially important during the launch operation. Checkout capability, integrated sequencing, the start system, monitoring and shutdown capability, and umbilical release are the design problems to be considered here.

Checkout includes checks on electrical circuitry, operation of valves, igniter continuity, sequencing, and even checks on checkers. All must be thought out in terms of the over-all concept for the system and translated into suitable ground operating equipment requirements. These considerations may, in turn, affect air-borne design. For example, to execute a countdown check on the guidance and control systems may involve gimbaling the engine, which creates a need for a compatible injector manifold arrangement to protect the injector from contamination by propellant sloshing.

The sequencing of the countdown is strongly influenced by engine firing requirements which involve such factors as bleeding of engine control systems, bleeding of pumps, pressurization of tanks, bleeding of boil-off and appropriate prefire temperature control for cryogenic propellants, and purging to obtain proper ignition conditions. There may also be requirements for filling thrust chamber jackets and release time requirements for umbilical connections. Furthermore, the kind of start system utilized and the associated requirements for special ground equipment must be considered.

The engine firing sequence is of such critical importance that special monitoring is generally desirable. Thus, if certain events do not take place in the proper sequence, a shutdown occurs. However, to return the missile to a safe condition, this shutdown capability, in turn, must be integrated with a recycling requirement on the entire launch control ground equipment.

The problem of engine ground support equipment is accompanied by special difficulties in a vehicle development program. Usually an extensive static firing program is required to integrate the engine properly into the airframe system, leading to many changes of the engine and of the start and ground operating equipment. Such changes should move toward design simplification and improved reliability, resulting finally in equipment and associated circuitry that is easy to service and replace. Basic elements or "building blocks" should be utilized and incorporated to achieve a patch board flexibility similar to that of general-purpose analog computers.

Any support system must also include requirements for loading propellants, and, if possible, loading is done in advance of the launch sequence. Loading accuracy is closely associated with outage control, and the requirements would be very stringent without a closed-loop propellant utilization system. Consideration must also be given to the effect that variations in propellant density have on engine operation. A suitable compromise must be made between environmental control by the support system, the compensation mechanism in the engine, and allowable shifts in engine operating characteristics. As another example, a fast-load capability is required for an operational fast-reaction weapon with cryogenic propellants, or air-borne weight and complexity penalties must be accepted from elaborate insulation devices.

8

FUNDAMENTAL FLIGHT DYNAMICS AND STAGING*

Albert R. Hibbs

8.1 VACUUM VELOCITY LAW

The vacuum velocity law can be derived from the law of conservation of momentum under the following assumptions.[1]

1. Only jet forces are acting.
2. The speed of ejected gas is adequately represented by a constant.
3. Acceleration of the motor case multiplied by time of motion of the gas through the burning chamber is small compared to the exhaust velocity.

A mathematical derivation will be carried out, using the following nomenclature:

m_b = mass of rocket after burning,
μ = mass of propellant ejected at time t,
μ_b = total mass of propellant ejected,
m_0 = total mass of rocket (before burning).

To show their relations,

$$m_0 = m_b + \mu_b \tag{8.1}$$

---

*This paper presents the results of one phase of research carried out at the Jet Propulsion Laboratory, California Institute of Technology, under Contract No. NASw-6, sponsored by the National Aeronautics and Space Administration.

$$m = m_0 - \mu \tag{8.2}$$

During the time interval dt, the mass $d\mu$ is ejected at a speed V_e relative to the rocket, and the rocket gains speed dv.

Just before dt, the momentum is

$$mv = (m_0 - \mu)v \tag{8.3}$$

Just after this time interval, the rocket and remaining propellant have the momentum

$$(m_0 - \mu - d\mu)(v + dv) \tag{8.4}$$

whereas the momentum of the ejected gas (with reference to a fixed frame) is

$$d\mu\,(v - V_e) \tag{8.5}$$

Since the momentum must be conserved,

$$(m_0 - \mu)v = (m_0 - \mu - d\mu)(v + dv) + d\mu(v - V_e)$$

saving only first-order terms gives

$$m\,dv = V_e\,d\mu \tag{8.6}$$

and integrating from the point $t = 0$, $v = 0$, $\mu = 0$ gives

$$v = V_e\,L_n\,\frac{m_0}{m_0 - \mu} \tag{8.7}$$

The exhaust speed V_e multiplied by the total mass of propellant ejected μ_b is called the "total impulse" of the rocket. It is the total momentum given to the propellant with reference to the rocket. Total impulse is an important parameter describing the performance of the propulsion system. One measure of the performance of the fuel used in the system is obtained by dividing the total impulse by the total weight of fuel available. This gives the "specific" impulse as

$$I_{sp} = \frac{V_e\,\mu_b}{w_b} = \frac{V_e}{g} \tag{8.8}$$

where w_b = weight of propellant
g = acceleration due to gravity

To achieve a large velocity gain, multiple-stage rockets are used. From a two-stage rocket, the total vacuum velocity gain under no gravity is

$$V = V_{e_1} L_n \frac{W_0}{\nu_1(W_0 - W_p) + W_{p_1}} + V_{e_2} L_n \frac{W_{p\,1}}{\nu_2(W_{p_1} - W_{p_2}) + W_{p_2}} \tag{8.9}$$

where W_0 = initial weight
W_{p_i} = payload weight of ith stage
ν_i = structure factor of ith stage

Let us investigate the optimum size arrangement between stages. It is assumed that exhaust velocities and structural factors are constant. To establish an optimum, let W_0/W_{p_2}, the over-all mass ratio, be a constant C, and we will vary W_{p_1} in order to obtain the maximum value of V.

Write

$$\frac{W_0}{W_{p_1}} = r_1 \tag{8.10}$$

$$\frac{W_{p_1}}{W_{p_2}} = r_2 \tag{8.11}$$

Then $r_1 r_2 = C$, and the stationary value is given by the solution of

$$\frac{\partial V}{\partial r_1} = 0 = V_{e_1}(1 - \nu_1)[\nu_2(r_2 - 1) + 1] - V_{e_2}(1 - \nu_2) - V_{e_2}(1 - \nu_2)[\nu_1(r_1 - 1) + 1] \tag{8.12}$$

If V_{e_1} equals V_{e_2} and ν_1 equals ν_2, this gives $r_1 = r_2$, and the velocity contribution from each stage is the same. For more general conditions, write $V = V_{e_1} L_n f_1 + V_{e_2} L_n f_2$, so that

$$f_i = \frac{r_i}{\nu_i(r_i - 1) + 1} \tag{8.13}$$

and write

$$\rho_i = \frac{\nu_i}{1 - \nu_i} \tag{8.14}$$

Then

$$f_i \nu_i = \frac{1}{1 + \rho_i/r_i} \tag{8.15}$$

The solution then takes the form

$$V_{e_2}\frac{r_1}{\rho_1} = \frac{1}{2}\left\{(V_{e_1} - V_{e_2}) + \left[(V_{e_1} - V_{e_2})^2 + \frac{4C}{\rho_1\,\rho_2 V_{e_1} V_{e_2}}\right]^{1/2}\right\} \tag{8.16}$$

and r_2 is obtained by interchanging all 1's and 2's. The term under the radical is the same for both r_1 and r_2. Let us call the radical K. Then

$$r_1 = \frac{\rho_1}{2V_{e_2}}\,(V_{e_1} - V_{e_2} + K) \tag{8.17}$$

$$r_2 = \frac{\rho_2}{2V_{e_1}}\,(V_{e_2} - V_{e_1} + K) \tag{8.18}$$

If V_{e_1} equals V_{e_2}, then r_1/ρ_1 equals r_2/ρ_2 and the mass ratios f are related to the structure factors ν by

$$\frac{f_1}{f_2} = \frac{\nu_2}{\nu_1}$$

for maximum velocity gain. If V_{e_1} does not equal V_{e_2}, the optimum condition is

$$\frac{f_1}{f_2} = \frac{\nu_2}{\nu_1} \cdot \frac{V_{e_1} - V_{e_2} + K}{V_{e_2} - V_{e_1} + K} \tag{8.19}$$

Since small values of ν and large values of V_e are characteristic of more efficient propulsion systems, this result says, in general, that the more efficient stages should have the larger mass ratios, and consequently larger contributions to the total velocity gain.

8.2 VERTICAL FLIGHT NEAR THE EARTH'S SURFACE

In deriving the vacuum velocity law, two factors have been omitted which are important near the earth's surface: gravity and air. To show how these factors affect the simplest type of motion, consider the flight of a vertical sounding rocket. The equation of motion is

$$m\frac{dv}{dt} = T - mg_0\left(\frac{r_0}{r}\right)^2 - \frac{\rho}{2}C_D S v^2 \tag{8.20}$$

where m = mass at time t
v = vertical speed = dr/dt
T = thrust at time t, a function of r and t
g_0 = acceleration due to gravity at the surface
r_0 = distance from the center of the earth to the surface
r = distance from the center of the earth to the rocket
ρ = density of the air, a function of r
C_D = drag coefficient, a function of r and v
S = frontal area of the rocket

The thrust measured in a static test stand is equal to $V_e\, d\mu/dt$, the exhaust velocity times the mass flow rate, but it depends on ambient pressure. Therefore, as the rocket rises through the atmosphere, the thrust varies.

8.3 MOTION OVER A SPHERICAL NONROTATING EARTH

In a description of the flight of a rocket over a spherical earth, it is convenient to use a cylindrical coordinate system (Fig. 8.1) fixed at the center of the earth. If the rotation of

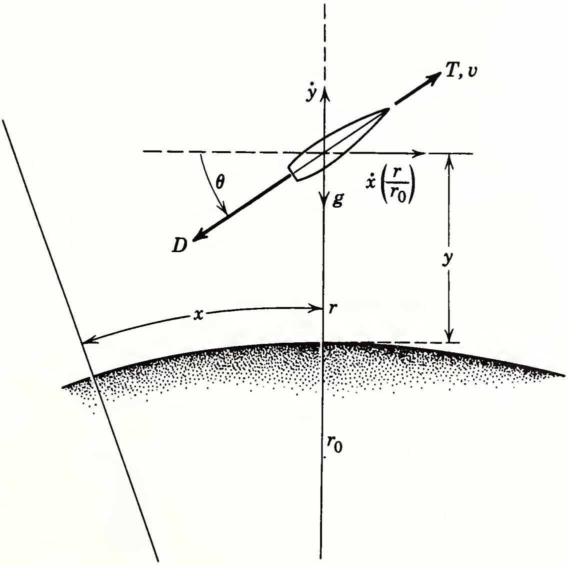

Fig. 8.1

the earth is neglected, the motion lies in a plane, and the two coordinates, r and ϕ, describe its position. The angle θ is is the angle between the direction of the velocity vector and the local horizontal.

Then the equations are

$$\frac{dv}{dt} = \frac{T - D}{m} - g \sin\theta \tag{8.21}$$

$$\frac{d\theta}{dt} = \left(\frac{v}{r} - \frac{g}{v}\right) \cos\theta \tag{8.22}$$

$$D = \frac{\rho}{2} C_D S v^2 \tag{8.23}$$

The first equation results from resolving the forces along the direction of the velocity vector. It is assumed that the thrust direction is exactly parallel to the instantaneous velocity, which implies that the rocket is being continually pitched over to follow its curving trajectory. Such a burning program is called a "gravity turn."

The second equation represents the resolution of forces perpendicular to the direction of the velocity vector. The first term is the centrifugal force divided by v since $v \cos\theta = rw = r\, d\theta/dt$. The gravitational acceleration is not a constant but is $g = g_0(r_0/r)^2$, where g_0 is the acceleration at the surface ($r = r_0$).

It is often convenient to define two other variables, x and y, where y measures altitude above the surface and x measures the curvilinear distance along the surface from the launch point to a point under the rocket (i.e., the range). These two quantities are defined by

$$\dot{x} = \frac{r_0}{r} v \cos\theta \tag{8.24}$$

$$\dot{y} = v \sin\theta \tag{8.25}$$

Although the gravity turn trajectory is very convenient to represent mathematically, alternate burning programs are often more useful. For launching of a satellite or an interplanetary probe, more optimum burning programs can increase the payload capacity of a given vehicle.

As already pointed out, the effect of the earth's rotation has been neglected. For most rockets during their burning phase, this effect can be introduced as a differential correction added on at the end of burning. However, if the rocket travels during burning over a distance comparable to the earth's radius, rotational effects become large enough to be included in the basic equations of motion.

8.4 MOTION IN AN INVERSE SQUARE FIELD

Once burning is terminated, only aerodynamic forces and gravity affect the motion of the missile. The aerodynamic forces will be neglected, although they have interesting consequences, even for satellite motion. It will be assumed that the gravitational field is central. That is, assume the central body (e.g., the earth) is spherical in its mass distribution and is the only body other than the missile in the universe. Furthermore, it will be assumed that the mass of the missile is negligible compared with the mass of the central body.

Under these assumptions the motion of the missile lies in a plane passing through the center of force and is conveniently described by the cylindrical coordinates r and ϕ. The gravitational force is represented as

$$F = -\frac{km}{r^2} \tag{8.26}$$

negative since it is directed inward, and inversely proportional to r^2. The constant k is actually GM, where G is the universal constant of gravity and M is the mass of the central body. Resolving the forces along and perpendicular to the radius vector r gives the two equations

$$m\left[\frac{d^2r}{dt^2} - r\left(\frac{d\phi}{dt}\right)^2\right] = -\frac{km}{r^2} \tag{8.27}$$

$$m\left(2\frac{dr}{dt}\frac{d\phi}{dt} + r\frac{d^2\phi}{dt^2}\right) = 0 \tag{8.28}$$

If the second of these is multiplied by r/m, we have

$$\frac{d}{dt}\left(r^2\frac{d\phi}{dt}\right) = 0 \tag{8.29}$$

or

$$r^2 \frac{d\phi}{dt} = H = \text{angular momentum} \qquad (8.30)$$

$$= \text{a constant}$$

Now we write

$$\frac{dr}{dt} = \frac{dr}{d\phi}\frac{d\phi}{dt} \qquad (8.31)$$

which is

$$\frac{H}{r^2}\frac{dr}{d\phi}$$

from the momentum equation. If $u = 1/r$ is substituted, this is

$$\frac{dr}{dt} = -H\frac{du}{d\phi} \qquad (8.32)$$

Furthermore,

$$\frac{d^2r}{dt^2} = -H^2u^2\frac{d^2u}{d\phi^2} \qquad (8.33)$$

Therefore, the first equation of motion can be written

$$\frac{d^2u}{d\phi^2} + u = \frac{k}{H^2} \qquad (8.34)$$

which gives

$$u = \frac{k}{H^2} + A\cos(\phi + \delta) \qquad (8.35)$$

By measuring ϕ from the point of maximum u, we can write this as

$$r = \frac{a(1 - \epsilon^2)}{1 + \epsilon\cos\phi} \qquad (8.36)$$

where

$$\epsilon = \frac{H^2A}{k} \qquad (8.37)$$

$$a = \pm\frac{1}{(k/H^2)(H^2A/k - 1)} \qquad (8.38)$$

This is the equation of a conic section with eccentricity ϵ. If it is an ellipse, a is the semimajor axis.

We have three constants in the equation of motion: k characterizes the strength of the field; H gives the angular momentum; and A is not defined physically. The other important constant, the energy, can be obtained in the following manner. Multiply the first differential equation by dr/dt, the second by $r(d\theta/dt)$, and add. The result can be integrated to give

$$\tfrac{1}{2}mv^2 - \frac{km}{r} = U = \text{constant} \tag{8.39}$$

where

$$v = \text{velocity} = \left[\left(\frac{dr}{dt}\right)^2 + r^2\left(\frac{d\theta}{dt}\right)^2\right]^{1/2} \tag{8.40}$$

This is the energy equation. Then $\frac{1}{2}mv^2$ is the kinetic energy, $-km/r$ is the potential energy, and the constant U is the total energy. In terms of this new constant,

$$\epsilon = \sqrt{1 + (2U/m)(H/k)^2} \tag{8.41}$$

$$a = \pm\frac{km}{2U} \tag{8.42}$$

The equation for r,

$$r = \frac{a(1 - \epsilon^2)}{1 + \epsilon \cos\theta} \tag{8.43}$$

gives an ellipse for $\epsilon < 1$, a parabola for $\epsilon = 1$, and a hyperbola for $\epsilon > 1$. The condition $\epsilon = 1$ is interesting because it makes the division between the orbits that are closed and those that never return. It is given by

$$1 + \frac{2U}{m}\left(\frac{H}{k}\right)^2 = 1 \tag{8.44}$$

or $U = 0$, which means

$$v = \sqrt{2k/r} = \sqrt{2GM/r} \tag{8.45}$$

This particular velocity is called escape velocity. It can be determined in a slightly different way from energy considerations. Suppose that the coasting flight of a missile begins at a distance r_1 from the center of the earth with speed v_1. Suppose that at its maximum distance r_2 its speed is negligible. The energy is conserved; therefore

$$\tfrac{1}{2}mv_1^2 - \frac{km}{r_1} = -\frac{km}{r_2} \tag{8.46}$$

or

$$v_1 = \left[2k\left(\frac{1}{r_1} - \frac{1}{r_2}\right)\right]^{1/2} \tag{8.47}$$

As r_2 approaches infinity, the trajectory approaches an escape trajectory and v_1 approaches $\sqrt{2k/r_1} = v_e$, the escape velocity.

It is interesting to note the speed requirements for travel to the moon starting near the surface of the earth. The ratio of distance to the moon to distance to the earth's surface (from the center) is about 60, so that

$$v_m = \left[\frac{2k}{r_1}\left(1 - \frac{r_1}{r_2}\right)\right]^{1/2} = v_e\left[1 - \frac{1}{60}\right]^{1/2} \simeq v_e\left(1 - \frac{1}{120}\right) \tag{8.48}$$

Thus a trip to the moon requires more than 99 per cent of escape velocity. Furthermore, a trip halfway to the moon requires an injection speed of

$$v \simeq v_e\left(1 - \frac{1}{60}\right) \tag{8.49}$$

The difference is $(1/120)v_e$, or less than 1 per cent of escape speed, which means that a speed error of about 208 mph (on the low side) out of a 25,000-mph total would imply going only halfway to the moon instead of all the way—a range error of 120,000 miles!

Another special speed is worth noting, the speed for a circular satellite orbit at a distance r_1 from the center of a central body. This orbit corresponds to an eccentricity of $\epsilon = 0$; therefore

$$v_c = \sqrt{k/r_1} = \frac{1}{\sqrt{2}}v_e \tag{8.50}$$

8.5 INTERPLANETARY FLIGHT

Travel to the planets requires not only escape from the gravitational field of Earth, but escape with enough excess speed to get out of Earth's orbit around the sun.

After the missile is sufficiently far from Earth that Earth's gravitational pull is small compared with that of the sun, we may consider the orbit as an ellipse around the sun. If the probe, traveling generally in the same direction as Earth, is moving faster than Earth, its sun-centered ellipse will carry it out toward Mars and the further planets. The missile must be launched at the correct time of day for its final motion to be in the same sense as Earth's.

If the missile is launched twelve hours later, its final motion (with respect to Earth) will be opposite to Earth's motion around the sun. Therefore, with respect to the sun, it will be moving more slowly than Earth. Its ellipse will carry it in toward Venus or Mercury.

Consider the first mission, a trip to Mars. If the speed after leaving Earth is great enough, aphelion will be out at the orbit of Mars. If launch takes place at the proper time of the year, Mars will be there to meet the missile. This situation corresponds to the minimum energy (and thus minimum speed) necessary to get from Earth to Mars. The resulting sun-centered trajectory is called the ''Hohmann'' transfer ellipse.

If the speed is greater than this minimum requirement, the missile will cross the orbit of Mars before it reaches aphelion. Again, a proper firing time will be required to make certain that Mars is at the intersection point when the missile goes by. In this circumstance the flight time required from Earth to Mars is less, and the distance between Earth and Mars at the time of intersection is less than that for the minimum-energy case. This fact may be quite important for such problems as communication, where the information rate depends on power loss, that is, inversely as the square of the communication distance.

Let us see what is required to establish a Hohmann ellipse toward Mars. On the average, Mars is about 50 million miles further from the sun than Earth. Thus the transfer ellipse, with perhelion at Earth, 93 million miles out, and aphelion at Mars, 143 million miles out, must have a semimajor axis a of $93 + \frac{1}{2}(50) = 118$ million miles.

Thus the energy is given by

$$U = -\frac{k_s m}{2a} \tag{8.51}$$

This is the energy required after leaving the gravitational field of Earth. The constant k_s is for the sun. Thus the total speed required is found from

$$\tfrac{1}{2}mv^2 - \frac{k_s m}{r_e} = -\frac{k_s m}{2a} \tag{8.52}$$

$$v = \left[\frac{k_s}{r_e}\left(2 - \frac{r_e}{a}\right)\right]^{1/2} \tag{8.53}$$

Now $\sqrt{k_s/r_e}$ is the speed of a body traveling in a circle around the sun at the distance r_e of Earth, in other words approximately the speed of Earth in its orbit, v_E. Therefore

$$\begin{aligned} v &= v_E\sqrt{2 - r_e/a} \\ &= v_E\sqrt{2 - 93/118} \\ &= 1.105v_E \end{aligned} \tag{8.54}$$

Now, since the missile starts on Earth, it has the Earth's speed v_E "for free" as it were. Therefore, all that is necessary is to add an increment of $0.105v_E$. Although this statement is true, it is somewhat misleading. It might be concluded that the total speed requirement is v_e (to escape from Earth) plus $0.105v_E$ (to get to Mars), giving a required rocket performance of

$$v_i = v_e + 0.105v_E \tag{8.55}$$

Actually, this conclusion is wrong. In leaving the gravitational field of Earth, the physical effect is a loss of energy, not speed. Thus, if we start with an initial speed v_i in excess of escape speed, the remainder Δv after leaving Earth's field is obtained from energy considerations

$$\tfrac{1}{2}v_i^2 m - \frac{km}{r_i} = \tfrac{1}{2}(\Delta v)^2 m \tag{8.56}$$

(The potential energy term is missing on the right, since the final r is infinite with respect to Earth.) This equation says

$$(\Delta v)^2 = v_i^2 - v_e^2 \tag{8.57}$$

If Δv is required to be $0.105v_E$, then

$$v_i = \sqrt{v_e^2 + (0.105v_E)^2} \tag{8.58}$$

To put in some numbers,

$$v_e \simeq 25{,}000 \text{ mph}$$
$$v_E \simeq 66{,}000 \text{ mph}$$

Thus

$$v_i \simeq 26{,}000 \text{ mph}$$

The improper addition of velocities instead of energies would have given 32,000 mph for this number.

The numerical constants required for careful work have been given by C. W. Allen.[2]

REFERENCES

1. L. Davis, Jr., J. W. Follin, Jr., and L. Blitzer, Exterior Ballistics of Rockets, D. Van Nostrand, Princeton, N. J., 1958.
2. C. W. Allen, Astrophysical Quantities, University of London, Athlone Press, London, 1955.

9

MISSIONS AND VEHICLE DESIGN

Warren H. Amster

9.1 INTRODUCTION

A rocket vehicle is a transportation device which differs from most other transportation equipment in several important respects. The vehicle, or portions of it, is expended in flight so that design and operations must be based on one-time use. Usually the vehicle configuration and the major subsystems are specifically designed to meet the special requirements of particular missions. In some cases major design features are incorporated for one particular flight. The design of rocket vehicles is, therefore, more closely related to the requirements of specific missions than is true of most other transportation vehicles. This chapter covers methods of determining approximate requirements for space missions within the solar system, and shows how these requirements influence the design of vehicles.

Most rockets to date have used the energy released from chemical reactions as a source of power and the gaseous reaction products, expanded through a nozzle, as a working fluid. Currently, there is intensive investigation of propulsion methods to supplement chemical rockets. These methods include nuclear rockets, electric propulsion by acceleration of charged particles, solar radiation pressure sails, solar heating of working fluids, and reaction from explosions of small nuclear bombs.[11-13] The discussion in this chapter applies primarily to chemical and nuclear rockets, but it is generally applicable to propulsion methods which provide thrust of the same order of magnitude as the vehicle weight.

9.2 ANALYSIS OF BALLISTIC FLIGHT

The flight of a rocket vehicle with a thrust-to-weight ratio near unity is characterized by short periods of rocket thrust and long periods of coasting. The powered flight trajectory equations include terms containing thrust and gravitational acceleration as functions of altitude, mass as a function of time, flight-path angle as a function of trajectory shaping, and drag as a function of Mach number, altitude, and velocity. Free-flight trajectories are described by the classic equations of motion of bodies in mutually attracting central force fields. General solutions to both types of equations are limited in their scope.[1]

The complexity of the equations for both powered and free flight has necessitated the widespread use of digital computers to obtain point by point trajectory solutions. These solutions can yield whatever accuracy is required, but each applies to specific flight conditions and it is difficult to draw general conclusions from them. When general conclusions on the influence of parameters are desired, they can be obtained by making simplifying assumptions that permit approximate analytical solutions. This procedure is used in Sections 9.2 and 9.3 to obtain approximations for launch burnout velocity, free-flight trajectories, and mission geometry.

The approximations used in this chapter are principally useful in obtaining rough numbers for vehicle size and staging. Experience with preliminary design of space vehicles has generally indicated that sound design decisions require greater accuracy than is afforded by these approximations. Digital computer solutions with analytical extensions are ordinarily necessary for detailed parametric design studies.

9.2.1 Powered Flight

A rocket vehicle launched from the ground ordinarily starts vertically to permit rolling to a desired launch azimuth and to avoid horizontal movement near the ground. After a vertical climb, usually around 10 sec in duration, the vehicle starts a programmed pitch maneuver. In the atmosphere it is usual to keep the vehicle axis oriented along the flight path in a "gravity turn." After leaving the atmosphere the pitch programs commonly used include gravity turn, constant attitude, and constant pitch rate. Upon shutdown of the last propulsion stage the vehicle will have "burnout" conditions of speed, altitude, range, and flight path angle. These conditions determine the path that the vehicle will continue to follow.[5, 9, 10]

Solutions to the powered-flight equations of motion are needed to find burnout conditions for a given vehicle or to determine what design will give desired burnout values. If the vehicle were operating in a vacuum without gravity, the burnout conditions could be calculated analytically by the following "vacuum velocity law" which is derived in Chapter 8

$$V_T = g \sum_{1}^{N} I_{sp_i} \ln m_i \qquad (9.1)$$

where V_T = theoretical vacuum velocity (ft/sec)

I_{sp_i} = specific impulse of the ith stage $\left[\dfrac{\text{thrust (lb)}}{\text{fuel flow (lb/sec)}}\right]$

m_i = mass ratio of ith stage $\left(\dfrac{\text{initial mass}}{\text{final mass}}\right)$

g = surface acceleration of gravity (32.2 ft/sec^2)

N = number of stages in vehicle

(There is a list of the symbols used in this chapter in Section 9.7.)

The rocket does not achieve this velocity, primarily because of gravity and drag forces and velocity from motion of the launch platform. The losses are difficult to estimate accurately because they arise from variations in the parameter.

A convenient approximation to launch losses will be sufficiently accurate for the purposes of this discussion. Experience with computer solutions has indicated that these losses are relatively invariant for vehicles with initial thrust-to-weight ratio around 1.5 performing a gravity turn to an approximate horizontal burnout. Acceptance of these restrictions is satisfactory for the design comparisons which follow. For this class of vehicles and trajectories, gravity losses are approximately 4600 ft/sec and drag losses are approximately 400 ft/sec. Total launch velocity loss is therefore $\Delta V_l = 5000$ ft/sec.

Rotation of the earth contributes to the burnout velocity of a space vehicle when viewed from an inertial reference. At the equator the earth has a velocity around 1500 ft/sec. The actual velocity contribution of earth rotation can be approximated from launch azimuth and latitude by the equation

$$\Delta V_\omega = \omega_E R_E \cos\psi \sin\phi \tag{9.2}$$

where ΔV_ω = velocity contribution of earth rotation (ft/sec)
ω_E = earth angular rotation (radians/sec)
R_E = earth radius (ft)
ψ = latitude angle
ϕ = launch azimuth angle from North

The approximate burnout velocity for the space vehicles under consideration here is

$$V_o = g\sum_1^N I_{sp_i} \ln m_i - \Delta V_l + \Delta V_\omega \tag{9.3}$$

9.2.2 Free Flight

During coasting flight outside the atmosphere the trajectory of a space vehicle is governed by the laws of motion of bodies with mutual gravitational attraction. The equations of motion are determined by conditions for conservation of energy and angular momentum. This subject is treated in greater detail in Chapter 8.[3] The case of several bodies with similar mass can be solved only by point by point integration. Most space vehicle problems can be approximated by a restricted case where one attracting body is considered at a time and the mass of the space vehicle is negligible compared to that of the attracting body. The analytical treatment of this case is considered here.

The equation for conservation of energy in this case is

$$V_1^2 - \frac{2GM}{r_1} = V_2^2 - \frac{2GM}{r_2} \tag{9.4}$$

where V_1 = vehicle velocity at condition 1
r_1 = distance of vehicle from center of mass of attracting body at condition 1
V_2 = vehicle velocity at condition 2

r_2 = distance at condition 2
GM = product of gravitational constant G, approximately 3.45×10^{-8} (ft^3/sec^2)/slug and mass of the attracting body M (slugs): (ft^3/sec^2)

The equation for conservation of angular momentum in this case is

$$V_1 r_1 \sin \beta_1 = V_2 r_2 \sin \beta_2 \tag{9.5}$$

where β_1 = angle of vertical to the velocity vector at condition 1
β_2 = angle at condition 2

The vehicle path is determined by the strength of the attracting field (GM), the speed (V_o), velocity vector angle from the vertical (β_o), and the distance of the vehicle from the center of mass (r_o). The subscript refers to conditions at the end of rocket burning. The quantity $\lambda = V_o^2 r_o/GM$ is a dimensionless parameter equal to twice the ratio of kinetic energy to potential energy. If λ is smaller than 2, the vehicle will follow an elliptical path with the attracting body at one focus. The special case of $\lambda = 1$ and $\beta_o = 90°$ results in a circular path. When λ equals 2, the path is parabolic with the vehicle just escaping from the attracting body. For λ larger than 2, the path is hyperbolic and the vehicle escapes with a residual velocity.

Figure 9.1 illustrates the kinds of paths that are traced. Equations 9.6 through 9.12 show some of the properties of the motion.

$$\lambda = \frac{V_o^2 r_o}{GM}: \begin{array}{ll} \lambda < 2 & \text{Elliptical path} \\ \lambda = 1 & \text{Circular path } (\beta_o = 90°) \\ \lambda = 2 & \text{Parabolic path} \\ \lambda > 2 & \text{Hyperbolic path} \end{array} \tag{9.6}$$

$$\text{Eccentricity } e = \sqrt{1 - \lambda(2 - \lambda)\sin^2 \beta_o} \tag{9.7}$$

$$\text{Perigee distance } r_{min} = \frac{1 - e}{2 - \lambda} r_o \tag{9.8}$$

$$\text{Apogee distance } r_{max} = \frac{1 + e}{2 - \lambda} r_o \tag{9.9}$$

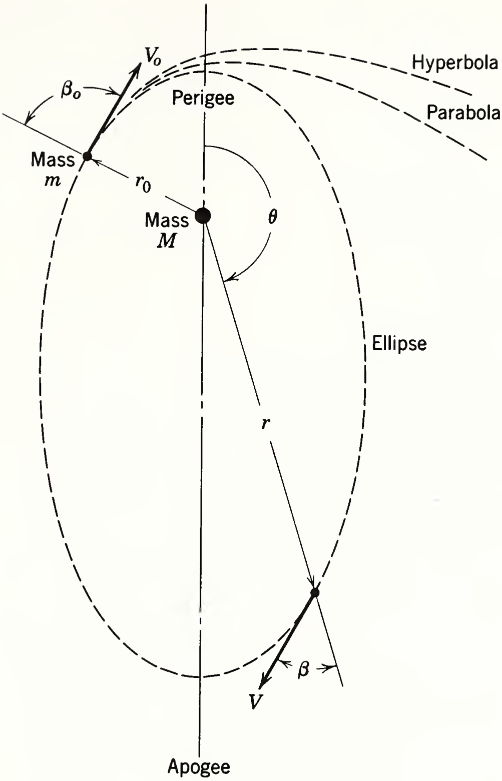
V_o
β_o
Hyperbola
Perigee
Parabola
Mass
m
r_0
Mass
M
θ
Ellipse
r
β
V
Apogee

Fig. 9.1 Motion of a particle in a central force field of inverse square intensity.

$$\text{Period } T = \frac{2\pi\left(\dfrac{r_o}{2-\lambda}\right)^{3/2}}{\sqrt{GM}} \tag{9.10}$$

$$\text{Velocity } V = V_o\left[1 + \frac{2}{\lambda}\left(\frac{r_0}{r} - 1\right)\right]^{1/2} \tag{9.11}$$

$$\text{Angle } \theta = \cos^{-1}\frac{1}{e}\left(\frac{1-e^2}{2-\lambda}\ \frac{r_o}{r} - 1\right) \tag{9.12}$$

These equations show that the free-flight motions of a vehicle near an attracting body are determined by initial conditions and the mass of the body. Vehicle motions near the various bodies in the solar system can usually be approximated by considering gravitational attraction of the body with the

TABLE 9.1
Physical Characteristics and Orbits of Sun, Moon, and Planets

		Physical Characteristics			Orbit				
Object	Sub-script	Radius R, ft	Gravitational Parameter GM, ft^3/sec^2	Rate of Rotation ω, radians/sec	Mean Orbit Radius r ft	Orbit Eccen-tricity e	Orbit Inclination i, deg	Mean Orbital Velocity V, ft/sec	Mean Angular Rate, η, radians/sec
Sun	S	2.283×10^9	4.679×10^{21}	. . .	. . .	. . .	. . .	. . .	. . .
Moon	L	5.702×10^6	1.727×10^{14}	2.661×10^{-6}	1.261×10^9	0.05490	28° 35′ to 18° 19′[a]	3.342×10^3	2.661×10^{-6}
Mercury		8.208×10^6	7.645×10^{14}	1.983×10^{-5}	1.899×10^{11}	0.2056	7° 0′ 14.2″	1.570×10^5	8.267×10^{-7}
Venus	V	2.036×10^7	1.145×10^{16}	7.930×10^{-5}	3.548×10^{11}	0.006794	3° 23′ 39.1″	1.149×10^5	3.238×10^{-7}
Earth	E	2.092×10^7	1.408×10^{16}	7.319×10^{-5}	4.905×10^{11}	0.01673	0	9.768×10^4	1.991×10^{-7}
Mars	M	1.086×10^7	1.515×10^{15}	7.088×10^{-5}	7.475×10^{11}	0.09337	1° 50′ 50.8″	7.882×10^4	1.054×10^{-7}
Jupiter		2.294×10^8	4.467×10^{18}	1.773×10^{-4}	2.552×10^{12}	0.04843	1° 18′ 19.9″	4.282×10^4	1.678×10^{-8}
Saturn		1.889×10^8	1.338×10^{18}	1.739×10^{-4}	4.679×10^{12}	0.05569	2° 29′ 42.2″	3.163×10^4	6.760×10^{-9}
Uranus		8.372×10^7	2.046×10^{17}	1.616×10^{-4}	9.409×10^{12}	0.04720	0° 46′ 22.9″	2.230×10^4	2.370×10^{-9}
Neptune		8.207×10^7	2.422×10^{17}	1.015×10^{-4}	1.474×10^{13}	0.008572	1° 46′ 26.5″	1.782×10^4	1.209×10^{-9}
Pluto		. . .	1.170×10^{16}	. . .	1.938×10^{13}	0.2486	17° 8′ 38.4″	1.554×10^4	8.019×10^{-10}

[a] Referred to equatorial plane.

greatest influence while neglecting more distant or smaller bodies. Data for calculation of these motions are given in Table 9.1.[2] The values given in Table 9.1 are known with varying degrees of accuracy. In the table they are uniformly rounded off to four significant figures for convenience in the type of computation for which they are intended. Examples of approximate methods for solution of typical mission requirements are given in Section 9.3.

9.2.3 Mission Equivalent Velocity

A rocket vehicle expels propellant mass to impart velocity to a payload. After rocket burnout the vehicle velocity varies in a manner to conserve total energy and angular momentum. Some missions require the addition of velocity increments by additional rocket thrust periods. The performance requirements of a mission can be measured by the sum of the velocity increments imparted to the payload. This value is frequently referred to as the "equivalent velocity" of a mission. Equivalent velocity is used to compare the difficulty of missions and as a means for evaluating the mission capabilities of space vehicles.

The establishment of equivalent velocity requires specification of an energy reference, since free-flight trajectories are based on energy and rocket capabilities are based on velocity. Several types of energy reference are possible, and the choice for any application depends on the kind of comparison that is desired. For the purposes of the vehicle parametric analysis in this chapter, a burnout altitude reference is very useful. The altitude selected for this purpose is not critical as long as it is used for all cases considered. A reference burnout altitude of 100 nautical miles was selected here as typical of burnout altitudes for two- or three-stage liquid-propelled vehicles.

The burnout altitude reference defines a launch burnout velocity to give the correct energy, when burnout occurs at an altitude of 100 nautical miles. By starting all missions with these launch conditions a valid vehicle comparison is obtained. Launch losses are also standardized corresponding to these burnout conditions. The use of another altitude as a reference would require that launch losses be adjusted accordingly.

An alternative to the altitude reference is a satellite orbit reference. Such a reference is used frequently in evaluating space maneuvering vehicles which are assumed to start from an orbit. Specification of launch losses is not necessary when using a satellite orbit reference.

9.3 MISSIONS FOR SPACE VEHICLES

The total spectrum of space missions is so broad that comprehensive treatment of all possibilities is beyond the scope of this chapter. However, missions fall into several classes with distinctive characteristics. These classes are defined by trajectory geometry, burning periods, and launch timing requirements. Four classes of missions are examined in Sections 9.3.1 through 9.3.4. Specific examples have been chosen from each of these classes to illustrate the analysis of mission requirements. The performance requirements for the examples chosen are expressed in terms of equivalent velocities. These equivalent velocity examples will later be used to determine the size of rocket vehicle needed to accomplish the missions selected as examples.

9.3.1 Ballistic Missiles

Ballistic missile trajectories are the simplest space vehicle flight path in principle. After ascent through the atmosphere, the missile burns out with λ and β_0 to place the missile nose cone on an elliptical path to intersect the target; λ must be less than 2 since the path returns to the earth's surface. Figure 9.2 shows a schematic ballistic missile trajectory. The powered-flight portion must have a specific pitch program and engine shutdown procedure to achieve the desired burnout velocity and angle. During free flight the nose cone is usually separated from the final stage. As the nose cone re-enters the atmosphere, it follows a ballistic trajectory modified by aerodynamic drag and lift forces. The precise impact point is determined by the powered, free-flight, and re-entry trajectories. However, the missile range is primarily dependent on the free-flight trajectory.

The maximum free-flight range of a ballistic missile can be approximated from the geometry of the elliptical flight

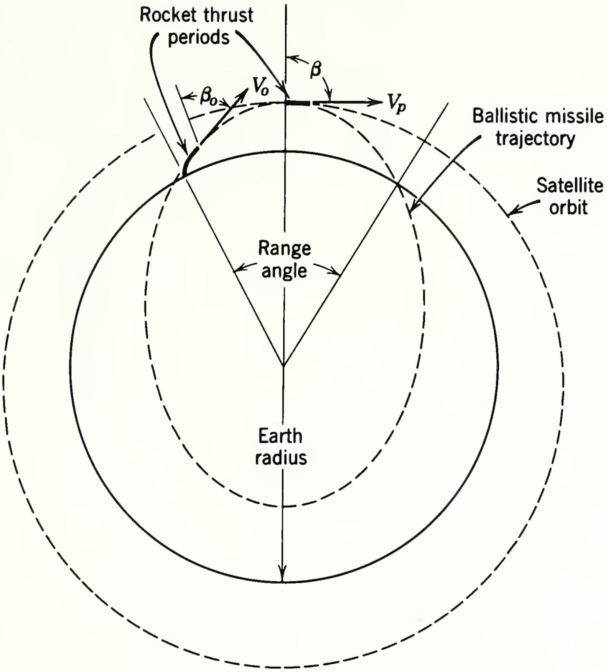
Rocket thrust periods
V_o
β_o
β
V_p
Ballistic missile trajectory
Satellite orbit
Range angle
Earth radius

Fig. 9.2 Trajectory of ballistic missile and earth satellite.

path and the intersections with the spherical earth surface. The equation for maximum range is

$$S = 2R_E \sin^{-1} \frac{1}{2g R_E / V_o^2 - 1} \tag{9.13}$$

where S = surface range (ft)
R_E = earth mean radius (ft)
g = earth surface gravity (32.2 ft/sec^2)
V_o = burnout velocity (ft/sec)

Figure 9.3 shows missile free-flight range as a function of angle and burnout velocity for a burnout altitude of 600,000 ft. The figure shows that there is no unique trajectory for a given range, but that there is a minimum required velocity for each range. The burnout angle corresponding to minimum velocity (or energy) increases with increasing range. At 1000 nautical miles range it is about 50° and at 6000 nautical miles range it is near 70°. As range increases, the curves of range versus

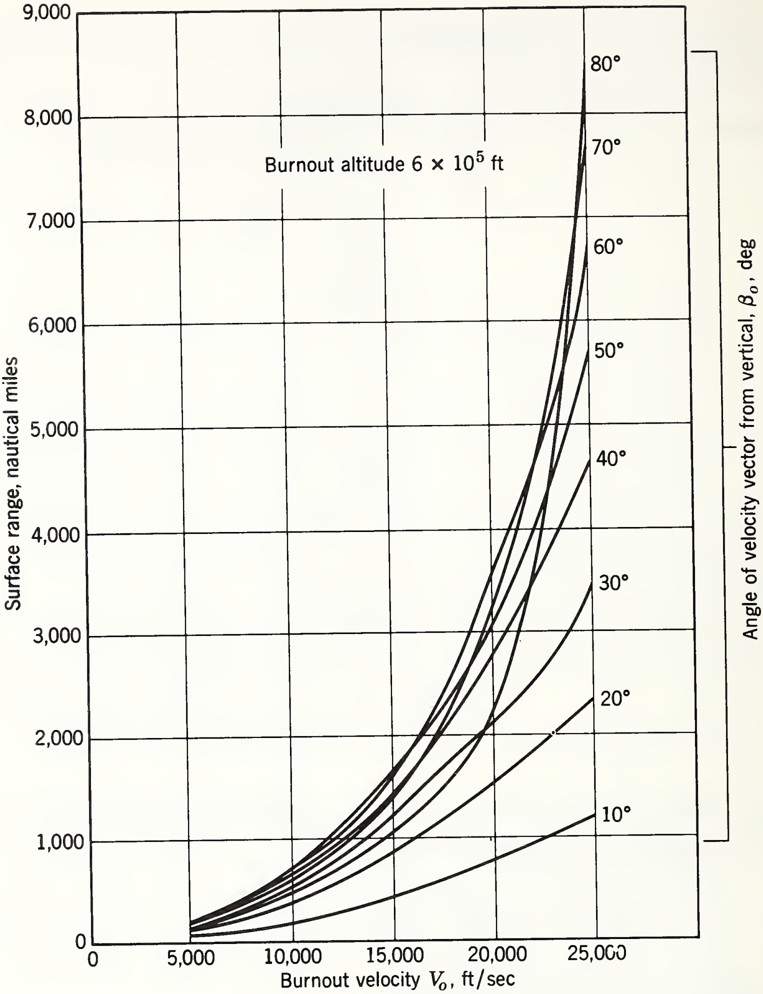

Fig. 9.3 Range of ballistic missile as a function of burnout velocity and angle.

velocity become steeper. Errors in burnout velocity will, therefore, have a greater effect on accuracy as range increases. At very long ranges trajectories are frequently lofted deliberately to reduce the impact error sensitivity to burnout velocity errors.

The mission example chosen to illustrate ballistic missile velocity requirements is a 6000-nautical mile minimum-energy trajectory. Figure 9.3 indicates a burnout velocity of

23,000 ft/sec at an altitude of 100 nautical miles. The curve used is the one corresponding to the lowest velocity for a 6000-mile range. The burnout angle is about 70°. Total mission velocity requirements are obtained by adding 5000 ft/sec to the burnout velocity for launch losses. Earth rotation velocity is not considered here because ballistic missiles can be launched on any azimuth.

9.3.2 Earth Satellites

A space vehicle in an elliptical free-flight trajectory which does not intersect the surface of the attracting body becomes a satellite. The vehicle will remain in the orbit unless attracted by another body, accelerated by rocket thrust, or decelerated by atmospheric drag. Powered-flight trajectories to achieve a satellite orbit may have continuous rocket burning or a period of coasting between thrust periods. For orbital injection altitudes up to a few hundred miles, the successive rocket stages can usually be burned one after the other. The final burnout conditions then determine the orbit. For injection altitudes above a few hundred miles it is usually necessary to have the final stage coast from launch burnout until a final injection thrust period. This type of trajectory is illustrated in Fig. 9.2.

The velocity of a satellite in a circular orbit can be found from eq. 9.6 by setting $\lambda = 1$.

$$V_c = \sqrt{GM_E/r_c} \tag{9.14}$$

where V_c = circular satellite velocity (ft/sec)
r_c = radius of satellite orbit (ft)
GM_E = gravitational field strength of the earth (ft^3/sec^2)

Elliptical satellite orbits are usually established by injecting near perigee. Orbital velocity at perigee can be found by combining eqs. 9.4 and 9.5 and noting that $\beta = 90°$ for both apogee and perigee.

$$V_p = \left[\frac{2GM_E}{r_p(1 + r_p/r_a)}\right]^{1/2} \tag{9.15}$$

where V_p = velocity at perigee (ft/sec)
r_p = perigee radius (ft)
r_a = apogee radius (ft)

If the satellite is injected directly into orbit at the end of rocket burning, the burnout conditions are identical with orbit conditions. If a coast period precedes injection, launch burnout should provide a coast apogee at the desired injection altitude. Launch burnout conditions required to achieve apogee at a desired altitude can be found from eq. 9.5 by noting that $\beta = 90°$ at apogee.

$$V_a = \frac{V_o r_o \sin \beta_o}{r_a} \tag{9.16}$$

where r_o = burnout radius (ft)
β_o = burnout angle (radians)
r_a = apogee radius (ft)
V_o = burnout velocity (ft/sec)
V_a = apogee velocity (ft/sec)

At apogee additional velocity must be added to achieve the desired orbit. The velocity increment required for injection into an orbit is, therefore,

$$\Delta V_I = \begin{cases} V_c - V_a & \text{(circular orbit)} \\ V_p - V_a & \text{(eccentric orbit)} \end{cases} \tag{9.17}$$

where ΔV_I = injection velocity increment (ft/sec)

Two satellite launching missions have been selected as examples. The orbits are circular with a 200- and 20,000-nautical mile altitude. Launch requirements are calculated

For a 200-nautical mile altitude circular orbit:

$$V_c = \left[\frac{1.408 \times 10^{16}}{(2.09 + 0.12) \times 10^7}\right]^{1/2} = 25{,}200 \text{ ft/sec}$$

$$V_o = \left[\frac{2 \times 1.408 \times 10^{16}}{2.15 \times 10^7 \left(1 + \dfrac{2.15 \times 10^7}{2.21 \times 10^7}\right)}\right]^{1/2} = 25{,}700 \text{ ft/sec}$$

Both satellite missions shown here have launch burnout horizontal at an altitude of 100 nautical miles, resulting in a minimum energy or Hohmann transfer to apogee at the desired orbital altitude.

$$V_a = 25{,}700\left(\frac{2.15 \times 10^7}{2.21 \times 10^7}\right) = 25{,}000 \text{ ft/sec}$$

$$\Delta V_{I_c} = 25{,}200 - 25{,}000 = 200 \text{ ft/sec}$$

Assuming 5000-ft/sec launch losses and no contribution from earth rotation, the total velocity required for a 200-nautical mile orbit is

$$V_t = 25{,}700 + 200 + 5000 = 30{,}900 \text{ ft/sec}$$

where V_t = total mission velocity required (ft/sec)

For a 20,000-nautical mile altitude circular orbit:

$$V_c = \left[\frac{1.408 \times 10^{16}}{(2.09 + 12.16) \times 10^7}\right]^{1/2} = 10{,}200 \text{ ft/sec}$$

$$V_o = \left[\frac{2 \times 1.408 \times 10^{16}}{2.15 \times 10^7\left(1 + \dfrac{2.15 \times 10^7}{14.25 \times 10^7}\right)}\right]^{1/2} = 33{,}800 \text{ ft/sec}$$

$$V_a = 33{,}800 \times \frac{2.15 \times 10^7}{14.25 \times 10^7} = 5100 \text{ ft/sec}$$

$$\Delta V_{I_c} = 10{,}200 - 5100 = 5100 \text{ ft/sec}$$

Thus for a 20,000-nautical mile orbit the total velocity required is

$$V_t = 33{,}800 + 5100 + 5000 = 43{,}900 \text{ ft/sec}$$

The satellite orbits discussed here have assumed a homogeneous spherical earth. The effects of the oblateness of the earth are outside this discussion.[6]

The detailed calculation of three-dimensional satellite launching trajectories requires a digital computer. The shaping of the launch trajectory and the orientation and timing for the injection thrust period can become quite complex. Some types of satellite orbits require out-of-plane maneuvers. The details of such maneuvers are beyond the scope of this chapter, but we should note that additional rocket performance is needed and that it will be reflected in the total mission velocity requirements.

9.3.3 Lunar or Satellite Intercept

The requirement for vehicle intersection with a satellite in orbit gives rise to an interesting class of missions. An artificial target satellite would not have sufficient gravitational attraction to affect the vehicle approach trajectory. The intersecting vehicle can be injected into the same orbit as the target or it can execute an in-plane or out-of-plane fleeting passage. The launch trajectories for each of these maneuvers would, in general, require different vehicle performance. To accomplish any of these maneuvers, the launch trajectory must be tailored to a particular revolution of the target satellite. The launching must be timed to account for the rotation of the earth, the position of the target orbit plane, and the location of the satellite in its orbit. The details of these maneuvers will not be discussed here. However, in the simple case of a co-orbital intercept performed entirely in the plane of the target satellite orbit, with the target in the most favorable position, the vehicle performance requirements are identical to those developed in Section 9.3.2 for satellite launching. For a fleeting apogee intercept with the same orbit geometry, the vehicle performance requirements are the same as for satellite launching but without the injection velocity increment, ΔV_I.

Lunar missions are a special case of satellite intercept. The launch geometry and timing considerations are similar to those for artificial satellites. However, in the vicinity of the moon, the vehicle path is influenced by the lunar gravitational field, and injection into the lunar orbit is not necessary.[4,7]

The geometry of lunar trajectories is illustrated in Fig. 9.4. The time of flight for a mission determines the angle through which the moon will travel from launch to arrival. On each day there will be a specified time when the earth has rotated to the correct position for launching from a particular site. The angle between the lunar orbit plane and the equatorial plane causes launch sites to be at different distances from the lunar plane at the proper launch time each day throughout a month. It is desirable to launch close to the lunar orbit plane for guidance and performance reasons. Therefore, days of the month when the launch site is nearest the lunar orbit plane are preferable for launching.

Figure 9.4 shows an elliptical trajectory corresponding to a two-day elapsed time for a lunar mission. The burnout conditions shown are typical for such a trajectory. For most of the transit time the vehicle motion is influenced insignifi-

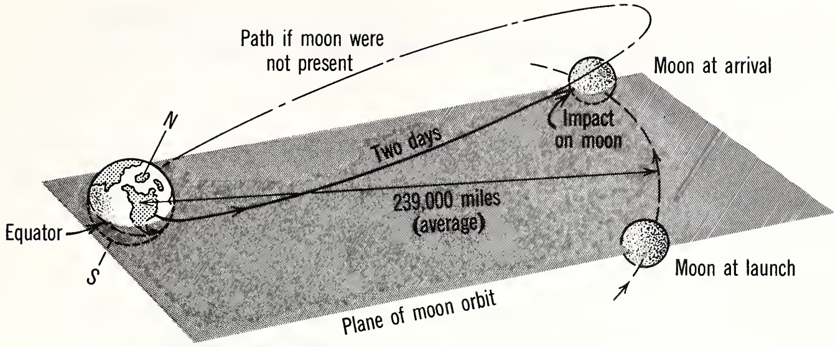

$V_0 = 36{,}000$ ft/sec
$\beta_0 = 70°$
$h_0 = 100$ nautical miles

Fig. 9.4 Typical lunar trajectory.

cantly by the presence of the moon. As the vehicle reaches the vicinity of the moon, the trajectory is altered by the lunar gravitational field.

Approximate lunar intercept trajectories can be calculated, using a simplified model which is compared with digital computer solutions.[14] The following assumptions are made.

1. The lunar orbit is circular.
2. The vehicle is launched in the lunar orbit plane.
3. The trajectory to the vicinity of the moon is not influenced by lunar gravity.
4. The trajectory in the vicinity of the moon is not influenced by the gravity of the earth.
5. The launch trajectory is either hyperbolic or elliptical, with a burnout velocity at least 100 ft/sec more than required for apogee at the lunar orbit. (The accuracy of the model improves with increasing launch velocity.)

By using this model, a lunar launch trajectory is calculated to reach the lunar orbit when the moon arrives at the intersection point. The vehicle velocity and flight path angle at the intersection with the lunar orbit are assumed as initial conditions for the lunar approach after transfer to a coordinate system moving with the moon. The vehicle trajectory as it is deflected by the moon or impacts on the surface can be calculated by the same equations used for motions in the earth gravitational field, but with a GM value for the moon.

The velocity of a vehicle impacting on the moon without terminal maneuvering can be found from eq. 9.4.

$$V_h = \sqrt{V_\infty^2 + 2GM_L/r_L} \tag{9.18}$$

where V_h = impact velocity (ft/sec)
V_∞ = approach velocity at $r = \infty$ (ft/sec)
GM_L = gravitational field strength of moon (ft^3/sec^2)
r_L = moon radius (ft)

For $V_\infty = 0$ the impact velocity is about 7800 ft/sec. A lunar landing would require a retrorocket to reduce the vehicle velocity by V_I plus gravity losses. A launch from the moon would require at least 7800 ft/sec plus gravity losses to leave the vicinity of the moon. The trajectory for a return trip from the moon to the earth can be calculated by using the simplified model of the earth-moon system. In general, earth-moon or moon-earth trajectories can be approximated by a two-part calculation where the unperturbed launch trajectory provides initial conditions for the terminal trajectory.

Three lunar missions are used as examples of vehicle design requirements. They are lunar impact, landing, and landing and return to earth. Total velocity requirements for these missions can be computed by treating the first two as successive steps in the later mission.

The launch burnout velocity at the 100-nautical mile altitude is selected to be 100 ft/sec more than required for apogee at the lunar orbit radius (207,000 nautical miles). From eq. 9.15,

$$V_o = \left[\frac{2 \times 1.408 \times 10^{16}}{2.15 \times 10^7 \left(1 + \frac{2.15 \times 10^7}{1.261 \times 10^9}\right)}\right]^{1/2} + 100 = 36{,}000 \text{ ft/sec}$$

Launch drag and gravity losses are assumed to be 5000 ft/sec and rotation of the earth contributes 1000 ft/sec, so total velocity for lunar impact is

$$V_t = 36{,}000 + 5000 - 1000 = 40{,}000 \text{ ft/sec}$$

The requirements for a lunar landing can be computed approximately from the launch conditions used for the lunar impact. The vehicle velocity at the lunar orbit altitude can be found from eq. 9.4.

$$V_{LO} = \left[36{,}000^2 - 2\times 1.408\times 10^{16}\left(\frac{1}{2.15\times 10^7} - \frac{1}{1.26\times 10^9}\right)\right]^{1/2}$$
$$= 3160 \text{ ft/sec}$$

The impact velocity on the moon's surface can be found from eq. 9.18.

$$V_h = \left[(3160)^2 + \frac{2\times 1.729\times 10^{14}}{5.72\times 10^6}\right]^{1/2} = 8400 \text{ ft/sec}$$

A retrorocket for landing would be required to remove the impact velocity plus gravity losses during rocket burning. Losses in landing on the moon depend on the nature of the landing maneuver and might typically be around 600 ft/sec. The total velocity required for the lunar landing would then be

$$V_t = 40{,}000 + 8400 + 600 = 49{,}000 \text{ ft/sec}$$

Return to the earth would require velocity to escape the lunar gravitational field and overcome launch losses. Assuming that the return launch trajectory is similar to the landing trajectory, the velocity requirement would be 8400 ft/sec launch burnout velocity plus 600 ft/sec losses. The total for the lunar landing and return would be

$$V_t = 49{,}000 + 8400 + 600 = 58{,}000 \text{ ft/sec}$$

9.3.4 Interplanetary Missions

Ballistic flight between the planets of the solar system may be analyzed to various levels of detail.[8, 15, 16, 17] Precise trajectories which account for orbital eccentricity and inclination, together with the perturbations from the planets, can be calculated very satisfactorily with a digital computer. The trajectory refinements which are essential for accurate navigation are usually not required in studies of vehicle velocity requirements for interplanetary flight. Useful approximations to trajectories and vehicle performance requirements for interplanetary missions can be computed by using a solar system model with simplifications similar to those of the lunar model in Section 9.3.3. The assumptions in using this model are:

1. Planets are in coplanar concentric orbits.

2. Vehicle trajectories lie in the common planetary orbit plane.
3. Launch trajectories are computed in the coordinate system of the departure planet and consider only its gravitational field.
4. Midcourse trajectories are computed in the coordinate system of the sun and consider only its gravitational field.
5. Terminal trajectories are computed in the coordinate system of the destination planet and consider only its gravitational field.
6. Transfer between heliocentric orbits and planet-centered trajectories occur at heliocentric vehicle velocities corresponding to intersection with the planetary orbits.

These assumptions yield good approximations to simple interplanetary missions because the planetary orbits are neither very eccentric nor very inclined. The relative angular positions of the planets in their orbits must be considered in calculating interplanetary trajectories. The method of calculation will be illustrated, using minimum energy or Hohmann's transfers between planets. Other transfers for shorter mission time at the expense of increased velocity requirements can be computed by the same methods.

Figure 9.5 shows an example of the geometrical configuration of the planets for a minimum energy transfer between circular concentric orbits. The time for a transfer is half

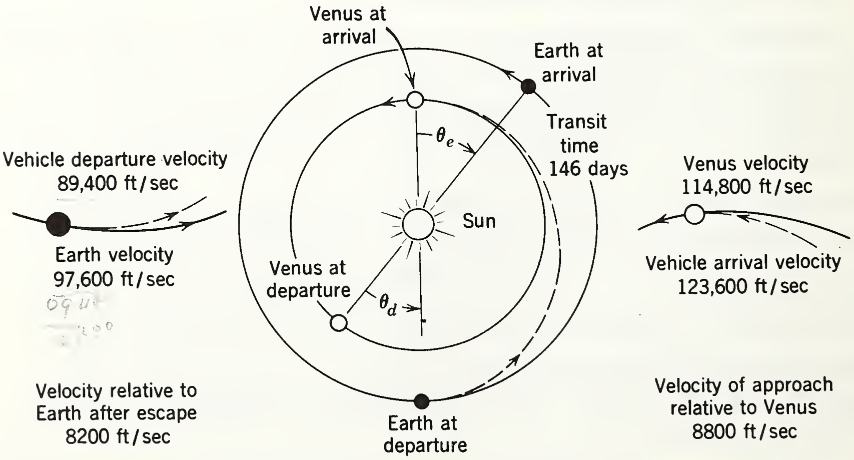
Venus at arrival
Earth at arrival
Transit time 146 days
θ_e
Sun
Venus at departure
θ_d
Earth at departure
Vehicle departure velocity 89,400 ft/sec
Earth velocity 97,600 ft/sec
Velocity relative to Earth after escape 8200 ft/sec
Venus velocity 114,800 ft/sec
Vehicle arrival velocity 123,600 ft/sec
Velocity of approach relative to Venus 8800 ft/sec

Fig. 9.5 Earth to Venus trajectory. Simplified solar system model.

the orbital period of an elliptical orbit with apogee at one planetary orbit and perigee at the other. This period can be computed from eq. 9.10.

$$T_m = \frac{\pi\left[(r_d + r_e)/2\right]^{3/2}}{\sqrt{GM_S}} \tag{9.19}$$

where T_m = minimum energy transfer time from r_d to r_e (sec)
r_d = radius from the sun of departure planet (ft)
r_e = radius from sun of destination planet (ft)
GM_S = gravitational field strength of sun (ft^3/sec^2)

The angular velocities of the planets can be found from the orbital velocity using eq. 9.14.

$$\dot{\theta}_d = \sqrt{GM_S/r_d^3} \tag{9.20}$$

$$\dot{\theta}_e = \sqrt{GM_S/r_e^3} \tag{9.21}$$

where $\dot{\theta}_d$ = angular velocity of departure planet (radians/sec)
$\dot{\theta}_e$ = angular velocity of destination planet (radians/sec)

The angular displacement of the planets during transfer is the product of eq. 9.19 with 9.20 and 9.21. At the start of transfer the departure planet is 180° from the required position of the destination planet at arrival. Therefore, the angular displacement of the planets at departure is

$$\Delta\theta_d = \pi\left[\left(\frac{r_d}{2r_e} + \frac{1}{2}\right)^{3/2} - 1\right] \tag{9.22}$$

where $\Delta\theta_d$ = angle of departure planet ahead of destination planet at departure (radians)

At the end of transfer the angular displacement between planets is

$$\Delta\theta_e = \pi\left[\left(\frac{r_e}{2r_d} + \frac{1}{2}\right)^{3/2} - 1\right] \tag{9.23}$$

where $\Delta\theta_e$ = angle of departure planet ahead of destination planet at arrival (radians)

The launch trajectory from the departure planet must have sufficient burnout velocity to escape with a desired residual velocity. Burnout velocity for launch from the earth can be computed from eq. 9.5.

$$V_o = \sqrt{V_r^2 + 2GM_E/r_o} \tag{9.24}$$

where V_r = residual velocity after escape (ft/sec)

The velocity of the vehicle around the sun after escape from the earth is the vector sum of the earth's orbital velocity plus the vehicle residual velocity after escape. This discussion will be confined to minimum energy transfers so that the initial vehicle flight path angle around the sun is $\beta = 90°$. For this case the resultant vehicle velocity is

$$V_s = V_E \pm V_r \tag{9.25}$$

where V_s = vehicle velocity with respect to the sun after escape (ft/sec)
V_E = orbital velocity of Earth around the sun (ft/sec)

The ± sign in this equation indicates that the residual velocity can either be directed in the direction of orbital motion or opposed to it. The plus sign will place the vehicle on a transfer outward toward the orbits of Mars and the outer planets. The minus sign will place it on an inward transfer toward the orbits of Venus and Mercury.

The initial transfer velocity required can be found from the geometry of the orbits of the departure and destination planets and the gravitational field strength of the sun.

$$V_s = \left[\frac{GM_S}{r_d}\left(\frac{2}{1 + r_d/r_e}\right)\right]^{1/2} \tag{9.26}$$

With the type of transfers used here, the vehicle would arrive at the destination planet exactly on the opposite side of the sun from departure. The vehicle velocity at the end of transfer can be found from eq. 9.5, with $\beta = 90°$ for both departure and arrival.

$$V_g = V_s (r_s/r_e) \tag{9.27}$$

where V_g = velocity around the sun at the end of transfer
r_e = radius from sun at the end of transfer

The velocity of approach to the destination planet can be found by considering the vehicle motion in a coordinate system moving with the planet.

$$V_k = |V_g - V_e| \tag{9.28}$$

where V_k = velocity of arriving vehicle with respect to destination planet
V_e = orbital speed of destination planet

Absolute values are used here because the speed of final approach to the planet is dependent on the initial relative speed, regardless of whether the vehicle overtakes the planet or is overtaken by it. The speed with which the vehicle enters the planetary atmosphere is obtained from eq. 9.4.

$$V_f = \sqrt{V_e^2 + 2GM_e/R_e} \qquad (9.29)$$

where V_f = speed at encounter with the atmosphere (neglecting the height of the atmosphere above the planet surface) (ft/sec)

GM_e = gravitational field strength of destination planet (ft^3/sec^2)

R_e = radius of destination planet (ft)

Landings on a planet require passage through the atmosphere so that the vehicle will be slowed by drag forces. The use of aerodynamic forces for deceleration and maneuvering will usually result in a lighter vehicle than is possible if rocket thrust alone is used. In computing total velocity requirements for interplanetary missions, it will be assumed that aerodynamic deceleration is used for any planetary landing.

The interplanetary mission examples which will be used for vehicle design requirements are minimum energy transfers from Earth to Venus and Mars and return. Figure 9.5 shows the geometry and coordinate transfers for the Venus mission. The initial transfer velocity for transfer from Earth to Venus is

$$V_s = \left[\frac{4.68 \times 10^{21}}{4.91 \times 10^{11}}\left(1 - \frac{1 - 3.56/4.91}{1 + 3.56/4.91}\right)\right]^{1/2} = 89{,}400 \text{ ft/sec}$$

V_E = 97,600 ft/sec (Earth orbital velocity)

V_r = 97,600 − 89,400 = 8200 ft/sec

$$V_o = \left[(8200)^2 + \frac{2 \times 1.408 \times 10^{16}}{2.15 \times 10^7}\right]^{1/2} = 37{,}100 \text{ ft/sec}$$

The total velocity for the Venus mission consists of the launch burnout velocity plus 5000 ft/sec launch losses and 1000 ft/sec assistance from Earth rotation. The total velocity is

Land on Venus: V_t = 37,100 + 5000 − 1000 = 41,100 ft/sec

Earth to Mars transfer is computed in the same way.

$$V_s = \left[\frac{4.68 \times 10^{21}}{4.91 \times 10^{11}}\left(1 + \frac{1 - 4.91/7.48}{1 + 4.91/7.48}\right)\right]^{1/2} = 107{,}200\ \text{ft/sec}$$

$$V_E = 97{,}600\ \text{ft/sec}$$

$$V_r = 107{,}200 - 97{,}600 = 9200\ \text{ft/sec}$$

$$V_o = \left[(9200)^2 + \frac{2 \times 1.408 \times 10^{16}}{2.15 \times 10^7}\right]^{1/2} = 37{,}200\ \text{ft/sec}$$

Land on Mars: $V_t = 37{,}200 + 5000 - 1000 = 41{,}200$ ft/sec

Velocity requirements for return from Mars or Venus are computed in the same way. For return from Venus the initial transfer velocity is the same as the arrival velocity from Earth.

$$V_s = 89{,}400\left(\frac{4.91}{3.56}\right) = 123{,}600\ \text{ft/sec}$$

$$V_V = 114{,}800\ \text{ft/sec}$$

$$V_r = 123{,}600 - 114{,}800 = 8800\ \text{ft/sec}$$

$$V_o = \left[(8800)^2 + \frac{2 \times 1.145 \times 10^{16}}{2.13 \times 10^7}\right]^{1/2} = 33{,}900\ \text{ft/sec}$$

Launching losses from Venus can be estimated by assuming the same burning time and trajectory shape as used for the earth launch. The surface gravity of Venus is approximately 0.86 that of Earth, so losses are estimated to be 4300 ft/sec compared to 5000 ft/sec for an earth launch. The total velocity requirement for a mission to Venus and return is

$$V_t = 41{,}100 + 33{,}900 + 4300 = 79{,}300\ \text{ft/sec}$$

Return velocity requirement from Mars can be computed in the same way.

$$V_s = 107{,}200 \times \frac{4.91}{7.48} = 70{,}400\ \text{ft/sec}$$

$$V_M = 79{,}000\ \text{ft/sec}$$

$$V_r = 79{,}000 - 70{,}400 = 8600\ \text{ft/sec}$$

$$V_o = \left[(8600)^2 + \frac{2 \times 1.52 \times 10^{15}}{1.128 \times 10^7}\right]^{1/2} = 18{,}500\ \text{ft/sec}$$

Launch losses from Mars can be estimated in the same manner as those for Venus. The surface gravity of Mars is 0.40 that of Earth, so launch losses are estimated as 2000 ft/sec. The total velocity requirement for a mission to Mars and return is

$$V_t = 41{,}200 + 18{,}500 + 2000 = 61{,}700 \text{ ft/sec}$$

9.3.5 Velocity Requirement Summary

The equivalent velocity requirements for the missions discussed in Sections 9.3.1 to 9.3.4 are summarized in Table 9.2. The total velocity values shown in the right-hand column are the sum of velocities corresponding to various phases of the missions. The values in each column are based on specific assumptions concerning the manner in which the mission is accomplished. The total velocity values are, therefore, not uniquely specified for each mission. The standardized assumptions and trajectories used in Sections 9.3.1 to 9.3.4 facilitate computation of equivalent velocity values for other missions, permitting direct comparison with those shown in Table 9.2.

Mission equivalent velocities are principally useful in over-all sizing of space vehicles. They can be unrealistic with vehicles which have solid propellant stages or liquid-propelled stages which cannot be restarted, for velocity increments must be added in specified amounts at specified points in a mission trajectory. The rocket stage which is available to provide thrust may not be sized to give the velocity increment needed next. Upper rocket stages using liquid propellants are frequently designed to restart for this reason. Solid propellant stages have not been developed with restart capability. Equivalent velocity as a measure of the performance requirement of a mission does not take this factor into account.

9.4 VELOCITY CAPABILITIES OF SPACE VEHICLES

Equivalent velocities as shown in Fig. 9.6 indicate the vehicle performance requirements for some typical space missions. The total velocity available from a space vehicle is found from eq. 9.1. This velocity is composed of the sum of

TABLE 9.2

Approximate Equivalent Velocity Requirements for Space Missions

	Mission	Launch Burnout[a]	Launch Loss	Land or Inject	Return Launch	Return Loss	Total
Ballistic missile	6,000-mile range	23,000	5,000				28,000
Earth satellite	200-mile altitude	25,700	5,000	200			30,900
	20,000-mile altitude	33,800	5,000	5,100			43,900
Moon	Impact	36,000	4,000[c]				40,000
	Land	36,000	4,000[c]	9,000			49,000
	Land and return[b]	36,000	4,000[c]	9,000	8,400	600	58,000
Mars and Venus	Land Mars or Venus[b]	37,200	4,000[c]				41,200
	Land Mars and return[b]	37,200	4,000[c]		18,500	2,000	61,700
	Land Venus and return[b]	37,100	4,000[c]		33,900	4,300	79,300

[a] Assuming launch burnout at 100-nautical mile altitude.

[b] Aerodynamic deceleration in planetary atmospheres.

[c] Earth rotation contributes 1000 ft/sec.

velocities from N stages. The velocity contributed by the ith stage can be expressed as

$$\Delta V_i = gI_{sp_i} \ln \frac{W_{O_i}}{\delta_i (W_{O_i} - W_{P_i}) + W_{P_i}} \tag{9.30}$$

where ΔV_i = total velocity gained by stage i (ft/sec)

δ_i = stage i structure factor $\left(\frac{\text{stage empty weight}}{\text{stage loaded weight}}\right)$

W_{O_i} = total weight at stage i ignition (lb)

W_{P_i} = stage i payload (lb)

Dividing by W_{O_i} gives

$$\Delta V_i = gI_{sp_i} \ln \frac{1}{\delta_i (1 - W_{P_i}/W_{O_i}) - W_{P_i}/W_{O_i}} \tag{9.31}$$

The total velocity for a multistage vehicle is ΣV_i. There is an optimum staging ratio for any combination of structure factors and specific impulse of each stage. Optimum staging gives the least total vehicle weight for a given payload, velocity, and number of stages. Solutions for optimum staging cannot be expressed in simple form, and an iteration procedure is required. Methods are known for determining optimum staging when structure factors and specific impulse are different for each stage.[18, 19]

A simple closed-form optimum staging solution can be obtained when structure factors and specific impulse are the same for all stages. It is shown in another chapter that the condition for minimum vehicle size in this case is obtained when each stage gains the same velocity. This case will be used here to illustrate the characteristics of a multistage vehicle. If all stages have equal values of I_{sp}, δ, and W_P/W_O, then for identical velocity gain for each stage

$$\frac{1}{(W_{P_i}/W_{O_i})^N} = P = \frac{\text{vehicle gross weight}}{\text{payload weight}} \tag{9.32}$$

The velocity capability of the over-all vehicle is N times the velocity contributed by each stage, as shown in eq. 9.30. Total vehicle velocity capability is, therefore,

$$V_T = NgI_{sp} \ln \frac{1}{\delta(1 - P^{-1/N}) + P^{-1/N}} \tag{9.33}$$

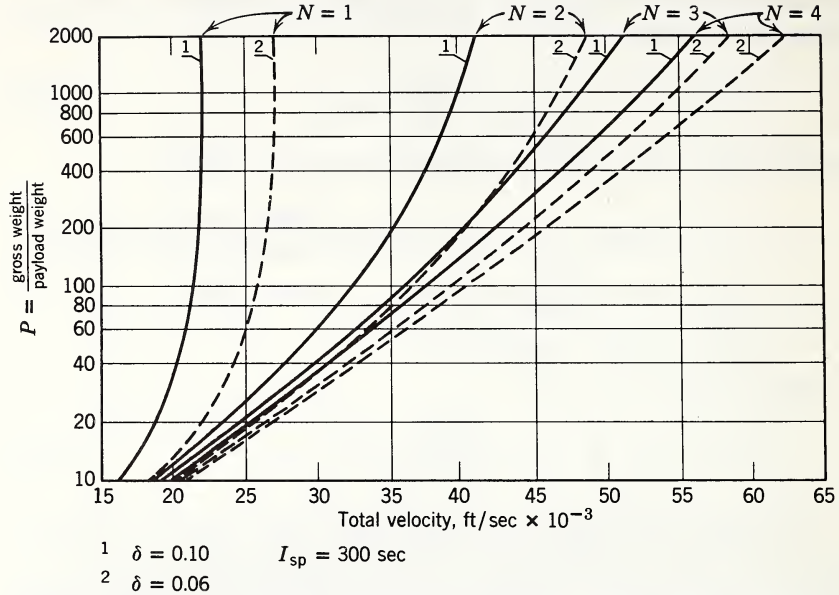

Fig. 9.6 Effect of staging and structure factor on vehicle payload ratio and velocity.

Figures 9.6 and 9.7 show curves plotted from eq. 9.33. These figures illustrate the effects of the principal parameters on which vehicle performance depends. The effects that are

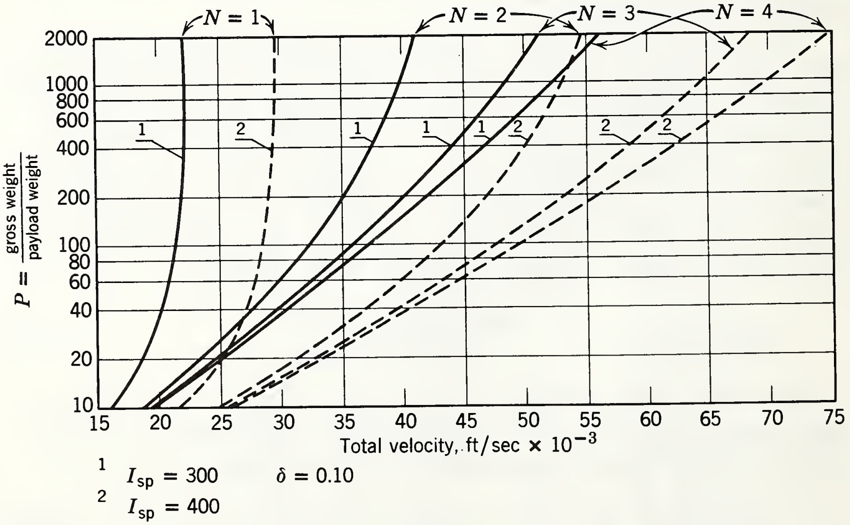

Fig. 9.7 Effect of staging and specific impulse on vehicle payload ratio and velocity.

neglected because of the simplified assumptions leading to eq. 9.33 will be discussed later.

Figure 9.6 shows the influence of structure factor and number of stages on performance. Curves for $\delta = 0.10$ and $\delta = 0.06$ are shown for $I_{sp} = 300$ sec and $N = 1, 2, 3, 4$. A vacuum specific impulse of 300 sec corresponds to common modern propellant combinations, of which liquid oxygen and kerosene is a typical example. Both curves for $N = 1$ rise steeply beyond $P = 100$, indicating that increased vehicle size is an unattractive means for performance improvement near the limits of one-stage vehicle velocity. Comparison of the curves for $\delta = 0.10$ and $\delta = 0.06$ shows that reduced structure factor results in modest performance gains at low velocities and increasing gains at higher velocities. Two stages offer significant performance advantages over one stage, even at modest velocities.

Three stages provide an improvement over two, but not as much improvement as between one and two. Four stages provide an even smaller improvement. The diminishing improvement in velocity capabilities shows that there is little to be gained beyond three or four stages. Performance improvement from a reduced structure factor also diminishes with an increased number of stages.

Figure 9.7 shows the influence of specific impulse on vehicle performance. Curves of V versus P are plotted for $\delta = 0.10$ and $I_{sp} = 300$ sec and 400 sec for $N = 1, 2, 3$, and 4. Specific impulse of 400 sec corresponds to high-energy propellants, of which liquid oxygen and liquid hydrogen are a typical combination. Increased I_{sp} displaces the curves appreciably, even in the low-velocity region. The performance improvement with increased I_{sp} increases with the number of stages in the region of large P values. The diminishing returns beyond three or four stages are still apparent. From the curves of Figs. 9.6 and 9.7, it appears that total velocities in the vicinity of 80,000 ft/sec will probably be attainable with large chemical rockets.

In most rocket designs it would be unusual for several stages to have identical structure factor and specific impulse. The rocket engines of upper stages usually have high nozzle expansion ratios, providing better vacuum specific impulse than a first stage with the same propellants. Specific impulse of the first stage varies in flight from sea level to vacuum conditions because of ambient pressure thrust reduction. The vacuum I_{sp} value for first stages is usually used in expressions such as eq. 9.33, since most of the stage velocity is gained at altitude during high acceleration.

The various stages of a multistage vehicle ordinarily have different structure factors. Increased stage size usually results in a lower structure factor. Both engine components and tanks become a smaller fraction of total stage weight as size increases. Weight-scaling laws for components such as thrust chambers, turbopumps, tanks, and engine mounts can be developed analytically. Complete stages are generally too complex for useful analytical scaling. However, experience with actual designs of rocket stages permits an empirical estimate of structure factor for a useful range of stage sizes. Figure 9.8 shows a band within which structure factors can be expected for modern rocket stages with thrust vector control.

Determination of the structure factor for a stage requires specifying which items are to be included in the stage weight and which in the payload. Stage weight is usually considered to include all items that are necessary for operation of the stage; it does not include some items necessary for mission accomplishment, but without which the stage would still function. Guidance equipment, tracking beacons, some power supplies, and range safety equipment are examples of items not

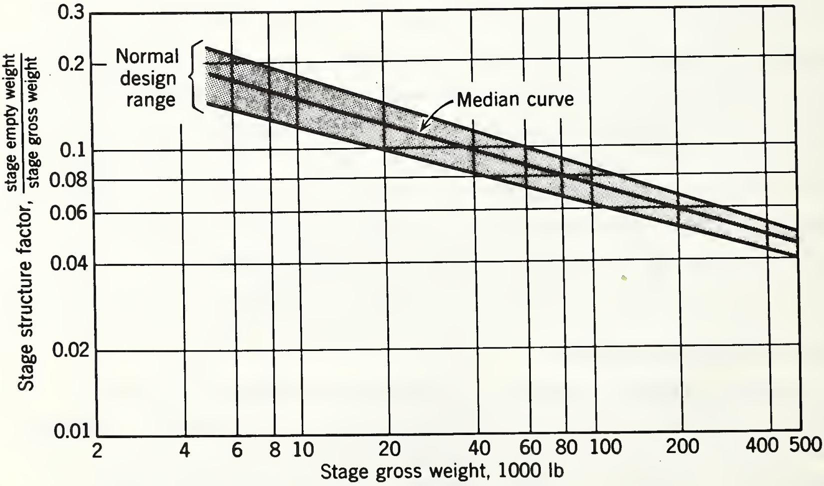

Fig. 9.8 Structure factor dependence on stage weight. Derived from empirical data on stages with thrust vector control.

ordinarily considered part of stage weight. Interstage structure is usually considered part of the stage to which it remains attached. If the interstage structure between the ith and (i + 1)st stages is separated after staging, it is usually considered part of the payload of the ith stage, but not part of the (i + 1)st stage weight.

Minimum values of P and corresponding staging ratios for vehicles with different I_{sp} and δ values for each stage can be determined.[18, 19] The methods used optimize designs for a specified equivalent velocity. The resulting staging ratios are not necessarily optimum for actual flight trajectories where losses for each stage are different. However, P has a flat optimum so it does not increase greatly over a considerable range of staging ratios. For this reason approximations to optimum staging ratios give P values which are adequate for many preliminary design purposes.

9.5 MISSIONS AND VEHICLE SIZE

Methods for determining mission equivalent velocity requirements are presented in Section 9.3. The performance capabilities of rocket vehicles in terms of total velocity may be found in Section 9.4. Estimates of the size of rocket vehicles needed for various missions can be obtained by combining these analyses. Table 9.3 shows the way that required vehicle weight-to-payload ratio varies with design characteristics for typical examples of space missions. The values in Table 9.3 were obtained from the curves of Fig. 9.7, using mission equivalent velocity values from Table 9.2. Weight-to-payload values for other missions can be obtained by the same methods.

The ballistic missile mission shows that additional stages do not improve performance significantly because velocity requirements are modest. For $I_{sp} = 400$ sec, P decreases only from 14 to 12 when the number of stages increases from two to four. In an actual vehicle, P might even increase because the smaller stages of the four-stage vehicle would probably have higher structure factors. The earth satellite missions have sufficient equivalent velocity to benefit appreciably from increased number of stages for $I_{sp} = 300$. The more ambitious lunar and interplanetary missions are possible only with a

TABLE 9.3

Approximate Vehicle Weight to Payload Ratios for Space Missions

(Structural factor $\delta = 0.1$)

		Vehicle Gross Weight to Payload					
	Number of Stages	N = 2		N = 3		N = 4	
	Specific Impulse I_{sp} sec	300	400	300	400	300	400
Ballistic missile	6,000-mile range	44	14	33	14	30	12
Earth satellite	200-mile altitude	77	20	50	16	44	16
	20,000-mile altitude	...	120	420	67	270	58
Moon	Impact	1200	65	205	44	150	39
	Land	...	330	1200	120	600	98
	Land and return[a]	...	...	...	400	...	260
Mars and Venus	Land Mars or Venus[a]	2000	78	250	49	180	47
	Land Mars and return[a]	...	...	...	680	...	390
	Land Venus and return[a]	...	...	...	...	...	...

[a] Aerodynamic deceleration in planetary atmospheres.

... = P > 2000.

combination of high-energy propellants, the advantages of staging, and large vehicle-to-payload weight ratios. The mission to land on Venus and return requires nearly 80,000-ft/sec velocity. In Table 9.3 this mission is shown to need a vehicle-to-payload weight ratio greater than 2000, even with four stages and $I_{sp} = 400$ sec. Examination of Figs. 9.7 and 9.8 indicates that this mission might be possible for very large vehicles in which the mean structure factor could be less than 0.10.

The use of an earth satellite space station as an intermediate step for such missions does not reduce the over-all vehicle-to-payload weight ratio. However, a space station permits departure from orbit with the combined payloads of several initial launch vehicles. The advantage of such a procedure is that payload size would not be limited by the capacity of the largest single first-stage vehicle available.

9.6 SYSTEM INTEGRATION OF VEHICLES, STAGES, AND PAYLOADS

Mission equivalent velocities and vehicle sizing are only one step in achieving a vehicle design. The full scope and detail required are indicated in many of the other chapters of this volume. Mission operating requirements frequently dictate basic design choices for propellants, rocket engines, structure, materials, control methods, staging sequence, power supplies, and payload arrangement. Interactions between these design choices usually necessitate consideration of the system as a whole to determine the best over-all design. Some of the factors involved will be considered here briefly. Besides design considerations for the vehicle as a whole, each stage has its own peculiar design problems (Fig. 9.9).

First-stage design is dominated by operation in the atmosphere with a steeply rising trajectory. The rocket engine expansion ratio and chamber pressure must be suitable for sea-level operation. A thrust-to-weight ratio above about 1.2 is desirable to reduce gravity losses, but values above 1.7 may cause aerodynamic heating or burnout acceleration problems. Staging in the atmosphere can cause stability and control problems.

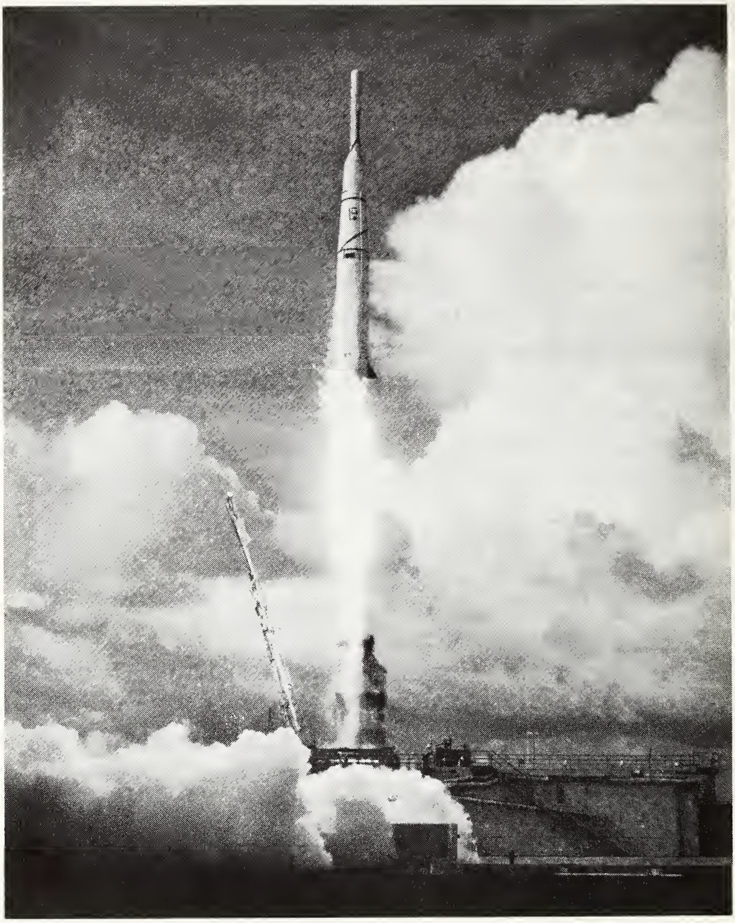

Fig. 9.9 Launching on August 7, 1959, of the three-stage Able 3 vehicle which placed the Explorer VI satellite into an eccentric orbit for space environment and propagation experiments. First-stage Thor missile, second-stage liquid-propelled AJ10-101A, third-stage solid-propelled ABL-248 A3.

Altitude stages can usually have thrust-to-weight ratios near 1.0 without serious gravity loss penalties. Provisions for altitude start, and sometimes restart, are typical system requirements. A coast period attitude control system is necessary for missions which require coasting. Long coast periods frequently require provision for temperature control (Fig. 9.10).

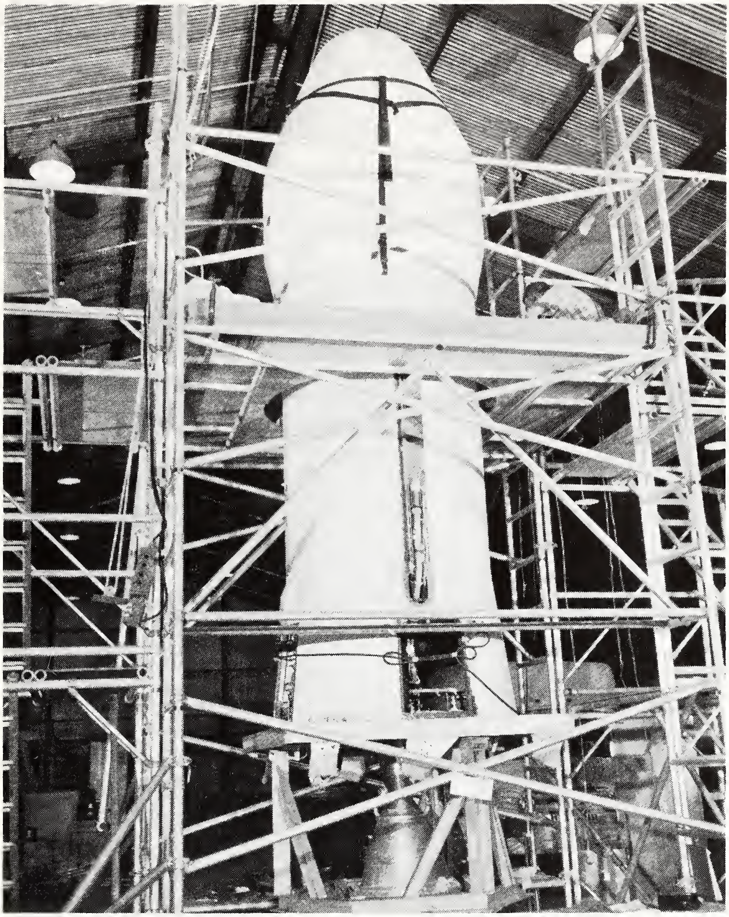

Fig. 9.10 Upper stage and payload cover of Transit II-A navigation satellite. The AJ10-104 stage is shown here during vertical checkout prior to assembly with the Thor first stage.

The final stage in any burning period must be capable of burnout velocity adjustment to required accuracy. Most liquid rockets can be shut down with an impulse repeatability corresponding to a few tenths of a second of full thrust. If this accuracy is not adequate, small vernier rockets must be provided to give precise velocity adjustment. For some precision lunar or interplanetary missions a midcourse velocity correction must be provided by vernier rockets fired from tracking data.

Vehicle payload is usually defined as equipment which is provided specifically for accomplishment of the intended mission. It may remain attached to the last powered stage or it may be separated, depending on specific objectives. Packaging techniques for this equipment depend on the nature of the mission to be accomplished.

For ballistic missiles, the primary payload packaging consideration is re-entry of the warhead into the atmosphere.

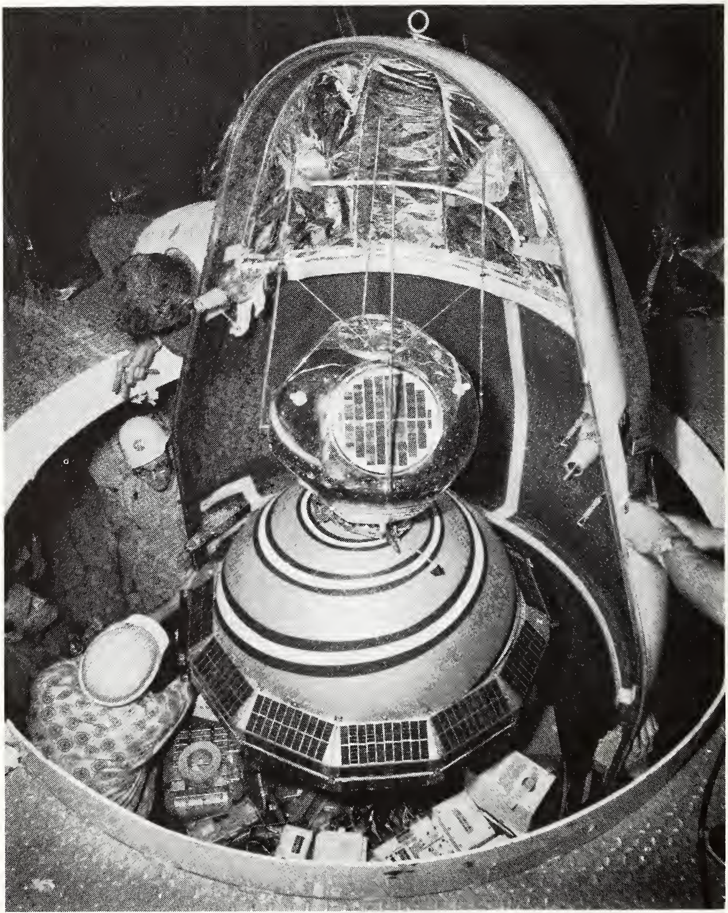

Fig. 9.11 Installation of payload cover for Transit II-A. The 36-in.-diameter main navigation satellite is shown with a 20-in.-diameter second payload containing scientific instruments. The cover protects the satellite during ascent and is jettisoned on leaving the atmosphere.

The re-entering vehicle must be suitably oriented and designed to withstand heating, drag deceleration, and lateral oscillations. Portions of the payload, usually including the guidance equipment, remain attached to the vehicle and are destroyed with it on encountering the atmosphere (Fig. 9.11).

Packaging of satellite, lunar, and interplanetary payloads can become quite complex, involving system interactions with the launch vehicle. The method of attitude orientation is an important characteristic of such payloads. Stabilization by spinning is attractive because of simplicity. However, spin stabilization imposes mass distribution requirements and imposes a fixed spin axis orientation. The alternative is attitude control to an inertial or electromagnetic signal reference by jets or reaction wheels. Such control imposes considerable equipment complexity. The choice of orientation method depends on details of the purpose of each mission. Power supply for extended duration is a major payload design problem. Solar, nuclear, chemical, and battery power each have their own advantages and problems which vary with different applications. Design of payloads of this type usually requires consideration of the interactions between attitude orientation,

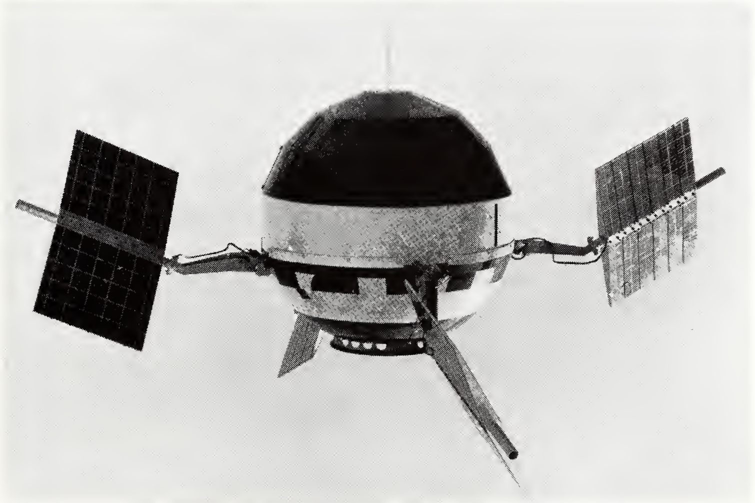

Fig. 9.12 Pioneer V solar satellite launched toward the orbit of Venus on March 11, 1960, by the Able 4 vehicle. Solar cell arrays provide power for experiments and transmitters. Color pattern is for temperature control. Antenna is located on top.

power supply, temperature control, and the achievement of basic mission objectives (Fig. 9.12).

The design of a complete vehicle for an intricate mission such as a lunar or planetary landing requires step-by-step consideration of a tremendous variety of detailed problems. Together, the total equipment for such a venture comprises a system so complex that it can be analyzed and tested only in parts, whereas in operation it must function as a whole. The accomplishment of this type of integrated operation is the essence of system engineering of space vehicles.

9.7 SYMBOLS USED IN THIS CHAPTER

GM = product of gravitational constant G and mass of the attracting body M ($\mathrm{ft}^3/\mathrm{sec}^2$)
I_{sp} = specific impulse (sec)
N = number of stages in multistage vehicle
P = gross weight to payload ratio
R = radius of body (ft)
S = surface range (ft)
T = period of orbit (sec)
V = velocity (ft/sec)
ΔV = velocity increment (ft/sec)
W = weight (lb)
e = orbital eccentricity
g = surface acceleration of gravity ($32.2\ \mathrm{ft}/\mathrm{sec}^2$)
i = orbit inclination
m = mass ratio
r = radius from center of attraction (ft)
β = angle of velocity vector to the line between the vehicle and the attracting body
δ = structure factor
η = mean angular rate of body in orbit (radians/sec)
θ = angle in orbit from perigee
$\Delta\theta$ = orbit angle difference
λ = dimensionless orbit parameter
ϕ = launch azimuth angle from north
ψ = latitude angle
ω = rate of rotation (radians/sec)

Subscripts

E = Earth
I = injection

L = moon
LO = lunar orbit
M = Mars
O = conditions at stage ignition
P = payload
S = Sun
T = theoretical or ideal value
V = Venus
a = apogee
c = circular satellite orbit
d = departure planet
e = destination planet
f = conditions at encounter with planetary atmosphere
g = heliocentric condition at end of transfer
h = impact conditions
i = ith stage of N-stage vehicle
k = conditions of approach to destination planet
l = contribution from launch losses
m = minimum energy transfer
p = perigee
r = residual conditions after escape
s = heliocentric conditions after escape
t = total value
0 = condition at stage ignition
1 = condition 1
2 = condition 2
ω = contribution from Earth rotation
∞ = condition at $r = \infty$

REFERENCES

1. H. S. Seifert, Space Technology, John Wiley and Sons, New York, 1959.
2. S. Herrick, R. M. Baker, Jr., and C. G. Hilton, "Gravitational and Related Constants for Accurate Space Navigation," Eighth International Astronautical Congress, Barcelona, Spain, October, 1957.
3. F. R. Moulton, An Introduction to Celestial Mechanics, Macmillan, New York, 1914.
4. R. W. Buchheim, "Motion of a Small Body in Earth-Moon Space," The RAND Corporation, RM-1726, June 4, 1956.
5. L. Davis, D. Follin, and L. Blitzer, Exterior Ballistics of Rockets, D. Van Nostrand, Princeton, N. J., 1958.

6. L. Blitzer, "On the Motion of a Satellite in the Gravitational Field of the Oblate Earth," Space Technology Laboratories, Report GM-TM-0165-00279, 1958.
7. R. W. Buchheim and H. A. Lieske, "Lunar Flight Dynamics," The RAND Corporation, Report P-1453, 1958.
8. H. Preston-Thomas, "Generalized Interplanetary Orbits," J. Brit. Interplanet. Soc., **2**, No. 2, 77-78 (1952).
9. H. S. Seifert, M. M. Mills, and M. Summerfield, "Physics of Rockets," Am. J. Phys., **15**, 1-21, 121-140, 255-272 (1947).
10. S. Rubin, "General Equation for Rocket Velocity," ARS Journal, 29, 219 (1959).
11. K. A. Ehricke, "Comparison of Advanced Propulsion Systems: Solar-Heating, Arc-Thermodynamic and Magnetohydrodynamic Systems," Convair Report AZK-002, 1957.
12. E. Stuhlinger, "Electrical Propulsion System for Space Ships with Nuclear Power Source," J. Astronautics, 149-152 (1955); 11-54 (1956).
13. J. H. Irving and E. K. Blum, "Comparative Performance of Ballistic and Low-Thrust Vehicles for Flight to Mars," Second Annual AFOSR Astronautics Symposium, Denver, Colorado, April 1958; published in Vistas in Astronautics, Vol. 2, Pergamon Press, New York, 1959.
14. A. B. Mickelwait and R. C. Booton, "Analytical and Numerical Studies of Three-Dimensional Trajectories to the Moon," Space Technology Laboratories, Report GM-TM-0165-00287, 1958.
15. K. A. Ehricke, "Interplanetary Mission Profiles," Convair Report AZM-023, 1958.
16. W. Hohmann, Die Erreichbarkeit der Himmelskoerper (Accessibility of Celestial Bodies), Oldenburg, Munich, 1925.
17. M. Vertregt, "Interplanetary Orbits," J. Brit. Interplanet. Soc., **16**, 326 (1958).
18. M. Vertregt, "A Method for Calculating the Mass Ratios of Step-Rockets," J. Brit. Interplanet. Soc., **15**, 95 (1956).
19. H. H. Hall and E. D. Zambelli, "On the Optimization of Multistage Rockets," ARS Journal, 28, 463 (1958).

10

STRUCTURE FUNDAMENTALS

A. Kaplan

10.1 INTRODUCTION

The principal functions of the missile structure are to maintain the proper space relationship between the missile components, to protect them from the external environment, and to maintain a desired external shape. These functions are to be performed with a reliability commensurate with that of the other components and with a minimum expense in weight. Thus, to an extent even greater than for other components, the structure is intimately concerned with all the components and functions of the missile system. Consequently, the first part of this chapter consists of a description of the trajectory characteristics which affect the missile structure. The second part discusses the resulting loads which act on the structure. Together these parts provide insight into the performance required of the structure and how this performance is affected by changes in the missile system. The final part of this chapter discusses the analysis and characteristics of some structural elements that are the most typical of ballistic missiles.

10.2 TRAJECTORY CHARACTERISTICS

In other chapters the characteristics of ballistic missile trajectories are analyzed in detail. In this section these characteristics will be reviewed, emphasizing the items that most strongly affect the structure.

10.2.1 Trajectory Shape

A typical ballistic missile flight (Fig. 10.1) starts off with a short vertical rise which serves primarily to clear the launching platform and to allow the launching transients to die out before starting the pitch program. On some missiles the vertical rise is also used to obtain the proper flight azimuth direction by rolling the missile, thus avoiding the problem of designing a rotating launcher.

Following the rise, the missile is pitched over into a "zero left" or "gravity" turn. This turn serves to minimize the aerodynamic forces acting on the missile by keeping the missile axis aligned with the velocity vector. The term "zero lift" indicates that during this turn the lateral aerodynamic force or lift is minimized, and the term "gravity" emphasizes that all the turning of the velocity vector is due to the force of gravity. This turn is continued throughout the sensible atmosphere, that is, to approximately 200,000 ft.

In making performance calculations, it is often assumed that the missile is pitched over instantaneously into the initial angle β_0 of the gravity turn. For a given missile this angle serves as a parameter to specify the entire gravity turn. In practice the instantaneous pitchover obviously cannot occur. Therefore, between the vertical rise and the gravity

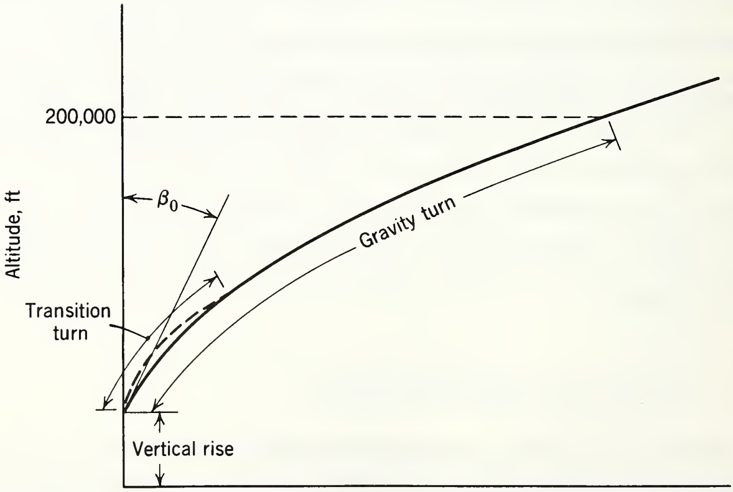

Fig. 10.1 Typical ballistic missile trajectory.

turn there is a so-called transition turn. This transition is designed to attain the ideal gravity turn as rapidly as possible without exceeding the pitching velocity and acceleration limits of the missile or its equipment.

After leaving the sensible atmosphere, the missile trajectory is shaped to achieve maximum performance as discussed in Chapter 9. Since the aerodynamic forces are negligible and the required maneuvering forces are low, the details of this shaping are of secondary interest for the structure.

10.2.2 Axial Acceleration

The second trajectory characteristic of interest is the total axial acceleration or, more specifically, the axial load factor N. This factor is obtained by dividing the total axial acceleration by g, the acceleration caused by gravity:

$$N = \frac{F - D}{W} \tag{10.1}$$

where F is the engine thrust
D is the total aerodynamic drag
W is the weight of the missile

The axial load factor N, when multiplied by the weight of a component, gives the axial force necessary to support that component in the missile. Starting from its launch value, the load factor (Fig. 10.2) increases continuously with time. The rate of increase is relatively small at first but becomes very large near stage burnout. Although the rate of change of weight (propellant consumption) and the thrust remain approximately constant, the decrease in the total weight causes the percentage rate of change of weight to increase.

Figure 10.2 compares time variations of axial load factor of two different vehicles. The first has an initial load factor of 1.5 and a burnout load factor of 15. The second is identical with the first except that the second-stage weight is doubled. Although this reduces the burnout load factor to 7.9, the load factor during most of the burning time is practically unchanged.

10.2.3 Dynamic Pressure

The next trajectory item of interest is the dynamic pressure q, expressed in equation form as

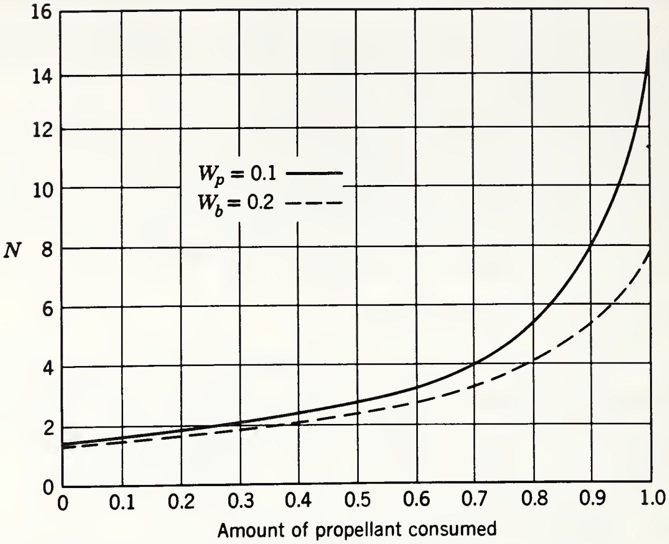

Fig. 10.2 Typical variation of axial load factor N.

$$q = \frac{1}{2} \rho U^2 \tag{10.2}$$

where ρ is the air density
U is the missile velocity

The parameter q is of interest since it is the dimensional factor to which all aerodynamic forces are proportional. In Fig. 10.3

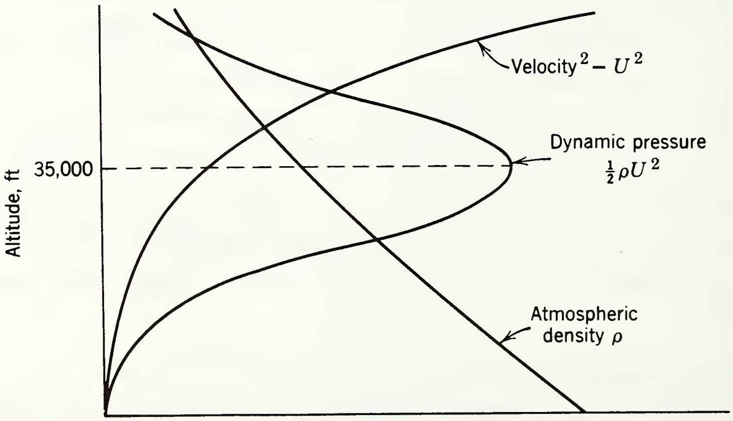

Fig. 10.3 Variation of dynamic pressure with altitude.

typical variations of ρ and U^2 with altitude are shown. The density ρ is, of course, an exponentially decreasing function of altitude, whereas U^2 increases at a rapidly increasing rate with altitude. The product q therefore starts off from zero, rapidly increases to a peak, and then rapidly dies off. For almost all nearly vertically rising missiles, this peak value occurs at approximately 35,000 ft, irrespective of the initial acceleration or acceleration history. Typical peak values for large missiles are from 5 to 30 psi. This value is primarily a function of the missile's initial load factor. For a given missile it is a function of the "lofting" of the trajectory, that is, the initial kick angle β_0 of the gravity turn. Decreasing β_0 will decrease the maximum value of q since any given velocity of the missile will then occur at a higher altitude.

10.2.4 Winds

So far we have been discussing an idealized trajectory through a stationary atmosphere. The vehicle, however, is also affected by the air movements which can be separated into two categories, the large-scale quasi-steady variation of the wind with altitude and the small-scale rapidly varying gusts or turbulence. The former can generally be treated as a static function or one that varies slowly with time, but treatment of the latter involves the dynamics of the vehicle system. These wind velocities vary considerably, depending on the location and the time of the year. In Fig. 10.4 is shown a profile[1] which has been used as a wind specification for several ballistic missiles. This profile is based on statistical data, and it is expected that its severity will not be exceeded more than 1 per cent of the time during the windiest season in the windiest part of the United States. However, the profile is representative of the wind conditions at the Air Force Missile Test Center, Cape Canaveral, during the winter. The important items in the profile are the maximum velocity of 300 feet/sec and the maximum shear of 0.045 ft/sec/ft. Later measurements with improved equipment have increased the shear value to 0.070 ft/sec/ft. The peak value of the wind is associated with the jet stream phenomenon and may occur anywhere in the range between 30,000 and 40,000 ft.

Because of the wind, a missile flying an ideal gravity turn no longer has its axis aligned with the air velocity. It is,

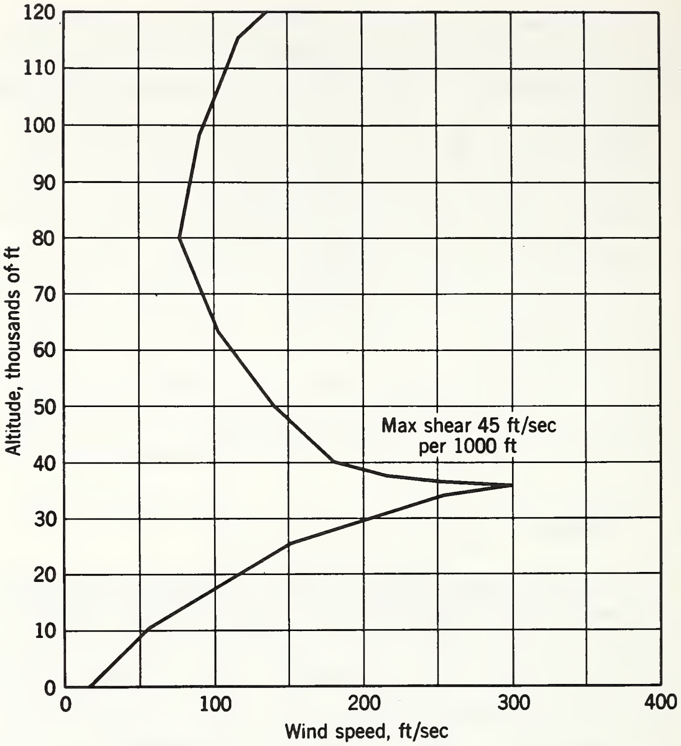

Fig. 10.4 Wind speed design profile. Maximum speed and associated maximum shear are likely to be exceeded only 1 per cent of the wintertime over the northeastern U.S.A.

therefore, subjected to lateral aerodynamic forces which tend to move the missile in the direction of the wind. It should be noted that the peak values of the wind and the dynamic pressure both occur at approximately the same altitude, 35,000 ft. This, then, is the altitude region in which the aerodynamic forces acting on the missile are at a maximum.

10.3 PRINCIPAL LOADS

10.3.1 Axial Load

The major force acting on the missile is the engine thrust F, which is counteracted by the inertia of the distributed mass of the missile and by the aerodynamic drag D. Within the structure this reaction results in a compressive load P_x vary-

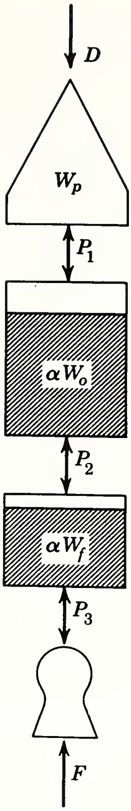

Fig. 10.5 Forces acting on a simplified missile.

ing along the length of the missile. The compressive load at station x is obtained by summing the forces acting forward of that station. Thus

$$\begin{aligned} P_x &= NW_x + D_x \\ &= (F - D)\frac{W_x}{W} + D_x \qquad (10.3) \\ &\approx F\frac{W_x}{W} + D_x \end{aligned}$$

where W_x and D_x are the weight and drag force, respectively, of the sections forward of station x.

Let us apply this equation to the idealized missile stage of

Fig. 10.5. It consists of a payload (or second stage) of weight W_p, a forward tank containing oxidizer of initial weight W_o, an aft tank containing fuel of initial weight W_f, and an engine weight W_e. The ratio of the weight of the fuel or oxidizer remaining at any given time to their initial weight is called α. Since this is an idealized missile, the structural weight has been minimized and, therefore, can be neglected. It will be assumed for simplicity that all the drag acts on the payload and that the thrust remains constant. Then the load P_1 acting between the payload and the forward tank is given by

$$P_1 = NW_p + D$$

The time variation of P_1 will be identical to that of the load factor N, except for a small peak due to drag near the time of maximum dynamic pressure. For a heavy streamlined payload (or second stage) this peak will be very small, but for a lightweight blunt payload it can be quite large.

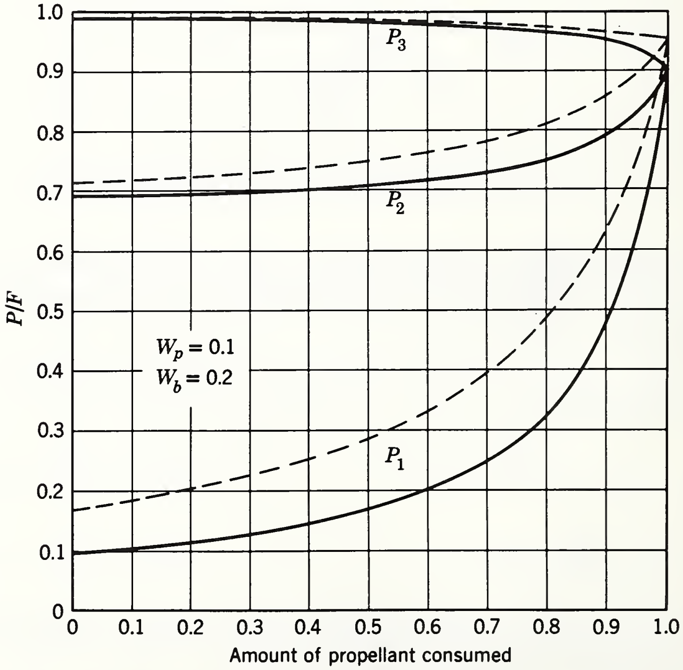

Fig. 10.6 Variation in axial loads.

$$\begin{aligned} P_2 &= P_1 + N\alpha W_o \\ &= P_1 + F\frac{\alpha W_o}{W} \\ &= P_1 + F\,\frac{\alpha W_o}{W_e + W_p + \alpha(W_o + W_p)} \end{aligned} \tag{10.4}$$

It can be seen that the second term actually decreases with time, so that P_2 increases more slowly than P_1. Similarly, P_3, the axial load at the bottom of the tank is given by

$$P_3 = P_2 + N\alpha W_f$$

$$P_3 = P_2 + F\,\frac{\alpha W_f}{W_e + W_p + \alpha(W_0 + W_p)} \tag{10.5}$$

If the thrust remains constant, P_3 will actually decrease slightly with time. The variation in loads is shown in Fig. 10.6 for typical values of

$$\frac{W_0}{W_f} = 2, \quad \frac{T}{W_b} = 1.65, \quad \frac{W_p}{W_b} = 0.01, \quad \frac{W_e}{W_b} = 0.01$$

where $W_b = W_e + W_0 + W_f$ is the launch weight of the first stage. The effect of an increase in payload weight is shown by the dotted lines which are plotted for $W_p/W_b = 0.02$. It can be seen that only the forward load P_1 is significantly affected by a 100 per cent increase in the payload weight. By contrast, doubling the thrust would have doubled all the loads. The variation of N for the two vehicles was shown in Fig. 10.2.

10.3.2 Bending Loads

Bending loads are due to the combination of lateral aerodynamic force or lift, the lateral component of the thrust vector used for control, and the inertia reaction to these forces, conceptually shown in Fig. 10.7. For bodies of revolution typical of ballistic missiles, the resultant of the lift force acts near the nose. Therefore, a lateral engine control force is required to maintain the attitude of the missile.

The total bending moment M_b at any station x can be expressed as

$$M_b\left(\frac{x}{l}\right) = f_l\left(\frac{x}{l}\right)L + f_f\left(\frac{x}{l}\right)F\,\delta \tag{10.6}$$

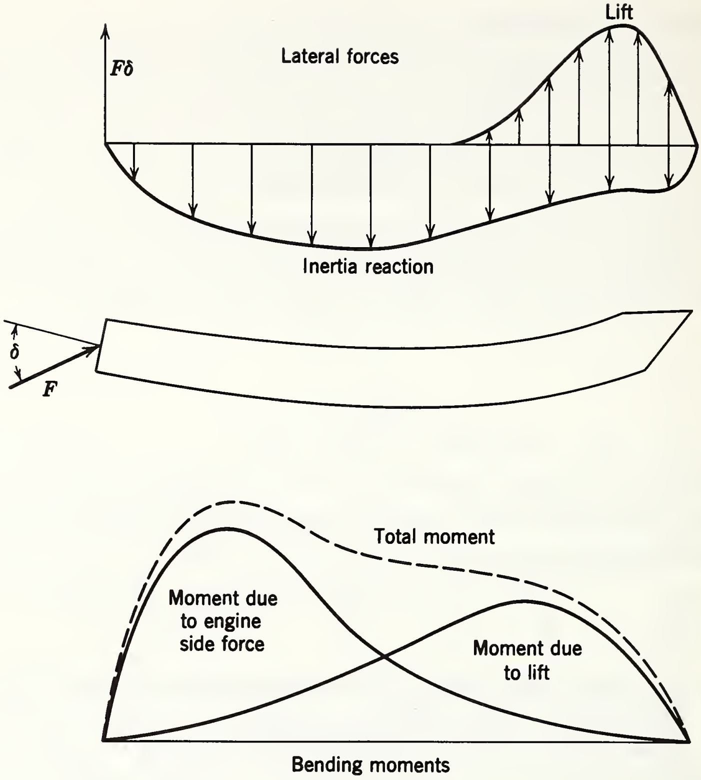
Lift
$F\delta$
Lateral forces
Inertia reaction
δ
F
Total moment
Moment due to engine side force
Moment due to lift
Bending moments

Fig. 10.7 Lateral forces and bending moments acting on a missile.

where f_l and f_f are nondimensional functions of the longitudinal mass distribution of the missile and f_l is additionally a function of the longitudinal lift distribution. Typical bending moment distributions are shown in Fig. 10.7. For the simple case of a uniform mass with the lift concentrated at the nose ($x = l$),

$$f_f\left(1-\frac{x}{l}\right) = f_l\left(\frac{x}{l}\right) = \left(1-\frac{x}{l}\right)\left(\frac{x}{l}\right)^2 \qquad (10.7)$$

For the trimmed condition (no pitching acceleration) $F\delta$ equals L and the maximum moment occurs at the center.

$$(M_b)_{max} = \frac{1}{4} lL \quad \text{(uniform mass distribution)} \qquad (10.8)$$

The mass distribution resulting in the largest moment is that in which all the mass is concentrated at the center. Then

$$(M_b)_{max} = \frac{1}{2} lL \quad \text{(mass concentrated at center)} \tag{10.9}$$

Because of a bending moment, the missile structure is subjected to a stress σ_b, which varies linearly across the section according to the well-known formula

$$\sigma_b = \frac{M_b c}{I} \tag{10.10}$$

where I is the moment of inertia of the cross-sectional area of the structure about its centroid and c is the distance from the centroid. If the structural members are located in a circle of radius r, then

$$I = \tfrac{1}{2} Ar^2 \tag{10.11}$$

where A is the cross-sectional area of the structural members, and the maximum bending stress is given by

$$\sigma_b = \frac{2M_b}{Ar} \tag{10.12}$$

Because of an axial load the structure is subjected to a uniform stress

$$\sigma_{axial} = \frac{P}{A} \tag{10.13}$$

If we denote by P_{eq} the axial load which causes the same stress as the maximum stress due to the moment M_b, then

$$P_{eq} = \frac{2}{r} M_b \tag{10.14}$$

Using the formula for $(M_b)_{max}$ for a uniform mass distribution, eq. 10.8,

$$P_{eq} = \frac{1}{2} \frac{l}{r} L \tag{10.15}$$

It is thus seen that, because the high values of the length-to-radius ratio l/r typical of ballistic missiles, lateral forces will cause much larger internal stresses or loads than would equal axial forces. Therefore, it is important that these lateral forces be minimized.

Ballistic missiles are generally symmetric about their longitudinal axis so that aerodynamic lift occurs only when there is an angle of attack between this axis and the relative air velocity. For a given missile this lift is proportional to the angle of attack, the dynamic pressure q, and a complicated function of the Mach number. As mentioned earlier, ballistic missiles are programmed to follow a gravity turn through the atmosphere so that, ideally, the angle of attack is zero. In practice, angles of attack can result from the approximations made in the pitch program and from errors in its execution caused by such things as gyro drift. However, the major cause of angles of attack during the gravity turn is the wind. Large angles of attack can also occur during the transition turn, which is why it is important to complete the turn early, before the dynamic pressure becomes large.

Lateral engine forces also occur as a result of guidance and program commands and control instabilities. However, except during the transition turn, these forces are generally small compared to those required to resist the overturning moment of the aerodynamic forces. Since the maximum wind velocity and the maximum dynamic pressure occur almost simultaneously at about 35,000 ft, this is also the point at which the missile is subjected to the maximum bending loads.

10.3.3 Thermal Loads

In flying through the atmosphere a missile is heated by aerodynamic friction. This aerodynamic heating rate is roughly proportional to ρU^3. Its variation with time is thus similar to that of the dynamic pressure, except that its peak is shifted to a later time. The temperature of an exposed structural element is proportional to the integral of the heating rate and inversely proportional to the element's heat capacity. Thus the rise in the temperature lags behind the rise in the heating rate. As the temperature becomes high, radiation from the structure becomes significant and serves to reduce the effective heating rate. For elements with low heat capacity, the maximum temperature is reached when equilibrium is attained between aerodynamic input and the radiation loss.

From this discussion it can be seen that the increase in temperature is small at the time of maximum dynamic pressure, but that the temperature typically is either approaching or has reached its peak value at the time of first-stage burnout.

Heating has two different effects on the missile structure. First, as a result of differential expansion, internal stresses are developed. These stresses have to be treated in the same way as stresses due to applied loads. The differential expansion may occur either as the result of uniform heating of two different materials or the nonuniform heating of a single material. In many cases, by careful detail design, these differential expansions and their effects can be minimized.

The second effect is the reduction of material strength because of the increased temperature. This requires the addition of more material to carry the same load or the substitution of a material resistant to high temperatures which, in general, will be less efficient.

However, in many cases, because of the transient nature of the heating, the more efficient solution to the temperature problem will be to avoid it through the use of insulation, radiation shields, or low-temperature ablating surfaces.

10.3.4 Internal Pressure

The largest part of the missile structure consists of the tanks which contain the propellants. For solid propellant systems these tanks are subjected to the full combustion pressure of the engine, whereas for pressure-fed liquid systems they are subjected to pressures considerably higher than the combustion pressure. For pump-fed liquid systems the tank pressure must be sufficient to prevent cavitation in the pumps. In addition to these pressure requirements, liquid-filled tanks must resist the hydrostatic pressure caused by the inertia of the fluid. For the most efficient use of the structure these tanks must also support the flight axial and bending loads. The internal pressure must, therefore, be considered both as a load and as a structural element. As a load, the pressure determines the thickness of the tank walls. As a structural element, the pressure supports an axial load equal to its value times the cross-sectional area of the tank (in a 10-ft-diameter tank, 1 psi will support an axial load of 11,000 lb) and, in addition, serves to increase the buckling resistance of the tank walls. Since the pressure is already required for the engines, this is a case in which something is obtained for nothing. If additional load-carrying capability is required, it is possible to further increase the pressure. However, in doing this it must be remembered that the weight of the tank and the pressurization gas will be increased, and so will the weight of the system used to supply the gas.

For solid propellant or pressure-fed systems the tank pressure requirement remains fairly constant in flight unless the thrust is programmed. For a pump-fed system the pressure requirement varies with time, but for simplicity in the system the pressure is usually regulated at either a constant gage or a constant absolute value. In the latter case, the gage pressure, which determines the stress in the tank walls, will increase as the missile rises through the atmosphere. By contrast, the hydrostatic component of the pressure is a maximum at launching and will decrease during flight despite the increase in the acceleration. For a cylindrical tank the product of the hydrostatic pressure at the bottom and the cross-sectioned area of the tank equals the total inertia reaction of the contents. The pressure is thus proportional to the second term of either eq. 10.4 or eq. 10.5. This, of course, does not hold for the second-stage tanks. Since they are still full at first-stage burnout, the maximum hydrostatic pressure occurs at that time. Fortunately, the small length-to-diameter ratio of most second-stage tanks tends to reduce the resulting high values of the hydrostatic pressure.

10.3.5 Dynamic Loads

The loads outlined so far are static or slowly varying loads which, fortunately, design most of the structure. In addition to these, there are a large number of rapidly varying or oscillating loads. These are more difficult to predict since they involve the detailed elastic characteristics of the structure and its interaction with the control system. Some typical dynamic loads are those caused by the rapid build-up and decay of engine thrust at launch and burnout, oscillation of the thrust about its steady-state value, sudden release at launch and staging, gusts, fuel sloshing, and control system oscillations. If neglected, these loads can often be catastrophic. However, by careful design of the system they can be kept within acceptable limits. For the structure this attempt to limit dynamic loads generally results in requirements being placed on its stiffness as well as on its strength. The subject of dynamic loads will be covered in detail in Chapters 8 and 16.

10.3.6 Summary of Flight Loads

This discussion of missile structural loads reveals that there are two primary critical conditions for the missile structure. The first occurs at, or near, the time of maximum dynamic pressure and is characterized by:

1. Large aerodynamic forces and moments.
2. Relatively low axial acceleration.
3. Low temperatures.
4. Sensitivity to trajectory shape and atmospheric conditions.
5. Critical locations being generally at the rear where the peak bending moments are superimposed on the relatively constant axial load, or at the extreme front where aerodynamic forces may be of prime importance.

The second condition occurs at stage burnout and is characterized by:

1. Small aerodynamic forces.
2. Large axial acceleration.
3. High temperatures.
4. Lack of sensitivity to wind conditions and, except for thermal effects, to changes in the trajectory shape.
5. Critical locations generally at the front since the axial loads there are at a maximum. In addition, the forward sections are affected the most by aerodynamic heating.

Secondary, but sometimes important, critical conditions occur at launching and during the transition turn.

10.3.7 Ground Loads

In addition to the flight loads discussed so far, the missile is also subjected to ground loads. These include loads caused by transportation, handling, erection, winds while erected, and possible enemy action. Because of the importance of missile weight, the philosophy in general is to design the missile structure for flight loads and then to design the ground-handling equipment so that these loads are not exceeded.

10.4 TYPICAL STRUCTURAL ELEMENTS

Having discussed missile trajectories and loads, it is now necessary to discuss some of the typical structural elements

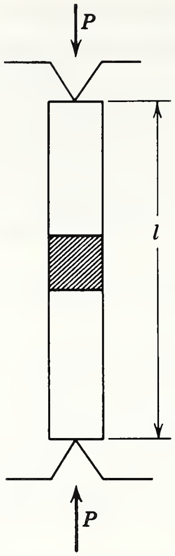

Fig. 10.8 Pinned-end column.

which are subjected to these loads. A missile is primarily made up of the tanks containing the propellants and the structures connecting the tanks together. In flight these are primarily subjected to axial compressive loads with some superimposed bending loads. In addition, the tanks are subjected to tensile loads caused by internal pressure. We will, therefore, study the analysis and design for minimum weight of two types of structures, a column designed by buckling and a pressure vessel designed by internal pressures, and finally a combination of the two.

10.4.1 Design for Buckling

The simplest example of a structure designed by buckling is the uniform solid column with pinned (hinged) ends shown in Fig. 10.8. For this column the buckling load P is obtained from the classical formula of Euler

$$P = \frac{\pi^2 EI}{l^2} \tag{10.16}$$

where E is the modulus of elasticity (Young's modulus) of the column material, l is the length, and I is the minimum centroidal moment of inertia of the cross section. The formula agrees very well with experimental results. If a square cross section of area A is assumed, then

$$I = \frac{1}{12} A^2 \tag{10.17}$$

On substituting this into eq. 10.17, the area required to support the load P can be obtained:

$$A = \sqrt{12Pl^2/\pi^2 E} \tag{10.18}$$

The corresponding stress at buckling, σ_{cr}, is given by

$$\sigma_{cr} = \frac{P}{A} = \left[\frac{\pi^2}{12} E \frac{P}{l^2}\right]^{1/2} \tag{10.19}$$

and the total weight W of the column is

$$W = \rho Al = \sqrt{12/\pi^2} \frac{\rho}{\sqrt{E}} l^2 \sqrt{P} \tag{10.20}$$

where ρ is the density of the column material. The weight per unit length and load, which can be taken as a measure of efficiency, is

$$\frac{W}{PL} = \frac{\rho}{\sigma_{cr}} = \sqrt{12/\pi^2} \frac{\rho}{\sqrt{E}} \sqrt{l^2/P} \tag{10.21}$$

It is seen that the required weight of the column increases as the square root of the load, the square of the length, and the ratio of the density of the material to the square root of its modulus.

The ratio ρ/E, which is proportional to the speed of sound in the material, is approximately the same for most structural materials as shown in Table 10.1. For these materials, since

$$\frac{\rho}{\sqrt{E}} = \sqrt{\rho}\,\sqrt{\rho/E} \tag{10.22}$$

the required column weight is proportional to the square root of the material density. Thus, the less dense the material, the lighter the column. The table also shows two notable exceptions to this rule. Fiberglas and beryllium both have the same density as magnesium, but Fiberglas has a modulus less than half that of magnesium whereas beryllium has a modulus over six times as large. This points up one of the big reasons for the interest in the development of beryllium. Fiberglas

TABLE 10.1

Density and Elastic Modulus for Common Structural Materials

Material	ρ, lb/in.^{3}	E, psi $\times 10^{-6}$
Magnesium	0.065	6.5
Aluminum	0.10	10
Titanium	0.16	16
Steel	0.28	28
Molybdenum	0.37	42
Fiberglas	0.065	2.5 - 3
Beryllium	0.065	41

used as a solid material is distinctly inferior to magnesium for buckling loads. It is only when its effective density is decreased by fabricating it as a sandwich with a lightweight core that it shows good performance.

The rule just given is also only true as long as the yield strength of the material is not exceeded. Above the yield stress of a material, the stress-strain curve is no longer linear and the effective value of the modulus reduces rapidly with increasing stress. Thus a simple column cannot support a stress significantly higher than the yield stress. From eq. 10.19 it is seen that as the design load P increases with no change in length, the stress at buckling increases and thus the efficiency of the column. This continues until the yield stress of the material is achieved. Thus for a heavily loaded column (large values of P/l^2), the yield stress as well as the ratio $\sigma/\sqrt{E}$ is important. This fact is shown in Fig. 10.9 where the ratio W/lP is plotted as a function of the loading parameter P/l^2 for various materials. It is seen that because of relatively low yield stresses of the lighter materials, magnesium and aluminum, they are efficient only for the smaller values of the loading parameter. However, this is generally the region of most interest for missile structures.

One obvious method of increasing the load-carrying efficiency of a column is to increase the moment of inertia I while maintaining a constant cross-sectional area, that is, by spreading the material in the column as far apart as possible. The cross section which does this is the hollow cylinder. This section is of particular interest for missiles because it can serve the function of providing an external surface for sections between tanks and also represents a tank

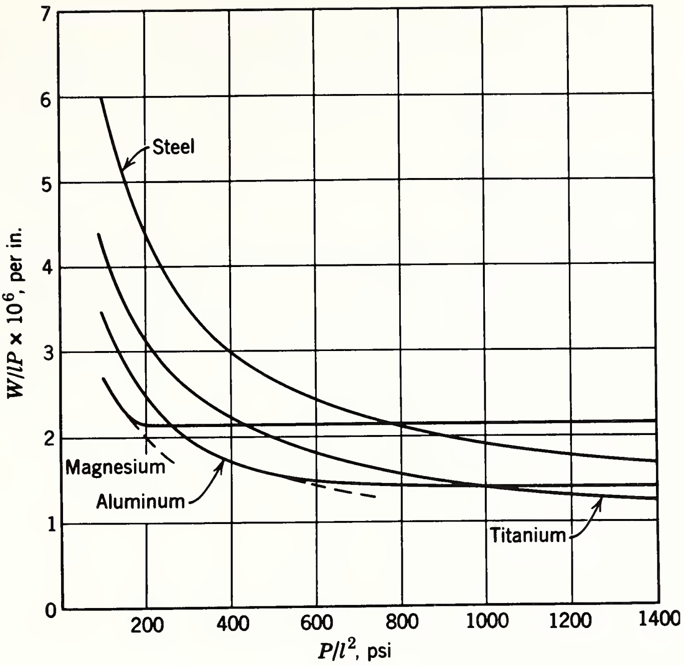

Fig. 10.9 Column efficiency of several structural materials.

itself when unpressurized. For a given cross-sectional area, the moment of inertia can be made as large as desired by increasing the radius r while decreasing the thickness proportionately. However, a point is soon reached at which, instead of buckling as an entire column, the thin skin of the cylinder buckles locally even when the cylinder is very short. For cylinders of reasonable length the theoretical buckling stress based on linearized elasticity theory is given by

$$\sigma_{cr} = \frac{1}{\sqrt{3(1-\mu^2)}} E\frac{t}{r} = 0.606E\frac{t}{r} \tag{10.23}$$

where μ is Poisson's ratio ($\mu \approx 0.3$ for most structural materials). However, in contrast with the case for the simple column, the agreement between theory and experiment is very poor, with the experimental results usually being less than half the theoretical value. Thus the design of thin-walled cylinders is based on empirical relations. One of the most convenient of these is due to Kanemitsu and Nojima.[2]

$$\sigma_{cr} = \left[9\left(\frac{t}{r}\right)^{0.6} + 0.16\left(\frac{t}{r} \cdot \frac{r}{l}\right)^{0.3}\right] E\frac{t}{r} \tag{10.24}$$

which is applicable for

$$500 \leq \frac{r}{t} \leq 3000$$

The term within the brackets replaces the theoretical value of 0.606. Except for small values of l/r, the length effect is small. It will, therefore, be neglected in what follows. Then

$$\sigma_{cr} = 9E\left(\frac{t}{r}\right)^{1.6} = \frac{P}{2\pi rt} \tag{10.25}$$

and the thickness required for a given load is

$$t = \left(\frac{r^{0.6}P}{18\pi E}\right)^{1/2.6} \tag{10.26}$$

The total weight of the column is

$$\begin{aligned} W &= 2\pi rtl\rho \\ &= 1.33r^{1.23}P^{0.385}\left(\frac{\rho}{E^{0.385}}\right)l \end{aligned} \tag{10.27}$$

and the weight per unit length and load is

$$\frac{W}{Pl} = 1.33\frac{\rho}{E^{0.385}}\left(\frac{r^2}{P}\right) \tag{10.28}$$

This equation is similar to that for the simple column, except that now the geometric parameter is the radius of the cylinder r rather than the length l. The measure of load intensity is provided by P/r^2, that is, by the pressure obtained when the load is divided by the included area of the cylinder. In addition, the weight is proportional to $\rho/E^{0.385}$ rather than $\rho/E^{0.5}$. This indicates an increased advantage for low-density materials.

If, for the required load intensity, the simple hollow cylinder is too heavy, it can be reinforced by longitudinal stiffeners (which act as simple columns) combined with frames or by a waffle- or sandwich-type construction. Each of these methods serves to decrease the effective ρ/E value of the cylinder wall.

10.4.2 Design for Tensile Loads— Pressure Vessels

The principal structural elements carrying tensile loads in a missile are the propellant tanks. The design of these for minimum weight is very important because of their large size. This importance is further emphasized in solid propellant and pressure-fed liquid systems where the tank pressures are equal to or greater than the combustion pressure. As a result, for these types of systems there is a very strong interaction between the engine and the propellant tank design.

For a given allowable normal stress and a given required volume, the tank shape of minimum weight is the sphere. In an ideal sphere of uniform thickness, the stress σ_s is the same at all points and at each point is equal in all directions parallel to the surface:

$$\sigma_s = \frac{pr}{2t} \qquad (10.29)$$

Or if σ is the allowable material stress:

$$t_s = \frac{pr}{2\sigma} \qquad (10.30)$$

where r is the radius of the sphere and p is the internal pressure. The weight of the tank W_s is then given by

$$\begin{aligned} W_s &= 4\pi r^2 t_s \rho \\ &= 2\pi r^3 p\left(\frac{\rho}{\sigma}\right) \qquad (10.31) \\ &= \frac{3}{2}\left(\frac{\rho}{\sigma}\right) pV \end{aligned}$$

where ρ is the density of the tank material and V is the volume of the tank.

Since a spherical shape provides the lightest-weight tank, it is often used for the small auxiliary tanks, particularly when the pressures are high. However, for the main propellant tanks, the large diameters required and the difficulties of joining two tanks will usually cause the system weight to be high. Therefore, cylindrical tanks with flattened spherical (ellipsoidal) closures are generally preferred.

For a cylinder the stress in the direction parallel to the axis is equal to that for a sphere, but the stress σ_c in the circumferential direction is twice that for a sphere:

$$\sigma_c = \frac{pr}{t} \tag{10.32}$$

Thus

$$t_c = \frac{pr}{\sigma} = 2t_s \tag{10.33}$$

and the weight W_c of a cylindrical section is given by

$$\begin{aligned} W_c &= 2\pi r t_c p \\ &= 2\pi^2 p \frac{\rho}{\sigma} \qquad (10.34) \\ &= 2\frac{\rho}{\sigma}\ pV \end{aligned}$$

Thus a cylindrical section of tank weighs 50 per cent more than an equivalent spherical tank of the same volume. For other shapes the equations for the weight of the tank differ only in the leading coefficients. It is seen that the weight of a tank is proportional to the product of its internal pressure and volume and the ratio of the material density to its maximum allowable normal stress. Thus, ideally, it makes no difference whether a given volume is obtained from a number of small tanks or from a single large tank.

This weight equation also points out another important consideration. The gas required to pressurize the propellant tanks is usually obtained from an auxiliary high-pressure tank. If the process of gas transfer is isothermal (pV = constant), eq. 10.22 indicates that the weight of this auxiliary tank will be equal to that of the main tanks. It is, of course, usual practice to reduce this weight by heating the pressurizing gas, but this equation emphasizes the fact that, in considering the use of pressure as a structural element, the weight of the pressurization supply system is a significant factor.

The pressure vessel stresses discussed up to now are the membrane stresses required to support the internal pressure. In addition to these, local bending and shear stresses are developed whenever there is a change in curvature or wall thickness, such as at joints, at the junction between a cylindrical section and a bulkhead, and at fittings and outlets. These stresses arise from the necessity of forcing continuity between sections which have different expansions under pressure. They are generally called discontinuity stresses. For materials which are "ductile," that is, which have large plastic deformation before failing, the peaks of the discontinuity stresses are relieved by local yielding. For these materials the discontinuity stresses to some degree can be neglected, particularly if the design factor of safety is large. However, for missiles, the importance of light weight has reduced the factor of safety and forced the use of high-strength materials not previously considered for pressure vessel use. These materials with higher strength generally do not behave in a ductile manner. To obtain these lightweight pressure vessels, there must be increased emphasis on the determination of discontinuity stresses and their reduction through proper transitions in shape and thickness.

In deriving the tank-weight equations, it was assumed that failure was a function of the maximum normal stress alone. Although this is at least approximately true, it has been demonstrated that some metals in certain hardness ranges can withstand a significantly higher maximum stress in the 2:1 stress field of the cylinder than in the 1:1 stress field of the sphere or the 1:0 stress field of the standard tensile test. In addition, many high-strength materials appear to behave in a ductile fashion in the standard tensile test but fail prematurely in a brittle fashion when subjected to the combined stresses typical of pressure vessels. Thus there is a great deal to be known about the behavior of high-strength materials in pressure vessels; and it is particularly dangerous to design lightweight pressure vessels solely on the basis of simple tensile test strength.

10.4.3 Combined Tension and Compression—Pressure Vessels as a Load Carrying Element

In addition to being required to act as pressure vessels, missile tanks are required to sustain flight and ground axial and bending loads. Sometimes they must do this while unpressurized, as for ground conditions or for first-stage flight of the upper stage of a solid propellant missile. Then the discussion in the section on compressive structures is directly applicable.

In most cases, however, the flight and pressure loads will act simultaneously. As discussed earlier, the internal pressure causes longitudinal tensile stresses in cylinders equal to half the circumferential stress. Thus, if the pressures are sufficiently high, the tank walls will always remain in tension and there is no problem of buckling. Since the wall thickness is primarily determined by the circumferential stress, the additional axial and bending loads will have little effect on the structure. This is, of course, typical of solid propellant and pressure-fed liquid propellant vehicles.

For intermediate or low pressures, the flight loads may cause compressive longitudinal stresses in the tank walls. We are then interested in the effect of the pressure on the longitudinal buckling stress of the tank. Investigations have been made of the simple monocoque cylinder.[3,4] These have shown a significant increase in the buckling stress (Fig. 10.10). However, results indicate that the increase in the buckling stresses reaches a limit as the pressure is raised. The sum of this increase in buckling stress and the longitudinal stress caused by pressure gives the total effect of the pressure in resisting external loads.

In case this is not sufficient, the simplest solution is to increase the tank wall thickness either with or without an increase in pressure. If the added strength required is large, a more efficient solution is to add longitudinal stiffeners. Although this configuration needs further study, initial investi-

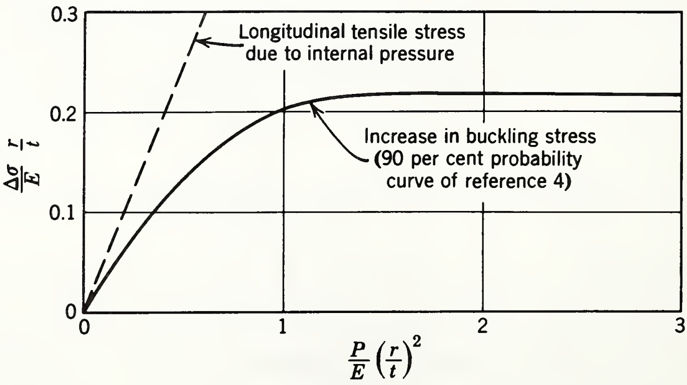

Fig. 10.10 Increase in compressive buckling stress caused by internal pressure.

gations[5] indicate that internal pressure has a greater effect on the buckling stress of a longitudinal cylinder than it does on a simple monocoque cylinder.

REFERENCES

1. N. Sissenwine, "Windspeed Profile, Windshear and Gusts for Design of Guidance Systems for Vertical Rising Air Vehicles," Air Force Surveys in Geophysics, 57, November 1954.
2. S. Kanemitsu and H. Nojima, "Axial Compression Tests of Thin Circular Cylinders," M.S. Thesis, Guggenheim Aeronautical Laboratory, California Institute of Technology, 1939. Reviewed in E. E. Sechler and L. G. Dunn, *Airplane Structural Analysis and Design*, John Wiley and Sons, New York, 1942, Chapter 8.
3. E. E. Sechler and Y. C. Fung, "Buckling of Thin-Walled Circular Cylinders Under Axial Compression and Internal Pressure," *J. Aeronaut. Sci.*, **24**, No. 5 (1957).
4. L. A. Harris, H. S. Suer, W. T. Skene, and R. J. Benjamin, "The Stability of Thin-Walled Unstiffened Circular Cylinders under Axial Compression Including the Effects of Internal Pressure," *J. Aeronaut. Sci.*, **24**, No. 8 (1957).
5. W. Thieleman, "New Developments in the Non-Linear Theories of Buckling of Thin Cylindrical Shells," paper presented at the Durand Centennial Conference on Aeronautics and Astronautics, Stanford University, August 5-8, 1959.

11

STRUCTURES: STATIC INTEGRATED ANALYSIS

Harry W. Johnson

11.1 INTRODUCTION

The design of a missile begins with the selection of a preliminary configuration and size based on side studies, and on past experience whenever possible. In the development program the preliminary design is revised and refined until it is capable of working properly and meeting all the system requirements. The extent to which the original configuration must be changed before the final form emerges depends on how well (and sometimes how luckily) all the requirements and interactions have been anticipated. Nothing is more discouraging or more difficult to accommodate than the discovery, after the design is well along, that a basic requirement either has been overlooked or, as is sometimes the case, has been added arbitrarily.

The purpose of this chapter is to examine some of the complicated interactions of the missile structure with the rest of the system and with the design environment, and to indicate how the structure, like other subsystems, must be integrated with the entire system. A computational technique, which was developed specifically to investigate some of these interactions, and to assist in performing missile-sizing studies and in making preliminary design decisions, will be discussed.

11.2 STRUCTURAL DESIGN REQUIREMENTS AND SYSTEM INTERACTIONS

A large variety of structural requirements exist and must be kept in mind during the design and development of a ballistic missile. These include general system requirements, functional requirements, and design criteria, proceeding from the general to the specific.

The structure must first be compatible with all other subsystems and contribute to the successful accomplishment of the mission for which it is designed and developed. Other general requirements include criteria for structural reliability and other economic considerations, such as critical materials, fabrication processes, maintainability, and useful lifetime—all of which must be consistent with the over-all system economics. It must be borne in mind that the minimum cost structure in the final analysis is not necessarily that costing the least number of dollars per pound of delivered hardware, but is that which contributes to the minimum cost of a successful operational system.

The structure must also fulfill such easily defined functional requirements as serving as a framework for mounting the payload and all subsystems in their proper places, and being capable of maintaining the required spatial arrangements and alignments during flight while transmitting thrust and control forces. Structure must likewise protect delicate components from the external environment, provide an acceptable over-all aerodynamic configuration, and include volumes large enough to contain the propellants which alone may exceed 90 per cent of the launch weight. For solid propellant engines the propellant storage tanks must also serve as combustion chambers. The structural design must further provide installation and maintenance accessibility to subsystem components, and yet incorporate suitable over-all handling characteristics.

Structural design criteria include the structural design philosophy and all the detailed rules by which the structure is to be developed and by which its performance can be evaluated. The structural philosophy must be consistent with other subsystem requirements. The degree of design conservatism to be employed must take into account such factors as the importance of structural weight to the system, the specific operational requirements, the time scale for the development, and the number of new concepts employed. Structural design criteria also specify appropriate strength and rigidity requirements to permit the proper functioning of all subsystems. Certain arbitrary quantities, such as factors of safety, and special structural design factors for fittings, castings, and other structural elements, are usually specified, as well as the structural allowables to be used.

In general, the structural design problem is to find a design solution which achieves all the objectives with a minimum number of compromises. Stating the design problem in a way that leads to its solution is not an easy matter, especially since some of the requirements are not easily translated into analytical forms. Because of the structure's multipurpose role, it is virtually impossible to know initially which of the numerous requirements have the strongest influence on its design. Side studies undertaken to investigate effects of individual parameters are always helpful, but they may also be misleading when taken out of context because they neglect interaction effects.

The propellant tanks in a liquid propellant missile present an excellent example of system interactions with the structure. Since the propellant tanks constitute a major portion of the structural weight of any stage, ample reason exists for being concerned with basic design features which minimize tank weight.

To illustrate some aspects of the problem, four possible but different bipropellant tank combinations, having nominally the same volumes, are illustrated in Fig. 11.1. Each can be contrasted in a number of ways.

11.2.1 Integral versus Nonintegral Structure

The tanks in Fig. 11.1a can scarcely be called integral because the intertank structure actually provides the structural continuity, whereas in each of the other configurations the load path includes the tank walls. Although not shown, it would also be possible to contain the propellants within an inner, nonintegral compartment even in the cylindrical tank configurations. The basic question is whether integral tanks are more or less advantageous to the entire system operation.

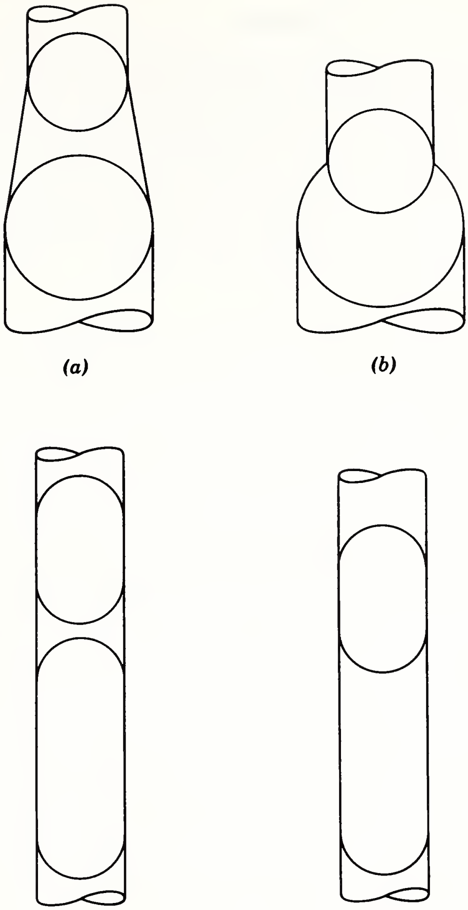

(a) (b) (c) (d)

Fig. 11.1 Four comparative bipropellant tank configurations: (a) separate spherical tanks with intertank structure, (b) nested spherical tanks with common bulkhead and no intertank structure, (c) separate cylindrical tanks with intertank structure, (d) nested cylindrical tanks with common bulkhead and no intertank structure.

11.2.2 Aerodynamic Forces

Each configuration presents different aerodynamic problems. The spherical tank configurations may cause higher drag than the slender cylindrical tank configurations, but the cylindrical configurations produce higher aerodynamic bending moments and stresses in the structure.

11.2.3 Aerodynamic Heating

The aerodynamic heating of the tanks in each configuration is different primarily because of different aerodynamic shapes and different amounts of tank surfaces exposed. Virtually no tank heating occurs for configuration a, whereas both the tanks in c and d are subjected to heating. Furthermore, the differing drags may cause the powered-flight trajectories and heat inputs to each configuration to differ.

11.2.4 Internal Pressures and Axial Loads

Tank pressures are required for at least three reasons: to force propellants into the pumps and prevent cavitation, to prevent propellant boiling in the tank, and to provide structural load-carrying capability for integral tank designs. The latter feature may occur gratis, at least in part, and is one of the advantageous features of integral tanks. The hydrostatic head for any axial acceleration is greater near the bottom of the cylindrical tank than in its equivalent spherical tank, and varies in an entirely different way with time as the acceleration and contents vary. There is virtually no axial load in the spherical tank walls a except owing to pressure stresses, whereas the lower tanks in each of the other configurations must support the weight of the forward tank by a combination of pressure and structural reactions. Another factor to be considered in the nested tank configurations b and d is that the pressures in each tank must be maintained in such a way to prevent bulkhead inversion. In d especially, the decision must be made, based on a number of factors, whether the common bulkhead should be concave downward or upward. Clearly, the internal pressures required by the four configurations may be quite different; therefore the skin gages required on the basis of geometry, pressure, and heating requirements will also differ. It should be noted that aerodynamic heating is also influenced by the skin thickness, which in turn depends on the heating.

11.2.5 Total Weights

The intertank structure weights, interstage structure weights, and pressurization system weights must all be considered in comparing the over-all system weights for different propellant tank configurations. Various side studies primarily concerned with the geometric influences have been made,[1] but such studies are more valuable for establishing trends than for determining actual system weights. Detailed weight comparisons for any specific design problem under consideration must take into account not only the factors already briefly mentioned but also the fact that different volumes may be required for different tank configurations due to some of these influences.

11.2.6 Fabricability

Each configuration presents different problems in fabrication, tooling, development effort, and in design change flexibility. For example, changing the volume of a spherical tank requires extensive redesign, but cylindrical tank volumes may be changed more easily if only elongated.

11.2.7 Handling and Transportation

The problems of handling and transporting large-diameter, short structural configurations are quite different from those for smaller-diameter, longer configurations. Road, rail, and aircraft size restrictions must be taken into consideration, as well as the handling facilities.

The foregoing qualitative comparisons of the alternative tank design concepts in Fig. 11.1 are by no means intended to be exhaustive but merely illustrate the necessity for understanding the entire system and how the structure is influenced by those considerations. They also point out some of the difficulties in making clear-cut design decisions.

11.3 PARAMETRIC MISSILE DESIGN ANALYSIS

Many parametric ballistic missile studies[2] have been devoted to performance investigations without considering much of the internal detail within the missile itself. Such studies establish the fundamental performance characteristics and gross sizes of systems, but bringing into being missiles which have the characteristics assumed in performance studies is a more difficult matter.

Although system analyses were first applied to design problems many years ago, as systems have grown more complicated, more specialized, and more expensive, the importance of thorough systems studies has increased proportionally. Moreover, the numerical computational capabilities of present high-speed electronic computers make possible parametric investigations which were not practical a decade ago.

Consequently, it is now possible to develop comprehensive analytical methods that take into account these many interactions. To be most useful, an analysis today should include the following features and capabilities.

1. It should include all identifiable subsystem interactions, environmental factors, and physical parameters necessary to define a complete system. It may be enlarged or reduced in content and scope from time to time to extend or limit its functions. Not only physical characteristics, but also logistics, costs, and other more intangible factors can be included as desired, although with concomitant increases in complexity.
2. It should possess the capability of seeking optima for the over-all system, based on arbitrary criteria which can be modified if desired.
3. It should be capable of indicating the effects on and changes within each subsystem due to input changes made in the analysis.
4. It should be able to show the performance trade-off or exchange ratios among the system variables and thereby disclose the strong and weak functions influencing system performance.
5. It should be capable of showing sufficient internal detail to give a fair definition of each subsystem analyzed and thereby assist in establishing specific preliminary designs.

Figure 11.2 indicates a much simplified block diagram of a program developed a few years ago at Space Technology Laboratories for the design analysis of liquid propellant rocket-powered long-range ballistic missiles. This analysis was the result of a large cooperative effort on the part of numerous people.[3-6] With appropriate modifications it has been used at different times to investigate one-, one-and-a-half-, two-, and three-stage missile and spacecraft booster vehicles, both liquid and solid propellant. It has played an important role in several missile programs by helping to establish missile sizes and stage ratios, preliminary structural

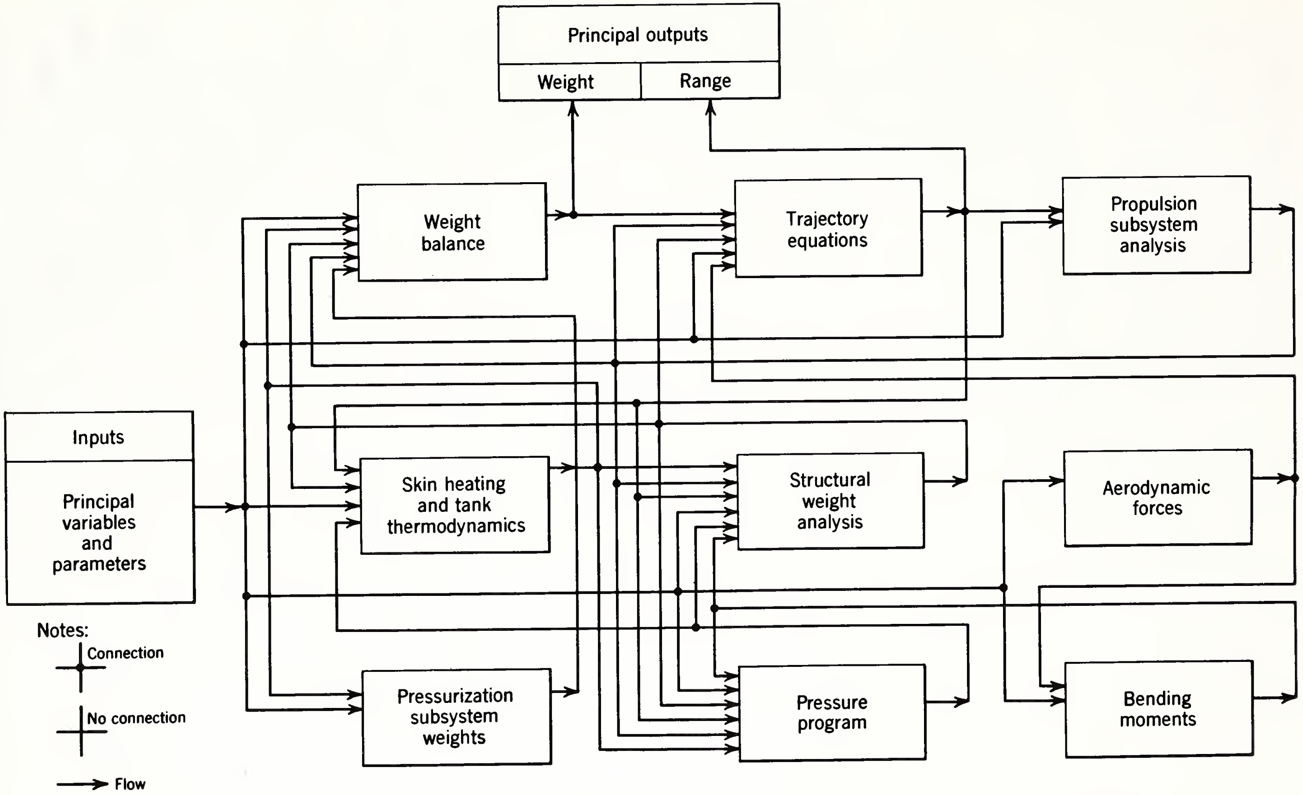
Principal outputs
Weight
Range
Inputs
Principal variables and parameters
Notes:
Connection
No connection
Flow
Weight balance
Skin heating and tank thermodynamics
Pressurization subsystem weights
Trajectory equations
Structural weight analysis
Pressure program
Propulsion subsystem analysis
Aerodynamic forces
Bending moments

Fig. 11.2 Simplified block diagram for generalized missile design analysis.

design details, and performance exchange ratios among the variables. For simplicity, and to highlight the basic philosophy instead of the details, Fig. 11.2 omits the numerous interconnections of individual quantities associated with each portion of the analysis and shows only the fundamental input-output relationships among the separately identified major portions of the analysis.

The underlying philosophy and method is to reduce the complicated system problem to a number of smaller and more manageable subsidiary, or component, analyses. Analytical expressions are then obtained to interrelate these component analyses, and also to relate them to the trajectory, the external environment, and the arbitrary quantities used to characterize the system. These quantities include such items as propulsion specific impulse, propellant weight flows and burning times, tank length to diameter ratios, stage weight ratios, material properties, allowable stresses, and factors of safety, residual propellant fractions, types of pressurization gas, and numerous other system characteristics which must be specified in advance. By means of these interrelating expressions, all component analyses are connected to each other in a self-consistent, closed network in such a way that output quantities from each analysis represent input quantities to other analyses, as appropriate. In this analysis the gross weight and range were selected as the principal outputs.

The analysis is set in motion after a set of boundary conditions or design constraints which characterize the system are specified, and after a set of initial conditions are selected. The missile is then "flown" on the computer, and the equations of motion along the trajectory are solved at specific times of flight. These trajectory details and external environmental factors are introduced to the component analyses, which in turn determine, by iterative computations, a self-consistent set of values for the internal variables such as tank pressure requirements, skin thicknesses and temperature histories, and subsystem weights. "Flights" are iterated, with each iteration incorporating certain revisions to the initial conditions, such as weights and skin gages, as determined in the preceding iteration. Trajectory parameters are also varied to produce maximum range, and the iteration procedures are continued until satisfactory convergence is obtained, as indicated by arbitrarily small changes in gross weight. The configuration obtained has the minimum gross weight and maximum range capability consistent with the set of arbitrary system characteristics on which the specific solution is based.

The design solution is defined in the principal outputs by gross weight and maximum range, and is further defined within the component analyses in terms of the weights of the stages and the principal subsystems, and by detailed subsystem characteristics such as tank pressures, skin thicknesses and temperature histories, the flight loads, and other trajectory details. By varying the input quantities, other design solutions can be obtained. Weight and performance exchange ratios among the quantities thus varied can then be obtained by comparing solutions.

The component analyses include the trajectory equations, a weight summary, and analyses to determine propellant tank details and other structural weights, propulsion system characteristics, pressurization system requirements, aerodynamic and control forces, and tank skin heating and internal thermodynamics.

Input data are termed principal variables and parameters. They include burning times and propellant flow rates, combustion chamber pressures, basic trajectory parameters, payload weights, guidance and control system weights, specific impulses, atmospheric properties, structural material allowables, safety factors, weight-scaling factors, and a variety of other details which must be entered into the component analyses.

The form of the analysis makes it possible to tailor the propulsion system to the specific needs of the mission by permitting the thrusts and engine weights to be results from, instead of inputs to, the analysis. Realistically, however, most liquid propellant vehicles are based on a relatively small number of engines whose performance characteristics and weights can be specified in advance. In most applications of this analysis existing propulsion system characteristics were used as input data.

The weights summed up in this analysis to determine the gross weight and stage weights are indicated in Table 11.1. Scaling laws and proportionality factors for the major components are determined from side studies and from analysis of existing systems. Efforts are made to linearize such relationships wherever feasible, while recognizing that lineariza-

TABLE 11.1
Weight Balance for Generalized Missile Design Analysis

Item (W_i)	Origin
Payload, fixed equipment, guidance and control electronics	Basic input
Structure:	
Intertank and interstage structures	Analysis
Thrust structure	Proportional to thrust
Fairings and secondary structure	Proportional to dry weight
Propellant tanks	Analysis
Pressurization system and gas	Analysis
Propulsion system	Analysis or basic input
Hydraulic system	Proportional to thrust
Propellants system	Proportional to thrust
Propellants (expended)	Proportional to propellants
Gross weight $= \sum_i W_i$	

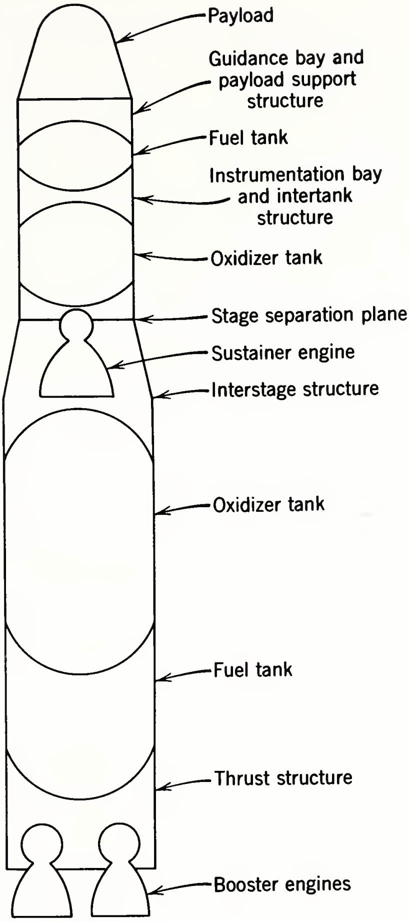
Payload
Guidance bay and payload support structure
Fuel tank
Instrumentation bay and intertank structure
Oxidizer tank
Stage separation plane
Sustainer engine
Interstage structure
Oxidizer tank
Fuel tank
Thrust structure
Booster engines

Fig. 11.3 Schematic diagram of two-stage tandem missile configuration.

tion may be accurate only in the vicinity of a given design point. For this analysis it is clear that the major computational effort is concerned with determining the propellant tanks and interconnecting structure details and weights. These structures interact most strongly with the vehicle performance requirements and cannot be described by simple weight-scaling laws.

It is not feasible to describe all the details associated with the entire analysis in this chapter, but the following general description of a propellant tank analysis will indicate some interesting aspects.

Propellant Tank Analysis. The propellant tank structural design and weight analysis can best be illustrated by a specific example. Shown in Fig. 11.3 is the schematic arrangement for a two-stage tandem missile. Obviously, in order even to set up the tank analysis, a number of assumptions must be made regarding the basic configuration. The assumptions made for this particular analysis are as follows.

1. All propellant tanks are integral and circular cylindrical. Second-stage tanks are completely independent of each other; first-stage tanks employ a common bulkhead separating the fuel and oxidizer compartments.
2. The oxidizer (liquid oxygen or LOX) tank is forward in the first stage and aft in the second stage; the fuel (RP-1) tank is aft in the first stage and forward in the second stage.
3. All tanks are assumed to be monocoque. Semi-monocoque construction could have been assumed without serious changes to the equations by using "equivalent monocoque" characteristics.
4. No external insulation is employed; given values of surface emissivities must be specified.
5. Existing propulsion systems are employed, having known weights, pressurization requirements, and specific impulse and thrust variations with altitude.
6. The tank walls are made of high-strength aluminum alloy; tensile and compressive strength variations with temperature must be specified.

These assumptions were entirely arbitrary; any or all can be changed to permit investigating other design concepts for comparison.

The assumed tank configurations must be simplified for purposes of analysis. Figure 11.4 shows the simplified equivalent for the first-stage tanks, consisting of a cylinder of length L, radius R, and length-to-radius ratio l_T, and having the same volume as the configuration it represents by employing the cylindrical equivalent length for the domed ends. The equivalent cylindrical tank is divided into two segments of lengths $K_o L$ and $K_f L$ for oxidizer and fuel, respectively, and expressions for weight take into account the actual bulkhead geometry and thickness requirements.

Skin thicknesses are determined at a number of axial stations in each tank segment, and the tank weight computation

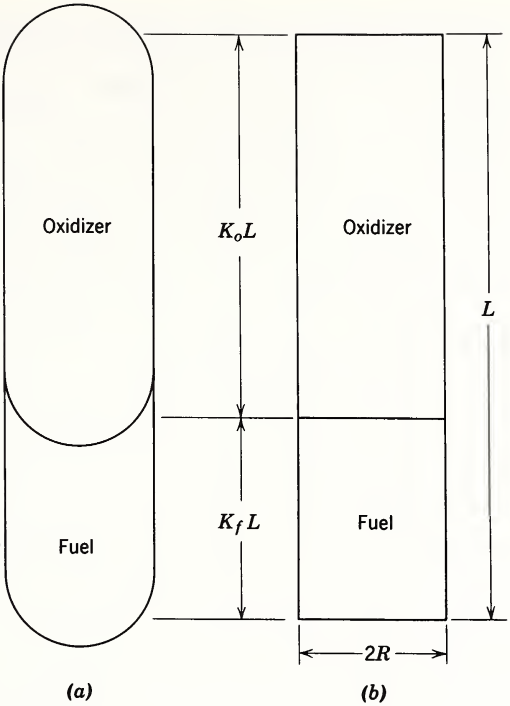

Equations

$$V = \frac{W_p}{\rho_p} = \frac{(1 + K_{RP})\omega_p t}{\rho_p}$$

$$= \pi R^2 L = \pi R^3 l_T$$

$$l_T = \frac{L}{R}$$

$$K_o = \left(\frac{W_o}{\rho_o}\right)\frac{1}{V}$$

$$K_f = \left(\frac{W_F}{\rho_F}\right)\frac{1}{V}$$

V = volume
ρ = weight density
W = weight
ω_p = propellant weight flow rate
t = burning time
K_{RP} = residual propellant factor

Subscripts

o = oxidizer
f = fuel
p = bulk mean

Fig. 11.4 Simplified tank configuration: (a) schematic configuration, (b) simplified configuration.

takes these variations into account. Only in this way can a minimum weight configuration be obtained, for the thickness requirements may vary significantly from top to bottom because of different temperature, pressure, and structural load requirements at each axial station. Furthermore, the skin thickness required at each station may vary with time during flight, and may have an even different value on the ground. Accordingly, the thickness requirements history at each axial station must be determined, and maximum values selected for the weight computation. In the present example, skin thicknesses were examined in six stations in each fuel and oxidizer tank for both ground and flight conditions. A minimum gage was also selected, based on fabrication and handling.

Ground condition. It was required that the tanks, although unpressurized, be capable of supporting the weight of the entire erected and unsupported missile for any possible combination of filled and unfilled tanks in both stages. Simultaneously, the vehicle was to be capable of withstanding the loads due to a specified lateral ground wind. Without internal pressures, the axial loads and bending moments on the tanks must be resisted solely by compressive stresses in the tank walls, so skin thicknesses must be selected to prevent buckling.

Flight conditions. In flight the tank skins must withstand hoop stresses from pressurization gas as well as the pressure of propellants at all stations beneath the liquid surfaces. These pressures may vary with time; so may the skin temperature and, therefore, allowable stress. Consequently, the entire pressure and temperature time history at each station must be examined in order to determine the maximum thickness required because of hoop tension. In this analysis the axial compressive strength of the tank skin is used at all times to assist the internal pressure in reacting the axial loads and bending moments. In addition, the incremental buckling strength due to the stabilizing effect of pressure is taken into account, and this depends on the pressure value and on the temperature-dependent modulus of elasticity and yield stress. Consequently, the compression load capability history at each station must also be computed, based on an appropriate allowable stress interaction relationship for axial load and bending moment. From this, the pressure requirement history due to structural loads is determined.

Minimum gage. Selection of a minimum skin gage is based on handling and fabrication considerations. This value represents a lower limit on thickness at each station.

Tank pressures. The gas pressures required in each tank may vary with time. Tank pressures are to prevent pump cavitation and propellant boiling, to provide some equivalent structural capability to withstand axial forces and bending moments, and to prevent reversal of common dividing bulkheads. The hoop tension stresses and skin gages are proportional to these pressurization requirements. Skin heating is related to thickness, so it also affects allowable stresses and required thickness. The values of pressure required are computed as a function of time in each tank for each separate requirement for pressure, and from these requirements a pressure envelope is obtained. However, the envelope pressure history may be physically impractical to achieve, if, for example, several extrema occur. To avoid this problem, a rational pressure schedule is selected to meet all the maximum requirements. The simplest pressure schedule, although not necessarily the only one or the best one that can be constructed, is a constant-pressure program.

Skin temperatures. Skin temperature histories are computed so that tensile and compressive stresses can be determined, as well as the heat transfer to the propellants and pressurization gas. The propellant temperature influences the vapor pressure, which in turn influences the pressure required to prevent pump cavitation. The heat balance history at each tank wall station takes into consideration aerodynamic convective heating, radiation, internal heat transfer to the liquids and gases, and the heat capacity of the skin. Skin thicknesses consistent with the pressure and buckling requirements must be employed in the heat balance, so this interaction must be accounted for in the analysis.

Typical results. Some of the results for the two-stage tandem missile configuration are illustrated in Figs. 11.5 and 11.6 for a specific design problem. The desired configuration was to have a range in excess of 5500 nautical miles, and preliminary sizing studies indicated a gross take-off weight in the vicinity of 200,000 lb for a payload of about 3500 lb and for residual propellant fractions of about 1 per cent. Table 11.2 summarizes some of the results for three designs nominally the same except for different residual propellant fractions. The first-to-second-stage weight ratio of usable propellants

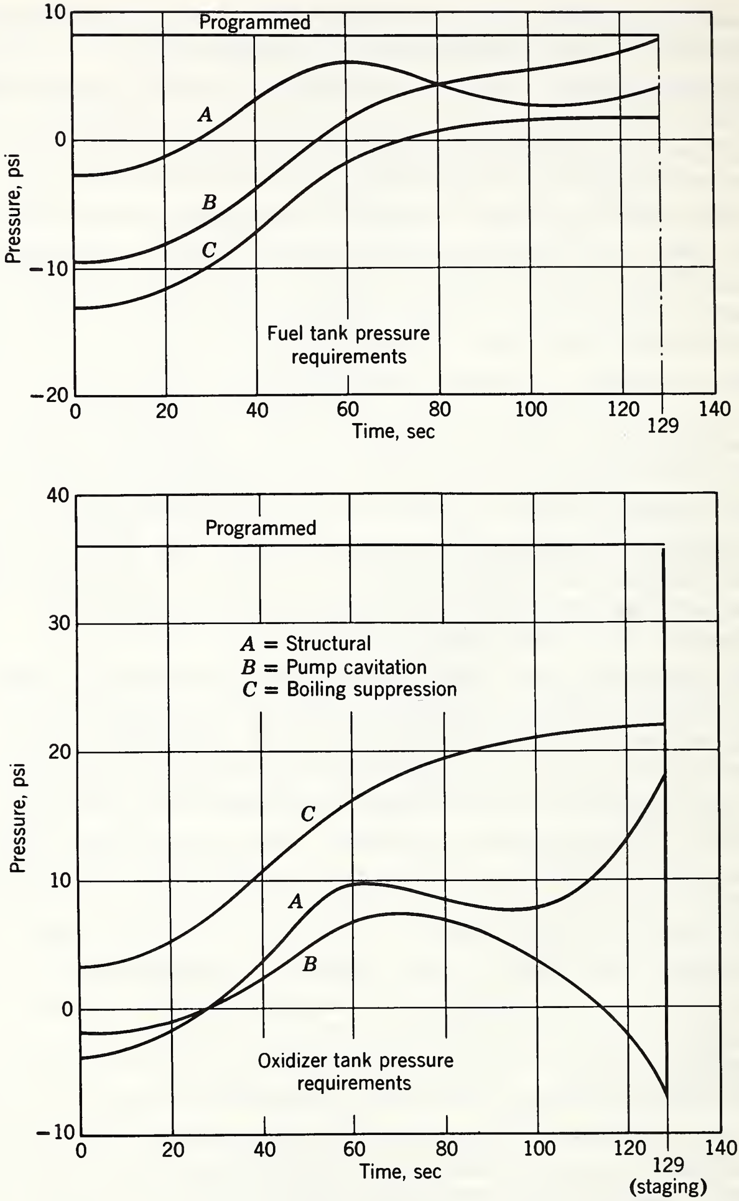

Fig. 11.5 Stage 1. Tank pressure requirements (1 per cent residual propellant configuration).

was set equal to 5 in each case, and hypothetical propulsion system characteristics were employed as input data.

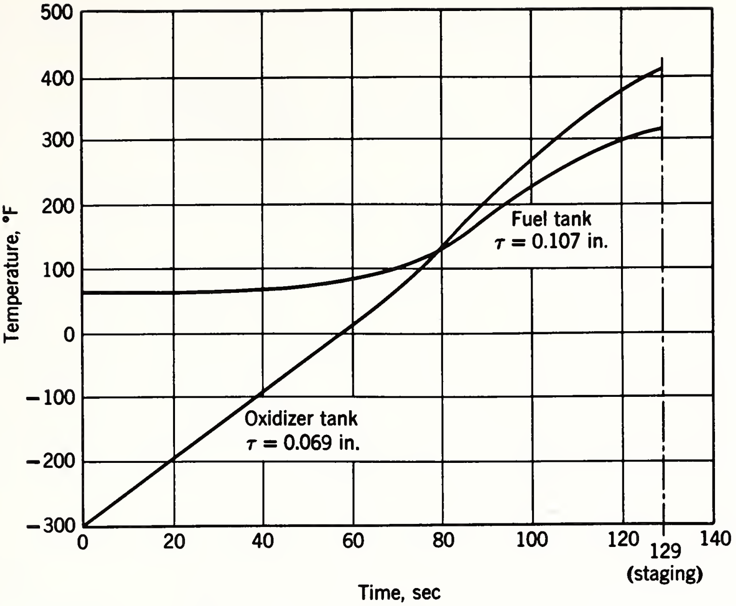

Fig. 11.6 Stage 1. Tank skin temperature histories (1 per cent residual propellant configuration).

The first-stage tank pressure requirements for the 1 per cent residual propellant case are presented in Fig. 11.5, and the skin temperature history at the top of each tank is shown in Fig. 11.6. In this study the first-stage tank pressure program selected to meet all requirements is a constant-pressure value equal to the maximum required value, which occurs at staging. The maximum skin temperatures are also observed to peak just prior to staging. Note in Table 11.2 that the maximum skin temperatures decrease with increasing gross weight, since the thrust program is fixed. Also note that the minimum skin gage of 0.025 in. was a limiting factor only for the forward end of the second-stage fuel tanks. For these configurations the front-to-rear variations in wall thicknesses for first-stage tanks were very small, and in the two lighter configurations there was no thickness change along the liquid oxygen tanks.

So far as the entire system is concerned, the generalized analysis results are useful in establishing performance and sizing relationships and performance exchange ratios based on vehicle design details which are internally consistent instead of arbitrarily assumed. To illustrate what is possible,

TABLE 11.2
Summary of Two-Stage Tandem Missile Design Features

Residual propellant fraction	0.005	0.01	0.02
Gross weight, lb	192,500	203,600	231,400
Maximum range, nautical miles	5,650	5,700	5,670
Jettisoned weight, lb	9,200	10,050	12,430
Burnout weight, lb	8,350	8,530	8,980
Tank weight, stage 1, lb	2,360	2,350	2,650
Tank weight, stage 2, lb	530	540	580
Pressurization weights (gas + bottles), lb			
Stage 1	325	340	380
Stage 2	65	70	75
Maximum skin temperatures, °F			
Lox tank	431	420	375
Fuel tank	363	321	271
Tank skin thicknesses, in.			
Stage 1 lox, forward/aft	0.077/0.077	0.069/0.069	0.067/0.073
fuel, forward/aft	0.104/0.107	0.107/0.110	0.114/0.116
Stage 2 lox, forward/aft	0.038/0.062	0.038/0.051	0.040/0.051
fuel, forward/aft	0.025/0.032	0.025/0.032	0.025/0.033
Tank pressures, psi			
Stage 1 lox	42.1	41.7	41.3
fuel	11.5	11.5	11.6
Stage 2 lox	39.7	38.6	37.7
fuel	29.4	29.6	30.1
Burning times, sec			
Stage 1	122	129	147
Stage 2	116	123	139
Initial thrust to weight ratio	1.51	1.43	1.26

additional studies of the same configuration were made for different launch weights and ranges. Figure 11.7 presents the weights and ranges of this family of vehicles as a function of residual propellant fraction. Similar plots could also be made for any of the internal details whenever such variations are of interest.

At this point it is important to recognize a few limitations on this or any other systems analysis. Clearly, the validity of any solution depends entirely on the validity of the individual component analyses, the correctness and completeness of the assumed interactions, and the input data. Although certain arbitrary functions can be and are programmed, in general the analysis requires relatively simplified relationships to be practical. Too much oversimplification tends to degrade the value of the results. Computational accuracy and convergence are also factors in the accuracy of the final results, although they have seldom been found to be limiting. Most important, perhaps, it must be emphasized that analyses of this kind should never be used to the exclusion of good judgment on the part of the designer.

Because of the nature of the analysis, results such as those

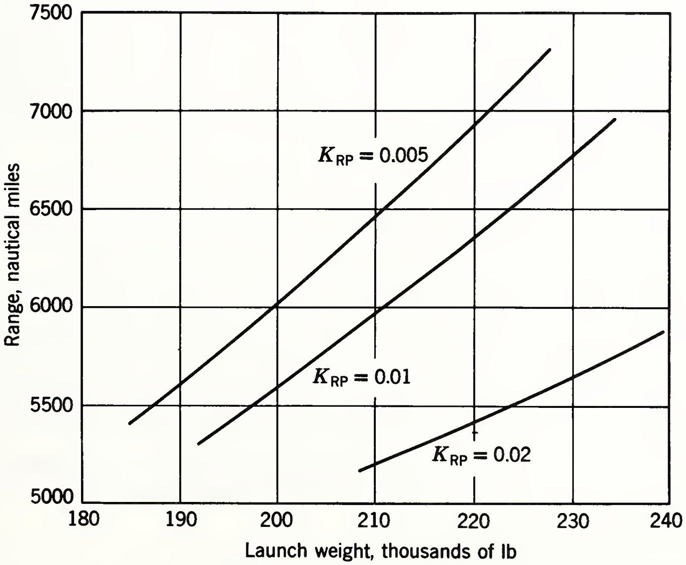

Fig. 11.7 Range versus launch weight two-stage tandem missiles, as a function of residual propellant fraction K_{RP}.

just described cannot represent an entirely accurate detailed design. For the structure the main value of the generalized analysis lies in establishing the most important system interactions, which may be useful later during the detail design, and in providing a rational preliminary definition of details. When a design is established, attention obviously becomes centered on the vehicle details instead of on the generalities. For example, the simplified structural description used in the generalized studies must be replaced by accurate physical descriptions so that the actual aerodynamics, temperatures, loads and their internal distributions, and structural allowables can be obtained accurately. Trajectories specifically applicable to the mission are used, and dispersions about the nominal are taken into account in establishing the final design conditions. Detailed structural analyses are performed to investigate the interactions of the actual structure with the external environment and with the other subsystems, based on detailed rather than generalized relationships.

REFERENCES

1. H. W. Baer, "Variations of Weight of Bulkhead—Intertank Structure with Bulkhead Height for Cylindrical Tanks in Series," Space Technology Laboratories, Report TM-59-0000-00376, July 20, 1959.
2. P. Dergarabedian and R. P. Ten Dyke, "Estimating Performance Capabilities of Boost Rockets," Space Technology Laboratories, Report TR-59-0000-00792, September 10, 1959.
3. M. V. Barton and P. Dergarabedian, "Generalized Missile Design and Performance Analysis," Transactions of the First Technical Symposium on Ballistic Missiles, Vol. 3, Aerodynamics and Structures, The Ramo-Wooldridge Corporation, GM01.1-266, June, 1956, pp. 225-256 (secret).
4. B. D. Fried and P. Dergarabedian, "Two Stage Missiles II," The Ramo-Wooldridge Corporation, Report CMCC GM16.1003, June 8, 1955 (confidential).
5. P. Dergarabedian, et al., "Two Stage Missiles III," The Ramo-Wooldridge Corporation, Report CMCC GM16.1014, March 3, 1955 (confidential).
6. P. N. Anderson, et al., "Two Stage Missiles IV," The Ramo-Wooldridge Corporation, Report CMCC GM16.1035, July 1, 1955 (confidential).

12

STRUCTURES: INTEGRATED DYNAMIC ANALYSIS

J. G. Berry, H. E. Lindberg,
and J. D. Wood

12.1 INTRODUCTION

In the previous chapters the in-flight loads have been determined by assuming the missile to be a rigid body. The interactions between the control system, propulsion system, aerodynamics, propellant motion, and the missile dynamic behavior have been neglected. The assumption of a rigid missile is necessary in the preliminary design phase in order to allow the computation of loads on which further design work can be based. However, once a preliminary structural design has been made, it is possible to compute the dynamic characteristics of the missile. Utilizing these dynamic characteristics, dynamic loads,* a revision to the initial load estimates, can be determined.

In this chapter the problem of determining dynamic loads will be discussed. Special attention will be given to the effects of subsystem interaction on dynamic loads and vice versa. A few technically important examples will be treated in some detail.

*Throughout this chapter the term "dynamic load" is used to designate those stresses, bending moments, shear forces, etc., which are generated by a time-dependent environment. The stresses, etc., are, of course, functions of time.

For purposes of the discussion which follows, a complete missile system is envisioned as being composed of the following subsystems: (a) airframe (structure) including propellants, (b) propulsion system, (c) control system, (d) payload (re-entry vehicle, satellite, etc.), (e) launch facilities. Each of these subsystems has its own peculiar dynamic characteristics which, from the dynamic loads point of view, are not exceptionally interesting. However, once these subsystems are interconnected, the picture may change completely. For example, a propulsion system generates a thrust which builds from zero to a more or less steady value and then later decays to zero. The time-dependent character of the thrust produces no startling behavior when acting on a rigid airframe; the situation can be dramatically different when the dynamic behavior of the airframe is considered. These types of dynamic interactions and their effect on dynamic loads are the central theme of what follows.

12.2 IN-FLIGHT DYNAMIC LOADS

In this section equations for the lateral motion of a liquid propellant missile will be developed. These equations, which include aerodynamic forces, control system dynamics, airframe dynamics, and propellant dynamics, can be used to compute dynamic loads for a variety of inputs. In addition, they can also be used to study control system stability (see Chapter 16).

12.2.1 General Considerations

A. Airframe dynamics—lateral bending. Experimental studies have established the fact that a missile airframe can be idealized as a nonuniform (in stiffness and mass distribution) beam for purposes of studying its lateral bending dynamics. Sometimes it may be necessary to represent an airframe as a collection of beams rather than as a single beam. However, such a representation poses no theoretical difficulties, although computational problems may develop.

It has been established, both theoretically and experimentally, that simple (Bernoulli-Euler) beam theory does not accurately represent the bending dynamics of airframes of the dimensions encountered in ballistic missiles. An adequate bending theory must account for the effects of shear deformation and, usually, the rotational inertia of beam elements. Such a theory, known as the Timoshenko beam theory, is available.

The Timoshenko equations are derived by writing the equilibrium and kinematic equations for a differential element of the beam as shown in Fig. 12.1. The beam has a number of spring-mass systems attached at distances l_j from the mass center. The reasons for including these systems will become clear later. Equilibrium of the lateral forces acting on the element requires that

$$\rho A\ddot{u} = \frac{\partial V}{\partial x} + \sum_{j=1}^{N} \Delta(x - l_j)(K_j \zeta_j + m_j a_x \psi_j) \tag{12.1}$$

where $\Delta(x - l_j)$ is the Dirac delta function defined by

$$\Delta(x - l_j) = 0 \quad \text{when} \quad x \neq l_j,$$
$$\int_{l_j - \epsilon}^{l_j + \epsilon} \Delta(x - l_j)\, dx = 1 \quad \text{as} \quad \epsilon \to 0 \tag{12.2}$$

Writing equilibrium of moments and dropping second-order terms gives

$$\rho I\ddot{\psi} = -\frac{\partial M}{\partial x} + V + P\frac{\partial u}{\partial x} - \sum_{j=1}^{N} \Delta(x - l_j)\, a_x m_j \zeta_j \tag{12.3}$$

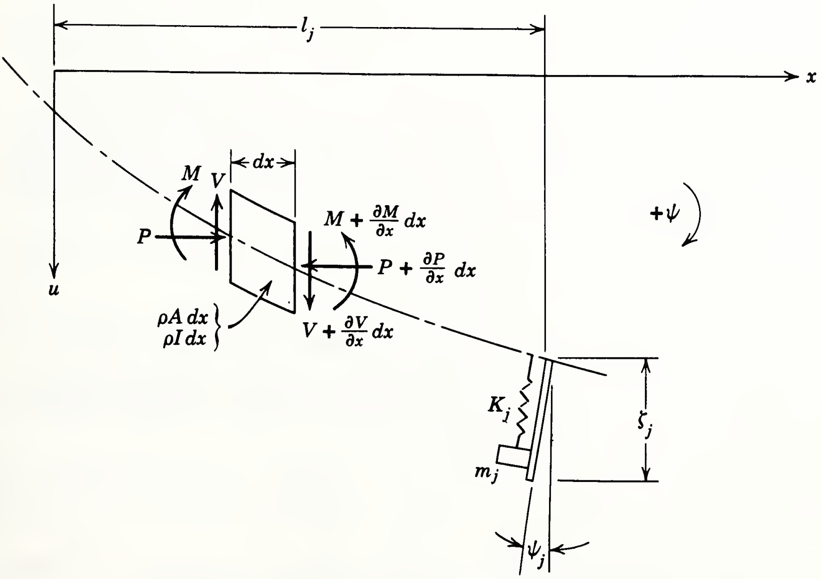

l_j
x
u
M
V
dx
P
$M + \frac{\partial M}{\partial x} dx$
$P + \frac{\partial P}{\partial x} dx$
$V + \frac{\partial V}{\partial x} dx$
$\rho A\, dx$
$\rho I\, dx$
$+\psi$
K_j
m_j
ζ_j
ψ_j

Fig. 12.1 Element of a Timoshenko beam.

where u = total deflection of beam, due to both bending and shear

ψ = slope of beam due to bending alone

ζ_j = displacement of jth attached spring-mass system relative to deflected position of beam

ρA = the mass per unit length

V = the shear force on a cross section

ρI = the mass moment of inertia per unit length of the beam cross sections

M = the bending moment on a cross section

P = the axial load in the beam at any section

$$= -a_x \int_x^{tip} \rho A \, dx - a_x \sum_{j=1}^{N_1} m_j$$

a_x = absolute acceleration of beam system in negative x direction

N_1 = number of spring-mass systems between x and missile tip

N = total number of spring-mass systems

Only the rotary inertia forces caused by the bending slope appear in eq. 12.2. The shear forces produce distortion only and not rotation of the beam elements. The moment curvature relationship for Timoshenko beam is the same as for a simple beam, namely

$$EI\frac{\partial\psi}{\partial x} = -M \tag{12.4}$$

where EI is the flexural rigidity of the beam. Because of the inclusion of shear deformation, another equation, describing the relationship of shearing forces to shearing deformations, is required. This relation is

$$KAG\left(\frac{\partial u}{\partial x} - \psi\right) = V + P\frac{\partial u}{\partial x} \tag{12.5}$$

where KAG is the shear rigidity of the beam, and $\partial u/\partial x - \psi$ is the shearing slope. Incorporating eqs. 12.4 and 12.5 into the equilibrium eqs. 12.1 and 12.3 yields the usual form of the Timoshenko beam equations:

$$\rho A\ddot{u} = \frac{\partial}{\partial x}\left[KAG\left(\frac{\partial u}{\partial x} - \psi\right) - P\frac{\partial u}{\partial x}\right] + \sum_{j=1}^{N}\Delta(x - l_j)(K_j\zeta_j + m_j\, a_x\,\psi_j)$$

$$\rho I\ddot{\psi} = \frac{\partial}{\partial x}\left(EI\frac{\partial\psi}{\partial x}\right) + KAG\left(\frac{\partial u}{\partial x} - \psi\right) - a_x \sum_{j=1}^{N}\Delta(x - l_j)\, m_j\,\zeta_j \tag{12.6}$$

These equations can be found in many standard texts on the vibrations of continuous systems (see, for example, reference 1). The provisions for attached springs and masses and the inclusion of the axial compression force $P = P(x)$ are not usually given explicitly in these texts. Inclusion of the axial compression force in the equations is important in missile applications because the axial acceleration of the missile in flight can substantially affect the bending dynamics. At this point it is useful to review briefly what is meant by normal modes and describe some of their properties. If an external force acting on the missile varies sinusoidally at a single frequency, and this frequency is slowly varied, we would observe a series of resonances at a number of discrete frequencies. At these frequencies the amplitude of vibration becomes quite large, and each point of the missile reaches its maximum displacement at the same time, describing a definite pattern in space. This pattern or mode shape is commonly called an eigenfunction or normal mode (given by $\phi_n(x)$, $\psi_n(x)$ here), and the frequency at which it occurs is called an eigenvalue. A very important property of these modes is that the motion of the missile in any one mode is independent of the motion taking place in any of the others, except through coupling from external forces (see later). This is due to the orthogonality property of the normal modes, and because of this independence it is usually expedient to describe the missile motion in terms of these modes.

The mathematical expressions which describe the orthogonality of the normal modes can be obtained directly from the differential equations of motion. The derivation of these orthogonality conditions is straightforward and follows the standard procedure given in many texts. The orthogonality conditions for eqs. 12.6 are

$$\int_l (\rho A\phi_m\phi_n + \rho I\psi_m\psi_n)\,dx + \sum_{j=1}^{N} m_j(\phi_{jm} + \zeta_{jm})(\phi_{jn} + \zeta_{jn}) = \begin{cases} M_n; & m = n \\ 0; & m \neq n \end{cases}$$

$$\begin{aligned} &\int_l EI\frac{d\psi_m}{dx}\frac{d\psi_n}{dx}\,dx + \int_l KAG\left(\frac{d\phi_m}{dx} - \psi_m\right)\left(\frac{d\phi_n}{dx} - \psi_n\right)dx \\ &- \int_l P\frac{d\phi_m}{dx}\frac{d\phi_n}{dx}\,dx + \sum_{j=1}^{N} K_j\zeta_{jm}\zeta_{jn} \qquad\qquad (12.7) \\ &+ a_x\sum_{j=1}^{N} m_j(\psi_{jm}\zeta_{jn} + \psi_{jn}\zeta_{jm}) = \begin{cases} M_n\omega_n^2; & m = n \\ 0; & m \neq n \end{cases} \end{aligned}$$

where $\phi_{jm} \equiv \phi_m(x)\big|_{x=l_j}$, that is, $\phi_m(x)$ evaluated at $x = l_j$, ζ_{jm} is the displacement of the jth mass in the mth mode, and the subscripts m and n refer to two different modes. The constant M_n is the generalized mass of the nth mode, ω_n is its circular frequency, and a_x is the axial acceleration of the missile. If we denote the amplitude of the nth mode at any instant of time by $q_n(t)$, these amplitudes can be used as generalized coordinates. Setting up the kinetic and potential energies in terms of these $q_n(t)$, and using orthogonality conditions 12.7, the equations of motion for the $q_n(t)$ can be reduced to the following form:

$$M_n\ddot{q}_n(t) + M_n\, 2b_n\omega_n\dot{q}_n(t) + M_n\omega_n^2 q_n(t) = Q_n(t) - \ddot{\delta}\int_0^b [z(\rho A_e)\phi_n - (\rho I_e)\psi_n]dz - K_{2n}[\ddot{\theta} + K_1(\dot{\delta} + \delta\omega_n{}^2)] - m_e\bar{z}\,a_x\delta\phi_n'(-l_e) = Q_n(t) + \overline{Q}_n(t) \tag{12.8}$$

where $Q_n(t)$ is the generalized force acting on the nth mode. This force can be found in the usual way by giving the nth mode a virtual displacement Δq_n and finding the work done by all the external forces acting on the missile. The presence of only one mode amplitude q_n in eq. 12.8 demonstrates the usefulness of the bending modes being independent of each other. K_1 and K_{2n} are defined later.

To return to the problem at hand, eqs. 12.6 can be solved, subject to appropriate boundary conditions, to yield a set of bending modes $\phi_n(x)$, $\psi_n(x)$.* For the missile in flight, the ends of the missile are free, and the engine can be treated as an integral part of the beam, clamped with zero control angle δ; disconnected from the missile altogether; or attached to the missile by some intermediate constraint. The resulting equations, showing the interaction between the bending and the control system, differ slightly depending on what representation of engine attachment is made for the computation of the bending modes. The equations that follow assume the modes to have been computed with the engine clamped at $\delta = 0$.

B. Propellant dynamics—sloshing. The description of the missile dynamics for missiles with liquid propellants is complicated by the interaction between the airframe and the propellants. As the missile bends and rotates, the liquid propel-

---

*Some practical procedures for computing the bending modes are discussed in reference 3.

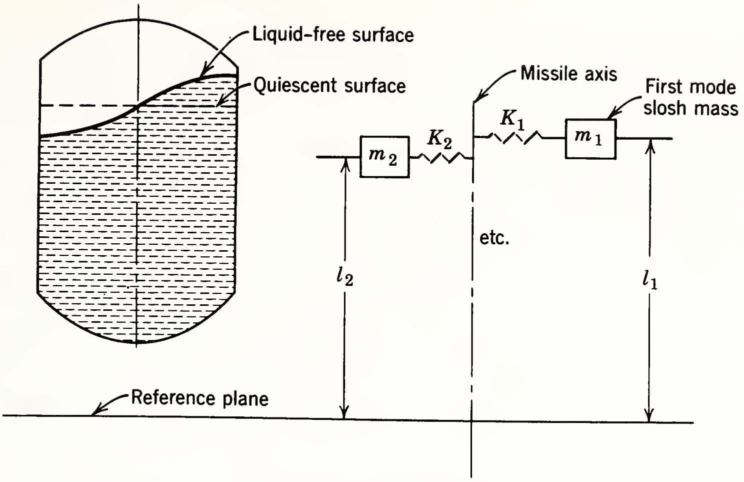

Fig. 12.2 Fluid sloshing.

lants move back and forth in their tanks as shown in Fig. 12.2, creating very appreciable forces on the missile.

It can be shown that only the fundamental (lowest frequency) mode of propellant motion contributes significantly to these forces. The fundamental mode of motion, depicted in Fig. 12.2 is called the "sloshing" mode. The resonant frequencies of these sloshing modes are usually quite low, and they interact severely with the autopilot. Furthermore, since the sloshing frequencies are considerably below the first free-free "bending" frequency of the missile structure, the external airframe rotates back and forth, essentially as a rigid body in some of the "sloshing" modes, in a direction opposite from the fluid sloshing in order to preserve angular momentum. This means that the interaction between sloshing and aerodynamics is also rather strong since the entire missile picks up an angle of attack during the sloshing motion. The interaction between aerodynamic forces and those missile modes that consist mainly of structural bending is not nearly as strong; only a local angle of attack is generated, and the resulting aerodynamic forces are usually negligible.

One possible scheme for eliminating the sloshing problem would be to divide the propellant tanks into small compartments, thereby increasing the slosh frequencies and reducing the sloshing forces. Unfortunately, because of weight considerations, such a procedure is generally highly impractical. However, small ring baffles are usually placed at various levels in the tanks. These baffles do not change the sloshing frequencies but do provide natural damping by creating turbulence in the regions of high liquid velocity.

The separate airframe and propellant dynamics may be combined to yield what are known as bending-sloshing modes. To obtain these combined modes, the fluid is treated as concentrated along the missile center line, and the sloshing modes in each tank are represented by attached springs and masses. The spring-mass systems are selected to give the correct slosh frequencies and horizontal force, and their attachment points are selected to give the same moments about the tank center of gravity as is produced by the fluid. The rotatory inertia assigned to the fluid, ρI in eq. 12.6, is adjusted so that the over-all inertia of the fluid in each tank is the same as that found by solving the fluid dynamics problem of a tank capped at the quiescent liquid surface. Equations 12.6, when coupled with appropriate equations defining k_j, will yield combined bending-sloshing natural frequencies and mode shapes. Those readers who wish to pursue the propellant dynamics problem further will find a discussion of the whole sloshing problem in reference 2.

C. Control system. The control system or autopilot is a very important part of a missile system. The thrusting missile is unstable in flight and would soon tumble hopelessly without a properly designed autopilot. The presence of structural bending vibrations makes this stability problem much more complicated. We can easily demonstrate this for ourselves by first taking a relatively rigid yardstick in the hand and balancing it upright by applying only vertical and lateral forces at its base. The yardstick is balanced with ease. If this yardstick is now replaced by a long flexible reed or wire, the task of balancing becomes very difficult.

The essential function of the autopilot is to sense the missile attitude and angular velocity and provide engine angular deflections, and hence a lateral component of the thrust, in accordance with these sensed quantities so as to maintain the missile at a desired attitude. The problems of control system design are treated extensively elsewhere in this text, so that in this chapter the autopilot will appear to a large extent as an unobtrusive black box. In order to provide the reader with something more concrete, however, a simplified hydraulic servo will be presented in block diagram form.

D. Propulsion system. The propulsion system characteristics will enter the equations of this section only in a fairly superficial way. The propulsion system is taken to consist of nozzles having mass and moment of inertia which rotate about gimbal points and thereby change the direction of a steady thrust vector.

12.3 SIMPLIFIED EQUATIONS OF MOTION

The equations of motion that follow assume that all slowly varying quantities such as missile mass, axial acceleration, liquid levels, mode shapes and frequencies, etc., can be treated as fixed. It must therefore be emphasized that the resulting equations are valid only for a few seconds at any selected point along the trajectory; however, this is sufficient to study "high" frequency in-flight dynamics.

12.3.1 Missile Deflections

In order to describe the motion of the missile in flight, it is necessary to know the motion of each section of the missile as a function of time. Once the engine start transient has damped out (this problem is considered in the next section), variations in axial forces at frequencies high enough to excite longitudinal vibrations (with the exception of engine noise, which is an entirely different type of problem) are very small so that all longitudinal deflections are neglected here. The position of each section of the missile can be described by two functions, $u(x, t)$, the lateral deflection of each point along the missile; and $\psi(x, t)$, the angle through which each section rotates relative to the moving axes. See Fig. 12.3.

These functions can be written as

$$u(x, t) = C_0(t) + xC_1(t) + \sum_{n=1}^{\infty} \phi_n(x)\, q_n(t) \qquad (12.9)$$

$$\psi(x_1 t) = C_1(t) + \sum_{n=1}^{\infty} \psi_n(x) q_n(t) \qquad (12.10)$$

where x is measured from the missile center of gravity.

The functions $\phi_n(x)$ and $\psi_n(x)$ are the sloshing-bending modes described earlier, and $q_n(t)$ are the generalized coordinates of these modes and represent the amplitude that must be assigned to each mode at any instant. The time functions $C_0(t)$ and $C_1(t)$ represent a rigid-body translation and rotation, respectively, of the missile. It is convenient to define these quantities so that the angular momentum of the entire missile (including sloshing, engine swiveling, and elastic bending) relative to the moving axes is zero. These quantities can be defined so that the total angular and lateral momentum with respect to the moving axes is independent of the engine deflection δ. To do this, C_0 and C_1 are adjusted so that any momentum created by engine motion is canceled by rigid-body motions of the missile as a whole. Applying this condition, C_0 and C_1 are given by

$$\begin{aligned} C_0 &= -\frac{m_e \overline{Z}}{M} \delta \triangleq -K_0 \delta \\ C_1 &= \frac{1}{I_c} (I_e + m_e l_e \overline{Z}) \delta \triangleq K_1 \delta \end{aligned} \qquad (12.11)$$

Where I_c is the mass moment of inertia of the entire missile (including engines) about the missile center of gravity, I_e is the mass moment of inertia of the swiveling engines about their gimbal points, and the other parameters are shown in Fig. 12.3.

With these definitions of C_0 and C_1, the total angular momentum depends only on q_n and θ. The contribution of q_n is found by first writing the equation of moment equilibrium between the inertia forces and moments and the moment due to the engine force for the missile deflected into an extreme position in the nth mode:

$$\begin{aligned} &\int_l (\chi \rho A \varphi_n + \rho I \Psi_n) dx + \sum_{j=1}^{N} \chi_j m_j (\varphi_{jn} + \zeta_{jn}) \\ &\qquad - (T_s + T_c) \frac{\varphi_n(-l_e)}{\omega_n{}^2} = 0 \end{aligned} \qquad (12.12)$$

where T_s and T_c are engine thrusts, described in more detail later. After multiplying through this equation by $\dot{q}_n$, inspection of the first two terms shows them to be the moment of momentum about the missile center of gravity caused by a coordinate velocity $\dot{q}_n$. This equation can then be used to determine the following simple expression for this momentum in the positive θ direction:

$$H_n = (T_s + T_c) \frac{\varphi_n(-l_e)}{\omega_n{}^2} \dot{q}_n \triangleq K_{2n} \dot{q}_n \qquad (12.13)$$

The contribution to the angular momentum produced by θ is merely

$$\frac{d}{dt}(I_c \dot{\theta}).$$

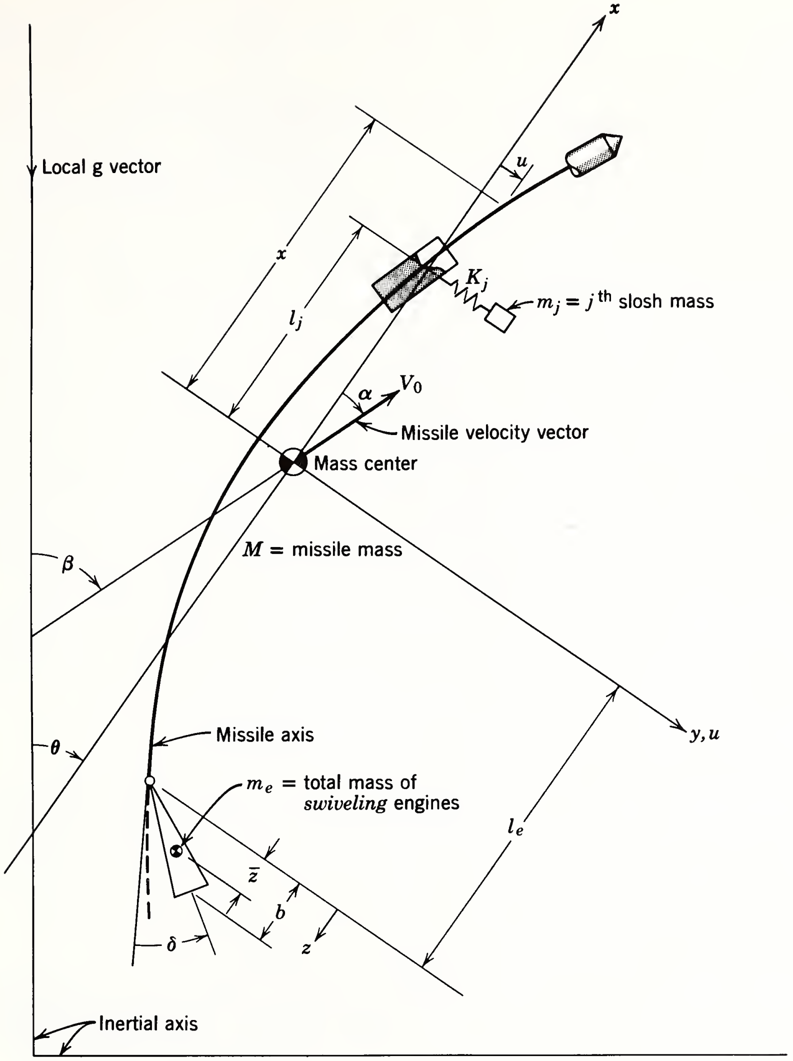
x
Local g vector
u
x
l_j
K_j
$m_j = j^{th}$ slosh mass
α
V_0
Missile velocity vector
Mass center
β
M = missile mass
θ
Missile axis
y, u
m_e = total mass of *swiveling* engines
l_e
$\bar{z}$
b
z
δ
Inertial axis

Fig. 12.3 Geometry and coordinate system.

12.3.2 Rigid-Body Equations

With the choice of coordinate system described above, the rigid-body equations for translation and rotation take on an extremely simple form. The external forces that must be considered in writing these equations are shown in Fig. 12.4.

Since there may be more than one engine, and not all the

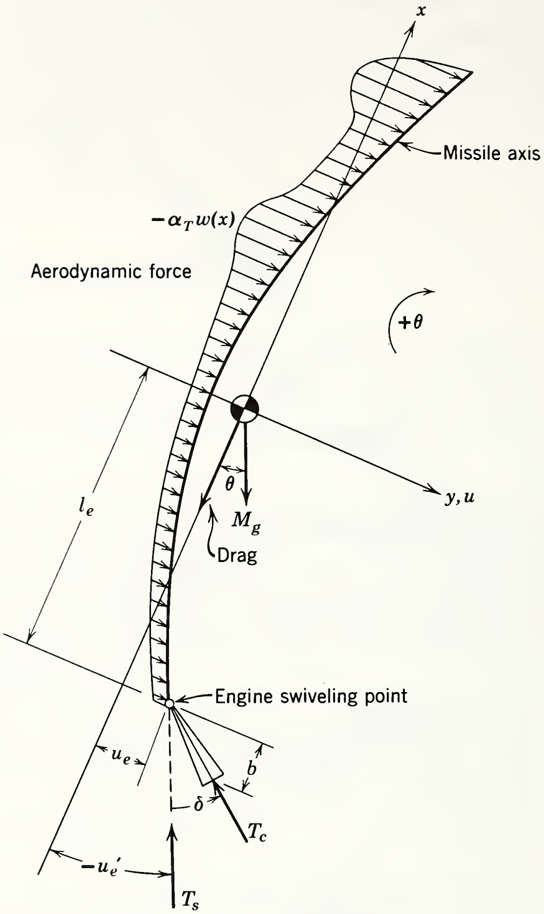
x
Missile axis
$-\alpha_T w(x)$
Aerodynamic force
$+\theta$
y, u
l_e
θ
M_g
Drag
Engine swiveling point
u_e
b
δ
T_c
$-u_e'$
T_s

Fig. 12.4 Forces acting on missile.

engines may swivel in each plane, the total thrust is broken into two components; T_c is the total thrust of the swiveling engines, and T_s is the total thrust of the engines stationary with respect to the tangent to the missile axis at the attach point.

The equations governing rotation (pitching) about the missile center of gravity is obtained by taking moments about the center of gravity with the result

$$\sum_{n=1}^{\infty} K_{2n}\ddot{q}_n + I_c\ddot{\theta} = -\alpha_T \int_l x\,w(x)\,dx + [T_c(\delta - u_e') - T_s u_e']\,l_e$$
$$-(T_c + T_s)u_e \qquad (12.14)$$

Here $$\alpha_T = \beta - \theta + \sum_{n=1}^{N} \alpha_n q_n + \frac{v_w}{V_0} + K_1\delta - K_0 \frac{\dot{\delta}}{V_0} \qquad (12.15)$$

is the total angle of attack producing aerodynamic forces. The velocity v_w is the component of atmospheric wind velocity perpendicular to the x-axis. The angle of attack due to the sloshing is represented by $\alpha_n q_n(t)$ where α_n is the angle through which the missile airframe rotates per unit of nth "slosh mode" (a bending-sloshing mode which consists mainly of sloshing) amplitude. The summation in eq. 12.14 is taken only over N such "slosh modes." It is implicitly assumed in eq. 12.14 that the aerodynamic force depends linearly on the angle of attack, and that $w(x)$ is the running load per unit angle of attack. The dependence of the aerodynamic forces on higher powers of α, and on other quantities, such as the angular velocity of the missile, are neglected here for simplicity. These additional forces are usually small, and for many studies it is legitimate to neglect them.

The angle u_e' (the prime indicates differentiation with respect to x) is the slope of the missile axis at the engine gimbal point. It is obtained by differentiating eq. 12.9 and evaluating at $x = -l_e$:

$$u_e'(t) = K_1\delta + \sum_{n=1}^{\infty} \phi_n'(-l_e)q_n \qquad (12.16)$$

The equation governing rigid-body translation is readily obtained by summing forces in the y direction (Fig. 12.4) with the result

$$M\ddot{y} = -\alpha_T \int_l w(x)\, dx + Mg\,\theta + (T_c + T_s)u_e' - T_c\delta \qquad (12.17)$$

where M is the total mass of the missile and g is the acceleration caused by gravity.

12.3.3 Missile Bending Equations

The bending equations (including sloshing) are most easily derived by first giving each mode a virtual displacement Δq_n and observing the work done by the forces acting on the missile. If this work is divided by the virtual displacement Δq_n, we obtain the generalized force Q_n to be used in

$$\ddot{q}_n + 2b_n\omega_n\dot{q}_n + \omega_n^2 q_n = \frac{Q_n}{M_n} + \frac{\overline{Q}_n}{M_n} \qquad (12.18)$$

where M_n is the nth generalized mass defined by eq. 12.7. The resulting generalized force is

$$Q_n = -\alpha_T \int_1 w(x)\,\phi_n(x)\,dx$$
$$- [T_c(\delta - u_c') - T_s u_e']\,\phi_n(-l_e) \qquad (12.19)$$

In eq. 12.18, ω_n is the circular frequency of the nth mode and b_n is the damping ratio. Damping ratio b_n is either determined experimentally by shaking an assembled missile, or assumed conservatively small (0.5 to 1 per cent of critical). It should be mentioned that the damping of a structure can seldom be represented in this way. In order that this representation be strictly correct, all damping forces would have to be of the viscous type (that is, proportional to velocity) and would have to be distributed along the length of the missile in the same way in which the mass and rotatory inertia are distributed, or in the same way in which an appropriate combination of the elastic forces are distributed. If the damping forces are distributed in any other way, application of Lagrange's equations would result in the equations of motion for the bending modes having velocity coupling through the viscous damping forces. That is, each equation corresponding to eq. 12.18 would have additional terms of the form $C_m \dot{q}_m$, where $m = 1, 2, \ldots$. For reasonably small values of damping, however, (corresponding to a few per cent of critical damping in any mode), these coupling terms have a negligibly small effect on the motion[3] and can be omitted as was done in eq. 12.18. Similarly, if the damping is of the hysteresis type rather than viscous, it can still be represented by an equivalent viscous damping ratio b_n for sufficiently small damping.

The force from the engine angular acceleration $\ddot{\delta}$ has been omitted for simplicity in eq. 12.18, but could easily be included in a more complete analysis as shown in eq. 12.8.

12.3.4 Control System and Engine-Swiveling Equations

The control system will be assumed to sense two quantities from gyros mounted on the missile airframe. These quantities are the attitude of the missile at the gyro station, given by $\theta_{FB} = \theta + u_g'$, and the angular velocity at that station, given by $\dot{\theta}_{FB}$, where

$$u_g' = K_1\delta + \sum_{n=1}^{\infty} \phi_n'(l_g)q_n(t) \qquad (12.20)$$

If the missile begins to go off course by building up an attitude θ, or if the gyros think the missile is going off course because the missile bends, giving rise to a u_g', the control system calls for a corrective engine angle, that is, a lateral thrust component. The engine command angle δ_c is formed as a linear combination of the difference between a desired attitude θ_c and the sensed attitude θ_{FB} and the sensed rate $\dot{\theta}_{FB}$. This is expressed by

$$\delta_c = K_\theta(\theta_c - \theta_{FB}) - K_R\dot{\theta}_{FB} \tag{12.21}$$

where K_θ and K_R are gain constants. This engine command signal is modified by compensation networks which shape the phase and amplitude of the signal to give satisfactory stability (see Chapter 16); the resulting signal δ_c is used to open a hydraulic valve, as shown in Fig. 12.5.

The fluid controlled by this valve flows into a hydraulic actuator which is connected directly to the engine bell. The position of the actuator rod δ_a is sensed and subtracted from the compensated engine command angle δ_c so that it is actually the error signal $\delta_c - \delta_a$ which determines the rate of flow in the valve. If the engine angle, as measured by the position

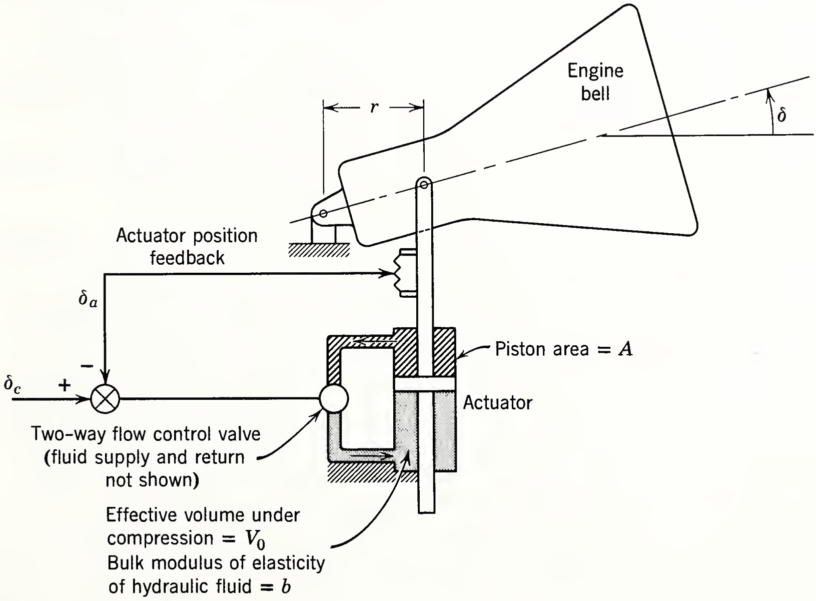
Engine bell
r
δ
Actuator position feedback
δ_a
−
δ_c
+
Piston area = A
Actuator
Two-way flow control valve (fluid supply and return not shown)
Effective volume under compression = V_0
Bulk modulus of elasticity of hydraulic fluid = b

Fig. 12.5 Schematic of autopilot actuator.

of the actuator rod, is the same as the command angle δ_c, no further fluid flows and the actuator does not move.

Going one step farther, if the compressibility of the hydraulic fluid is taken into account, there is an apparent compressibility flow which must be subtracted from the flow initiated by the error signal $\delta_c - \delta_a$. This entire process is represented conveniently in block diagram form in Fig. 12.6. The variable s, used in this diagram, is the usual Laplace operator. (The reader not familiar with Laplace transforms is referred to Chapter 16 where a brief resumé of this theory is given.)

From Fig. 12.6 it is clear that the control flow in the valve is proportional to K_v except for a small delay or valve action time τ. From this flow rate the compressibility flow Q_c is subtracted and the resultant flow is divided by Ar (defined by Fig. 12.5) and integrated (multiplied by 1/s) to give the actuator position δ_a, as shown. The difference between the engine position δ and the actuator position δ_a is multiplied by the equivalent torsional spring constant K_a of the actuator to give the torque acting on the engine bell. Following around the hydraulic loop, this torque divided by Ar gives the pressure in the hydraulic cylinder. This pressure, multiplied by the effective volume V_0 under compression and divided by the bulk modulus of elasticity b of the fluid, gives the change in volume of the fluid caused by the pressure. The rate of change (multiply by s) of volume is the compressibility flow Q_c. The torque acting on the engine bell causes it to move according to

$$I_e\ddot{\delta} + B_e\dot{\delta} + K_e\delta = K_a(\delta_a - \delta), \tag{12.22}$$

where K_e is the torsional spring constant between the engine bell and the missile airframe (caused by bellows, pendulum action resulting from axial acceleration, etc.) and B_e represents any viscous damping present. Equation 12.22 is given in block diagram form in Fig. 12.6. This equation is the only equation in this development of the integrated dynamic equations which is basically incomplete. Many terms have been omitted from the other equations, but they were omitted because they were small. In the case of eq. 12.22, however, all the interactions between engine swiveling, bending, and rigid-body dynamics have been neglected for the sake of expediency. These interactions are important in relation to other effects

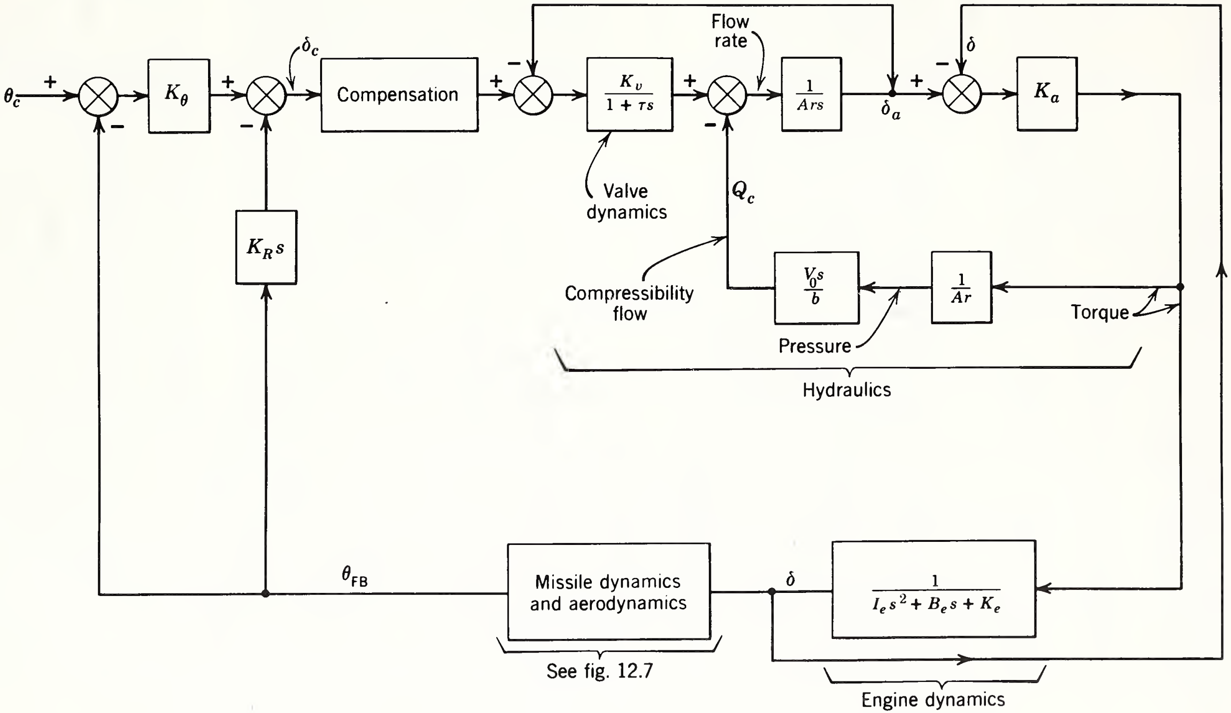
θ_c
+
−
K_θ
+
−
δ_c
Compensation
+
−
$\frac{K_v}{1 + \tau s}$
Valve dynamics
+
−
Flow rate
$\frac{1}{Ars}$
δ_a
+
−
δ
K_a
Q_c
$K_R s$
Compressibility flow
$\frac{V_0 s}{b}$
$\frac{1}{Ar}$
Pressure
Torque
Hydraulics
θ_{FB}
Missile dynamics and aerodynamics
See fig. 12.7
δ
$\frac{1}{I_e s^2 + B_e s + K_e}$
Engine dynamics

Fig. 12.6 Block diagram of autopilot and engine dynamics.

included in the analysis, but most of them arise in a manner so subtle that Lagrange's equations must be resorted to to demonstrate their existence. Such a procedure is lengthy but straightforward, and the enterprising reader can derive the more complete engine-swiveling equation given by

$$\begin{aligned}&[I_e - K_0 m_e \bar{z} - K_1 (I_e + m_e l_e \bar{z})]\ddot{\delta} + m_e \bar{z} a_x (\delta - u_e') \\ &\quad + (I_e + m_e l_e \bar{z})\ddot{\theta} + m_e \bar{z} a_y + \sum_{n=1}^{\infty} \ddot{q}_n \int_0^b (\rho A \phi_n z - \rho I \psi_n)\, dz \\ &\quad = K_a(\delta_a - \delta) - B_e \dot{\delta} - K_\delta \delta \qquad (12.23)\end{aligned}$$

where b is the distance from the engine gimbal to the nozzle exit plane, a_x and a_y are the rigid-body accelerations in the x and y directions, and K_δ is the spring constant between the engine bell caused by a direct spring action, such as from a bellows. In spite of its being incomplete, the use of eq. 12.22 in conjunction with the other equations developed here would generally give adequate engineering information concerning in-flight dynamics.

12.3.5 Block Diagrams

Following the procedure used for the control equations, we can convert the bending and rigid-body equations into Laplace notation and draw a block diagram which represents these equations completely. Such a diagram is given in Fig. 12.7. Only one block representing a typical bending-sloshing mode is shown in this diagram; however, it is understood that there are as many such blocks as there are modes being used. In most cases inclusion of the "slosh modes" (one for each tank) and two or three bending modes is sufficient. The summation signs given on the paths leading out of the bending-sloshing block indicate that a summation is to be made over the modes of the quantities in question.

A study of Fig. 12.7 is enlightening in that the flow of cause and effect of each subsystem on the other can be seen without having to interpret several equations simultaneously. In addition, several significant quantities such as the engine lateral force caused by bending and the total angle of attack α_T (see eq. 12.15) and their effect on the system become apparent. The complexity of Fig. 12.7 detracts somewhat from its usefulness if we do not care to follow all the details; therefore,

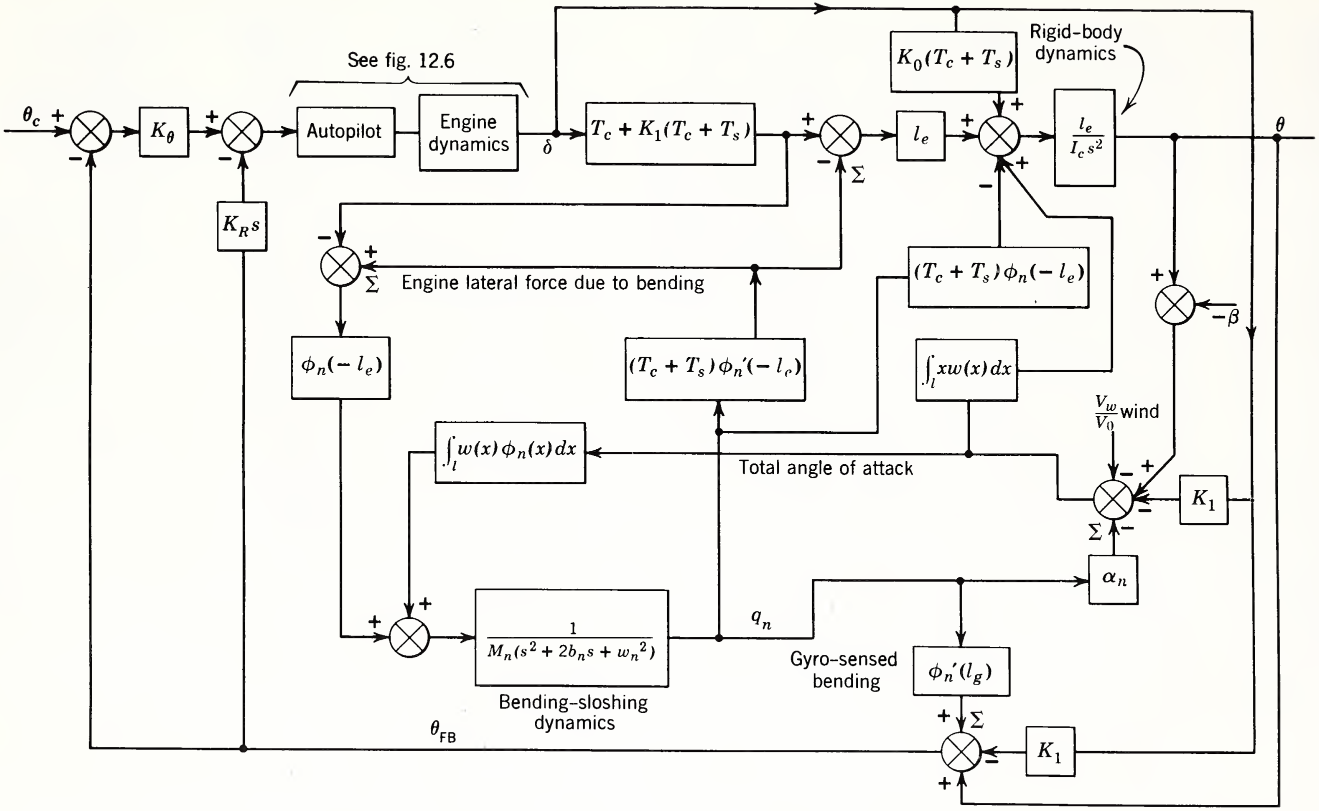
θ_c
+
−
K_θ
+
−
$K_R s$
See fig. 12.6
Autopilot
Engine dynamics
δ
$T_c + K_1(T_c + T_s)$
$K_0(T_c + T_s)$
Rigid-body dynamics
l_e
$\frac{l_e}{I_c s^2}$
θ
Σ
Engine lateral force due to bending
$\phi_n(-l_e)$
$(T_c + T_s)\phi_n'(-l_c)$
$(T_c + T_s)\phi_n(-l_e)$
$\int_l xw(x)\,dx$
$\int_l w(x)\phi_n(x)\,dx$
$-\beta$
$\frac{V_w}{V_0}$ wind
Total angle of attack
K_1
α_n
$\frac{1}{M_n(s^2 + 2b_n s + w_n^2)}$
Bending-sloshing dynamics
q_n
Gyro-sensed bending
$\phi_n'(l_g)$
K_1
θ_{FB}

Fig. 12.7 Block diagram showing detailed in-flight interactions.

a functional diagram showing only the directions of the interactions is given in Fig. 12.8.

12.3.6 Use of Equations

The in-flight dynamics equations developed herein have many uses. From the standpoint of the control system engineer, their most important use is to allow him to study the stability of the missile in flight and to indicate the form of autopilot compensation required to obtain stability. The structural dynamicist sees them as a tool to determine the dynamic loads on critical sections of the missile. These loads arise from autopilot limit cycles, discrete and random gusts, staging transients, and other rapid maneuvers where the action time is of the order of the period of one of the bending modes.

For the control engineer these equations are complete as they are (with the exception of the simplifications), but the structural dynamicist must modify them slightly to insure satisfactory convergence of modal solutions, that is, a series expansion in terms of normal modes. This happens because the control engineer is interested only in displacements,

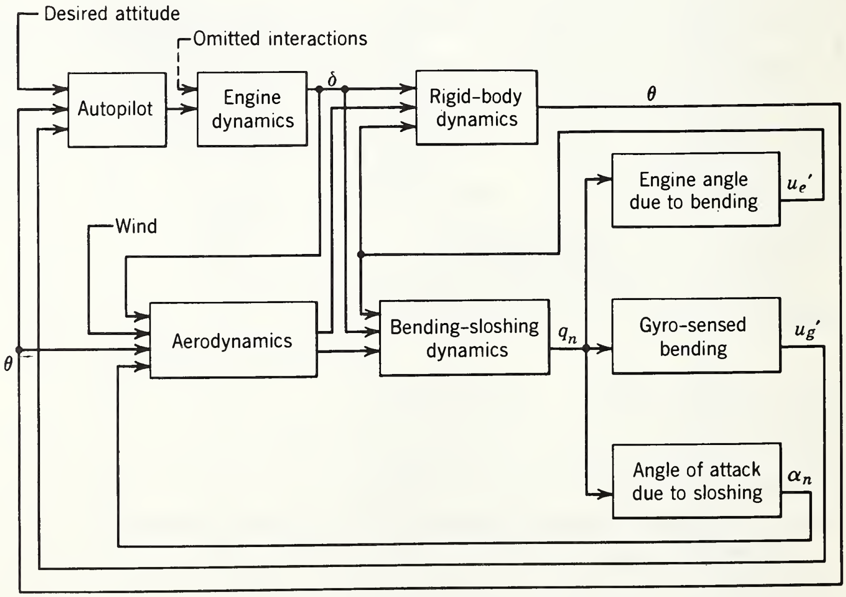
Desired attitude
Omitted interactions
Autopilot
Engine dynamics
δ
Rigid-body dynamics
θ
Engine angle due to bending
u_e'
Wind
Aerodynamics
Bending-sloshing dynamics
q_n
Gyro-sensed bending
u_g'
θ
−
Angle of attack due to sloshing
α_n

Fig. 12.8 Functional block diagram.

whereas the structural dynamicist is interested in bending moments and shear forces as well. The convergence of series expansions of bending moments and shear forces is very poor for a beam with a concentrated load (the engine force), and even in the absence of any dynamic effects at all, many modes would be needed to obtain satisfactory accuracy. On the other hand, series expansions of displacement and slope converge quite rapidly.

The difficulties associated with computing bending moments and shear force can be minimized by employing the so-called "mode acceleration" technique.[4] The essential feature of this method is that it separates the pseudostatic loads (loads found by rigid-body techniques) from the loads arising from the dynamic response of the missile. Thus, the poor convergence caused by discontinuities in the loading, such as a concentrated force, are taken into the pseudostatic load, and the additional load caused by dynamic bending converges much faster. For example, the bending moment at any station, along a missile, can be written as

$$M(x,t) = M_s(x,t) - \sum_{n=1}^{\infty} m_n(x) \frac{\ddot{q}_n(t)}{\omega_n^2} \tag{12.24}$$

where $M_s(x,t)$ is the pseudostatic load neglecting dynamic bending, and $m_n(x)$ is the nth eigenfunction representing the bending moment at any station. The same moment expressed without the use of the mode acceleration procedure is given by

$$M(x,t) = \sum_{n=1}^{\infty} m_n(x) q_n(t) \tag{12.25}$$

which converges more slowly because of the absence of ω_n^2 in the denominator. Equation 12.24 assumes small damping and can easily be derived from eq. 12.25 by using

$$\ddot{q}_n + \omega_n^2 q_n = \frac{Q_n}{M_n} \tag{12.26}$$

Solving for q_n from eq. 12.26 and substituting into eq. 12.25, we obtain

$$M(x,t) = \sum_{n=1}^{\infty} \frac{m_n(x) Q_n(t)}{\omega_n^2 M_n} - \sum_{n=1}^{\infty} m_n(x) \frac{\ddot{q}_n(t)}{\omega_n^2} \tag{12.27}$$

But $\sum_{n=1}^{\infty} \frac{m_n(x)Q_n(t)}{M_n\omega_n^2}$ is simply the moment that results if the system of forces, including rigid-body inertia forces, giving rise to $Q_n(t)$ is applied "statically" since it comes from the solution of eq. 12.26 for $\ddot{q}_n = 0$. Thus eq. 12.27 is identical with eq. 12.24. A term $\sum_{n=1}^{\infty} m_n(x)\frac{2b_n\dot{q}_n}{\omega_n}$ would appear on the right-hand side of 12.24 if damping were present in eq. 12.26, but the damping ratios b_n are usually quite small, and these terms can be neglected.

12.4 ILLUSTRATIVE EXAMPLE

The interaction between control system dynamics and airframe bending dynamics can force the control system into a nonlinear mode of operation which results in a limit cycle. In such a situation the control system causes the engines to gimbal continuously, searching for the correct trim condition, that is, the control system "hunts" for the correct engine swivel angle δ. The data in Table 12.1 illustrate the effects that a control system limit cycle can have on dynamic loads. The data were taken from an actual case (time of flight corre-

TABLE 12.1
Dynamic Loads Generated by a Control System Limit Cycle

$\frac{X}{L}$	$\frac{M_{LC}}{M_D}$
0	1.00
0.1	1.06
0.2	1.12
0.3	1.20
0.4	1.27
0.5	1.30
0.6	1.32
0.7	1.28
0.8	1.04
0.9	1.01
1.0	1.00

$\frac{X}{L}$ = axial missile station measured from the missile tip.

M_{LC} = total bending moment, control system limit cycle.

M_D = total design bending moment, no limit cycle.

sponds to maximum dynamic pressure) in which the damping in the control system hydraulics became negative for large engine angular velocities $\dot{\delta}$. The negative damping caused a limit cycle whose frequency was near the first bending frequency of the missile. The control system had to be redesigned to eliminate the limit cycle.

12.5 PRELAUNCH-POSTLAUNCH DYNAMIC LOADS

In Section 12.2 the equations necessary for the computation of in-flight dynamic loads were developed. The important elements of the in-flight loads problem are the control system, the airframe bending dynamics, and the in-flight aerodynamics. In this section two types of problems are considered. The first is concerned with the interactions between airframe bending dynamics and ground wind aerodynamic forces. The second type of problem has to do with the interactions between the axial or (longitudinal) airframe dynamics and the propulsion system.

These problems fall into a general class known as prelaunch, postlaunch problems, depending on whether the dynamic loads occur before or as a result of releasing the missile.

12.5.1 Wind-Induced Oscillations

A. Theoretical considerations. A missile in the prelaunch condition, that is, erected on a launch pad (Fig. 12.9), may be exposed to ground winds which give rise to flow around the missile of large Reynolds number R* ($R > 10^6$ based on the missile diameter). In such a flow the boundary layer on the missile is turbulent and, as a consequence, random pressure fluctuations act on the missile. These random pressure fluctuations create random lift and drag forces which in turn can induce large, oscillating displacements and bending moments in the missile.

In an air flow perpendicular to a circular cylinder, such as a missile, a great variety of changes occur with an increasing

---

*The Reynolds number R is defined to be $R = Ud/\nu$, where U is the undisturbed velocity of flow, d is the missile diameter, and ν is the kinematic viscosity of the flowing liquid.

Reynolds number. Details of these changes can be found in reference 4 and other texts in fluid mechanics. Briefly, if R is in the range of 40 to 150, the "shedding" of vortices is regular. The eddying motion in the wake is periodic both in space and time, and the flow can be approximated by the well-known Karman vortex street. The range of R between 150 and 300 is a transition range, in which the vortex shedding is no longer regular. For $R > 300$, the vortex shedding is "irregular." A predominant frequency can be determined, but the amplitude is random. Finally, at R of order 10^5, the separation point of the boundary layer moves rearward on the cylinder and the drag coefficient decreases appreciably. The flow in the wake at these large Reynolds numbers becomes so turbulent that the vortex street pattern is no longer recognizable.

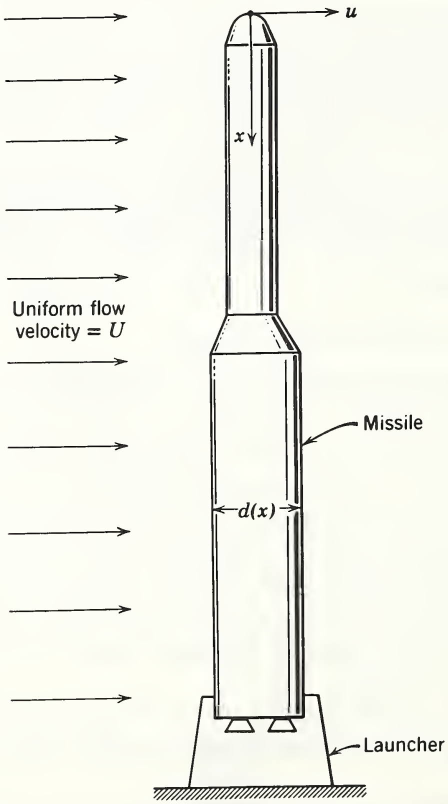

Fig. 12.9 Missile exposed to ground winds.

Experimental results for flow around cylinders when R is larger than 10^5 are presented in reference 5.

Consider the lateral motion of the missile in Fig. 12.9. The applied lift force per unit length along the missile can be written as

$$L(x,t) = q(x)\, d(x) C_L(t) \qquad (12.28)$$

where q(x) is the dynamic pressure, d(x) is the diameter, and $C_L(t)$ is the lift coefficient which varies randomly with time. Actually, C_L is a function of Reynolds number as well as of time. Therefore C_L, at each missile station, depends on the diameter of the missile at that station. The dependence of C_L on R and t is such that it is not possible, in general, to express C_L as a product or sum of a function of R and a function of t. However, the experimental data of reference 5 indicates that C_L is not a strong function of R, at least for limited ranges of R in excess of 5×10^5. Therefore, it is reasonable to assume that a value of C_L, associated with a Reynolds number based on a representative missile diameter, should be adequate for eq. 12.28. This conclusion, being founded on the data of reference 5, is only valid for two-dimensional flow. The three-dimensional flow characteristics around the tip of a missile have a substantial effect on the total lift and drag forces. However, in the absence of detailed wind tunnel data on particular missiles, the procedure developed herein is the best available. On the basis of limited experimental data, it can be anticipated that the results obtained will be conservative.

The lift force of eq. 12.28 is a random function of time since $C_L(t)$ is random in time. Problems involving random time variations are usually more conveniently treated in the frequency domain than in the time domain. The frequency representation of a random function is known as its power spectral density. Figure 12.10 is a typical power spectral density of lift force on a uniform cylinder. The frequency parameter, $S = \omega d / 2\pi U$, used in Fig. 12.10 is known as the Strouhal number; the curve is normalized such that

$$\int_0^\infty F(S)\, dS = 1 \quad \text{or} \quad \int_0^\infty F\left(\frac{\omega d}{2\pi U}\right) d\omega = \frac{2\pi U}{d}$$

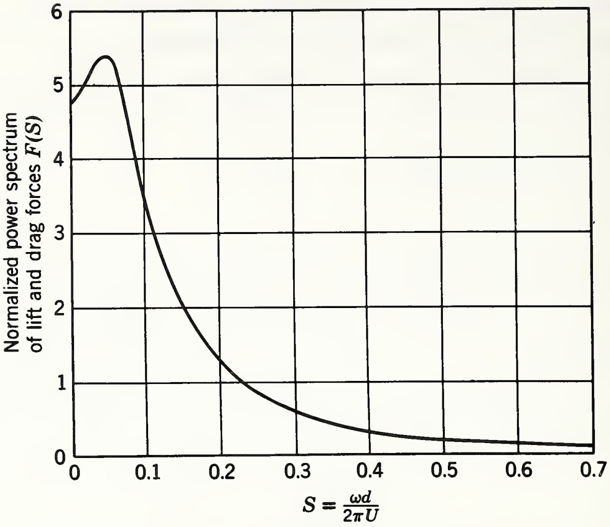

Fig. 12.10 Normalized power spectrum for the lift force and drag force at Reynolds number 1.39×10^6.

By definition, if $P(\omega)$ is the power spectral density of the lift coefficient $C_L(t)$, the mean square value of C_L is given by

$$\int_0^\infty P(\omega)\, d\omega = \overline{C_L{}^2} \tag{12.29}$$

By comparing the latter two equations, the normalizing factor $K = P(\omega)/F(S)$ is evident and

$$P_L(\omega) = \frac{d\overline{C_L{}^2}}{2\pi U} F(S) \tag{12.30}$$

Similarly, the power spectral density of the drag force is given by

$$P_D(\omega) = \frac{d\overline{C_D{}^2}}{2\pi U} F(S) \tag{12.31}$$

where $\overline{C_D{}^2}$ is the mean square value of the drag coefficient. The expressions for the motions of a missile resulting from random lift and drag forces are developed as follows. The displacement response of the missile, which is assumed to be a linear structure, can be expressed in terms of its principal modes as

$$u(x,t) = \sum_{n=1}^{\infty} \phi_n(x)\, q_n(t). \tag{12.32}$$

The generalized coordinates $q_n(t)$ are determined from

$$\ddot{q}_n + 2b_n\omega_n\dot{q}_n + \omega_n^2 q_n = \frac{Q_n(t)}{M_n} \tag{12.33}$$

where the generalized force is

$$Q_n(t) = \int_1 f(x,t)\phi_n(x)\, dx$$

and M_n is the generalized mass of the nth mode. By assuming that the forcing function can be decomposed to

$$f(x,t) = F(x)T(t),$$

the generalized force becomes

$$\begin{aligned} Q_n(t) &= T(t)\int_1 F(x)\phi_n(x)\, dx \\ &\equiv T(t)W_n \end{aligned} \tag{12.34}$$

where

$$W_n = \int_1 F(x)\phi_n(x)\, dx \quad \text{and} \quad F(x) = q(x)\,d(x)$$

For such a forcing function it is possible to find an extremely simple expression for the root mean square (rms) of the time response of the missile by assuming that the damping ratios b_n are small. The function $T(t)$ is assumed to be random and expressible in terms of a power spectral density $P(\omega)$.

To obtain the response, first notice that if $T(t)$ equals $a \cos \omega t$, the steady-state solution of the equation of motion is

$$q_n = \frac{aW_n \cos(\omega t + \theta_n)}{M_n\omega_n^2\left\{\left[1-\left(\frac{\omega}{\omega_n}\right)^2\right]^2 + \left(2b_n\frac{\omega}{\omega_n}\right)^2\right\}^{1/2}} \tag{12.35}$$

The corresponding displacement is

$$u(x,t) = a\sum_n \frac{W_n\phi_n(x)\cos(\omega t + \theta_n)}{M_n\omega_n^2\left\{\left[1-\left(\frac{\omega}{\omega_n}\right)^2\right]^2 + \left(2b_n\frac{\omega}{\omega_n}\right)^2\right\}^{1/2}} \tag{12.36}$$

The mean square response (which will be needed as explained later) is defined to be

$$\overline{u^2(x)} = \frac{\omega}{2\pi} \int_t^{t+2\pi/\omega} u^2(x,\tau)\, d\tau \tag{12.37}$$

$$\overline{u^2(x)} = \frac{\omega a^2}{2\pi} \int_t^{t+2\pi/\omega} \sum_n \sum_m \frac{W_n W_m \phi_n \phi_m \cos(\omega t + \theta_n) \cos(\omega t + \theta_m)}{M_n M_m \omega_n^2 \omega_m^2 \{(\omega, n)\}^{1/2} \{(\omega, m)\}^{1/2}} \tag{12.38}$$

This equation can be integrated by term to yield

$$\overline{u^2(x)} = \frac{a^2}{2} \sum_n \sum_m \frac{W_n W_m \phi_n \phi_m \cos(\theta_n - \theta_m)}{M_n M_m \omega_n^2 \omega_m^2 \{(\omega, n)\}^{1/2} \{(\omega, m)\}^{1/2}} \tag{12.39}$$

Equation 12.39 is the mean square response to a force distribution fixed in space and varying sinusoidally with time at frequency ω. If $T(t)$ is considered as a concentrated force acting on a unit dashpot, the average power dissipated is $a^2/2$, that is

$$\overline{E} = \frac{1}{t} \int_0^t T^2(\tau)\, d\tau = \frac{a^2}{2}$$

Similarly, if $T(t)$ is a random force acting on a unit dashpot, a power spectral density $P(\omega)$ can be defined for this force (with certain restrictions) such that the average power dissipated by frequency components in the range ω, $\omega + d\omega$ is $P(\omega)\, d\omega$. Thus, if a random force of the form given by $f(x,t)$ acts on the missile, its response can be obtained by using eq. 12.39 and superimposing the responses from each frequency component of the random force, that is, replace $a^2/2$ by $P(\omega)\, d\omega$ and integrate over all frequencies:

$$\overline{u^2(x)} = \int_0^\infty \sum_n \sum_m \frac{W_n W_m \phi_n \phi_m \cos(\theta_n - \theta_m) P(\omega)}{M_n M_m \omega_n^2 \omega_m^2 \{(\omega, n)\}^{1/2} \{(\omega, m)\}^{1/2}}\, d\omega \qquad (12.40)^*$$

---

*The manipulations which led to eq. 12.40 have been essentially intuitive and without mathematical justification. However, a mathematically rigorous treatment of the same problem yields exactly eq. 12.40.

It is the nature of random processes that only a statistical description is meaningful. It is quite often impossible to construct the statistics needed for a complete description; however, the mean square value, which is the second statistical moment, is usually obtainable. If the statistics of a random process are gaussian, the mean square value provides a complete description. It is for these reasons that the particular manipulations leading to eq. 12.40 were undertaken.

In evaluating the integral in eq. 12.40, a simplification can be made if the damping ratios b_n are small and if $P(\omega)$ is a smooth function as compared to the resonant peaks of the structure. In such a case, the largest contributions to the integrand are those terms for which $n = m$ because near each resonance $\omega \approx \omega_n$ the radicals in the denominator become very small. By neglecting the terms for which $n \neq m$,

$$\overline{u^2(x)} = \int_0^\infty \sum_n \frac{W_n^2 \phi_n^2 P(\omega)}{M_n^2 \omega_n^4 \left\{\left[1-\left(\frac{\omega}{\omega_n}\right)^2\right]^2 + \left(2b_n \frac{\omega}{\omega_n}\right)^2\right\}} dw$$

or

$$\overline{u^2(x)} = \sum_n \frac{W_n^2 \phi_n^2}{M_n^2 \omega_n^4} \int_0^\infty \frac{P(\omega)}{\left[1-\left(\frac{\omega}{\omega_n}\right)^2\right]^2 + \left(2b_n \frac{\omega}{\omega_n}\right)^2} dw \qquad (12.41)$$

If $P(\omega)$ is a constant, no further assumptions need be made because each term in the foregoing equation is easily integrated. Remembering that the integrand is a function with very steep peaks at each ω_n, we can make another simplifying assumption. Since the integrand has these steep peaks near $\omega = \omega_n$, the main contribution to the integral comes when $P(\omega) = P(\omega_n)$; thus a good approximation results if $P(\omega)$ is taken as $P(\omega_n) =$ constant for each term. Then

$$\overline{u^2(x)} = \sum_n \frac{W_n^2 \phi_n^2(x)}{M_n^2 \omega_n^4} \frac{\pi \omega_n}{4b_n} P(\omega_n) \qquad (12.42)$$

Substituting for $P(\omega_n)$ from eq. 12.30 yields

$$\overline{u^2(x)} = \frac{d\overline{C_L}^2}{8U} \sum_n \frac{W_n^2 \phi_n^2(x)}{b_n M_n^2 \omega_n^3} F(S_n) \qquad (12.43)$$

It follows from 12.4 that the mean square bending moment along the missile in the lift plane is

$$\overline{M^2(x)} = \frac{d\overline{C_L^2}}{8U} \sum_n \frac{W_n^2 \left[EI(x)\,\frac{d\psi_n}{dx}\right]^2}{b_n M_n^2 \omega_n^3} F(S_n) \qquad (12.44)$$

The mean square response in the drag plane can be obtained from this expression if $\overline{C_L^2}$ is replaced by $\overline{C_D^2}$.

The other wind force acting per unit length along the missile is the steady-stage drag force defined as

$$F_{DS}(x) = C_{DS}\,q(x)\,d(x) \qquad (12.45)$$

where C_{DS} = steady-state drag coefficient
$q(x)$ = dynamic air pressure at station x

For purposes of analysis, the responses in the drag and lift planes are added vectorally. For example, the peak displacement of the missile at station x is defined as

$$u_{max}(x) = [(u_{DS} + 3u_{OD})^2 + (3u_{OL})^2]^{1/2} \qquad (12.46)$$

where u_{DS} = steady-state drag displacement
u_{OD} = root mean square value of the oscillatory drag displacement
u_{OL} = root mean square of the oscillatory lift displacement

It is assumed that the oscillatory lift and drag displacements have "normal" distributions. The root mean square values of these responses are equivalent to the standard deviations (sigma) since the "means" are zero.

The use of 3 σ (3 times root mean square) values in eq. 12.46 implies that 99.73 per cent of the time the peak oscillating lift and drag displacements will be less than the 3 σ value. Equation 12.46 also implies that the oscillatory components of the lift and drag displacement reach their maximum at the same time, which is certainly conservative.

B. An example. An indication of the magnitude of bending moments which may be induced by a strong ground wind acting on a large ballistic missile may be obtained from Table 12.2. In this case a typical intercontinental ballistic missile is assumed to be erected on a surface launcher in the vertical position and exposed to a uniform steady 60-mph wind. The steady-state drag coefficient is assumed to be 0.55, and the

TABLE 12.2
Bending Moments in a Typical Missile Exposed to a Uniform 60-mph Wind

Distance from Missile Base, in.	Bending Moments, in. lb. × 10^{-5}			
	M_{DS}	$3M_{OD}$	$3M_{OL}$	M_R
0	15.07	19.54	63.50	72.32
150	9.82	14.10	44.80	51.59
350	4.84	7.33	23.80	26.75
650	0.80	0.78	2.52	2.97

predominant component of oscillatory response in both the drag and lift planes is at the first bending mode frequency of the missile. The bending moments at several points along the missile are shown in Table 12.2.

As can be seen from these figures, a strong ground wind can easily impose loadings on a missile which could be catastrophic if not taken into account in the structural design of the airframe or if the missile is not otherwise protected. These figures also indicate the fallacy of using just the steady-stage drag response as a design criteria, since the maximum oscillatory components greatly exceed the steady-state response.

12.5.2 Launching in a Wind

A. Solution of the problem. In the prelaunch condition, the missile is bent over by a steady wind and is also oscillating in its various constrained modes because of the vortex shedding previously discussed. The transients that occur in the postlaunch or free-free condition depend very strongly on the deflected shape and velocity of the missile just before release. It would be desirable to find the initial condition that gives the highest postlaunch loads, but with the missile oscillating in several modes with random phase, it is impossible to say a priori what condition would give the largest loads. It seems evident, however, that for any given constrained mode the resulting free-free loads will be largest if the missile is released when it is bent over to its maximum value. Loads indicative of the most severe postlaunch loads likely to occur can be obtained if the postlaunch transients are computed using as initial conditions the missile bent into each of its constrained modes which have appreciable amplitude because of wind-induced oscillations. This means a separate computation for each prelaunch (constrained) mode and a computation for the initial static deflection caused by steady drag.

As an example of the procedure involved in computing the postlaunch transients, consider a case in which the missile is bent into a deflection curve given by $y_0(x)$ as shown in Fig. 12.11. The function $y_0(x)$ could represent any of the displacements discussed earlier, but for this example it will be assumed to be due only to a steady wind. The procedure to be followed here is to represent the missile in the postlaunch condition in terms of its free-free modes $\phi_n(x)$, $\psi_n(x)$ with generalized coordinates $q_n(t)$. Assuming that the free-free modes (ϕ_n, ψ_n) have been obtained from eqs. 12.6, the problem is to determine the generalized coordinates appearing in eqs. 12.9 and 12.10, that is, solve eq. 12.18 subject to the ap-

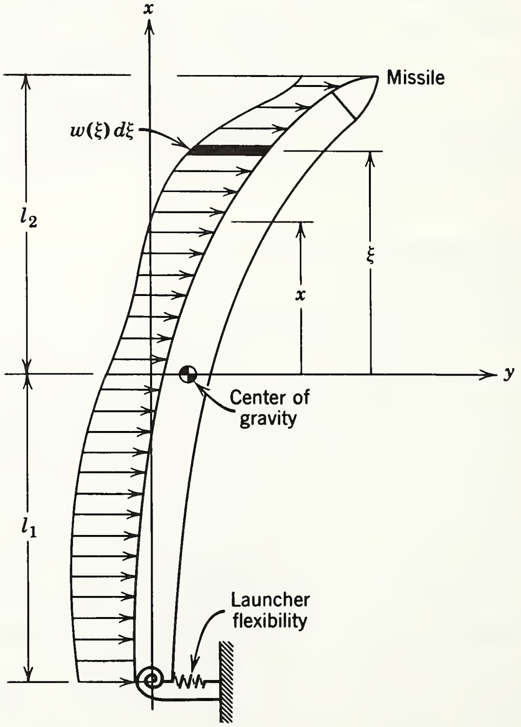

Fig. 12.11 Coordinate system of constrained missile.

propriate initial conditions. For the sake of convenience, the pertinent equations are collected here:

$$u(x,t) = C_0(t) + xC_1(t) + \sum_{n=1}^{\infty} \phi_n(x)\, q_n(t) \tag{12.9}$$

$$\psi(x,t) = C_1(t) + \sum_{n=1}^{\infty} \psi_n(x) q_n(t) \tag{12.10}$$

$$EI\frac{\partial \psi}{\partial x} = -M \tag{12.4}$$

$$KAG\left(\frac{\partial u}{\partial x} - \psi\right) = V \tag{12.5}$$

$$\ddot{q}_n + 2b_n\omega_n\dot{q}_n + \omega_n^2 q_n = \frac{Q_n}{M_n} \tag{12.18}$$

The term involving P has been dropped from eq. 12.5. The axial load P does not affect the bending dynamics for the problem being considered. The generalized force Q_n is given by Fig. 12.11. Here

$$Q_n = \int_1 w(x)\, \phi_n(x)\, dx \tag{12.47}$$

and is independent of time since $w(x)$ is assumed to arise from a steady wind. The solution of eq. 12.18 is

$$q_n(t) = \left(a_n - \frac{Q_n}{M_n\omega_n^2}\right) e^{-b_n\omega_n t}\left(\cos \omega_n t - \frac{b_n}{\omega_n} \sin \omega_n t\right) + \frac{Q_n}{M_n\omega_n^2} \tag{12.48}$$

where $q_n(0)$ equals a_n, $\dot{q}_n(0)$ equals zero, and b_n is assumed to be small, that is, the damped and undamped natural frequencies are essentially equal. It only remains to determine the constants a_n. To this end, the initial bending moment $M_0(x)$ and shear force $V_0(x)$ caused by the steady wind are computed from (see Fig. 12.11)

$$-M_0 = \int_x^{l_z} w(\xi)(\xi - x)\, d\xi \tag{12.49}$$

$$V_0 = \int_x^{l_z} w(\xi)\, d\xi \tag{12.50}$$

Equations 12.9, 12.10, 12.4, and 12.5 may be combined to yield the following expansions for M_0 and V_0:

$$-M_0(x) = EI \sum_{n=1}^{\infty} a_n \psi_n'(x) \tag{12.51}$$

$$V_0(x) = KAG \sum_{n=1}^{\infty} a_n (\phi_n' - \psi_n) \tag{12.52}$$

where the prime denotes differentiation with respect to x. The constants in these expansions may now be determined with the aid of eq. 12.7, that is,

$$\begin{aligned} \int_l EI\psi_m'\psi_m'\,dx & \\ + \int_l KAG\,(\phi_m' - \psi_m)(\phi_n' - \psi_n)\,dx &= M_n\omega_n^2 \qquad m = n \\ &= 0 \qquad\quad\; m \neq n \end{aligned} \tag{12.53)*$$

Equation 12.51 is now multiplied by ψ_m' and eq. 12.52 is multiplied by $\phi_m' - \psi_m$; the results are added and integrated over the length of the missile to yield

$$\begin{aligned} \int_l [M_0\psi_m' + V_0(\phi_m' - \psi_m)]\,dx &= \int_l EI\psi_m' \sum_{n=1}^{\infty} a_n\psi_n'\,dx \\ &+ \int_l KAG(\phi_m' - \psi_m) \sum_{n=1}^{\infty} a_n(\phi_n' - \psi_n)\,dx \end{aligned} \tag{12.54}$$

A comparison of eqs. 12.54 with 12.53 yields immediately

$$a_n = \frac{1}{M_n\omega_n^2} \int_l [M_0\psi_n' + V_0(\phi_n' - \psi_n)]\,dx \tag{12.55}$$

with the a_n's determined, it is now possible to compute the bending moments and shear forces generated as a result of launching a missile in a wind.

B. An example. Because the moment at the base $x = -l_1$ is the maximum moment in the constrained condition, while the moment at this station is zero for all of the free-free modes, the convergence of the initial moment expressed in terms of free-free modes is understandably poor. However, such an expansion has been made using the bending modes of an actual missile, and convergence to a reasonable engineering accuracy was obtained using six bending modes. Figure 12.12 shows a plot of

---

*The terms corresponding to the sloshing coordinates and P have been dropped from eq. 12.7. Experience has shown that sloshing and P are not important in the problem being considered.

$$\sum_{n=1}^{N} EI(x)\, a_n \frac{d\psi_n(x)}{dx}$$

for values of N from one to six. The actual initial moment $M_0(x)$ is also shown, and it can be seen that convergence is good for sections away from the base. Near the base, the maximum loads occur before launching so that the poor convergence here is not important. An indication of the convergence during the postlaunch transient is given by Fig. 12.13, which shows the maximum value of $M(x,t)$ incurred during the transient at several stations of the missile.

Again, N is varied from one to six in this figure, and it can be seen that the additional moment due to the sixth mode is not too large. These computations were made with no postlaunch damping (that is, $b_n = 0$). When the damping was in-

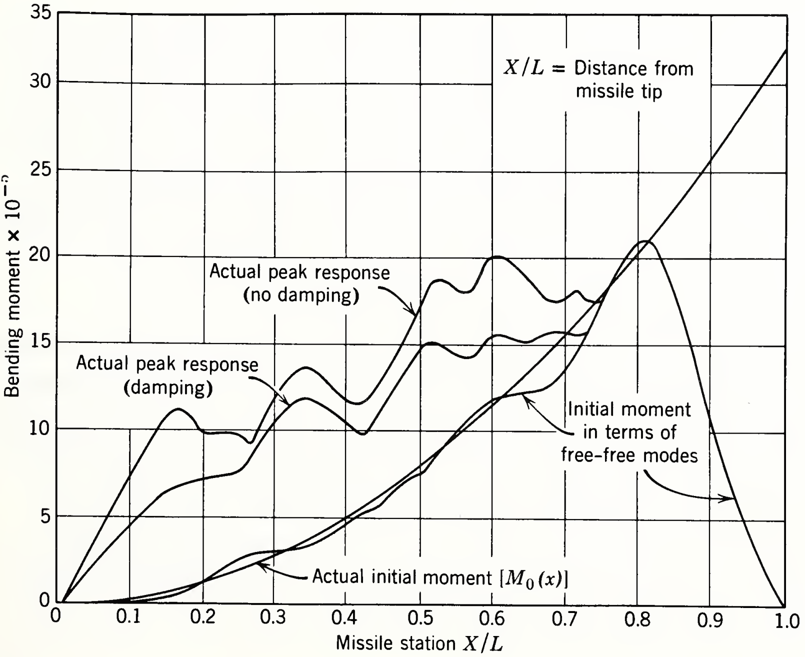

Fig. 12.12 Absolute maximum bending moments at launch.

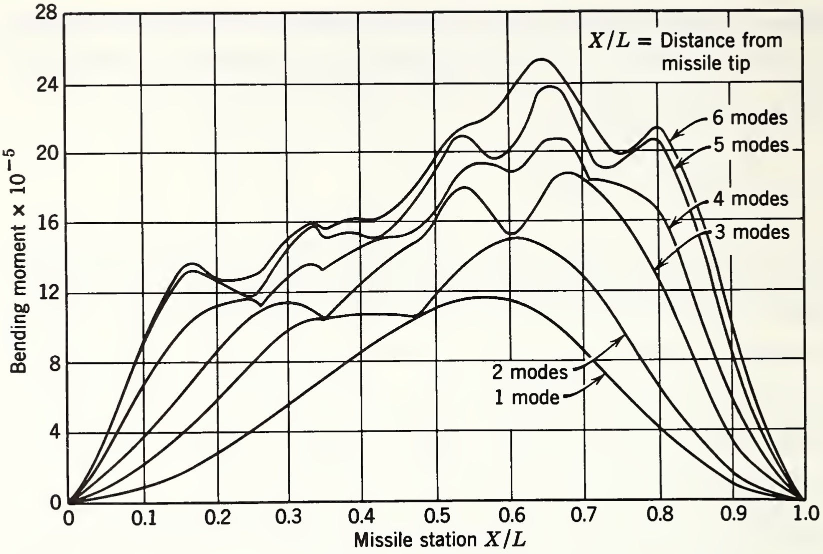

Fig. 12.13 Absolute sum of peak mode responses of bending moments due to sudden release from initial deflection.

cluded, the convergence was better, particularly near the center of the missile where the lower free-free modes contribute strongly to the moment. At these stations, moments caused by the higher modes were damped out by the time the moments caused by the lower modes became in phase. A comparison of the peak postlaunch moments with and without damping is shown in Fig. 12.12. The amount of damping used in the analysis was

$$b_n = 0.02$$

Figure 12.12 also indicates the importance of the postlaunch transient. Notice that in the prelaunch condition the bending moments near the tip of the missile are quite small, whereas during the postlaunch transient the bending moments become quite appreciable because of the unloading wave induced by the sudden release. The characteristic dip in the moment curve at station 0.44 of Fig. 12.12 is caused by a sudden reduction in the flexural rigidity of the missile at this station. These postlaunch moments designed the forward section of the missile of this example.

12.5.3 Effects of Thrust Build-up

In this section the problem of determining the dynamic loads generated by an engine start transient is considered. This problem differs from those discussed in previous sections in that the longitudinal rather than the bending dynamics of the airframe is involved.

A. Theoretical considerations. Consider a missile erected on and attached to a launch stand (see Fig. 12.14). At time t = 0 the engines are started, generating a time dependent thrust F(t). The problem is to determine the response of the airframe to F(t).

Experimental data have confirmed that the longitudinal dynamics of a missile airframe are adequately represented by simple, one-dimensional, beam theory. Therefore, the longitudinal response of the missile is determined from

$$a^2(x)\,\frac{\partial^2 u(x,t)}{\partial x^2} = \frac{\partial^2 u(x,t)}{\partial t^2} \tag{12.56}$$

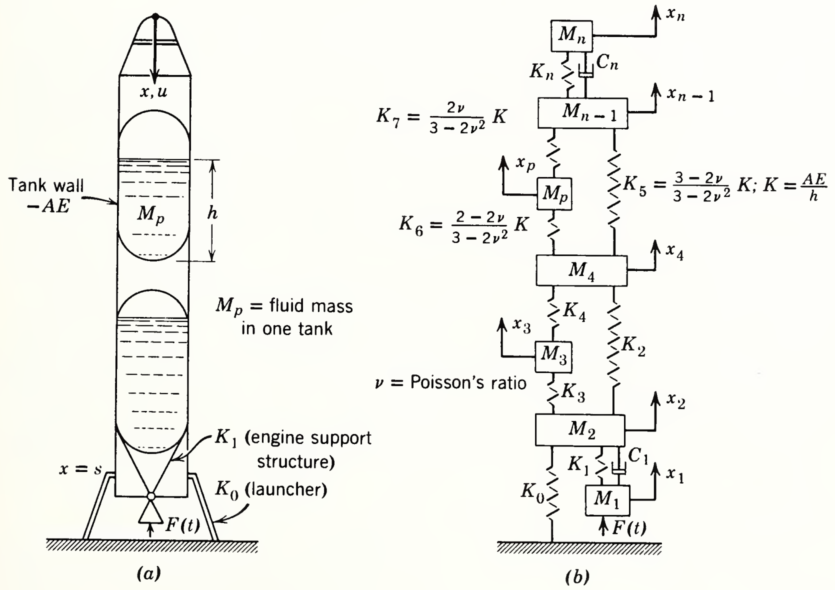
x, u
Tank wall $-AE$
M_p
h
M_p = fluid mass in one tank
$x = s$
K_1 (engine support structure)
K_0 (launcher)
$F(t)$
(a)
x_n
M_n
K_n
C_n
x_{n-1}
M_{n-1}
$K_7 = \frac{2\nu}{3-2\nu^2} K$
x_p
M_p
$K_5 = \frac{3-2\nu}{3-2\nu^2} K;\ K = \frac{AE}{h}$
$K_6 = \frac{2-2\nu}{3-2\nu^2} K$
M_4
x_4
K_4
x_3
M_3
K_2
ν = Poisson's ratio
K_3
M_2
x_2
K_1
C_1
x_1
K_0
M_1
$F(t)$
(b)

Fig. 12.14 (a) Inboard profile of a missile. (b) Spring-mass analog of a missile.

subject to the boundary conditions. Here

$$\frac{\partial u(o,t)}{\partial x} = 0 \quad \frac{\partial u(s,t)}{\partial x} = -\frac{1}{A(s)E}\left[F(t) + K_0 u(s,t)\right] \qquad (12.57)$$

where $a^2(x) = \dfrac{EA(x)}{m(x)}$

E = modulus of elasticity
$A(x)$ = cross-sectional area of the load carrying portion of the airframe
$m(x)$ = mass per unit length of the airframe
$u(x,t)$ = axial displacement of the airframe
x = axial coordinate measured from the missile tip
K_0 = spring constant of the launcher

A direct integration of eq. 12.56 is usually quite difficult, especially when the effects of liquid propellants are included. Therefore, rather than attempt a direct solution of eq. 12.56, it is far more convenient to replace the continuous airframe by a lumped spring-mass analog. A typical decomposition of an airframe into a spring-mass system is shown in Fig. 12.14.

The general procedure used to arrive at such an analog is to divide the airframe into a number of sections, replacing the distributed mass of each section by a single mass placed at the center of gravity of each section; the masses are joined by springs whose stiffnesses are equal to the stiffness of the airframe structure between the masses. The inclusion of propellant effects requires special treatment. The hydrostatic pressure created by the effective weight of accelerating propellants causes the propellant tanks to bulge, which in turn shifts the center of gravity of the propellant mass. A computation of these events leads to expressions for effective spring constants of the form given by K_5, K_6, and K_7 of Fig. 12.14.

The equations of motion of the spring-mass analog can be written by inspection. Some of these equations are

$$M_n\ddot{x}_n + K_n(x_n - x_{n-1}) + C_n(\dot{x}_n - \dot{x}_{n-1}) = 0$$

$$M_{n-1}\ddot{x}_{n-1} + K_7(x_{n-1} - x_p) + K_5(x_{n-1} - x_4) + K_n(x_{n-1} - x_n) + C_n(\dot{x}_{n-1} - \dot{x}_n) = 0$$

$$M_p\ddot{x}_p + K_6(x_p - x_4) + K_7(x_p - x_{n-1}) = 0 \qquad (12.58)$$

$$M_4\ddot{x}_4 + K_4(x_4 - x_3) + K_2(x_4 - x_2) + K_6(x_4 - x_p)$$
$$+ K_5(x_4 - x_{n-1}) = 0$$

$$M_2\ddot{x}_2 + K_1(x_2 - x_1) + C_1(\dot{x}_2 - \dot{x}_1) + K_2(x_2 - x_4)$$
$$+ K_3(x_2 - x_3) + K_0x_2 = 0 \qquad x_2 \leq \frac{W}{K_0}$$

$$M_2\ddot{x}_2 + K_1(x_2 - x_1) + C_1(\dot{x}_2 - \dot{x}_1) + K_2(x_2 - x_4)$$
$$+ K_3(x_2 - x_3) + W = 0 \qquad x_2 > \frac{W}{K_0}$$

where $W = \sum_{i=1}^{n} M_i g$

The limits on the last two equations of 12.58 account for the possibility of the missile separating from the launcher. The solution of these equations provides axial loads F_n, for example,

$$F_n = K_n(x_n - x_{n-1}) + C_n(\dot{x}_n - \dot{x}_{n-1})$$

and accelerations $\ddot{x}_n$ for different sections of the missile. Since the coordinates originate from the equilibrium position, the absolute acceleration of any mass will be $\ddot{x}_n + g$, where g is the acceleration caused by gravity. Similarly, the total axial load at station n equals $K_n(x_n - x_{n-1}) - m_n g + C_n(\dot{x}_n - \dot{x}_{n-1})$. This choice of coordinates is made in order to eliminate the necessity of computing initial displacements and setting them as initial conditions on a computer. The initial displacements for the equations here are all zero, whereas if all spring deflections were measured from their free length, the deflection of each spring under the weight of the masses above it would have to be used to determine initial conditions. In a more complicated model with springs spanning across several masses, solution of the static problem is more tedious so that the use of coordinates measured from equilibrium is even more strongly indicated.

In many engine thrust transient response problems the effect of damping in the missile is very important. Hence, an estimate of the modal damping (possibly an experimental value) for the structure is necessary to determine the values of dashpots C_n, which are located between masses as shown in Fig. 12.14. If the modal damping b_n in the missile is small, it can be shown (reference 6) that a good approximation for b_n is given by

$$b_n = \sum_{j=1}^{P} C_j \frac{[\phi_n(x_j) - \phi_n(x_{j+1})]^2}{2\omega_n M_n} \tag{12.59}$$

where b_n = per cent of critical viscous damping in the nth mode

C_j = dashpot constant at station j

P = total number of dashpots

$\phi_n(x_j) - \phi_n(x_{j+1})$ = relative displacement in dashpot j, for the nth mode.

ω_n = circular frequency of nth mode

M_n = generalized missile mass for the nth mode

$= \sum_{i=1}^{N} m_i \phi_n^2(x_i)$

N = total number of masses

The foregoing equation provides the necessary values of the dashpot constants to maintain the desired modal damping. A set of P simultaneous equations are formed with P dashpot constants, C_j as unknowns.

Equations 12.58 can be written in matrix form as follows:

$$[A]\{\ddot{x}\} + [B]\{\dot{x}\} + [C]\{x\} = 0 \tag{12.60}$$

where [A] = mass matrix

[B] = damping matrix

[C] = stiffness matrix

{ } = a column matrix

For purposes of computing longitudinal modes and natural frequencies, the damping is assumed to be negligible, and the time dependence of the displacements is sinusoidal with frequency ω. Equation 12.60 then takes the form

$$([C] - \omega^2[A])\{x\} = 0 \tag{12.61}$$

Equation 12.61 is the classical form for an eigenvalue problem in matrix notation. The solution of 12.61 yields the natural frequencies ω_n and mode shapes $\phi_n(x)$. With the mode shapes available, the response of the spring-mass analog can be written as

$$u(x, t) = \sum_{n=1}^{N} \phi_n(x)\, q_n(t) \tag{12.62}$$

with the generalized coordinates $q_j(t)$ given by

$$\ddot{q}_n(t) + 2 b_n \omega_n \dot{q}_n(t) + \omega_n^2 q_n(t) = \frac{F(t)\, \phi_n(x_1)}{M_n} \tag{12.63}$$

Equations 12.62 and 12.63 are valid, independent of whether the missile is resting on or has left the launcher, the only

TABLE 12.3

Effect of Damping and Release Time on Missile Axial Loads due to Launch and Engine Thrust Transients

Case	Missile Station	Maximum Compressive[a] Axial Load
A: Release at 77% of full thrust $b_n = 1\%$ $n = 1, 2, 3, 4$	125 tip	1.0[b]
	250	4.5
	400	12.2
	800	38.8
B: Release at 100% of thrust $b_n = 1\%$	125	2.1
	250	11.1
	400	27.5
	800	64.5
C: Release at 100% of thrust $b_n = 0$	125	3.8
	250	18.0
	400	45.0
	800	73.5
D: Release after a 1-second hold $b_n = 1\%$	125	1.9
	250	9.7
	400	24.0
	800	59.0

[a] Loads are normalized to b and occur after release (post-launch).

difference being that the mode shapes ϕ_n are different in each case.

Equations 12.62 and 12.63 may not represent the most convenient form of the solution. In fact, it is often much faster to solve eqs. 12.58 directly on an analog computer rather than attempt a modal solution.

B. An example. Table 12.3 shows the effects of damping and release time on missile axial loads caused by launch and engine thrust transients. The axial loads occur in a large ballistic missile just after launch when the release time is specified at a per cent of the full engine thrust. A typical engine thrust build-up curve is shown in Fig. 12.15 with release times of the missile which correspond to the cases of Table 12.3. To compare cases B and D, the differences in the loads are caused by the transients of the engine thrust which are generated in part by the rate of build-up. In case D these transients are nearly damped out, and hence for this case the results may be obtained by simply applying a step load to the end of a free-free missile of magnitude T – W, where T is the 100 per cent thrust value and W is the total weight of the missile. To compare cases A and B, the differences in the axial loads is mainly caused by the differences in the rigid-body accelerations. The effect of damping is clearly indicated in cases B and C. Although the axial loads of Table 12.3 indicate that it is advantageous to release the missile at the lowest thrust level, the combination of axial and lateral loads may indicate the necessity for a different time of release. An over-all

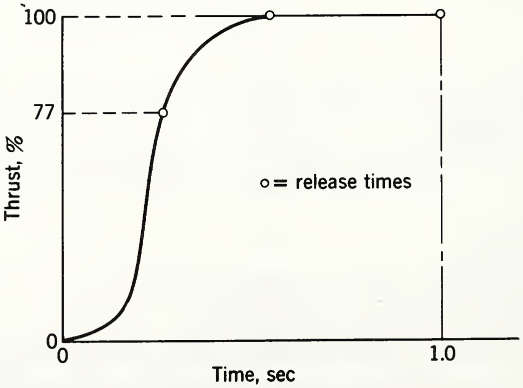

Fig. 12.15 Engine thrust build-up curve.

loads picture must be examined before a release time can be specified. The lateral loads will dominate the axial loads in certain sections of the missile and vice versa. Therefore, if the lateral loads are predominant, which is usually the case at sections near the tip of the missile, it may be necessary to launch at a time when some of the contributors to lateral loads are damped out, that is, effects of engine thrust differential, which have not been treated here.

REFERENCES

1. S. Timoshenko, Vibration Problems in Engineering, D. Van Nostrand, Princeton, N. J.
2. R. M. Cooper, "Dynamics of Liquids in Moving Containers," ARS Journal, **30**, No. 8 (1960).
3. R. L. Bisplinghoff, H. Ashley, and R. L. Halfman, Aeroelasticity, Addison-Wesley Press, Reading, Mass., 1955.
4. Y. C. Fung, The Theory of Aeroelasticity, John Wiley and Sons, New York, 1955.
5. Y. C. Fung, "Fluctuating Lift and Drag Acting on a Cylinder in a Flow at Supercritical Reynolds Numbers." Bulletin 26th Shock and Vibration Symposium, Dept. of Defense, 1958.
6. H. E. Lindberg, "Effect of Support Conditions and Shaker Arrangements in Beam Vibration Testing," 4th Symposium on Ballistic Missiles and Space Technology, University of California, Los Angeles, 1959.

13

ESTIMATING PERFORMANCE CAPABILITIES OF BOOST ROCKETS

P. Dergarabedian and R. P. Ten Dyke

13.1 INTRODUCTION

In a parametric study of boost rockets, the term boost rocket includes rockets launched from the surface of the earth for the purpose of achieving near-orbital or greater velocities.

The parameters studied can be divided into two categories, vehicle design parameters and trajectory parameters. Vehicle design parameters describe the physical rocket and include such quantities as weights, thrusts, propellant flow rates, drag coefficients, and the like. A set of these parameters would serve as a basic set of specifications with which to design a vehicle. Trajectory parameters include such quantities as impact range, apogee altitude, and burnout velocity. Trajectory parameters can serve, although not uniquely, as specifications for a missile system as well. A particular vehicle system can perform many missions, and any one mission can be performed by many vehicles. We usually think of missions in terms of trajectory parameters and vehicles in terms of design parameters, and the problem becomes to relate the two.

The simplest relation is found in the well-known equation:

$$V_i = I_i g \ln r_i \qquad (13.1)$$

where I_i = stage i specific impulse, thrust divided by flow rate of fuel
g = gravitational constant = 32.2 ft/sec^2
r_i = stage i burnout mass ratio, initial mass divided by burnout mass
V_i = velocity added during stage i

If several stages are used, the total velocity is the sum of the velocities added during each stage. Certain assumptions are used in the derivation of the rocket equation which limits its usefulness for boost rockets. They are (a) no gravitational acceleration, (b) no drag, and (c) constant specific impulse. When it becomes necessary to include these effects, the most frequent technique is to solve the differential equations of motion by use of a computing machine. Since some of the inputs to the problem are not analytic, such as drag coefficient versus Mach number, the machine uses an integration technique which virtually "flies" the missile on the computer. In this manner impact range, apogee altitude, burnout velocity, burnout altitude, and so forth can be determined as functions of vehicle design parameters.

The same vehicle can be flown on many paths, so it is necessary to provide the machine with some sort of steering program. The most frequently used program for the atmospheric portion of flight is the "zero-lift" turn. Assuming that the rocket thrust vector is aligned with the vehicle longitudinal axis, the vehicle attitude is programmed to coincide with the rocket velocity vector. For this reason the zero-lift trajectory is frequently referred to as the "gravity turn." If a rotating earth is used, the thrust is aligned with the velocity vector as computed in a rotating coordinate system. Since the missile is launched with zero initial velocity, a singularity exists for the velocity angle at the instant of launch. All gravity turn trajectories, regardless of burnout angle, must launch vertically. For that reason, a mathematical artifice (an initial "kick" angle) is applied to the velocity vector a few seconds after launch to start the turn.

Most problems can be solved by the computer very quickly, and the accuracy of the results is almost beyond question. But there are disadvantages as well. First, the actual computer time consumed may be small, but the time required to prepare the input data and arrange for computer time can be rather long in comparison. Secondly, the accuracy required of results for preliminary design purposes is rather different from that required for, let us say, targeting purposes; and the high accuracy offered by the digital machine frequently goes to waste. Finally, it is one thing to be able to feed the computer one set of data and have a set of answers returned and quite another to be able to view an analytic relation or graph and get a "feel" for the whole system. For these reasons simplified, even if approximate, solutions to the problem of determining trajectory parameters for boost vehicles are quite useful.

Two techniques may be employed to determine approximate solutions to the differential equations of motion. One technique uses approximation before the equations are solved. The original model is transformed into a simpler one for which the solutions are known. In this case we must make a priori guesses as to the accuracy lost in simplification. However, the digital computer has provided the tool for making approximations after solution. The model which is simplified is the solution, not the set of differential equations; and the accuracy of the approximations can be readily observed. The latter technique has been employed in this study.

The differential equations are helpful in showing which variable will be important to consider. A short, theoretical analysis, given in Section 13.7, has shown that the following missile design parameters, together with a burnout velocity angle, will determine a trajectory.

I = vacuum specific impulse; vacuum thrust divided by flow rate
r = mass ratio
N_0 = ratio of initial (launch) thrust to lift-off weight
$C_{DM}A/W_0$ = drag parameter; C_{DM} is the maximum value for drag coefficient versus Mach number, A is the reference area, and W_0 is the lift-off weight of missile.
I_s/I = ratio of initial specific impulse to vacuum specific impulse
t_b = burning time $= (I_s/N_0)(1 - 1/r)$ for constant weight flow rate

The trajectory parameters studied are

V_b = burnout velocity
β_b = velocity burnout angle (with respect to local vertical)
h_b = burnout altitude from the earth's surface
x_b = surface range at burnout
R = impact range

It is clear from the number of parameters studied that it would be impossible to simply plot the results. Therefore, simplification and codification of the results have been a significant part of the study. Results are presented in two forms: (a) a set of general equations for determining V_b, h_b, and x_b versus β_b for selected ranges of missile design parameters (where necessary "constants" used in the equations are presented in graphical form) and (b) a simple equation for maximum impact range as a function of missile parameters, together with many of its derivatives.

In addition, a table of equations of several free-flight trajectory parameters based on the Kepler ellipse is included. These equations are well known but are included for convenience. These formulas, together with burnout conditions determined from the computer study, will aid in the solution of a large variety of the problems frequently encountered in preliminary design.

The free-flight trajectory for a vehicle is defined by the velocity and position vectors at burnout. The velocity vector is defined in terms of its magnitude* V_b and its angle with respect to the local vertical β_b. The position vector is defined by an altitude h_b and surface range x_b; V_b, h_b, and x_b are determined as functions of β_b and the vehicle design parameters.

13.2 VELOCITY VERSUS BURNOUT ANGLE

By using eq. 13.1 the "theoretical" burnout velocity may be determined for a vehicle. We define the quantity V_L as being the loss in velocity caused by gravitation and atmosphere,

$$V_b = V^* - V_L \tag{13.2}$$

where

*The term velocity will refer to the magnitude of the velocity vector. If the vector is meant, velocity vector will be used.

$$V^* = \Sigma V_i = \Sigma I_i g \ln r_i \tag{13.3}$$

An empirical equation for V_L in terms of vehicle design parameters has been derived by comparing results of several hundred machine trajectory calculations assuming single-stage vehicles, a gravity turn, and a spherical, nonrotating earth:

$$V_L = (gt_b - K_{gg})\left[1 - K_g\left(1 - \frac{1}{r}\right)\left(\frac{\beta_b}{90°}\right)^2\right] + K_D\frac{C_{DM}A}{W_0} + K_a \tag{13.4}$$

It will be convenient to discuss the equation term by term, so we will designate the three components as follows:

$$V_g = \text{gravitational loss} = (gt_b - K_{gg})\left[1 - K_g\left(1 - \frac{1}{r}\right)\left(\frac{\beta_b}{90°}\right)^2\right] \tag{13.5}$$

$$V_D = \text{drag loss} = K_D\frac{C_{DM}A}{W_0} \tag{13.6}$$

$$V_a = \text{nozzle pressure loss} = K_a \tag{13.7}$$

13.2.1 Gravitational Loss

The gravitational loss was determined by setting the drag equal to zero and flying the vehicle to several burnout angles. The term gt_b is the gravitational loss to be expected from a vertical flight in a constant gravitational field. A realistic gravitational field varies in an inverse square of the distance from the earth's center, so the term actually overestimates this loss. For ranges of vehicles using currently available propellants, the differences between the amount gt_b and the correct gravity loss will be small; and for this equation the difference has been included as the constant K_{gg}. The term $\left[1 - K_g\left(1 - \frac{1}{r}\right)\left(\frac{\beta_b}{90°}\right)^2\right]$ fits a curve as a function of β_b. The constant K_g was determined by a least-squares curve-fitting technique and usually resulted in a curve fit which was within 30 ft/sec of the machine results. This form was found to fit actual results better than a more obvious choice, $K \cos \beta_b$. The latter resulted in maximum differences of 300 ft/sec.

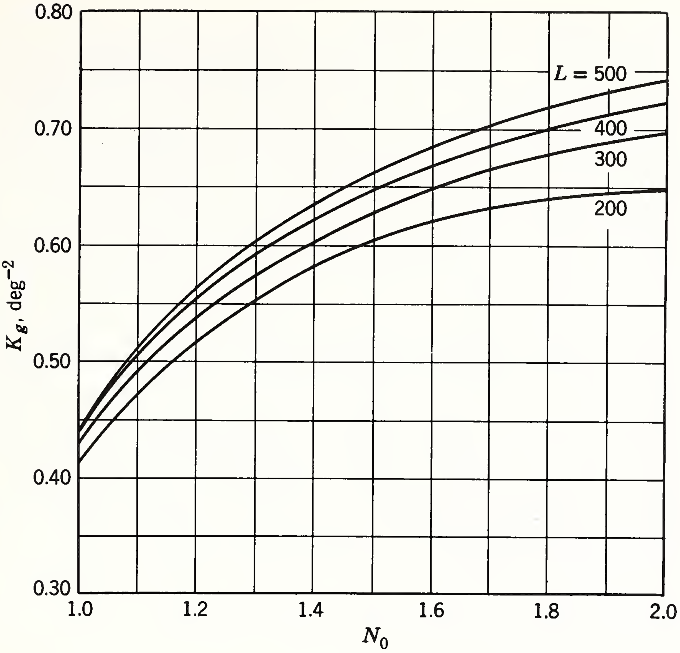

Fig. 13.1 K_g versus vacuum specific impulse I and initial thrust to weight ratio N_0.

Curves for K_g versus I and N_0 are found in Fig. 13.1, and a curve for K_{gg} versus I is found in Fig. 13.2.

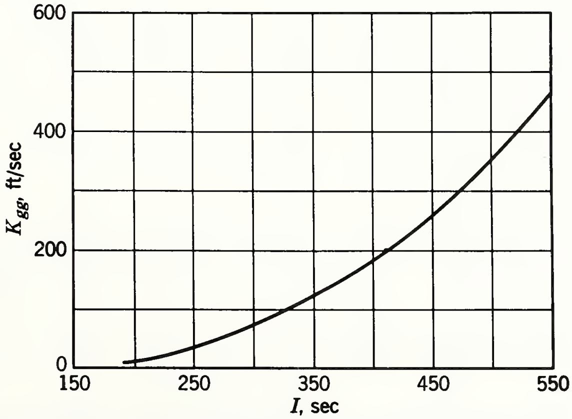

Fig. 13.2 K_{gg} versus vacuum specific impulse I.

13.2.2 Drag Velocity Loss

The velocity lost to drag is proportional to the quantity $C_{DM} A/W_0$. The symbol C_{DM} has been chosen as a single parameter to define all drag curves. The reasons for this choice are (a) most realistic drag curves have approximately the same form, except for the absolute magnitudes of the values, and (b) the greater portion of the drag loss occurs early in powered flight, where C_D attains a maximum. The actual drag curve used in the machine trajectory calculation is shown in Fig. 13.3. The empirical constant K_D was obtained by computing the difference between burnout velocities for similar vehicles with and without drag. All comparisons were made for identical burnout angles. The constant was found to be a function of I_s/N_0, β_b, and N_0. However, K_D was so weakly dependent on N_0 that this effect was disregarded for simplicity in presenting the results. In Fig. 13.4 K_D is shown as a function of I_s/N_0 and β_b.

13.2.3 Nozzle Pressure Loss

For the same propellant flow rate, the effective thrust at sea-level ambient pressure is less than in a vacuum. This

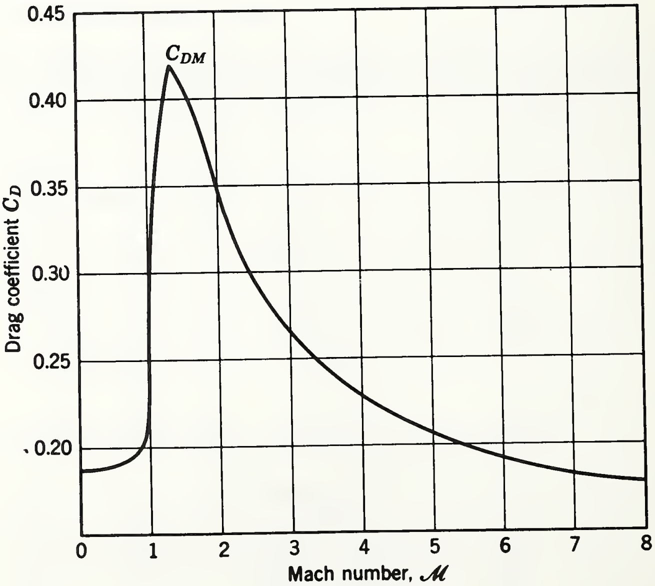

Fig. 13.3 Drag coefficient C_D versus Mach number.

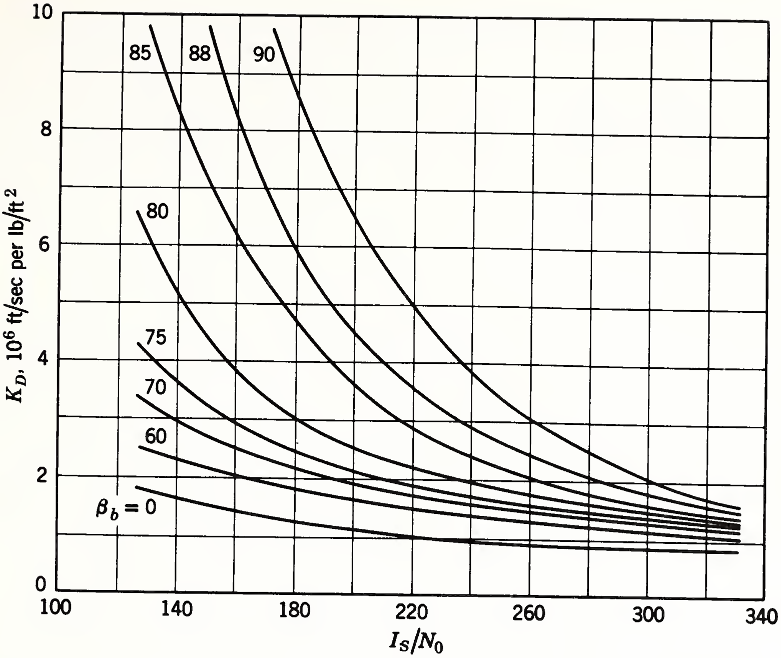

Fig. 13.4 K_D versus burnout velocity angle β_b and ratio of sea-level specific impulse to initial thrust to weight ratio, I_s/N_0.

may be thought of as a change in specific impulse. The ratio of sea level to vacuum specific impulse is dependent on the chamber pressure, nozzle area expansion ratio, and ratio of specific heats for the combustion products. Thrust coefficient tables are readily available to provide this information. It was again assumed that the greater portion of the losses would occur early in flight, and all losses were computed for vertical trajectories. The results are given in Fig. 13.5 where K_a is plotted as a function of I_s/I.

13.2.4 Accuracy of Results

Accuracies to within 150 ft/sec should be expected with these results. Occasionally, cases may exist which exceed these limits. First, drag curves may not actually be similar to the one selected for this study. Secondly, simplification of the results to a form that will facilitate rapid computation has necessitated several approximations. It is believed that the results as presented will be more useful in preliminary design

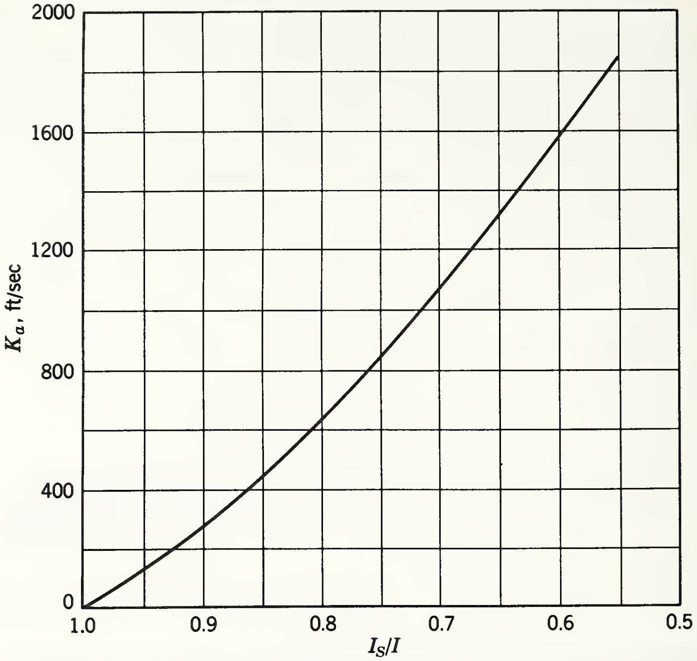

Fig. 13.5 K_a versus ratio of sea level to vacuum specific impulse, I_s/I.

than extremely accurate results. Guessing that the typical first stage is designed to achieve about 10,000 ft/sec, the accuracy of 150 ft/sec amounts to 1.5 per cent.

13.2.5 Application to More Than One Stage

All computations were performed for single-stage vehicles, but the results may be applied to multistage vehicles.

If the first stage can be assumed to burn out at greater than 200,000 ft at a velocity angle less than 75°, the drag losses may be assumed to have occurred during first stage. It is important to note that the constant K_D will be determined on the basis of the velocity burnout angle for the first stage. For multistage vehicles, this may be 5 to 15° less than the angle at final-stage burnout; but for β_b less than 75°, the drag losses are relatively insensitive to β_b, and any reasonable estimate will probably be satisfactory.

Under almost any circumstances the nozzle pressure loss can be considered to occur during the first stage. Constants applicable to the first stage should be used.

The most significant velocity loss from succeeding stages will be gravitational loss. Since the velocity angle will be more constant during succeeding stages, it is usually satisfactory to assume a constant value between the assumed burnout of the first stage and the desired final burnout angle. Then the velocity loss for succeeding stages may be computed by

$$V_{L2} = g\left(\frac{R_e}{R_e + \bar{h}}\right)^2 t_{b2} \cos \bar{\beta} \qquad (13.8)$$

where $\bar{\beta}$ is an intermediate velocity angle, $\bar{h}$ is an "average" altitude for second-stage powered flight, and the subscript 2 refers to succeeding stages. The difference between burnout angles of the first stage and that for the final burnout will depend on the thrust pitch program selected for succeeding stages. For a ballistic missile, where impact range is the desired result, holding the thrust vector constant with respect to a stationary inertial coordinate system has been found to yield greater ranges than the gravity turn. For this case the change in β from first-stage burnout to final burnout will be comparatively small. In contrast, many satellite missions require that burnout angles approach or equal 90°. Under these circumstances a gravity turn or one in which the vehicle is pitched downward is a more likely trajectory. The resulting difference in burnout angles between first and final stages will be rather large.

In any trajectory in which thrust is not aligned with velocity, some energy will be expended in "turning" the velocity vector. The proportion of the thrust which goes to increasing the velocity varies as the cosine of the angle of attack, so for small angles of attack the loss will be small.

13.2.6 Effect of the Earth's Rotation

The significant parameter in determining performance is the inertial velocity. Thus the velocity of the launch point must be considered in any realistic calculation. A simple, albeit approximate, correction may be made by vectorially adding the inertial velocity vector of the launch point to the vehicle velocity vector at burnout. In several comparisons between this approximate technique and that of a machine trajectory for an eastward launch on a rotating earth, this approximation underestimated the actual burnout velocity. It has not been determined whether this is generally true; but based on the few comparisons we would expect the approximation to tend toward conservative results.

13.3 BURNOUT ALTITUDE VERSUS BURNOUT ANGLE

The burnout altitude is a particularly important parameter in determining payload capabilities for low-altitude satellites with circular orbits. As with the rocket equation, a closed-form expression may be derived for the distance traversed by an ideal rocket in vertical flight (constant g, no drag, constant specific impulse):

$$h^* = gIt_b \left(1 - \frac{\ln r}{r-1}\right) - \frac{gt_b^2}{2} \qquad (13.9)$$

It was found that this form could be modified to account for drag, nozzle pressure, and burnout angle:

$$h_b = \left[h^* - \frac{(V_D + V_a)t_b}{2}\right]\left[1 - \left(\frac{\beta}{K_h}\right)^2\right] \qquad (13.10)$$

where

$$K_h = 93 + \frac{28}{r}\left[1 + 5(2 - N_0)^2\right] \quad 1 \le N_0 \le 2 \qquad (13.11)$$

Equation 13.10 assumes that the drag and nozzle pressure losses are averaged over the duration of flight. This is not exactly true, but the approximation has proved to be satisfactory because the correction is small. The constant K_h has been determined empirically. Accuracies for eq. 13.10 have been found to agree with machine calculations to about 20,000 ft.

In calculating values for multistage vehicles, eq. 13.10 will yield the altitude of burnout for the first stage. The additional altitude achieved during succeeding stages may be calculated using the first-stage burnout velocity as computed by eq. 13.4 and the following relation derived by integrating $Ig \ln r - gt \cos\beta$ at a constant, average flight path angle $\overline{\beta}$:

$$\begin{aligned} h_{b2} &= h_{b1} + V_{b1}t_{b2}\cos\overline{\beta} \\ &\quad + \left[gI_2t_{b2}\left(1 - \frac{\ln r_2}{1 - r_2}\right) - \frac{gt_{b2}^2\cos\overline{\beta}}{2}\right]\cos\overline{\beta} \qquad (13.12) \end{aligned}$$

where the subscripts 1 and 2 refer to the first and second stage, respectively. This form may be extended to cover additional stages. Again, an intermediate value for the flight path angle $\overline{\beta}$ may be selected between the estimated first-stage burnout flight path angle and the desired final burnout angle.

No correction is suggested for use with a rotating earth. In several comparisons with machine trajectories, assuming an eastward launch on a rotating earth, the altitude value for the nonrotating earth was approximately equal to that for the rotating earth.

13.4 BURNOUT SURFACE RANGE

The surface range at burnout may be determined by the following empirical expression:

$$x_b = 1.1h^* \frac{\beta_b}{90^\circ} \tag{13.13}$$

The surface range is the least important of the trajectory parameters in determining gross vehicle performance. However, it is important in that it adds to the impact range of a surface-to-surface ballistic missile. Again, no correction is offered for the rotating earth because, for reasonably short flight duration, the increased inertial velocity of the vehicle and the velocity of the launch point may be assumed to cancel. Equation 13.13 has been found to yield surface range at burnout within an accuracy of about 10 per cent.

For multistage vehicles the same technique used in determining altitude may be applied:

$$x_{b2} = x_{b1} + (h_{b2} - h_{b1}) \tan \overline{\beta} \tag{13.14}$$

13.5 FREE-FLIGHT TRAJECTORY

The calculation of the burnout conditions of a vehicle is only an intermediate step in determining its performance. Performance is usually measured in terms of impact range, apogee altitude, or some other end condition. Since all vehicles in free-flight follow a Kepler ellipse, values for range, apogee altitude, and the like may be determined from the burnout conditions by using equations yielding these values in closed form. A number of these equations are listed in Table 13.1.

TABLE 13.1
Miscellaneous Formulas for Kepler Ellipse

$\sigma = \dfrac{R_e + h_b}{R_e}$	$\epsilon = \sqrt{1 - 2\lambda \sin^2 \beta + \lambda^2 \sin^2 \beta}$
$\lambda = \dfrac{V_b^2 \sigma_b}{gR_e}$	R_e = earth radius = 20.9×10^6 ft
Conservation of energy	$V^2[t] - \dfrac{2gR_e^2}{z} = \text{constant}$
Conservation of angular momentum	$Vz \sin \beta = \text{constant}$
Impact range angle from burnout	$\psi = \pi - \sin^{-1} \dfrac{1 - \lambda\sigma \sin^2 \beta_b}{\epsilon} - \sin^{-1} \dfrac{1 - \lambda \sin^2 \beta_b}{\epsilon}$
Velocity required to obtain impact range	$V_b = \left[\dfrac{gR_e}{\sigma} \cdot \dfrac{1 - \cos \psi}{\sigma \sin^2 \beta_b + \sin \beta_b \sin (\psi - \beta_b)} \right]^{1/2}$
Apogee altitude	$h_a = \dfrac{\sigma R_e \lambda \sin^2 \beta_b}{1 - \epsilon} - R_e$
Velocity required to obtain apogee altitude	$V_b = \left\{ \dfrac{2gR_e}{\sigma} \quad \dfrac{1 - \sigma/\sigma_a}{1 - [(\sigma/\sigma_a) \sin \beta_b]^2} \right\}^{1/2}$
	$\sigma_a = \dfrac{R_e + h_a}{R_e}$
Period for complete elliptic orbit	$T = \dfrac{2\pi r_b^{3/2}}{(2 - \lambda)^{3/2} (gR_e^2)^{1/2}}$
Time to apogee from burnout	$t_a = \dfrac{T}{2\pi} \left(\sqrt{1 - \epsilon^2} \quad \cot \beta_b + \cos^{-1} \dfrac{1 - \lambda}{\epsilon} \right)$

13.6 RANGE EQUATION

Experience in the optimization of performance of medium- and long-range missiles at Space Technology Laboratories has shown that the trajectory which consists of a short period of vertical flight followed by a gravity turn to staging and a constant attitude (thrust angle with respect to launch coordinate system) throughout subsequent stages of flight yields a near-optimum range trajectory.

In the case of a single-stage missile, the constant-attitude portion of the trajectory is initiated at an altitude of approximately 150,000 ft. The velocity angle of the missile at burnout is optimized for maximum range. An examination of the trajectory equations shows that the range of a missile is determined by specifying the same vehicle design parameters investigated in the previous section. (In determining the empirical equation, however, only one value of the ratio I_s/I was used, based on a chamber pressure of 500 psi, an expansion ratio of 8, and a γ of 1.24.) This study was performed at a different time from that in the preceding section, and a slightly different drag curve was assumed, but it is not expected that the results will be significantly different for this reason.

Machine calculations were performed to determine maximum range of vehicles launched from a spherical, nonrotating earth. Here impact range is measured from the launch point rather than from the burnout point. Computer data have been used to plot a curve which shows the quantity V^* as a function of missile range. Even with a large variation in vacuum specific impulse, varying from 200 to 1000 sec, all the data points fall essentially on a single curve for a given N_0 and $C_{DM}A/W_0$. For any other values of N_0 and $C_{DM}A/W_0$ similar results are obtained. Figure 13.6 shows the mean curve obtained for $N_0 = 1.5$ and $C_{DM}A/W_0 = 0.000265$.

The results of Fig. 13.6 have been replotted in Fig. 13.7 on semilog paper, together with a curve given by

$$R = D(e^{V^*/Bg} - 1) \tag{13.15}$$

For ranges varying from 400 to 6000 nautical miles it can be seen that eq. 13.15 represents the curve obtained from the machine calculations rather accurately. We have found that the parameter B is very insensitive to changes in N_0 and $C_{DM}A/W_0$, whereas the parameter D is fairly sensitive to such changes. The values of the parameters in Fig. 13.6 are $D = 80$ and $B = 208$.

The parameter B determines the slope of the fitted curve, and the parameter D determines the displacement. However,

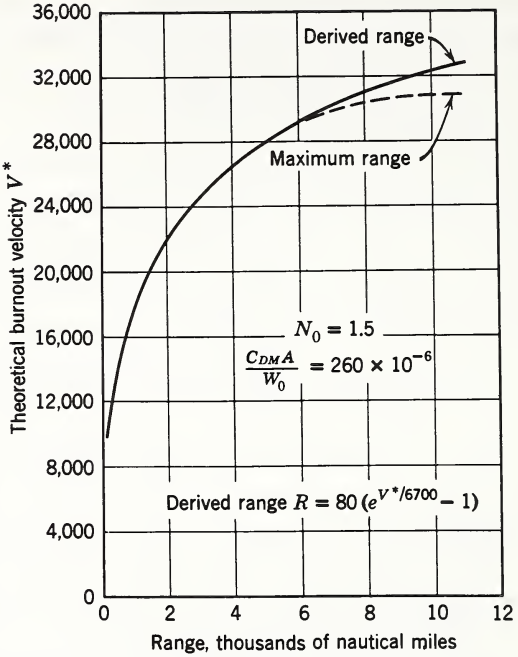

Fig. 13.6 Range versus theoretical burnout velocity V^*.

the two constants must be treated as a pair. Many curves might be fitted to the empirical data, giving better accuracies in some ranges and poorer accuracies in others. We have arbitrarily selected the value of 208 sec for B, and all values of D have been determined on this basis. If another value for B is selected, new values for D must be derived. Figure 13.8 shows D as a function of N_0 for various values of $C_{DM}A/W_0$.

The results of eq. 13.15 can be extended for use from 400 to 10,800 nautical miles (halfway around the earth) by the following argument. Burnout angles were selected to maximize range. For ranges beyond 6000 nautical miles the use of maximum-range trajectories results in very large-range misses for errors in burnout speed. This can be seen by the slope of the curve in Fig. 13.7. Lofting the trajectories so that the burnout velocity increases as determined with eq. 13.15 results in an increase of about 5 per cent above the maximum-range burnout velocity for the 10,800-nautical mile range. At the same time, the lofting decreases the miss from

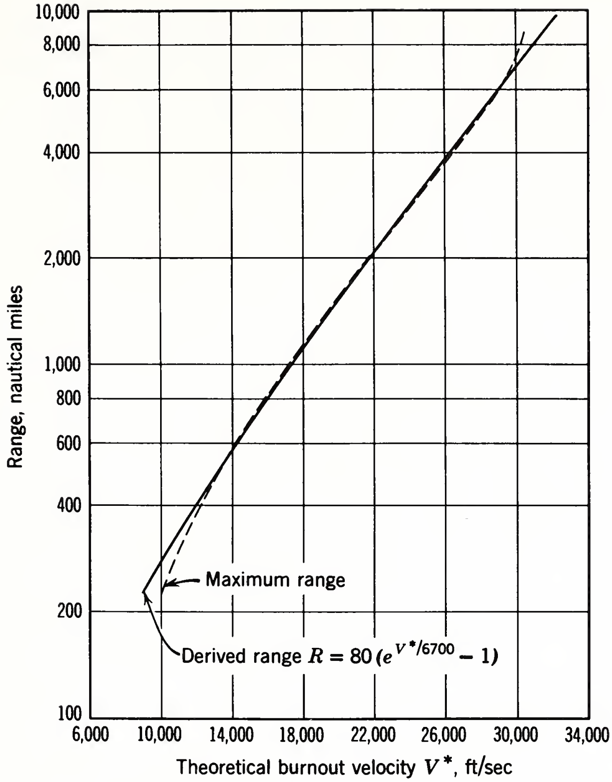

Fig. 13.7 Range versus theoretical burnout velocity V*.

about 10 nautical miles to less than 2 nautical miles for an error in the burnout speed of 1 ft/sec. For design purposes it appears that deviation from the maximum-range trajectory for ranges beyond 6000 nautical miles is reasonable and, in fact, desirable.

In the case of two-stage missiles we note that

$$V^* = I_1 g \ln r_1 + I_2 g \ln r_2$$

Thus for two-stage missiles eq. 13.15 becomes

$$R = D\,(r_1^{I_1/B}\, r_2^{I_2/B} - 1) \qquad (13.16)$$

By differentiating eq. 13.16 we may obtain a number of exchange ratios, some of which have been derived and are presented in Table 13.2.

TABLE 13.2
Summary of Exchange Ratios Derived from Simplified Range Equation

Single-Stage Vehicles

R (nautical miles) = $D(r^{I/B} - 1)$

$$\frac{\partial r}{\partial V_b} = \frac{R + D}{Bg}$$

$$\left.\frac{\partial R}{\partial W_b}\right|_{W_0} = -\frac{I(R + D)}{BW_b}$$

$$\frac{\partial R}{\partial W_0} = \frac{I(R + D)}{BW_0}$$

$$\frac{\partial R}{\partial I} = \frac{(R + D)\ln r}{B}$$

$$\left.\frac{\partial W_0}{\partial W_b}\right|_{\frac{C_{DM}A}{W_0}} = r\left[1 - \frac{B}{I} \cdot \frac{RN_0}{D(R + D)} \cdot \frac{\partial D}{\partial N_0}\right]^{-1}$$

$$\left.\frac{\partial W_0}{\partial W_b}\right|_{N_0,\ \frac{C_{DM}A}{W_0}} = r$$

$$\frac{\partial W_0}{\partial W_L} = \frac{W_0}{W_L}$$

Two-Stage Vehicles[a]

R (nautical miles) = $D\left(r_1^{I_1/B}\, r_2^{I_2/B} - 1\right)$

$$\frac{\partial R}{\partial V_b} = \frac{R + D}{Bg}$$

$$\frac{\partial R}{\partial W_j} = -\frac{I_1(R + D)}{BW_{b1}}$$

$$\frac{\partial R}{\partial W_{b2}} = -\frac{I_2(R + D)}{BW_{b2}} + \frac{\partial R}{\partial W_j}$$

[a] Numerical subscripts refer to stages and are in order of burning period.

TABLE 13.2 (Continued) Two-Stage Vehicles (Continued)

$$\left.\frac{\partial R}{\partial W_{01}}\right|_{r_1/r_2} = \frac{I_2(R + D)}{BW_{01}}$$

$$\left.\frac{\partial R}{\partial W_{01}}\right|_{W_{02}} = \frac{I_1(R + D)}{BW_{01}}$$

$$\left.\frac{\partial R}{\partial W_{01}}\right|_{W_{01} - W_{02}} = \frac{I_1(R + D)}{BW_{01}} \left(1 - r_1 + \frac{I_2 r_1}{I_1}\right)$$

$$\frac{\partial R}{\partial I_1} = \frac{(R + D) \ln r_1}{B}$$

$$\frac{\partial R}{\partial I_2} = \frac{(R + D) \ln r_2}{B}$$

$$\left.\frac{\partial W_{01}}{\partial W_j}\right|_{\frac{C_{DM} A}{W_0}} = r_1\left[1 - \frac{B}{I_1} \cdot \frac{RN_0}{D(R + D)} \cdot \frac{\partial D}{\partial N_0}\right]^{-1}$$

$$\left.\frac{\partial W_{01}}{\partial W_{b2}}\right|_{\frac{C_{DM} A}{W_0}} = r_1 r_2\left[1 - \frac{B}{I_2} \cdot \frac{RN_0}{D(R + D)} \cdot \frac{\partial D}{\partial N_0}\right]^{-1}$$

$$\left.\frac{\partial W_{01}}{\partial W_j}\right|_{N_0,\ \frac{C_{DM} A}{W_0}} = r_1$$

$$\left.\frac{\partial W_{01}}{\partial W_{b2}}\right|_{N_0,\ \frac{C_{DM} A}{W_0}} = r_1 r_2$$

$$\frac{\partial W_{01}}{\partial W_L} = \frac{W_{01}}{W_L}$$

Equation 13.16 has been checked many times against results of machine computation. To date, the equation has been accurate to about 5 per cent of the range. It has been found that the equation is useful in two ways. First, if the missile under study has no close counterpart and no machine data are available, a value for D as found in Fig. 13.8 is used. Frequently, however, a vehicle is studied for which a small amount of machine data is or can be made available. In this case the value of D is derived by solving eq. 13.16 "backward." Once a value of D has been determined for the particular missile system, the calculation of perturbations of this missile system may be made using eq. 13.16 and the D value thus derived.

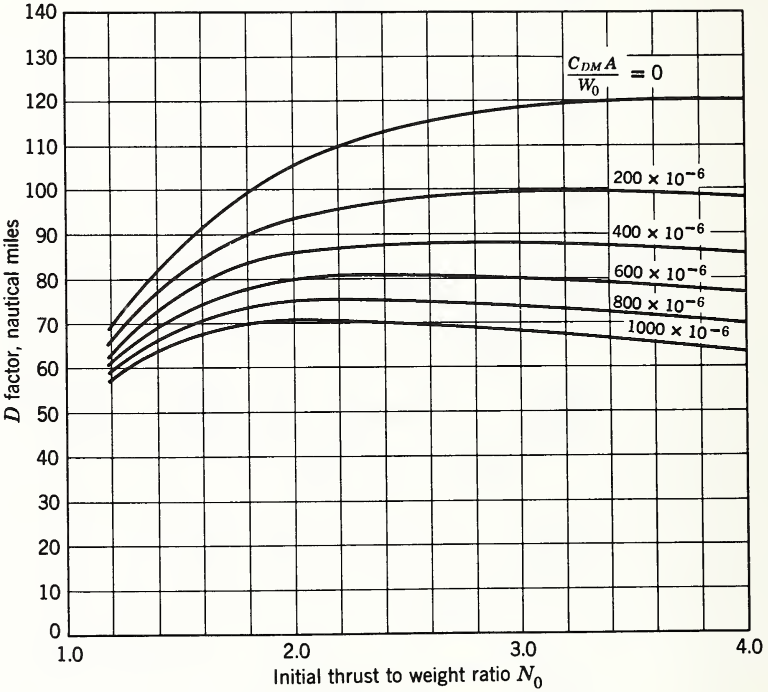

Fig. 13.8 D factor versus initial thrust to weight ratio for various $C_{DM}A/W_0$.

13.7 SELECTION OF MISSILE DESIGN PARAMETERS

In determining the performance of a rocket, we are confronted with complicated differential equations of motion. Accurate solutions are obtained only by using a digital computer. However, we can obtain a large amount of information about such things as gravitational and atmospheric effects on the performance of boost rockets by a term-by-term examination of the equations without the computer. The basic equation of motion is

$$\ddot{\underset{\sim}{z}} = n[z,t]\underset{\sim}{\kappa}[t] + \underset{\sim}{\alpha}[z,\dot{\underset{\sim}{z}},m] \tag{13.17}$$

where $\underset{\sim}{z}$ = radius vector from earth center to missile
n = thrust-to-mass ratio = $F[z]/m[t]$
t = time
$m[t]$ = mass of missile
$\underset{\sim}{\kappa}$ = unit vector in the direction of thrust
$\underset{\sim}{\alpha}$ = $\underset{\sim}{\alpha}$[gravitation] + $\underset{\sim}{\alpha}$[drag]

Here

$$\underset{\sim}{\alpha}[\text{gravitation}] = -\frac{gR_e^2}{z^2}\cdot\frac{\underset{\sim}{z}}{z} \tag{13.18}$$

$$\underset{\sim}{\alpha}[\text{drag}] = -\frac{1}{2}\frac{\rho V^2 C_D A}{m}\cdot\frac{\underset{\sim}{V}}{V} \tag{13.19}$$

where C_D = drag coefficient, a function of Mach number
R_e = radius of earth
$\underset{\sim}{V}$ = vehicle velocity relative to the atmosphere
A = reference area
ρ = air density

By replacing α with the terms for $\underset{\sim}{\alpha}$ [gravitation] and $\underset{\sim}{\alpha}$ [drag] and dividing by g,

$$\frac{\ddot{\underset{\sim}{z}}}{g} = \frac{F}{W}\frac{[z]}{[t]}\underset{\sim}{\kappa}[t] - \frac{R_e^2}{z^2}\frac{\underset{\sim}{z}}{z} - \frac{1}{2}\rho V^2\frac{C_D A}{W[t]}\cdot\frac{\underset{\sim}{V}}{V} \tag{13.20}$$

We assume that thrust in a vacuum is proportional to the weight flow rate. Thrust as a function of altitude is taken as the vacuum thrust corrected for ambient pressure:

$$F[z=\infty] = F_\infty = I\dot{W} \tag{13.21}$$

$$F[z] = F_\infty\left[1 - \frac{p[z]}{p_s}\left(1 - \frac{I_s}{I}\right)\right] \tag{13.22}$$

where $p[z]$ = ambient pressure
p_s = ambient pressure at sea level
I_s/I = ratio of sea-level thrust to vacuum thrust for identical flow rates.

Values for I_s/I may be calculated from tables showing thrust coefficient versus expansion area ratio, ratio of specific heats for exhaust products, and chamber pressure. Defining N_0 as ratio of initial thrust to initial weight and assuming constant $\dot{W}$, we can write the equation of motion in terms of missile design parameters:

$$\frac{\ddot{\underset{\sim}{z}}}{g} = N_0 \frac{I}{I_s} \frac{1}{1-\frac{N_0}{I_s}t}\underset{\sim}{\kappa} - N_0 \frac{\left(\frac{I}{I_s}-1\right)\frac{p}{p_s}}{1-\frac{N_0}{I_s}t}\underset{\sim}{\kappa} - \frac{R_e^{\,2}}{z^2} \cdot \frac{\underset{\sim}{z}}{z} - \frac{1}{2}\rho V^2 \frac{C_D A}{W_0\left(1-\frac{N_0}{I_s}t\right)} \cdot \frac{\underset{\sim}{V}}{V} \tag{13.23}$$

In some cases flow rate will not be constant, but we assume it to be so during the first several seconds of flight. By forming the dot product of $\underset{\sim}{V}/V$ with $\ddot{\underset{\sim}{z}}$, integrating for a gravity turn (thrust aligned with velocity), and assuming a spherical, nonrotating earth,

$$\frac{V_b}{g} = I \ln r - \int_0^{t_b} \frac{N_0\left(\frac{I}{I_s}-1\right)\frac{p}{p_s}}{1-\frac{N_0}{I_s}t}\,dt - \int_0^{t_b} \frac{R_e^{\,2}}{z^2}\cos\beta\,dt - \int_0^{t_b} \frac{\frac{1}{2}\rho V^2 C_D A}{W_0\left(1-\frac{N_0}{I_s}t\right)}\,dt \tag{13.24}$$

We define the velocity lost to gravitation, drag, and atmosphere as the following integrals:

$$V_g = g\int_0^{t_b} \frac{R_e^{\,2}}{z^2}\cos\beta\,dt \tag{13.25}$$

$$V_D = g\int_0^{t_b} \frac{\frac{1}{2}\rho V^2 C_D A}{W_0\left(1-\frac{N_0}{I_s}t\right)}\,dt \tag{13.26}$$

$$V_a = g \int_0^{t_b} \frac{N_0 \left(\frac{I}{I_s} - 1\right) \frac{p}{p_s}}{1 - \frac{N_0}{I_s} t} \, dt \tag{13.27}$$

and the design velocity

$$V^* = Ig \ln r$$

So the burnout velocity becomes

$$V_b = V^* - V_g - V_D - V_a \tag{13.28}$$

It is apparent that the velocity lost is intimately tied in with the trajectory itself. Forming the dot product of $\ddot{\underset{\sim}{z}}/g$ with a unit vector normal to the velocity, and again assuming a gravity turn and nonrotating earth, we obtain

$$\dot{\beta} = \frac{g}{V} \frac{R_e^2}{z^2} \sin \beta - \frac{V \sin \beta}{z} \tag{13.29}$$

For low velocity the turning rate is large, and the greater portion of turning is to be expected early in the trajectory. However, the amount of turning to be achieved is limited by the desired burnout angle. Therefore it is frequently necessary to keep $\sin\beta$ (therefore β) rather small during the early portion of the trajectory to prevent too much turning. The trajectory can be thought of as consisting of three segments: (a) a portion during which the vehicle flies steeply, (b) a period of turning, and (c) a portion in which the velocity angle remains relatively constant.

For the early portion of flight, the velocity can be approximated by

$$V \approx (N_0 - 1) g t \tag{13.30}$$

For a given burnout angle the start of the period of turning will depend primarily on the initial thrust to weight ratio N_0. Thus, for low values of N_0 (near 1.0), the initial portion of flight will be at a lower velocity and the turning rate will be increased. To achieve the same burnout angle as that for a higher value of N_0, the initial portion of the trajectory must be steeper (lower β).

The turning rate for a gravity turn is zero when the vehicle velocity equals that required for a circular satellite orbit at the same altitude.

13.7.1 Gravity Loss

We can use the foregoing to gain insight into the behavior of the velocity lost to gravitation and atmosphere. In vertical flight the gravity loss should be proportional to t_b. For a trajectory burning out at angle β_b the gravity loss will be some fraction of that lost in purely vertical flight; and we would expect that fraction to depend on N_0 and the proportion of total mass consumed as propellant $(1 - 1/r)$.

It is sometimes proposed that the velocity lost to gravitation is not really lost at all but that it is converted into potential energy. It may be observed, however, that a vehicle in powered flight is not a conservative system. A ballistic missile does not burn impulsively (that is, all the propellant is not burned on the ground). Some of the fuel is used to lift the unburned fuel, so that the vehicle always ends up at some finite altitude above the earth. Energy is imparted to the expended propellants by raising unburned propellant to some finite altitude.

One way to see what happens is to consider the following comparison of two single-stage vehicles which are identical in all respects except thrust. Figure 13.9 compares vertical trajectories for the two vehicles. With vehicle 1 we assume an infinite thrust (impulsive burning) and with vehicle 2 a finite thrust. Vehicle 1 burns out all its propellants at the surface of the earth, achieves a theoretical velocity V^*, rises, returns to earth, and impacts at the same velocity. For vehicle 2,

$$V_b = V^* - gt_b \tag{13.31}$$

$$V_{\text{impact}} = V^* - gt_b + gt_j \tag{13.32}$$

$$V_{\text{impact}} = V^* - gt_b\left(1 - \frac{t_j}{t_b}\right) \tag{13.33}$$

where t_b = burning time for vehicle 2
t_j = time from burnout altitude to impact on re-entry

Here t_j will always be less than t_b, for it takes a time t_b to get from a velocity of 0 to V_b, whereas it takes a time t_j to get from a velocity of V_b to V_{impact}, where $V_{\text{impact}} > V_b$. The kinetic energy of vehicle 1 at impact will be essentially proportional to the square of its impact velocity V^*. The kinetic energy of vehicle 2 will be essentially proportional to the

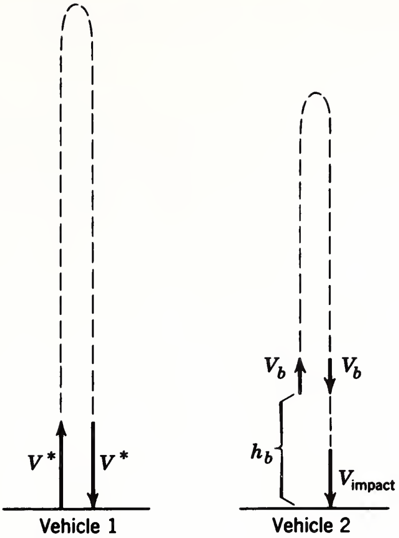

Fig. 13.9 Comparison of impulsive and finite thrust for vertical trajectory. (Constant gravitational field and no atmosphere.)

square of its impact velocity, and V_{impact} will always be smaller than the theoretical velocity of vehicle 1. As the thrust-to-weight ratio of vehicle 2 increases, V_{impact} gets closer to V^*, and hence gravity losses decrease. In actual missiles, the thrust-to-weight ratio will be closer to one than infinity because the weights of engines and structural components will increase with increased thrust. We reach a point where the advantage of higher thrust in terms of velocity losses is offset by increase in burnout weight.

We see that not all the velocity loss goes into gaining altitude; some is lost to the expended propellants. By substituting the appropriate numerical values for an existing vehicle into these equations, it was determined that around 25 per cent of the velocity loss went into gaining altitude; 75 per cent was lost as equivalent energy to the expended propellants. This calculation presents a good argument for holding the burnout altitude as low as possible. It is true that low-burnout altitudes mean larger drag effects, but these are relatively small when compared to gravity losses. Aerodynamic effects, of course, lead to heating, and heating often means an increase in structural weight, but gravitational losses are still a prime concern.

13.7.2 Drag Loss

The drag loss, eq. 13.26, is dependent on the ratio $C_D A/W_0$, ρ, and V^2. The air density ρ is dependent on altitude and, for qualitative purposes, can be considered to exponentially decay with altitude:

$$\rho(z) = \rho_s e^{-k(z - R_e)} \tag{13.34}$$

The dependency of the drag losses on V^2 will be significant during late portions of flight if the trajectory is flat (low) and high velocities are achieved below, say, 150,000 ft. However, the effect of V^2 for most "normal" trajectories is not important because these values occur when the vehicle is beyond the atmosphere. The greatest erosion of velocity occurs when C_D is near its peak and early in flight when ρ is of the same magnitude as ρ_s. In a typical trajectory with an initial thrust-to-weight ratio of 1.2, the vehicle achieved Mach 1 in 80 sec at about 30,000 ft, where the density is approximately 0.37 times that at the earth's surface.

It would be expected that for equivalent trajectories the velocity loss to drag would be sensitive to N_0. There are two effects. For high N_0 higher velocities are achieved at lower altitudes, and hence the density for Mach 1 velocity is large. But for high N_0 the duration of time through which the drag forces are acting is reduced, and the effects will tend to cancel. It turns out that drag losses are very insensitive to N_0.

For the most part, V_D depends on $C_{DM}A/W_0$, N_0/I_s, and β at burnout. Because the trajectory changes little with variation in $C_{DM}A/W_0$, the losses can be expected to be proportional to this quantity. C_{DM} (the maximum C_D) is the single parameter selected to be characteristic of all drag curves for reasons stated elsewhere in this paper. The term I_s/N_0 is equivalent to $W_0/\dot{W}$, which determines the change in $C_{DM}A/W[t]$ with time. For the same initial weight the missile with lower I_s/N_0 will have less weight at the time when the drag forces become most important. The burnout angle β is a measure of the proportion of the total trajectory contained in the atmosphere. As β is increased, the density associated with each velocity is increased, and the resulting velocity loss is greater.

As the trajectory becomes very flat and high velocities are achieved at low altitudes, the effect of V^2 and the long duration of the drag force combine to increase the drag loss to very high values. It is not expected that such trajectories are realistic, as aerodynamic heating may preclude extremely flat burnout angles. Flat burnout angles may be achieved if the thrust is reduced to increase the total time of powered flight. Usually, thrust levels that are sufficient to boost the vehicle at launch yield comparatively short over-all burning times. Thrust may be reduced by throttling a single-stage vehicle or, more profitably, by staging. If either of these techniques is not sufficient, and if flat burnout velocities are required, a coast period may be inserted between burning periods. If restart capabilities are not available or not desirable, the remaining alternative is to fly the vehicle steeply during an early portion of flight and pitch down after sufficient altitude has been achieved, yielding a negative angle of attack. In this type of trajectory considerable velocity (and payload) is lost in turning the velocity vector when the magnitude of the velocity is high. To date, no approximation has been found to determine these ''turning losses''; the only realistic approach has been to use the computing machine.

13.7.3 Nozzle Pressure Loss

The term V_a results from the fact that thrust is lost when the nozzle pressure in the exit plane is less than the ambient pressure. This loss is frequently thought of in terms of a reduction in specific impulse. The amount of the thrust loss as a function of trajectory parameters is dependent only on the ambient pressure, so the total velocity loss occurs early in powered flight.

The integral shows that the nozzle pressure loss should also be proportional to N_0. However, an increase in N_0 increases the rate at which altitude is achieved, reducing the duration of flight time at high ambient pressure by an amount also dependent on N_0; and the two effects tend to cancel. The effect of I_s/N_0, or the change in vehicle weight with time, is less significant with the nozzle pressure loss than with the drag loss because the largest percentage of nozzle pressure loss occurs early in powered flight.

13.8 SYMBOLS USED IN THIS CHAPTER

A = vehicle reference area for drag calculations

B = empirical parameter in simplified range equation

C_D = drag coefficient, function of Mach number

C_{DM} = maximum drag coefficient

D = empirical parameter in simplified range equation

F = thrust (lb)

g = gravitational constant, 32.2 ft/sec^2

h = burnout altitude measured from the earth's surface

$\bar{h}$ = intermediate altitude between first-stage burnout and final burnout to compute velocity loss in succeeding stages

h^* = burnout altitude for vertical trajectory neglecting atmospheric effects

I = vacuum specific impulse, vacuum thrust divided by flow rate of fuel

I_s = sea-level specific impulse, sea-level thrust divided by flow rate of fuel

i = index denoting stage measured from launch

K_a = empirical constant used to determine V_a

K_D = empirical constant used to determine V_D

K_g = empirical constant used to determine V_g

K_{gg} = empirical constant used to determine V_g

M = Mach number

m = mass of vehicle

N_0 = initial thrust-to-weight ratio, launch thrust divided by launch weight

n = thrust-to-mass ratio, a function of time

p = atmospheric pressure, a function of altitude

p_s = atmospheric pressure at sea level

R = impact range

R_e = radius of earth = 20.9×10^6 ft

r = burnout mass ratio = stage initial weight (mass) divided by stage burnout weight (mass)

T = total period of elliptic orbit

t = time

t_a = time from selected trajectory conditions to apogee

t_b = burning time

t_j = time from reaching burnout altitude to impact on re-entry

$\underset{\sim}{V}$ = vehicle velocity vector

V^* = theoretical velocity as determined by rocket equation
V_a = velocity lost to nozzle pressure
V_b = magnitude of burnout velocity
V_D = velocity lost to drag
V_{impact} = velocity at impact
V_g = velocity lost to gravitation
V_L = total velocity lost = $V_a + V_D + V_g$
$V[t]$ = magnitude of velocity as function of time
W_0 = vehicle initial weight
W_b = vehicle final (burnout) weight
W_j = weight jettisoned between stages of two-stage vehicle
W_p = weight of payload (includes guidance and other weights which do not vary with last stage size)
$W[t]$ = weight of vehicle, function of time
x_b = surface range at burnout
$\underset{\sim}{z}$ = radius vector to vehicle from earth center
z = magnitude of $\underset{\sim}{z}$
β_b = angle between vehicle velocity vector at burnout and local vertical
$\bar{\beta}$ = selected β between those for first-stage and final-stage burnout to be used in determining velocity losses and altitude gains
ϵ = eccentricity of free-flight ellipse
$\underset{\sim}{\kappa}$ = unit vector aligned with thrust
λ = nondimensional parameter = $V_b^2 \sigma / g R_e$
γ = ratio of specific heats of combustion products
ρ = atmospheric density, function of altitude
σ = nondimensional parameter = $R_e + h_b / R_e$
ψ = impact range angle
$\left.\frac{\partial u}{\partial v}\right|_w$ = partial derivative of u with respect to v with w held constant
[ ] = brackets indicating functional notation

REFERENCES

1. Burton D. Fried, "On the Powered Flight Trajectory of an Earth Satellite," Jet Propulsion, 641-643 (1957).
2. Burton D. Fried and John M. Richardson, "Optimum Rocket Trajectories," J. Appl. Phys., **27**, No. 8, 955-961 (1956).
3. Burton D. Fried, "Corrections to Comments on the Powered Flight Trajectory of a Satellite," Jet Propulsion, 342-343 (1958).
4. D. F. Lawden, "Optimal Flight Trajectories," Jet Propulsion, 1263 (1957).

14

TRAJECTORY ANALYSIS

A. B. Mickelwait

14.1 INTRODUCTION

This chapter is intended as an introduction to that important part of system design which selects the mode of flight for a space vehicle. In these early days of space flight, it is apparent that trajectory studies are the focal point for much of the preliminary systems analysis which brings together the trajectory-dependent properties of the propulsion system, guidance system, and the basic mission requirements. Although the problems discussed in this chapter are restricted to simple examples that may be treated analytically, the applications met in practice usually rely heavily on complex computer simulations. Nevertheless, an individual's intuition can be greatly strengthened by a thorough understanding of the analytically simpler approximate models for various space missions.

Two trajectory areas will not be discussed in this chapter, namely, powered flight and atmospheric re-entry. Both of these problem areas have peculiar characteristics and ranges of physical phenomena of their own so that they deserve separate attention. This chapter will study the so-called free-flight portion of a space flight; that is, that portion of flight bounded by main propulsive burning and regions with large atmospheric forces. Of course, as flight modes become more sophisticated, the free-flight or ballistic region will contain multiple coasting periods punctuated by high-level vernier firings so that the distinction between the various regimes will become more diffuse.

14.2 UNIFORM GRAVITATIONAL FIELD

First, let us consider a problem which, although unrealistic, exhibits many important ideas related to trajectory analysis that will be needed in later sections. Let us consider a vehicle launched to intercept an object moving along a flat surface at constant velocity, and assume in addition that the gravitational field through which the vehicle moves is constant (see Fig. 14.1). Initially, at $t = 0$, the target has an X coordinate equal to d_0, and the vehicle is at $X_0 = 0$, $Y_0 = 0$ with an initial velocity v_0 at an angle β_0 with respect to the vertical, as indicated in Fig. 14.1. This model simulates closely the problem of hitting a moving or stationary target on the surface of a rotating earth where the vertical and horizontal distances involved are so small that both the earth's curvature and variation in gravitational field with altitude can be ignored.

The first problem is to determine what initial velocity and launch angle will successfully intercept the moving target as a function of various initial conditions. The necessary relationships are obtained by requiring that the X coordinate of the target X_t equals the X coordinate of the vehicle X_v when the Y coordinate Y_v equals 0, in other words, when the vehicle

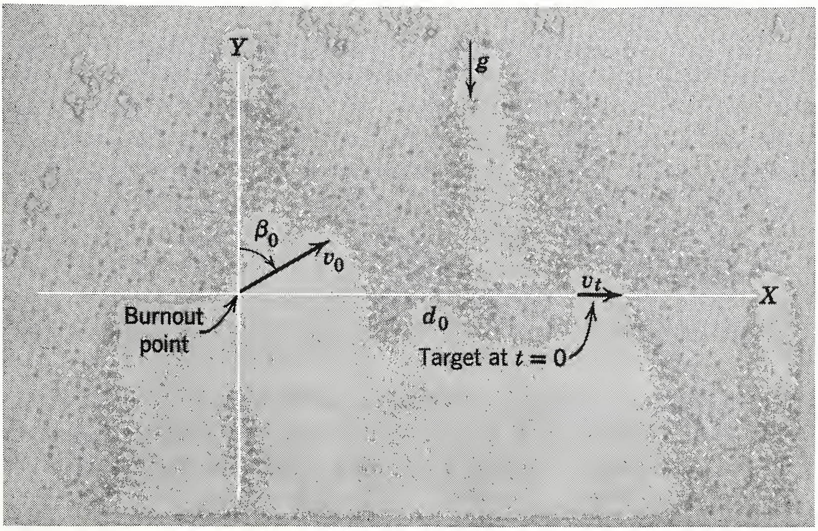

Fig. 14.1 Uniform gravitational field.

has returned to the surface. Then the following equation, often referred to as a "hit" equation, is obtained.

$$v_0 = \frac{v_t}{2 \sin \beta_0} \left[1 + \left(1 + \frac{2gd_0}{v_t^2} \tan \beta_0 \right) \right]^{1/2} \tag{14.1a}$$

For

$$v_t = 0$$

we have

$$v_0 = \sqrt{2gd_0/\sin \beta_0} \quad \text{(the flat, nonrotating case)} \tag{14.1b}$$

Equation 14.1 relates the required velocity at take-off to the flight path angle at launch, the initial position of the target, and its rate of motion along the surface. From eq. 14.1 we can see that for a fixed d_0 and v_t there is a launch angle β_0 that yields a minimum v_0. If the energy available from a given amount of propellant in a boost vehicle is independent of the angle of launch, launching at this β_0 that corresponds to minimum v_0 will allow the largest payload to be delivered to the target. It is also important to notice that at this minimum the magnitude of the velocity required is insensitive to small changes in the launch angle, which implies that small errors in launch angle at this minimum do not affect the accuracy of the trajectory.

The determination of sensitivity of a trajectory to small changes in launch conditions is the second general problem of interest. Since the accuracy of any real guidance system is finite, it is desirable to know how trajectory shaping can vary the response of a vehicle to various errors in initial conditions. If we define the miss M in this problem as equal to $(X_v - X_t)$ when the vehicle returns to the target surface, $Y_v = 0$, then M is given by

$$M = (X_v - X_t) = \frac{2v_0 \cos \beta_0}{g} (v_0 \sin \beta_0 - v_t) - d_0 \tag{14.2}$$

Differentiating eq. 14.2 with respect to initial velocity v_0 and initial flight path angle β_0, respectively, we find the miss coefficients or sensitivity of M to errors in initial conditions as

$$\frac{\partial M}{\partial v_0} = \frac{2}{g_0} (v_0 \sin 2\beta_0 - v_t \cos \beta_0) \tag{14.3}$$

$$\frac{\partial M}{\partial \beta_0} = \frac{2v_0}{g} (v_0 \cos 2\beta_0 + v_t \sin \beta_0) \qquad (14.4)$$

From eq. 14.4 it follows that the angular miss coefficient will vanish when

$$\cos 2\beta_0 \left(1 + \frac{2gd}{v_t^2} \tan \beta_0\right)^{1/2} = -1 \qquad (14.5)$$

Equation 14.5 can only be satisfied if the initial flight path angle is greater than 45°. On the other hand, we notice that as the target velocity v_t goes to 0 (see eq. 14.1b), the familiar stationary target flat-earth case, this maximum payload angle approaches 45°. If we set the target velocity equal to the velocity of an object rotating with the earth's surface, our crude model exhibits most of the properties of a short-range missile launched on a rotating earth. In particular, we see that the rotation of the earth has moved the position of minimum velocity and zero in sensitivity to flight path angle away from 45° toward a flatter, more depressed trajectory.

From eq. 14.3 it follows that the velocity miss coefficient, or sensitivity of miss to initial errors in velocity, can vanish as well. This occurs when

$$\tan \beta_0 = \frac{-v_t^2}{2gd_0} \qquad (14.6)$$

which can only be satisfied if d_0 is less than 0, that is, if the vehicle at launch leads the target by a distance d_0. On the other hand, from eq. 14.5 it follows that when $\partial M/\partial v_0$ equals zero,

$$\frac{\partial M}{\partial \beta_0} = \frac{2v_0^2}{g} \qquad (14.7)$$

and, hence, the flight path angle miss coefficient cannot vanish simultaneously. The trajectory designer in this case would, therefore, be faced with the problem of balancing velocity errors against payload weight and angular errors to arrive at an optimum mode of flight. This is the normal situation found in the design of all but the most pathological trajectories.

The guidance constraints on trajectory shaping could proceed with the properties of the guidance system for this situation being summarized by σ_v, $\sigma_{\beta v}$, $\sigma_{v\beta}$ which are the variances of v and β, respectively, at burnout; or, in other words, a statistical statement of the ability of the guidance system to control the burnout quantities v_0 and β_0. The $1 - \sigma$ miss M would be given by

$$M = \left[\left(\frac{\partial M}{\partial v_0} \right)^2 \sigma_v^2 + \left(\frac{\partial M}{\partial \beta_0} \right)^2 \sigma_\beta^2 + 2 \frac{\partial M}{\partial v_0} \frac{\partial M}{\partial \beta_0} \sigma_{v\beta} \right]^{1/2} \tag{14.8}$$

Notice that, in general, the quantities σ_v, σ_β, and $\sigma_{v\beta}$, as well as the miss coefficients $\partial M/\partial v_0$ and $\partial M/\partial \beta_0$, are also functions of v_0 and β_0. Guidance systems normally have differing abilities to control a vehicle, depending on the powered-flight geometry or equivalently on the velocity and flight path angle at burnout. The important idea here is that the miss coefficients at burnout provide a convenient way to relate terminal conditions to the performance of a given guidance system for optimization through trajectory shaping.

To continue further and make this simple model more realistic, the errors in position control should be noted. So far we have assumed the burnout position to be at the origin $X = 0$, $Y = 0$. In actual fact, of course, the vehicle will launch from some other point and burn out with position errors δX, and δY around the nominal $X = 0$, $Y = 0$. These errors can be calculated in this situation in a fashion similar to the velocity errors by

$$\frac{\partial M}{\partial X_0} = 1 \tag{14.9}$$

$$\frac{\partial M}{\partial Y_0} = \tan \beta_0 - \frac{v_t}{v_0} \sec \beta_0 \tag{14.10}$$

It should be noted that the sensitivity to a burnout error in the vertical direction is increased over and above a simple geometrical displacement. It is true, in general, that trajectories are more sensitive to position errors in the direction of the gravity field than in lateral directions.

Before the error analysis for this mission is complete, the effect of geophysical uncertainties will have to be considered. In this instance, the geophysical uncertainties can be summarized by variations in g in eq. 14.2, and the resulting miss coefficient is

$$\frac{\partial M}{\partial g} = - \frac{d_0}{g} \tag{14.11}$$

which is independent of the particular trajectory shown. As will be seen later, this is not true for the actual gravity field.

In this simple model we have indicated briefly some of the interactions between propulsion and guidance properties as they are affected by the mode of flight. As will be shown subsequently, the ideas brought out here carry over into the more complex missions.

14.3 MOTION IN GENERAL GRAVITATIONAL FIELD

The complete description of the motion of a space vehicle, of course, requires taking into account all the gravitational forces of the earth, sun, moon, planets, etc., acting simultaneously. However, for many practical problems it is sufficient to consider the effect of only one force center at a time. For instance, when describing the motion of long-range ground-to-ground vehicles, or low-level earth satellites, the motion is almost entirely governed by the attracting force of the earth F_E when

$$F_E = -\frac{GM_E}{r^2} \tag{14.12}$$

and GM_E is the product of earth's mass M_E and the universal gravitational constant G,* and r is the radial distance to the center of the earth. The equations of motion and their solutions are given in numerous mechanics texts and are reproduced here only for reference:

$$\frac{d^2r}{dt^2} = -\frac{GM}{r^2} + r\left(\frac{d}{dt}\right)^2 \tag{14.13}$$

$$\frac{d}{dt}\left(r^2\frac{d\theta}{dt}\right) = 0 \tag{14.14}$$

As is well known, eqs. 14.13 and 14.14 have first integrals which are interpreted physically as conservative of energy and angular momentum, namely,

$$E = \frac{1}{2}v^2 - \frac{GM}{r} = \text{constant} \tag{14.15}$$

---

*In English units $GM_E = 1.4077 \cdot 10^{16}\ \mathrm{ft}^3/\mathrm{sec}^2$.

$$J = r^2 \frac{d\theta}{dt} = \text{constant} \tag{14.16}$$

where E is the energy of the vehicle per unit mass and J is the angular momentum of the vehicle per unit mass. Since E and J are constants, they may be written in terms of conditions at any point along the ballistic trajectory and in particular in terms of conditions at burnout; thus

$$E = \frac{1}{2} v_0^2 - \frac{GM}{r_0} \tag{14.17}$$

$$J = r_0 v_0 \sin \beta_0 \tag{14.18}$$

In addition to the two first integrals, the integration of the equations of motion may be carried one step further and the equation of the path obtained as

$$r = \frac{J^2}{GM[1 + e \cos(\theta)]} \tag{14.19}$$

in which θ is measured from perigee (see Fig. 14.2) and e is the eccentricity of the orbit. Since the equations of motion, eqs. 14.13 and 14.14, are of second degree, four arbitrary constants are needed to completely specify the trajectory. In our case, we may choose r_0, v_0, β_0, and θ_0, where θ_0 is the

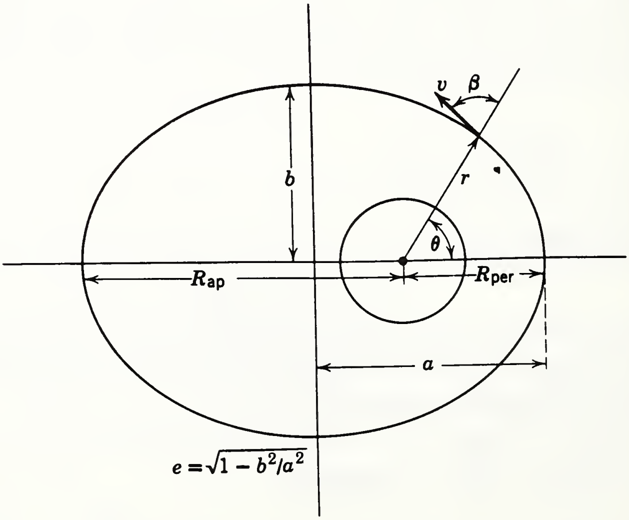

Fig. 14.2 Geometry of satellite orbit.

angular position of the burnout point (see Fig. 14.2). Then any other constants associated with the trajectory can be written as functions of these four as has been done in eqs. 14.17 and 14.18. Although not demonstrated here, eq. 14.19 for $r = r(\theta)$ is the equation of a conic section, ellipse, parabola, or hyperbola. The eccentricity e may be written in terms of E and J as

$$e = \left[1 + \frac{2EJ^2}{(GM)^2}\right]^{1/2} \tag{14.20}$$

The eccentricity may be used to characterize the type of conic section the vehicle is moving on since when

$$\begin{array}{ll} e = 0 & \text{circle} \\ e < 1 & \text{ellipse} \\ e = 1 & \text{parabola} \\ e > 1 & \text{hyperbola} \end{array} \tag{14.21}$$

We have included $e = 0$, the circular orbit, as a distinct case, although it is really a special case of elliptical orbits, because of the large number of space missions that are designed to be circular or near circular. Notice in eq. 14.19 that as $e \to 0$

$$r = \frac{J^2}{GM} = \text{constant} \tag{14.22}$$

A number of relationships of practical significance may be derived with ease for circular orbits and are listed here:

$$R = -\frac{GM}{2E} \tag{14.23}$$

$$T = 2\pi\sqrt{R^3/GM} = 2\pi\frac{GM}{v_0{}^3} \tag{14.24}$$

$$E = -\frac{1}{2}\frac{GM}{r_0} = -\frac{1}{2}v_0{}^2 \tag{14.25}$$

in which R is the circular radius and T the orbital period. It is apparent from eqs. 14.23 and 14.25 that the total energy to mass E must be negative for circular orbits, leading to an alternative method of determining the conic section to which the trajectory belongs:

$$\begin{aligned} E &< 0 \quad \text{ellipse} \\ E &= 0 \quad \text{parabola} \\ E &> 0 \quad \text{hyperbola} \end{aligned} \tag{14.26}$$

If E is equal to or larger than zero, then eqs. 14.26 are physically reasonable since eq. 14.17 for vehicle energy may be satisfied even though r approaches infinity, that is, even though the vehicle escapes to infinity. On the other hand, if E is smaller than zero, the term GM/r in the energy expression can never vanish since v would then be imaginary and, therefore, the vehicle must be on an orbit that stays within a finite distance from the force center.

The range of applications of this simple one-body model is wide. For example, the elliptical equations apply to surface-to-surface vehicles, earth satellites, lunar satellites (when GM_e is replaced by GM_M for the moon), and an interplanetary orbit during the time the vehicle is well away from planetary forces. The parabolic trajectory, which occurs for only a unique initial energy, is that escape trajectory requiring the minimum energy for escape from the earth or any other force center. Setting E equal to zero in eq. 14.17, we have for minimum escape velocity V_{esc} on a parabolic trajectory

$$V_{esc} = \sqrt{2GM_E/r_0} \tag{14.27}$$

A typical value of velocity for escape from the earth, with a burnout altitude of 200 nautical miles is $V_{esc} = 35{,}600$ ft/sec and is, therefore, a minimum requirement for interplanetary trajectories. Hyperbolic orbits, on the other hand, describe either the earth escape phase of an interplanetary flight or the approach phase to the moon or some other planetary body. In all cases, of course, the vehicle is really moving through a multiforce region, and the applications already mentioned represent only approximations to the actual physical situation.

In order to finish the mathematical machinery necessary to describe completely the one-body motion, we note that eq. 14.19 is a description of r as a function of the central angle θ. It is often convenient, however, to have a description of r and θ as functions of time along the orbit. These may be obtained from eqs. 14.13 and 14.14:

$$t = \int_{r_0}^{r_1} \frac{dr}{\left(2E + \frac{2\mu_E}{r} - \frac{J^2}{r^2}\right)^{1/2}} \tag{14.28}$$

$$\theta = \int_{r_0}^{r_1} \frac{J\,dr}{r^2\left(2E + \frac{2\mu_E}{r} - \frac{J^2}{r^2}\right)^{1/2}} \tag{14.29}$$

where $\mu_E = GM_E$.

The integrations in eqs. 14.28 and 14.29 can be carried out in closed form, but the expressions they yield are awkward and are not necessary for the further development here.

14.4 ELEMENTARY TRAJECTORY AND GUIDANCE ANALYSIS FOR GROUND-TO-GROUND VEHICLES

As one application of the ideas presented in Section 14.3 consider the trajectory design problem of long-range flight from point to point on the earth's surface. Note that for most flights the trajectory is elliptical, although an interesting example of hyperbolic trajectories near the earth's surface is provided by interceptor vehicles launched from a satellite orbit toward a stationary or moving target near the earth. For an elliptical trajectory, eq. 14.19 describing $r = r(\theta)$ can be rewritten in terms of initial conditions, which is a convenient form for this particular application. The "hit" equation analogous to that of Section 14.2 then becomes

$$\frac{r_0}{r_1} = \frac{1 - \cos\theta}{\lambda \sin^2 \beta_0} + \frac{\sin(\beta_0 - \theta)}{\sin \beta_0} \tag{14.30}$$

in which $\lambda = r_0 v_0^2/GM_E$, r_0 and r_1 are the initial and final radii, respectively, and θ is the central angle between r_0 and r_1. The dimensionless quantity λ is twice the ratio of kinetic energy to potential energy at burnout and, from the previous statements about correlation of conic section with energy (eq. 14.26), can be used also to determine the type of conic on which the vehicle moves.

In particular,

$\lambda = 1$	circle
$\lambda < 2$	ellipse
$\lambda = 2$	parabola
$\lambda > 2$	hyperbola

It should be noted that the variable λ is the only place where the central force field affects the equation, and it enters as GM_E/r_0, that is, as the potential and not as the force.

Equation 14.30 is approximate in the sense that no consideration is made of (a) earth's rotation, (b) noncentral gravity forces, (c) atmospheric drag, if r_0 and r_1 are within the atmosphere. Nevertheless, this "hit" equation is adequate for most design effort.

In a fashion similar to Section 14.2, eq. 14.30 can be inverted to solve for the velocity as function of β_0, r_0, and range angle θ as follows:

$$v_0^2 = \frac{GM_E}{r_0} \frac{1 - \cos\theta}{[(r_0/r_1)\sin^2\beta_0 + \sin(\theta - \beta_0)\sin\beta_0]} \tag{14.31}$$

A study of eq. 14.31 as a function of β_0 shows that for fixed θ, r_0, and r_1 a minimum exists in v_0. Furthermore, as the range angle θ is decreased, the critical β_0 approaches 45° as for the flat-earth model in Section 14.2.

The important miss coefficients can be determined from the "hit" equation as soon as a criterion of miss is established. Here let the miss M be $R(\delta\theta)$, where R is the earth's radius, $\delta\theta$ equals $\partial\theta/\partial q_i$, δq_i, and δq_i is one of the error sources. Then, for instance, we have the initial-speed error δv_0, altitude error δr_0, and flight path angle error $\delta\beta_0$:

$$\frac{\partial M}{\partial q_i} = R\frac{\partial\theta}{\partial q_i}$$

$$\frac{\partial M}{\partial v_0} = \frac{2R}{v_0}[\sin\theta + \tan\beta_0(1 - \cos\theta)] \tag{14.32}$$

$$\frac{\partial M}{\partial r_0} = 2\tan\beta_0 - \frac{\sin(\beta_0 - \theta)}{\sin\beta_0} \tag{14.33}$$

$$\frac{\partial M}{\partial \beta_0} = 2R\left[1 + \frac{\sin(\theta - 2\beta_0)}{\sin 2\beta_0}\right] \tag{14.34}$$

In these miss coefficients we have chosen to let $r_0 = r_1 = R$; that is, burnout and intercept both occur at the earth's surface. For most applications this approximation is good to about 10 per cent since r_1 and r_0 usually do not differ much either from each other or from the earth's radius R. Let us see under what conditions these may vanish.

The velocity sensitivity vanishes if

$$\tan \beta_0 = \frac{-\sin \theta}{1 - \cos \theta} \tag{14.35}$$

that is, if θ is greater than 180°, which is another way of saying if the vehicle leads the target as with the flat-earth case in Section 14.1.

The flight path angle sensitivity on the other hand vanishes if

$$\tan 2\beta_0 = \frac{-\sin \theta}{1 - \cos \theta} \tag{14.36}$$

that is, if θ is less than 180° and, therefore, the trajectory cannot be shaped to make the velocity and angular sensitivities occur simultaneously. As θ approaches zero, the minimum β_0 approaches 45° in agreement with the flat-earth result in Section 14.1. On the other hand, in the ranges between zero and 180°, the minimum β_0 moves from 45° toward 90° as, for instance, when θ equals 90° or 5400 nautical miles, the zero in $\partial M/\partial \beta_0$ occurs at $\beta_0 = 72.5°$.

The effect of the earth's rotation will be to move the minimum still further toward higher β_0. We have seen in Section 14.2 how the target motion flattens the minimum velocity and minimum angular sensitivity trajectory away from the classical 45° case. This is true, of course, only if the vehicle is launched easterly—that is, chasing the target. In this case, the time of flight is reduced by a flatter trajectory and, therefore, the distance the target moves during the flight is also reduced. Launching westerly will naturally produce the opposite effect; the longer flight time will reduce the required range to the target and, therefore, the effect of earth's rotation will be to elevate the minimum velocity and angular sensitivity trajectory above that already given by eq. 14.36.

In a fashion analogous to Section 14.2, the designer can choose the mode of flight by considering the effectivness of the guidance system in controlling burnout variables and the capability of the vehicle to achieve various velocities. The analysis has been highly simplified here since the effect of nonguidance dispersions on vehicle accuracy will probably also enter into the trajectory shaping. It is apparent that a ballistic vehicle will suffer displacements by winds when reentering the atmosphere. It is also apparent that these displacements will be minimized as the time required for re-entry is reduced. That is, decreasing β_0 or lofting the trajectory will decrease re-entry dispersions. In addition, differentiating the "hit" eq. 14.30, the geophysical miss coefficients can be derived. For instance, the effect of uncertainties in GM/R are given by

$$\frac{\partial M}{\partial (GM/R)} = \frac{1}{GM/R^2}\left[\tan\beta_0 (1 - \cos\theta) + \sin\theta\right] \tag{14.37}$$

The effect of survey error in leveling the launch coordinate system in the plane of the trajectory is given by

$$\frac{\partial M}{\partial E} = 2R\left[(1 - \tan\beta_0) + \frac{\sin(\theta - 2\beta_0)}{\sin^2\beta_0} + \frac{\sin(\beta_0 - \theta)}{2\cos\beta_0}\right] \tag{14.38}$$

where the angle δE expresses the tilt of the launch coordinate system.

When the various geophysical, geodetic, and re-entry error sources are all considered, it is discovered that in each instance the miss coefficients decrease as the trajectory is lofted above minimum velocity trajectory. The designer must then balance the accuracy requirements and response of guidance system versus fuel and payload requirements before arriving at the most desirable mode of flight.

14.5 EARTH SATELLITE ORBITAL ANALYSIS

The orbital problems associated with earth satellite missions are usually different from the problems of ground-to-ground vehicle design. For the missions flown to date, the desire has been to obtain a given orbital shape and orientation with a reasonable probability rather than to intercept a moving point either on the earth's surface or in space. As the mission objectives become more complex and satellite rendezvous is attempted, the satellite mission problems will then become similar to the moving-point intercept problem.

Orbital parameters that can be used to define the orbital shape are semimajor axis and eccentricity. Closely related orbital parameters are apogee, perigee, period, and inclination. Inclination—that is, tilt of the orbit plane with respect to equatorial plane—is not of interest here, but it can be determined in terms of burnout parameters by using simple spherical trigonometric considerations. To determine apogee and perigee in terms of semimajor axis a, and eccentricity e, we note from Fig. 14.2 that the semimajor axis a is given by

$$a = \frac{R_{ap} + R_{per}}{2} \tag{14.39}$$

R_{ap} and R_{per} can be evaluated from eq. 14.19 and substituted into eq. 14.3 to give

$$a = \frac{GM_E}{-2E} \tag{14.40}$$

one of Kepler's laws that is a very useful relationship in satellite work.

Recalling the definition of eccentricity e, namely,

$$e = \left[1 + \frac{2EJ^2}{(GM_E)^2}\right]^{1/2} \tag{14.41}$$

and eliminating J from eq. 14.19, we find

$$R_{ap} = a(1 + e) \tag{14.42}$$

$$R_{per} = a(1 - e) \tag{14.43}$$

which determine apogee and perigee distance in terms of semimajor axis and eccentricity.

The orbital period may be obtained by integrating eq. 14.28 from R_{per} to R_{ap} to give

$$T = 2\pi\sqrt{a^3/GM_E} \tag{14.44}$$

By using eq. 14.40, the period can be rewritten as

$$T = \frac{\pi GM_E}{\sqrt{(-2E)^3}} \tag{14.45}$$

The eqs. 14.40 through 14.45 and the defining equations for J, E, and e in Section 14.2 serve to complete the specification of useful orbital parameters in terms of initial conditions.

Since one of the basic problems in satellite mission design is accuracy of control of apogee, perigee, and period, we now proceed to determine the dispersion in apogee, perigee, and period resulting from errors in burnout quantities. Referring to eqs. 14.42 and 14.43, we find

$$\frac{\partial R_{ap}}{\partial \beta_0} = a\frac{\partial e}{\partial \beta_0} = \frac{a(1-e^2)}{e} \cot \beta_0 = R_{ap}\frac{1-e}{e} \cot \beta_0 \tag{14.46}$$

$$\frac{\partial R_{per}}{\partial \beta_0} = -a\frac{\partial e}{\partial \beta_0} = \frac{-a(1-e^2)}{e} \cot \beta_0 = R_{per}\frac{1+e}{e} \cot \beta_0 \tag{14.47}$$

$$\frac{\partial R_{ap}}{\partial v_0} = \frac{\partial a}{\partial v_0}(1+e) + a\frac{\partial e}{\partial v_0} = \frac{2R_{ap}\sin\beta_0}{e\sqrt{aGM_E(1-e^2)}}(R_{ap}-r_0) \tag{14.48}$$

$$\frac{\partial R_{per}}{\partial v_0} = \frac{\partial a}{\partial v_0}(1-e) - a\frac{\partial e}{\partial v_0} = \frac{2R_{per}\sin\beta_0}{e\sqrt{aGM_E(1-e^2)}}(r_0-R_{per}) \tag{14.49}$$

$$\frac{\partial R_{ap}}{\partial r_0} = \frac{R_{ap}}{er_0^2}\left[(a-r_0) + (a+r_0)e\right] \tag{14.50}$$

$$\frac{\partial R_{per}}{\partial r_0} = \frac{R_{per}}{er_0^2}\left[(r_0-a) + (a+r_0)e\right] \tag{14.51}$$

$$\frac{\partial T}{\partial \beta_0} = 0 \tag{14.52}$$

$$\frac{\partial T}{\partial v_0} = \frac{3aTv_0}{GM_E} \tag{14.53}$$

$$\frac{\partial T}{\partial r_0} = \frac{3aT}{r_0^2} \tag{14.54}$$

From eqs. 14.46 to 14.54, some important design theorems can be deduced immediately. The first-order sensitivity of apogee and perigee distance to errors in initial flight path angle β_0 vanishes if injection into orbit occurs at $\cot \beta_0 = 0$; that is, when $\beta_0 = \pi/2$ at apogee or perigee. On the other hand, the sensitivity of apogee to errors in initial-velocity magnitude is maximum for injection at perigee and vanishes, where it obviously must, if injection occurs at apogee itself. Quite frequently the guarantee of control of perigee is more important than control of apogee. Since the earth's atmosphere decreases exponentially with altitude, the interaction of the atmosphere with a vehicle in an elliptical orbit can be assumed to occur in the neighborhood of perigee alone. As a consequence, the lifetime of a satellite in an elliptical orbit can be strongly influenced by a relatively small change in perigee height. Therefore, it becomes more important to ensure accurate control of perigee height than apogee height when injecting into orbit. The obvious mode of injection will favor injection close to perigee itself to minimize the effect of injection errors. From the propulsion point of view—that is, maximizing the useful payload weight that can be injected into an orbit with a given semimajor axis—it is also desirable to inject at perigee.

Let us assume that the last burning period gives the vehicle an impulsive velocity increment Δv_0; then the change in total energy and, therefore, semimajor axis is given by

$$\Delta E = v_0 \, \Delta v_0 \tag{14.55}$$

From this expression, it is clear that the largest energy increment ΔE from a given velocity increment Δv_0 can be attained when the vehicle has its largest velocity v_0, in other words, at perigee.

It is frequently of interest to place a satellite in an orbit with period that is commensurate with the earth's rotational period so that the satellite will reappear over a given region with a regular frequency. This design constraint makes control of period important. The ability of a given guidance system to control period depends, according to eqs. 14.52 to 14.54, principally on the ability to control burnout velocity v_0.

In this discussion we have ignored errors from variations in r_0 as summarized in eqs. 14.50, 14.51, and 14.54, since the errors in r_0 from launch guidance are usually small compared to velocity vector error. In addition, the error in r_0 is usually strongly correlated with angular errors. Therefore, a meaningful design analysis which takes r_0 errors into account utilizes this correlation.

The foregoing eqs. 14.46 to 14.54 are adequate for elliptical orbits but present difficulties of interpretation for circular or near-circular orbits. Since this class of satellite missions is becoming of more practical importance, we present here the analogous expressions that are appropriate for circular orbits. These expressions are derived by computing the semimajor axis and eccentricity for the near-circular orbit produced by small changes in β_0, v_0, and r_0 from those of a circular orbit.

Let $(R_{ap} - R_{per})/2$ be the measure of deviation from circularity. Then

$$\frac{R_{ap} - R_{per}}{2} = ae \tag{14.56}$$

Now let the small change in v_0 be Δv_0. Then

$$\begin{aligned} a' &= R\left(1 + \frac{2\Delta v_0}{v_0}\right) \\ e' &= \frac{2\Delta v_0}{v_0} \end{aligned} \tag{14.57}$$

where a' and e' are orbital parameters for the near-circular orbit and R is the radius of the circular orbit. Then by substituting into eq. 14.56

$$\frac{R_{ap} - R_{per}}{2} = \frac{4R}{v_0}\Delta v_0 \tag{14.58}$$

Let the small change in β_0 be $\Delta\beta_0$. Then

$$\begin{aligned} a' &= R \\ e' &= \Delta\beta_0 \end{aligned} \tag{14.59}$$

By substituting into eq. 14.56

$$\frac{R_{ap} - R_{per}}{2} = R|\Delta\beta_0| \tag{14.60}$$

Notice that the deviation from circularity for flight path angle errors is independent of the sign of $\Delta\beta_0$ in the limit of circular orbits.

Also of interest for circular orbits is the period error which, from eq. 14.53, is simply

$$\Delta T = \frac{\partial T}{\partial v_0}\Delta v_0 = \frac{3T}{v_0}\Delta v_0 \tag{14.61}$$

Take, for example, a vehicle in a circular orbit whose period coincides with the earth's rotational period (24-hr satellite). Then

$$\frac{\partial T}{\partial v_0} = 23 \text{ sec/(ft)(sec)}$$

Since the earth revolves about $\frac{1}{4}°$/min, the apparent drift of a 24-hr satellite over one day as seen by an earth observer would be 0.1°. Evidently if there is a need for long-term stability in positioning capability, the accuracy of control of velocity must be somewhat better than 1 ft/sec.

The logical next step in satellite orbital analysis is to relax the assumption that the controlling gravitational field is as given by eq. 14.12; that is, a single $1/R^2$ force field. A more realistic look at the earth shows it to have an irregular surface density and, therefore, fluctuations in external gravity. The extremes of these fluctuations appear to run from -0.01 to $+0.02$ ft/sec². Although these are extremely small accelerations by most standards, they can be significant if they have an opportunity to act over an appreciable length of time. One way of handling the irregularities in earth's gravity is to expand the gravitational potential U in a harmonic series as a function of latitude ϕ as follows,

$$U = \frac{GM_E}{R}\left[\frac{R}{r} + J\left(\frac{R}{r}\right)^3\left(\frac{1}{3} - \sin^2\phi\right) + \frac{8}{35}D\left(\frac{R}{r}\right)^5 P_4 + \dots\right] \tag{14.62}$$

where $P_4 = \frac{1}{8}(35 \sin 4\phi - 30 \sin^2\phi + 3)$
R = mean equatorial radius
ϕ = latitude
r = distance from the center of the earth

and J and D are constants determining the strength of the higher harmonics. In particular

$$J = 1.64 \cdot 10^{-3}$$
$$D \simeq 9.10^{-6}$$

This expansion is in latitude only, and longitude-dependent terms have been omitted. Recently, however, careful observations of the motion of several satellites over a period of several years indicates that a longitude-dependent term does, in fact, exist and eventually should be included in the harmonic expansion. Little is known as yet about the amplitude of other harmonic terms that must certainly exist, except that they are probably small.

The mathematical machinery for handling these angular dependent terms in U is quite complex and is usually done in an approximate fashion. For our purposes it is sufficient to look at the effects of the J term, or oblateness. Since J is small, in a good approximation the satellite orbit will still be an ellipse but will have slowly changing orbital parameters. When the equations of motion, eqs. 14.13 and 14.14, are rewritten to include the J term in the force, it is straightforward to show that energy to mass is still a constant and that the component of angular momentum along the earth's polar axis is also a constant. From these two facts it can be shown that the semimajor axis a and eccentricity e of the satellite orbit are unaffected by oblateness—that is, the shape of the orbit as determined by a given set of initial conditions is the same as for a spherical earth.

The major effect of oblateness, then, appears in the orientation of the plane of the orbit and the position of the major axis. So far we have avoided discussion of three-dimensional characteristics of satellite orbits. However, the description of an orbit is completed with a statement of the inclination of the orbital plane with respect to some fixed plane, the position where the orbital plane intersects this fixed plane (line of nodes), and the orientation of the semimajor axis a in the orbital plane itself. The usual choice for the reference plane is the earth's equatorial plane.

The oblateness term causes the plane of the orbit to precess slowly around the polar axis and the orbital ellipse to rotate slowly in its own plane. If we let λ be the angle the orbit plane precesses around the polar axis in one revolution of the satellite, then

$$\lambda = \frac{2\pi JR^2 \cos i}{a^2(1 - e^2)^2} \tag{14.63}$$

where i is the inclination of the orbit plane with respect to the equator. If we let ψ be the angular amount the major axis rotates in the orbital plane in one revolution of the satellite, then

$$\psi = \frac{2\pi JR^2}{a^2(1 - e^2)^2}\left(2 - \frac{5}{2}\sin^2 i\right) \tag{14.64}$$

Certain facts are obvious from examination of eqs. 14.63 and 14.64. First, these effects are small. For a low-level satellite, orbiting below 200 miles, the amount of precssion per day is about 0.15°, and the rotation of perigee (or apogee) in its own plane is about 0.3° per day. For low-level satellites these effects can easily be masked by atmospheric perturbations—that is, unpredictable density effects can cause orbital changes of this magnitude. However, these effects have considerable practical importance for high-altitude satellites that are unaffected by drag while their orbit planes remain stationary in inertial space. In these cases considerable care must be taken to shape the orbit to counteract the oblateness perturbations. In a more general sense, the oblateness term is significant because careful observations of satellite orbits can lead to a refined value for J which, in turn, is directly related to the flattening of the earth and is of great geodetic interest.

Including the higher harmonics in the earth's field does not complete the description of the gravitational field traversed by the satellite. A complete description includes the gravity fields of the sun, the moon, and all the planets. The planets' fields can be ignored for all applications because of their small mass and distance. However, for certain satellite orbits the effects of the sun and moon are of great significance. For example, the perigee height of Explorer VI, which had an initial apogee height of 24,000 miles, was lowered from 150 miles by the lunar-solar perturbations to a point where atmospheric drag significantly reduced the satellite's lifetime. Without the lunar-solar perturbations its lifetime would have been twenty years instead of, in fact, about two years. To be more precise, if the effect of the moon or sun on perigee is averaged over one month, the rate of change of perigee per orbital revolution is given by

$$\Delta R_{\text{per}} = \frac{-15}{4}\left(\frac{GM_D}{GM_e}\right)\frac{a^4}{R_D}\,\pi e\,(\sqrt{1-e^2})\,\sin 2\omega\,\sin^2 i \tag{14.65}$$

where GM_D applies to the sun or the moon, R_D is the apparent orbital radius of the sun or moon with respect to the earth, and ω is the angular position of perigee measured in the satellite orbit plane from the line of intersection with the equatorial plane.

The only major perturbation not considered so far is the effect of atmospheric drag on the satellite orbit. For elliptical orbits, the effect of drag can be qualitatively described as concentration of the drag force in the neighborhood of perigee with each satellite revolution removing some energy from the orbit. Since the vehicle is passing through perigee when energy is removed, the only change in the orbit will be to reduce apogee height. By the time the orbit has reached circularity, it is in its final stages of decay and the vehicle will spiral in rapidly. The major problem remaining is not how to compute drag effects but how to gain an accurate knowledge of the atmosphere itself. Enough has been learned recently from sounding rockets and satellites to establish that large atmospheric changes occur diurnally with latitude and sporadically with solar flares. Evidently the atmosphere above 100 miles is a time-dependent phenomenon requiring a more sophisticated model than has been established to date.

15

CONTROL SYSTEM THEORY AND COMPONENTS

J. R. Burnett

15.1 INTRODUCTION

First, this chapter discusses control systems, but does not present rigorous proofs. It is designed to be a general survey with emphasis on the results and cornerstones of control theory. There are many excellent textbooks in which proofs and more details may be found.

Second, the following material is concerned only with systems that can be characterized by sets of linear differential equations with constant coefficients. There are more significant problems today that lie outside of this restriction, but there is also much less known about the theory. The theory of nonlinear systems is in part based on linear theory, so it is entirely appropriate to consider linear theory first.

Third, most control theory results have been obtained within the framework of electrical engineering technology. Consequently, the nomenclature is heavily rooted in this area.

15.2 CONTROL SYSTEM THEORY

Control system theory is a mathematical tool for the analysis and synthesis of control systems. It allows concise statements of the dynamic behavior of entire systems or portions of entire systems to be made. It leads to clear understanding of the dynamic operation of systems and consequently to reasoned approaches to control problems.

Linear systems will be considered here, as nonlinear control theory is imperfectly understood today. Dynamic behavior implies behavior as a function of time or the time solution of differential equations. The dynamic behavior of linear systems can be characterized by sets of linear differential equations. In general, it is difficult to look at a set of differential equations and readily gain insight about the operation of the system. Control system theory is based on an integral transformation, known as Laplace transform, of sets of differential equations. The rate of learning can be more rapid since differential equations involve solving polynomials, whereas transform techniques can, in part, circumvent the polynomial problem.

Control system theory is related to differential equations and their formulation and solution, electric network theory, complex variable theory—mapping, poles and zeros—and vibration theory.

15.2.1 Review of Differential Equation Description of Systems

Electric circuit elements obey the following relationship:

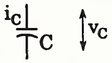

$$v_C = \frac{1}{C} \int i_C \, dt \quad \text{or} \quad i_C = C\frac{dv_C}{dt} \tag{15.1}$$

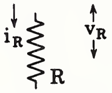

$$v_R = Ri_R \quad \text{or} \quad i_R = \frac{1}{R} v_R \tag{15.2}$$

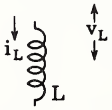

$$v_L = L\frac{di_L}{dt} \quad \text{or} \quad i_L = \frac{1}{L} \int v_L \, dt \tag{15.3}$$

whereas, in a similar fashion,

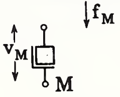

$$v_M = \frac{1}{M} \int f_M \, dt \quad \text{or} \quad f_M = M\frac{dv_M}{dt} \tag{15.4}$$

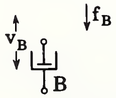

$$v_B = \frac{1}{B} f_B \quad \text{or} \quad f_V = Bv_B \tag{15.5}$$

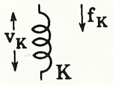

$$v_K = \frac{1}{K}\frac{df_K}{dt} \quad \text{or} \quad f_K = K \int v_K \, dt \tag{15.6}$$

15.2.2 Steady-State Sinusoidal Solution of Differential Equations

Given a specific input to any system that can be described by a set of linear differential equations, the output can always be computed at least in principle. For various reasons which will be made clear later, let us investigate steady-state sinusoidal solutions of linear differential equations.

From Fig. 15.1, below,

$$v_o(t) = i(t)R + \frac{1}{C}\int i(t)\,dt \tag{15.7}$$

$$v_o(t) = \frac{1}{C}\int i(t)\,dt \tag{15.8}$$

Let $$v_i(t) = V\cos\omega t = \frac{V}{2}\left(e^{j\omega t} + e^{-j\omega t}\right) \tag{15.9}$$

Since the differential equation is linear, superposition holds. Consequently, solving it for $(V/2)e^{j\omega t}$ as a forcing function by symmetry yields the $(V/2)e^{-j\omega t}$ solution and then the solution of the problem.

Assume a solution of the form

$$i(t) = I_+ e^{j\omega t} + I_- e^{-j\omega t} \tag{15.10}$$

where I_+ and I_- are complex quantities. Then

$$\frac{V}{2}e^{j\omega t} = I_+ e^{j\omega t} R + \frac{I_+}{C}\int e^{j\omega t}\,dt$$

$$\frac{V}{2}e^{j\omega t} = I_+ e^{j\omega t}\left(R + \frac{1}{j\omega C}\right) \tag{15.11}$$

$$I_+ = \frac{V}{2(R + 1/j\omega C)} = \frac{V}{2Ze^{-j\theta_Z}} \qquad Z = \sqrt{R^2 + 1/\omega^2 C^2} \tag{15.12}$$

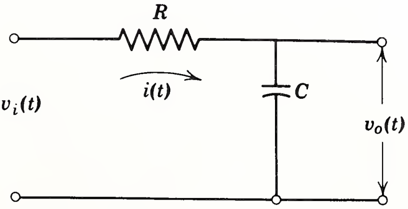

Fig. 15.1

$$I_- = \frac{V}{2(R - 1/j\omega C)} = \frac{V}{2Ze^{+j\theta_Z}} \qquad \vec{Z} = Ze^{-j\theta_Z} \tag{15.13}$$

Hence

$$i(t) = \frac{V}{2Z}\left(e^{j\omega t}e^{j\theta_Z} + e^{-j\omega t}e^{-j\theta_Z}\right)$$

$$= \frac{V}{Z}\cos(\omega t + \theta_Z) \tag{15.14}$$

This gives in shorthand notation,

$$I(j\omega) = \frac{V_i(j\omega)}{Z(j\omega)} \tag{15.15}$$

and

$$\frac{V_o}{V_i}(j\omega) = \frac{1}{1 + j\omega RC} \tag{15.16}$$

The expression $(V_o/V_i)(j\omega)$ may be better understood from Figs. 15.2 and 15.3 and eqs. 15.17 and 15.18:

$$v_i(t) = V_i \cos \omega t \tag{15.17}$$

$$v_o(t) = V_o \cos(\omega t + \theta) \tag{15.18}$$

As ω is varied, $(V_o/V_i)(j\omega)$ is the expression which enables V_o/V_i and θ to be calculated. In other words, it relates the transfer of the input signal to the output of the network.

The table indicates values of θ and V_o/V_i as ω is varied. Two forms of plotting this information are presented. Both

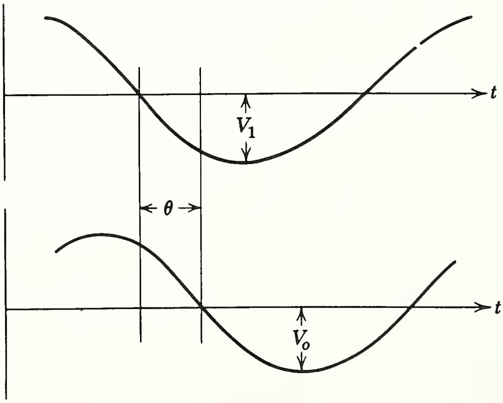

Fig. 15.2

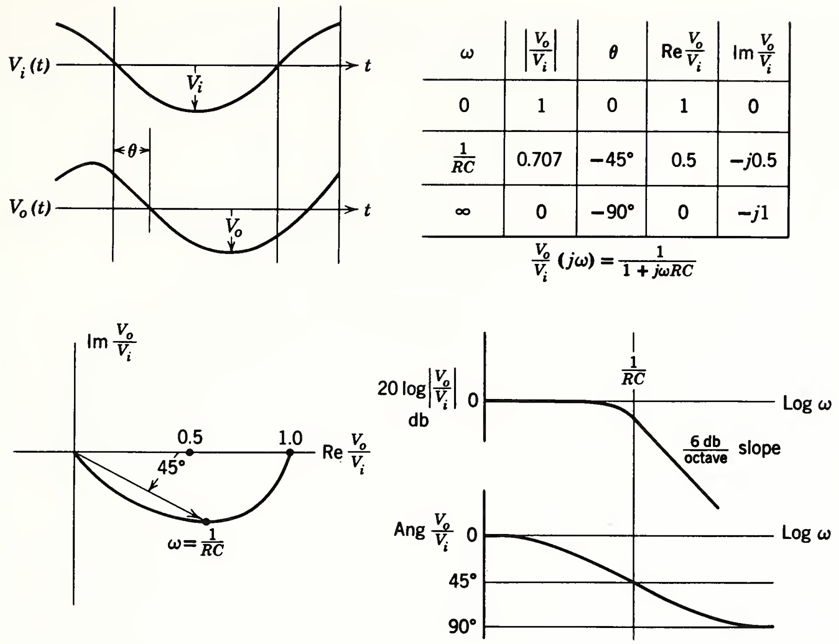

ω	$\left\|\frac{V_o}{V_i}\right\|$	θ	Re $\frac{V_o}{V_i}$	Im $\frac{V_o}{V_i}$
0	1	0	1	0
$\frac{1}{RC}$	0.707	−45°	0.5	−j0.5
∞	0	−90°	0	−j1

$$\frac{V_o}{V_i}(j\omega)=\frac{1}{1+j\omega RC}$$

Fig. 15.3

types of plots are used extensively in control work, and both present exactly the same information.

This analysis gives the following results:

1. Steady-state sinusoidal solutions involve only algebraic manipulation of differential equations. These solutions are far simpler than for other types of inputs.
2. Steady-state sinusoidal response is readily instrumented for experimental measurement.
3. In general, these solutions are obtained by the substitutes

$$\frac{di}{dt}\sim Ij\omega \qquad \int i\,dt\sim\frac{I}{j\omega}$$

15.3 TRANSFER FUNCTIONS

The expressions for steady-state sinusoidal solutions of differential equations are readily written in the form output/input = F(jω). The F(jω) characterizes the system

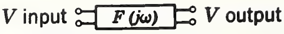

Fig. 15.4

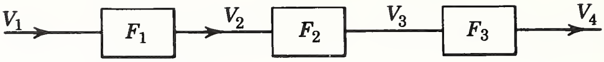

Fig. 15.5

such that, for any amplitude and frequency of input signal, the output can be readily determined, as drawn schematically in Fig. 15.4. F(jω) is known as the transfer function of the system and is defined as the frequency relationship between the input and output of interest in a system.

There are two general methods of obtaining transfer functions. The first is by computation starting from the differential equations of the system and solving them for the desired ratio, as previously illustrated.

The second method is by experimental measurement. One form of measurement involves a sinusoidal generator at the input and suitable instrumentation at the output.

Transfer functions can be rather useful in obtaining the performance of large systems. This usefulness can be best illustrated by considering the conditions shown in Fig. 15.5. If it is assumed that it is easy to obtain F_1, F_2, and F_3, what would be the relationship between V_4/V_1? If the addition of F_2 to F_1 does not change V_2, that is, the system F_2 does not load the system F_1, and if F_3 does not change V_3, then

$$\frac{V_4}{V_1} = F_1F_2F_3 \tag{15.19}$$

Summing devices are given by

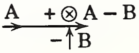

which from Fig. 15.6 gives

$$E = V_1 - V_2 \tag{15.20}$$

$$V_2 = FE \tag{15.21}$$

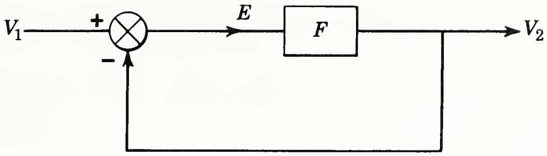

Fig. 15.6

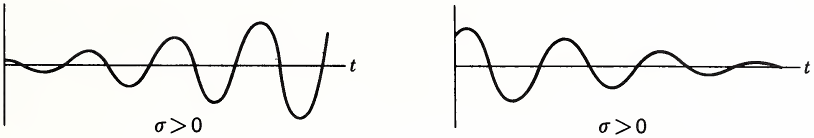

Fig. 15.7

15.4 COMPLEX FREQUENCY DOMAIN

It is entirely reasonable to try a solution of the form e^{+st} where $s = \sigma + j\omega$ in the differential equations of interest:

$$E_i e^{+st} = IRe^{+st} + \frac{I}{C} \int e^{+st}\, dt$$

$$= IRe^{+st} + \frac{Ie^{st}}{sC} \tag{15.22}$$

$$E_i = I\left(R + \frac{1}{sC}\right) = I \frac{1 + RsC}{sC} \tag{15.23}$$

$$I = E_i \frac{sC}{1 + RsC} \tag{15.24}$$

$$\mathrm{Re}\, e^{(\sigma + j\omega)t} = e^{\sigma t} = \cos \omega t \tag{15.25}$$

The behavior of eq. 16.25 is graphically interpreted in Fig. 15.7.

So far all the results have been various aspects of the Laplace transform which is expressed as

$$F(s) = \int_0^{\infty} e^{-st} f(t)\, dt \tag{15.26}$$

Aside from certain mathematical refinements, if we perform the Laplace transform of differential equations, it is equivalent to the following replacement of terms:

$$\frac{di}{dt} \sim sI(s), \quad i \sim I(s), \quad \int i\, dt \sim \frac{I(s)}{s}$$

The Laplace transform then has the very powerful property of causing a differential equation to become an algebraic equation, a tremendous simplification. Further, if s equals $j\omega$, the steady-state sinusoidal solution results. This solution also results without solving the characteristic polynomial of the system.

Since F(s) is an algebraic function, it must be the ratio of two polynomials in s:

$$F(s) = \frac{a_0 + a_1 s + a_2 s^2 \ldots a_n s^n}{b_0 + b_1 s + b_2 s^2 \ldots b_k s^k}$$

$$= K\frac{(s+z_0)(s+z_1) \ldots (s+z_n)}{(s+p_0)(s+p_1) \ldots (s+p_k)}$$

The values $-z_n$ are known as the zeros of F(s), and the values $-p_k$ are known as the poles of F(s). It then follows that the poles, zeros, and a multiplicative constant completely characterize a linear system. Furthermore, all that has been said about transfer functions $F(j\omega)$ hold for F(s). Poles and zeros can be plotted as shown in Fig. 15.8.

A number of Laplace transforms and theorems are shown in Table 15.1.

15.5 FEEDBACK CONCEPT

15.5.1 Transfer Function Diagram

Elementary feedback systems can be characterized by the diagram shown in Fig. 15.9. The signals in the feedback sys-

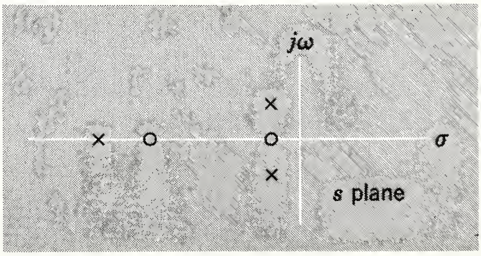

× = pole
o = zero

Fig. 15.8

tem have been characterized by Laplace transforms; R(s) and T(s) are the inputs, R(s) is the desired input, T(s) is the undesired input, E(s) is the error signal, C(s) is the output signal. The inverse transforms of these signals would be given by the corresponding lower-case letter. For example:

$$\mathcal{L}^{-1}[R(s)] = r(t) \tag{15.27}$$

The quantities $F_1(s)$, $F_2(s)$, and H(s) are transfer functions which characterize those parts of the system. The summers and the transfer functions are assumed to obey the no-loading restriction. That is, the summer after R(s) does not change R(s).

The block diagram (Fig. 15.9) is actually a picture of the following set of equations:

$$E(s) = R(s) - C(s)H(s) \tag{15.28}$$

$$C(s) = E(s)F_1(s)F_2(s) + T(s)F_2(s) \tag{15.29}$$

TABLE 15.1

Laplace Transforms and Theorems

f(t)	F(s)	Time Plot	Pole-Zero Location
$\frac{df(t)}{dt}$	$sF(s)$		
$\int f(t)\,dt$	$\frac{F(s)}{s}$		
e^{-at}	$\frac{1}{s+a}$	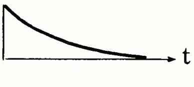	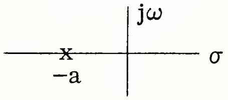
cos bt	$\frac{s}{s^2+b^2}$	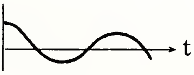	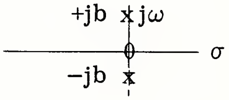
e^{-at} cos bt	$\frac{s+a}{(s+a)^2+b^2}$	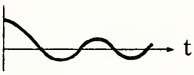	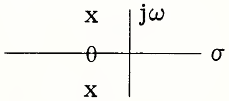

This set may be solved for the output, as illustrated in Fig. 15.10.

15.5.2 Main Advantages of Feedback

There are three main advantages of feedback which will be illustrated, but it must be considered that $F_2(s)$ is commonly known as the ''fixed'' part of the system as it may involve a power element to move the load, and that any system is subject to more inputs than desired. It must also be realized that any feedback system can in principle be replaced by the diagram illustrated in Fig. 15.11. The question of the advantages of feedback involve a comparison of the performance of the systems.

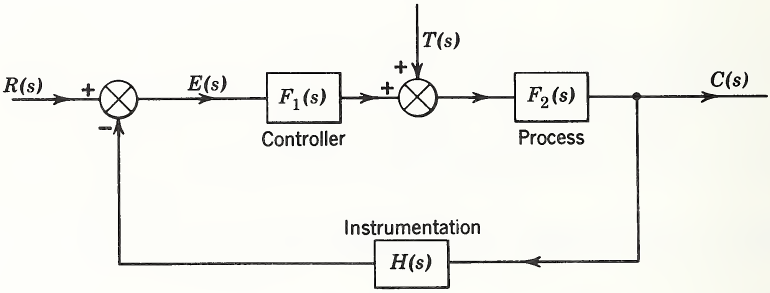

Fig. 15.9

$$C(s) = \underbrace{\frac{RF_1F_2}{\underbrace{1 + HF_1F_2}_{\text{Loop gain}}}}_{\text{Signal part of output}} + \underbrace{\frac{TF_2}{1 + HF_1F_2}}_{\text{Noise part of output}}$$

Fig. 15.10

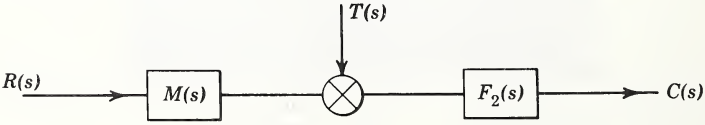

Fig. 15.11

1. Feedback reduces the sensitivity of the over-all transfer function to changes in parts of the system. Let us assume that $F_2(s)$ is a power element and is subject to considerable change in its transfer function as temperature, loads, time, etc., change. Let us also assume that $T(s)$ is zero for this discussion, giving the following results.

With Feedback

$$\frac{dC}{C} = \frac{1}{1 + HF_1 F_2} \frac{dF_2}{F_2} \tag{15.30}$$

Without Feedback

$$\frac{dC}{C} = \frac{dF_2}{F_2} \tag{15.31}$$

Obviously, a large loop gain $(HF_1 F_2)$ with respect to unity can materially reduce the variations in dC/C as $dF_{2/F}$ change.

2. Feedback changes the effects of noise or disturbances. If we consider $T(s)$ to be a disturbance in the system, at the output, the signal-to-noise ratio is then:

With Feedback

$$\frac{s}{N} = \frac{R(s)}{T(s)} F_1(s) \tag{15.32}$$

Without Feedback

$$\frac{s}{N} = \frac{R(s)}{T(s)} M(s) \tag{15.33}$$

In designing the loop, if F_1 is a large number the s/N ratio is increased. Further, a large F_1 is still compatible with reasonable values of C/R. Without feedback, a large M is probably quite undesirable.

3. Feedback changes the effects of inputs on outputs. The implication here is that the poles and zeros which relate inputs to outputs can be moved about by feedback. This is obvious from an examination of C/R, which is the most valuable effect. In many control systems the C/T transfer function is completely unstable. The inclusion of a feedback loop can stabilize the system.

As an illustrative example of feedback as defined in paragraph 1, assume that

$$F_1 = 100, \quad H = 1, \quad F_2 = 2, \quad \Delta F_2 = -0.1$$

$$\frac{\Delta C}{C} = \frac{5\%}{191}$$

A 5% decrease in F_2 gives an over-all decrease of 191 times less.

In the case described in paragraph 3, assume the following:

$$F_2 = \frac{1}{s+1}, \quad F_1 = 10, \quad H = 1, \quad R(s) = 0$$

$$\frac{C}{T} = \frac{1}{s+1} \quad \text{(no feedback)}$$

$$\frac{C}{T} = \frac{1/(s+1)}{1 + 10/(s+1)} = \frac{1}{s+11}$$

As shown in Fig. 15.12 the feedback changed the pole at −1 to −11.

15.5.3 Cost of High Loop Gain

The price paid for the benefits which arise from high loop gain is often engineering that controls the feedback and makes the system stable:

$$\frac{C}{R} = \frac{F_1 F_2}{1 + HF_1 F_2} \tag{15.34}$$

$HF_1 F_2$ is a frequency dependent function. Assume that $HF_1 F_2$ equals −1 at a frequency ω_1. Then

$$\frac{C}{R} = \frac{F_1 F_2}{0} \tag{15.35}$$

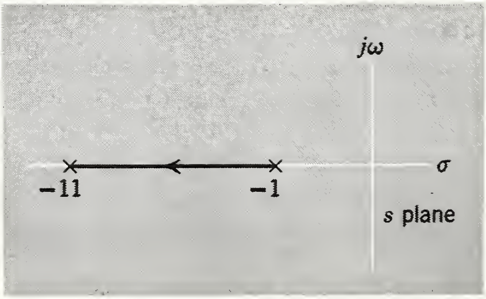

Fig. 15.12

This implies a finite output with zero input. Such a condition means that the frequency ω_1 is being sustained by the system which is oscillating or unstable.

15.6 STABILITY

15.6.1 Stability Measurement

Stability of a system may be measured or computed by considering a unit impulse input to the system. A unit impulse has a transform of one. In mechanics terms it is similar to a hammer blow. Stability is defined in terms of the time response of the system as represented in Fig. 15.13.

15.6.2 Stability Tests

Stability depends on the location of the poles of the transfer function C/R(s). If any poles are on the $j\omega$ axis or in the right-half s plane (Fig. 15.14b), the system is unstable. One pole at the origin is considered stable. Analytically, in a feedback system C/R can be expressed as a transfer function, factored, and stability determined. In practice, this is most tedious, involving finding the roots of high-order polynomials.

Nyquist diagrams, Bode diagrams, and root loci plots are extensively used to study stability of systems. Nyquist diagrams are a polar plot of the open-loop transfer function with ω as a parameter (Fig. 15.15). Lack of encirclements of $-1 + j0$ indicates stability.

Let $F_1 F_2 = \dfrac{1}{s(s+1)} \qquad H = 1$

This may also be tested analytically (eq. 15.36 and Fig. 15.16):

$$\frac{C}{R} = \frac{K/s(s+1)}{1 + K/s(s+1)} = \frac{K}{s^2 + s + K} \tag{15.36}$$

Bode plots are a form of Nyquist diagrams (Fig. 15.17). Stability is indicated by the same criteria as that of a Nyquist plot; $-1 + j0$ is equivalent to 0 db and 180°.

Stability is obtained in systems by changing loop gains or by inserting networks which change the frequency characteristics of the loop gain.

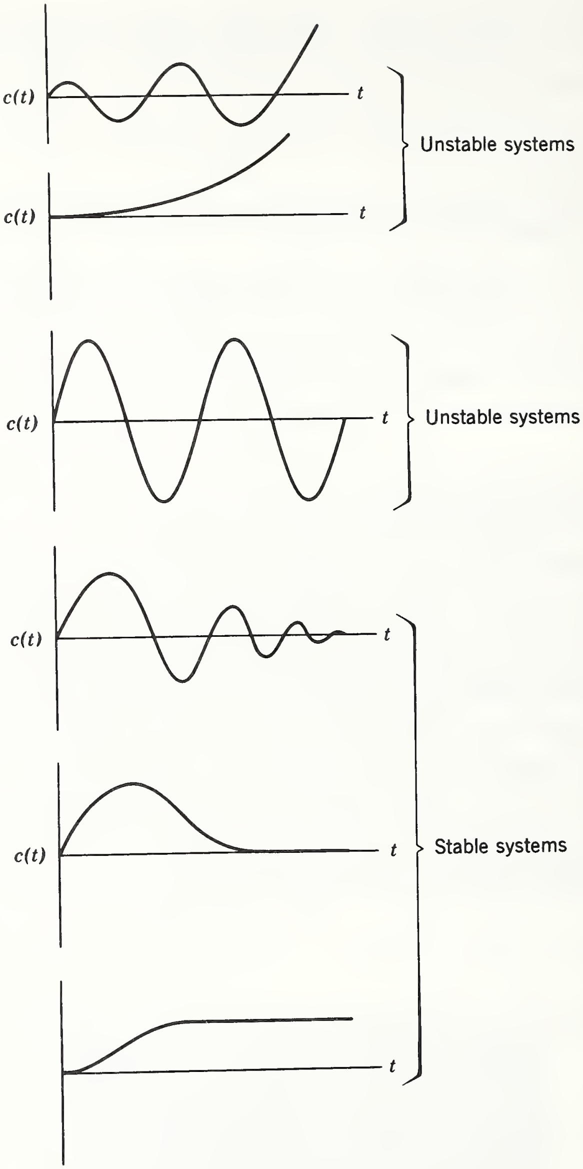

Fig. 15.13

Suppose that $$F_1 F_2 = \frac{K}{(s-1)(s+2)} \tag{15.37}$$

$$\frac{C}{R} = \frac{K}{s^2 + s - 2 + K} \tag{15.38}$$

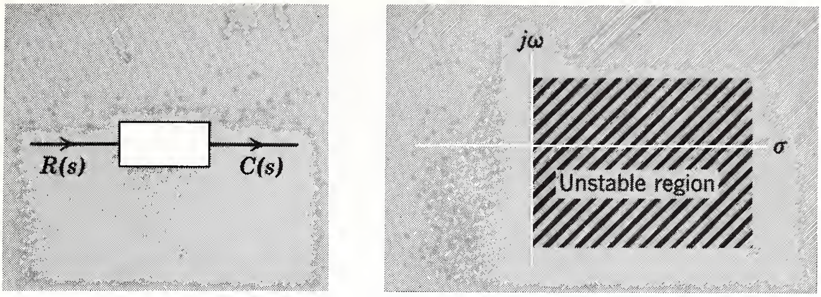
R(s)
C(s)
jω
σ
Unstable region

(a)

(b)

Fig. 15.14

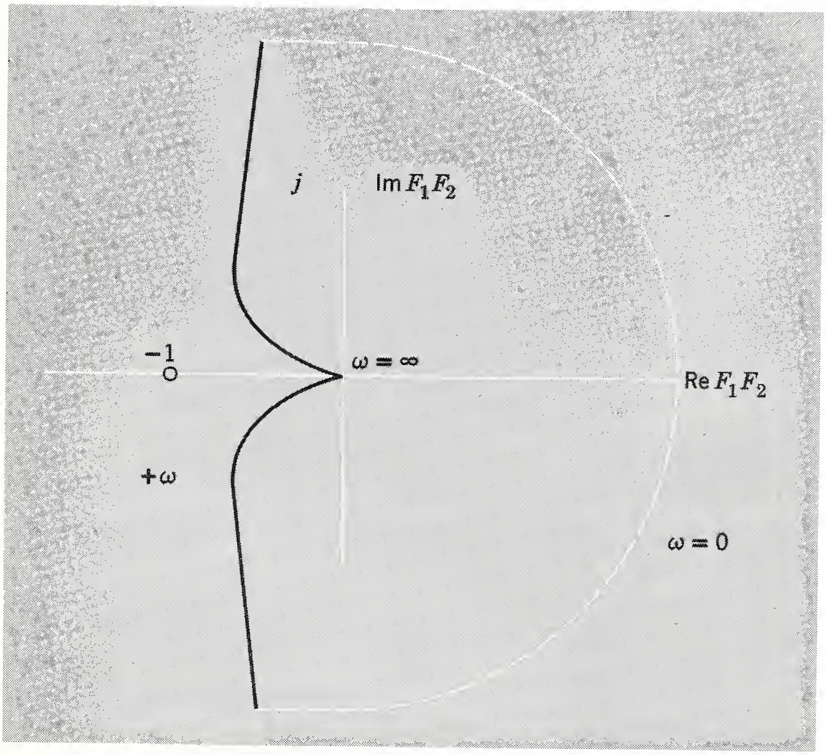

Fig. 15.15 Since the plot does not enclose −1 + j0, the system is stable.

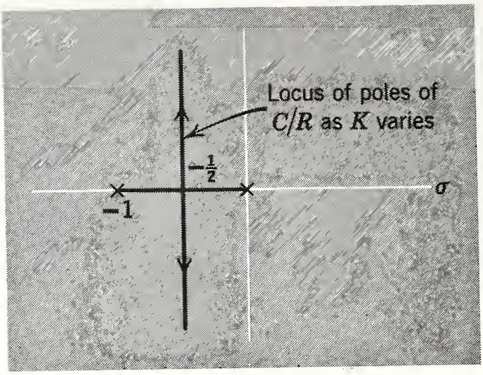
Locus of poles of
C/R as K varies
$-\frac{1}{2}$
-1
σ

Fig. 15.16

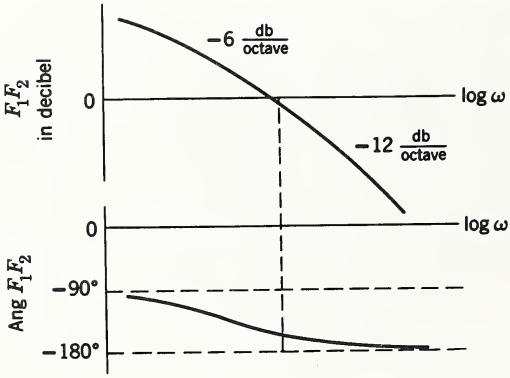

Fig. 15.17

If K is greater than two, the system is stable (Fig. 15.18). Again let

$$F_1 F_2 = \frac{K}{s^2} \tag{15.39}$$

$$\frac{C}{R} = \frac{K}{s^2 + K} \tag{15.40}$$

This is the locus of a variable frequency oscillator. Compensate by

$$\frac{K}{s^2} = \frac{s+1}{s+10} \tag{15.41}$$

Over a certain region of K the system is stable (Fig. 15.19).

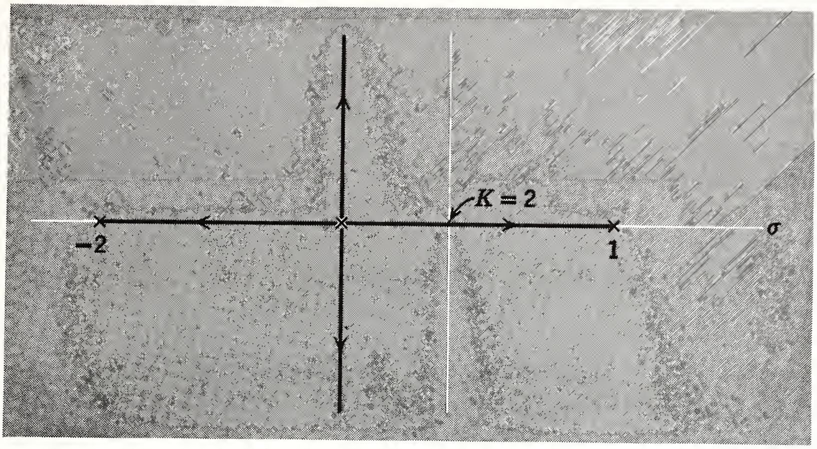

Fig. 15.18

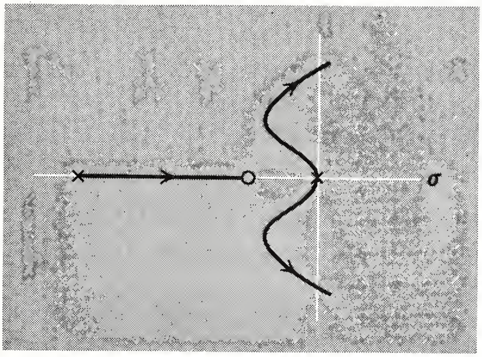

Fig. 15.19

A very important stability consideration, originated by H. W. Bode, may be outlined as follows. There is a relationship between gain and phase shift of a transfer function. A simple consequence of this relationship is that for a constant-slope gain frequency curve (gain in decibels versus log ω) the phase shift is equal to

$$\phi = k15^\circ$$

where k is equal to slope of line in decibels per octave.

Furthermore, stability tests indicate that 180° phase lag and 0 db gain is a critical point that should be avoided with some margin. An adequate margin is 30°, giving a phase lag of 150°. This corresponds to a decrease of 10 db per octave and is illustrated in Fig. 15.20.

A large amount of gain may be needed from zero to, say, 1 radian/sec. There is usually no excuse for using feedback unless considerable loop gain is used. Assume that this is 40 db. Then 4 octaves of frequency are required to cut the system off in a stable fashion. As indicated in Fig. 15.20, the frequency characteristic must be controlled to sixteen times the useful band of the over-all system.

Another way of stating the price for a stable feedback system is to say that the gain-frequency characteristics must be controlled to a frequency which is K times the useful bandwidth of the system. This number K is larger than unity and increases as the loop gain increases.

15.7 BALLISTIC MISSILE CONTROL SYSTEMS

A block diagram of a ballistic missile control system showing the components and parameters affecting the system, is presented in Fig. 15.21. The control system is necessary because

1. Parameter variation of the aerodynamics would make a profound difference in the transfer function so that guidance would not be as effective.
2. The transfer function from winds to θ_0 behaves as $1/(s + a)(s - b)$ at low frequencies, and the feedback is required to stabilize the system.

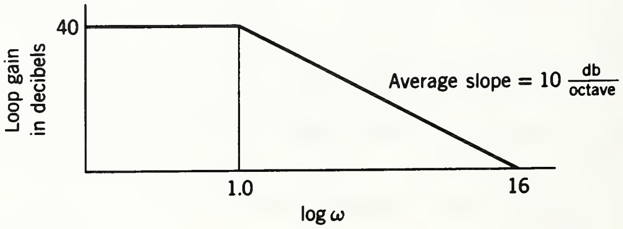

Fig. 15.20

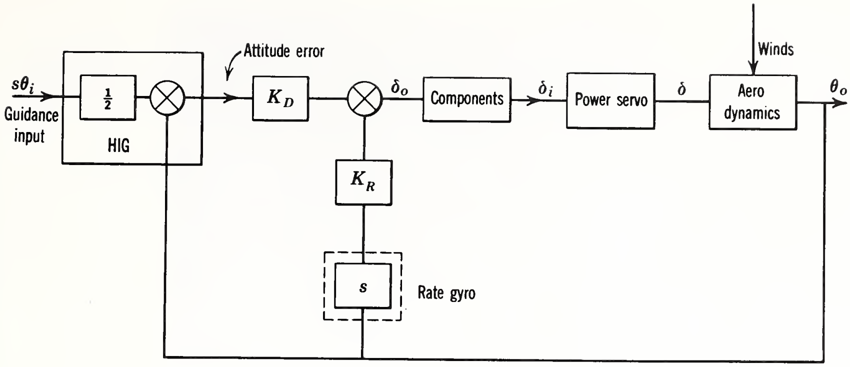
$s\theta_i$
Guidance input
$\frac{1}{2}$
HIG
Attitude error
K_D
δ_o
Components
δ_i
Power servo
δ
Winds
Aero dynamics
θ_o
K_R
s
Rate gyro

Fig. 15.21

15.7.1 Description of System

The rigid-body aerodynamics are of the form

$$\frac{\theta}{\delta} = \frac{K}{(s + a)(s - b)} \tag{15.42}$$

The effect of the position of the components and the rate gyros (Fig. 15.21) is to make

$$\frac{\delta_o}{\theta_o} = K_D + K_R s \tag{15.43}$$

This equation is given graphically in Fig. 15.22.

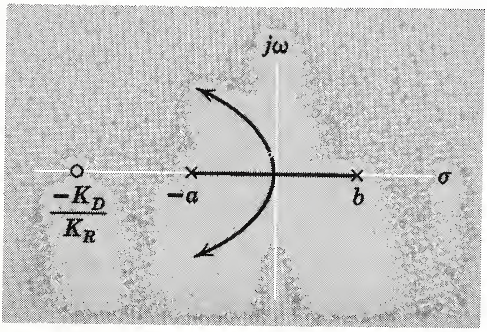
$j\omega$
σ
$\frac{-K_D}{K_R}$
$-a$
b

Fig. 15.22

15.7.2 Bending

Assume that Fig. 15.23 represents the shape of a missile when its first bending mode is excited. The time representation of the shape after an impulse input is then

$$e^{-\zeta\omega_1 t}\cos\omega_1 t\sin x$$

Clearly, a gyro located at x_1 has an output

$$e^{-\zeta_1\omega_1 t}\cos\omega_1 t\sin x$$

Then

$$\frac{\theta_o}{\delta}(s) = \frac{K_1\cos x\,(s+\zeta_1\omega_1)}{s^2+2\zeta_1\omega_1 s+\omega_1^2} \tag{15.44}$$

for this effect alone.

In general, a missile has many modes which are not sinusoidal in x whereby

$$\frac{\theta_o}{\delta}(s) = \frac{K}{(s+a)(s-b)} + \sum_{k+1}^{n}\frac{K_k(s+\zeta_k\omega_k)f^1(x)}{s^2+2\zeta_k\omega_k s+\omega_k^2} \tag{15.45}$$

when n is commonly in the range 3 to 5. The damping factors ζ_k are usually small.

The effect of bending can be shown (Fig. 15.24) by adding the X term to the pole-zero plot. There are several zeros which belong in Fig. 15.24 and can be located anywhere, depending on the numbers.

15.7.3 Sloshing

The fluid in the various tanks can be represented by a series of mass-spring-damper combinations (Fig. 15.25). The effect of sloshing is shown on the pole-zero plot in Fig. 15.26. In general, the damping factors are quite small and the frequencies are usually smaller than the bending frequencies.

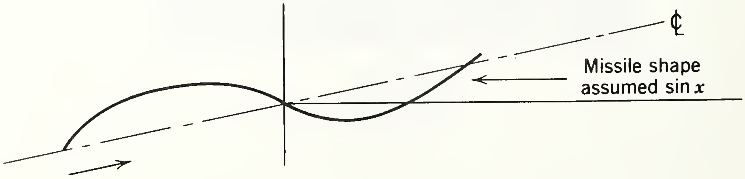

Fig. 15.23

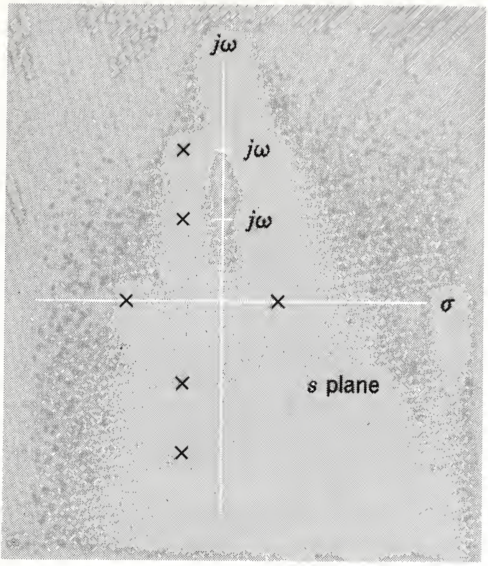

Fig. 15.24

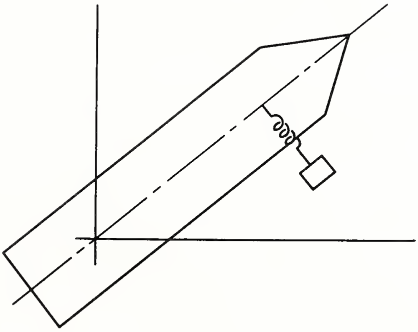

Fig. 15.25

15.7.4 Power Servos

Power servos take an electrical engine angle command δ_i, and cause an engine angle δ. These servos are commonly hydraulic. The δ/δ_i transfer is of the form

$$\frac{\delta}{\delta_i} = \frac{K}{(s+c)(s^2 + 2\zeta_n \omega_n s + \omega_n{}^2)} \tag{15.46}$$

and is shown in Fig. 15.27 on the pole-zero plot.

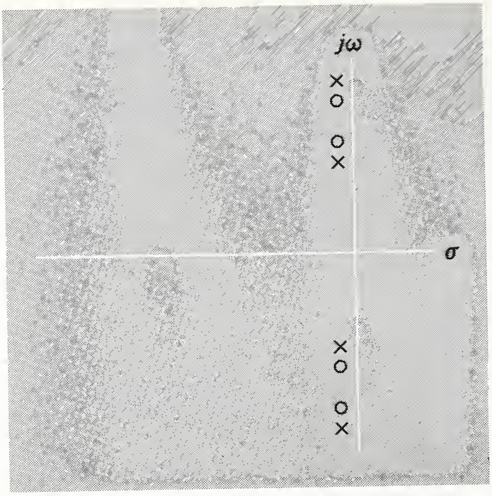

Fig. 15.26

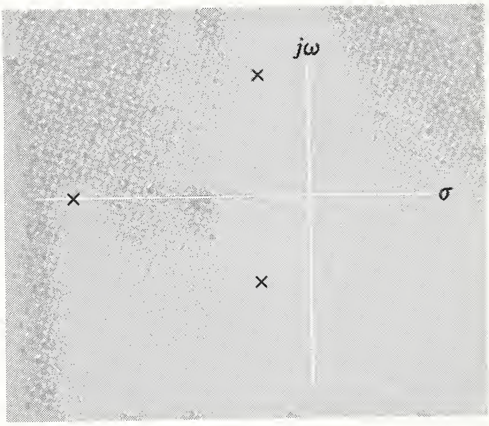

Fig. 15.27

15.7.5 Tail Wags Dog

This effect occurs when the reaction forces from accelerating the motor balance the side force produced by the thrust, resulting in zero angular acceleration of the main body. This produces a transfer function of the form:

$$\frac{s^2\theta_o}{\delta} \approx K_3(s^2 + \omega_{TWD}{}^2) \qquad \omega_{TWD} = \sqrt{T/ml}$$

shown in the pole-zero plot in Fig. 15.28.

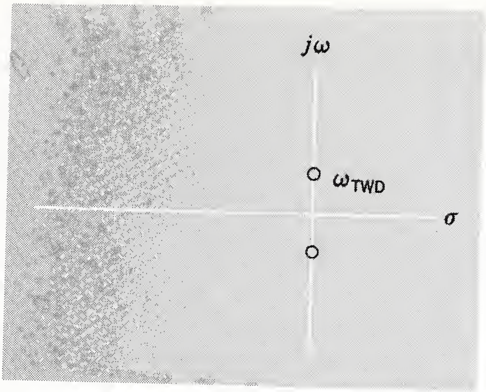

Fig. 15.28

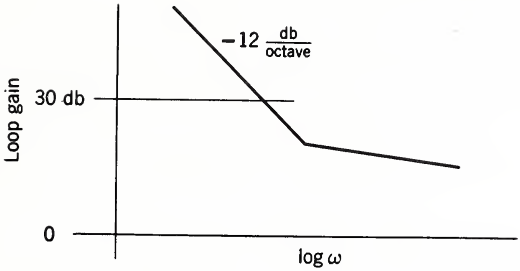

Fig. 15.29

The loop gain effect is illustrated in Fig. 15.29.

15.7.6 Pole-Zero Diagram

A summary of the effects of bending, hydraulics, sloshing, power servos, and tail wags dog is shown on the pole-zero plot of Fig. 15.30.

15.8 INPUTS

Inputs to control systems can be described as a particular time function by a corresponding transform or by other means, including statistical information. The specific set of inputs for one missile control system will probably never be duplicated in another missile of the same type. The control engineer has to find suitable bounds on the inputs such that, with

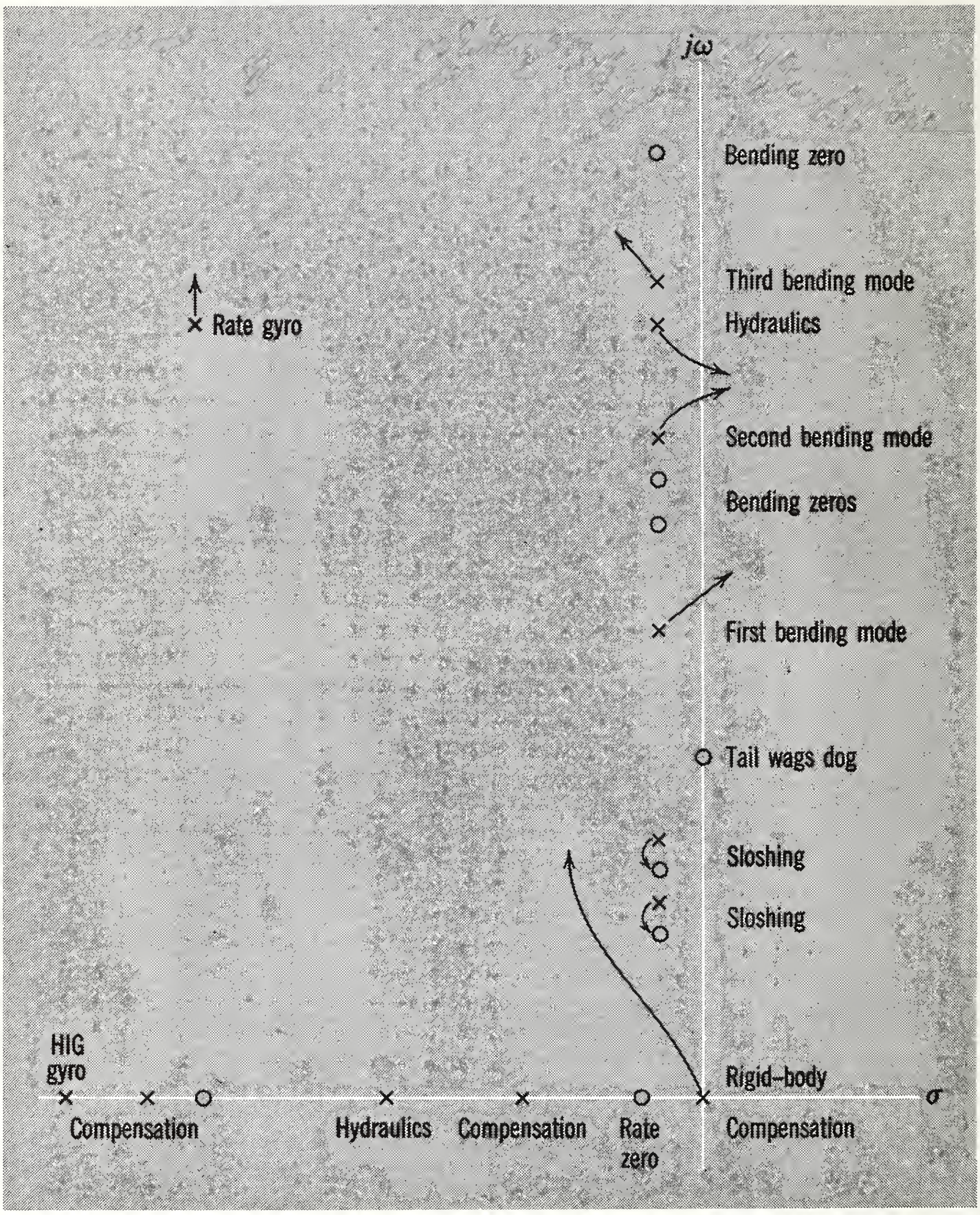
jω
Bending zero
Third bending mode
Hydraulics
Rate gyro
Second bending mode
Bending zeros
First bending mode
Tail wags dog
Sloshing
Sloshing
HIG gyro
Rigid-body
σ
Compensation
Hydraulics
Compensation
Rate zero
Compensation

Fig. 15.30 Single-axis ballistic missile control system pole-zero diagram.

a reasonable expectancy, a particular missile can be controlled for any combination of input events. An example of this process can be found by examining the approach used in designing a control system to fly through atmospheric winds.

One type of statistical description of wind information is given by Sissenwine (Fig. 15.31a). It is essentially of the envelope of wind velocities that are exceeded only 1 per cent of the time. Analytically, or with the aid of an analog computer, the control system can be "flown" through the wind envelope with various other disturbances such as gyro drift and thrust perturbations. The essential result is a curve of engine angle required to fly through the wind as a function of K_D (Fig. 15.31b). Since there is a very obvious limitation to the amount of engine angle available, this result enables a range of K_D to be determined, lessening the effect of an unwanted disturbance. This value of K_D must, of course, be compatible with stability and bandwidth requirements for guidance.

Treatment of guidance inputs is best accomplished by another means. Here a study of the guidance system yields a power density spectrum (Fig. 15.32) of the ensemble of guidance signals. Then the bandwidth of the control system must be large enough to accommodate the significant frequency range of the guidance inputs. Usually the value of K_D arrived at by stability and wind conditions is more than adequate in terms of guidance bandwidth.

15.9 OTHER CONSIDERATIONS

One other very important problem must be kept in mind, the one associated with the fact that all the missile parameters change with time and some of the changes are rather radical. Aerodynamics, bending frequencies, sloshing frequencies, accelerations, to mention but a few, are among these variables. The usual technique in handling this problem is to consider the design of the control system at discrete points in time along the trajectory. If the time variations are not too rapid, this is a valid approach.

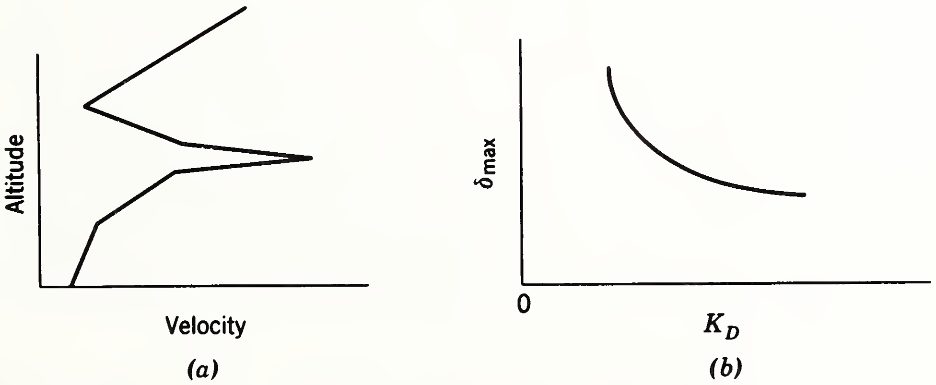

Fig. 15.31 (a) Sissenwine profile, (b) Engine angle versus loop gain.

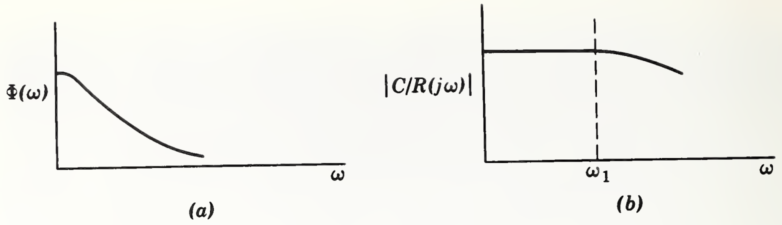

Fig. 15.32 (a) Guidance spectrum, (b) control system transfer function.

One result of this analysis is the discovery that various design parameters of the control system require changes with time or trajectory point to achieve the requirements. A typical change is in the values of K_D and K_R. Another typical change is in the parameter values of the compensation networks. These changes can be accomplished by the use of a programmer. The programmer can be a device that activates switches at prescribed points in time or velocity. Programmers can also be used to supply an open-loop input to the control system before formal guidance begins. This means of trajectory control is far less precise than a guidance system.

15.10 SUMMARY

1. Control systems are composed of elements that can be described by sets of linear differential equations.

2. Laplace transform-steady-state sinusoidal analysis of these elements leads to transfer function descriptions of the various elements. This analysis can be checked by sinusoidal testing.

3. Feedback theory shows that sensitivity to changes in portions of the system can be minimized; that effects of disturbances can be lessened; and that the dynamic characteristics of portions of the system can be changed. Ballistic missile control systems make use of all these reasons (to mention a few of the reasons): (a) The variations of the system are minimized for guidance. (b) Effects of winds can be lessened. (c) The missiles are dynamically unstable without a control system.

4. Having chosen the loop gain to satisfy 3, it is then necessary to design filters, etc., to stabilize the system. This re-

sults in the need to control the gain frequency characteristics for a considerable frequency range above that necessary to accommodate guidance spectra.

5. It may be necessary to make discrete variations in the control system parameters by means of programmers.

16

RADIO GUIDANCE FUNDAMENTALS

R. B. Muchmore

16.1 INTRODUCTION

This chapter is not written for the guidance expert; it is an attempt to cover some of the fundamental principles of radio guidance operation at a college physics level, emphasizing measurement procedures which are the basis of any radio guidance system. The coverage will (a) include some of the simpler aspects of electromagnetic theory as used in radio guidance; (b) show how these principles of electromagnetic wave propagation can be used in direction finding, ranging, and velocity measurements; (c) discuss fundamental errors in measurement, not errors in equipment; and (d) give an example of a hypothetical tracking system design.

The emphasis is on fundamentals, not detailed analysis or synthesis of radio guidance equipment. Radio circuit design is much too large a subject to be encompassed within the limitations of this chapter. No details are given of how to design radio receivers, transmitters, decoders, modulators, etc. Similarly, the problems of computation and control as distinct functions in guidance systems are not covered because they have been discussed in other chapters in this book. To repeat, then, what is covered here is a brief review of the basic principles of radio tracking methods as used in radio guidance systems, with some indication of how the limitations of these methods are recognized when applied to the measurement of position and velocity.

16.2 ELECTROMAGNETIC THEORY

To understand radio measurements we must understand something of the principles of electromagnetic wave propagation, since it is by measurement of some property of these waves propagated through the space between vehicle and reference point that we deduce facts concerning the vehicle's position and velocity.

16.2.1 Geometric Optics

To solve many of the problems of radio guidance the full form of the electromagnetic equations is not required. It suffices to use the geometric optics approximation[1,2] which involves the solution of the scalar wave equation

$$\nabla^2\Psi + k^2n^2\Psi = 0 \tag{16.1}$$

where $k = 2\pi/\lambda$, λ is the free-space wavelength, and n is the index of refraction; Ψ can represent the magnitude of either the electric field or the magnetic. The medium is assumed to be isotropic. The geometric optics method for finding an approximate solution to this equation is to set

$$\Psi = Ae^{-ikS} \tag{16.2}$$

where A is an amplitude factor, S is a phase factor, and A and S are real functions of position in the medium. Substituting eq. 16.2 into eq. 16.1 and assuming that $\nabla^2A/Ak^2 \ll n^2$, we obtain

$$|\nabla S|^2 = n^2 \tag{16.3}$$

Provided ∇^2A/Ak^2 remains finite, eq. 16.3 gives an approximate solution which becomes exact in the limit as k becomes infinite, that is, λ approaches zero. Equation 16.3 is commonly called the equation of the eikonal.

It is possible to show that the general solution to eq. 16.3 is a family of surfaces upon which S is constant. Since S is the phase factor in eq. 16.2, these surfaces for S equal to a constant are surfaces of constant phase in the field. It is also possible to show that lines everywhere orthogonal to these surfaces are parallel to the direction of energy flow; these lines are commonly called rays and are the lines ordinarily drawn to represent the passage of light in a geometric optics graphical construction. The equation of the rays is

$$\frac{d}{d\sigma}(n\vec{t}) = \nabla n \tag{16.4}$$

where $d\sigma$ is an element of length along the ray and $\vec{t}$ is a unit vector in the direction of $d\sigma$. This equation can be used to trace the passage of a ray through any medium for which n as a function of position is known. Once the rays have been determined, S can be found from

$$S(\vec{r}) = \int_{\vec{r}_0}^{\vec{r}} n\,d\sigma + S_0 \tag{16.5}$$

where $\vec{r}_0$ is the initial point, S_0 is the initial value of S, and the integral is along the ray path.

To illustrate the application of these principles to a very simple yet important case, consider the example of radio waves coming to the surface of the earth from outside the atmosphere. Assume for the present that the atmosphere is horizontally stratified—that is, ∇n is directed vertically down. For simplicity, assume a plane earth. Let $\vec{j}$ be a unit vector in the direction of ∇n and take the vector product of $\vec{j}$ with both sides of eq. 16.4. We obtain

$$\frac{d}{d\sigma}(n\vec{j} \times \vec{t}) = 0 \tag{16.6}$$

which implies that $n\vec{j} \times \vec{t}$ is constant along the ray. The constant vector $n\vec{j} \times \vec{t}$ can be shown to be perpendicular to the incremental vector $d\vec{t}$ in the following way. Equation 16.4 can be rewritten as follows:

$$\frac{d}{d\sigma}(n\vec{t}) = \frac{dn}{d\sigma}\vec{t} + n\frac{d\vec{t}}{d\sigma} = \nabla n \tag{16.7}$$

Solving for $d\vec{t}/d\sigma$ we have

$$\frac{d\vec{t}}{d\sigma} = \frac{\nabla n}{n} - \frac{1}{n}\frac{dn}{d\sigma}\vec{t} \tag{16.8}$$

Now take the dot product of both sides of this equation with the constant vector $n\vec{j} \times \vec{t}$:

$$\frac{d\vec{t}}{d\sigma} \cdot \left(n\vec{j} \times \vec{t}\right) = \nabla n \cdot \left(\vec{j} \times \vec{t}\right) - \frac{dn}{d\sigma}\vec{t} \cdot \left(\vec{j} \times \vec{t}\right) \tag{16.9}$$

$$= 0 \tag{16.10}$$

The step from eq. 16.9 to 16.10 can be made because ∇n and $\vec{j}$ are colinear and, of course, $\vec{t}$ is colinear with itself. Therefore, the two vector products on the right side of eq. 16.9 both yield zero, showing that the vector increment $d\vec{t}$ is always normal to the constant vector $n\vec{j} \times \vec{t}$. Since this constant vector is always normal to both $d\vec{t}$ and ∇n, we deduce that the increment $d\vec{t}$ lies always in the plane of ∇n and $\vec{t}$. Thus, if the gradient of n has a constant direction, the rays must be plane curves. Equation 16.6 can then be reduced to

$$\frac{d}{d\sigma}(n \sin\gamma) = 0 \tag{16.11}$$

where γ is the angle between the ray and ∇n.

Equation 16.11 is Snell's law in optics which states that the index of refraction times the sine of the angle of incidence is a constant along a ray. This law can be used to find refraction in the atmosphere. For instance, in Fig. 16.1 the spacing of the lines represents the density of atmosphere with density decreasing in the vertical direction. A ray incident on the top of the atmosphere at an angle γ_0 passes through the atmosphere, keeping the product $n \sin\gamma$ constant. It thus bends downward as indicated, the angle of incidence at the surface of the earth being γ_s. This phenomenon is obviously of importance for radio location methods, since the apparent direction of the source as measured at the surface of the earth is not the true direction to that source. For a source at infinity and for a plane earth the error angle ϵ (the difference between γ_s and γ_0) is given by

$$\epsilon \simeq (n - 1)\tan\gamma_0 \tag{16.12}$$

This equation is approximately true over a spherical earth where the angle of incidence is not greater than about 75°.

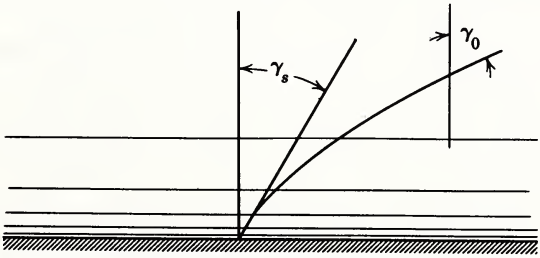

Fig. 16.1

In the troposphere the index of refraction n in the microwave portion of the spectrum varies with meteorological factors from approximately 1.000340 to about 1.000470 at the surface of the earth at sea level. The quantity $N = n - 1$ decreases approximately exponentially with altitude dropping to 1/e of its surface value at something like 27,000 ft.

At certain frequencies the effect just described is important, not only in the troposphere but also in the ionosphere. In the ionosphere the index of refraction is a function of frequency and is given by[3]

$$n \simeq \sqrt{1 - (81N_e{}^2/f^2)} \tag{16.13}$$

where N_e is the number of electrons per cubic meter and f is frequency in cycles per second. It is obvious that for accurate direction finding, from the point of view of this factor alone, as high a frequency as possible should be used since this reduces the index of refraction and the refraction bending.

16.2.2 Diffraction

Although the geometric optics solutions are adequate for many purposes, there are certain instances in which a full vector wave equation solution must be used. These instances are, of course, those for which the geometric distances involved are not large compared to the wavelength. In these instances the approximation of vanishing wavelength is not valid and we must seek other solutions to the problem.

To pick a specific example which is simple, yet very important practically, consider the radiation of energy from a parabolic mirror. Figure 16.2 shows the situation encountered. A parabolic mirror is illuminated from its focal point by an electromagnetic source illustrated in the figure as an electric dipole. The common approximate method of solution for this problem follows. Geometric optics are used to trace rays from the source to the mirror and then back to some arbitrary plane P which is commonly taken as the plane coinciding with the mirror aperture. By the well-known properties of parabolic mirrors every ray, in traversing the distance from the source to this plane, travels an equal distance. Thus plane P at the aperture is an equiphase front as defined earlier.

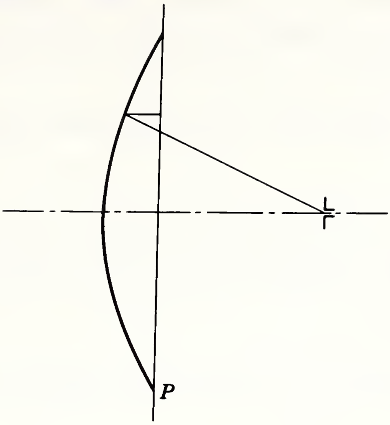

Fig. 16.2

As a simple approximation we can assume that the amplitude A over this plane is everywhere constant. At this point in the analysis we shift from geometric optics to a wave solution. The distant field at a point p (see Fig. 16.3) a great distance from the mirror can be obtained from Huygen's principle. According to this principle each element of the aperture of the mirror (indicated by the irregular outline at the origin in Fig. 16.3) radiates a spherical wave. At a great distance (point p) the total field is given simply as the summation of the fields from each of these elementary areas in the aper-

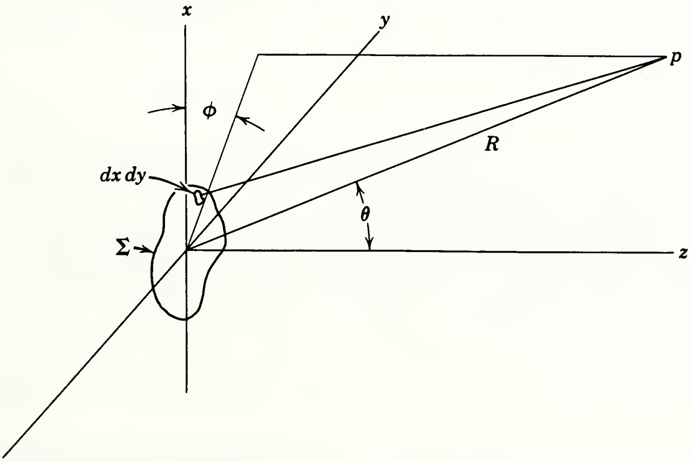

Fig. 16.3

ture. From the element dxdy in Fig. 16.3, taking proper account of the geometry in the figure and accounting for phase shifts, the field at point p is given for small θ by[4]

$$E_p \simeq \frac{i}{\lambda R} \exp(-ikR)\ F(x, y) \exp\left[ik \sin\theta (x \cos\phi + y \sin\phi)\right] \, dx\,dy \tag{16.14}$$

where F(x, y) is a function giving amplitude and phase of the field in the aperture. The total field is obtained by integrating over the aperture Σ:

$$E_{pt} \simeq \frac{i \exp(-ikR)}{\lambda R} \iint_\Sigma dx\,dy\ F(x, y) \exp(ik_x x + ik_y y) \tag{16.15}$$

where $k_x = k \sin\theta \cos\phi$, $k_y = k \sin\theta \sin\phi$. From eq. 16.15 it is evident that the strength of the electric field at a far point is given approximately by the two-dimensional Fourier transform of the field across the aperture of the mirror. For instance, if F(x, y) is constant over an aperture which is circular and of radius a, the far field is given approximately by the integrated value

$$E_{pt} \simeq K \frac{J_1(ka \sin\theta)}{ka \sin\theta} \tag{16.16}$$

where K is a constant of proportionality which involves the total power radiated, the wavelength, and the distance between the antenna and the observation point (as well as certain constant phase factors).

16.2.3 Antenna Beamwidth and Gain

The beamwidth of the antenna may be deduced from eq. 16.16. A useful empirical equation which takes into account a certain amount of deviation between theory and practice gives the beamwidth, that is, the angular variation between points where the total power received at p has dropped to one-half, as

$$BW \simeq 0.6 \frac{\lambda}{a} \tag{16.17}$$

The reader may check that eq. 16.16 gives a value slightly less than this.

Antenna gain is defined as the ratio of the power radiated in a given direction by the actual antenna to the power that would be radiated in that direction by a hypothetical isotropic source. Ordinarily, unless otherwise specified, the gain is given in the direction of the maximum power radiation, that is, the maximum gain is quoted.

An antenna placed in a radiation field and used as a receiver will absorb a certain amount of the energy incident on it. This absorption is usually specified in terms of the equivalent cross-sectional area of the antenna where equivalent cross-sectional times energy density per unit area in an incident plane wave gives the total power available at the antenna terminals. Antenna cross-sectional area σ is related to antenna gain by[5]

$$G = \frac{4\pi\sigma}{\lambda^2} \tag{16.18}$$

16.3 RADIO MEASUREMENTS

For guidance purposes, the measurement capabilities of radio systems are of primary importance. We shall take up in order (a) direction finding, (b) ranging, (c) velocity measurements, and (d) angular rate measurements.

16.3.1 Direction Finding

Direction-finding techniques take advantage of the fact that in the distant field of a radiator the phase fronts are, in the absence of perturbations in the propagation medium, very nearly plane and of equal amplitude over large areas. A simple means for finding the normal to the phase front, and hence the direction along the rays, is diagrammed in Fig. 16.4. Two receiving antennas are shown schematically a distance d apart. The signals from these two antennas are brought to a point midway between them where the phase difference is measured. A phase front (surface of constant S, see Section 16.2.1) is shown at the instant of passing through one of the antennas. The signal picked up by the other will be delayed in phase by the angle ϕ where

$$\phi = kx = \frac{2\pi d \sin\alpha}{\lambda} \tag{16.19}$$

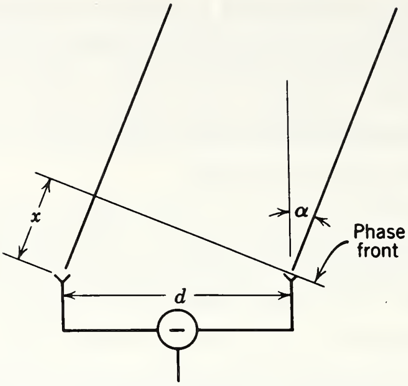

Fig. 16.4

This error is shown plotted in Fig. 16.5 as a function of α, the angle of incidence, and is a periodic function of α (corresponding to going round and round the measurement point). Note also that the peak amplitude of the quantity ϕ can be much greater than π if d/λ is large; obviously α is determinable from a measurement of ϕ in this case only if the proper cycle of ϕ can be chosen. A system such as this is ordinarily operated in such a way that ϕ is known to within one cycle—for instance, within $-\pi$ and π as drawn in Fig. 16.5. The point α_a can then be found from eq. 16.19 as

$$\begin{aligned}\alpha_a &= \sin^{-1}\frac{\lambda}{2d} \\ &= \frac{\lambda}{2d} \quad \text{if } d \gg \lambda\end{aligned} \tag{16.20}$$

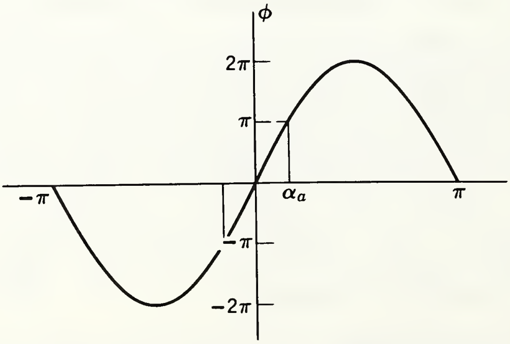

Fig. 16.5

Certainly if ϕ is known to be within one particular 2π range of Fig. 16.5, with the scheme of Fig. 16.4 the normal to the phase front can be found and the apparent position of the source determined. (The source is presumed always to be radiating a spherical wave in a homogeneous isotropic medium; thus the direction of normals to the phase front are radial lines toward the source. In a nonhomogeneous medium —for instance, the stratified atmosphere treated in section 16.2—the rays are curved and the measurement described here gives only an apparent direction of the source and not its true direction.) This scheme for direction finding is commonly called a phase comparison or interferometer system.

Another common method for direction finding makes use of a so-called lobing technique. Figure 16.6 shows two antenna beams A and B and an incoming ray at an angle α with respect to the symmetry axis. We note from the figure that the amplitude received on antenna A is equal to that received on antenna B along the symmetry axis, but that these two powers are different in other directions. A plot of received signal strength versus α is given in Fig. 16.6 on the assumption that the amplitude of the signal from A is subtracted from the amplitude of the signal from B. Between the two peaks of the curve, in the range marked α_r, the angle of incidence of the ray can be unambiguously determined. Again, the angle must be determined to within this range by some other means.

Either of these two systems could be made self-tracking by mounting the antenna on an appropriately designed servo mount and using the signal of either Fig. 16.5 or Fig. 16.7 as

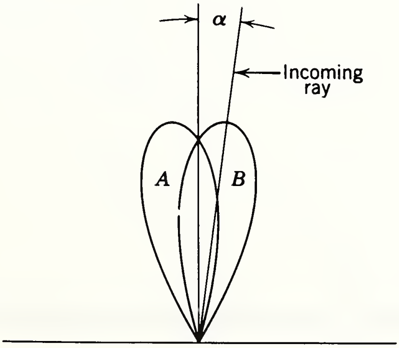

Fig. 16.6

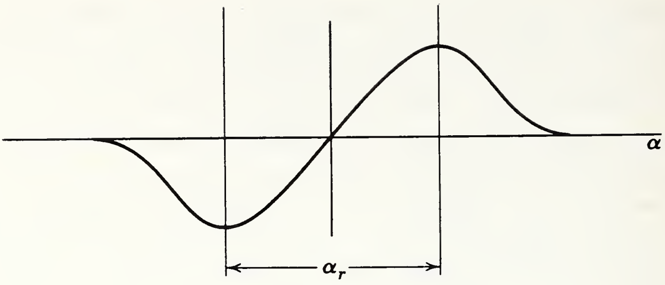

Fig. 16.7

the error signal to control the servo. Thus the antenna system could be aligned so as always to point in the direction along the ray and normal to the phase front.

With a direction finder operating from the surface of the earth to find the direction of a ray coming from above the atmosphere, there is an important distinction between a system which tracks automatically and one for which the direction of arrival is computed from measurements made by the phase comparison method. This is illustrated in Fig. 16.8; the two antennas are on the surface of the ground, and the phase difference between them is given by k_g times x, where k_g is the propagation constant appropriate to the atmosphere at the ground surface. This value of k can be used in conjunction with the measured phase shift to calculate the angle α_g, which is the angle of incidence at the ground or the apparent source direction.

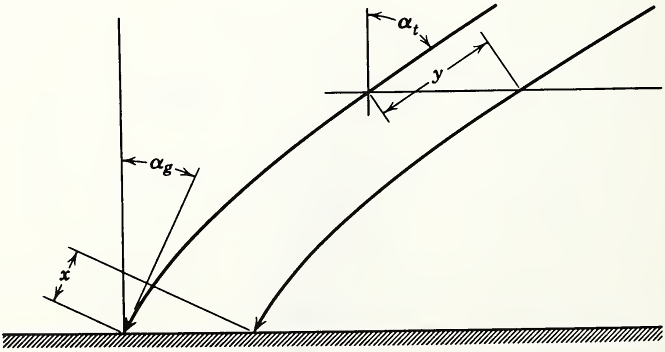

Fig. 16.8

Consider now, however, a plane P parallel to the ground but above the atmosphere. The phase shifts between ray intersections of this plane and the ground are equal for the two rays, so that if the two antennas were raised above the atmosphere and placed on this plane, they would measure precisely the same phase difference as they do on the ground. The phase difference now, however, is proportional to k_a times y, with k_a now the propagation constant above the atmosphere. By using this value of k and the same phase shift, the angle α_t, the true angle of incidence, can be calculated. Obviously, we can make a measurement on the ground, use the value of k appropriate above the atmosphere, and calculate the true angle of arrival, not the apparent angle of arrival. For a horizontal stratified atmosphere and a very distant source this correction is thus automatically made without any knowledge of the propagation constant at the bottom of the atmosphere. An automatic tracking system, however, can only line itself up along the direction of the ray as it reaches the antenna. It will thus indicate the direction α_g which can only be corrected by making measurements of the propagation constant in the atmosphere and then calculating, using Snell's law.

16.3.2 Ranging

All systems of ranging depend on knowing the velocity of propagation and the time of transit. We solve for distances simply by multiplying the rate times the time.

To determine range, then, some distinctive signal is transmitted to one end of the path, either passively reflected or actively retransmitted back to the other end of the path, and the time of transit is measured. Pulses are a common distinguishable signal form. Figure 16.9 shows a time versus

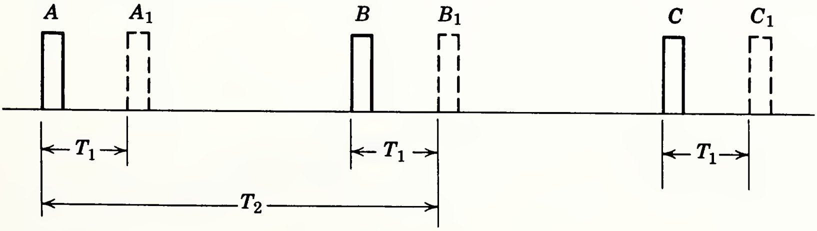

Fig. 16.9

amplitude plot of a hypothetical pulse-ranging system. The pulses A, B, C, are transmitted in sequence and, ordinarily, at equal periods of time. The time to travel to the target and back might be represented, for instance, by the time T_1, shown in Fig. 16.9. The dashed pulse shapes on the figure would then be the return signals from the target, and they would occur at the instants A_1, B_1, C_1, etc. The total range to the target and back would then be obtained by multiplying the time interval T_1 by the velocity of propagation c.

There is a possibility of ambiguity, however. Unless we have a priori knowledge to the contrary, it is possible that the total time of transit may have been the time T_2, equal to a complete period of the repetitive pulse form, plus a time equal to the additional T_1; or it could, of course, mean T_1, plus any multiple of the period of the repetitive pulse. These possible ambiguities are generally by-passed in the ordinary pulse system by making the interpulse period so long that signals which have traveled far enough to make their range ambiguous have decayed in amplitude to such a low figure that they are very seldom found above the noise in the return signal.

A similar situation can be arranged by using sine wave modulation as shown in Fig. 16.10. The sine wave labeled I can be assumed to be the transmitted modulation waveform, and the sine wave labeled II can be taken as the returned

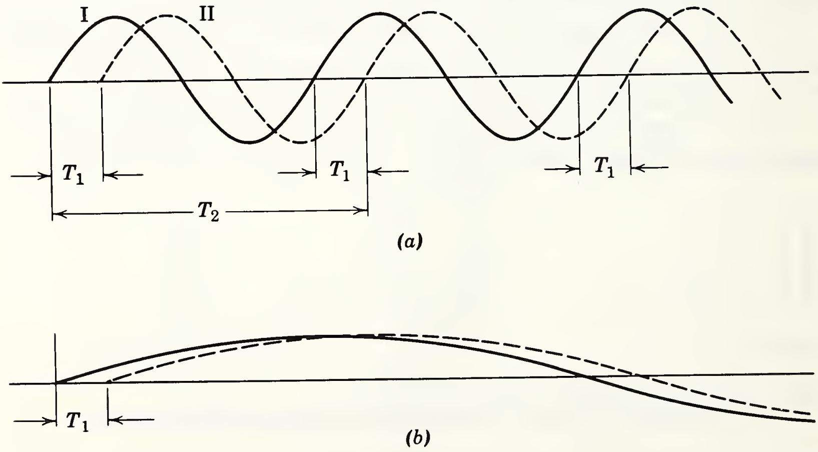

Fig. 16.10

modulation waveform. Again there is a possibility of ambiguity in range. The time T_1 may represent the range, but on the other hand the time T_2 may also represent the range, corresponding to a complete 2π phase shift in the return signal in addition to the extra shift represented by T_1. Ambiguities of this sort may be resolved by simultaneously modulating the signal with sine waves of several different frequencies. For instance, in B of Fig. 16.10, a very long-period sine wave may be transmitted in addition to the short-period sine wave of A. The time T_1 represents less than one period, and so does the time T_2. Thus we could distinguish between the cycles in trace A by comparing the trace obtained on B. By using sine waves of longer and longer periods we can, in principle, distinguish between ambiguities to some maximum range. The same principles could, of course, be used with pulse ranging, but here it has the disadvantage that multiple-period pulses are not easily distinguishable unless different types of modulation are used for the different periods. Sine waves, naturally, can be separated out by means of filters in the receivers.

16.3.3 Velocity Measurements

Velocity measurements are based on use of the Doppler principle.[6] In its relativistic form this principle states that the received frequency f is given in terms of transmitted frequency f_0 by

$$f = f_0 \frac{(1 - v/c \cos\theta)}{\sqrt{1 - v^2/c^2}} \tag{16.21}$$

where v is the relative velocity along the line of sight between transmitter and receiver, c is the velocity of propagation, and θ is the angle between the line of sight and the velocity vector. The source and receiver are assumed to be moving apart; if they are moving together, the minus sign in the numerator becomes a plus sign. A common Doppler measuring scheme is to transmit a carrier at frequency f_0 to the moving vehicle. It is received there with a Doppler shift. This Doppler shifted frequency is then transmitted back to the ground where it is received with another Doppler shift of the same size; thus the signal returning to the ground has a double Doppler shift. By comparing transmitted and received frequencies, and using eq. 16.21, we can deduce the vehicle velocity.

It is also possible, of course, to find velocity by measuring range by one of the schemes given earlier and then differentiating this range as a function of time. It should be noted that this measurement is exactly equivalent to the Doppler shift measurement described, at least in principle, because the range measurement is essentially a measurement of phase of a returned wave relative to a transmitted wave. However, the rate of change of phase with time is the velocity required, but it is also frequency, and it can be shown that the frequency so determined is precisely that given by eq. 16.21.

16.3.4 Angular Rate Measurement

We can measure angular rate by determining the rate of change of angular position of a tracking antenna. This measurement determines only the rate of change of apparent direction to the source if there is a refraction error in the atmosphere. It also has inherent in it any errors from noise in the tracking servo or from inaccuracies in following.

Another method of determining angular rate is to measure the Doppler difference frequency between signals received at a pair of antennas, such as the pair in Fig. 16.4. The phase difference between these antennas is given by eq. 16.19, which, when differentiated to give frequency, yields

$$\text{Doppler difference frequency} = \frac{\dot{\phi}}{2\pi} = \frac{d\,\dot{\alpha}\cos\alpha}{\lambda} \qquad (16.22)$$

This frequency is called a Doppler difference because it represents the difference between the Doppler frequency received at one antenna and that received at the other. If these two frequencies are different, the difference is proportional to the angular rate of the source measured about an axis perpendicular to the line connecting the two antennas.

16.4 RADIO GUIDANCE ERRORS

16.4.1 Equipment Errors

There are a number of errors in radio guidance systems which are not subject to analysis; they must be evaluated individually and can only be determined by actual test of the equipment concerned. These errors include servo jitter, nonlinearity in circuits, drifts in amplitude or phase which might be caused by temperature or aging, etc. In evaluating these errors beforehand, the best guide for the designer is experience with similar equipment. Knowledge of how best to minimize such errors is often empirical because, although they are frequently among the most important errors in a system, they are not fundamental in the sense that improvements in technique make possible a reduction in errors. The errors discussed here are fundamental in that they are manifestations of physical laws for equipment operating in an earth environment.

16.4.2 Propagation Errors

The refraction error in a horizontally stratified atmosphere was discussed in Section 16.2. In addition to this average or long-term error there will be other more or less random changes in the apparent direction of the source. These random perturbations are caused by winds, convection, and turbulence in the atmosphere.

A simple phenomenological model for these changes follows. Assume that the atmosphere—either the troposphere or the ionosphere—contains blobs or cells in which the index of refraction is slightly different from the average. If a ray is drawn through such an atmosphere, a crude representation of the index of refraction along the ray might be that shown in Fig. 16.11. The average index is indicated, and there are small perturbations about the average. These small perturbations represent the blobs referred to previously.

In this crude model the index is assumed constant at some random value throughout any individual blob and then constant at some other random value for the next blob. In some one given blob of length l_0, the phase perturbation in traversing it is

$$\delta\phi_1 = \frac{2\pi l_0 \, \delta n}{\lambda} \tag{16.23}$$

where δn is the index of refraction perturbation. If the total path length through the medium is L, the mean square phase perturbation is the mean square for one blob times the total number of blobs in the path, or

$$\overline{\delta\phi^2} = \frac{4\pi^2 l_0^2\,\overline{\delta n^2}}{\lambda^2}\,\frac{L}{l_0} = \frac{4\pi^2 L l_0\,\overline{\delta n^2}}{\lambda^2} \tag{16.24}$$

This is the mean square phase perturbation induced in one path.

For a phase comparison system the error will be proportional to the difference in phase over two paths. Thus the mean square error will be proportional to twice the mean square single-path error as determined from eq. 16.24 times one minus the correlation coefficient when the correlation coefficient expresses the degree of correlation between the signals transmitted along the two paths shown in Fig. 16.11. The mean square difference error $\delta\phi_{12}$ is

$$\overline{\delta\phi_{12}^2} = \frac{8\pi^2 L l_0\,\overline{\delta n^2}}{\lambda^2}(1 - \rho_{12}) \tag{16.25}$$

The quantity ρ_{12} is the normalized correlation coefficient.

The mean square error in angle of arrival may be obtained from eqs. 16.25 and 16.19 by assuming that the angle α is small so that the sine equals the angle. To first order in α, the mean square angle of arrival is obtained as

$$\overline{\alpha^2} \simeq \frac{\lambda^2\,\overline{\delta\phi^2}}{2\pi^2 d^2}(1 - \rho_{12}) = \frac{2 L l_0\,\overline{\delta n^2}}{d^2}(1 - \rho_{12}) \tag{16.26}$$

If the assumption is made that the correlation between ray paths is negligible, eq. 16.27 is obtained as

$$\alpha^2 \simeq \frac{2 L l_0\,\overline{\delta n^2}}{d^2} \tag{16.27}$$

This assumption is tantamount to saying that the base line length (see Fig. 16.4) is large compared to the mean blob size l_0 in the atmosphere.

This analysis can be shown[7] to be correct to first order in phase perturbation when the quantity $\delta\phi$ is much less than 2π. To the same order of approximation, the amplitude variations seen in the resultant wave are of smaller order and thus become very small indeed. When this first-order approximation cannot be made, that is, when $\delta\phi$ is of the order of 2π

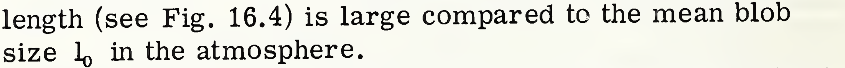

Fig. 16.11

or more, no simple analysis can be made to show what the results will be. About the only simple result that can be quoted is for the case when $\delta\phi$ is very large. Then $\delta\phi \pmod{2\pi}$ can be shown to be a random quantity uniformly distributed from zero to 2π, and the amplitude of the resultant wave will have the Rayleigh distribution.

Under ordinary conditions in the troposphere on line of sight paths the first-order theory just presented is quite valid. However, in considering the ionosphere, this analysis is not valid when the quantity δn becomes large. From eq. 16.13 can be written

$$n = 1 - \delta n \cong \sqrt{1 - 81N_e^2/f^2} \simeq 1 - \frac{40.5N_e^2}{f^2} - \cdots$$

and for certain values of N_e/f, δn can be near unity. (Imaginary values of n correspond to no transmission into the ionosphere; see Mitra.[3]) For δn large, the phase perturbation and, of course, correspondingly, the amplitude perturbation become large, and the simplified theory no longer holds.

Representative tropospheric blob sizes, a dimension often called the scale length in the atmosphere, are of the order of a few hundred meters.[8] In the F region in the ionosphere these lengths are of the order of several kilometers.[9]

16.4.3 Signal-to-Noise Ratio Errors

Thus far it has been tacitly assumed that the signals received by the tracking or direction-finding antennas are uncontaminated by locally generated noise. This approximation is only valid when the received signal power is much greater than the internally generated noise. The well-known expression for power received is[10]

$$P_r = \frac{P_t G_t \sigma_r}{4\pi R^2} \tag{16.28}$$

where P_r is the received power, σ_r is the absorption cross section of the antenna (see eq. 16.18), P_t is the power transmitted from the source, G_t is the gain of the source antenna, and R is the range from source to receiver. The power received is to be compared with the internally generated noise in the receiver which is[11]

$$P_{noise} = FkTB \tag{16.29}$$

where F is the receiver noise figure, that is, the ratio of actual noise to theoretical noise at the input stage temperature, k is Boltzmann's constant, T is temperature in degrees Kelvin, and B is receiver bandwidth. As an example of an error induced by a finite signal-to-noise ratio, the ranging error in a system which measures range by determining the phase difference between a transmitted and returned sine wave may be approximately evaluated in the following manner. Consider Fig. 16.12 which shows a small section of the zero crossing of the returned sine wave as it would be seen if there were no noise in the receiver circuits. The time $t = 0$ has been taken as the reference time at which this returned sine wave crosses zero in the positive-going direction. This situation corresponds to that shown in Fig. 16.10.

Actually, the received signal will be perturbed by some unknown amount of noise. If we can assume that the receiver bandwidth is narrow, this noise voltage appears more or less as a constant value over the very limited time interval shown in Fig. 16.12. Thus the actual signal plus noise will be indicated by the line through the zero axis which crosses at the different time indicated by the point τ. This time τ is the timing error in determining the range to the target.

We can evaluate τ in the following way; from the figure it is equal to

$$\tau = \frac{E_n}{S} \tag{16.30}$$

Where E_n is the noise voltage which has been added to the signal voltage and S is the slope of the sine wave as it crosses the origin. The slope may be evaluated as

$$\text{slope} = S = A\omega_0 \cos \omega_0 t \Big|_{t=0} = A\omega_0 \tag{16.31}$$

where it has been assumed that the sine wave representing the return signal can be given in the form $A \sin \omega_0 t$, and the

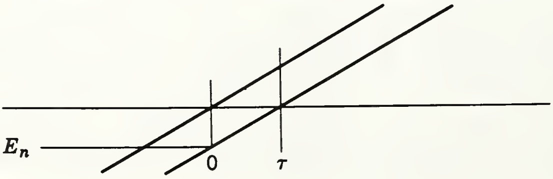

Fig. 16.12

slope is, of course, the derivative of this evaluated at the point t = 0. The noise voltage in the circuit, E_n, can be specified only in some statistical manner; assume that we know its mean square value which is proportional to the total noise power. The mean square error in timing, $\overline{\tau^2}$, is

$$\overline{\tau^2} = \frac{\overline{E_n{}^2}}{A^2\omega_0{}^2} = \frac{1}{2\frac{S}{N}\omega_0{}^2} \tag{16.32}$$

where the quantity S/N has been entered to represent the power signal to noise ratio at this point in the circuit. Thus the mean square error in timing is inversely proportional to the signal-to-noise ratio which we might, of course, expect and is inversely proportional to the square of the radian frequency of the ranging modulation. The mean square error in range is then obtained by multiplying the mean square error in timing by the square of the velocity of light. In terms of root mean square values,

$$\delta R \simeq \frac{c}{\omega_0\sqrt{2S/N}} \tag{16.33}$$

Now the expression just derived gives the error for one single independent determination of the range (round-trip range). In practice, we will measure not just a single zero crossing but many zero crossings. The net error is obtained by dividing eq. 16.33 by the square root of the number of independent measurements made:

$$\delta R_a \simeq \frac{c}{\omega_0\sqrt{2KS/N}} \tag{16.34}$$

where δR_a represents the root mean square error from an average determination of range and K is the number of independent range determinations which have been averaged together.

A range measurement will be independent of another range measurement if sufficient time has elapsed between the two measurements for the noise voltage to be substantially independent at the two times. An approximate criterion for the time lapse is a period between range determinations greater than or equal to the reciprocal of the bandwidth of the electrical filter in the ranging circuit. Here, of course, we must use the narrowest effective filter in the circuit. When the only noise in the system is the internally generated noise, given by eq. 16.29, signal-to-noise ratio is obtained by dividing eq. 16.28 by eq. 16.29.

Perhaps it should be pointed out here that in certain types of systems the internally generated noise is not the controlling noise in the system. An example of this is a system in which the input amplifier is perhaps a maser or parametric amplifier, with an equivalent internal noise temperature T, in eq. 16.29, of no more than 50 to 100° K. If a well-designed antenna which feeds this amplifier is then pointed toward certain portions of the sky, or perhaps toward the earth, the external noise will control. That is, the noise generated in the galaxy or the noise generated simply by thermal motion of the electrons in the earth will be controlling. The earth has a temperature, of course, roughly equal to 300° K. The sky background has an equivalent noise temperature which depends on frequency and position in the sky.[12]

A similar formula may be derived for pulse ranging systems. In general, any ranging system behaves in approximately the same manner. Differences in methods of measuring time delay or phase and differences in averaging procedures will produce minor differences in the range error formulas. However, the general functional form as shown in eq. 16.34 will always apply; range error is proportional to measurement error, inversely proportional to the square root of averaging time, and inversely proportional to the square root of the power signal to noise ratio.

The root mean square Doppler measurement error can be obtained in a very similar way under the same assumptions and is given by

$$\delta v = \frac{c}{4\pi K_1 \sqrt{K_2 S/N}} \qquad (16.35)$$

where it is assumed that the returned Doppler shifted frequency is determined by counting cycles (and fractions of cycles) for a certain period of time and K_1 is the number of cycles counted per measurement; K_2 is the number of such independent measurements made. Doppler difference errors would have the following form, with Δ as the difference velocity error:

$$\Delta \simeq \frac{1}{\pi K_1 \sqrt{K_2 S/N}} \qquad (16.36)$$

The assumption has been made that the noise sources in the two separate channels are completely independent, which would be true, for instance, if the noise were internal noise generated in separate and independent preamplifiers placed at the two separate antennas. If the noise were partially correlated, as would be true, for example, when external noise was overriding and the two antennas were pointing at the same portions of the sky, a different treatment of the problem would be necessary and would account for this correlation. In this instance the over-all noise would be lower.

It is obvious that even without any equipment errors it is not possible to achieve unlimited accuracy in direction and rate finding. There are inherent limiting errors, both in the atmosphere and in the internally generated noise in the equipment. Both of these are fundamental in nature and cannot be eliminated by improved design. We can only minimize them by increasing signal-to-noise ratio, increasing averaging time, and increasing space averaging, that is, base line length.

16.4.4 Ground Reflection Errors

Another important error in direction-finding systems is that produced by ground reflection. Figure 16.13 shows an antenna of height h above the ground. There are two possible rays that can reach the antenna from a source at a great distance away at an angle of elevation β. One is the direct ray to the antenna, and the other is the ground-reflected ray; thus two signals are produced in the antenna. One of them is represented in Fig. 16.14 as the vector voltage E, that comes from the direct ray. The reflected ray is indicated as α times E where α is the complex reflection coefficient for the ground

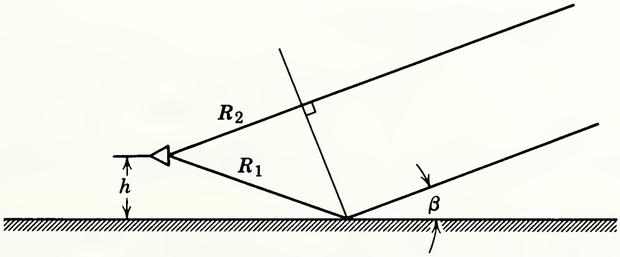

Fig. 16.13

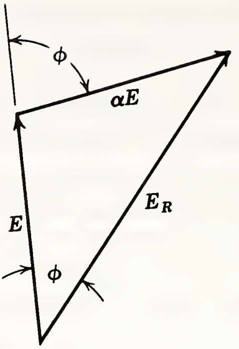

Fig. 16.14

surface. The net voltage appearing in the antenna circuit then is the vector sum of these two, E_R. The phase difference between the direct ray and the resultant is the angle θ.

From the geometry of Fig. 16.13 we can show that the distances R_1 and R_2 in Fig. 16.13 are given by

$$R_1 = \frac{h}{\sin\beta} \tag{16.37}$$

$$R_2 = R_1 \cos 2\beta = \frac{h}{\sin\beta} - 2h \sin\beta \tag{16.38}$$

The phase difference between the two rays at A is given by

$$\phi = \frac{2\pi(R_1 - R_2)}{\lambda} = \frac{4\pi h \sin\beta}{\lambda} \tag{16.39}$$

Now from the vector diagram of Fig. 16.14 the phase error in the measured voltage to first order can be obtained as

$$\theta \simeq |\alpha| \left[\frac{4\pi h |\alpha|}{\lambda}\right]_{2\pi} \tag{16.40}$$

The notation $[\ ]_{2\pi}$ means modulo 2π.

In a phase comparison system an error can be produced in determining elevation angle if the ground reflection conditions are different at the two ends of the base line. In an amplitude comparison system an error is produced because the amplitude of the resultant E_R is not the same as the amplitude of the direct ray. Looked at another way, the antenna is seeing signals coming apparently from two different directions, one in the direction of the true source and one in the direction of its mirror image which is below the ground surface. The ground reflection can be minimized by treating the ground surface so that it has poor reflective properties, and by increasing the directivity of the antenna so that it discriminates against the ground reflected ray. Either of these expedients is equivalent to reducing the value of $|\alpha|$ in eq. 16.40.

Only a partial list of the errors in direction-finding systems has been given. In designing or analyzing such a system, deviations from the ideal principle of operation assumed must be accounted for. The extent and detail of such analyses are conditioned by the accuracy required of the system and by the exact measurement methods to be used.

16.5 SYSTEM DESIGN FOR A HYPOTHETICAL SYSTEM

To illustrate some of the principles already mentioned, assume a desire to calculate the performance of an interferometer-type tracking station located at the surface of the earth but used to track satellites above the atmosphere. Its use for guidance purposes might be, for instance, to control orbit perturbation maneuvers. Take the following parameter values.

1. Angle of incidence, vertical. We assume, perhaps unrealistically, that the system is to evaluate the angle to the satellite only as it is passing directly overhead.
2. We take the base line length for the interferometer to be $d = 2000$ ft.
3. Assume a wavelength of $\lambda = 1/2$ ft (this corresponds very nearly to a frequency of 2000 mc/sec.)
4. Take the receiver noise figure to be equal to 6 db; this is a factor of 4.
5. Assume that the range to the satellite in the vertical overhead position is 5000 nautical miles (note that 1 nautical mile equals 6080 ft).
6. Let the sinusoidal ranging subcarrier period be equal to $T_t = 10^{-4}$ sec.
7. Assume an averaging period for the measurement of 1 sec.
8. Take the tropospheric turbulence scale length to be equal to 500 ft. Note here that the turbulent portion of the

troposphere is of the order of 10,000 ft thick over the portions of the earth's surface that are roughly sea level. This turbulent portion of the troposphere extends somewhat higher in absolute altitude above high-altitude regions. It is perhaps a reasonable approximation to assume it to be 10,000 ft thick, regardless of the elevation of the ground below. This assumption will tend to give slightly pessimistic results for tracking systems located on high mountain peaks or high plateaus.

9. Assume that the ground antenna gain is equal to 30 db. This is a factor of 1000.

10. We take the satellite antenna gain equal to 0 db, that is, a factor of unity. We assume this since it may be necessary to communicate with or to track a satellite, regardless of its attitude with respect to the ground. We assume here a satellite that may be tumbling, as distinct from one that might be attitude-controlled. In the latter case we might be able to point an antenna toward some selected portion of the ground, and thus it would be possible to have a higher antenna gain.

11. Take the power in the satellite transmitter to be 10 mw, which is in line with the idea that power in a space vehicle is very costly in propulsion effort and in the weight and complexity of power supplies which must be carried aloft.

12. Take the bandwidth of the receiver on the ground to be 100 cps, thus tacitly assuming that there is a tracking filter, that is, a filter of constant width which follows a variable-frequency received signal in the ground circuitry. This assumption is in line with advanced practice which makes use of such devices to obtain the ultimate in sensitivity. Note that this filter makes the noise independent over a period of approximately 10^{-2} sec and thus in 1 sec there are about 100 independent measurements of range possible.

13. Take variation in index of refractivity of the troposphere to be $\delta n/n = 1/2 \times 10^{-6}$.

14. As for other constants required in calculations, Boltzmann's constant equals 1.374×10^{-23} joules/°K. We ordinarily use $T = 300°K$ as the ambient temperature on the surface of the earth. The velocity of light is very nearly 10^9 ft/sec. At a frequency of 2000 mc/sec we may ignore the effect of the ionosphere.

The first calculation that we ordinarily make is a calculation of signal-to-noise ratio. If the signal-to-noise ratio is too low, there is not much point in going further. By making use of eqs. 16.28 and 16.29, the signal-to-noise ratio is

$$\frac{S}{N} = \frac{(0.01)(1)(10^3 \cdot (1/2)^2/4\pi)}{4\pi(5000 \cdot 6080)^2 \cdot 4 \cdot (1.37 \cdot 10^{-23})(300)(100)} \qquad (16.41)$$

$$= 10.4$$

Equation 16.18 has been used to compute effective cross-sectional area of the ground antenna for reception. For the present example we have a signal-to-noise ratio of approximately 10; this is neither too large nor too small. It has been tacitly assumed here that the signal-to-noise ratio on the ground-to-satellite link is sufficiently high that it does not degrade the transponded satellite-to-ground signal. Because ground power is relatively cheap compared to satellite power, the ground-radiated power can be economically increased to the point where this statement is true.

By using eq. 16.34 the accuracy to which the range to the satellite can be determined can be calculated, obtaining from this equation

$$\delta R = \frac{10^9}{2\pi(10^4)\sqrt{2(100)(10.4)}} \simeq 349 \text{ ft} \qquad (16.42)$$

Actually, this equation gives the inaccuracy in determining range for the full round trip. The one-way error is half of this, or approximately 175 ft.

Assume that in making the velocity measurement the radiated carrier frequency of 2000 mc/sec is used, not the ranging subcarrier. From eq. 16.35 is obtained

$$\delta v = \frac{10^9}{4\pi(2 \times 100^7)\sqrt{(100)(10.4)}} \simeq 0.125 \text{ ft/sec} \qquad (16.43)$$

In making use of this formula, K_1 has been set equal to 2 × 10^7, the number of cycles in a 1/100 sec counting interval, whereas K_2 has been set equal to 100, the number of independent measurements, according to the noise bandwidth, which can be made in the 1-sec interval.* This is a high order of accuracy of measurement; there may be bias errors

*Note that a different division of counting and averaging intervals will reduce the error still further. If we count for a full second K_1 becomes 2 × 10^9 and K_2 is 1. This is a net factor of ten better in overall accuracy. It should be evident that very careful balancing of measurement times, signal-to-noise ratios,etc., is required in obtaining an optimum design. Also, for any serious optimization, the relatively simple approach used here may be inadequate.

of one sort or another in the actual circuitry which will produce errors greater than the ultimate limiting accuracy produced by the signal-to-noise ratio in the system.

Next, the error in determining angle induced by the presence of noise in the system can be evaluated. Use is made of eq. 16.33, interpreting it in a slightly different way. To recall how the interferometer system operates, in essence the difference in range is measured. This difference is the same within a constant factor as the difference in phase between signals arriving at two separate antennas. Equation 16.33 gives the error in determining the difference in range; in the way this equation was derived, this error was the difference in range between zero range and out to the target and back. This error may also be interpreted as the difference in range between two signals from the target as used in determining angles in the interferometer. Interpreting the equation in this manner, then, and inserting a factor of $\sqrt{2}$ to account for independent errors on each leg, the error in angle of arrival becomes

$$\delta\alpha = \frac{\delta R'}{d} = \frac{\dfrac{10^9}{2\pi \cdot 2 \cdot 10^9 \sqrt{(100)(10.4)}}}{2000} \simeq 1.2 \cdot 10^{-6} \text{ radians} \tag{16.44}$$

where $\delta R'$ is interpreted as being the error in determining difference in range at the two ends of the interferometer base line. We use, in the equation for range error, not the ranging subcarrier but the actual carrier frequency, since this is ordinarily used in making this determination. Again we also use $K = 100$; there are approximately 100 possible independent measurements of range difference in a 1-sec interval when the system bandwidth is 100 cps/sec. This error, eq. 16.44, can be compared with the error induced by the troposphere by making a calculation based on eq. 16.27.

$$\delta\alpha = \frac{\sqrt{2} \cdot (10{,}000)(500) \cdot 1/2 \cdot 10^{-6}}{2000} \simeq .79 \cdot 10^{-6} \text{ radians} \tag{16.45}$$

In the present example, at any rate, the errors induced by possible tropospheric fluctuations are roughly the same order of magnitude as those induced by the signal-to-noise ratio fluctuations in the measurement. This is perhaps the way the system should be designed since the tropospheric fluctuations cannot be reduced by any method available to the designer short of increasing the base line length or raising his equipment above the troposphere. The signal-to-noise ratio errors can, of course, be reduced simply by using larger antennas either in the vehicle or on the ground, by using more power, by improving the noise figure of the receiver, etc.

It is of interest to calculate the actual physical size of the ground antenna required by this system. Making use of eq. 16.18 and noting that the reception cross section of an antenna is ordinarily approximately equal to its actual geometrical or physical cross section when viewed normal to the axis (for at least the commonly used parabolic reflector antenna), with the parameters above, is obtained

$$\begin{aligned}\text{Radius of antenna reflector} = r &= \sqrt{\sigma_r/\pi} \\ &= \sqrt{(1/2)^2(1000)/4\pi^2} \\ &\simeq 2.5\ \text{ft} \qquad (16.46)\end{aligned}$$

Here the ground antennas are a very reasonable size, being 5 ft in diameter. It is apparent that we could, by increasing this by a factor of 2 or 3, increase signal-to-noise ratio very appreciably and thus decrease some of the errors just calculated.*

We have by no means given a complete analysis of this particular system; indeed this material should be considered only a rough first approximation to any such analysis. It does illustrate, however, the sorts of calculations that must be made, the magnitudes of the numbers that are likely to be used in these calculations, and the magnitudes of the answers. The accuracies quoted are probably achievable in the field without undue complication in the actual circuitry and equipment design. It must be reiterated that these errors as calculated here are to be considered as fundamental errors,

---

*An ideal antenna has been assumed for this calculation. Actually an antenna "efficiency" of 0.5 to 0.7 is more nearly practicable. This means that the theoretical gain and cross-sectional area figures will only be realized with an antenna from 1/0.5 to 1/0.7 times as large as indicated by the formula.

errors that cannot be reduced simply by improving circuitry design or by improving circuitry components. In this light, of course, it is also possible that the errors calculated here may not be realized because of errors in actual circuitry components. Again, it is beyond the scope of this chapter to treat actual receivers, transmitters, circuits—all subjects for a far larger volume than this one. However, remember that the errors in the actual practical component must be very carefully controlled if the accuracy fundamentally inherent in this system is to be attained.

16.1 CONCLUSION

Radio guidance systems depend for their operation on a simple application of certain principles of electromagnetic wave propagation as typified by the approximate solutions of geometric optics. All the common principles of operation for radio guidance systems are easily understood and explained on the basis of this simple picture of electromagnetic wave propagation. The primary problem in applying these methods of radio measurement lies in proportioning the general design and dimensions of the equipment so that the internal inadequacies of circuitry are secondary and the external nonreduceable sources of noise are controlling, at least if the ultimate in sensitivity of measurement is desired. Also necessary are adequate power signal-to-noise ratios and, possibly adequate control of the ground reflections.

REFERENCES

1. H. Bremmer, "Propagation of Electromagnetic Waves," Handbuch der Physik, Vol. 16, Springer-Verlag, Berlin, 1958, pp. 423-638.
2. A. Marêchal, "Optique Geomêtrique Generale," Handbuch der Physik, Vol. 24, Springer-Verlag, Berlin, 1956, pp. 44-170.
3. S. K. Mitra, The Upper Atmosphere, second edition, The Asiatic Society, Calcutta, 1952, p. 180.
4. S. Silver, Microwave Antenna Theory and Design, Radio Laboratory Series, Vol. 12, McGraw-Hill, New York, 1949, p. 173.
5. S. Silver, Loc. cit., p. 4.
6. C. L. Temes, "Relativistic Consideration of Doppler Shift," IRE Trans. on Aeronaut. Navigational Electronics, ANE-6, 37 (1959).
7. A. D. Wheelon, "Near Field Corrections to Line-of-Sight Propagation," Proc. IRE, 43, 1949 (1955).
8. J. W. Herbstreit and M. C. Thompson, "Measurement of the Phase

of Radio Waves Received over Transmission Paths with Electrical Lengths Varying as a Result of Turbulence," Proc. IRE, 43, 1391 (1955).

9. M. Spencer, Proc. Phys. Soc. (London), B68, 493 (1955).
10. D. E. Kerr, Propagation of Short Radio Waves, Radio Laboratory Series, Vol. 13, McGraw-Hill, New York 1951, p. 31.
11. H. T. Friis, "Noise Figures of Radio Receivers," Proc. IRE, 32, 419 (1944).
12. H. C. Ko, "The Distribution of Cosmic Radio Background Radiation," Proc. IRE, 46, 208 (1958).

17

INERTIAL GUIDANCE FOR BALLISTIC VEHICLES

W.T. Russell

17.1 INTRODUCTION

Inertial guidance is based on the measurement of vehicle acceleration by instruments mounted within the vehicle. It has the advantage of being entirely self-contained. There are none of the line-of-sight limitations or propagation disturbances found in radar guidance, nor is dependence placed on clear weather for star sightings. No radiation to or from the vehicle is needed. The technique has the disadvantage that for long flight durations the velocity and position errors may become quite large. Inertial guidance is based on simple applications of Newton's laws, but it is only in the last ten years that the basic sensing instruments have been developed with sufficient accuracy to make the method competitive with other means. Much of the development has been dome for military weapons systems and performance figures, and details of specific systems remain classified information. The general principles are, however, no more classified than the principles of radar, control system theory, and classical mechanics.

Inertial guidance systems can be classified into two broad categories. First are systems for operation at essentially constant altitude. They are used in airplanes, surface ships, and submarines. Such systems are really two-dimensional insofar as inertial operation is concerned, and they use altimeters for measurement of the vertical or third dimension. Almost all the literature on inertial guidance pertains to this class of system.[1-4] The second class of inertial guidance system is intended for use in rocket-propelled vehicles in which altitudes and vertical velocities are great and operation beyond the earth's atmosphere is necessary. This is the typical application for space flight, and only this class of system will be discussed in this chapter.[5]

The basic conceptual elements of inertial guidance systems are an attitude reference, a vector accelerometer, a computer, and a clock. The attitude reference is a mechanical device which is carried within the vehicle and which establishes the reference frame for determining the direction of the acceleration. At the start of the flight it is placed at some known orientation, and during the flight it either maintains this orientation or is rotated in a known manner relative to it. At present all practical attitude references employ gyroscopes. The vector accelerometer measures the three components of the acceleration of the vehicle. Normally three single-degree-of-freedom instruments are employed, mounted so that their input or sensitive axes are orthogonal. The computer is used to integrate acceleration to obtain velocity and position, to calculate the effects of gravity, and to compute steering and engine thrust commands. The clock furnishes time information which is used to compute the motion of the earth or of other bodies in space. These four conceptual elements are not necessarily separate pieces of hardware. For instance, integration and other computing tasks are often done in the accelerometer. In addition to these elements ground equipment is needed at the launch point to orient the attitude reference, to insert instructions into the computer, and to check out and prepare the air-borne equipment for launch.

Associated with the guidance system, but conceptually distinct, is the vehicle control system which physically steers the vehicle and maintains the pitch, roll, and yaw angles at the proper values in the presence of external disturbances. The control system changes the direction of the vehicle thrust vector (usually by changing the vehicle attitude) as commanded by the guidance system. Functional elements of the guidance system and of the control system are frequently mechanized together.

To perform successful inertial navigation and guidance, a detailed quantitative knowledge is needed of the shape of the earth, of gravity fields, and of the location of objects on the earth or in space. These subjects are frequently included in a discussion of inertial guidance, but they are really part of the science of mapping and geophysics and will not be discussed here.

In this chapter some of the important characteristics of gyroscopes, accelerometers, stabilized platforms, and vehicle control systems are presented. The effect of gravity on the inertial guidance problem is considered, and the broad subject of guidance schemes for rocket-propelled vehicles is explored. Finally, an example of an inertial guidance system for a ballistic vehicle is presented.

17.2 GYROSCOPES

17.2.1 Description

Gyroscopes are invariably used to establish the air-borne attitude reference for inertial guidance systems.[6] For precision systems the gyros are usually mounted upon a servo-driven stabilized platform. They serve as precision instruments which sense small rotations relative to inertial space. They thus operate as angular error detectors over a very small range around their reference or null positions. Gyros for inertial systems of medium accuracy or gyros that form the attitude reference of the vehicle control system are frequently mounted directly to the vehicle structure. However, the vehicle itself is controlled in attitude so that it serves as a large stabilized platform for the structure-mounted gyros. The gyros considered here can be contrasted with aircraft instrument gyros which have wide angular capability but low accuracy. The gyros can also be contrasted with large gyros which are used primarily to furnish a resisting torque to a forced precession rather than to remember a reference orientation.

Gyros can be classified as having a single degree of freedom or two degrees of freedom. Each class has its proponents, but the relative advantages and disadvantages of the two types are probably overshadowed by differences among specific designs. Single-degree-of-freedom gyros can be further classified as rate gyros, integrating gyros, and undamped gyros. At the present time commercially available gyros that are suitable for guidance systems weigh from 1 to 3 lb and have a maximum linear dimension of about 5 in. However, rapid progress is being made in the development of smaller and more accurate instruments.

Gyro operation is based on the familiar physical fact that when a torque is applied to a spinning wheel so as to change the direction of the spin axis (angular momentum vector), the spin axis tends to align itself with the torque vector. Stated another way, a torque applied perpendicular to the spin axis causes the spin axis to rotate about an axis perpendicular to the spin and torque axes. This rotation is called precession. Conversely, when the axis of a spinning wheel is forcibly precessed, the wheel exerts a torque about an axis perpendicular to the spin and precession axes. In the absence of any torque, the gyro spin axis does not rotate relative to inertial space.

17.2.2 Two-Degrees-of-Freedom Gyros

Figure 17.1 is a schematic of a two-degrees-of-freedom gyro. The gyro wheel is mounted on spin bearings in the in-

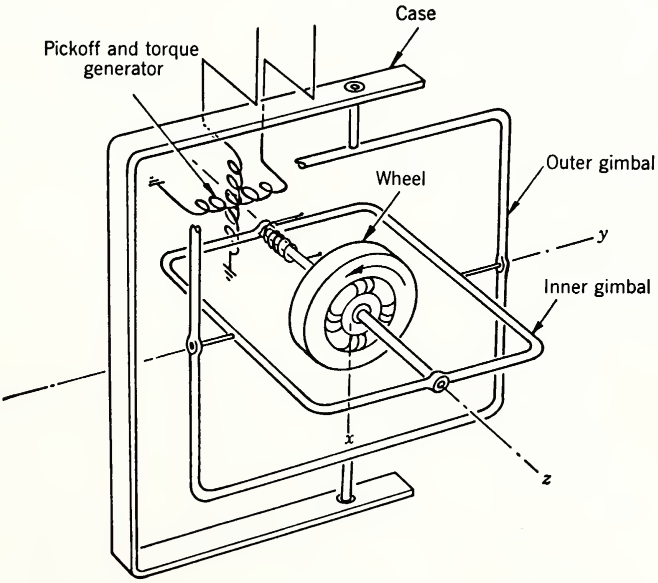

Fig. 17.1 Two-degrees-of-freedom gyro.

ner gimbal and is driven at a constant angular velocity by the spin motor. Bearings between the inner and outer gimbal and the outer gimbal and case permit the case to have rotational freedom relative to the inner gimbal. A pickoff is provided between the inner gimbal and the case to sense the relative angular motion about the two sensitive axes (x and y in Fig. 17.1). A torque generator is used to apply known torques to the wheel and inner gimbal. Prior to flight, the gyro wheel is brought up to speed and torques are applied to precess the inner gimbal to the reference or zero position of the pickoff. During flight, any small motion of the case relative to inertial space about one of the sensitive axes is detected by the pickoff, and this signal is used to drive a platform servo motor which rotates the case to its original orientation relative to the spin axis.

Any stray or uncertainty torques acting about a sensitive axis will cause a precession which is termed a drift rate. This drift represents a loss in attitude reference and is an instrument error. Torques that can cause drift arise from gimbal unbalances, from friction in the gimbal bearings, and from reaction torques in the pickoff, torque generator, and the leads used to conduct power to the spin motor and to elements of the pickoff mounted on the inner gimbal. The prime problem in gyro design is to make the uncertainty torques as small as possible.

The essential features of operation of all types of gyros can be explained by classical rigid-body mechanics.[7] Using symbols defined at the end of this section, we find that the equations of motion of the inner gimbal are

$$\vec{T} = \frac{d\vec{H}_t}{dt} \tag{17.1}$$

$$\vec{H}_t = I_{xx}\,\omega_x\,\vec{i} + I_{yy}\,\omega_y\,\vec{j} + (I_{zz}\,\omega_z + H)\,\vec{k} \tag{17.2}$$

Substituting eq. 17.2 into 17.1 and expressing in component form gives

$$T_x = I_{xx}\,\dot{\omega}_x + \omega_y\,\omega_z(I_{zz} - I_{yy}) + \omega_y H \tag{17.3}$$

$$T_y = I_{yy}\,\dot{\omega}_y + \omega_x\,\omega_z(I_{xx} - I_{zz}) - \omega_x H \tag{17.4}$$

$$T_z = I_{zz}\,\omega_z + \omega_x\,\omega_y(I_{yy} - I_{xx}) \tag{17.5}$$

These equations are in terms of an orthogonal coordinate system (shown in Fig. 17.1) which is fixed in the inner gimbal and directed along the principal axes of inertia. It is assumed that the spin angular velocity of the wheel relative to inertial space is a constant; that is, coupling between the inner gimbal and wheel through the spin motor is neglected. The last terms on the right in eqs. 17.3 and 17.4 are much larger than the others so that in approximate form the gyro equations are

$$T_x = \omega_y H \tag{17.6}$$

$$T_y = -\omega_x H \tag{17.7}$$

One of the interesting motions of a gyro is called nutation. Its essential features can be seen by considering the solution of eqs. 17.3, 17.4, and 17.5 for no external torques and for ω_z assumed (or constrained by instrument construction) to be zero:

$$0 = I_{xx}\dot{\omega}_x + \omega_y H \tag{17.8}$$

$$0 = I_{yy}\dot{\omega}_y - \omega_x H \tag{17.9}$$

In these equations I_{xx} includes the outer gimbal inertia. The solution of the equations represent a conical motion of the spin axis such that a point on the spin axis moves in an ellipse:

$$\omega_y = A \sin(\beta t + \phi) \tag{17.10}$$

$$\omega_x = \sqrt{I_{yy}/I_{xx}}\ A \cos(\beta t + \phi) \tag{17.11}$$

$$\beta = \sqrt{H^2/I_{xx} I_{yy}} \tag{17.12}$$

The initial conditions fix A and ϕ; β is called the nutation frequency. In practical instruments damping torques act on the inner gimbal and nutation frequencies are kept high; consequently, nutation is seldom an important factor. The complete analysis including gimbal dynamics and nonorthogonal gimbals becomes quite complicated.[8]

Figure 17.2 is a schematic of the two-degrees-of-freedom gyro manufactured by the Arma Division, American Bosch Arma Corporation. The inner gimbal consists of a spherical shell or float which contains the gyro wheel assembly. The float is suspended in a liquid which has the same density as the float. The float is centered in the case by fine suspen-

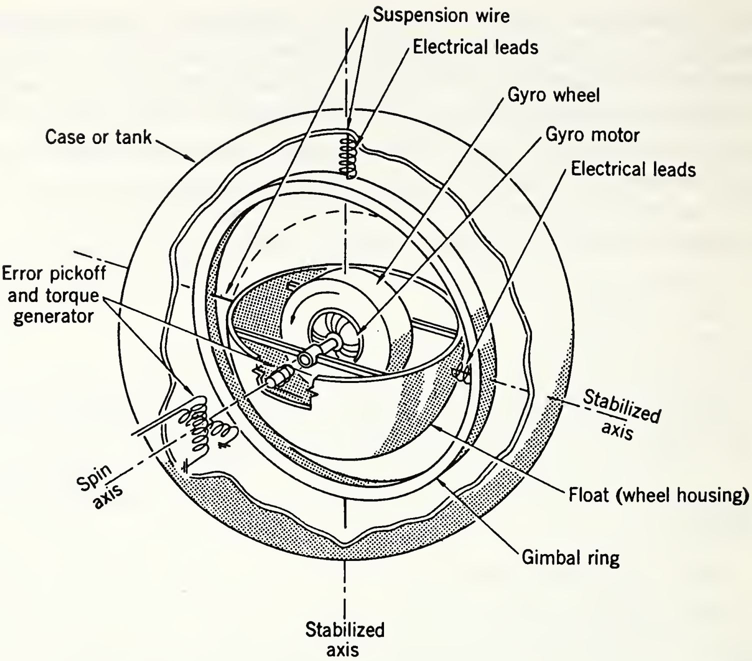
Suspension wire
Electrical leads
Gyro wheel
Gyro motor
Electrical leads
Case or tank
Error pickoff and torque generator
Stabilized axis
Spin axis
Float (wheel housing)
Gimbal ring
Stabilized axis

Fig. 17.2 Arma-type two-degrees-of-freedom gyro.

sion wires and by an intermediate gimbal which is also at neutral buoyancy in the fluid. This method of suspension elim-

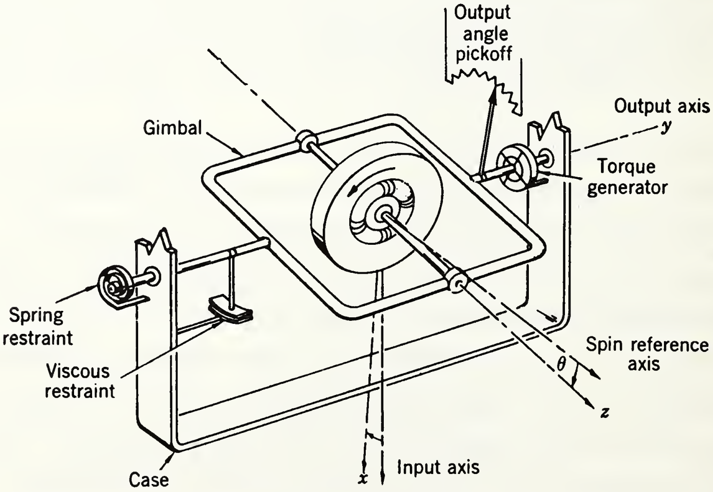
Output angle pickoff
Gimbal
Output axis
y
Torque generator
Spring restraint
Viscous restraint
Spin reference axis
θ
z
Case
x
Input axis

Fig. 17.3 Single-degree-of-freedom gyro.

inates the gimbal bearings which can be a source of uncertainty friction. A two-degrees-of-freedom electromagnetic pickoff and a torquer are employed. The gyro is intended for use on stabilized platforms, and for the small motions encountered with a proper servo design the suspension wires have a negligible spring torque. Since the gyro operates about a null, the net precession caused by the fluid damping torques is zero. As in any gyro it is necessary to minimize torques arising from such causes as unsymmetrical fluid currents, from static unbalance of the float or gimbal, and from residual torques in the suspension wire when the pickoff signal is at a null. Gyro temperatures must be controlled so that the flotation fluid is within the proper density range for buoyancy of the float.

17.2.3 Single-Degree-of-Freedom Gyros

Figure 17.3 is a schematic of a single-degree-of-freedom gyro (SDF). It contains a single gimbal which is free to rotate relative to the case about the output or y-axis. The spin axis z is perpendicular to the output axis. The spin reference axis is fixed in the case and by definition is coincident with the spin axis when the pickoff or output signal is at its null or reference value. The angle between these axes is called the output angle θ. The input axis is fixed in the gyro case perpendicular to the output and spin reference axes. It is coincident with the x-axis when the output angle is zero. The principal input quantity is a rotation of the case, relative to inertial space, about the input axis. This rotation is transmitted to the gimbal and wheel through the gimbal bearing and constitutes a forced precession of the gyro wheel. The forced precession makes the gyro wheel exert a torque, called the gyroscopic torque, upon the gimbal about the output axis. This torque is balanced by the inertial reaction torque of the gimbal, by a viscous restraint torque proportional to gimbal angular velocity relative to the case, and by a spring restraint torque proportionto gimbal angle relative to the case. Depending on which term is predominant, the SDF gyro is termed an integrating or position gyro, or a rate gyro. Known external torques can be applied to the gimbal by means of a torque generator. As with the two-degrees-of-freedom gyro, uncertainty and bias torques of various origins exist, causing gyro drift.

The input-output relationship for the gyro can be obtained from eq. 17.4. The relationship involves motion of the case; therefore a coordinate conversion between the axes fixed in the case and those fixed in the gimbal is necessary. This relationship is

$$\omega_y = \dot{\theta} + \omega_o \tag{17.13}$$

$$\omega_x = \omega_i \cos\theta - \omega_s \sin\theta \tag{17.14}$$

$$\omega_z = \omega_s \cos\theta + \omega_i \sin\theta \tag{17.15}$$

The T_y term of eq. 17.4 becomes

$$T_y = -b\dot{\theta} - k\theta + T_e \tag{17.16}$$

Substitution of these relationships into eq. 17.4 gives

$$\begin{aligned} H\omega_i \cos\theta + T_e = {} & I_{yy}\ddot{\theta} + b\dot{\theta} + k\theta + H\omega_s \sin\theta + I_{yy}\dot{\omega}_o \\ & + (I_{xx} - I_{zz})\left[\tfrac{1}{2}\sin 2\theta(\omega_i^2 - \omega_s^2) + \omega_s\omega_i \cos 2\theta\right] \end{aligned} \tag{17.17}$$

The last term in this equation must be modified if the principal axes of inertia of the gimbal and wheel are not coincident with the spin and output axes. The term should be considered in analyzing some gyro drift effects, but is is generally unimportant and will be omitted in what follows. For small output angles eq. 17.17 thus becomes

$$H\omega_i + T_e = I_{yy}\ddot{\theta} + k\theta + b\dot{\theta} + H\omega_s\theta + I_{yy}\dot{\omega}_o \tag{17.18}$$

The last two terms on the right are cross-coupling terms which must be considered in the design of the stabilized platform or of the complete system using the gyro. Since the gyro operates about a null, the values of ω_i, ω_s, and ω_o can usually be considered as those obtained from operation in the platform servo loop plus the sinusoidal and random oscillation arising from vibration. With oscillations of proper phase relationship, the cross-coupling terms and the noncommutativity of finite rotations can cause a gyro drift.[9-11] The T_e term acts on the gyro like an input angular rate and hence acts to change the reference orientation of the gyro. The torque T_e consists of that obtained from the torque generator plus all extraneous, uncertainty, and other torques which are undesirable and contribute to gyro drift or noise in the output. Physically this torque moves the inner gimbal against the inertia, viscous, and spring restraints to give an output angle and hence output signal. This signal drives a servomotor which rotates the platform at an angular rate such that the gyro torque $H\omega_i$ just balances the applied torque T_e and the spring-restraint torque.

If the cross-coupling terms are omitted, the gyro transfer function becomes

$$\theta = \frac{H\omega_i + T_e}{I_{yy} s^2 + bs + k} \tag{17.19}$$

A typical rate gyro might have a characteristic function with an undamped natural frequency of about 25 cps and a damping factor of about 0.5 critical. Rate gyros are frequently used for stabilization in a missile control system but are normally not used in inertial guidance systems. For an integrating or position gyro the spring restraint is negligible and the transfer function becomes

$$\theta = \frac{H}{b}\,\frac{\omega_i}{s}\,\frac{1}{(I_{yy}/b)\,s+1} + \frac{T_e}{bs}\,\frac{1}{(I_{yy}/b)\,s+1} \tag{17.20}$$

A typical value for the time constant I_{yy}/b is about 1 or 2 msec. This delay is unimportant for most applications, and therefore the output signal for input motions is essentially proportional to the time integral of the input angular velocity or to the small input angle turned from the reference position:

$$\theta = \frac{H}{b} \int \omega_i \, dt = \frac{H}{b}\,\theta_i \tag{17.21}$$

Undamped gyros usually have a gas or hydrodynamic output axis bearing in which the damping term and the spring term are small. In this case the output signal for input motions is essentially proportional to the time integral of the input angle:

$$\theta = \frac{H\omega_i}{I_{yy} s^2} \tag{17.22}$$

$$\theta = \frac{H}{I_{yy}} \int \theta_i \, dt \tag{17.23}$$

Single-degree-of-freedom gyros develop a resisting torque about the input axis when forcibly precessed. In an integrating gyro this torque is small and can usually be neglected in platform servo analysis. However, it may be of prime importance in an undamped gyro.

In simplified form the torque is

$$T_x \approx \omega_y H \approx \dot{\theta} H \approx \frac{H^2}{b}\omega_i \frac{1}{(I_{yy}/b)s + 1} \approx \frac{H^2}{I_{yy}} \frac{\omega_i}{s} \qquad (17.24)$$

Figure 17.4 is a schematic drawing of the hermetic integrating gyro (HIG) originally developed by Dr. C. S. Draper at the Instrumentation Laboratory, Massachusetts Institute of Technology.[12] Various commercial versions differ in mechanical detail and in the type of signal generator and torque generator used, but the family resemblance is quite strong. The gyro wheel is contained in a hermetically sealed float which is suspended in a fluid at neutral buoyancy. A shaft attached to the float carries the rotor elements of the signal and torque generators. Jewel pivots are provided at either end of the shaft to center the float. The fluid is quite viscous and, since the fluid is at neutral buoyancy, the jewel pivots have negligible radial forces and thus contribute negligible friction torques about the output axis. Means are provided for balancing the float and for temperature control. The instrument is simple in concept, but to achieve high precision extreme care must be taken in design and fabrication detail.

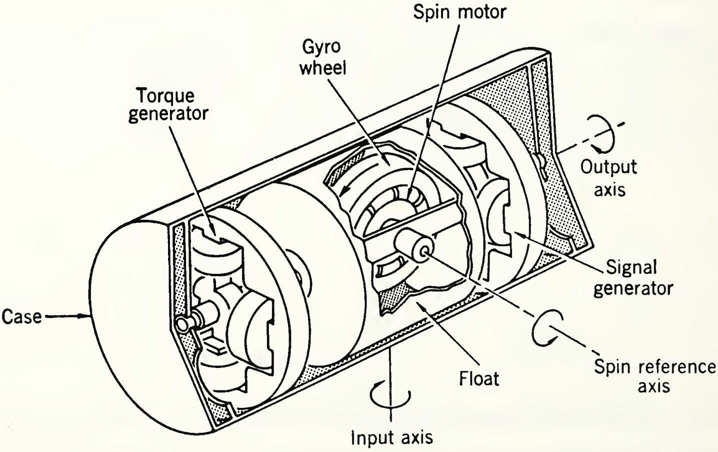

Fig. 17.4 HIG gyroscope.

17.2.4 Gyroscope Drift

Gyro drift is a subject which deserves special mention. Drift rate effects are frequently classified into three groups. First are those that are independent of applied translational acceleration. These include spring torques from power and signal leads to the float or reaction torques from the signal and torque generators. The second group includes those proportional to the acceleration. The chief source of drift here is the static unbalance of the inner gimbal assembly, that is, the displacement between its center of mass and its center of support or buoyancy. The third group consists of drift rates proportional to the square of acceleration. This is commonly called the nonisoelastic or compliance effect. Figure 17.5 shows the situation schematically. The applied acceleration causes inertia force components to act on the center of mass. These forces cause displacements of the center of mass relative to the center of support that are proportional to the compliances of the wheel and gimbal assembly in the respective directions. If the compliances C_x and C_z are unequal, the displacement vector will have a component normal to the vector acceleration and a torque will result. By using the coordinates and nomenclature shown in Fig. 17.5, this torque can be calculated as

$$F_z = ma_z = ma \sin \phi$$

$$F_x = ma_x = ma \cos \phi$$

$$\delta_z = C_z F_z = C_z ma \sin \phi$$

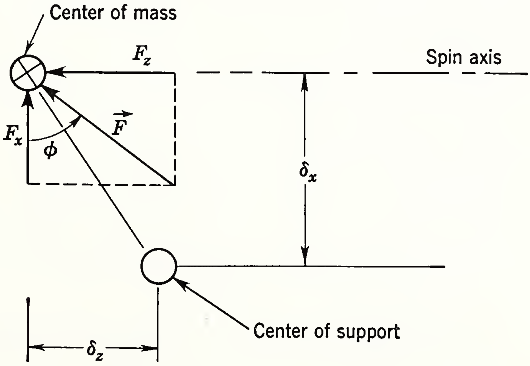

Fig. 17.5 Compliance effects.

$$\delta_x = C_x F_x = C_x ma \cos \phi$$

$$T_y = F_x \delta_z - F_z \delta_x$$

$$T_y = \frac{m^2 a^2 \sin 2\phi}{2} (C_z - C_x) \qquad (17.25)$$

The nonisoelastic torque is at a maximum when the applied acceleration is midway between the input axis and spin axis. Note that a steady drift can arise from this source when the applied acceleration is oscillatory.

Usually for a given specific gyro a portion of the gyro drift is repeatable. That is, the individual gyro can be calibrated, and suitable compensation torques can be applied. The remaining portion is not repeatable and is the part that is generally called the random or uncertainty drift. The equations just given neglect the effect of the frequency of the applied acceleration on drifts. In practice, internal resonances of the gyro occur at frequencies above a few hundred cycles per second, and in a complete analysis all these internal dynamic effects should be included.

A typical value of angular momentum for a precision gyro is 10^6 dyne-cm-sec. If the drift rate is to be less than, say, 0.2°/hr (10^{-6} radians/sec), by eq. 17.7 the uncertainty torques must be less than 1 dyne-cm.

17.2.5 Nomenclature Relating to Gyroscopes

b	Linear viscous drag coefficient
H	Spin angular momentum of gyro wheel
H_t	Total angular momentum
I_{xx}, I_{yy}	Principal moments of inertia of inner gimbal and wheel
I_{zz}	Principal moments of inertia of inner gimbal
k	Spring coefficient
s	Laplace transform variable
T	Torque applied to the inner gimbal
T_e	External torques acting on a single-degree-of-freedom gyro; includes known torques from the torque generator and uncertainty or nonlinear effects which cause drift
ω_x, ω_y, ω_z	Angular velocity components of the inner gimbal with respect to inertial space
β	Nutation frequency

ω_i , ω_s , ω_o	Angular velocity components of the inner gimbal with respect to inertial space along the input axis, spin reference axis, and output axis respectively.
θ	Angle between the gimbal and case in a single-degree-of-freedom gyro
$\theta_i = \int \omega_i \, dt$	Angle turned about the input axis relative to inertial space

17.3 ACCELEROMETERS

Three single-degree-of-freedom orthogonally mounted accelerometers are commonly used to measure the vector acceleration of rocket-propelled vehicles. They must work over a very wide range of input values with great precision and under severe conditions. Figure 17.6 is a schematic of an accelerometer which shows the basic elements involved.

The instrument operates by applying force to a seismic mass inside the instrument case so that except for instrument dyanmics the acceleration of the mass is equal to the acceleration of the case. The force used to accelerate the mass along the input axis is measured in terms of some physical quantity which is proportional to the force. For instance, if the force generator is a simple spring, force is measured by the deflection of the spring. A common force generator is ob-

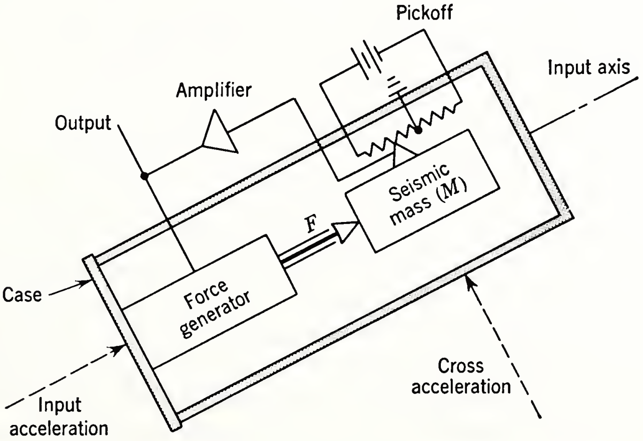

Fig. 17.6 Basic accelerometer.

tained by applying current to a coil in a magnetic field. As shown in the figure, the current is obtained by feedback from a pickoff which is sensitive to the relative motion between the mass and case along the input axis.

For a nonrotating instrument, Newton's law applied to the mass is

$$a = F/M + g \tag{17.26}$$

where a = acceleration of seismic mass along input axis
F = all nongravitational forces acting on seismic mass along input axis
M = mass of seismic mass
g = component of gravity along the input axis.

This equation, which will be called the acceleration equation, shows that an accelerometer does not measure acceleration but rather the difference between acceleration and gravity. This difference, which is equal to the quantity F/M, has been called thrust acceleration a_t. The nomenclature stems from the fact that F/M for the accelerometer is equal to the corresponding quantity for the complete missile, that is, to the sum of the nongravitational forces acting on the missile, divided by the instantaneous mass of the missile. Most of the nongravitational force acting on a rocket-propelled missile is thrust, hence the term thrust acceleration. To obtain the acceleration, gravity must be calculated in the computer and added to thrust acceleration. Gravity acceleration is a function of position in space and of time, in the sense that the relative positions of the planets change with time. It is important that the meaning of the terms in eq. 17.26 be made quite clear.

Acceleration as used here is acceleration relative to any specified freely falling reference frame, that is, to a frame which is acted upon by gravitational mass attraction forces only. The free-fall reference frame most frequently used is one located at the center of the earth and therefore freely falling in the sun's gravitational field (plus that of the moon and planets). A free-fall reference frame moving with a satellite is useful for flights in the vicinity of a satellite. For ballistic missile use a free-fall reference frame which has the velocity and position of the missile at termination of powered flight is useful. This frame is called the correlated frame and its velocity, as a function of time, is called the correlated velocity. It should be noted that an accelerometer which is freely falling, as for instance in a satellite, will have a zero output.

Gravity, in eq. 17.26, means the difference in the gravitational force per unit mass between the location of the accelerometer and the location of the free-fall reference frame. For flights near the surface of the earth, with a free-fall reference frame at the earth's center, this difference in gravity is due almost entirely to the earth's gravity field, and the difference in the sun's gravity field at the two locations can be neglected. For flights near a satellite the difference in gravity between the satellite and the accelerometer may be negligible. In this case the thrust acceleration measured by the accelerometer is essentially the actual acceleration relative to the satellite. An accelerometer mounted vertically on the surface of the earth measures the upward "thrust acceleration" of the support on the case of the instrument. Gravity acceleration is a computed downward quantity. The difference between these quantities is the centrifugal acceleration of the instrument caused by the rotation of the earth on its axis. It should be noted that some authors use the term "gravity" to denote the combination of gravitational attraction and the centripetal acceleration due to the rotation of the earth.

The time integral of the acceleration is the velocity, that is, the velocity of the accelerometer relative to the free-fall reference frame. The time integral of thrust acceleration and gravity acceleration are called thrust velocity and gravity velocity.

It is important that all the forces acting on the seismic mass along the input axis be measured. For instance, any static friction between the mass and its support will lead to errors. However, perfectly linear constraint forces, as for instance from fluid damping, will only affect instrument dynamics because the time integral of such forces will be zero. The instrument case must be stiff so that it will not deflect under cross acceleration and thereby make the accelerometer sensitive to a component of cross acceleration.

Figure 17.7 is a schematic of a practical type of instrument based on the HIG gyro construction described in Section

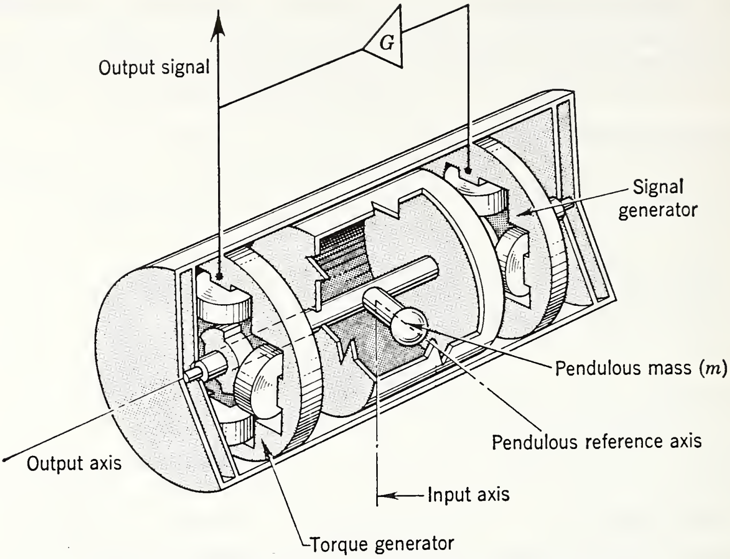

Fig. 17.7 Constrained pendulum accelerometer.

17.2. The seismic mass exists in the form of a pendulum, and the force generator is an electromagnetic torque generator. The pickoff is the signal generator. Flotation virtually eliminates uncertainty friction torques at the pivots. Because of the pendulous mass, acceleration of the instrument along the input axis creates a torque about the float pivot axis. This torque causes rotation of the float and a consequent signal generator voltage proportional to θ. This voltage is used to generate a current which is applied to the torque generator to give a torque which "constrains" the pendulum and keeps θ small. The current I is thus proportional to acceleration along the input axis. The gain of the feedback system must be kept quite high so that deflection of the pendulum under high input acceleration is small. Otherwise, a "cross-talk" torque is developed which is proportional to the product of the acceleration along the pendulous reference axis and the sine of the deflection angle θ. Instruments of this type, called force feedback pendulums or constrained pendulums, are available commercially. Inaccuracies can arise if the zero set or gain of the elements in the feedback loop drift from their calibrated values.

Velocity and position are the quantities of interest in space navigation, rather than acceleration. Increased accuracy and reliability may sometimes be obtained by performing integration in the accelerometer and in effect turning it into a velocimeter. Basically, this is done by making the force acting on the seismic mass proportional to a rate of some kind. For instance, the current fed to the torque generator in Fig. 17.7 might be applied in pulses of constant area but variable rate. Pulse rate is then proportional to acceleration and total number of pulses to velocity.

Another practical instrument, one used by the Germans in the V-2 rocket of World War II, is the pendulous gyro accelerometer (PGA). This integrating accelerometer is essentially a force feedback pendulum in which the force generator is a gyroscopic element. Figure 17.8 is a schematic of such an instrument based on the HIG gyro construction. The output of the signal generator is fed to the servomotor which rotates the gyro case about the input axis at a rate such that the torque developed by the gyro element just equals the pendulous torque. The steady-state torque balance about the float axis is essentially

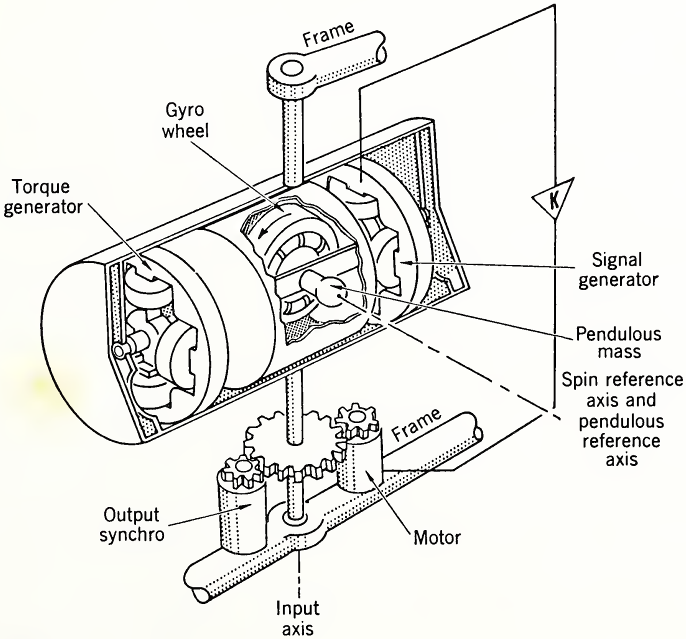
Frame
Gyro wheel
Torque generator
K
Signal generator
Pendulous mass
Spin reference axis and pendulous reference axis
Frame
Output synchro
Motor
Input axis

Fig. 17.8 Pendulous gyro accelerometer (PGA).

$$H\omega_i = mla_t \tag{17.27}$$

where ml is the pendulosity and the other symbols have been defined previously. Hence,

$$\theta_i = \int \omega_i \, dt = \frac{ml}{H} \int a_t \, dt = \frac{ml}{H} v_t \tag{17.28}$$

The angular rate of the gyro case is thus proportional to thrust acceleration, and the total angle turned by the gyro case is proportional to thrust velocity. As with the instrument of Fig. 17.7, the gain of the feedback loop must be kept high so that θ is very small. The PGA has the advantage that the principal scale factor depends only on mechanical parameters and on the wheel angular momentum, and both quantities can be made very stable. Since the case rotates, the cross-talk error reverses with each revolution. The torque generator of the gyro can be used to apply additional torques to the gyro float, adding to the pendulous torque. In this way gravity may be added to the thrust acceleration to give vehicle acceleration and velocity as outputs.

17.4 STABILIZED PLATFORMS

A stabilized platform is commonly used as the attitude reference for inertial guidance systems.[13, 14] Gyroscopes are mounted on the platform and serve as error detectors for rotation of the platform from the initial reference orientation. The output signals of the gyros are used to drive torque motors which serve to keep the platform at the reference orientation. It is convenient to mount the accelerometers upon the platform so that they measure acceleration directly in terms of the reference frame in which navigation is accomplished. Figure 17.9 is a schematic of a typical stabilized platform. The gimbal rings and bearings serve as a ball-and-socket joint which permits the vehicle to rotate in any way about the platform. The figure shows a conventional or "outside-in" gimbal system in which the gimbal rings are external to the platform. An alternative design which is called "inside-out" has small gimbals located near the center of mass of the platform. The order of gimbaling shown in the figure is roll, yaw, and pitch and is convenient for ballistic missiles in which the launch is vertical and large pitch mo-

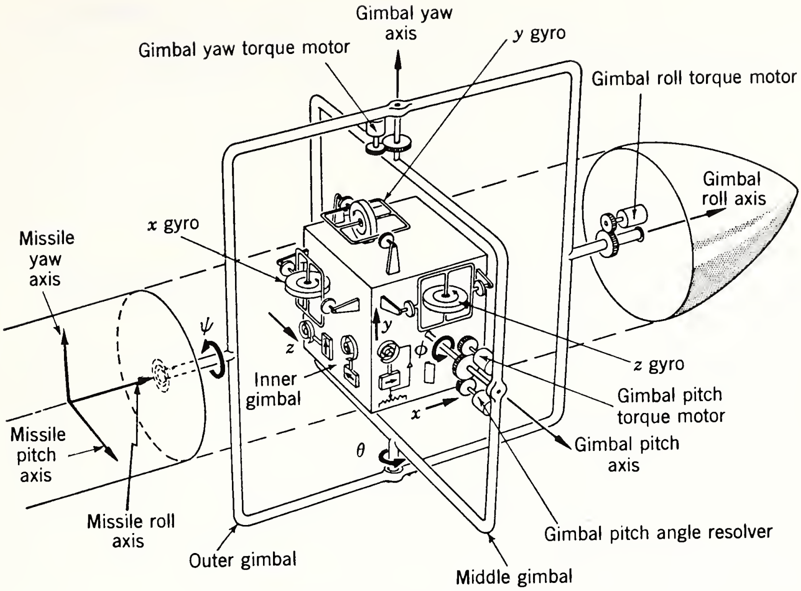
Gimbal yaw axis
Gimbal yaw torque motor
y gyro
Gimbal roll torque motor
Gimbal roll axis
Missile yaw axis
x gyro
ψ
z
y
φ
Inner gimbal
x
z gyro
Gimbal pitch torque motor
Missile pitch axis
θ
Gimbal pitch axis
Missile roll axis
Outer gimbal
Gimbal pitch angle resolver
Middle gimbal

Fig. 17.9 Stabilized platform.

tions are used. Other configurations are, of course, possible. One with pitch on the outside, an intermediate gimbal, and an azimuth gimbal for the inner platform is frequently used.

In the figure the platform axes (x, y, z) are shown parallel to the gimbal axes, which in turn are shown parallel with missile pitch, roll, and yaw axes. In the orientation shown, an output of the y gyro indicating a small rotation about the platform y-axis should be fed to the yaw torque motor to turn the platform about the gimbal yaw axis, thereby returning the platform to its original position. In a similar way, the output of the x gyro is fed to the gimbal roll torque motor. If, however, the platform is rotated to some angle ϕ about the pitch or z-axis relative to the position shown in the figure, the output of the x and y gyros must be resolved into components along the gimbal yaw and roll axes for proper operation of the servos. If resolution is not used, the gain in the yaw and roll servo loops is decreased and cross coupling is introduced. In a kinematic sense, at least, resolution will be proper if the three gyro outputs, which are the components along the platform axes of a small rotation, are resolved into components along the three gimbal axes. Angular rates (or small rotations) about the platform x-, y-, and z-axes resolved along the gimbal yaw axis, the normal to the gimbal yaw and pitch axes, and the gimbal pitch axis are

$$\dot{\theta} = \omega_y \cos \phi + \omega_x \sin \phi \tag{17.29}$$

$$\dot{N} = -\omega_y \sin \phi + \omega_x \cos \phi \tag{17.30}$$

$$\dot{\phi}_1 = \omega_z \tag{17.31}$$

The normal component is resolved along the gimbal pitch axis and gimbal roll axis and becomes

$$\dot{\psi} = \dot{N} \sec \theta \tag{17.32}$$

$$\dot{\phi}_2 = \dot{N} \tan \theta \tag{17.33}$$

The proper equations are thus

$$\dot{\psi} = \sec \theta(\omega_x \cos \phi - \omega_y \sin \phi) \tag{17.34}$$

$$\dot{\phi} = \dot{\phi}_1 + \dot{\phi}_2 = \omega_z + \tan \theta(\omega_x \cos \phi - \omega_y \sin \phi) \tag{17.35}$$

$$\dot{\theta} = \omega_y \cos \phi + \omega_x \sin \phi \tag{17.36}$$

If the missile yaws to 90°, the figure indicates that the gimbal roll axis and gimbal pitch axis become parallel and that one degree of freedom is lost. This situation is called gimbal lock and is prevented in vehicles in which large yaw motions are found by the addition of a fourth gimbal. In ballistic vehicles or spacecraft yaw motions are not large, and the resolution through the angle θ can usually be omitted. In the equations just given this is equivalent to making θ equal zero. Resolution of the x and y signals through the angle ϕ is done by a synchro resolver mounted on the gimbal pitch axis. Pickoffs can be used to obtain the gimbal angles, which can be used as the attitude reference for the vehicle control system. If this is done and if the vehicle has a large roll motion, as it might, for instance, during a vertical rise, additional resolution similar to that just described will be needed between the platform angles and the pitch and yaw axes of the missile attitude control system.

The design of the platform servos is a challenging problem in that high performance must be obtained with small weight and power consumption. Disturbing torques acting upon the platform include friction at the gimbal bearings and unbalances of the platform itself. Unbalance includes the effect of nonisoelastic deformation, as was explained in the section on gyros. In the servo design consideration must be given to compliance in the gimbal structure and to the shock mounts upon which the gimbal system may be mounted. Figure 17.10 is a simplified block diagram of one loop of the three-dimensional servo. A more sophisticated diagram would include the cross coupling through the gyros, eq. 24.17, and the feedback torque from the gyros caused by the forced precession, eq. 17.24. The latter effect may be predominant for an undamped gyro.[15] The loop senses an error in position but applies a correction torque which results in an acceleration. Some form of damping is thus required and is generally obtained by networks.

The assembly, consisting of the stabilized platform, the accelerometers, and the auxiliary electronics is sometimes called an inertial measurement unit (IMU). The accelerometers need not be oriented with their input axes parallel to the gyro input axes but may be directed to minimize the effect of various component errors or to satisfy the requirements of the guidance scheme (Section 17.7).

The platform must be aligned quite accurately at the start of the flight to some known external reference frame. One way that this can be done is to set the three gimbal angles to the desired values. This orients the accelerometers relative to the vehicle structure, which in turn must be oriented relative to the external reference frame. A much more accurate method is to level the platform by the use of precision levels or by outputs of the navigation accelerometers, and to orient it in azimuth by optically sighting on a mirror mounted on the platform from a theodolite external to the vehicle.

The earth rotates relative to inertial space, and to keep the

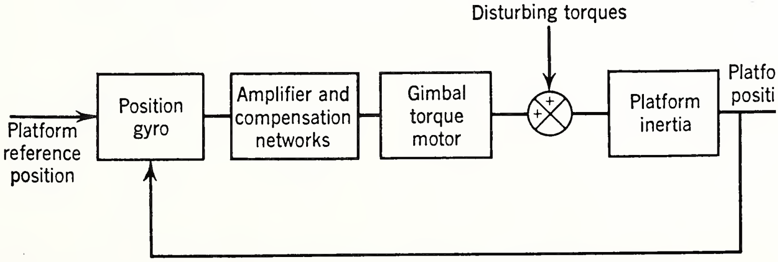

Fig. 17.10 Platform stabilization servomechanism.

platform properly aligned to an earth-fixed reference frame prior to launch, the gyros must be torqued at earth rate. The torquing signals can be obtained from the theodolite and the levels which then operate as error detectors in the alignment or erection loops.

17.5 ATTITUDE CONTROL SYSTEM

The purpose of the vehicle control system is to maintain the vehicle attitude or direction of the thrust vector at some commanded value. The control system is necessary no matter what type of guidance is used, that is, radio or inertial. Steering can be done in many ways. The German V-2 rocket employed fins in the airstream as well as carbon vanes in the rocket jet. Steering jets whose thrust line is perpendicular to the main engine thrust can be used. If disturbing torques are very small, as they may be in space flight, the control torques required are small and might be obtained from moving masses or even from control of the radiation pressure from the sun. A common method used for powered flight is to hinge the main rocket thrust chambers. Figure 17.11 is a schematic of the yaw channel for a vehicle employing this method of steering.

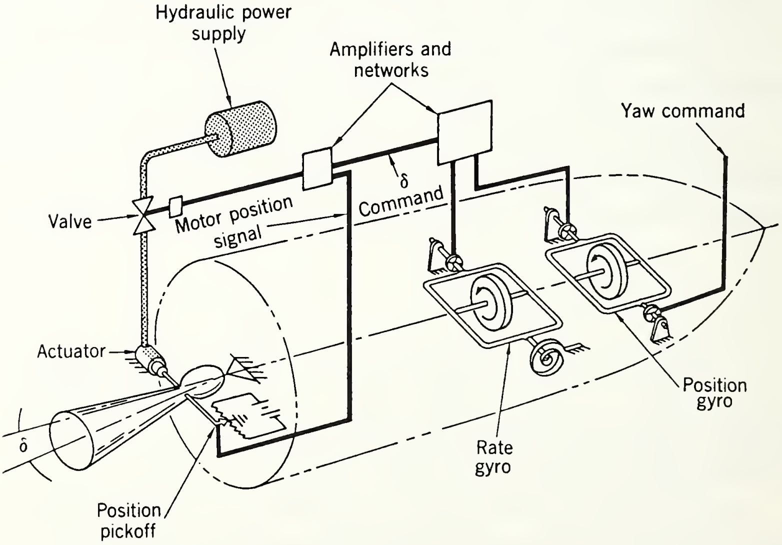
Hydraulic power supply
Amplifiers and networks
Yaw command
Valve
Motor position signal
δ Command
Actuator
δ
Position pickoff
Rate gyro
Position gyro

Fig. 17.11 Missile control system (yaw axis).

The roll and pitch control loops are similar to those in Fig. 17.9. However, if the missile has only one main rocket nozzle, auxiliary jets are required for roll control.

An angular error in vehicle attitude will result in an output from the position gyro. This output signal is amplified and sent to the power servomechanism as a thrust chamber position command. The signal is compared with the actual position obtained from the position pickoff, and any difference results in operation of the hydraulic valve. Hydraulic pressure is applied to the actuator to move the thrust chamber until the position, as measured by the pickoff, just equals the commanded signal. The rotated thrust vector causes an angular acceleration of the complete vehicle which results in an angular velocity and elimination of the angular position error. As just described, the control loop is oscillatory, and therefore some means must be provided for damping. For a short stiff vehicle, a lead network can be used in series with the position gyro output. For a flexible vehicle, however, bending of the structure causes severe problems, which may be overcome by using a properly placed rate gyro. The gyro should sense the rigid-body angular rate and should be located so that it is insensitive to bending. Other sensors such as angle-of-attack meters or accelerometers may be used in the control loop. Steering commands from the guidance system can be applied to the torque generator of the position gyro. The attitude control system turns the missile so that the attitude rate is essentially equal to that commanded.

The principal disturbing torques acting upon the vehicle arise from aerodynamic disturbances, from the effect of moving masses within the vehicle, and from thrust misalignments. The control system must cope with rapidly varying parameters such as vehicle inertia, mass, and aerodynamic forces and moments. Static friction in the nozzle hinges may be high and the structural supports may be quite flexible, thus complicating the dynamics. It is important that the power requirements and the weight of the control system be as small as possible.

The system performance must adequately limit the angle of attack and make possible light vehicle structure. All these requirements and the complete vehicle interactions make the design of an optimum system a very challenging task.

In conventional aircraft, a man is frequently used as an error detector in the control loop. Because of the difficult conditions involved, it seems unlikely that he will be so used in spacecraft.

17.6 GRAVITY

To accomplish inertial navigation in a region containing gravity fields, some method must be used for calculating gravity acceleration. If the path of the vehicle can be accurately predicted, the effects of gravity can be precalculated. In this instance, guidance during flight would be done in terms of thrust acceleration and its time integrals only. As the path of a specific vehicle becomes difficult to predict (relative to the accuracy requirement), it becomes necessary to make a gravity computation during flight.

Figure 17.12 shows, with an exaggerated scale, the powered-flight trajectory of a space vehicle. A rectangular coordinate system with the origin in the vicinity of the trajectory and with the y-axis vertical can be used to express the components of gravity relative to a free-fall reference frame at the center of the earth as follows:

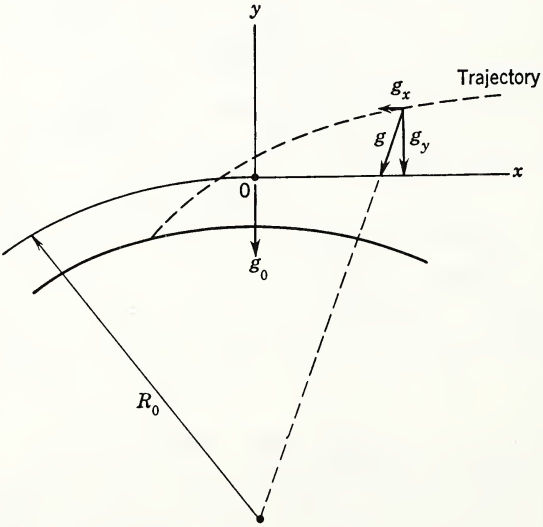

Fig. 17.12 Geometry of gravitation.

$$g_x = -g\frac{x}{R} = -\frac{g_0 R_0{}^2 x}{[x^2 + z^2 + (R_0 + y)^2]^{3/2}} \tag{17.37}$$

$$g_y = -g\,\frac{y + R_0}{R} = -\frac{g_0 R_0{}^2 (y + R_0)}{[x^2 + z^2 + (R_0 + y)^2]^{3/2}} \tag{17.38}$$

The g_z term is similar to g_x but for simplicity will be omitted here; x can be taken in the nominal plane of the trajectory and the problem considered in two dimensions. These equations are nonlinear, and their mechanization requires considerable computer complexity. Simple linear approximations which are valid near the origin of coordinates are

$$g_x = -\frac{g_0}{R_0}x \tag{17.39}$$

$$g_y = -g_0\left(1 - \frac{2y}{R_0}\right) \tag{17.40}$$

The acceleration equations in component form are

$$\ddot{x} = a_{tx} + g_x \tag{17.41}$$

$$\ddot{y} = a_{ty} + g_y \tag{17.42}$$

Block diagrams for the solution of these linear equations are shown in Fig. 17.13. The x channel has negative feedback and two integrations and thus has a sinusoidal response to an input disturbance. The y channel has positive feedback, and an input disturbance leads to a diverging value of y.

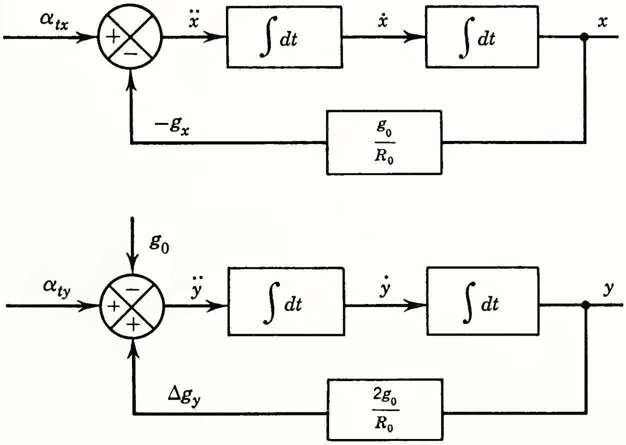

Fig. 17.13 Gravity computer.

The effect of the approximation in the gravity computer can, of course, be calculated for a given trajectory. Additional terms to include the nonspherical gravity field of the earth can be included as necessary. If the acceleration free-fall reference frame is located in a satellite, for example, the gravity components which give the difference in gravity between the location of the accelerometer and the reference frame will, of course, differ from those given in eqs. 17.37 and 17.38. Because the satellite moves rapidly the gravity components will vary with time.

The effect of the gravity computation on position and velocity error buildup caused by accelerometer or initial-condition errors is of considerable interest.[16, 17] It can be investigated analytically in terms of perturbation equations. These simply state that a small change in vehicle acceleration is equal to a small change in the measured thrust acceleration plus a change in the computed value of gravity acceleration. The gravity perturbation is composed of computer mechanization error and perturbations caused by using an erroneous position in calculating gravity. To consider only the latter here, the perturbation equations are

$$\Delta\ddot{x} = \Delta a_{tx} + \Delta g_x = \Delta a_{tx} + \frac{\partial g_x}{\partial x}\Delta x + \frac{\partial g_x}{\partial y}\Delta y \tag{17.43}$$

$$\Delta\ddot{y} = \Delta a_{ty} + \Delta g_y = \Delta a_{ty} + \frac{\partial g_y}{\partial y}\Delta x + \frac{\partial g_y}{\partial y}\Delta y \tag{17.44}$$

The differential coefficients are functions of space which can be obtained from eqs. 17.37 and 17.38. They should be evaluated along the unperturbed path of the vehicle. However, this method leads to differential equations with time-varying coefficients which cannot be solved in closed form. For flights in a region of a few hundred miles breadth, the coefficients can be evaluated at one point in the vicinity of the trajectory with accuracy adequate for our purposes. This procedure gives the following equations for the perturbation in position caused by thrust acceleration perturbation or accelerometer error:

$$\Delta\ddot{x} + \frac{g_0}{R_0}\Delta x = \Delta a_{tx} \tag{17.45}$$

$$\Delta\ddot{y} = \frac{2g_0}{R_0}\Delta y = \Delta a_{ty} \tag{17.46}$$

The physical meaning of these equations is easy to determine. For example, a positive error in vertical position leads to a calculated value of gravity acceleration which is too small and thus to a calculated value of vehicle acceleration which is too large. This acceleration error in turn integrates into an even larger positive position error.

The solution to eqs. 17.45 and 17.46 for constant values of thrust acceleration perturbations (accelerometer bias or zero offset) are

$$\Delta x = \frac{\Delta a_{tx}}{g_0/R_0} \left(1 - \cos \sqrt{g_0/R_0}\, t\right) \tag{17.47}$$

$$\Delta y = \frac{\Delta a_{ty}}{2g_0/R_0} \left(\cosh \sqrt{2g_0/R_0}\, t - 1\right) \tag{17.48}$$

The terms for initial-condition perturbations are similar to these. Near the surface of the earth the sinusoidal oscillation has a period of about 84 min, that is, $2\pi\sqrt{R_0/g_0} \approx 84$ min.

Position errors caused by accelerometer errors other than a constant bias can be calculated by well-known methods. An offset in the attitude reference will cause a cross-coupling error, thus $\Delta a_{tx} = \beta a_{ty}$, where β is the attitude reference error. A gyro drift rate thus gives an increasing position error.

These perturbations or error equations illustrate a basic limitation of inertial guidance for long periods of flight, namely, that errors in the vertical direction increase exponentially with time. However, errors in the horizontal direction caused by accelerometers are oscillatory with a period of 84 min. This makes practical two-dimensional inertial systems for aircraft and ships which can employ altimeters to measure altitudes. For flight times less than about 10 min, eqs. 17.47 and 17.48 can be approximated by the simple equations,

$$\Delta x = \Delta a_{tx} \frac{t^2}{2} \qquad \Delta \dot{x} = \Delta a_{tx} t \tag{17.49}$$

$$\Delta y = \Delta a_{ty} \frac{t^2}{2} \qquad \Delta \dot{y} = \Delta a_{ty} t \tag{17.50}$$

which are those that would be obtained by ignoring the feedback error from the gravity calculation. They are also those that would be obtained for navigation in a constant gravity field.

17.7 GUIDANCE SCHEMES

The term guidance scheme denotes the equations, coordinate systems, and general methods used to calculate steering and thrust termination commands for the vehicle. Guidance is needed to compensate for disturbances that act on the missile during flight. Principal disturbances encountered are variations in the rocket thrust, nonstandard atmospheric conditions, and misalignments in the thrust vector.

Several forms of ballistic or near-ballistic flight can be identified. First, and probably most important, is the powered launch of a vehicle followed by free fall or a ballistic trajectory. The simplest example is a projectile fired from a gun. Here guidance is accomplished by the constraint of the gun barrel, and thrust is terminated when the projectile leaves the muzzle. Causes of dispersion can be placed into two groups. First are those arising during the travel of the projectile in the barrel. These include the azimuth, elevation, and muzzle velocity dispersions, all of which might be called the "guidance" error. The second group consists of nonstandard atmospheric conditions which affect the ballistic part of the trajectory. In an unguided rocket the burning period is prolonged until the rocket fuel is exhausted. Steering is done passively by means of aerodynamic moments acting on stabilizing fins or on the spinning rocket body. It could be said that the gun barrel is extended to the burnout point of the rocket. In a guided rocket the velocity and position are measured during powered flight; thrust is terminated and steering accomplished so that at the time of motor shutoff the vehicle has the proper motion to follow a ballistic path to its destination. As with the gun-launched projectile, dispersions consist of those existing at motor shutoff and those arising during the unpowered flight of the vehicle. For space vehicles the unpowered flight may be largely out of the atmosphere, and aerodynamic effects will contribute less to dispersion than would a guidance system if it were operated during this period.

Other classes of ballistic flight which may require guidance are re-entry into the atmosphere and landing for spacecraft, the flight in space under very low accelerations, and the landing on the moon or a planet without atmosphere. Guidance equipment may be needed to measure and control short periods of rocket thrust which are used to change orbits or to make corrections in velocity during space flight. Free fall in outer space is a special case in which accelerometers have no output and in which position and velocity can be calculated solely from initial conditions and knowledge of the gravity field.

Associated with the concept of guidance schemes is that of the standard or reference trajectory. Such a trajectory is one that a standard or nominal missile would follow under standard or nominal aerodynamic conditions. The path of any specific missile should follow the standard trajectory rather closely. In general, the specific paths will be statistically distributed about the standard, which in some sense will be a mean of the distribution. The standard trajectory is chosen to optimize such conflicting requirements as vehicle range, weight, aerodynamic heating, re-entry considerations, ground handling, and guidance accuracy. A typical standard trajectory consists of a vertical rise followed by a gravity turn (zero lift) and then a constant-attitude flight until burnout.

The guidance scheme must be chosen to optimize a number of conflicting characteristics. Included in these are accuracy, flexibility in changing trajectories, nature and magnitude of disturbances encountered, complexity of the computer as it affects reliability, weight and power consumption, and complexity of preflight ground computation. Steering of the vehicle is based on measurements made within the vehicle; consequently, guidance is a closed-loop process which includes, as a subsystem, the missile control system. This guidance loop must have proper stability and high enough gains so that dynamic lags occurring at motor shutoff are not excessive. The design of a guidance scheme is truly a systems problem for which the specific mission, the available hardware, and detailed characteristics of the over-all vehicle system must be considered.

If the earth were nonrotating and spherical, the missile trajectory would lie in a plane. The real oblate earth has a gravity field which makes the trajectory slightly nonplanar. However, this effect is small and will not be considered further here. For inertial guidance applications near the rotating earth, it is convenient to visualize trajectories in nonrotating coordinates. With this point of view target points and launch points on the earth are moving eastward over the surface of the earth with a velocity equal to the earth's surface velocity. If the launch point and target are both on the equator, the trajectory will lie in a plane. If the vehicle is fired over a pole, the target is moving normal to the trajectory plane and hence the vehicle must be ''aimed'' at the location of the target at the predicted time of impact. The vehicle will have an initial velocity normal to the free-fall trajectory plane because of the eastward motion of the launch point. This velocity must be canceled by aiming the missile to the west of the target, so that at burnout the velocity vector will lie in a plane containing the burnout point, the center of the earth, and the target at the moment of impact. Because of this initial lateral velocity, the path of the missile does not lie in a plane during all the powered flight and, because it does not, a lateral component of gravity will exist.

For a rotating earth the lateral position of the target at impact will depend on the total time of flight, which in turn will depend on the velocity and position at motor shutoff. Lateral steering must be done before thrust termination, and since the moment of shutoff is not known before it occurs, some form of prediction must be used to steer so that the downrange and lateral components of miss are zero at the same time.

17.8 BALLISTIC MISSILE EXAMPLE

To help clarify some of the concepts and methods of inertial guidance, an example will be given in terms of the German V-2 rocket of World War II. The example is not an optimum design but serves to point out some of the salient features. Similar concepts, and in fact an almost identical method, could be used for the powered flight necessary to place an earth satellite in orbit or to launch a spacecraft to the moon or a nearby planet.

Figure 17.14 shows the standard trajectory for the missile. Burnout is at 70 sec, after which the missile follows a ballistic path to the impact point. Guidance will be carried out during powered flight. Dispersions occurring during un-

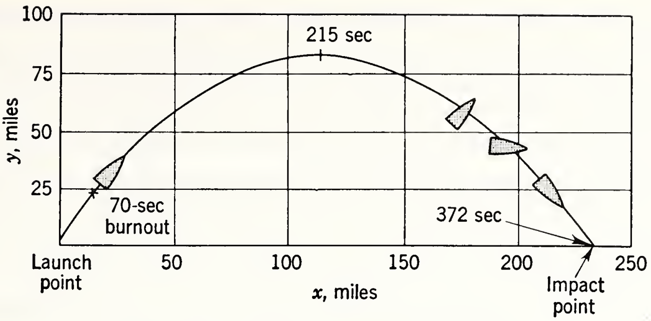

Fig. 17.14 V-2 standard trajectory.

powered flight should be small and will be neglected. Figure 17.15 gives additional detail on the powered portion of the trajectory. The trajectories shown are calculated for a nonrotating earth. The shape for a rotating earth would depend on the launch point-target combination but would differ from those shown in minor details only. The guidance system will utilize an inertial measurement unit such as that shown in Fig. 17.9. The platform will be accurately aligned to the ver-

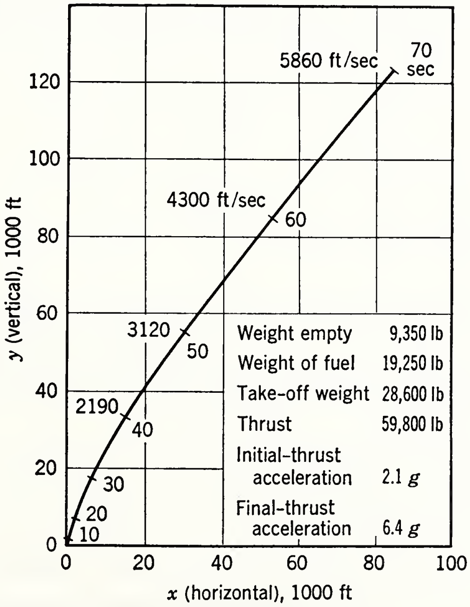

Weight empty	9,350 lb
Weight of fuel	19,250 lb
Take-off weight	28,600 lb
Thrust	59,800 lb
Initial-thrust acceleration	2.1 g
Final-thrust acceleration	6.4 g

Fig. 17.15 V-2 standard trajectory (powered flight).

tical prior to launch by means of force feedback pendulums which also act as the navigation accelerometers. The platform pitch will be accurately oriented in azimuth so that for a nominal missile the velocity vector will have the proper direction at motor shutoff. The missile will be launched vertically and will then follow a pitch attitude program which gives a zero-lift trajectory for the nominal missile. Steering will be done laterally or in yaw in such a way that the integrated output of the z accelerometer is essentially zero. No z or lateral computation of gravity will be made since it is a small effect which can be precalculated. The stabilized platform gimbal angles will be used as the attitude reference for the control system. Figure 17.16 is a schematic of the steering computer. The angle commanded by the pitch programmer is compared with the gimbal pitch angle to give a pitch-steering command to the missile control system. The overall guidance loop is illustrated in Fig. 17.16 by the feedback from the missile control system through missile dynamics to the inertial measurement unit.

Lateral and pitch steering having been accomplished, the remaining problem is to terminate the missile thrust at the proper time so that the missile will hit the intended impact point. If for a specific missile the thrust is less than stand-

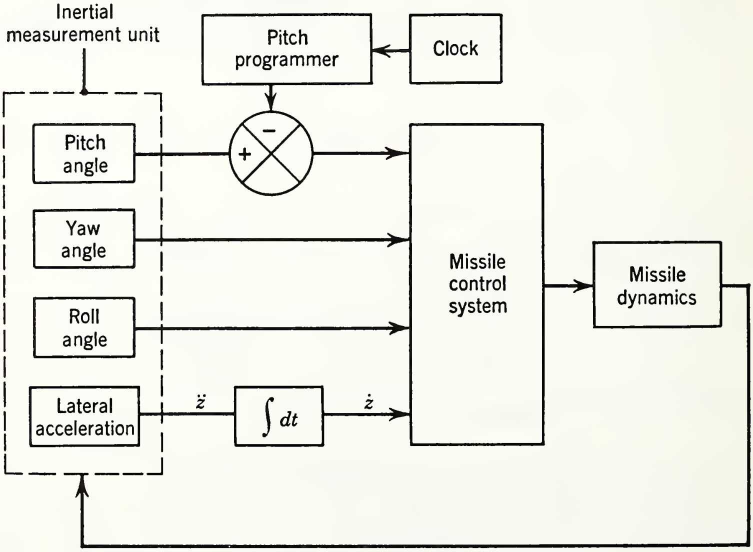
Inertial measurement unit
Pitch programmer
Clock
−
+
Pitch angle
Yaw angle
Roll angle
Lateral acceleration
$\ddot{z}$
$\int dt$
$\dot{z}$
Missile control system
Missile dynamics

Fig. 17.16 Steering computer.

ard (or the drag is greater than standard), the actual trajectory will lie beneath that shown in Fig. 17.15. Powered flight for slightly longer than 70 sec will be required in this case to achieve the proper terminal velocity and position. On the other hand, if the thrust is higher than standard, the trajectory will lie above that shown in Fig. 17.15, and the proper terminal velocity will be achieved earlier than 70 sec. The proper combination of shutoff values can be obtained by considering the effects on target miss of small changes in the horizontal and vertical components of position and velocity. For instance, an increase of 1 ft/sec in the horizontal velocity components at shutoff will result in a range 300 ft greater than standard. To express this analytically, the range of the missile is expanded as a function of position and velocity components about the standard shutoff point:

$$R - R_s = \frac{\partial R}{\partial x}(x - x_s) + \frac{\partial R}{\partial y}(y - y_s) + \frac{\partial R}{\partial \dot{x}}(\dot{x} - \dot{x}_s) + \frac{\partial R}{\partial \dot{y}}(\dot{y} - \dot{y}_s) + \dots \tag{17.51}$$

R designates range, the s subscript designates standard burnout conditions, and the partial derivative coefficients are evaluated at the standard shutoff point. These constant coefficients for the trajectory example of Fig. 17.14 are

$$\begin{aligned} \frac{\partial R}{\partial x} &= C_x = 1\frac{\text{ft}}{\text{ft}} & \frac{\partial R}{\partial \dot{x}} &= C_{\dot{x}} = 300\,\frac{\text{ft}}{\text{ft/sec}} \\ \frac{\partial R}{\partial y} &= C_y = 0.7\frac{\text{ft}}{\text{ft}} & \frac{\partial R}{\partial \dot{y}} &= C_{\dot{y}} = 220\,\frac{\text{ft}}{\text{ft/sec}} \end{aligned} \tag{17.52}$$

A computer which continuously calculates the downrange miss at the target is shown in Fig. 17.17. A linear gravity computation term can be identified by comparison with Fig. 17.12. Prior to the start of the flight, values of the standard burnout conditions, x_s, etc., are fed into the computer along with values of the coefficients, C_x, etc., which are calculated for the particular range desired. At some zero time for guidance (which should be within a few seconds of the actual lift-off time of the missile) the accelerometers are connected to the computer, and torquing of the gyros at earth rate is stopped. Position and velocity components relative to the launch point

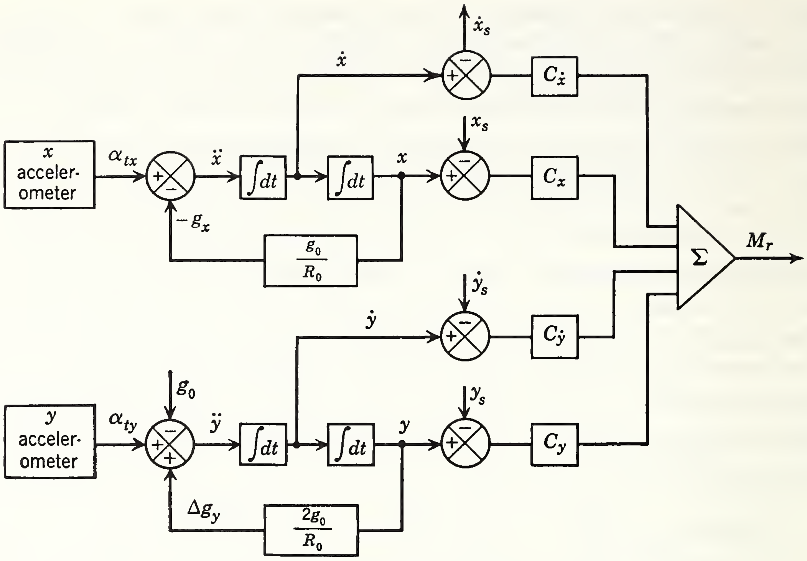

$\dot{x}_s$
$\dot{x}$
$C_{\dot{x}}$
x_s
x acceler-ometer
α_{tx}
$\ddot{x}$
$\int dt$
$\int dt$
x
C_x
$-g_x$
$\frac{g_0}{R_0}$
Σ
M_r
$\dot{y}_s$
$\dot{y}$
$C_{\dot{y}}$
g_0
y_s
y acceler-ometer
α_{ty}
$\ddot{y}$
$\int dt$
$\int dt$
y
C_y
Δg_y
$\frac{2g_0}{R_0}$
+
−

Fig. 17.17 Motor shutoff computer.

then appear in the channels indicated in the figure, and the computer calculates the downrange miss M_r. Early in the flight the calculated value will be grossly in error because only linear terms are used in the expansion. Near shutoff, however, the computation will be quite accurate. The thrust of the missile is terminated when the computed range miss becomes zero.

The guidance scheme presented should be evaluated from several standpoints. For example, the need for the gravity computer should be investigated. If the actual missile flight is sufficiently close to the nominal flight, the effect of gravity can be precalculated with sufficient accuracy and no gravity computer is necessary. On the other hand, and especially for extreme accuracy, additional terms in the gravity expansion may be necessary. If the variation in missile thrust is large, higher-order terms may be needed in the expansion of the motor shutoff equation (eq. 17.51). Refinements in the guidance scheme would include means of compensation for time of flight variations. The design of the system should include an error analysis of all the principal components so that a proper balance in design complexity can be obtained. For example, high accuracy in the shutoff computer is meaningless if the accelerometers are low-accuracy devices.

As a simple example of an error analysis, the effect of a scale factor error in the y accelerometer will be calculated. Figure 17.15 shows that the vertical component of velocity at burnout is about 4500 ft/sec. The thrust velocity in the vertical direction is this value minus the gravity velocity, or

$$\dot{y}_t = 4500 - (-32.2)(70) = 6750 \text{ ft/sec}$$

In the same way, the thrust displacement in the y direction is

$$y_y = 125{,}000 - (\tfrac{1}{2})(-32.2)(70)^2 = 204{,}000 \text{ ft}$$

A scale factor error of, say, 0.1 per cent in the y accelerometer thus gives thrust velocity and thrust position errors of

$$\Delta\dot{y}_t = \Delta\dot{y} = 6.75 \text{ ft/sec}$$

$$\Delta y_t = \Delta y = 204 \text{ ft}$$

The vehicle velocity and position errors are equal to the thrust values because the gravity feedback term of eq. 17.46 can be neglected for this short time of flight, and gravity computer errors are not being considered. By using the range or error coefficients given for the shutoff equation, eqs. 17.51 and 17.52, the total range miss caused by the scale factor error becomes

$$\Delta R = (220)(6.75) + (0.7)(204) = 2160 \text{ ft}$$

Additional analyses would show that the x accelerometer is more sensitive to errors than the y accelerometer, and that in terms of the present state of the art the accelerometers are generally more critical than the gyros.

17.9 SOUNDING ROCKET PROBLEM

17.9.1 Problem Definition

To obtain a further appreciation of guidance system synthesis and system trade-offs, the guidance equation for a vertical sounding rocket will be investigated. For simplicity, aerodynamic and earth rotation effects will be neglected and gravity will be assumed constant at 32 ft/sec^2.

The mission requires that the peak altitude reached be controlled to within ±2000 feet of a preset value. The rocket is known to have uncertainties in its burning characteristics. Therefore, an accelerometer and a computer will be needed to command rocket engine shutoff (also called burnout or cut-off) when a suitable velocity and altitude are attained. The principal problem to be considered here is that of the form of the shutoff equation. It should be as simple as possible and yet meet the peak altitude accuracy specification.

17.9.2 Standard Powered Trajectory

The standard powered trajectory to be used is defined by constant values of the rocket effective exhaust velocity c, the mass burning rate $\dot{m}$, and the initial mass M. Integration of Newton's law with zero initial conditions gives the following trajectory equations:

$$\text{acceleration} \quad a = a_t + a_g = \frac{c\dot{m}}{M} \, \frac{1}{1 - \dot{m}t/M} - 32 \qquad (17.53)$$

$$\text{velocity} \quad v = v_t + v_g = c \ln \frac{1}{1 - \dot{m}t/M} - 32t \qquad (17.54)$$

$$\text{altitude} \quad h = h_t + h_g = ct \left(1 - \frac{1 - \dot{m}t/M}{\dot{m}t/M} \ln \frac{1}{1 - \dot{m}t/M} \right) - \frac{1}{2} gt^2 \qquad (17.55)$$

The first terms in eqs. 17.53, 17.54, and 17.55 are called the thrust terms (t subscript) and the second the gravity terms (g subscript). Accelerometers measure thrust acceleration only; the gravity terms must be calculated in flight.

The numerical values for the standard powered trajectory and the design point peak altitude are

Total mass at liftoff	$M = 28{,}600$ lb
Mass burning rate	$\dot{m} = 275$ lb
Effective exhaust velocity	$c = 7040$ ft/sec
Burning time	$t = 70$ sec

ILLUSTRATIVE PROBLEM (Part 1)

The first calculation is to determine the numerical value of the quantities in eqs. 17.53, 17.54, and 17.55 at standard shutoff (i.e., t = 70 sec), giving

$$\begin{aligned} a &= a_t + a_g = 207 - 32 = 175 \text{ ft/sec}^2 \\ v &= v_t + v_g = 7870 - 2240 = 5630 \text{ ft/sec} \\ h &= h_t + h_g = 225{,}200 - 78{,}400 = 146{,}800 \text{ ft} \end{aligned} \qquad (17.56)$$

The velocity and altitude at shutoff are, of course, the initial conditions for the free-flight portion of the trajectory.

17.9.3 Perturbation Equations

Rocket characteristics cannot be predicted exactly before a flight; however, the actual values will cluster about a known average value with some known measure of dispersion. Usually the standard values (as in the first calculation) are taken to be equal to these average values.

To design the computing scheme it is necessary to calculate the variation (or dispersion) in burnout velocity and position caused by variation in c, $\dot{m}$, and M. If the variation is only a few per cent of the standard, this functional relationship can be expressed by linear perturbation equations which are simply the first-order terms in a Taylor's series expansion of velocity and position about the standard burnout point. For example,

$$\delta v \approx \frac{\partial v}{\partial c}\,\delta c + \frac{\partial v}{\partial \dot{m}}\,\delta \dot{m} + \frac{\partial v}{\partial t}\,\delta t + \frac{\partial v}{\partial M}\,\delta M$$

ILLUSTRATIVE PROBLEM (Part 2)

It is now necessary to obtain linear perturbation equations for velocity and altitude as functions of t, c, $\dot{m}$, and M. For convenience, the variations are expressed in c, $\dot{m}$, and M as ratios of their standard values, giving

$$\delta v \approx v_t \frac{\delta c}{c} + a_t t \frac{\delta \dot{m}}{\dot{m}} - a_t t \frac{\delta M}{M} + a_t \delta t - 32\delta t \qquad (17.57)$$

$$\delta h \approx h_t \frac{\delta c}{c} + (t v_t - h_t)\frac{\delta \dot{m}}{\dot{m}} - (t v_t - h_t)\frac{\delta M}{M} + v_t \delta t - 32t\,\delta t \qquad (17.58)$$

In each of these equations the sum of the first four terms is the variation in the thrust velocity or position, and the last term, which depends only on time, is the variation in the gravity quantity.

For simplicity in carrying out the further analysis it will be assumed that the only rocket characteristic which varies is the mass burning rate, i.e., $\delta M = \delta c = 0$.

ILLUSTRATIVE PROBLEM (Part 3)

Now obtain numerical values for the coefficients in eqs. 17.57 and 17.58. For later reference, also write the equations for variations in thrust velocity:

$$\delta v \approx 14{,}490 \frac{\delta \dot{m}}{\dot{m}} + 175\,\delta t \tag{17.59}$$

$$\delta v_t \approx 14{,}490 \frac{\delta \dot{m}}{\dot{m}} + 207\,\delta t \tag{17.60}$$

$$\delta h \approx 325{,}700 \frac{\delta \dot{m}}{\dot{m}} + 5630\,\delta t \tag{17.61}$$

Since these linear equations will be used to evaluate the approximations used in various guidance equations, it is necessary to investigate their range of validity. This can be done by comparing the linear results with exact values of δv, etc., as functions of δt and $\delta \dot{m}$ obtained from natural logarithm tables. It can also be done by calculation of the second-order terms in the series expansion. As an example, for small variations in $\dot{m}$ and t, the per cent error in δv_t given by eq. 17.60 is about equal to the per cent variation in $\dot{m}$ or t.

17.9.4 Peak Altitude

The peak altitude reached by the rocket is given by

$$p_a = h_a + \frac{v_a^2}{2g} \tag{17.62}$$

where p_a = peak altitude (velocity = 0)
h_a = altitude at burnout
v_a = velocity at burnout

The a subscript denotes actual quantities at burnout in contrast to the standard values which carry no subscript. The design point peak altitude is

$$p = h + \frac{v^2}{2g} = 146{,}800 + \frac{(5630)^2}{64} = 642{,}200 \text{ ft}$$

A computing scheme could be designed to calculate v, h, and p continuously, based on the accelerometer output. Rocket shutoff could be commanded when the calculated value of p equaled the desired value which was preset into the computer. The disadvantage of such a scheme is the complexity required to perform integrations and multiplications of large numbers with high accuracy.

An alternate approach is to calculate peak altitude deviation as a function of deviation in velocity and position from standard burnout values. When the peak altitude deviation is zero, rocket shutoff is commanded. This technique simplifies the rocket-borne computer but increases the preflight ground computation because standard values of burnout velocity and position must be calculated and set into the computer prior to flight.

ILLUSTRATIVE PROBLEM (Part 4)

To obtain an equation for the perturbation in peak altitude as a function of perturbations in burnout velocity and altitude, the general technique is to expand eq. 17.62 as a Taylor's series. In this simple case there is only one second-order term and this should be included. Also write the equation with numerical coefficients for the design point peak altitude:

$$\delta p = \delta h + \frac{v}{g}\,\delta v + \frac{1}{2g}\,(\delta v)^2 \qquad (17.63)$$

$$\delta p = \delta h + 176\,\delta v + 0.0156(\delta v)^2 \qquad (17.64)$$

17.9.5 Shutoff Equations

The computing scheme from which the rocket shutoff command is obtained should be as simple as possible and yet be consistent with the system accuracy requirement. Usually the over-all accuracy is specified, and the guidance system designer must allocate accuracies to the various subsystems after considering all pertinent factors. It is pointless, for example, to make the computer very accurate if the accelerometer is rather inaccurate.

There are many ways by which the cutoff command can be generated, and some will now be explored. The equation which is satisfied to yield the shutoff command is called the ''shutoff'' equation or the ''hit'' equation. An exact shutoff condition in the sense that there is no computational error is given by eq. 17.63 with $\delta p = 0$.

ILLUSTRATIVE PROBLEM (Part 5)

Draw a block diagram (Fig. 17.18) for a computer to solve eq. 17.63 and to obtain δv and δh continuously during flight. The input to the computer is the output of the accelerator. A means for obtaining the gravity term and suitable integrators and multipliers must be provided. The computer output is δp, and cutoff occurs when δp equals zero. Quantities set into the computer before flight are standard burnout values of h, v, g, and the coefficients of δv and $(\delta v)^2$ which correspond to the desired peak altitude.

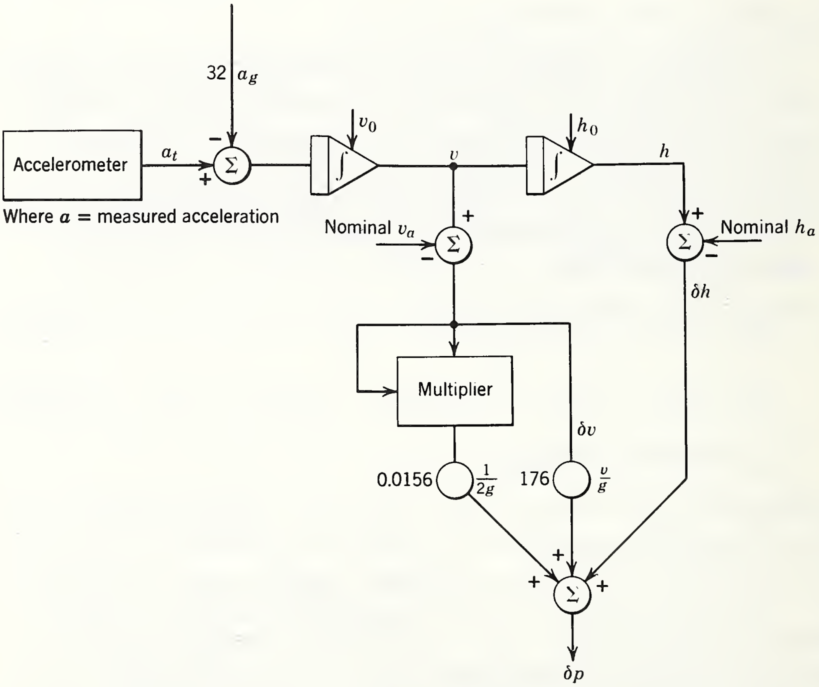
32 a_g
v_0
h_0
Accelerometer
a_t
−
+
Σ
∫
v
∫
h
Where a = measured acceleration
Nominal v_a
+
−
Σ
+
Nominal h_a
Σ
−
δh
Multiplier
δv
0.0156
$\frac{1}{2g}$
176
$\frac{v}{g}$
+
+
+
Σ
δp

Fig. 17.18 Block diagram for a computer to solve Illustrative Problem (Part 5). Note: If the g term is not considered as a constant, the nonlinear or $g = g_0\left(\frac{R_0}{R_0 + h}\right)^2$ term must be included.

The exact shutoff equation of Illustrative Problem (Part 5) is probably more complicated than is needed. To evaluate the situation, the variation in actual cutoff velocity, position, and time as a function of $\delta\dot{m}/\dot{m}$ is needed. Remember that variation in these quantities is defined as the difference between the actual value at shutoff and the standard value.

ILLUSTRATIVE PROBLEM (Part 6)

Solve eqs. 17.59, 17.61, and 17.64 to obtain values for δv, δh, and δt at actual shutoff ($\delta p = 0$) as functions of $\delta\dot{m}/\dot{m}$. Suggestion: Ignore the quadratic term in eq. 17.64 in this solution; it has a very small effect. The answers are

$$\delta t \approx -78.9\,\frac{\delta\dot{m}}{\dot{m}}$$

$$\delta v \approx +674.8\,\frac{\delta\dot{m}}{\dot{m}} \tag{17.65}$$

$$\delta h \approx -120{,}800\,\frac{\delta\dot{m}}{\dot{m}}$$

These values are approximate because they are based on linear expansions of the logarithmic functions.

Typically, rockets have variations in $\dot{m}$ of about 3 per cent. With this variation the functions of Illustrative Problem (Part 6) show that the quadratic term in eq. 17.64 contributes about 6 ft to the peak altitude term. Six feet are negligible in terms of the system specification, and in order to simplify the computer the quadratic term can be eliminated from the shutoff computation. The shutoff equation thus becomes

$$\delta h + \frac{v}{g}\,\delta v = 0. \tag{17.66}$$

A further computer simplification could be obtained by eliminating the δh term and commanding shutoff when δv equals zero. The peak altitude error involved in this approach will now be calculated.

ILLUSTRATIVE PROBLEM (Part 7)

Solve the cutoff equation

$$0 = \delta v = \delta v_t - 32\,\delta t \tag{17.67}$$

together with eqs. 17.59 and 17.61 to obtain δh and δt at actual shutoff as functions of $\delta\dot{m}/\dot{m}$. What is the error in peak altitude as a function of $\delta\dot{m}/\dot{m}$, using this simplified shutoff scheme The equation is

$$\delta p \approx -140{,}400 \frac{\delta\dot{m}}{\dot{m}}$$

For $\delta\dot{m}/\dot{m}$ of 3 per cent, this computing arrangement, although simple, still leads to large system errors and cannot be used without relaxing the system specification.

Other shutoff schemes might be considered. For example, shutoff could be commanded when δt equals zero, that is, cutoff by a simple preset timer. Or shutoff might be commanded when δv_t equals zero, that is, by the output of an integrating accelerometer only. Analysis like that used in Illustrative Problem (Parts 6 and 7) will show that in both cases, and even for small values of $\delta\dot{m}/\dot{m}$, the resulting peak altitude error is unacceptably large. The computing scheme could be simplified if the rocket thrust were controlled by the output of the accelerometer to a standard value. However, this requires generating a standard acceleration program in the guidance system and usually complicates the rocket engine so that the over-all missile system becomes less optimum.

A little reflection on the shutoff problem will show that the burnout altitude and velocity can be considered as functions of time, thrust velocity, and effective exhaust velocity only. Because of this and for the special case in which the exhaust velocity does not vary, an accurate but simple computing scheme is possible.

ILLUSTRATIVE PROBLEM (Part 8)

Express peak altitude as a function of thrust velocity, exhaust velocity, and time. Then obtain a linear perturbation equation of variation in peak altitude as a function of variation in shutoff time and thrust velocity. Calculate numerical coefficients for the design point trajectory:

$$p = ct - \frac{Mv_t}{\dot{m}} + \frac{v_t^2}{2g} \qquad (17.68)$$

$$\delta p = \left(\frac{v_t}{g} - \frac{M}{\dot{m}} + \frac{Mv_t}{\dot{m}a_t t}\right)\delta v_t + \left(c - \frac{Mv_t}{\dot{m}t}\right)\delta t \tag{17.69}$$

$$\delta p = 198.44\,\delta v_t - 4653.9\,\delta t \tag{17.70}$$

ILLUSTRATIVE PROBLEM (Part 9)

Draw a computer block diagram for the solution of eq. 17.70. Suggestion: Consider the equation in the following form:

$$\frac{\delta p}{198.4} = \int_0^t \left(a_t - \frac{4654}{198.4}\right) d\tau - \left(v_{ts} - \frac{4654}{198.4}\,t_s\right) \tag{17.71}$$

where the s subscript denotes standard preset values of thrust velocity and burning time. For the design point peak altitude of Illustrative Problem (Part 1), $v_{ts} = 7870$ ft/sec and $t_s = 70$ sec.

Shutoff eq. 17.69 and the computer of Illustrative Problem (Part 9) have the same form as eq. 17.67 and the computer of Illustrative Problem (Part 7), but the coefficients are different. This is not surprising since with $\dot{m}$ as the only rocket variable, h can be expressed as a function of v and t and, consequently, eliminated from eq. 17.62.

The computing approximation in eq. 17.69 stems from linearization of the coefficients. The error involved is not as easy to calculate as it was in eq. 17.66 where the error was given exactly by the term $(\delta v)^2/2g$. Equation 17.57 cannot be used in the error analysis method of Illustrative Problem (Part 6) because eq. 17.57 contains the same linearization approximations that are to be evaluated in eq. 17.69. Consequently, second-order terms must be included in the analysis, or the problem must be solved numerically for a range of values of $\dot{m}$. In practice, the latter approach must invariably be used in order to achieve the required accuracy of analysis and in order to study the effects of atmospherics and of time-varying parameters.

ILLUSTRATIVE PROBLEM (Part 10)

Solve the shutoff equation 17.70 together with the thrust part of eq. 17.54 for a range of values of $\Delta\dot{m}/\dot{m}$ to obtain the values of Δt and Δv_t at actual shutoff. Use a finite difference form of eq. 17.68,

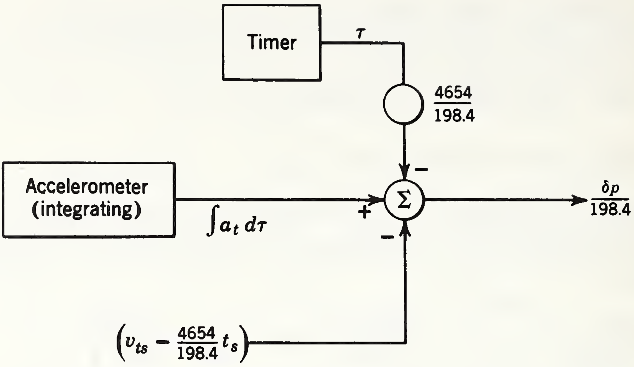

Fig. 17.19 Block diagram for a computer to solve Illustrative Problem (Part 9).

$$\Delta p = f(\Delta \dot{m}, \Delta t, \Delta v_t)$$

to determine peak altitude errors caused by the approximation in the shutoff equation. Consider round-off errors at all steps in the calculation. Equation 17.56, for example, has insufficient significant figures. For $\Delta \dot{m}/\dot{m} = 3\%$,

$$\Delta t = -2.2917 \text{ sec}$$

$$\Delta v_t = -53.75 \text{ ft/sec}$$

$$\Delta p = -40 \text{ ft}$$

The block diagram for eq. 17.71 is given in Fig. 17.19.

The optimum set of guidance coefficients for an accurate missile system with many random variables affecting guidance accuracy is usually determined by a cut and try process which involves the definition of "optimum" and the probability distributions of the various dispersions. The three-dimensional case, including steering equations and a rotating earth, is analyzed in a manner similar to that used in these problems but is, of course, much more complicated.

REFERENCES

1. J. M. Slater and D. B. Duncan, "Inertial Navigation," Aeronaut. Eng. Rev., 15, No. 1, 49-52 (1956).
2. W. Wrigley, R. B. Woodbury, and J. Hovorka, "Inertial Guidance," Institute of Aeronautical Sciences Preprint 698, presented January 31, 1957.

3. P. J. Klass, "Inertial Navigation," Aviation Week, Special Report, **64,** Nos. 1-4, Jan. 2, 32-35; Jan. 9, 42-43; Jan. 16, 94-99; Jan. 23, 76-77 (1956).
4. D. B. Duncan, "Analysis of an Inertial Guidance System," Jet Propulsion, **28,** No. 2, 111 (1958).
5. W. T. Russell, "Inertial Guidance for Rocket-propelled Missiles," Jet Propulsion, 28, No. 1, 17 (1958).
6. J. M. Slater, "Gyroscopes for Inertial Navigators," Mech. Eng., **79,** No. 9, 832 (1957).
7. H. Goldstein, Classical Mechanics, Addison-Wesley Press, Reading, Mass., 1950.
8. B. T. Plymale, et al., "Nutation of a Free Gyro Subjected to an Impulse," J. Appl. Mech., **22,** 365 (1955).
9. R. H. Cannon, Jr., "Kinematic Drift of Single-Axis Gyroscopes," American Society of Mechanical Engineers Paper 57-A-72 (to be published in Journal of Applied Mechanics).
10. R. M. Stewart, "Some Effects of Vibration and Rotation on the Drift of Gyroscopic Instruments," ARS Journal, **29,** No. 1, 22-28 (1959).
11. L. E. Goodman and A. R. Robinson, "Effect of Finite Rotations on Gyroscopic Sensing Devices," J. Appl. Mech., **25,** No. 2, 210 (1958).
12. C. S. Draper, W. Wrigley, and L. R. Grohe, "The Floating Integrating Gyro and Its Application to Geometrical Stabilization Problems on Moving Bases," Institute of the Aeronautical Sciences Preprint 503, presented January 25, 1955.
13. R. H. Cannon, Jr., and D. P. Chandler, "Stable Platforms for High-Performance Aircraft," Aeronaut. Eng. Rev., **16,** No. 12, 42 (1957).
14. C. S. Draper and R. B. Woodbury, "Geometrical Stabilization Based on Servo-Driven Gimbals and Integrating Gyro Units," Massachusetts Institute of Technology, presented at Advisory Group for Aeronautical Research and Development, Symposium on Guidance and Control, Venice, Italy, September 24-28, 1956.
15. J. P. Jagy, "How Industry Solved the Air-Bearing Gyro Stabilization Problem," Missiles and Rockets, **3,** 84 (1958).
16. J. J. Gilvarry, S. H. Browne, and I. K. Williams, "Theory of Blind Navigation by Dynamical Measurements," J. Appl. Phys., **21,** 753-761 (1950).
17. S. H. Browne and J. J. Gilvarry, "Theory of Errors in Automatic Navigation with Integrating Accelerometer Systems," U.S. Air Force Project RAND, a report published by The RAND Corporation, R-154, May 5, 1952.
18. C. S. Draper, W. Wrigley, J. Hovorka, Inertial Guidance, Pergamon Press, New York, 1960.

18

RE-ENTRY AND RECOVERY

J. R. Sellars

18.1 INTRODUCTION

When the first ballistic missiles were in the planning stage, it was recognized that among the many problems requiring solution the re-entry problem was the one for which people were most hesitant to give a definite development schedule. Although most scientists were convinced that the problem would ultimately be solved, it definitely required breakthroughs in the state of the art, and breakthroughs are notably difficult to schedule. Now, in retrospect, it is evident that the real breakthrough was in seeing that no breakthrough was ever needed. Practically all problems have yielded to conventional analysis or experimentation, and much of the analysis even existed in the very early days of great doubt. The problem was partly that people were hesitant to believe that the conventional laws could be extrapolated so far and still give answers of reasonable accuracy.

Today the re-entry problem is solved, even for the recovery of satellites, although improvements in technique will continue to be made. Some of these improvements are, in fact, vital because the tendency is always to obtain the last ounce of effective payload from every missile firing so that future plans for both ballistic and space missions will not be able to accommodate an inefficient solution of the re-entry problem.

The following pages are intended to suggest the scope of some of the re-entry problems, to give a general notion of the behavior of re-entry bodies, and finally to discuss briefly the mechanics of breaking an orbit to recover a satellite. The satellite re-entry problem is sufficiently different from a regular ballistic re-entry to warrant a special section.

18.2 GENERAL TRAJECTORY CONSIDERATIONS

For analysis, the re-entry portion of a re-entry vehicle trajectory is usually divided into three regions. The first is at an extremely high altitude, that is, where the re-entry vehicle (generally called a nose cone) is first affected by the atmosphere. The second region is where the nose cone experiences extremely high heating and deceleration. The third is a region of "slow fall" where the aerodynamic forces are comparable to the force of gravity and the nose cone actually begins to cool.

Throughout the first region there are sufficient forces on the nose cone to start it oscillating extremely slowly and thereby greatly reducing its angle of attack (if it is a statically stable nose cone). These same forces, however, do not reduce the velocity; in fact, the velocity may even increase slightly because of gravitational acceleration. It is during this time that an attitude control system begins to operate. As the nose cone oscillates around its neutral (i.e., zero angle of attack) position, the attitude control (in a typical design) damps this motion by means of air jets actuated by a servo which picks up the output of a set of rate gyros.

At an altitude of approximately 200,000 feet, depending somewhat on the design, the drag of the missile will be just equal to the acceleration due to gravity, and the maximum speed of the nose cone will be reached. From this point on, the drag builds up so rapidly that the gravity term can be neglected completely in an analysis of the motion for most purposes. During this time the high decelerations and heating rates associated with re-entry are encountered. The last phase of the trajectory is a slow fall to the surface of the earth. In this region the major problem is aerodynamic stability, and gravity can no longer be neglected.

Examination in greater detail of the second region of the trajectory, which has high deceleration and high heating, will delineate the more important parameters and give some intuitive notion of their importance. Typical re-entry conditions are generally expressed by specifying a re-entry velocity V_E and an angle of the trajectory ψ_E measured from the local horizontal (see Fig. 18.1). There is, of course, no definite point of re-entry into the atmosphere, but for purposes of heating think of a re-entry point at the point where the velocity V reaches its maximum value. From here on a simple equation for the deceleration of the nose cone may be written if we neglect the gravity term:

$$\frac{W}{g}\frac{dV}{dt} = -C_D A \frac{\rho V^2}{2} \tag{18.1}$$

To integrate this equation, a law for the variation of density with altitude must be established, such as

$$\rho = \rho_0 e^{-\beta y}$$

Here ρ_0 and β are constants. Values which give a reasonably accurate fit between a 50,000-ft altitude and a 300,000-ft altitude are $\rho_0 = 0.0034$ slug/ft³ and $\beta = 1/22{,}000$ ft.

Introducing this law in eq. 18.1 and noting that the incremental change in altitude is related to the incremental change in time by

$$dy = -V \sin \psi \, dt$$

gives

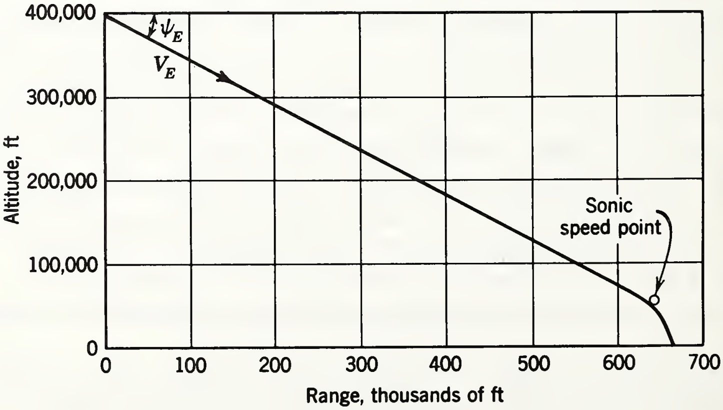

Fig. 18.1 Re-entry trajectory schematic.

$$\frac{dV}{dy} = \frac{-g}{2(W/C_D A)\sin\psi}\,\rho_0 e^{-\beta y} \tag{18.2}$$

Since we are neglecting the effect of gravity compared to aerodynamic forces, it is consistent to regard ψ as a constant because gravity is the only force tending to curve the path. With this approximation, eq. 18.2 immediately integrates to

$$V = V_E \exp \frac{-g\rho_0 e^{-\beta y}}{2\beta(W/C_D A)\sin\psi} \tag{18.3}$$

The "entry velocity" V_E is properly the maximum velocity reached by the nose cone; however, in a "no gravity" system it becomes the velocity at infinite altitude.

Here appears the important parameter $W/C_D A$ which plays a strong role in determining the heating of a re-entry body. Exactly why this parameter has such an important role will be shown later.

From eq. 18.3 it can be seen that varying $W/C_D A$ simply varies the altitude (density) at which a particular fraction of re-entry occurs. Since $W/C_D A$ varies the altitude at which a particular velocity is reached, it is instructive to ask whether it varies the time history in other ways—for example, does it vary the time between two given velocities. This question can be answered by solving for the density in eq. 18.3 and substituting it in eq. 18.1, obtaining

$$\frac{dV}{dt} = -\beta V_E^2 \sin\psi \left(\frac{V}{V_E}\right)^2 \log\frac{V_E}{V} \tag{18.4}$$

This equation shows that dV/dt (at a particular velocity) is independent of $W/C_D A$ and, therefore, the time from one value of V to another is independent of $W/C_D A$. Equation 18.4 provides a simple expression for the maximum value of the deceleration. Differentiating, we find that

$$\left(\frac{dV}{dt}\right)_{\max} = \frac{\beta V_E^2 \sin\psi}{2e} \tag{18.5}$$

and this occurs when

$$\frac{V}{V_E} = e^{-1/2} = 0.61$$

Equation 18.5 shows that for typical 5500-nautical mile re-entry conditions ($V_E = 23{,}500$, $\psi_0 = 20.7°$) the maximum deceleration is about 58 g. At this condition the component of gravity along the trajectory is only about 1/3 g, so neglecting gravity gives fairly accurate results during the time when the most significant velocity changes are taking place.

Thus two things are now established: the density occurring at a particular velocity may be varied within some limits as $W/C_D A$ is varied; however, the time between two velocities is not affected, nor, it follows, is the maximum acceleration. This means, in effect, that as we halve $W/C_D A$ we merely start decelerating at densities which are half as large and subsequently go through the same deceleration pattern but at a higher altitude. These considerations then hold down to a velocity or, more properly, a deceleration so small that gravity can no longer be ignored.

Since a body with a low $W/C_D A$ slows to a low velocity at high altitude, it then drops slowly through the remaining altitude. During this time wind drift may be significant and accuracy may suffer; it may also be more vulnerable. At this point there is a temptation to say that the highest possible $W/C_D A$ is desirable; however, the next section shows that a high $W/C_D A$ adversely affects heating. Consequently, a particular design is always a compromise of sorts between accuracy and the severity of the heating problem.

18.2.1 Heating Laws

Before examining heating laws in detail, it may be helpful to establish some general features to improve understanding of the effect of trajectory parameters. Because of the limitations of this book, proofs of all statements cannot be presented here, but perhaps they will establish an intuitive notion of why things work as they do.

For a given nose cone geometry, the local laminar and turbulent heat rates at a particular point on the surface vary approximately according to the following laws:

$$q_L \sim V^3 \rho^{1/2} \text{ Btu/(ft}^2\text{)(sec)}$$

$$q_T \sim V^{3.5} \rho^{0.8} \text{ Btu/(ft}^2\text{)(sec)} \tag{18.6}$$

where q is the heat rate per unit area measured in Btu per square foot per second, and the subscripts L and T signify "laminar" and "turbulent," respectively.

If the density associated with a particular velocity can be lowered arbitrarily by changing $W/C_D A$, it should be possible to lower the heating to some acceptable level, especially when we remember that the total time of heating is unaffected by changes in $W/C_D A$. Indeed, Q, the total amount of heat added per unit area to the surface of a nose cone (integrating the heat rate over the period of re-entry), is found to depend on $W/C_D A$ whether the flow is laminar or turbulent:

$$Q_L \sim \left(\frac{W}{C_D A}\right)^{1/2} \frac{V_E^2}{\sin^{1/2} \psi_E}$$

$$Q_T \sim \left(\frac{W}{C_D A}\right)^{0.8} \frac{V_E^{2.48}}{\sin^{0.2} \psi_E} \tag{18.7}$$

These last equations make it quite clear why bodies with low $W/C_D A$'s have been considered. However, as mentioned before, the use of a low $W/C_D A$ has some unfortunate consequences. For a $W/C_D A$ of about 1000 lb/ft^2, the impact is very nearly at sonic speeds. For a $W/C_D A$ of about 100 to 120 lb/ft^2, sonic velocity occurs at about 45,000 ft and almost 90 sec are required for the rest of the trajectory. During this time wind drift is a significant factor.

18.3 FLOW AROUND BODIES AT HYPERSONIC SPEEDS

As a body moves through the air at speeds many times that of sound, the air ahead of the body receives very little warning that a body is approaching. As a result, there is a sudden compression of the air very near the surface of the body and a flowing around the body of a thin layer of high-speed, high-temperature air. This layer is called the shock layer. It is drawn approximately to scale for a hemisphere moving at Mach 20 in Fig. 18.2. At the nose it is separated from the body by about one-fifteenth the radius of the body.

If we consider that all the incoming air is suddenly turned to flow parallel to the body, ignoring small gradients and flow angles within this thin layer, it is easy to calculate the normal pressure which the body must exert. If we consider a point at angle θ from the nose, and if we consider that the

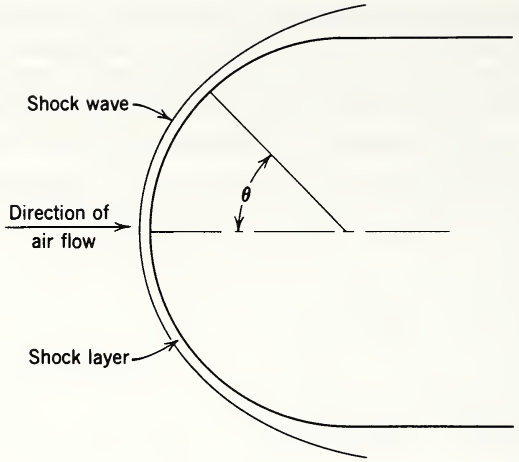

Fig. 18.2 Schematic of flow over hemisphere at very high speeds.

shock layer is essentially parallel to the body at this point, the mass flow per unit area crossing the shock layer is

$$\rho_\infty V_\infty \cos\theta$$

At the same time this mass has a velocity in the normal direction of $V_\infty \cos\theta$, giving a momentum flux per unit area of

$$\rho_\infty V_\infty^2 \cos^2\theta$$

Equating this momentum flux to the pressure difference across the (thin) shock layer in the normal direction yields

$$p - p_\infty = \rho_\infty V_\infty^2 \cos^2\theta \tag{18.8}$$

This is the so-called Newtonian pressure law. It is remarkably accurate over the nose portion of bodies with well-defined radii of curvatures.

For other than hemispheres, of course, the angle θ is to be interpreted as the angle the local body normal makes with the flow direction.

Equation 18.8 indicates that the pressure at the stagnation point of a body ($\theta = 0$) is equal to

$$p_s = p_\infty + \rho_\infty V_\infty^2 \tag{18.9}$$

Since this pressure is also the stagnation point pressure behind a normal shock, it is possible to write a more accurate estimate of this pressure which allows for the fact that the shock layer has finite thickness. If we approximate the flow from behind the normal shock to the stagnation point by assuming it is uncompressible flow, we obtain

$$p_s = p_\infty + \rho_\infty V_\infty^2\left(1 - \frac{1}{2\Delta}\right) \qquad (18.10)$$

Here Δ is the ratio of density after the shock to before the shock. This number is a function of velocity and altitude (density), but typically it varies from 10 to 20 for air in cases of interest ($M > 15$). This illustrates the fact that the Newtonian pressure law (eq. 18.8) is quite accurate. As might be expected, if the density ratio approached infinity, the shock layer would be of vanishing thickness and the Newtonian formula would become exact.

In order to take part of this inaccuracy into account, the so-called "modified" Newtonian pressure distribution is often used. This is

$$\frac{p - p_\infty}{p_s - p_\infty} \equiv \cos^2\theta \qquad (18.11)$$

where p_s is calculated by exact formulas or an improved approximation such as eq. 18.10.

Concepts such as the one just described are useful and exact enough for many cases. However, for bodies with more complicated shapes, such as the one in Fig. 18.3, more sophisticated methods must be applied to predict the pressure distribution along the cylinder or flare portion of the body.

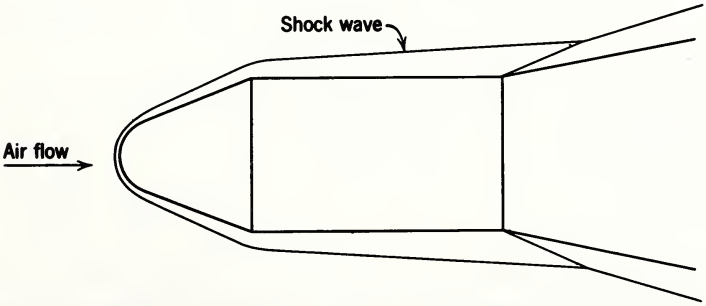

Fig. 18.3 Schematic of nose cone with shock wave pattern.

18.4 HEAT TRANSFER CALCULATIONS

The last section illustrated how, in principle, forces and moments on simple bodies could be calculated. This section will illustrate some of the steps that go into calculating laminar heat transfer over bodies of revolution. Consider the axisymmetric body with the coordinate system shown schematically in Fig. 18.4. It has been shown[2] that the laminar heat transfer at any point (x_0, r_0) is given by

$$q = \frac{0.355}{p_r^{2/3}} \frac{\rho_e u_e (H_e - H_w)}{\tilde{R}_e^{1/2}} \text{ Btu/(ft}^2\text{)(sec)} \tag{18.12}$$

with

$$\tilde{R}_e = \frac{\int_0^{x_0} \rho_e u_e \mu_e r^2 \, dx}{\mu_e^2 r_0^2} \tag{18.13}$$

Here ρ is density in slugs per square foot, H is enthalpy in Btu per slug, Pr is the Prandtl number (0.71 for air), μ is the viscosity in slugs per foot per second. The subscript e refers to conditions at the "edge" of the boundary layer; the subscript w refers to the air conditions at the wall. In the vicinity of the stagnation point we may write

$$u = \frac{du}{dx} x$$

Using this expression and noting that $r = x$ at this point, we may simplify R_e:

$$R_e \simeq \rho_e \frac{du}{dx} \frac{x^2}{4 \mu_e} \tag{18.14}$$

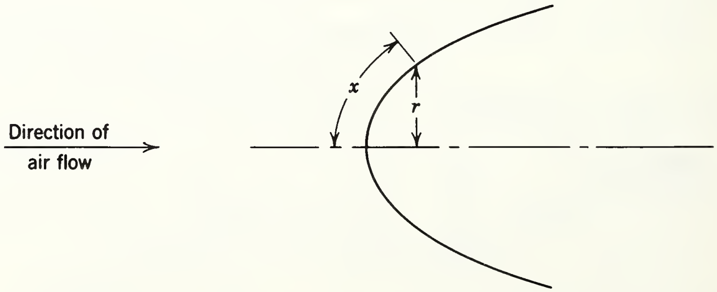

Fig. 18.4 Coordinate system for boundary layer problems of axisymmetric bodies.

All properties are evaluated at the stagnation point. Thus, at the stagnation point, eq. 18.12 becomes

$$q = \frac{0.71}{P_r^{2/3}} \left(\rho_e \mu_e \frac{du}{dx}\right)^{1/2} (H_e - H_w) \tag{18.15}$$

The density is given by calculating the stagnation density after a normal shock, taking into account the dissociation of the air. It is tabulated in various places. The value of viscosity is also tabulated as a function of the state variables.[3,4] A plot of the results shows that a reasonable fit at high temperatures is given by

$$\mu = 5 \times 10^{-8} H_e^{0.33} \text{ slug/(ft)(sec)} \tag{18.16}$$

With this information the one remaining unknown is the value of du/dx, which can be determined from the known pressure distribution. Suppose we are interested in determining the heat transfer to a spherical nose of radius R. First, we note that Euler's equation just outside the boundary layer near the stagnation point is

$$\rho u \frac{du}{dx} + \rho v \frac{du}{dy} = -\frac{\partial p}{\partial x} \tag{18.17}$$

Differentiating with respect to x, and noting that $u = v = 0$ at the stagnation point, we obtain

$$\left(\frac{du}{dx}\right)^2 = -\frac{1}{\rho_s} \frac{\partial p^2}{\partial x^2} \tag{18.18}$$

If we use the Newtonian pressure distribution law in the simplified form

$$p = p_s \cos^2 \theta = p_s \left(1 - \frac{x^2}{2R^2} + \ldots\right)$$

we obtain

$$\left(\frac{du}{dx}\right)^2 = \frac{p_s}{\rho_s} \cdot \frac{1}{R^2} \tag{18.19}$$

As an example, let us estimate the heat transfer to the stagnation point of a sphere 6 in. in radius moving at 20,000 ft/sec at a 50,000-ft altitude:

$$\rho_\infty = 3.6 \times 10^{-4}\ \text{slug/ft}^3 \qquad p_\infty = 237\ \text{lb/ft}^2$$

$$H_e \simeq \frac{V^2}{2J} = 256{,}000\ \text{Btu/slug}$$

$$H_e - H_w \simeq H_e \qquad \text{for wall temperatures that are low}$$

$$\rho_e \simeq \rho_\infty \times (\text{density ratio across a normal shock at the given altitude and speed})$$

$$\rho_e = \rho_\infty \times (11.8) \text{ from reference 3}$$

$$\rho_e = 4.25 \times 10^{-3}\ \text{slug/ft}^3$$

$$\mu \simeq 5 \times 10^{-8}\,(256{,}000)^{0.33} = 3 \times 10^{-6}\ \text{slug/(ft)(sec)} \quad \text{(using formula 18.16)}$$

$$p_s \simeq \gamma p_\infty M^2 \left(1 - \frac{1}{2 \times \Delta}\right) =$$

$$= 1.4 \times 237.0(20)^2 \left(1 - \frac{1}{2 \times 11.8}\right)$$

$$= 126{,}000\ \text{lb/ft}^2$$

$$\frac{du}{dx} = \frac{1}{R}\sqrt{p_s/\rho_s} = \frac{1}{0.5}\sqrt{126{,}000/(4.25 \times 10^{-3})}$$

$$= 10{,}900\ \text{(ft/sec)/ft} \qquad \text{(using eq. 18.15)}$$

$$q = \frac{0.71}{(0.71)^{2/3}}\sqrt{4.25 \times 10^{-3} \times 3 \times 10^{-6} \times 10{,}900}\,(256{,}000)$$

$$q = 2650\ \text{Btu/(ft}^2\text{)(sec)}$$

This heat rate is about five times the heat rates commonly encountered in rocket nozzle throats.

Since the air which is at the edge of the boundary layer at the stagnation point expands isentropically as it flows around the body, we can calculate the properties of this air at any point around the body where we know the pressure by the use of a Mollier diagram. If we do so, we can perform the integration indicated in eq. 18.3. The result enables us to calculate the distribution of heat transfer rates over the body. Figure 18.5 shows this distribution for a hemisphere at very high speeds, assuming that the pressure distribution is given by the (modified) Newtonian formula (eq. 18.8). According to this approximation the heat transfer drops almost to zero at

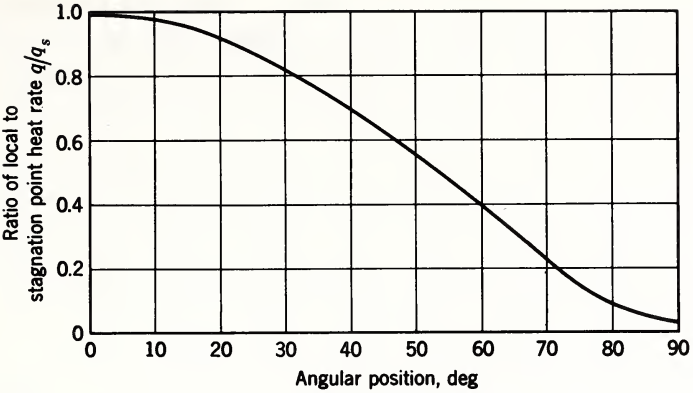

Fig. 18.5 Theoretical laminar heat transfer distribution on a hemisphere.

the 90° point on the hemisphere, which follows from the fact that the pressure drops almost to zero there. Actually, the heat transfer equals about 5 per cent of the value at the stagnation point.

With turbulent flow the theories do not give rise to such compact formulas. However, on modern ballistic missiles, except near the stagnation point, the flow is such that most of the heat is transferred through a turbulent boundary layer. Since a detailed treatment of turbulent flow adds nothing to the general concepts we are examining here, further discussion of it is omitted.[5]

18.5 HEAT PROTECTION SYSTEMS

A number of schemes are available to protect the payload of a ballistic missile from the extreme heating produced during re-entry. From the heat protection point of view, one of the most important characteristics of ballistic re-entry is its short duration; most of the heat is absorbed in about 30 sec or less—after which the payload must be protected for periods of time ranging from 10 sec to 80 sec before the impact.

One of the simplest and most straightforward schemes of heat protection is the use of a heat sink. A slab of copper 1 in. thick can absorb about 10,000 Btu/ft^2 before it melts if the heat rates are low. If the heat rates are sufficiently high, however, the surface will melt before this point of absorption is reached because the heat cannot be conducted fast enough to the interior of the slab. This fact illustrates one of the problems of such a scheme; the heat rates must be kept to reasonable levels to avoid melting the surface of the heat shield.

Another scheme which has certain applications is the radiant shield. As the surface of the shield is heated by the airstream to high temperatures, the shield radiates the energy back until some equilibrium temperature is reached. If the emissivity of the body is taken to be unity, a good rule of thumb for estimating this radiation is

$$q_{\text{rad}} = \frac{1}{2}\left[\frac{T(°\text{R})}{1000}\right]^4 \ \text{Btu/(ft}^2\text{)(sec)} \qquad (18.20)$$

A temperature of 2000°R, therefore, could support a heat transfer rate of a mere 8 Btu/(ft^2)(sec), which is very low compared to rates of several thousand Btu per square foot per second commonly encountered in ballistic re-entries on some parts of the body. On the other hand, winged vehicles moving at high speed in the upper atmosphere do have such heat transfer rates, so there radiation cooling is a practical means of dissipating energy. Because of the fourth-power dependence of radiation on temperature, however, if surface temperatures of 5000-6000°R can be achieved, this radiation is significant even when compared to re-entry heat transfer rates.

Still other schemes involve the flow of liquids or gases through the surface. These schemes, called transpiration cooling, are distinguished by their high heat protection efficiency per pound of fluid actually used. Water, for instance, will absorb over 1000 Btu/lb as compared to only 200 Btu/lb for a copper heat shield. In addition, the flow of steam off the surface prevents much heat from reaching the surface in the first place, thus effectively multiplying the cooling power of the water several times over. The beauty of this scheme is, unfortunately, marred by the complexity, reliability, and weight of the associated pumping equipment. Also, a uniformly porous surface that will not plug up must be constructed. If a single point plugs up, the hot air may burn through there.

A scheme which combines many of the advantages of the radiation shield and transpiration cooling devices is the so-called ablating shield, a solid shield which may reach such high surface temperatures that the surface actually melts or evaporates. Surface temperatures of 5000°R are actually achievable along with the transpiration cooling effect as the evaporated mass moves away from the surface. Effective values of heat absorption of 5000 to 10,000 Btu/lb are possible with certain of these materials.

In order to compare such materials with, say, a solid heat shield, we may calculate how much heat would be absorbed by a cool solid surface on a given trajectory. Then we may ask how many pounds of a particular heat shield material would have been required to protect the body on such a trajectory. For comparative purposes, we do not have to ask how the material copes with this heat pulse; some may do it acting as a solid shield, some may radiate most of the heat, some may "block" the flow of heat as fluid evaporates, and some may merely melt and run along the surface. We define a parameter Q^*, which will be a rough figure of merit for a material, by the ratio of the heat that would have been added to a cold wall by the flow to the number of pounds of material we found necessary to shield this heat. Thus

$$Q^* = \frac{Q \text{ (heat added by flow to cold wall)}}{w \text{ (pounds of heat shield necessary)}} \text{ Btu/lb}$$

This parameter depends in actuality on many things: whether the boundary layer is laminar or turbulent, the re-entry velocity, the shape of the body, etc. However, it is sufficiently constant to make it a usable concept, if attention is confined, for instance, to high $W/C_D A$ bodies re-entering at ICBM velocities.

The effect of this parameter on the design of nose cones is illustrated by Fig. 18.6. Thus a significant improvement was made possible when values of this parameter were raised from 150 to 200 Btu/lb (solid heat shields) to 5000 Btu/lb, which is a value that has been achieved with certain materials in arc and flight tests.

18.6 SATELLITE RE-ENTRIES

Now let us give attention to the re-entry of satellites from a low-altitude orbit. For our purposes it would be sufficient to specify some angle and velocity as the satellite enters the

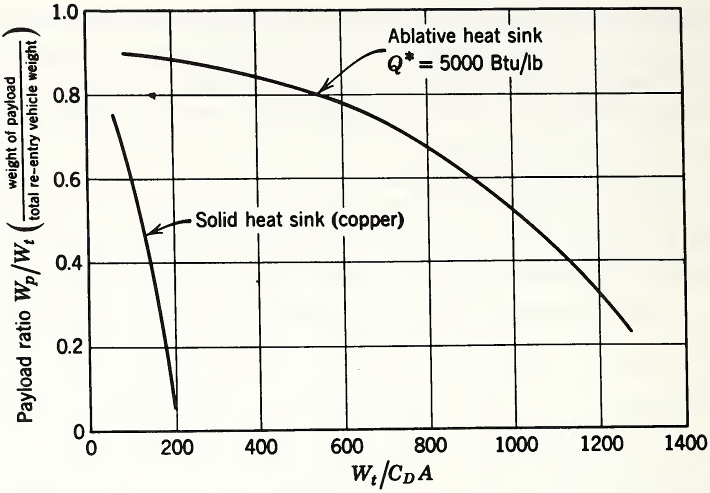

Fig. 18.6 Effect of heat shield material on nose cone design.

"edge" of the atmosphere. However, it is instructive to see how a satellite arrives at this point. Consider a satellite which is in a circular orbit. To break this orbit a retrorocket must be fired to slow down the satellite; this puts it on an elliptic orbit that intersects the earth's atmosphere at some angle with the local horizontal.

A plot of the retrorocket velocity required as a function of re-entry angle is shown in Fig. 18.7 for a 200-nautical mile orbit. It is seen that a re-entry at 3° demands about twice as large a retrorocket as one at 1°. Above 3° the size of the retrorocket goes up enormously. Thus we conclude that re-entries from low-altitude orbits will generally be at low angles. As can be seen from Fig. 18.8, this means that re-entry velocities will not vary much but that the range angle (the angle around the earth from the point where the retrorocket is fired to where the satellite re-enters) will be rather large, corresponding to 5000 to 8000 nautical miles. Thus a retrorocket fired over Australia would bring a satellite down over the United States, if it were on an orbit which crossed from Australia to the United States.

Other curves of interest in trying to pick out a precise landing spot for a satellite are shown in Fig. 18.9. Here for the case in question at an entry angle of 2°, an error in retrorocket imparted velocity of only 1 ft/sec would cause the sat-

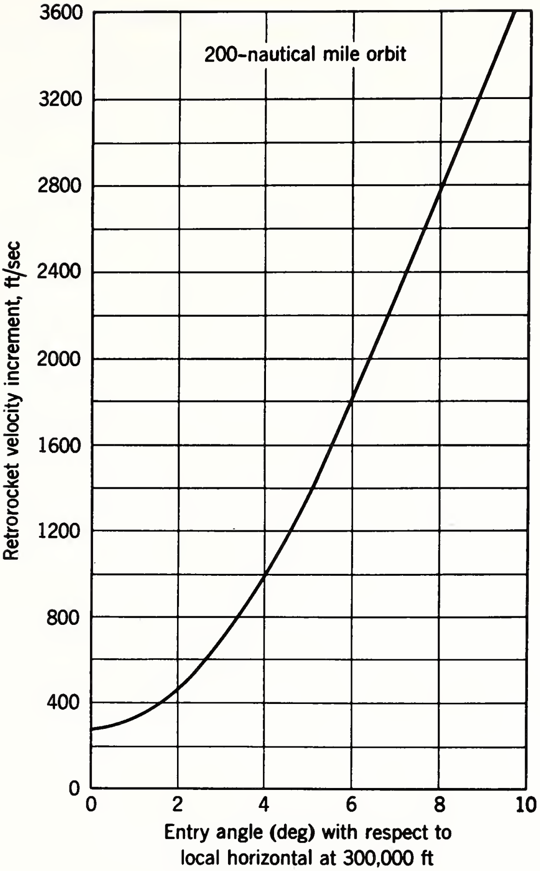

Fig. 18.7 Retrorocket velocity increment and retrorocket orientation, both as a function of entry angle.

ellite to miss the expected landing spot by some 10 nautical miles. Similarly, an error in orientation of the retrorocket of 1° would cause a 30-nautical mile miss in the expected landing spot, which means that very precise control of the velocity changes might still cause intolerable errors in the landing site. Therefore it is suggested that ultimately some maneuvering capability will have to be provided to land satellites on designated airfields.

Figure 18.10 shows the approximate amounts of heat per square foot encountered in a satellite re-entry. These are to be compared to typical values of about 6000 Btu/ft^2 which are encountered by a low $W/C_D A$ ballistic nose cone at 5500-

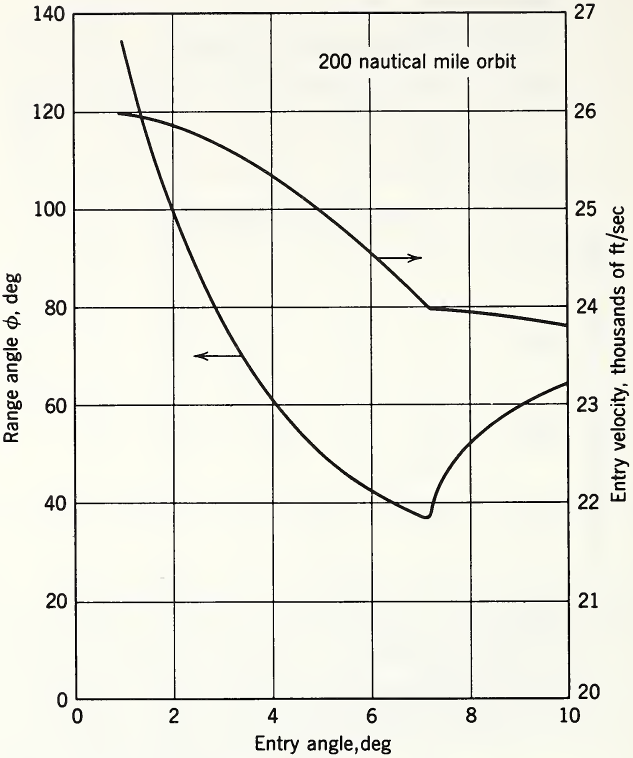

Fig. 18.8 Range angle and entry velocity, both as a function of entry angle.

nautical mile range. Figure 18.11 shows a time profile of a very flat re-entry. Note that the periods of time run about ten times as long as for a ballistic re-entry.

Turning now to re-entry at velocities near escape speed, such as a moon rocket would have, we face a somewhat different condition. If a satellite re-enters the atmosphere very steeply, say at 90°, then the peak g's go over 400. On the other hand, if we hit the high atmosphere (400,000 ft) at less than about 4°, we pierce it and proceed back into space for another few days. This means that a guidance system must function so as to bring the capsule in between an angle of 4° and some angle low enough not to produce excessive g's. This angle is found to be between 5° and 6°, leaving a very tight corridor only about 8 nautical miles wide which the guidance system must hit.

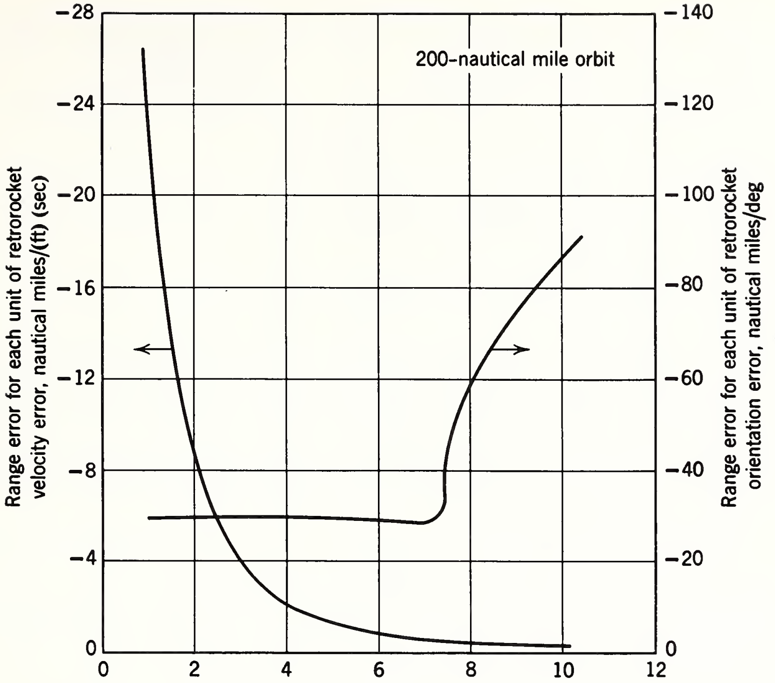

Fig. 18.9 Range error due to errors in retrorocket orientation and velocity increment, both as a function of entry angle.

To "open up" the narrow guidance corridor, several schemes may be used. For instance, a capsule can be designed so that its drag coefficient can be varied. Then, as it plunges into the atmosphere, it can be streamlined more and more to prevent the deceleration from reaching more than some fraction of the value it would have reached without such drag modulation. By such a scheme, if we can vary the drag coefficient by a factor of 10, the deceleration can be reduced to about 60 per cent of the unmodulated case.

A more effective way of reducing deceleration is by the use of lift. In this scheme the vehicle does a gentle pull-out as it enters the atmosphere.

Thus the body stays at very high altitudes (in low-density air) until it slows to a point at which it can proceed to lower altitudes without great drag forces. Figure 18.12 illustrates these results. Obviously, the allowable angular corridor is opened considerably. The linear tolerance on the guidance

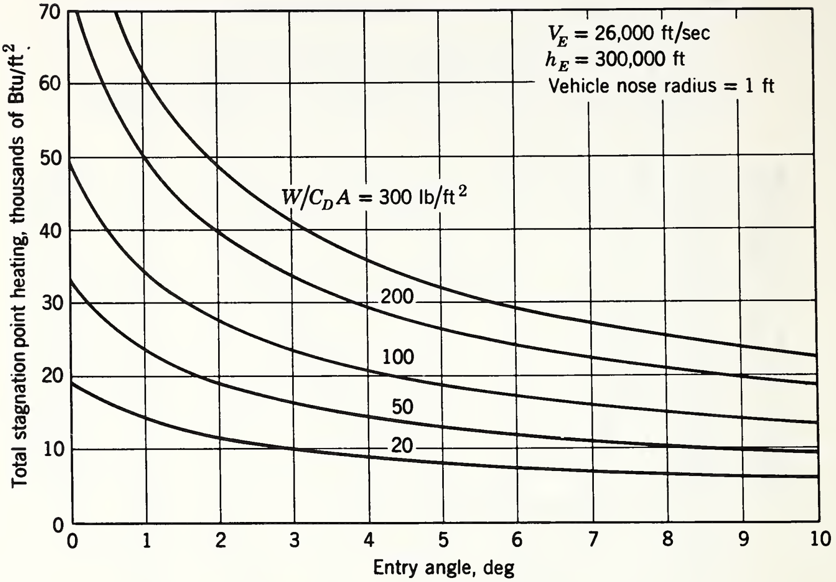

Fig. 18.10 Total stagnation point heating as a function of entry angle for various W/C_DA's.

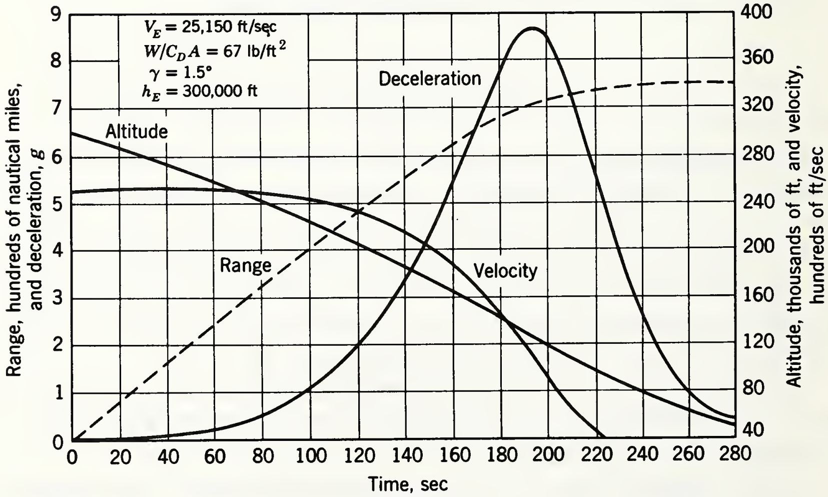

Fig. 18.11 Trajectory parameters for a pure ballistic re-entry from a low-altitude satellite.

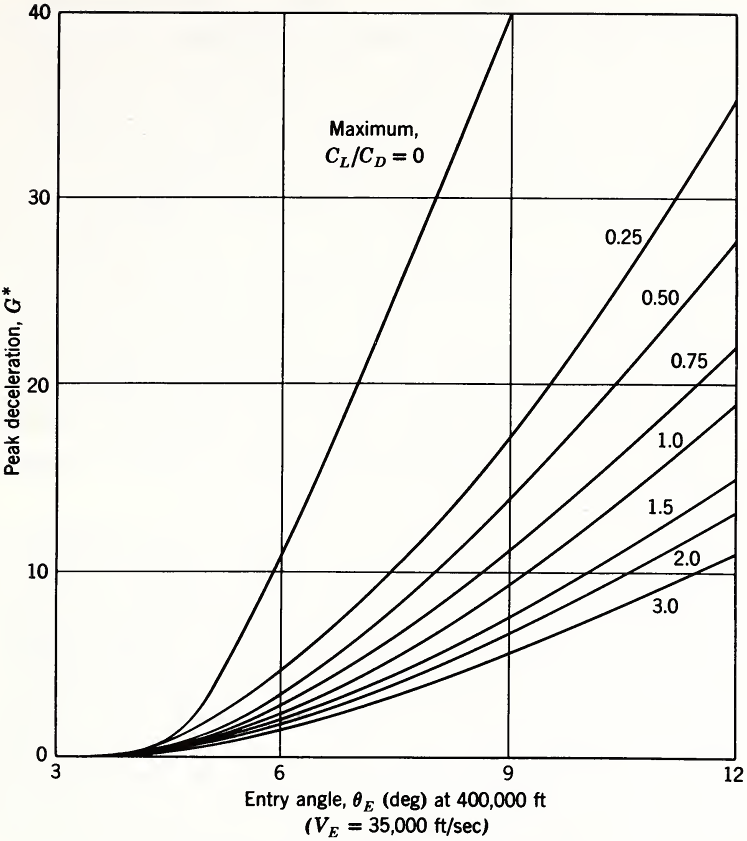

Fig. 18.12 Reduction of peak re-entry g's by use of lift.

system corresponding to this is relieved to about 80 nautical miles from the 8 nautical miles previously mentioned. Over and above this, the lift may now be used for a certain amount of maneuvering which will assist in picking out a landing site. As a matter of fact, there is nothing in principle to prevent the use of both a drag modulation scheme and a lifting body.

18.7 SATELLITE HEAT SHIELDING TECHNIQUES

The combination of low heating rates and extremely long heating times, which are encountered by both classes of manned re-entry vehicles (i.e., low-altitude satellite re-entry and re-entry at escape velocity), necessitates a review of the philosophy of heat shield design. Some present-day ICBM nose cones utilize the heat sink, or absorption, technique to ensure survival of the payload. This technique is thought to be unacceptable for a manned re-entry body because of the excessive weight of heat sink material required (effective heat capacity = 150 Btu/lb for copper) and because the insulation weight required to provide a tolerable temperature environment for the human passenger will be prohibitive. Even if a beryllium heat sink (effective heat capacity = 1000 Btu/lb) is employed, a large amount of insulation will still be required, and in addition the system is complicated by the requirement that the heat sink be jettisoned after the heating period. Because the heat sink retains the heat it has absorbed, the shield must be discarded to prevent the internal capsule temperature from becoming unendurable as time passes, including possibly time after landing.

Because of the comparatively low heating rates associated with satellite re-entry, it has been proposed that radiation alone be used to dissipate the heat. In this solution very high-drag bodies are employed, and the heat rates are generally reduced to less than 8 Btu/(ft^2)(sec). Thus a metal surface radiating at 2000°R is capable of dissipating the heat. This method has the disadvantage of leading to very large bodies which must be made very light, or to the use of drag brakes or similar devices. Very flat entry angles must be employed as well, with a subsequent large dispersion. Because of these problems, the ablating heat shield technique is believed to offer the best solution to the problem.

The ablating material does not constitute a major portion of the weight of a satellite; in fact, it is expected to be less than 10 per cent of the total. In any case, most of the material will be required simply to cover the large area of the satellite with a minimum thickness of heat-resistant material. If we were to attempt to cover the entire surface of the satellite with a material like fiberglass (120 lb/ft^3), it would be found that only a very thin layer could be spread over the entire surface of the satellite without an excessive weight penalty. Actually, most of the material would be needed in the nose area leaving a very thin layer to cover the sides. This thin layer would not stand heating for 300 to 500 sec; conduction into the material would heat and weaken it, possibly causing it to fail structually. A large amount of insulation would also be required behind the material to prevent heat from reaching the interior of the satellite. These considerations seem to indicate that a very low-density, poorly conducting material is needed so that thick layers of it can be applied for a low cost in weight. However, low-density materials do not usually have high resistance to shear or buckling forces, although they can be made to take moderate compressive loads.

On the other hand, since the dynamic pressures associated with satellite re-entry are very low (5 to 8 psi maximum), the shear forces turn out to be very small. Thus we can imagine materials that combine adequate strength and sufficient thickness to produce good insulation. As a corollary they may also have very high surface temperature so that radiation dissipates a large fraction of the heat.

REFERENCES

1. H. Julian Allen and A. J. Eggers, Jr., "A Study of the Motion and Aerodynamic Heating of Missiles Entering the Earth's Atmosphere at High Supersonic Speeds," NACA RM A53D28, 1958.
2. L. Lees, "Laminar Heat Transfer over Blunt-Nosed Bodies at Hypersonic Flight Speeds," Jet Propulsion, **26**, 259-269 (1956).
3. Saul Feldman, "Hypersonic Gas Dynamic Charts for Equilibrium Air," Avco Research Laboratory Report, January 1957.
4. Everett Braus and Martin Zlotnick, "Transport Coefficients of Air to 8000° K," Avco Research and Advanced Development Division Report, September 1958.
5. Peter Rose, Ronald F. Probstein, and Mac C. Adams, "Turbulent Heat Transfer through a Highly Cooled, Partially Dissociated Boundary Layer," J. Aeronaut. Sci., **28**, No. 12, 751-760 (1958).
6. R. L. Phillips and C. B. Cohen, "The Use of Drag Modulation to Reduce Deceleration Loads during Atmospheric Entry," ARS Journal, **29**, No. 6, 414-422 (1959).
7. L. Lees, F. W. Hartwig, and C. B. Cohen, "The Use of Lift During Entry into the Earth's Atmosphere," ARS Journal, **29**, No. 9 (1959).
8. George E. Solomon, "The Nature of Re-entry," Astronautics (1959).

19

AUXILIARY SUBSYSTEMS

D. E. Shonerd

19.1 INTRODUCTION

19.1.1 Scope

Auxiliary subsystems are loosely defined in three different ways. In the broadest definition the auxiliary subsystems consist of all portions of the ballistic or space rocket systems except the missile, that is, the support systems are the gun and the missile is the bullet. Another common definition states that the auxiliary subsystems perform all functions that are necessary to insure a successful mission for the vehicle. A third definition specifies the scope of auxiliary subsystems to include those functions required to launch the vehicle and to monitor the success of the vehicle's mission after launching.

Under the launch complex for a ballistic or space vehicle is a vast, complicated, and expensive array of mechanical, electrical, and structural elements. There are miles of pipe, conduits, and reinforcing rod; hundreds of pumps and valves for liquids and gases; hundreds of instruments for detecting, measuring, recording, converting, or transmitting signals; highly automated checkout equipment for sequencing and monitoring the missile and payload before flight; and trucks, forklifts, cranes, hoists, and elevators for handling and assembling the missile. This array is a part of the auxiliary support system required for the program.

Auxiliary subsystems are of critical interest in the development of any ballistic or space vehicle system for three reasons.

1. The availability of funding. The supporting subsystems in general require approximately 85 per cent of the total funding for a ballistic or space vehicle system.
2. There are difficult technical problems associated with support equipment which must be solved on a timely basis if severe restrictions or limitations to the complete system are not to occur.
3. The longest lead times are always required for auxiliary support systems, such as test facilities, handling equipment, and trained personnel to operate the system.

To achieve a well-integrated set of auxiliary subsystems to support a ballistic or space mission requires a high degree of technical and management effort. At the time the rocket vehicle arrives at the launch site for its countdown and testing phases, the auxiliary subsystems must have already proceeded through their own testing phases. Accordingly, although the rocket vehicle is undergoing its design, fabrication, and component test phases in preparation for flight test, the auxiliary support systems must go through design, fabrication, and component tests and complete functional tests. In general, this development cycle for auxiliary support systems precedes the development cycle for the missile and results in the freezing of technical interfaces at earlier dates than would be desirable from the standpoint of development of the rocket vehicle. Sufficient flexibility of design must be incorporated into auxiliary supporting systems to accommodate the changes in the rocket vehicle which invariably occur after final freeze dates on the auxiliary subsystem.

19.1.2 Problem Areas

The basic problem areas in the creation of auxiliary subsystems consist of the interaction of costs and lead times coupled with the new technical problems that have to be solved in order to support the particular space or ballistic rocket mission. The new concept of concurrency in the development of space or weapon systems has emphasized the importance of the development of auxiliary subsystems. Planning for concurrency has shown clearly that the longest lead times and largest costs exist with the support equipment and facilities. Although auxiliary subsystems are intended to support and assist in achieving a successful rocket flight, the concept of concurrency introduces important limits to the scope of the mission because of the early freeze dates and long lead times. For example, in an integrated weapon system there are, in addition to the missile, the facilities required for operation and maintenance, the transportation and handling system, the communication system for command control and for logistic support, the industrial complex for production, and, finally, the training facilities for the personnel required to operate and maintain the weapon system. Similarly, a space rocket research system also consists of the facilities and equipment required to check out and monitor the rocket while it is on the ground, the handling equipment required to bring the rocket to the launch site and support it during the missile countdown, and finally the data acquisition equipment required to monitor the missile and payload during its flight.

The cost breakdown for a typical rocket space research mission or for a weapon system is shown in Table 19.1. This type of broad cost segregation has been found to apply generally to most of the current programs. For a typical research project the 15 per cent of total funds for the missile is allocated for the purchase of existing rocket stages, for the design and development of the interstage structures and separation mechanisms, and for the procurement of the research payloads. The 40 per cent for facilities would include a new launch pad, a new or modified work tower and umbilical tower, a new or modified blockhouse and modifications to laboratory buildings for the final preparation of the vehicle. The 45 per cent of funds allocated for ground support equipment would

TABLE 19.1
Typical Cost Summary

Missile	15%
Facilities	40%
Ground support equipment	45%

include the transportation and handling equipment, the checkout and test equipment, launch control consoles, the data acquisition and data reduction equipment, and the new or modified downrange tracking equipment required for the particular mission.

For a ballistic missile system the cost breakdown of 15 per cent for the missile and 85 per cent for the auxiliary subsystems includes the entire initial cost for research, development, production, and activation of the system. Accordingly, the 15 per cent of total funds allocated for the missile includes the hardware required for flight testing and for the operational weapon system. The 40 per cent funding for facilities includes those blockhouses and launch complexes required for the Research and Development (R & D) program, and the production, command, and launch complex facilities required for the operational system. The auxiliary equipment which accounts for 45 per cent of the total funds encompasses communication systems, transportation and handling systems, checkout, monitoring, and sequencing equipment required for development and production, and the maintenance and training equipment required for the weapon system.

Generally, the majority of difficult scheduling problems arise with auxiliary support systems. In Fig. 19.1 is shown a

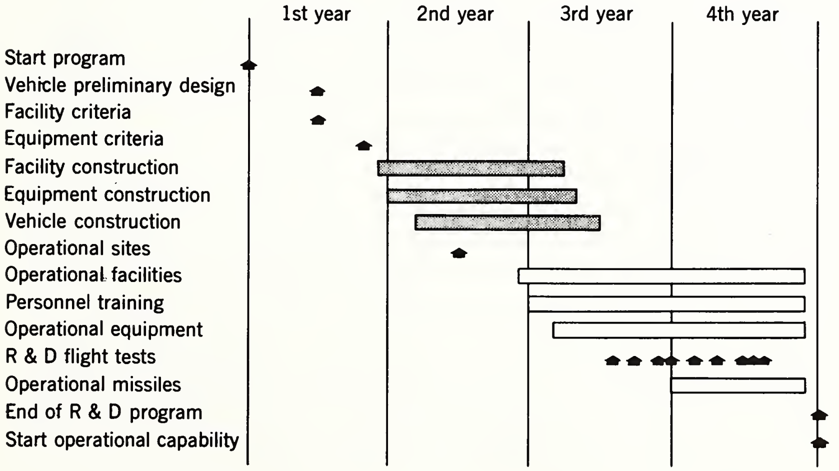

Fig. 19.1 Typical program schedule.

typical program schedule. This schedule illustrates a typical orderly progression from an established concept at the beginning of the first year to an operational or research capability at the end of the fourth year. Based on the philosophy of concurrency, this program proceeds through the following steps: (a) a preliminary design phase leading to the establishment of technical design criteria, (b) the construction of the vehicles, facilities, and equipment required for R&D testing, (c) the complete system flight testing, and (d) the construction of operational missiles and equipment facilities and the training of the personnel required.

The philosophy of concurrency also introduces the concept of "buy before fly." This is clearly illustrated in Fig. 19.1. At the end of the first system flight test in the third quarter of the third year, all operational facilities and operational support equipment have been procured. Midway through the flight test program the production cycle of operational missiles must be begun. Clearly, design changes introduced from the experience gained in the system flight test can only result in a retrofit or a modification program to the operational system after the end of the development program.

Incorporation of flexibility plus growth potential in auxiliary support systems is emphasized by the programming of "buy before fly." For example, the criteria for supporting facilities for the R&D program must be frozen at the end of the vehicle preliminary design period. Similarly, the final support equipment criteria must be frozen midway through detailed design period for the missile. Since it is clear that there will be changes in design to the missile after the supporting facilities and equipment facilities are frozen, the auxiliary subsystems must be made as flexible as possible. Such flexibility permits manufacture of facilities and equipment, and the training of personnel for the operational system, to begin approximately a year before the freeze date of the operational missiles. In a tightly integrated research or weapon system, changes to the missile "downstream" will always cause changes to the supporting subsystems. These changes can only be accommodated in an expeditious manner if flexibility has been introduced early in the design of the support systems, making them usually nonoptimum.

In other words, when the operational or research system is finally activated, inefficiency in the supporting systems will become evident because of the built-in allowance for growth which was incorporated earlier in the program. For example, if the original concept for a ballistic research rocket planned to use the highest-performance solid propellant available, considerations of potential safety problems will suggest a Class 9 explosive for the propellant. The criteria that have been established for R&D facilities and for operational usage will reflect this assumption of Class 9 explosives very strongly. The supporting buildings will be isolated by established safe separation distances. Expensive earth barricades and reinforced concrete construction will be built in accordance with standard safety regulations. If midway through the system test program it is found that this high-performance solid rocket propellant is a Class 2, the facilities under construction are clearly more expensive and awkward than would be required for the final system.

Another important aspect of program scheduling, implied with the lead times shown in Fig. 19.1, is the requirement for installation, checkout, and testing of the auxiliary subsystems before their use with the rocket vehicle. For example, the R&D facility construction is shown as starting at the beginning of the second year and ending approximately three months before the first R&D flight test. Included in this sixteen-month period is not only the fabrication of the equipment but also its installation, the inspection and checkout of the equipment subsystems, and finally functional testing to make sure that the entire auxiliary subsystem is ready to support the research or weapon mission. To support this very important test program for the auxiliary subsystem, special inert laboratory missiles may be required so that the functional testing is complete in every detail. Similarly, with the operational equipment a lead time of approximately twenty months is required, since the installation and checkout will be under field conditions, and even more extensive functional tests must be made to insure that this equipment will perform its operational role.

The most important impact of the early freeze dates for supporting equipment and facilities is in the rigidity introduced in the missile development program. Even the most intelligent use of flexibility in the design of the supporting subsystems cannot anticipate changes that will occur in an R&D program. Unfortunately, the change that might be highly desirable in the over-all goal of the program may not be practicably introduced because of the inertia of all the supporting equipment and facilities. For example, the incorporation of a new and better tracking beacon in a research payload may not be possible because the sequencer and monitor equipment in the launch control consoles cannot be ready in time, or because the downrange tracking facilities cannot be modified in time to meet the schedule for the research mission.

The inertia introduced into a ballistic rocket development program by the early freeze dates of supporting subsystems is the result of the massive array of back-up subsystems which are required to implement the auxiliary support systems. For example, there is the test support equipment required for the functional test of the auxiliary support systems; there are the training programs required to supply the personnel for operating and maintaining the auxiliary support systems; there are the tools, jigs, and fixtures required to fabricate and install the auxiliary subsystems at the launch site; there are the contractual procedures which must be used for the incorporation of changes into the complex of contractors and subcontractors who will be working on a ballistic or space rocket system.

The orderly progression of a development program through the key steps as shown in Fig. 19.1 can only be achieved if key decisions are made in a timely manner throughout that development program. Typical key decisions and their required dates for this hypothetical development program are shown in Table 19.2. These key decisions establish the course and nature of the system through the progression of

TABLE 19.2

Typical Key Decision Dates

System concept	48 months
R&D facilities	42 months
R&D equipment	40 months
R&D missiles	37 months
Test plan	36 months
Operational sites	30 months
Operational facilities	24 months
Operational equipment	20 months
Operational missiles	12 months

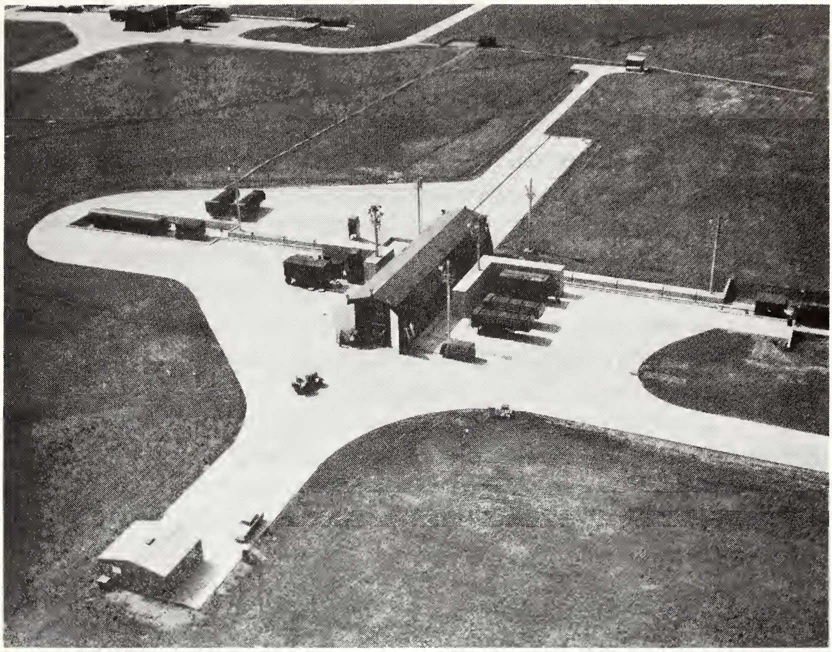

Fig. 19.2 Thor launch complex.

study phases, hardware phases, and testing programs. These key decisions and their required dates are the most important management tool that exists in an R&D program. The failure to meet one of these key decision dates may be the first clear indication of an inescapable slippage in the entire program.

The study and testing phases of any R&D program are intended to supply the data required to make the key decisions on a timely basis. For example, preliminary design is intended to make those trade-off studies required for decision on a final design configuration. Environmental and functional tests of components and subsystems are intended to provide the data required for decisions regarding the cancellation of back-up programs and for the incorporation of the particular equipment in the operational system.

The typical key decisions seen in table 19.2 must always be made at a time in the over-all development program when the data available is insufficient for an optimum decision. Any ballistic or space vehicle program must begin with a decision regarding the over-all concept for the program. This may be a definition of the space mission or a definition of the operational requirements which the weapon system must meet. Following the establishment of the program concept, the initial feasibility trade-off and preliminary design studies begin. Midway through this study phase the design for the facilities required for the R&D program must be frozen. Clearly, 42 months prior to the activation of the weapon system there are many unanswered questions which will influence the type of R&D facilities that may finally be required. However, because of the long lead time needed for the contractual procedures and also the design and construction of brick-and-mortar facilities, this decision to freeze must be made.

Decisions freezing the supporting equipment required for the R&D program must also be made before the completion of the design of a rocket vehicle. The long lead time for equipment items is required for fabrication, component testing, installation, checkout, and final functional testing before its end use.

After approximately eleven months of study and design, the configuration for the rocket vehicles required for the first R&D testing phase must be established. This key decision must take into consideration the problems associated with introducing changes into the facilities and equipment that were frozen several months earlier. Following the design freeze for the R&D missiles, or approximately eighteen months before the first flight testing, a complete general test plan must be established. This test plan must also reflect the facilities and equipment that will be available to support the test activities.

TABLE 19.3
Typical Support Functions

Transportation and handling
Environmental control
Sequencing and monitoring
Launch control
Telemetering
Tracking during flight
Recovery
Safety

Key decisions relative to the operational phase of the weapon system must, in general, be made before starting complete system testing. During the fabrication of the test facilities, test equipment, and R&D missiles, but before the key system flight test, the key decisions regarding the operational sites and the operational facilities must be made. Key decisions for the operational missiles, in general, must also be made part way through the system test program and before a high confidence level can be established regarding the functional capabilities of the system.

19.2 OBJECTIVES OF AUXILIARY SUBSYSTEMS

19.2.1 Typical Support Functions

Broadly, the objectives of the auxiliary subsystems are to provide the supporting functions that are necessary to insure a successful flight for the ballistic or space vehicle. The basic categories are the support functions for the missile while it is on the ground, and the monitoring functions while the missile is on its flight mission. Typical support functions are shown in Table 19.3.

The supporting functions begin at the factories where the missile components are first manufactured; these include the inspection and checkout facilities required to make sure that the individual air-borne components and subsystems meet the design requirements. After the components and subassemblies are assembled into a missile, the support systems play a greater and more complex role. During the several weeks in which a missile is undergoing checkout and countdown at the launch site, the prelaunch preparations rely heavily on the auxiliary subsystem facilities and equipment. The checkout of the missile, the monitoring during the launch countdown, the flight monitoring, and the recovery of data capsules of the missile are all important examples of supporting functions.

Other supporting functions have a less direct application to the missile and may in some instances limit the timing or nature of the mission of the ballistic or space vehicle system. For example, analyses of safety problems start concurrently with the design of the missile. Selection of a launch site will be strongly dependent on safety considerations, and the operational flight paths will be determined to a large extent by range safety considerations. Further safety rules influence strongly the design of all facilities and equipment associated with the launching of missiles.

19.2.2 Meteorological Effects

As another example, the missile range meteorology plays a very important role during the countdown, both in long-range forecasting and in the determination of meteorological data, such as air density, winds, pressure-altitude relationships, refractive index, and relative humidity occurring during the flight of the missile.

19.2.3 Missile Monitoring

A number of difficult technical problems arise in the design and development of support equipment and facilities which may strongly influence the nature of the mission for the complete weapon or space vehicle system. For example, the type of early developmental flight tests that will be made are generally established by carefully monitoring the conditions in and around the missile during its flight. The ability to analyze failures or to evaluate the success of the mission depends on the data available from the monitoring system. The tracking accuracy of the available optical and radar equipment is not good enough to answer satisfactorily many of the re-entry problems of ballistic nose cones. The limited number of channels that may be telemetered or recovered in data capsules is not sufficient to establish clearly the causes of missile malfunctions. The meteorological data concerning the upper atmosphere is never complete enough to satisfy the requirements for evaluating the nature of the ballistic trajectory. Accordingly, research programs are underway in all these areas to advance the ''state of the art'' for the purpose of improving the probability of successful missions for ballistic and rocket vehicle systems.

The support system for transporting and handling the missile involves a variety of equipment at contractors, plants, at assembly sites, and at the launch complex. Compatibility between the carts and trailers for components and the jigs and fixtures for missile assembly must be established. Similarly, compatibility between the transporter and erector and the launcher and work tower must exist. It is only through careful design of the transportation and handling equipment that the loading conditions on the missile on the ground can be limited to less than the flight-induced loads.

19.2.4 Environmental Control

Environmental control includes the equipment required to maintain temperature, pressure, humidity, shock vibration, fungus, and sand and dust to those levels specified by system considerations. The concept of designing equipment and facilities to withstand nuclear detonations introduces highly complex technical problems of shock isolation, nuclear radiation attenuation, and overpressure resistance. In many instances, the inability to control the environment will cause design changes to the missile.

19.2.5 Sequencing and Monitoring

The sequencing and monitoring functions become more difficult the nearer the missile comes to the launch countdown. Many of the components and subsystems of a ballistic rocket vehicle may be manually tested, using standard test meters and recording equipment. However, after a guidance system has been mated, for example, to a solid propellant rocket motor, safety considerations dictate that most of the functional testing be done remotely with carefully controlled automatic sequences. Similarly, after the missile is readied for launching, safety considerations require that all monitoring of the performance of all elements of the air-borne system be done remotely. The sequencing and monitoring equipment used for this functional check during the final phases of the launch countdown may become very complex because of the nature of the instrumentation on the missile.

19.3 DESCRIPTION OF TYPICAL AUXILIARY SUBSYSTEMS

19.3.1 Launch Complex

In Table 19.4 is shown a list of typical support equipment and facilities. These may be categorized in terms of those items required to ready the missile before launching and those required for monitoring functions while the missile is on its flight mission. They may also be categorized in terms of

TABLE 19.4
Typical Support Equipment and Facilities

Transporter-erector
Launcher
Blockhouse
Static test stands
Checkout and launch consoles
Assembly jigs and fixtures
Telementry ground stations
Recovery capsules
Pumping facilities for liquid propellants
Optical and radar tracking facilities

their long lead times, the large cost associated with their design, construction, and checkout, and in terms of the typical technical problems which may be encountered in the program required to develop these items of supporting equipment and supporting facilities.

The blockhouse of a typical ballistic missile launch complex is a good example of the complex type of brick and mortar installation which must be designed and constructed before the initiation of a flight test program. A typical blockhouse is dome-shaped and windowless, and may be as much as 200 ft in diameter and 40 ft to 50 ft in height. It is usually a two-story building with two protective layers of thick reinforced concrete roof and walls. These two layers of reinforced concrete may be separated by a 10- to 12-ft layer of sand. The first floor of the blockhouse will usually contain the personnel ready rooms, the instrumentation, repair rooms, and the power equipment required to operate the equipment in the blockhouse. The second floor will usually house all the command control equipment, and may include some of the quick-look data-recording equipment. This floor is the main operation center of the launch complex during the checkout, countdown, and launch procedures. Periscopes and television receivers are used to obtain a full view of the missile. Other equipment includes the operating consoles, the communication terminal equipment, and the racks of electrical gear required for recording and monitoring data.

In Fig. 19.2, is a typical example of the Thor launch complex. The lead time for such facilities was considerably longer than that required for any of the payloads or vehicles used in the research or operational programs. In general, some design limitations were placed on the rockets and on the vehicles because of the nature of the supporting equipment and the facilities available.

In Fig. 19.3 is shown a Thor operational missile being erected for simulated firing. The transporter-erector holding the missile is typical of the handling support equipment required for this semi-mobile operation. The problems of defining technical interfaces between the missile and the transporter and between transporter and the launcher must be solved very early in the research program.

In Fig. 19.4 is shown a typical work stand for a space vehicle system. The design of this work stand, including the positioning of the work platforms, was frozen before the final details of rocket configuration were known. The design criteria for a work stand of this type must be prepared by the rocket and payload designers since the functions to be per-

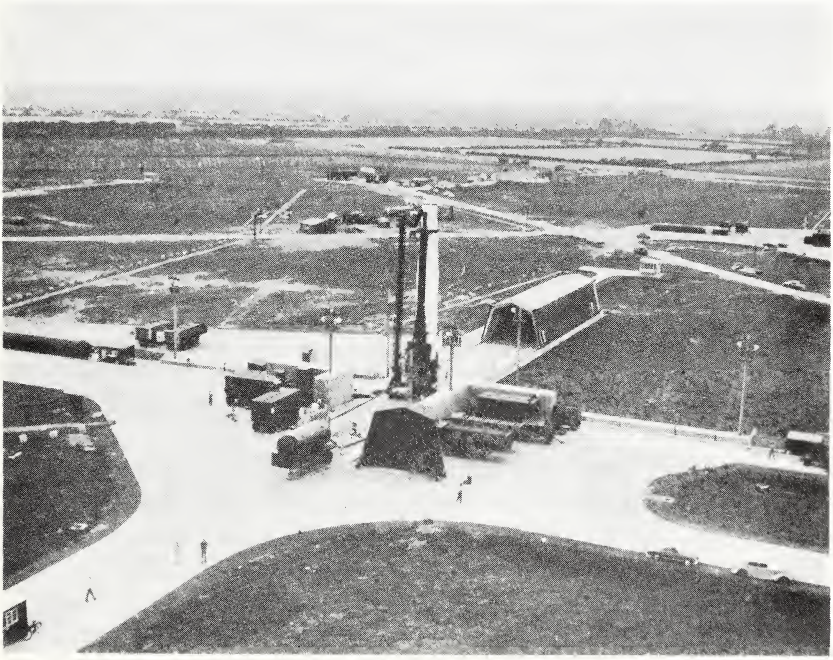

Fig. 19.3 Thor operational missile being erected.

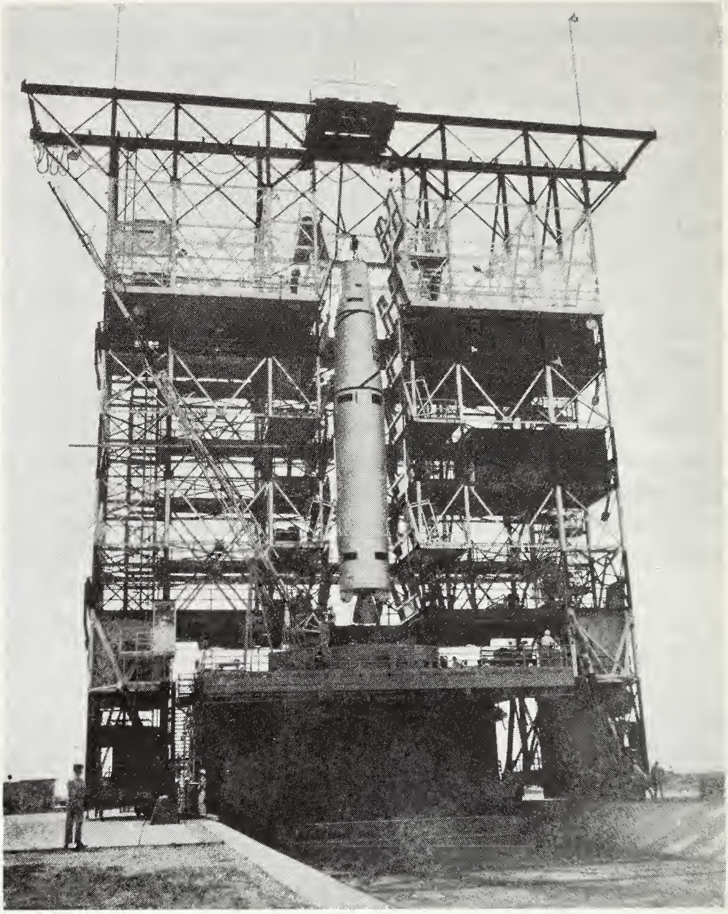

Fig. 19.4 Work stand for space vehicle system.

formed are intimately connected with the details of the design, propulsion and guidance systems, and research payload.

In Fig. 19.5 is shown the complete launch complex for the Atlas intercontinental ballistic missile. The blockhouse, the work tower, and the launch stand are typical examples of the large, complex facilities and equipment required for a ballistic vehicle using liquid propellant rocket engines. The lead time for these facilities and equipment includes not only the design, fabrication, and checkout, but also a testing program to determine the functional adequacies of the supporting systems. In Fig. 19.6 is shown another view of the launch pad

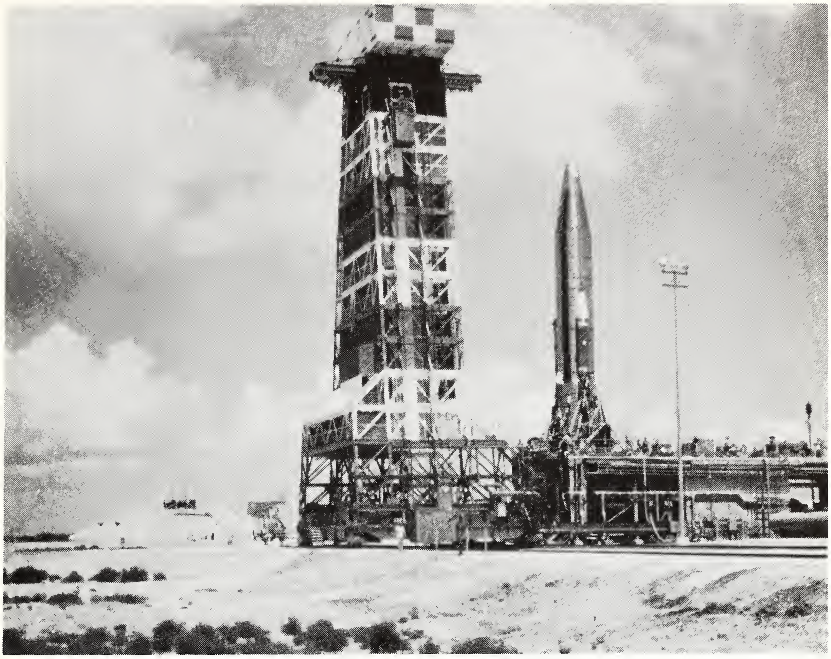

Fig. 19.5 Launch complex for Atlas missile.

and work tower for the Atlas missile. The missile transporter is midway in its erection cycle for placing the Atlas on its launch stand. In Fig. 19.7 the Atlas transporter has completed its erection cycle and the Atlas is in position on its launch stand.

Typical support equipment on the launch stand for the Titan missile is shown in Fig. 19.8. The work tower has been lowered in the foreground. The Titan missile is setting on its launch stand with the umbilical tower providing the only connection to the missile.

A typical range station for data acquisition is shown in Fig. 19.9. All test programs must tailor their data acquisition requirements to the facilities and equipment that are available at the flight test ranges.

In Fig. 19.10 is shown typical equipment which will be found in the blockhouse for ballistic rocket programs. It shows typical reporting equipment for quick-look data and for monitoring the status of the missile during the prelaunch and

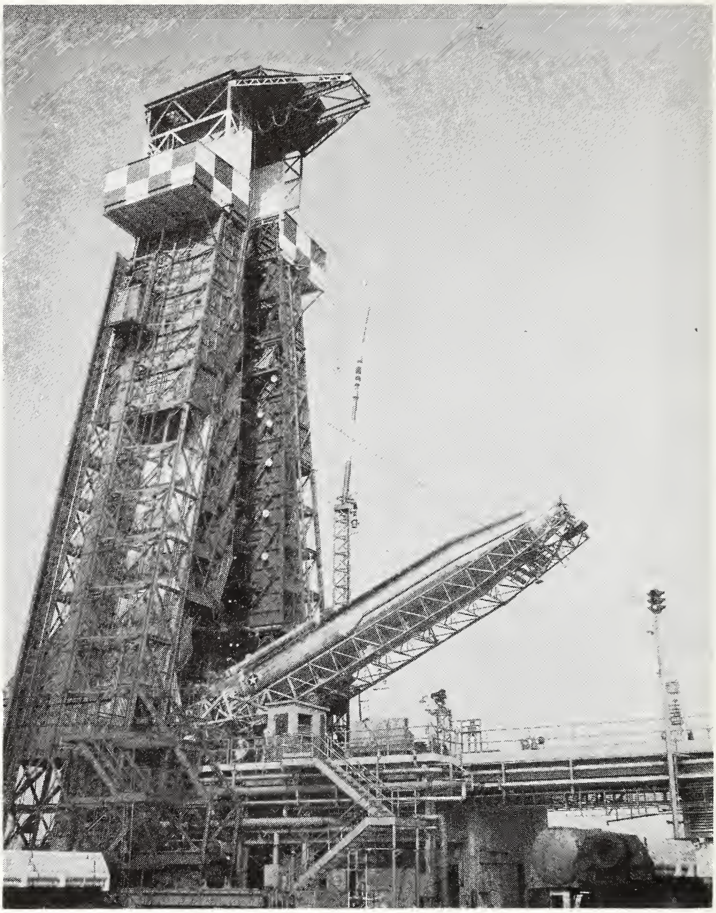

Fig. 19.6 Atlas missile being erected on launch pad.

launch countdown, and the various monitoring and command consoles required for the launch countdown.

19.4 COUNTDOWN PROCEDURES

19.4.1 Two-Year Countdown

There are several types of countdowns that are of critical importance in the development of a ballistic vehicle system. There is the widely publicized launch countdown that requires several hours or several days at the launch site with the

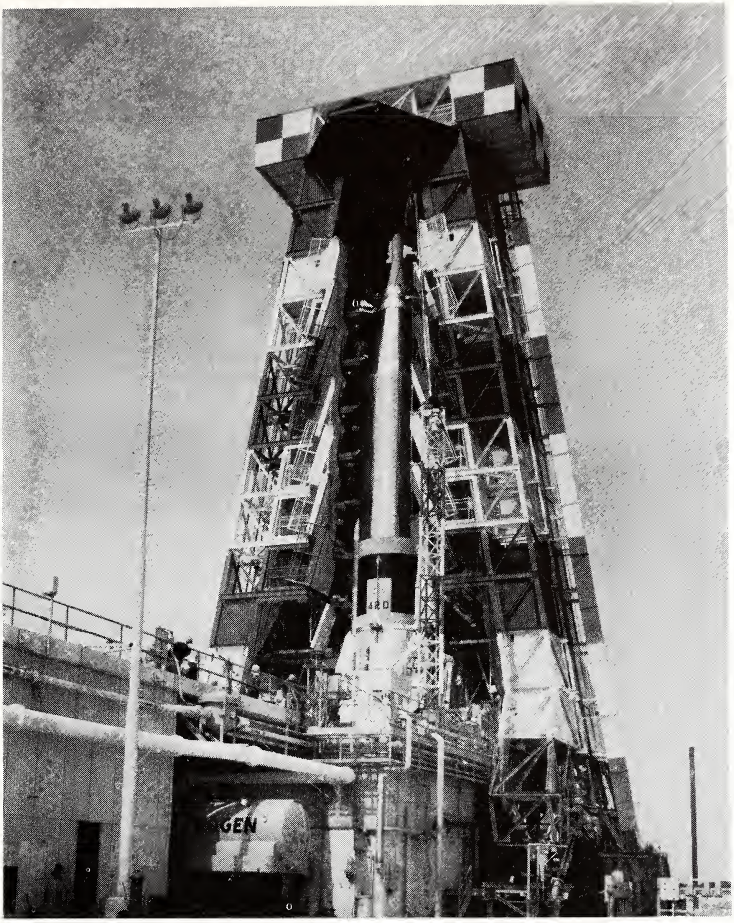

Fig. 19.7 Atlas missile in fully erected position on launch pad.

missile on the launcher. The second countdown is the two-to four-week countdown which starts when the missile arrives at the missile firing base. The third countdown, which is even harder to plan, is the one-to two-year countdown which starts with the first fabrication and testing of components of the missile or the supporting equipment.

The term "two-year countdown" is used to emphasize the high degree of planning and coordination which is necessary to have all elements of a weapon system functioning properly in the final use. While the missile and its payload perform their final objectives during the flight, the supporting equip-

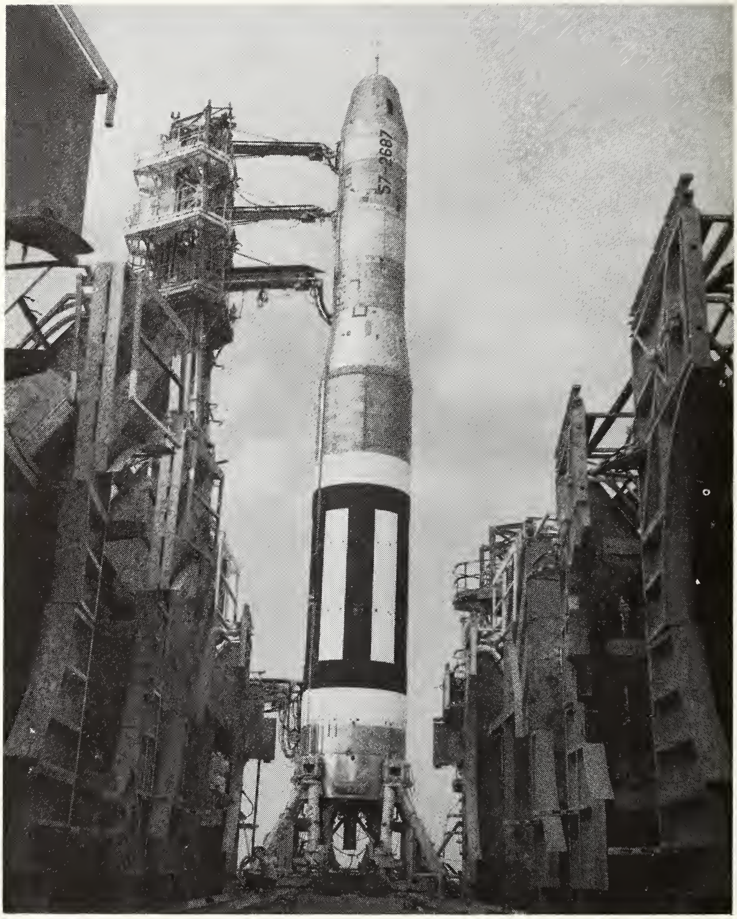

Fig. 19.8 Typical support equipment on Titan launch stand.

ment may perform their final objectives many weeks or months before the flight. To insure success of the entire program these auxiliary subsystems must have been functionally tested and modified, if necessary, long before the actual flight of the rocket vehicle. The two-year countdown is the backbone of the closely integrated planning which leads to successful completion of a ballistic rocket research or weapon system program.

As an example of a two-year countdown, consider a piece of transportation equipment for a ballistic weapon system. Approximately two years before the first flight test of the

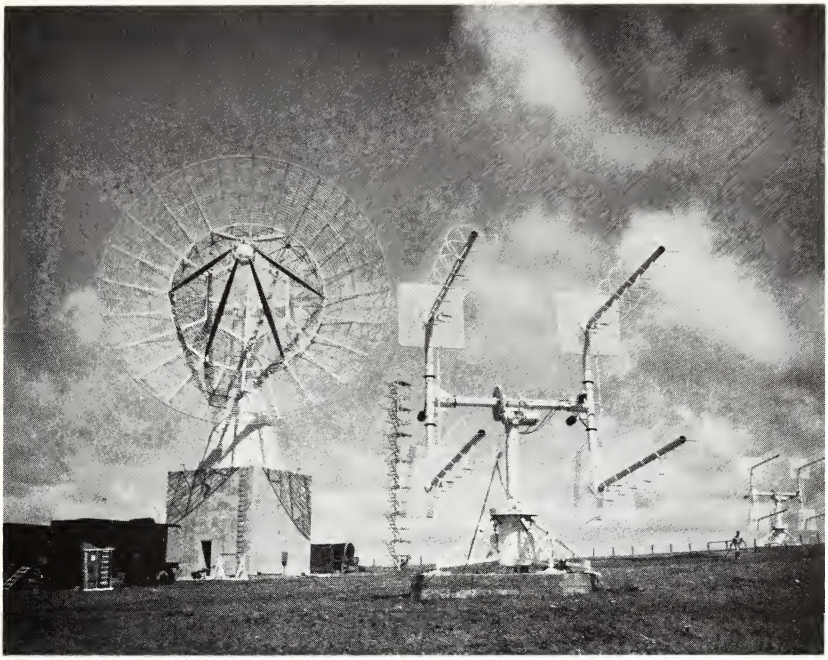

Fig. 19.9 Typical range station for data acquisition.

weapon system, the design criteria for this handling equipment are made final. The preliminary and final design are then completed in the next six to eight months and the first prototype equipment is fabricated. Approximately six months before the first flight test, this equipment is then functionally checked and run through a test program of its own to determine its applicability for the weapon system testing. Finally, approximately two months before flight test, this equipment will be shipped to the flight test base, and compatibility and checkout tests will be made at the launch site. After the missile arrives at the launch site, additional compatibility testing and dry runs are made, utilizing all elements of the weapon system. Finally, at the end of this two-year countdown, this particular element of the auxiliary support system is used for the one or two hours required to transport and handle the missile in preparation for the actual launch.

The development of nose cones for ballistic re-entry vehicles is another example of several-year countdown products. Extensive model testing in wind tunnels, shock tubes, heated

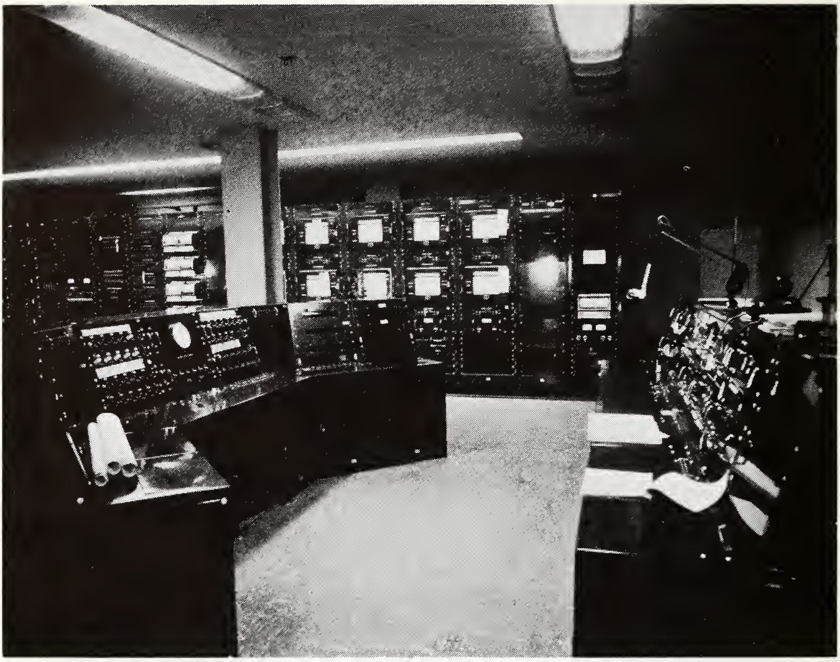

Fig. 19.10 Equipment in blockhouse of ballistic rocket program.

jets, rocket exhausts, and plasma jets began several years before the first programmed full-scale flight test. The subscale tests were followed by larger-scale flight tests using multistage rocket vehicles especially for that purpose. Finally, after this many-faceted program of developmental testing, the first confirmatory full-scale flight test using the ballistic rocket systems were made. It is important to note that the long lead time items in this program for the development of a re-entry nose cone were for the supporting subsystems. The facilities and laboratory equipment required to conduct the shock tube and wind tunnel tests had to be designed and fabricated before the start of testing. Similarly, the auxiliary subsystems to support the multistage rocket re-entry test vehicles had to be studied many months before the first launch of this test vehicle. Finally, plans for the instrumentation and data acquisition equipment for studying the re-entry phenomena on the full-scale launches were made long before the launches.

One of the most important philosophies underlying a two-year countdown is the premise that no untried equipment, facilities, or procedures can be checked out for the first time at the flight test base. Through bitter experience it is almost axiomatic that critical errors will occur if changes in procedures or equipment are made while the rocket is on the launcher. Since very tight schedules are maintained for all firings from flight test bases, it is not acceptable to have delays of several days or weeks because of malfunctions in auxiliary support equipment. Because the supporting equipment may be as technically sophisticated as the rocket vehicle itself, completely separate test programs are required to assure functional acceptance of the support equipment.

19.4.2 Prelaunch Countdown

A prelaunch countdown includes that four- to six-week period, starting with the delivery of the missile to the flight test base and usually ending with a complete dry run of the launch countdown. The missile is usually delivered to the base as a group of disassembled components. Each of these components must be throughly inspected and tested for functional acceptance. As the components are assembled into the subassemblies—such as guidance, control, and instrumentation—the subsystems must undergo extensive compatibility and functional testing. Finally, the subsystems are joined together, and a complete checkout and test of the air-borne system is made. The usual approach during this prelaunch countdown period is to perform a complete checkout and calibration of all systems in laboratory environment before delivery of the missile to the launcher. Because of the tight scheduling and launching at flight test bases, it is necessary that this prelaunch countdown be carefully planned and scheduled on a daily or hourly basis.

Midway through the prelaunch countdown period the missile will be taken from the laboratory assembly area to the launcher. On the launcher additional compatibility and functional tests will be made, utilizing mechanical, electrical, pneumatic, and hydraulic connections at the launch complex. In general, on the launcher the complete series of component subsystems and complete system tests are again repeated to insure compatibility with the new launch environment.

A prelaunch countdown usually culminates in a complete dry run of the actual launch countdown. The dry run is basically a complete system test performed in accordance with a rigid time-based sequence of procedures. All procedures except irreversible actions, such as safety and arming, are performed during this dry run.

19.4.3 Launch Countdown

After the extensive preparation of the two-year countdown and the prelaunch countdown, the actual launch countdown may be anticlimatic. This countdown usually requires two days. On the launch minus one day, most of the work is involved in readying the various ordnance systems that are aboard a rocket vehicle. A rocket vehicle will contain a relatively large quantity of explosive components, including explosive bolts, prima cord or shaped charge destruct units, pyrotechnic flares, and squibs and igniters. The installation of these explosive elements are usually performed after all system testing has been completed. Other activities which may be performed on launch minus one day are preparing and load-testing the rocket power supplies and purging of the rocket propellant systems.

The final countdown for support systems does not end with the flight of the missile from its launcher. Many of the downrange data acquisition systems may be in operation several months or hours after the launch countdown in the block house has reached T minus 0.

In spite of the extensive planning and pretesting there are usually circumstances that require minor deviations in the countdown procedures. These may be rocket or range technical difficulties or uncontrollable operational factors. A well-rehearsed countdown procedure is required if these minor deviations are to be handled expeditiously without reducing the probability of a successful flight mission.

19.5 DATA ACQUISITION

19.5.1 Telemetry

One of the most important functions of the auxiliary support system is the acquisition of data during the flight of the missile. In order to establish the nature of the functional performance of the missile, it is necessary to monitor continuously many channels of information concerning the propulsion, guidance, control, and payload subsystems of the missile. In addition to these missile parameters, it is also necessary to know the trajectory of the missile and the characteristics of the atmosphere through which the missile is traveling.

Various systems of telemetry are used in almost all ballistic or research rocket flights. Transducers placed aboard the missile measure the selected parameters and provide an electrical analog output proportional to the value measured. The various telemetry systems, such as frequency modulation, amplitude modulation, and pulse code modulation, are systems for transmitting this measured value to the ground where it may be recorded and analyzed. The selection of a particular telemetry system will depend on the following factors.

1. Nature of the parameters to be measured.
2. Weight and space available on the missile.
3. Nature of the receiving equipment available at the flight test site.
4. Nature of data reduction available at the flight test site.
5. Type of analysis which must be performed on the data.

The various systems have certain advantages in terms of frequency of response, accuracy of data, compatibility with digital systems, ease and speed of data reduction, and cost of transmitting and receiving equipment.

Early decisions affecting the entire development program must be made to provide an adequate telemetering support system. For example, in the typical program shown in Fig. 19.1 the facility criteria released during the first year must include any new telemetering ground stations that may be required for the R&D flight tests or the operational capability. Similarly, the key decisions shown in Table 19.2 relative to R&D equipment, R&D missiles, and the test plan are all intimately connected with the type of telemetry system to be used. The data-recording and data reduction equipment in the blockhouse must also be closely tied in with the type of telemetry system to be used.

The location of the antenna and transducers aboard the missile may dictate certain aspects of the design of the entire missile. For example, if transducers must be imbedded within the grain of a solid propellant rocket motor, this will have an early effect on the design of the grain and case of that motor. The antenna located in fins or stabilized skirts may dictate the the type of material used and also the structural configuration of the fin. The location of antennas in re-entry vehicles also strongly influence the over-all configuration of the nose cone.

The test plan, developed approximately two years before the first R&D test, must spell out in detail the nature of the channels which must be telemetered to the ground. Accordingly, all technical characteristics of the telemetry support system must be established at this time. Although a limited number of changes may be made after the test plan is finalized, these changes may result in a reduction of reliability, an increase in cost, and a delay in the development schedule for the complete system. Since it is necessary to run a complete testing program on the telemetry system before it is used on a missile, two years is not unusually long for the design, fabrication, and functional, environmental, and compatibility testing that must be performed before the first complete missile flight test.

19.5.2 Recovery

The recovery of a missile or of a data capsule from within a missile is a technique commonly used to acquire information concerning the functioning of the missile during its flight. In many cases identical data may be telemetered to the ground and also recorded in onboard data capsules which are recovered after the flight. The addition of a supporting system to recover a data capsule will cause significant changes to be made to the missile and to the ground support system.

In typical data capsule recovery systems, the missile-borne sequencing starts at the beginning of the re-entry phase. The ejection system may be armed at altitudes of greater than 200,000 ft and the capsule ejected very soon thereafter. The capsule must then be designed to withstand re-entry environments. The total sequence may involve the ejection of several parachutes to assure the survival of the capsule during the re-entry. Additional functions in the sequence will be the ejection of dye markers to pinpoint its position in the sea or on land, the ejection of floats, and the energizing of some type of transmitter to assist in the search for the capsule. On the ground the supporting system will include the boats, airplanes, or ground vehicles required to search for the capsule, the data reduction equipment required to handle the recorded data within the capsule, and the checkout and monitoring equipment required to see that the data capsule is functioning properly during the launch countdown. For a typical overwater flight, a fleet of ships may be required to cover the projected impact areas for the flight. The supporting communication system to maintain safety and the coordination of this fleet of ships during the countdown of the flight of a ballistic rocket is another supporting subsystem which must be provided.

There have been many types of beacons used to assist in the recovery of data capsules. These include radio transmitters, flashing lights, pyrotechnic flaters, radioactive transmitters, and even olfactory transmitters. Each of these types of beacons has been used with varying degrees of success. The parameters that must be used in the selection of a transmitter include the following.

1. The length of time the beacon must transmit.
2. The range required for the transmitted signal.
3. The air-borne weight and volume that can be allocated for the beacon.
4. The environmental conditions that will occur while the beacon must operate.

The radioactive source technique for recovery of data capsules was pioneered at the Holloman AFB, New Mexico. Its primary advantage is in the minimum weight and high reliability of a radioactive element as a transmitter. The total weight for most applications was less than 2 oz and the reliability is almost 100 per cent since there is no known way to cause a radioactive element to stop transmitting. High-energy gamma rays are used in this recovery technique since ranges of approximately one-quarter mile can be achieved with radioactive sources. A good source for high-energy gamma rays is cobalt 60. The cobalt 60 may be encapsulated in a tiny machine screw and this machine screw attached to the missile payload or fin during the last phases of the launch countdown. After impact, Geiger counters or scintillometers are placed aboard light aircraft or helicopters and a search of the impact area is made. A thousand square miles may be searched in an eight-hour period using this technique. After finding the radioactive scource and the data capsule, it is necessary to remove the source, using 4-ft to 6-ft tongs before taking the data capsule for data reduction. The radioactive sources are stored in lead pigs weighing several hundred pounds. Radioactive source recovery technique is not usually used when photographic film is carried in the data capsule. The weight of lead shielding required to prevent destruction of the film by radioactive eminations usually offsets the weight and reliability advantage of the radioactive technique.

19.5.3 Tracking

The problem of tracking the vehicle during its flight has been undergoing study for many years. The position, velocity, acceleration, and attitude of the missile relative to three mutually perpendicular axes are required throughout the entire trajectory. In addition, event data, such as stage separation, flare ejection, or rocket ignition, should be detected by ground tracking equipment. Radar skin tracking and radar tracking of beacons carried aboard the missile are commonly used methods for determining position, velocity, and acceleration. For position data of highest accuracy, ballistic cameras are often used. In this technique the missile is flown at night with a flashing light aboard the nose cone. The ballistic camera has a fixed photographic plate which photographs the flashing light and the star background. The camera-aiming direction is determined from analysis of the star tracks, and the position of the missile is then determined from the analysis of data from at least three of the ballistic cameras.

The manner in which tracking requirements may influence the entire missile and the supporting subsystems is exemplified by the Hypersonic Test Vehicle program at Holloman AFB. The Hypersonic Test Vehicle was a two-stage solid propellant rocket round which was fired to obtain aerodynamic data at hypersonic Mach numbers and high Reynolds numbers.

The first stage had an acceleration of 100 g, and the second stage had a peak acceleration of 200 g. The round reached velocities of approximately 7000 ft at altitudes of a few thousand feet above the ground. In order to correlate the data obtained aboard the missile, it was necessary to know the velocity and position of the missile accurately. On the initial flights of the missile, multiple fixed cameras and tracking phototheodolite camera stations and tracking radar stations were used. During the very high acceleration of the round, none of the optical or the radar stations was able to stay locked on the vehicle. Because of launcher tip-off and thrust misalignment, many of the fixed cameras did not retain the vehicle within their field of view. Accordingly, no information from the ground tracking systems was obtained on the first flights.

Two possible new techniques were proposed for obtaining trajectory data for the Hypersonic Test Vehicle. The first was to place a radar tracking beacon aboard the missile so that automatic lock-on for the radar tracking ground stations would result. The other technique proposed was to place a flashing light or pyrotechnic flare aboard the missile and to use fixed plate ballistic cameras and night launches to provide the trajectory data. The ballistic camera approach was selected because of the excessive amount of weight required to carry a radar beacon in the missile. Pyrotechnic flares were carried on the tail fins of the hypersonic test vehicle, and the auxiliary ballistic cameras had carefully timed shutters to provide a timing reference on the film.

At least three ballistic cameras were used, permitting calculation of a complete three-dimensional trajectory for the rocket. On a typical film would appear continuous star tracks with lengths depending on how long the camera shutters were open. A dotted image would appear when the flares and the rocket ignition of the two-stage vehicle were interrupted by the shutters on the camera. The correlation of the various camera plates was achieved by the shutter interruptions and by the flash of the ignition in the first and second stages of the rocket. Accurate acceleration, velocity, and position data were obtained by using this technique.

The ballistic camera tracking technique is widely used at most flight test bases for very accurate tracking data. A flashing light is commonly carried aboard the missile so that no shutters are required on the camera. The ballistic camera technique requires, of course, that night launches be used and that the flashing light be visible to the camera regardless of the roll or pitch attitude of the missile. The launches are further limited to clear nights when cloud formations will not interfer with the visibility of the flashing lights or pyrotechnic flares.

The tracking requirements for the Hypersonic Test Vehicle caused major modifications of the missile, the launcher, the checkout and sequencing equipment, and of the ground-based tracking equipment. The missile fins were redesigned to accommodate the pyrotechnic flares. The complete weight and balance of the vehicle was altered. The launcher and umbilical were modified to permit the checking and ignition of the flares before launch. The firing console was modified to incorporate new procedures resulting from the addition of flares on the missile. Complete new camera pads were required, and the shuttered ballistic cameras were redesigned and fabricated for the program. This supporting subsystem played a major role in determination of the schedules and results obtained from this research program.

19.5.4 Angle of Attack

In addition to the characteristics of a missile trajectory, the angle of attack of the missile during its flight is also of considerable importance. The angle of attack is an aerodynamic parameter—the angle between the missile longitudinal axis and the relative wind vector. Accordingly, in addition to the missile velocity and attitude in space, the relative atmospheric wind must also be considered. The angle of attack may be measured by pivoted vanes which are located on booms extending from the front of the nose cone, or by appropriately spaced pressure orifices placed on the nose cone. If upper atmosphere wind data is available, the angle of attack may also be computed by determining the missile velocity vector in space coordinates by ground tracking, and the missile attitude in space by output from its guidance system.

Several sources of inaccuracy are inherent in the technique of using a nose cone boom with a vane to measure the angle of attack of a missile. The boom deflects because of the aerodynamic loads at angle of attack, the response of the vane depends on the frequency of the change of the angle of attack of the missile, and there are errors associated with the telemetering of the vane position relative to the boom. This technique correctly measures the aerodynamic angle of attack since the vanes automatically sense the resultant of the relative wind vector and the missile velocity vector.

Another method of measuring the true aerodynamic angle of attack is to place four or five pressure orifices in the nose of the missile. However, this method requires extensive wind tunnel testing because the correlation of the measured pressure with angle depends strongly on the Mach number of the missile. In addition to the large number of data channels that must be transmitted to the ground and interpreted, there is the problem of none cone shape. Any change to the shape of the nose cone necessitates a completely new set of calibration runs in a wind tunnel. Accordingly, this support system may cause postponement of a desirable change to a nose cone shape because a wind tunnel program must be scheduled for accurate calibration of the angle-of-attack system.

The third commonly used technique for determining angle of attack depends on three sets of data independently derived. The first set is the velocity and position along the trajectory derived from ground tracking or telemetered accelerometer data. The second set is the missile attitude in space derived from optical tracking or from gyro pick-off data telemetered from the missile. The third set of data is the relative atmospheric wind derived from meteorological data acquisition. By mathematically combining the data on missile attitude along the trajectory and the missile velocity and wind vectors, the aerodynamic angle of attack may be computed. Relatively large inaccuracies result because of difficulty in establishing atmospheric winds at the exact time of the missile flight. Meteorological data is usually taken two to five hours before the flight and gust conditions cannot be forecast accurately.

19.6 RANGE SAFETY

19.6.1 Analysis of Normal Trajectory

Range safety calculations and analyses begin at the earliest phases of missile and auxiliary support system design. Before a flight test program can be planned, it must be established that the probability is very small that the missile will deviate from its normal flight and endanger personnel. The ultimate selection of a flight test site is often determined solely by the range safety analysis.

The range safety calculations begin with a detailed analysis of the normal trajectory of the missile. Because of the many small perturbations that may influence a completely successful launch of a missile, there will be an envelope of the trajectories for a normally functioning missile. A large number of trajectories must be computed with small changes made to such parameters as thrust misalignment, launcher tip-off at separation of stages, and atmospheric winds. In Fig. 19.11 is shown a typical range safety problem for a two-stage research rocket. The normal trajectory, including the boost phase for the first stage, the boost phase for the second stage, the coasting phase to summit altitude, and the fall to impact, will be influenced by the five functions shown. The radius of the allowable impact area is computed by assuming that each of the five forcing functions acts independently of the others. Accordingly, the probability of landing within a certain impact circle is computed by computing a root mean square sum

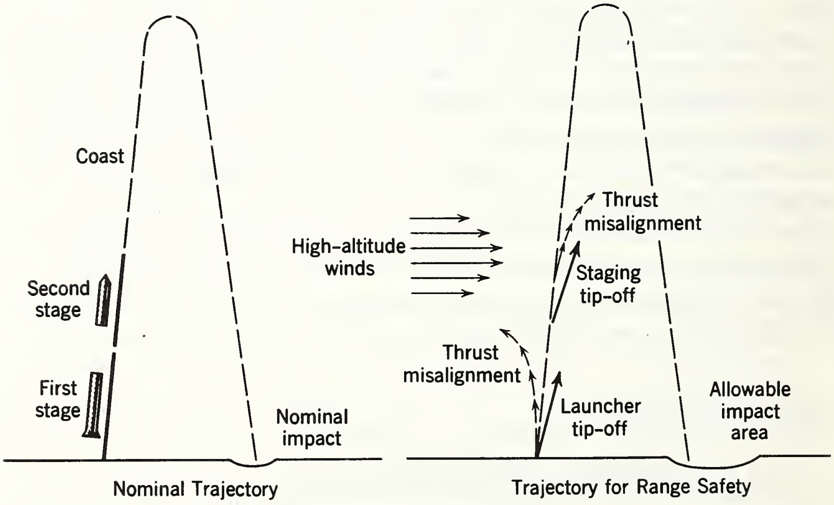
Coast
Second stage
First stage
Nominal impact
Nominal Trajectory
High-altitude winds
Thrust misalignment
Staging tip-off
Thrust misalignment
Launcher tip-off
Allowable impact area
Trajectory for Range Safety

Fig. 19.11 Typical range safety problem for a two-stage research rocket.

of the probable deviations resulting from launcher tip-off, thrust misalignment of first stage and of staging tip-off, thrust misalignment of the second stage, and high-altitude winds.

In addition to computing an allowable impact area, an envelope of the position of the missile during the two boost phases must be provided to the range safety officer. If the tracking data during the flight shows that the missile is deviating from the allowable envelope, the range safety officer will usually elect to blow up the missile.

The influence of high-altitude winds on ballistic rockets must be carefully considered. A guided vehicle may automatically compensate for the drift and angle of attack induced by high-altitude winds. The trajectory of an unguided missile may be strongly influenced. If an unguided rocket is accelerating under rocket thrust and is aerodynamically stable, a curvature of the flight patch will be induced by winds since the thrust vector will be rotated relatively to the missile velocity vector. If, for example, in the problem shown in Fig. 19.11, the second stage is coasting in a region of high-altitude winds the missile will assume an angle of attack relative to the winds; if the second-stage rocket is ignited at that time, the thrust vector will be inclined to the trajectory and the missile trajectory will be curved. It is a usual design requirement with multistage unguided sounding rockets that no ignition of any stage occur in the region of high upper atmospheric winds.

The range safety equipment that must be carried aboard every missile subtracts from the amount of equipment that may be carried for research. In addition to range safety tracking beacons, fail-safe explosive equipment must be carried to allow the range safety officer to destroy the missile, if necessary. Provisions for range safety equipment must be included in the earliest design layouts made for any ballistic or space vehicle system. In addition to the equipment required aboard the missile, there must be the checkout and handling equipment at the launcher, the range safety monitoring consoles in the blockhouse, the range safety receivers and transmitters on the ground, and the range safety tracking equipment which may include both radar and optical ground stations. This entire range safety auxiliary subsystem must be tested for functional acceptability before its use in the flight test of a ballistic rocket.

19.6.2 Failure Trajectory Analysis

In addition to the determination of an envelope of normal missile trajectories, a failure trajectory analysis must also be made for the range safety officer. The failure trajectory analysis is required to estimate the impact area of the missile for all possible types of failures, and to estimate the amount of time available to the range safety officer for a decision regarding destruction of the missile after it leaves the envelope of normal trajectories. This analysis must recommend to the range safety officer how rapidly and completely the missile is to be blown up in order to prevent it from landing beyond a safe impact area.

Typical types of malfunctions which must be analyzed for any ballistic rocket system are the following.

1. Guidance failure during boost.
2. Blow up of the first stage of a multistage rocket.
3. Structural failure of the interstage connector of a multistage rocket.
4. Aerodynamic instability of the vehicle.
5. Failure of the launcher, causing large tip-off angles at launch.
6. Nozzle failures, causing large thrust misalignment.

Each of these types of failures must be analyzed to predict the possible impact zone and the time required for the missile to reach unsafe impact areas.

19.7 SUMMARY

Auxiliary support systems require continuous technical and management attention during the development of a ballistic or space vehicle system. The supporting systems are usually time-determining in the development program and also require the expenditure of approximately 85 per cent of the total funds for a program. The technical problems involved in the design of the auxiliary support systems will often cause trade-offs which change the mission for the complete vehicle system.

20

THE MISSILE AS AN INTEGRATED SPACE VEHICLE SYSTEM

K. Brown

20.1 INTRODUCTION

The preceding chapters have discussed the elements of vehicle design, including propulsion, structures, vehicle staging, performance analysis, radio guidance, inertial guidance, control, re-entry, and recovery. The objective of this chapter is to study the conceptual problem of analyzing all these elements of a missile or space vehicle system as an integrated whole. An analysis of a system as a whole, if sufficiently quantitative, serves to define better the design requirements and specifications for the various subsystems. More importantly, a systems analysis can serve as a guide to making decisions when the design requirements of the several subsystems are in apparent conflict with each other. The analysis can serve to reduce some element of the design problem to comparatively precise terms so that experience and expert opinion can more easily be brought to bear on the remainder.

The first step in a systems analysis is to define clearly the objective of the system in functional terms and then to see whether the system meets these terms.

The analysis can be broken down into the following steps.

1. A definition of system objectives in quantitative terms, or system value.
2. A definition of general requirements, that is, the requirements for a system with maximum system value.
3. A synthesis of a system which can meet the defined requirements.
4. A definition of subsystem requirements to meet the general system requirements.
5. A definition of interfaces between the subsystems.
6. Detailed subsystem specifications.

Of these six steps for arriving at detailed subsystem specifications, the first two, the definition of system value and the definition of the general requirements for the system with maximum system value, could be defined as the performance parameters and will be considered together.

20.2 PERFORMANCE PARAMETERS

In attempting to understand the concept of system value for a ballistic missile system, it is helpful to start by enumerating the basic elements of performance for such a system. Such elements include (a) range, (b) payload weight, (c) accuracy (defined as circular error of probability), (d) reliability, (e) readiness, (f) vulnerability (including hardness, dispersion, reaction time, exposure time, and penetration).

All these elements must then be integrated in complex fashion with operating manpower requirements, operational flexibility, and cost. Obviously, some of these elements of performance may conflict. For example, a given missile can carry a large weight (payload) for a relatively short distance (range) or a smaller weight for a longer distance. Reliability and accuracy may also be in conflict.

If we wish to derive the maximum value from the complete system, it would be necessary to balance properly these various conflicting elements of performance. More specifically, it would be desirable to define a quantitative function of an analytical value corresponding to the maximum value.

This quantitative function is the system value previously defined.

Ideally, we would try to define such a system value function in terms of the basic elements of performance just listed: range, payload, accuracy, and so forth, and then to select the requirements for range and payload that maximize the system value function. Also ideally, these requirements for the basic performance parameters would then be used to specify subsystems requirements. In practice, however, it is difficult to achieve this much quantitization; the variables are too complex. It becomes necessary, therefore, to devise an analytical model that approximates the real system as closely as possible. Such a system model is in many ways analogous to the wind tunnel model used in aerodynamic testing. We perform an analysis on the model and then attempt to interpret the analysis in terms of a full-scale situation. For example, the broad objective of a ballistic missile system is to be, with a high degree of probability, capable of destroying an enemy target whenever called upon. The system value could be considered as the probability of destroying targets. The system value can be further simplified to the probability that a single missile, when called upon to do so, will destroy a single assigned target. In a simplified model an analysis would show that the maximum system value (destroying the target with one missile) can be achieved if the following factors occur with a high probability.

1. Survival of enemy attack on the ground.
2. Readiness.
3. Reliable operation in flight.
4. Survival of enemy countermeasures in flight.
5. Survival of atmospheric heating during re-entry.
6. Ability to achieve the necessary damage when the nose cone actually hits the target.

These probabilities can be considered as essentially independent events because they occur at different times, from before take-off to target impact. Therefore, a simple multiplication of the probabilities of each event, shown in equation form in Fig 20.1, is reasonably accurate in describing the total probability of destroying the target with one missile. This basic equation can thus be used to balance the

$$(P_{\text{DESTROYING TARGET WITH ONE MISSILE}}) =$$

$$(P_{\text{SURVIVAL ON GROUND}}) \times (P_{\text{READY TO GO}}) \times (P_{\text{RELIABILITY}}) \times$$

$$(P_{\text{SURVIVAL AT RE-ENTRY}}) \times (P_{\text{NECESSARY DAMAGE WHEN HIT}}) \times$$

$$(P_{\text{SURVIVAL OF ENEMY COUNTER MEASURES}})$$

Fig. 20.1

various requirements for the optimum ballistic missile system. For example, the highest probability of achieving damage when the nose cone hits the target can be achieved by constructing an accurate and precise guidance system; however, this may introduce into the design a complexity that would tend to reduce reliability. The desire for accuracy can be balanced against the necessity for reliability.

Thus a model of even this simple kind can be used conceptually and, as shown in a later example, quantitatively, to weigh and balance the various elements of system design and to achieve a maximum system value. However, the model presented here omitted several elements of the problem, such as the cost of development; therefore the analysis is incomplete.

20.3 OVER-ALL SYSTEMS ANALYSIS

Following the establishment and evaluation of the performance or so-called strategic parameters, it is necessary to make a systems synthesis or systems analysis of the complete system, including establishment and definition of the detailed subsystem requirements, which are often referred to as the system-controlling parameters. Table 20.1 shows a partial list of typical parameters, but in a complete ballistic missile system there are hundreds. Varying these parameters in a process of engineering synthesis will give a number of possible functional configurations that will satisfy the detailed requirements. These chosen functional and para-

TABLE 20.1

Missile and Geodetic Factors

Stage thrust (as a time variable)
Total flow rate, mass ratio versus time
Vernier thrust and flow rate
Missile take-off weight
Missile dry weight
Propulsion specific impulse
Engine and vernier decay impulses
Engine and vernier burning times
Drag coefficient versus Mach number
Drag coefficient versus control means
Missile and nose cone drag areas
Missile and nose cone normal force coefficient and areas
Missile and nose cone moment coefficient and areas
Center of pressure versus attitude
Center of gravity travel
Booster programmed tilt time and kick angle
Guidance initiation times
NPSH versus time and acceleration
Autopilot steering gains, pitch, and yaw
Autopilot time constants and rates
Accelerometer constants
Minimum radar elevation angle
Staging sequence parameters
Duration of gravity turn
Re-entry angle
Nose cone weight
Local heating boundaries

Look angle boundaries

Guidance weight per unit of circular error probability

Staging constants

Earth constants

Launch point constants

Atmosphere distribution (pressure and speed of sound as a function of altitude

Wind profile

metric configurations can be translated into physical ensembles involving block, interaction, and circuit diagrams, inboard and outboard profiles, computer logic tables, overall kinematics and space layouts, major structural arrangements, crude weight and inertial distribution tables, and other physical summaries. The systems design and analysis effort can then be programmed in the following manner.

1. The definition of key problems and problem areas.
2. The corresponding choice of solution methodology.
3. The enunciation of research objectives and development milestones.
4. The establishment of the guidelines necessary for an operational concept (silo, ground support equipment, mobility, transport, communication).
5. The establishment of technical budgets, such as reliability and weight budgets.
6. The establishment of test philosophy and gross test objectives, numbers of ground and flight tests.
7. The specification of necessary facilities.
8. The preliminary programming, selection of numbers of missiles, and subsystems.

A development program can then be prepared with known problem areas, projection times, and cost and anticipated schedules.

With the program outlined and the system established, the next step is to formulate the system and subsystem design criteria and the associated detail specifications. To accomplish this, continuous refinement of the system and subsystem design is necessary to establish trade-offs between various subsystem requirements and to make explicit significant interfaces. An assessment must also be made of the environment to be encountered throughout transport, silo storage, and trajectory flight.

All significant subsystems must be constructed to a functional design, to a performance criterion, and to a model specification. Such design criteria should include pertinent geophysical and meteorological data, standard and nonstandard atmospheric models, structural loading envelopes, and materials selection and fabrication processes.

In the preceding chapters the detail design analyses for most of the major systems of a complete ballistic missile system have been presented. When applicable, many problems relating to interface have also been discussed. It is the intent in this chapter to present a broad philosophical look at a few additional areas that must be considered in the broad coverage of the complete integrated analysis of a ballistic missile or space vehicle system.

20.3.1 System and Subsystem Testing

A well-planned over-all test program will minimize major design failures that occur in operational flights. The spectrum of tests required to develop a highly reliable ballistic weapon is very wide, starting with functional testing of the smallest parts under environmental conditions and ending with actual flight tests of the complete vehicle. A complete testing program would include the following.

1. Laboratory component tests.
2. Cold-flow laboratory work.
3. Aircraft tracking tests for early guidance work.
4. Rocket attenuation experiments on microwave signals.
5. Shock tube.
6. Arc tunnel.
7. Wind tunnel research.
8. Drop test and re-entry experiments.
9. Thrust chamber and engine development tests.
10. Battleship, captive, and flight readiness firings.
11. Dynamic and structural.
12. Autopilot static and dynamic testing.

13. Sled.
14. Shake table and centrifuge operations.

At each higher and generally more complicated and expensive level of testing, benefits are realized from the testing at lower levels. The interrelation of all tests must be reviewed, and a system of feedback to the design process is a definite requirement.

20.3.2 Reliability

As discussed in Section 20.2, reliability plays an extremely important role in performance parameters because it directly affects range, accuracy, payload, and readiness. Reliability is also an important system-controlling parameter and a specific design parameter.

From an over-all system approach it is necessary to establish quantitative reliability requirements and a reliability apportionment for the vehicle, its propulsion and guidance, the power supply, re-entry vehicle, instrumentation systems, and all other major and subsystems. To establish reliability predictions and procedures, a typical five-step evaluation testing program consists of (a) design and development tests, (b) acceptance tests, (c) flight proofing tests, (d) qualification tests, (e) production monitoring tests.

A reliability model should be established for each component or system and an assessment made of the reliability implication of an alternate design. In these reliability design analyses, the factors of derating, redundant circuits, provision for parameter drift producibility and simplicity, standards, packaging, and the human element should be included.

20.3.3 Advanced Missile Studies

In advanced missile studies the desirable characteristics of the weapon system should first be determined. Starting with only the general constraints, the probability of success of a given flight with high reliability and logistic simplicity, the complete spectrum of technically feasible propellant combinations, guidance systems, and re-entry vehicles must be studied parametrically. Beginning with the functional relationship of accuracy and warhead yield required to achieve a given destructive effect with a given probability, the optimization process simultaneoulsy determines the necessary booster weight for a particular propellant combination, the necessary aerodynamic properties of the re-entry vehicle, the associated warhead size, and the general properties of the required guidance system. Advanced studies of this type use the following items of information.

1. Geophysical uncertainties and their dependence on mode of flight.
2. Atmospheric winds and density fluctuations and their influence on re-entry vehicles.
3. Influence of the ionosphere and troposphere on various radio guidance systems.
4. Structural requirements and stage sizes for various fuel combinations.
5. Payload capabilities of various propellants flown to a given range with different velocities.

Finally the various combinations of propellants and guidance systems should be optimized with respect to ground support equipment, reliability, and reaction to counter measures.

20.3.4 Lunar and Interplanetary Missions

Although lunar or interplanetary mission differs from the ballistic missile system because such parameters as readiness, fast reaction capability, and operational concepts do not apply, some specific parametric studies are necessary for such missions. In addition to payload weights and vehicle configurations, there is now added the additional parameter of flight mission. For example, the early guidance studies were influenced by vehicle calculations which indicated that only limited weight could be allocated to guidance systems. Such weight limitations clearly ruled out the use of available ballistic missile guidance systems and led to the design of several systems combining autopilot components with a versatile radio system that measured Doppler shift for tracking, transmitted telemetry, and received and executed commands. Analysis of vehicle and guidance dispersions showed that the vehicle control executed during powered flight could not in itself furnish sufficient accuracy and had to be augmented by a simple midcourse correction. The firing of a number of small vernier rockets mounted on the payload could be utilized to provide this midcourse corrective thrust. The problem of determining from incomplete tracking data the optimum number of rockets to mount on the payload and the optimum number to fire in flight requires a mathematical solution. Such analyses have extended the theory of control systems in the area of final-value control.

Because early vehicle guidance systems did not have enough flexibility to compensate for changes in launch time, it was necessary to determine the probability of carrying out the mission at various launch times compared with the probability of launching the vehicle as a function of time. This process in turn made it necessary to integrate the entire countdown procedure and the launch procedure with the complete system to maximize the probability of being able to launch a vehicle in a given launch interval.

In determining orbits for satellites around the earth, moon, or planets, many trajectory characteristic studies are required to establish an optimum orbit using the available guidance and vehicle characteristics. Because of the effect of guidance and vehicle dispersion, which is nonlinear, an entire family of dispersed trajectories should be considered in the selection of the nominal orbits that are optimum.

In the over-all systems analysis of interplanetary flights, such interrelated factors as the following must be considered.

1. Effect of the uncertainty in the astronomical unit.
2. Possibility of measuring the astronomical unit by a probe.
3. Relationship between launch conditions and terminal conditions at the planet.
4. Transmission distances for communication.

20.4 SPECIFIC DESIGN PARAMETERS

The problem of cooling electronic equipment may be used to illustrate how a simple systems model can be a guide in delineating subsystem requirements when the several subsystems interact. This cooling problem confronts every systems designer, particularly early in the life cycle of a system. The failure rate of the system components increases rapidly as the temperature (Fig. 20.2a) of electronic components increases. Also, as shown in Fig. 20.2b, the reliability of the complete system can be considered as a function of the product of the failure rate of individual elements (N_{fr}), and the time in which these elements must perform within the stated specification. If the failure rate increases, which corresponds to a temperature increase in Fig. 20.2a, the reliability decreases. Thus it seems desirable to provide adequate cooling for the electronic equipment and maintain a low failure rate.

On the other hand, the refrigeration necessary to cool the electronic equipment also weighs something, and a missile or space vehicle system is very sensitive to weight. The weight of the cooling equipment (Fig. 20.2d) is inversely related to temperature; therefore, if the allowable temperature is high, the cooling equipment weight can be small.

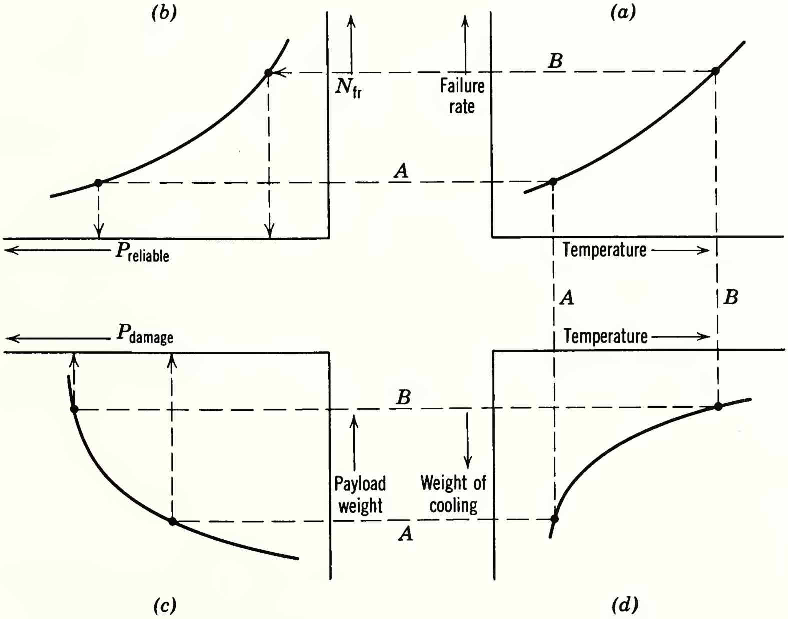

N_{fr} = Product of failure rate of individual elements

Fig. 20.2

When the weight parameter is considered, it is necessary immediately to introduce the size of payload carried in the vehicle. For ballistic missiles the weight of the payload is directly proportional to the probability of achieving damage at the target. As shown in Fig. 20.2c, the probability of damage increases as the payload weight increases.

If all these individual elements are evaluated together, it is possible to arrive at a specific design point that maximizes the product of reliable operation and probability of achieving damage and, in effect, maximizes the system value. This evaluation is represented by the connecting lines A and B of Fig. 20.2. If the electronic equipment is cooled to the corresponding temperature at A (Fig. 20.2a), the reliability of the system will be high (Fig. 20.2b). This low temperature can be achieved only by heavy cooling equipment (Fig. 20.2d) which would reduce the payload capability. With a low payload the probability of damage (Fig.20.2c) will be low. If the electronic equipment were allowed to run at the higher temperature of B (Fig. 20.2a), the failure rate would increase and the reliability (Fig. 20.2b) would decrease considerably. However, with this higher temperature the weight of cooling equipment would be reduced (Fig. 20.2d) and, in turn, this reduction would allow an increased payload. With an increased payload (Fig. 20.2c) the probability of damage would be considerably higher.

From these two interconnecting curves, A and B, based entirely on the temperature of electronic cooling equipment, it is shown that as the reliability increases the probability of damage decreases. Therefore, there must lie somewhere between these two sets of conditions a point that is optimum, or a point at which the product of these terms is maximized. Both terms are found in the definition of the model of system value.

20.5 CONCLUSION

It is apparent that even the approximate model of a ballistic missile system can be used as a conceptual framework within which to examine a specific and detailed problem, as illustrated in the example of the cooling of electronic equipment in the system, in Section 20.4. The difficult task of defining the objectives and the system value requires a conceptual approach in sufficiently quantitative terms to permit the construction of an analytical model. Such a model, in turn, can be used as a working tool to obtain a definition of the design requirements that will maximize the value of the system for its intended use.

To avoid erroneous conclusions from this kind of analysis, it is necessary to understand clearly the effect of these elements of the total problem that are not explicitly incorporated in the analytical model. The generality of the model can be expanded to such a point that the model becomes a statement of a hypothetical problem. On the other hand, the scope of the model can be narrowed to such a point that it omits so many important elements of the problem that the analysis is misleading rather than clarifying.

INDEX

Ablating material, 468
Acceleration, 126
  axial, 209
Accelerometers, 415
Advanced missile studies, 510
Aerodynamic forces, 235
  heating, 236
Airframe dynamics, 254
Alcohol, properties as nuclear propellant, 94
Ammonia, properties as nuclear propellant, 94, 99, 100
Angle of attack, 498
Angular rate measurement, 386
Antenna beam width and gain, 378
Attitude control systems, 424
Autopilot, 260
  actuator, 267
  and engine dynamics, 269
Auxiliary subsystems, 470
Axial acceleration, 209
Axial load, 212, 236
  factor, 209

Ballistic flight analysis, 169
Ballistic missile control system, 362
Ballistic missile trajectories, 176
Bending equations, dynamic, 265
Bending loads, 215
Bending moment at launch, 287
Beryllium, as reactor material, 97
Bipropellant tank configurations, 235
Blockhouse for rocket program, 485
Boost rocket capability, 296
Buckling, 222
Burnout altitude versus burnout angle, 306
Burnout angle versus velocity, 299
Burnout surface range, 307
Burnout velocity, 92, 102, 171
  of nuclear rockets, 101, 102

Centrifugal pump, 65
Characteristic length, 37
Characteristic velocity, 26, 36, 125
Charge neutralization, 133
Checkout, 153
Chemical rockets, compared with nuclear rockets, 92, 101, 102, 103
Circular probable error, 6
Combustion chamber, 45
Combustion pressure level, 46
Complex frequency domain, 351
Compressibility flow, 268
Concurrency, 10, 471, 474

Conservation law for enthalpy and kinetic energy, 20
Conservation of energy, 122
Conservation of momentum, 122, 155
Control system, 260, 266
  ballistic missile, 362
  bending, 364
  inputs, 367
  nuclear rocket reactor, 106, 107
  pole-zero diagram, 367
  power servos, 365
  sloshing, 364
  stability, 357
  stability measurements, 357
  stability tests, 357
  summary, 370
  tail wags dog, 366
  theory, 345
Coordinate system, 263, 284, 407
Core design, 97, 115, 117
Core power density, 104, 105, 114, 117
Countdown, 153
  launch, 492
  prelaunch, 491
  procedures, 486
  two years, 486

Damping, missile axial loads, 293
Data acquisition, 492
Decay power, 111
  flight tests, 112
  static testing, 112
Deceleration, 449
De Laval nozzles, 24
Density of structural materials, 224
Differential coefficients, 428
Differential equations, description of control systems, 346
  steady state sinusoidal solution, 347
Diffraction, 376
Direction finding, 379
Doppler principle, 385
Drag curves, 302
Drag loss, 320
Drag velocity loss, 302
Dynamic loads, 220, 253
  control system limit cycle, 274
Dynamic pressure, 209

Earth satellite orbital analysis, 336
Earth satellites, 179
Earth's rotation effect, 305
Electrically propelled rocket, 120
  performance properties, 124
Electromagnetic theory, 373
Electromagnetic thrust devices, 127
Electronic equipment cooling, 512
Electrostatic propulsion, 128
Electrostatic thrust devices, 128
Electrothermal thrust devices, 127
Elementary trajectory, 333
Elliptical trajectory, 330, 333
Engine alignment, 149
  balancing, 146
  calibration, 146
  swiveling equation, 266

Engine alignment
  transient operation, 150
Engineering of interface problems, 144
Enthalpy and kinetic energy, 20
Entry velocity, 451
Environmental control, 481
Equation of motion, 261
Escape velocity, 163
Euler formula, 222
Exchange ratios, 312
Exhaust velocity, 36

Failure rate, 513
Failure trajectory, 502
Feedback, advantages, 354
  concept, 352
Fission density distribution, 107, 108
Flight, free, 171
  powered, 169
  trajectory, 169
Flight dynamic loads, 254
Flight dynamics, airframe, 254
  control system, 260
  propellant sloshing, 258
  propulsion system, 260
Flight loads, 221
Flight near Earth's surface, 158
Flow, hypersonic speeds, 453
Flow around bodies, 453
Flow dynamics, 48
Flow geometry, 48
Fluid sloshing, 259
Forces acting on missile, 264
Free flight, 171
  motion, 173
  trajectory, 299, 307
Fuel element base material, for nuclear rockets, 94, 97

Gas velocity as a function of pressure ratio, 21
General operational requirement, 5
General trajectory considerations, 449
Geodetic and missile factors, 507
Geometric optics, 373
Geometry of satellite orbit, 330
Gimbaling, 148
Gimbal-mounted rocket engine, 72
Graphite, fuel element base material, 95, 96, 97, 104
  neutron moderator, 97
  rocket reactor reflector moderator, 97
  thermal strain effects, 104
Gravitational loss, 300
Gravity, 426
  loss, 318
  turn, 208
Ground loads, 221
Ground reflection errors, 393
Ground support system association, 12
Ground support system integration with missile, 13
Guidance, nuclear rockets, 109
Guidance analysis, 333
Guidance schemes, 430
Guidance system synthesis, 437
Gyros, input-output, 410
  single degree of freedom, 409

Gyros, input-output
  two degrees of freedom, 405
Gyroscope drift, 413
Gyroscopes, 404

Heating laws, 452
Heat shield, 460
  material, 462
Heat shielding, satellite, 467
Heat sink, 459
Heat transfer, 456
Heat protection system, 459
High loop gain, 356
Hohmann ellipse, 165
Hydrogen, as nuclear propellant, 94, 97, 98, 99, 100
Hydrostatic pressure, 219
Hyperbolic trajectory, 333

Impulse turbine, 63, 66
Impulse-weight ratio, 35
Impulsive and finite thrust, 319
Inertial guidance elements, 403
Inertial guidance missile example, 432
Inertial guidance systems, 402
Inertial navigation, 426
Inertial space, 423
Inertial velocity, 305
Inputs, 367
Instrumentation of nuclear rockets, 112, 113
Insulation, 468
Integral versus non-integral structure, 234
Integrated weapon system, 472
Integration, payloads, 199
  stages, 199
  vehicle, 199
Intercept, lunar and satellite, 181
Interface problems, 11
Internal pressure, 219, 236
Interplanetary and lunar missions, 511
Interplanetary flight, 164
Interplanetary missions, 185
Inverse square field, 161

Jetavator, 76
Jet vane, 75
Jet velocity, 20

Kepler ellipse, 308
Kepler's law, 337

Laplace transform, 346, 353
Lateral binding, 254
Launch complex, 481, 482
Launch countdown, 492
Launching in wind, 283
Liquid propellant properties, 94
Liquid propellant rocket engine, 54
  definition, 54
  pressure fed, 55, 58
  turbopump fed, 57, 60
Liquid rocket ballistic missile system, 139
Liquid rocket design procedure, 38
Loads (see type)
Lunar and interplanetary missions, 511
Lunar or satellite intercept, 181

Macroscopic absorption cross section, 96, 97
Mass flow through nozzle, 25
Mass ratio, rocket vehicles, 92
  variation with specific impulse, 93
Materials for nuclear rocket reactor, 93, 98
Maximum range capability, 145
Maximum thrust, 19
Meteorological effects, 480
Miss coefficient, 334
Missile and geodetic factors, 507
Missile axial loads, damping and release time, 293
Missile bending equations, 265
Missile deflections, 261
Missile design parameters, 314
Missile monitoring, 480
Missile parametric design analysis, 237
Missile structure, trajectory characteristics, 207
  trajectory shapes, 208
Missile subsystems, 2, 3
Missile transporting and handling, 480
Mission, examples of lunar, 184
  interplanetary, 185
  lunar, 182
  lunar and interplanetary, 511
  size, 197
  space vehicles, 176
  to Mars, 165
  velocity, 175
Mission equivalent velocity, 175
Mixture ratio control, 146
Moderators, nuclear rocket reactors, 97
Modules of elasticity, structural materials, 224
Molecular weight, 23, 57
Momentum theory, 17
Motion in an inverse square field, 161
Motion in general gravitational field, 329
Motion over a spherical nonrotating earth, 159

Neutron and gamma ray radiation, 110
Neutrons, nuclear rocket reactors, delayed, 105, 106, 107
  fast, 97
  prompt, 106
  moderators, 97
Newtonian pressure law, 454
Niobium carbide, 95, 96
Normal trajectory, 499
Nozzle area ratio, 28
Nozzle pressure loss, 302, 321
Nuclear energy, introduction, 90
Nuclear power, aircraft, 90
  naval vessels, 90
  rockets, 90, 118
Nuclear propulsion, thrust-to-weight ratio, 98
  Vehicle design, 108
Nuclear radiation leakage, 108, 110
Nuclear rocket, materials, 93
  performance, 98, 103
  propellants, 93

Nuclear rocket
  schematic, 91
  start-up, 105
  testing, 109, 114
  vehicle design, 108, 109
Nuclear rocket design problems, 103, 108
Nuclear rockets, 90, 118
Nuclear system performance, 101

Oblateness, 342
Octane properties, 94
Operations analysis, 5
Optimization, 4
Orbital analysis,
  earth satellites, 336
Orbital parameters, 336
Orbits, satellite, 179
Outage, 146, 147, 154
Over-all systems analysis, 506

Parabolic mirror, 376
Parameters, performance, 504
  specific design, 512
Parametric design analysis, 237
Parametric studies, 7
Parametric study, boost rocket, 296
Performance capability of boost rockets, 296
Performance parameters, 504
Perturbation equations, 439
Plasma, general theory, 120
Plasma engine, 127
Plasma propulsion, introduction, 119
Platform, stabilized, 420
Platform servos, 422
Post launch dynamic loads, 275
Power density, 100, 104, 114, 117
Powered flight, 169
Power requirements for nuclear rockets, 104
Prelaunch countdown, 491
Prelaunch dynamic loads, 275
Preliminary design, 138
Pressure ratio, 28
Pressure vessels stresses, 227
Principle of concurrency, 10
Principle structural loads, 212
Probabilities, 505
Probability damage, 513
Probability reliability, 513
Process of iteration, 8
Products of combustion, 57
Program schedule, 473
Propagation errors, 387
Propellant, nuclear rockets, 93, 94, 97
Propellant flame temperature, 57
Propellant injector design, 47
Propellant loading, 153, 154
Propellant loading bias, 147
Propellant mixture ratio, 57, 67
Propellant sloshing dynamics, 258
Propellant specific impulse, 55, 58, 99
Propellant stay time, 70
Propellant tanks, 55
  analysis, 244
Propellant utilization, 146
Properties of liquid propellants, 94

Propulsion interface, 138
Propulsion interface concept, 138
Propulsion system, 260
Pump, cavitation, 65
  centrifugal, 65
  discharge flow, 63
  external leakage, 65
  inlet head, 65
  internal leakage, 65
  operation, 63
  output head, 63
  suction head, 65

Radiation after shutdown of nuclear rockets, 112
Radiation in nuclear rockets, 95
  structural design, 105, 108
  test facilities, 111
Radio guidance, equipment errors, 386
  errors, 386
  fundamentals, 372
  system design, 395
Radio measurements, 379
Range capability, 145
Range distribution function, 145
Range equation, 308
Range safety, 499
Range station, 485
Ranging, 383
Rate gyro, 411
Ratio of specific heats, 57
Reaction of a fluid jet, 16
Reactor design, 103
Reactor heat transfer, 114
Reactor performance, 98
Reactors in nuclear rockets, 103, 108
Reactor specific power, 99
Recovery, 494
Re-entry and recovery, 448
Re-entry vehicle trajectory, 449
Refractory metals, 95, 96
Relativistic speeds, 126
Release time, missile axial loads, 293
Reliability, 510
Resonance, 257
Retrorocket, 185, 462
  velocity, 463
Rhenium, 95, 96, 97
Rigid body equations, 262
Rocket propulsion, basic parameters, 43
  design criteria, 34
  design procedures, 43
  performance criteria, 34
Rocket prototype model, 50
Rocket specifications, 50
Rocket thrust, 16
Rocket vehicle performance, 54, 55

Satellite, orbits, 179
  re-entry, 461
  velocity, 179
Satellite heat shielding, 467
Satellite or lunar intercept, 181
Schedules, 473
Seismic mass, 418
Sequencing and monitoring, 481
Shock wave, 455
Signal to noise ratio errors, 389
Sine wave modulation, 384
Single stage vehicles, 304, 312
Sloshing dynamics, 258

Snell's law, 375
Solid propellant, advances, 79
  burning rate, 81
  other characteristics, 82
  properties, 84
  rocket design, 86
  rocket motor design, 85
  rocket motor operation, 80
  rocket trends, 88
Space vehicles, velocity, 191
Specific design parameters, 512
Specific heat ratio, 22
Specific impulse, 34
  influence on performance, 195
  of nuclear rockets, 92
Specific propellant consumption, 35
Spherical nonrotating Earth, 159
Stability, 357
Stabilized platform, 420
Staged rockets, 103
Stages, number, 195
Staging, 151
  problems, 151
Standard powered trajectory, 438
Structural design requirements, 233
Structural dynamic equations, use, 272
Structural elements, 221
Structural fabricability, 237
Structural loads, 212
Structural system interactions, 233
Structural weights, 236
Structure factory staging, 196
Structure fundamentals, 207
Structures, integral versus nonintegral, 234
  dynamic analysis, 253
  static, 232
Subsystem testing, 509
Supersonic nozzle contour, 24
Support equipment, 482
Support facilities, 482
Support functions, 479
Support system considerations, 152
Support system interactions, 152
Synthesis of system interfaces, 142
System model, 505
System optimization, 145
System performance, 144
Systems engineer, 14
Systems engineering, application, 4
  concept, 4
  definition, 1
  economic considerations, 9
  interface, 11
Systems synthesis, 506
System testing, 509
System value, 505

Tandem missile configuration, 243
Tandem missile design features, 250
Tanks, flight conditions, 246
  ground condition, 246
  handling and transporting, 237
  minimum gage, 246
  pressure, 247
  skin temperatures, 247
Tantalum, 95, 96, 97
Telemetry, 492

Tensile loads, 227
Tension and compression, combined, 229
Terminal statistics, 145
Test facilities for nuclear rockets, 110, 111
Testing program, 509
Test programs for nuclear rockets, 109, 114
Theory of gases, 23
Thermal loads, 218
Thermal neutron, 95, 96
Thermal strain in nuclear rocket reactors, 104, 105, 107
Thrust build-up, dynamic effects, 289
Thrust chamber, combustion chamber, 69
  cooling device, 57, 69, 71 72
  definition, 69
  injector, 69, 70
  nozzle, 55, 69
Thrust coefficient, 28, 36
  analytical definition, 30
Thrust law, 19
Thrust-programmed rocket, 103
Thrust-to-weight ratio, 169
Thrust vector control, 72, 148
Timoshenko beam theory, 255
Total impulse, 156
Tracking, 496
Trajectories, ballistic missiles, 176
  lunar geometry, 182
Trajectory, analysis, 324
  characteristics, 207
  considerations, 144
Trajectory
  elliptical, 330, 333
  failure, 502
  free flight, 299, 307
  hyperbolic, 333
  lunar launch, 183
  normal, 499
  parameters, 296
  re-entry vehicle, 449
  shape, 208
Transfer functions, 349, 352
Transient operation, 150
Tungsten, 95, 96, 97
Turbine, impulse, 63, 66
Turbopump, 63
  bootstrap operation, 60
  direct drive, 63, 66
  gas generator, 60, 67
  geared drive, 67
Two-stage vehicles, 312
Two-year countdown, 486
Typical support functions, 479

Uniform gravitational field, 325
Uranium-tungsten system, 95

Vacuum specific impulse, 298, 301
Vacuum velocity law, 155
Vehicle, size, 197
Vehicle path, 172
Velocity, burnout, 171
  burnout angle, 299
  capabilities of space vehicles, 191
  free flight, 171
  Mars or Venus, 190
  measurements, 385
  miss coefficient, 327
  mission equivalent, 175

Velocity
  satellite, 179
  summary, 191
Vertical flight, 158

Weapon system integration, 472
Weight balance, missile design, 242
Wind, launching, 283
Wind-induced oscillations, 275
Winds, 211

Zirconium carbide, 95, 96

Date Due

SCIENCE ROOM MAY 14 '62

Due	Returned	Due	Returned
MAY 29 '62 ML	MAY 16 '62	APR 21 '69 RD	APR [illegible] 2 1969
JUN 5 '62 ML	MAY 31 '62		
AUG 3 '62 ML	JUL 28 '62 ML		
OCT 30 '62 ML	OCT 31 '62 ML	OCT 31 '69 RD	
FEB 24 '63 ML	FEB 24 '63 ML		DEC 5 '69 RD
MAR 12 '63 ML	MAR 14 '63	DEC 05 1988 NOV 20 1990	DEC 08 1988 NOV 20 1990
OCT 11 '63 ML	OCT 1 '63	APR 20 1991	APR 24 1991
NOV 22 '63 ML	NOV 14 '63		
JAN 31 '64 ML	JAN 22 '64		
APR 6 '64 ML	MAR 25 '64		
APR 15 '64 ML	APR 18 '64		
JUN 22 '64 ML	MAY 28 '64		
JUN 14 '64 ML	JUN 4 '64		
NOV 17 '64 ML	NOV 17 '64		
DEC 1 '64 ML	DEC 1 '64		
DEC 15 '64 ML	DEC 12 '64		
MAR 4 '65 ML	MAR 3 - '65 ML		
APR 1 1 '65 ML	APR 13 '65 ML		
MAR - 3 '66 ML	MAR - 3 '65		

3 1262 00002 8901

KEEP CARD IN POCKET

SITY OF FLORID

268

IT IS IMPORTANT THAT
CARD BE KEPT IN POCKET